A. Lerman
D. Imboden
J. Gat
Editors

Physics and Chemistry of LAKES

Second Edition



Springer



Physics and Chemistry of Lakes

Edited by

Abraham Lerman, Dieter M. Imboden
and Joel R. Gat

With Contributions by

L. Chou, W. Davison, S.J. Eisenreich, J.R. Gat
J. Hamilton-Taylor, K.C. Hornbuckle, S.W. Hostetler
D.M. Imboden, R. Ishiwatari, D. Mackay
F.T. Mackenzie, M. Meybeck, P.A. Meyers, J. Schnoor
W. Stumm, S. Vink, P. Vlahos, T.C. Winter
R. Wollast, A. Wüest

With 176 Figures and 48 Tables

Springer-Verlag
Berlin Heidelberg New York London Paris
Tokyo Hong Kong Barcelona Budapest

Prof. Abraham Lerman
Department of Geological Sciences
Northwestern University
Evanston, Illinois 60208
USA

Prof. Dr. Dieter M. Imboden
Swiss Federal Institute of Technology (ETH)
and Swiss Federal Institute for
Environmental Science and Technology (EAWAG)
8600 Dübendorf
Switzerland

Prof. Joel R. Gat
Department of Environmental Sciences and Energy Research
The Weizmann Institute of Science
76100 Rehovot
Israel

Physics and Chemistry of Lakes
ISBN-13:978-3-642-85134-6

Lakes. Chemistry, Geology, Physics
ISBN-13:978-3-642-85134-6 e-ISBN-13:978-3-642-85132-2
DOI: 10.1007/978-3-642-85132-2

Library of Congress Cataloging-in-Publication Data. Physics and chemistry of lakes/edited by Abraham Lerman, Dieter Imboden, and Joel Gat; with contributions by L. Chou . . . [et al.]. – 2nd ed. p. cm. Rev. ed. of: Lakes – chemistry, geology, physics. c1978. Includes bibliographical references (p.) and index. ISBN-13:978-3-642-85134-6
1. Lakes. 2. Limnology. I. Lerman, Abraham. II. Imboden, Dieter M., 1943– . III. Gat, Joel, 1926– IV. Chou, Lei, 1953– . V. Lakes – chemistry, geology, physics. GB1603.2.L34 1995 551.48'2 – dc20 95-6098

This work is subject to copyright. All rights are reserved, whether the whole or part of the material is concerned, specifically the rights of translation, reprinting, reuse of illustrations, recitation, broadcasting, reproduction on microfilm or in any other way, and storage in data banks. Duplication of this publication or parts thereof is permitted only under the provisions of the German Copyright Law of September 9, 1965, in its current version, and permission for use must always be obtained from Springer-Verlag. Violations are liable for prosecution under the German Copyright Law.

© Springer-Verlag Berlin Heidelberg 1978, 1995
Softcover reprint of the hardcover 2nd edition 1995

The use of general descriptive names, registered names, trademarks, etc. in this publication does not imply, even in the absence of a specific statement, that such names are exempt from the relevant protective laws and regulations and therefore free for general use.

Typesetting: Best-set Typesetter Ltd., Hong Kong

SPIN: 10125632 32/3136/SPS – 5 4 3 2 1 0 – Printed on acid-free paper

Preface

Nearly 17 years have passed since the publication by Springer-Verlag of *Lakes: Chemistry, Geology, Physics* in 1978, edited by Abraham Lerman. That volume was among the first to focus on the role and interest of sciences other than biology in natural and man-made lakes. Strong emphasis in the book was placed on the sediments and sedimentary processes in lakes, in recognition of their role as recorders of historical information on geologically short- and long-term scales, and, perhaps somewhat farsightedly, of the expanding role that studies of lake sediments were to play as archives for palaeoclimatic reconstructions.

Since the late 1970s, there has been a great increase in the awareness of the environmental fragility of lake systems that include not only the water, sediments and land, but living plant and animal communities, as well as human populations that are often deeply integrated in their lake environment. Changes for the worse in lake systems – sometimes dramatic, such as the desiccation of the Aral Sea – have been increasingly and justifiably attracting more attention to lake-water and sediment pollution from various industrial, municipal or agricultural sources, their harmful and even deadly effects on lake biota, and health hazards to humans that are often associated with poor waste-disposal practices.

In a world greatly concerned with the consequences of all aspects of global change, and its natural and man-made causes, lakes are a relatively small, but from a human perspective important, component of the global environment. Human societies living near lakes depend on a great variety of things associated with them, ranging from aesthetic and recreational demands, to economic infrastructures, and the reliance on lakes as sources of water and ameliorators of local climate. Even those aspects of human activity that are perceived today as damaging the lake environment have some of their rationale rooted in our behaviour due to ignorance in the past. Making lakes receptacles of various kinds of wastes, or producing profound changes in endemic ecosystems – these are the types of harmful effects on lakes that people have begun to realize relatively recently.

A global inventory of lakes includes bodies of fresh and saline waters. Among the latter, there are very big lakes containing brackish to saline brines, such as the Caspian, Aral and Dead Seas, the Great Salt Lake, and other saline lakes on all the seven continents. For freshwater lakes alone, their total surface area is less than 1% of the ice-free continental surface, about 855 000 km^2. The total volume of freshwater lakes, estimated at about 125 000 km^3, is dominated by a few large water bodies and a great number of smaller lakes. The ten biggest lakes in the world account for about 61% of the total volume of freshwater lakes, and a slightly greater fraction, two-thirds or 67%, includes the lakes having a volume greater than 1 km^3. Thus, a sizeable one-third of freshwater lakes represents a large number of small water bodies. In general, the greater the volume of a lake, the longer it takes to renew its water by inflow and outflow. At the other end of the spectrum, the bigger freshwater lakes have water renewal or residence times of hundreds of years, grading down to very short times (days) at some arbitrary cutoff volume of the smaller lakes. Globally, the mean water residence time for lakes with out-

flow is between 5 and 6 years, and this figure is one of the measures of the water flow rate through lakes. Its significance to the hydrological regimes of the continents lies in the similarity of the freshwater lakes and continental glaciers at present, about 122 000 km^3, that through melting or growth affect the lake water budgets.

The present volume, *Physics and Chemistry of Lakes*, is a sequel to the 1978 volume. It reflects some of the very extensive research done since the late 1970s, continuously driven by the growing interest in lakes. The choice of the title of this volume, and of the individual subject matter of the 10 chapters written by 20 authors, was determined in part by the editors' views of the material that would make a useful and thematically consistent collection, and, to a greater extent, by the willingness and readiness of our colleagues to put their time and efforts into this project.

The individual chapters of the book deal with processes occurring in the lake water column, and at the boundaries between the lakes and their neighbouring environments, such as the sediments, atmosphere, and watersheds. The reader will note some differences in the book titles, authorship, and chapter contents between the earlier, 1978, *Lakes: Chemistry, Geology, Physics*, and this volume. The latter has fewer chapters dealing with lake sediments alone, and it devotes more space to human impacts on lake systems.

The book starts with an overview of the global geographical distribution and geological settings of lakes (M. Meybeck), updating and expanding the time-honoured classification of G. E. Hutchinson.

Four chapters deal primarily with physical and hydrological aspects of lakes, focusing on the hydrological regimes of lakes and their controlling mechanisms (T. C. Winter); relationships between climate, and the thermal and hydrological regimes of lakes (S. W. Hostetler); mixing mechanisms that interact with the main chemical, geological and biological processes in lakes (D. M. Imboden and A. Wüest); and the stable isotopes in lake water, and their uses as hydrological tracers that provide important information on the hydrology and climate of lake-watershed systems (J. R. Gat).

Three chapters discuss primarily the chemical aspects of human impact on lake systems, including the occurrences and behaviour of volatile organic substances (P. Vlahos, D. Mackay, S. J. Eisenreich, and K. C. Hornbuckle); atmospheric deposition of acids in lake basins (W. Stumm and J. Schnoor); and the behaviour of trace metals, as driven by the oxidation and reduction cycles in lakes (J. Hamilton-Taylor and W. Davison).

Two chapters address the interactions between lake sediments and water. One discusses fundamental inorganic and biogeochemical processes in sediments and water of coastal saline lakes (F. T. Mackenzie, S. Vink, R. Wollast, and L. Chou). The other presents an overview of the origins and diagenesis of organic compounds in lake sediments (P. A. Meyers and R. Ishiwatari).

We believe that this book serves a diverse professional readership, as both a working reference and teaching text. It addresses both scientists and engineers concerned with lake studies, and it can be used as a textbook by students specializing in different fields of limnology. The earlier volume, *Lakes: Geology, Chemistry, Physics*, has lived up to the expectation of serving a dual function as a reference text for research workers in various lake-related disciplines and a text for advanced students. We hope the new *Physics and Chemistry of Lakes* will professionally stimulate the readers' interest in lakes by presenting a selection of fundamentally important subjects that underlie an interdisciplinary approach to our understanding

of the environmental issues of lake systems and their evolution under different conditions of global change.

Evanston, Illinois, USA
Zürich, Switzerland
Rehovot, Israel
March 1995

Abraham Lerman
Dieter M. Imboden
Joel R. Gat

Contents

1 Global Distribution of Lakes
M. MEYBECK 1

1 Introduction 1
2 Background Material and Approaches to Global Lake Census 2
2.1 Data Used 2
2.2 Approaches to Global Lake Census 5
3 General Laws of Lake Distribution 5
3.1 Lake Density 5
3.2 Limnic Ratio 7
4 Distribution of Lakes of Tectonic Origin 8
5 Lakes of Glacial Origin 8
5.1 Lake Densities 8
5.2 Global Deglaciated Area 11
5.3 Total Number of Glacial Lakes 12
6 Fluvial Lakes 12
7 Global Distribution of Crater Lakes 13
8 Global Distribution of Saline Lakes 14
8.1 Coastal Lagoons 14
8.2 Salinized Lakes due to Evaporation 15
9 Global Lake Distribution 15
9.1 Extrapolation Approach 17
9.2 Lake Type Approach 17
9.3 Climatic Typology Approach 19
9.4 Lake Distribution in Endorheic Areas 21
9.5 Global Dissolved Salt Distribution in Lakes 23
10 Major Changes in Global Lake Distribution in the Geological Past 24
10.1 Lake Ages 24
10.2 Historical Changes 25
10.3 Postglacial Changes 25
11 Discussion and Conclusions 29
References 32

2 Hydrological Processes and the Water Budget of Lakes
T.C. WINTER 37

1 Introduction 37
2 Hydrological System with Regard to Lakes 37
2.1 Interaction of Lakes with Atmospheric Water 38
2.2 Interaction of Lakes with Surface Water 44
2.3 Interaction of Lakes with Subsurface Water 45
2.4 Change in Lake Volume 58
3 Summary 58
References 60

3 Hydrological and Thermal Response of Lakes to Climate: Description and Modeling
S.W. HOSTETLER 63

1 Introduction 63
2 Hydrological Response 63
3 The Hydrological Budget 67
4 Hydrological Models 68
5 Thermal Response 68
5.1 Energy Budget and Energy Budget Models 69
5.2 Models and Modeling 72
6 Use of Models to Link Lakes with Climate Change 74
7 Input Data Sets 74
8 Sample Applications 75
9 Summary 79
References 79

4 Mixing Mechanisms in Lakes
D.M. IMBODEN and A. WÜEST 83

1 Transport and Mixing 83
2 Lakes as Physical Systems 84
3 Fluid Dynamics: Mathematical Description of Advection and Diffusion 86
3.1 Equations of Fluid Motion 86
3.2 Turbulence, Reynolds' Stress, and Eddy Diffusion 87
3.3 Vertical Momentum Equation 89
3.4 Nonlocal Diffusion and Transilient Mixing 90
4 Density and Stability of Water Column 91
4.1 Equation of State of Water 91
4.2 Potential Temperature and Local Vertical Stability 93
5 Energy Fluxes: Driving Forces Behind Transport and Mixing 94
5.1 Thermal Energy 96
5.2 Potential Energy 97
5.3 Kinetic Energy 98
5.4 Turbulent Kinetic Energy Balance in Stratified Water 100
5.5 Internal Turbulent Energy Fluxes: Turbulence Cascade 101
6 Mixing Processes in Lakes 103
6.1 Waves and Mixing 104
6.2 Mixing in the Surface Layer 107
6.3 Diapycnal Mixing 112
6.4 Boundary Mixing 115
6.5 Double Diffusion 120
6.6 Isopycnal Mixing 123
7 Mixing and Its Ecological Relevance 129
7.1 Time Scales of Mixing 129
7.2 Reactive Species and Patchiness 132
7.3 Mixing and Growth: The Search for an Ecological Steering Factor 134
References 135

5 Stable Isotopes of Fresh and Saline Lakes
J.R. GAT 139

1 Introduction 139
1.1 Isotope Separation During Evaporation 141

2 Small-Area Lakes 143
2.1 Seasonal and Annual Changes 144
2.2 Deep Freshwater Lakes 146
2.3 Transient Surface-Water Bodies 148
3 Interactive and Feedback Systems 151
3.1 Network of Surface-Water Bodies 151
3.2 Recycling of Reevaporated Moisture into the Atmosphere 152
3.3 Large Lakes 153
3.4 Large-Area Lakes with Restricted Circulation 154
4 Saline Lakes 154
4.1 Isotope Hydrology of Large Salt Lakes 157
4.2 Ephemeral Salt Lakes and Sabkhas 157
5 Isotopic Paleolimnology 161
6 Conclusions: From Lakes to Oceans 162
References 162

6 Exchange of Chemicals Between the Atmosphere and Lakes
P. Vlahos, D. Mackay, S.J. Eisenreich, and K.C. Hornbuckle 167

1 Introduction 167
2 Air–Water Partitioning Equilibria 168
3 Diffusion Between Water and Air 169
4 Volatilization and Absorption: Double-Resistance Approach 170
5 Factors Affecting Mass-Transfer Coefficients 171
6 Partitioning of Chemical to Particulate Matter in Air and Water 172
6.1 Air 172
6.2 Water 172
7 Atmospheric Deposition Processes 173
7.1 Dry Deposition 173
7.2 Wet Deposition 174
8 Specimen Calculation 174
8.1 Step 1: Physicochemical Properties 174
8.2 Step 2: Mass-Transfer Coefficients 174
8.3 Step 3: Sorption in Air and Water 175
8.4 Step 4: Equilibrium Status 175
8.5 Step 5: Volatilization and Deposition Rates 175
9 Role of Air–Water Exchange in Lake Mass Balances 176
10 Case Studies 176
10.1 Mass Balance on Siskiwit Lake, Isle Royale 176
10.2 Mass Balance on Lake Superior 177
10.3 Air–Water Exchange in Green Bay, Lake Michigan 179
10.4 Air–Water Exchange in Lake Superior 180
11 Conclusions 182
References 182

7 Atmospheric Depositions: Impact of Acids on Lakes
W. Stumm and J. Schnoor 185

Abstract 185
1 Introduction: Anthropogenic Generation of Acidity 185
1.1 Genesis of Acid Precipitation 186
2 Acidity and Alkalinity: Neutralizing Capacities 190
2.1 Transfer of Acidity (or Alkalinity) from Pollution Through the Atmosphere to Ecosystems 192

3 Acidification of Aquatic and Terrestrial Ecosystems 194
3.1 Disturbance of H^+ Balance from Temporal or Spatial Decoupling of the Production and Mineralization of the Biomass 194
3.2 In Situ H^+ Ion Neutralization in Lakes 195
3.3 Krug and Frink Revisited 197
4 Brønsted Acids and Lewis Acids: Pollution by Heavy Metals, as Influenced by Acidity 198
4.1 Cycling of Metals 199
4.2 Pb in Soils 199
5 Impact of Acidity on Ecology in Watersheds 200
5.1 Soils 200
5.2 Lakes 200
5.3 Nitrogen Saturation of Forests 201
6 Critical Loads 202
6.1 Critical Load Maps 203
6.2 Models for Critical Load Evaluation 205
7 Case Studies 207
7.1 Chemical Weathering of Crystalline Rocks in the Catchment Area of Acidic Ticino Lakes, Switzerland 208
7.2 Watershed Manipulation Project at Bear Brooks, Maine 210
8 Summary 212
References 213

8 Redox-Driven Cycling of Trace Elements in Lakes
J. Hamilton-Taylor and W. Davison 217

1 Introduction 217
2 Major Biogeochemical Cycles and Pathways 218
3 Iron and Manganese 219
3.1 Transformations and Cycling 219
3.2 Iron and Manganese Compounds as Carrier Phases 220
4 Sediment-Water Interface 225
4.1 Diffusive Flux from Sediments 226
4.2 Evidence of Little or No Diffusive Efflux from Sediments 227
4.3 Transient Remobilization 227
4.4 Diffusive Flux into Sediments 228
5 Pathways Involving Redox Reactions Directly: Case Studies 229
5.1 Arsenic 230
5.2 Chromium 235
5.3 $^{239,240}Pu$ 237
5.4 Selenium 239
6 Pathways Involving Redox Reactions Indirectly: Case Studies 242
6.1 ^{137}Cs 242
6.2 Stable Pb, ^{210}Pb, and ^{210}Po 244
6.3 Zinc 249
7 Summary and Conclusions 257
References 258

9 Comparative Geochemistry of Marine Saline Lakes
F.T. Mackenzie, S. Vink, R. Wollast, and L. Chou 265

1 Introduction 265
2 General Characteristics of Marine Saline Lakes 265
3 Comparative Sediment-Pore-Water Reactions 269

3.1 Mangrove Lake, Bermuda 269
3.2 Solar Lake, Sinai 275
4 Conclusions 276
References 277

10 Organic Matter Accumulation Records in Lake Sediments
P.A. MEYERS and R. ISHIWATARI 279

1 Introduction 279
1.1 Significance of Organic Matter in Lake Sediments 279
1.2 Origins of Organic Matter to Lake Sediments 280
1.3 Alterations of Organic Matter During Deposition 280
1.4 Similarities and Differences Between Organic Matter in Sediments of Lakes and Oceans 282
1.5 Dating of Lake-Sediment Records 283
2 Indicators of Sources and Alterations of Total Organic Matter in Lake Sediments 283
2.1 Source Information Preserved in C/N Ratios of Sedimentary Organic Matter 283
2.2 Source Information from Carbon-Stable Isotopic Compositions 285
2.3 Source Information from Nitrogen-Stable Isotopic Compositions 288
3 Origin and Alterations of Humic Substances 290
4 Sources and Alterations of Lipid Biomarkers 292
4.1 Alteration of Lipids During Deposition 293
4.2 Changes in Sources vs Selective Diagenesis 293
4.3 Effects of Sediment Grain Size on Geolipid Compositions 295
4.4 Source Records of Alkanes in Lake Sediments 296
4.5 Preservation and Degradation of Fatty Acids in Lake Sediments 297
4.6 Sources and Diagenesis of Sterols in Lake Sediments 300
4.7 Origins and Significance of Polycyclic Aromatic Hydrocarbons in Lake Sediments 303
4.8 "Free" and "Bound" Geolipid Fractions of Lake Sediments 305
5 Sources and Alterations of Pigments in Lake Sediments 306
6 Sources and Diagenesis of Lignins and Their Derivatives 308
7 Diagenesis of Carbohydrates and Proteins in Lake Sediments 309
8 Paleolimnological Organic Geochemistry 311
8.1 Organic-Matter Record in the Laurentian Great Lakes of North America 311
8.2 Organic-Matter Record in Lake Biwa, Japan 315
8.3 Organic-Matter Record in Greifensee, Switzerland 317
8.4 Organic-Matter Record in Lake Washington, Washington, USA 319
8.5 PAH Records of Greifensee and Lake Washington Sediments 320
9 Organic Geochemical Records of Ancient Lakes 321
10 Summary 322
References 323

Subject Index 329

Lake Index 333

List of Contributors

L. Chou
Laboratoire d'Océanographie
Université Libre de Bruxelles
Campus de la Plaine, CP-208
1050 Brussels, Belgium

W. Davison
Institute of Environmental and
Biological Sciences
Lancaster University
Lancaster LA1 4YQ
UK

S.J. Eisenreich
Gray Freshwater Institute and
Department of Civil Engineering
University of Minnesota
P.O. Box 100
Navarre, MN 55392
USA

J.R. Gat
Department of Environmental
Sciences and Energy Research
Weizmann Institute of Science
76100 Rehovot
Israel

J. Hamilton-Taylor
Institute of Environmental and
Biological Sciences
Lancaster University
Lancaster LA1 4YQ
UK

K.C. Hornbuckle
Gray Freshwater Institute and
Department of Civil Engineering
University of Minnesota
P.O. Box 100
Navarre, MN 55392
USA

S.W. Hostetler
US Geological Survey
ERL-C
200 SW 35th
Corvallis, OR 97333
USA

D.M. Imboden
Swiss Federal Institute of Technology
(ETH) and Swiss Federal Institute
for Environmental Science
and Technology (EAWAG)
8600 Dübendorf
Switzerland

R. Ishiwatari
Department of Chemistry
Tokyo Metropolitan University
Hachioji-shi, Tokyo
Japan

D. Mackay
Department of Chemical Engineering
and Applied Chemistry
University of Toronto
200 College Street
Toronto, Ontario M5S 1A4
Canada

F.T. Mackenzie
Department of Oceanography
School of Ocean and
Earth Science and Technology
University of Hawaii
1000 Pope Road, MSB 525
Honolulu, HI 96822
USA

M. Meybeck
Laboratoire de Géologie Appliquée
Université de Paris 6
Place Jussieu
75257 Paris Cedex 05
France

P.A. Meyers
Department of Geological Sciences
and Center for Great Lakes
and Aquatic Science
University of Michigan
1006 C.C. Little Building
Ann Arbor, MI 48109-1063
USA

W. Stumm
Institute for Water Resources
and Water Pollution Control (EAWAG)
Swiss Federal Institute
of Technology (ETH)
Zurich
Switzerland

J. Schnoor
Department of Civil and
Environmental Engineering
University of Iowa
Iowa City, IO
USA

S. Vink
Department of Oceanography
School of Ocean and
Earth Science and Technology
University of Hawaii
1000 Pope Road, MSB 525
Honolulu, HI 96822
USA

P. Vlahos
Department of Chemical Engineering
and Applied Chemistry
University of Toronto
200 College Street
Toronto, Ontario M5S 1A4
Canada

T.C. Winter
US Geological Survey
Water Resources Division
Mail Stop 413, Box 25046
Denver, CO 80225-0046
USA

R. Wollast
Laboratoire d'Océanographie
Université Libre de Bruxelles
Campus de la Plaine
CP-208, 1050 Brussels
Belgium

A. Wüest
Swiss Federal Institute
for Environmental Sciences
and Technology (EAWAG)
8600 Dübendorf
Switzerland

1 Global Distribution of Lakes

M. MEYBECK

1 Introduction

The distribution of lakes over continents has been addressed by geographers since the eighteenth and nineteenth centuries, and the last great lakes were explored by explorers and scientists in Africa only 100 years ago: Lake Malawi (C. Boccaro, 1616; D. Livingstone, 1850), Lake Tanganyika (R.F. Burton, J.H. Speke, 1858), Lake Victoria (J.H. Speke, 1858), Lake Albert (S. Baker, 1864), Lake Edward (H. Stanley, 1875), and Lake Rudolf now Turkana (S. Teleki and von Höhnel, 1888). In other continents, lake exploration was achieved earlier: Great Slave Lake was named by S. Hearne in 1771 and Great Salt Lake was named by J. Bridger and E. Provost in 1824 (Encyclopedia Britannica 1962). In South America, some maps of the early nineteenth century still present a huge mythic lake in the upper Branco, the Rio Negro tributary originating from the Guyana Shield. In Asia, all great lakes of central Asia, such as Issyk-Kul and Hovsgol, have been known to Chinese and Russian scholars for a long time, whereas the Caspian Sea and Aral Sea had already been described by Greek historians. Lake Kivu (2370 km^2) was the last of the major lakes to be "discovered" by von Götzen in 1894. After this, it can be said that most of the lake exploration phase was achieved, although a few important lakes have still been described more recently, such as crater Lake Wisdom (95 km^2) in New Guinea (Ball and Glucksman 1978). The twentieth century has seen the development of limnology in all continents, and numerous monographies can be found for most major lakes of the planet, e.g., for Lake Tanganyika (Coulter 1991), Lake Chad (Carmouze et al. 1983), Lake Issyk-Kul (Romanovsky 1990), the Aral Sea (Létolle and Mainguet 1993), and Lake Titicaca (Dejoux and Iltis 1992).

Laboratoire de Géologie Appliquée, Université de Paris 6, Place Jussieu, 75257 Paris Cedex 05, France

Despite major improvements in our scientific knowledge of lakes, however, there still remain some gaps for the most southern patagonian lakes, the Tibetan lakes, and the upper Amazon floodplain lakes at the foot of the Andes.

During the past decade, earth and biological sciences have evolved to a global perspective within the International Global Biosphere and Geosphere Programme. The global lake distribution (number, area, and volume), which interested only geographers 100 years ago (Penck 1894), is now being reconsidered for many reasons. Lakes are one of the most easily available water resources (Soviet IHP 1978). Lakes, and the various shallow water bodies named wetlands, cover millions of km^2 of continental area and are essential components of regional (e.g., central Asia) and global water balances (Soviet IHP 1978). In global biogeochemical cycles, lakes are now seen as major regulators in the carbon, nitrogen, and phosphorus cycles through various processes: sedimentation of detrital organic matter, production of autochthonous organic matter, precipitation of carbonates, and precipitation of evaporites (Mulholland and Elwood 1982; Hammer 1986; Risacher 1992; Downing et al. 1993; Meybeck 1993). Lakes are also recognized as major sedimentological features in which stored material can be used to decipher recent climatic evolution up to the past million years (Löffler 1987; Gray 1988), and as models to understand past geological evolution such as rift opening (Tiercelin and Mondeguer 1991). Lakes have always been studied extensively by biologists, and most limnology books have actually been written by them, such as the *Treatise of Limnology*, by Hutchinson (1957), which is still a reference book for many limnological items including non-biological items. In recent years, a new concern of biologists has been the study of lake endemism at a global scale, which is closely linked to lake distribution, origins, and ages. Finally, lake censuses are needed as soon as certain lakes are

considered as endangered water resources that should be protected and preserved from human activities.

Recent lake censuses started 25 years ago in the former Soviet Union, then in Scandinavia, North America, and now they are in progress in many regions such as in Europe (EEA 1994). However, very few authors have considered the problem on a global scale. Hutchinson (1957) and Fairbridge (1968) still quote Penck (1894) in this regard. The most recent attempt on a global census is still the one of Tamrazyan (1974), which is actually an extrapolation of a general census of Soviet lakes. The only comprehensive lake census on a global scale is the work of Herdendorf (1982, 1984, 1990), on great lakes, i.e., lakes exceeding 500 km^2 which considers 253 lakes. Tamrazyan has estimated that the total lake number amounts to many millions.

The major objectives of this review are to: (1) determine the lake distribution laws at local, regional, and global scales, i.e., the distribution per lake area classes, (2) identify the specific distribution for major lake types according to their various origins, (3) study their distribution according to major climatic features, (4) examine the links between lake distribution, geology, and geomorphology, and (5) consider the lake distribution in the recent geological past (since the last glacial age). Only natural lakes are considered here.

2 Background Material and Approaches to Global Lake Census

2.1 Data Used

For this study the Encyclopedia Brittanica's (1962) definition of lakes is used: "a mass of stillwater situated in a depression of the ground without direct communication with the sea." For much smaller lakes ($A_o < 0.1\,km^2$) and lakes located in floodplains, there is a continuum between lakes and water bodies without continuous and permanent vegetation cover and wetlands. Natural lakes are those found in natural depressions not excavated by humans, such as ponds, nor resulting from the construction of dams such as impoundments and reservoirs. Some environmental administrations have set a lower limit to lake volume for lake census, of the order of 1000 m^3 (1 acre-foot; R. Wetzel, pers. comm.). This can be an operational definition in lake management. The Aral Sea and Caspian Sea are, of course, considered here as lakes, but not the Baltic Sea or Black Sea, which are in direct connection with the world oceans.

Three sets of data have been used: (1) Herdendorf's global census of great lakes, (2) local or regional census including smaller lakes (i.e., lakes $A_o < 10\,km^2$), and (3) lake registers and limnological literature.

Herdendorf's review, published in various forms in 1982, 1984, and 1990, included a full set of all lakes exceeding 500 km^2 (defined as "great lakes") giving their exact location, lake origin, area, volume, and even salinity, whenever this information is available. It also included shallow and/or saline lakes that are subject to great size variations such as Lake Eyre in central Australia, or Tonle Sap (Grand Lac) in Cambodia. This set is nearly comprehensive, apart from Lake Sarykamish (1470 km^2 according to Savvaitova and Petr 1992), southwest of the Aral Sea, which is missing. The Aral Sea and Caspian Sea areas used here are those given by Herdendorf, and were valid in the 1950s prior to major human activities.

Local and regional censuses have been taken from various sources, through personal communication of administration reports thanks to many colleagues. The most complete and extended census is the one done for the whole territory of the former Soviet Union (22.3 million km^2) by Domanitsky et al. (1971), also published by Nezhikhovsky (1973) and quoted by Tamrazyan (1974) and Romankevich and Artemyev (1985). It concerns all lakes ranging from the Caspian (374 000 km^2) to lakes of 0.1 km^2. Although some confusion occurs for lakes exceeding 100 km^2 in the two Russian quotations, Herdenforf's census of lakes can be used to cross-check these data. The results proposed in Table 1 are a synthesis of all these sources. For the smaller lakes ($A_o < 1\,km^2$), Soviet sources allocate 2 814 727 lakes, corresponding to 159 322 km^2. These are made up here as follows: 300 000 lakes (78 000 km^2) for the 0.1–1.0 km^2 class; 2 500 000 lakes (65 000 km^2) for lakes less than 0.1 km^2. A more detailed account of central Asian lakes of the former Soviet Union has been established, based on Nikitin's data (1977) quoted by Savvaitova and Petr (1992), over a 2.2 million km^2 territory. Another very useful census was found for China in Shuncai (1988) with data of all lakes as small as 1 km^2. The Federal Indian Government (Anonymous 1990) also made a detailed census of all lakes and reservoirs down to 1 km^2. A new European census

Table 1. Regional lake distributions (see text for explanations)[a]

Lake area class (km^2) Country (area, million km^2)		0.1	1	10	10^2	10^3	10^4	10^5	Total lake area (km^2)	Limnic ratio (%) (4)
USSR (3)(5)										
(22.3)	d_L		13 500[b]	1 650	106	7.6	0.54	0.18		
	A_o		78 000[b]	87 075	55 913	42 324	43 830	133 500	440 000 (3)	2.3(3)
	n		300 000[b]	36 896	2 360	159	12	4		
Canada (6)										
(9.96)	d_L		44 000[b]	4 400[b]	450[b]	52[b]	3.1	0.7		
	A_o		114 000[b]	114 000[b]	117 000[b]	136 000	88 000	270 000	833 000	8.4
	n		440 000[b]	44 000[b]	4 500[b]	523[b]	31	7		
China (7)										
(9.56)	d_L		1 500[b]	250	36	11.6	1.25	0		
	A_o		3 600[b]	9 100	12 300	29 900	29 300	0	84 400	0.88
	n		14 000[b]	2 383	341	111	12	0		
USA (1)										
(9.35)	d_L		3 750[b]	375[b]	48[b]	5.9	0.75	0.11		
	A_o		9 100[b]	9 100[b]	11 700[b]	14 219	13 064	57 750	115 000	1.2
	n		35 000[b]	3 500[b]	450[b]	55	7	1		
India (8)										
(3.255)	d_L		200[b]	40	12.3	4.9	0.92	0		
	A_o		200[b]	468	1 440	5 760	4 140	0	12 000	0.37
	n		800[b]	130	40	16	3	0		
Argentina (9)										
(2.7)	d_L		5 500[b]	630[b]	61	5.9	1.85	0		
	A_o		3 900[b]	4 400[b]	4 536	3 603	7 320	0	23 800	0.88
	n		15 000[b]	1 700[b]	166	16	5	0		
Scandinavia (2)										
(1.11)	d_L		47 000	7 400	975	91	5.4	0		
	A_o		13 600	21 500	28 200	26 200	15 120	0	104 600	9.4
	n		52 500	8 273	1 087	101	6	0		
Total										
(58.2)	A_o		222 000[b]	245 700[b]	231 000[b]	252 000	200 800	461 000	1 610 600	2.77

d_L, Lake density (number per M km^2); A_o, total lake area (km^2); n, total lake number.

[a] Small numbers in parentheses following countries: (1) Including Alaska, excluding lakes Superior, Huron, Erie, and Ontario counted in Canada, extrapolated from Van der Leeden et al. (1989); (2) Norway, Sweden, Finland only (EEA 1994); Thörneloff, personal communication); (3) Caspian not counted; from Domanitskiy et al. (1970) and Nezhikhovskiy (1973); (4) for total lake area >0.1 km^2; (5) Aral Sea area estimated to 68 000 km^2; (6) with Laurentian Great Lakes, except Lake Michigan, estimated from Gilliland et al. (1973) and Herdendorf (1984); (7) Shuncai (1988); (8) Anonymous (1990a); (9) IARH (1992).

[b] Values estimated.

(EEA 1994) also provides some very precious census information for a dozen countries of western and eastern Europe, including Norway, Finland, Yugoslavia, Georgia, etc.

Another source of information is the limnological monographs on lakes of a given country such as in Great Britain (Burgis and Morris 1987), France (Delebecque 1898), Victoria State in Australia (Williams 1964), Japan (Kurata 1990), and outer Mongolia (Egorov 1993). In these cases the lake distribution was not always presented with simple boundaries (1–10–100 km^2, etc.) or in metric units, and had to be reestablished here. A recent example of this source is presented in Table 2 for Indonesia from Nontji (1994) and Giesen (1994); however, this is not taken into account in the documented regions listed in Table 1.

Table 2. Lake densities in various areas[a]

Lake are class (km^2) Country (area, million km^2)		0.001	0.01	0.1	1	10	10^2	10^3	10^4	Limnic ratio (%)
Great Britain (1) 0.232	d_L	158 000	63 000		6700	850	85	0	0	1.0
Southern Europe (2) 1.09	d_L			5 800[b]	450	200	53	4.5	0	0.33
Victoria (Australia) (3) 0.228	d_L				360[b]	285	70	0	0	0.27
France (4) 0.55	d_L				294	163	13	0	0	0.09
Nonglaciated USA (5) 6.3	d_L				60[b]	10[b]	4	1.9	0	0.09
ELA (Canada) (6) 0.005	d_L		←	200 000	→					
0.28	d_L					450[b]	140	25	3.6	1.86
Alaska (USA) (7) 1.5	d_L					1300[b]	130	11.3	1.3	1.7
Central Asia (8) 2.2	d_L			2100[b]	450[b]	105	11.8	1.8	1.36	0.56
Japan (9) 0.37	d_L				1350[b]	192	62	10.8	0	0.68
Indonesia (10) 1.9	d_L				>121	123	24.2	5.8	0.53	0.32
Outer Mongolia (11) 1.56	d_L				2100	160	9.5	5.1	0.64	1.1
Tibet (12) 1.2	d_L					299	172	37	2.5	2.0

d_L, Lake density [number per million km^2]. There is no lake >10 000 km^2 in this set, except Lake Urs (Mongolia). Limnic ratio may be rough estimates.

[a] Small numbers in parentheses following countries: (1) Recalculated from. Burgis and Morris (1987); includes glaciated Scotland; (2) nonglaciated countries: Moldavia, Georgia, and former Yugoslavia from EEA (1994); France without Lake Geneva, see below; Hungary, recalculated from Szesztay (1966); (3) recalculated from Williams (1964); (4) this work, based on Delebecque (1898), includes glaciated Alps and Pyrenees (Lake Geneva not counted); (5) all states, excluding Florida, Louisiana, Alaska, and glaciated states, computed from Van der Leeden et al. (1989); (6) Experimental Lakes Area (Ontario), Cleugh and Hauser (1971); (7) computed from Van der Leeden et al. (1989); (8) computed from Nikitin (1977) quoted by Savvaitova and Petr (1992); (9) computed from Kurata (1990); (10) computed from Giesen (1994) and Nontji (1994); (11) Egorov (1993); (12) Jin Xiangcan et al. (1990).

[b] Values estimated.

For Canada we took into account the distribution presented by Gilliland (1973) for lakes exceeding 100 km^2, and by Hammer (1988) for all Saskatchewan lakes exceeding 10 km^2. A very detailed account of small lakes (0.01–1 km^2) of the Experimental Lakes Area (ELA) in western Ontario can be found in Cleugh and Hauser (1971).

In the United States a detailed state-by-state list of all lakes exceeding 10 $miles^2$ (approximately 25 km^2) is found in the Water Encyclopedia (Van der Leeden et al. 1989), and numerous distributions have been calculated from this data base.

Although not generally specified, it is likely that most of these censuses are still derived from very long and tedious measurements on maps. Remote sensing, and particularly radar imagery, are now used as in the Amazon floodplain, for

which the distribution has also been recalculated from Sippel et al. (1993).

The third type of basic material is the general limnological publications in which numerous lake descriptions can be found. The most useful set is published by the International Lake Environment Committee (ILEC), located in Otsu, Japan, which has already published four registers of world lakes of all sizes (ILEC 1988, 1989, 1990, 1991). The Unesco report on water balance of lakes and reservoirs (Unesco 1974) is also a precious source of data as well as publications of Hutchinson (1957), Lerman (1974), Lerman and Hull (1987), the World Water Balance (Soviet IHP 1978), the Encyclopedia of Geomorphology (Fairbridge 1968), and special symposia such as that organized by IAHS (1973).

The basic data used here, including the extrapolation made for smaller lakes discussed in Section 3, are presented in Table 1 for extended regions (former USSR, Canada, China, USA, India, Argentina, and Scandinavia), and in Table 2 for local censuses. The distribution of continental area used here is taken from Baumgartner and Reichel (1975). The total nonglaciated continental area is estimated to be 133 million km^2 (Greenland and Antarctica excluded).

2.2 Approaches to Global Lake Census

Three types of independent approaches are used here: (1) a lake-type approach based on lakes origins, (2) an extrapolation of known regional censuses listed in Table 1, and (3) a climatic approach based on lake distributions in homogeneous temperature and runoff environments.

In all three approaches, the lake distribution has been estimated with a top-down process starting from the Caspian, with a log scale of lake area, i.e., $>100\,000\,km^2$, then $10\,000-100\,000\,km^2$, $1000-10\,000\,km^2$, $100-1000\,km^2$, etc. A very careful consideration of smaller lakes has been made, because a myriad of small lakes can account for as much as a few great lakes. Thanks to Herdendorf's census, the three first lake categories are completely known at the global scale and are always used as true information in the three approaches.

The first approach includes global estimates of lake distribution for various lake categories. Hutchinson (1957) has listed 76 different lake origins, some of them being as difficult to differentiate as those resulting from tectonic movements or from volcanic activity, and others being known for only few specimens. Therefore, these origins have been grouped into: rift lakes (Hutchinson's type 9), all other tectonic lakes (types 1–8), all lakes of glacial origin (types 23–42), coastal lagoons (types 64 and 65), crater lakes (types 10–14, 16), and all lakes of fluvial origin (types 49–59). The rest have been grouped into a miscellaneous category that includes, among others, landslide lakes (types 20–22), other dam lakes (types 18, 19, 69–72), solution lakes (types 43–47), deflation lakes (types 60–63), etc. Man-made lakes (Hutchinson's types 73 and 74) are not considered here. Six specific distributions are estimated here starting with larger lakes based on Herdendorf's census, then extrapolated to the smaller lake sizes on the basis of other collected information.

The extrapolation approach is necessary only for approximately 75 million km^2 of nonglaciated continental area, half of it being arid and semiarid, because reliable censuses are presently available for 58 million km^2 (Table 1). The climatic approach is based on the lake distribution in five climatic zones: deglaciated, temperate, dry and arid, wet tropics, and desert. These zones are derived from a global map of 14 zones based on average air temperature and surface water runoff used in the computation of river budgets to oceans (Meybeck 1979, 1988). This approach has been specially adapted to provide information for possible changes in lake distribution due to global climatic changes.

Finally, a differentiation has been made between lakes with river outlets connected to oceans (exorheic drainage) and other lakes, either without outlets such as the Dead Sea or Lake Chad, or with outlets connected to saline lakes such as Lake Titicaca (endorheic drainage).

3 General Laws of Lake Distribution

3.1 Lake Density

Lake density (d_L) is simply defined as the number of lakes found in a given lake-size category divided by the total area on which the census is performed. In order to permit comparisons between censuses, lake density is expressed in lake number per million km^2. It varies from less than 0.01 for lakes exceeding $100\,000\,km^2$ found on continents (the

Caspian is the only specimen presently) to more than 100 000 for lakes between 0.01 and 0.1 km^2 on glacial shields. Lake densities are given in Tables 1 and 2.

Each census can be expressed as a relation between lake densities and lake sizes (Fig. 1). The most striking feature is a regular increase in densities from large lakes to small lakes, as in China, Scandinavia, or India: This increase is roughly tenfold when going from one lake-size category to the next smaller category at a log scale. This variation is not new, and was already presented by Wetzel (1990). This relationship can be defined as $\log(d_L) = b \log(A_o) + a$, where d_L is the density and A_o is the lake size, with b close to -1. When looking closer, however, it is found that the slope b can vary from one census to another and within a given census.

In a few censuses, the slope b is slightly lower than -1 (from -1.1 to -1.6), i.e., the corresponding total area found within one lake-size category increases toward smaller lakes. This is found for lakes between 1 and 10 000 km^2 for the former Soviet Union (Table 1), and between 10 and 10 000 km^2 for Scandinavian lakes. In such regions the very small lakes (area <0.01 km^2) could be numbered by millions such as for the tundra ponds (Hobbie 1980).

In many instances an opposite trend is observed where $-1 < b < 0$. In this case there is a marked decrease in total lake area when stepping down from large lakes to smaller lakes. This is particularly observed in dry and semiarid countries, such as China, Japan, India, southern Europe (Tables 1 and 2; Fig. 1), which have very little or no lakes of glacial origin.

There are some obvious exceptions to these regular trends, due to the excessive volume of some large lakes. In these cases total lake area is by far greater than for smaller lakes. A good example is provided by the former Soviet Union census, where total lake area extends from 87 000 km^2 (1–10 km^2 area class) to 43 000 km^2 (1000 km^2–10 000 km^2 area class), and then jumps to 133 500 km^2 and 374 000 km^2 for the 10 000 km^2–100 000 km^2 and >100 000 km^2 area classes, due to the enormous size of the Aral Sea (66 000 km^2) and the Caspian Sea (374 000 km^2). For the former Soviet Union these two water bodies should therefore be considered as outliers in the territorial distribution, but they fit well with the global distribution of large lakes based on Herdendorf's census (Fig. 1). A similar exception can be made for the five Laurentian Great Lakes. They are found across the boundary between the Canadian shield and sedimentary lowlands, and presently represent approximately 245 000 km^2. When Lake Michigan is attributed to the United States' distribution and lakes Superior, Huron, Erie, and Ontario are attributed to Canada alone,

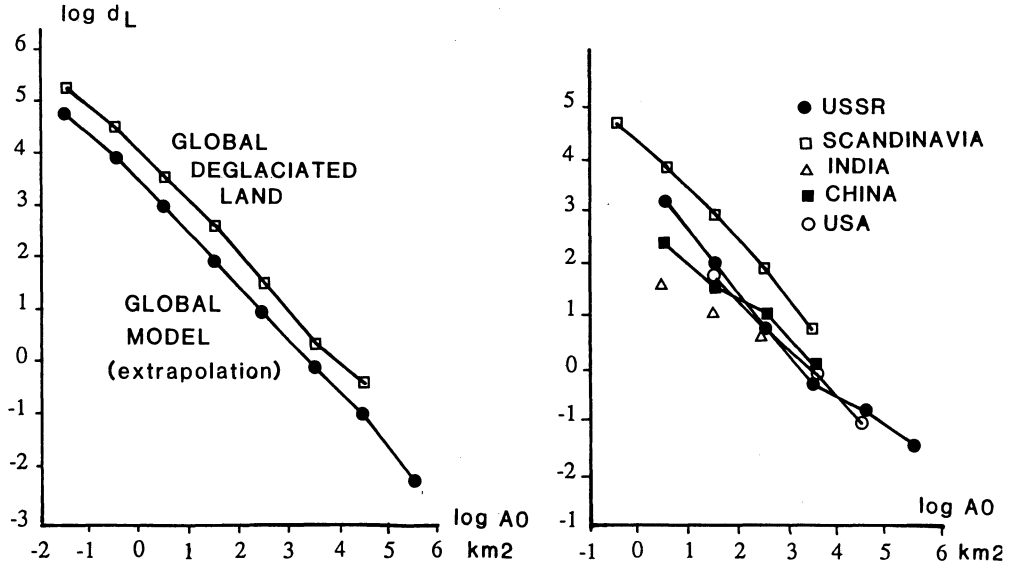


Fig. 1. Evolution of lake density (lake number per million km^2) with lake area classes from 0.01–0.1 km^2 to 10^5–10^6 km^2. *Left* Estimate for global deglaciated land (18 million km^2) and for global land area, ice caps excluded (133 million km^2). *Right* Regional estimates from known censuses. Note the log–log scale. The Caspian Sea (374 000 km^2) has been counted in the former USSR census

they are responsible for an increase by three- to fourfold of the total area expected to be found in the 10 000–100 000 km^2 class. When these largest lakes are distributed over the whole continental area, they only exceed the expected area in this class by a factor of 1.5.

In many cases the published census does not give the total lake area in each area class, and this figure must be estimated from the total lake number. The average lake size must therefore be estimated. This problem has already been considered by Tamrazyan (1974), who attributed to the geometrical center of each class the unique factor 2.4, i.e., the average lake size is 2.4 km^2 in the 1–10 km^2 class, 24 km^2 in the 10–100 km^2 class, etc. This factor has been checked here on the available data set for lake populations exceeding $n = 100$ in any area class, and for which the exact total area was known: Over 17 determinations, the class center ranges from 2.1 to 3.8, with a median at 2.6 and 70% of the population between 2.4 and 2.8. Because the number of determinations available to Tamrazyan was only 4, a value of 2.6 has been chosen here. Another question was the extrapolation of Herdendorf's census of lakes between 500 and 1000 km^2 to lakes between 100 and 1000 km^2. It was found in two countries that there were approximately eight times more lakes in the whole class (1–10) than in the partial class (5–10).

The determination of lake densities for smaller lake classes that are undocumented is also a necessary step. Usually, it is done first on the basis of the variation of densities for greater lake classes, i.e., the slope coefficient b, then taking into account the density variations documented in similar regions listed in Tables 1, 2, and 4.

3.2 Limnic Ratio

The limnic ratio (LR, expressed in percent) is defined as the ratio between total lake area over total documented area on which the census has been performed. The LR varies over more than two orders of magnitude from less than 0.1% for France, without Lake Geneva, or for the nonglaciated part of the United States, to more than 10% in some deglaciated shields (Tables 1 and 2). The limnic ratio must be at least determined on a complete lake census down to $A_o = 1\,km^2$. In deglaciated regions for which the slope coefficient $b < -1$, a census of 0.1–1 km^2 and even of 0.01–0.1 km^2 should also be considered. If these data are lacking, they should be estimated as stated above. When the distribution of total lake area is known for each class, they are summed to determine LR.

In regions not formerly glaciated during the last glacial age, approximately 115 million km^2 (see Sect. 5), the limnic ratio depends on three independent factors: climate, tectonics, and lithology. When no major rift occurs, LR is clearly a function of climate and lithology: LRs are very low (<0.1%) for arid or dry regions such as the nonglaciated conterminous United States, or for regions rich in carbonate rocks where water easily percolates such as in France and most of southern Europe. China (LR = 0.88%), India (LR = 0.37%), and Argentina (LR = 0.88%) are examples of lower LR, due to their general aridity. The low LR value of Japan (0.68% including tectonic Lake Biwa; 0.50% without it) is probably linked to the perviousness of its rocks. A similar observation is made for Indonesia, for which LR is only 0.32% with tectonic Lake Toba and 0.26% without it.

The occurrence of rifts and/or major tectonic movements can lead to an unexpected limnic ratio in relatively arid areas such as Kenya and Israel. In central Asia (Nikitin 1977), the LR is estimated to be 0.56% when tectonic lakes (Issyk-Kul, Sarykamish) are included, and less than 0.20% without them.

In areas formerly glaciated, LRs are generally much higher and depend on bedrock type and relief. In lowland crystalline shields, the LR generally exceed 8% (Table 4). In Kola peninsula and Karelia, the LR could even reach 20%, although if Lake Ladoga, an obvious outlier in the distribution, is discarded, LR drops to 13%. In some subarctic regions of Siberia and Canada, the LR can even exceed 50%, due to the myriads of arctic ponds of very small area (1 ha) resulting from permafrost melting (Hobbie 1980). These shallow water bodies are probably not taken into consideration in the Soviet census that stops at 0.1 km^2 (10 ha). In sedimentary lowlands where the glacial scour was less effective, lakes are not as numerous and extended: LR for the South Baltic states, i.e., Denmark, Poland, Estonia, and Latvia, is only estimated to be 2.2%. In formerly glaciated mountainous regions, LR is 8.6% for the Alps (3440 km^2 lake area for 40 000 km^2 total area formerly glaciated by Würm glaciers) and 3% for Patagonia.

4 Distribution of Lakes of Tectonic origin

Tectonic lakes are a prominent feature of global lake distribution in terms of volume and permanence, and to a lesser extent, of area. Hutchinson lists nine major types of tectonic lakes, such as relict seas, upwarping reversing drainage, and tectonic graben or rift lakes (type 9). For the purpose of this chapter, the first eight types are classified as *tectonic lakes*, whereas *tectonic graben lakes* are considered separately, due to their great depth. The Caspian Sea is also considered separately, due to its primary position with regard to many parameters (volume, area, total salt mass), but not for salinity and maximum depth. It is the remnant of a very old tectonic depression, the Parathetys, which, together with the Black Sea, has been connected and disconnected (lacustrine phases) to the Mediterranean Sea and world oceans during the past 5 million years (Stanley and Wezel 1985). Because of its great size (374 000 km^2 presently; Herdendorf 1984, 1990), it has been named a sea, as with the Aral Sea, although actually it clearly corresponds to the definition of a lake.

As already mentioned, Herdendorf's census (1984) of great lakes was first used to assess the distribution of tectonic lakes. However, the difference between tectonic lakes and other categories, such as volcanic lakes or glacial lakes, is not always clear-cut, and this author reports many lakes of mixed origin such as volcano-tectonic or glacial-tectonic lakes. We have considered Lake Toba (Sumatra) and Atitlan (Guatemala) to be part of the volcanic caldera lakes. Lake Kivu (Zaire and Rwanda) is seen as a tectonic graben lake, although it is also a relatively recent volcanic dam. Lakes Champlain and Taymir have been considered as glacial, and Lake Taupo, as tectonic. Some intelligent guesses had to be made since the exact origin of lake was not known to Herdendorf: All Patagonian lakes in highlands are considered to be of glacial origin, and most central Asian lakes are considered to be of tectonic origin. All lakes greater than 10 000 km^2 listed by Herdendorf have thus been attributed to a given origin, and 11 lakes between 1000 and 10 000 km^2 remain of undetermined origin, and have been reclassified here as miscellaneous lakes.

Compared with glacial lakes, fluvial lakes, or coastal lagoons, lakes of tectonic origin are less clustered in lake provinces. However, the East African Rift is the location of most present-day deep tectonic graben lakes (from north to south): Dead Sea (Israel), Asal and Abhe (Djibouti), Abaya (Ethiopia), Turkana (former Rudolf, Kenya), Edward (Uganda–Zaire), Albert (Uganda–Zaire), Kivu (Zaire–Rwanda), Tanganyika (Zaire–Tanzania–Burundi–Zambia), and Malawi (former Nyasa, Malawi–Mozambique–Tanzania). Beyond this list the major graben lakes are located in central Asia: Baikal (Russia), Issyk-Kul (Kirghistan), Alakol (or Alakul, Kazakstan), Hovsgol (or Khubsugul, Mongolia). Most other important deep tectonic lakes likely to be of graben origin are also located in regions where tectonic activity is presently important such as in Japan (Lake Biwa), Nevada (Tahoe and Pyramid lakes), and Himalaya (Lake Pangong). Table 3 lists the major tectonic lakes in two categories: graben lakes and all others.

Most other tectonic lakes result from mountain uplift, faulting, etc. The most extended lakes are: Lake Victoria in East Africa, caused by a slight uplift of its western side (its former connections with Lake George are still marked by extended wetland), Lakes Chad (Chad), Maracaibo (Venezuela), Nicaragua (Nicaragua), Urmia (Iran), and Great Salt Lake (Utah).

The total area of tectonic lakes exceeding 1000 km^2 is approximately 776 000 km^2, 48.2% for the Caspian Sea only, 19.2% for all graben lakes, and 32.6% for other tectonic types. When the total volume of large tectonic lakes is considered, these figures are different: Total volume is estimated to be approximately 135 000 km^3, (57.7%) for the Caspian Sea alone, 37.9% for all graben lakes (i.e., mostly Tanganyika and Baikal), and 4.4% for other lakes. If the Caspian Sea is disregarded, three graben lakes hold 84% of the total volume of tectonic lakes: Baîkal, Tanganyika, and Malawi. The estimated global distribution of tectonic lakes is presented in Table 9 (total area 900 000 km^2).

5 Lakes of Glacial Origin

5.1 Lake Densities

Depending on the types of rock and relief recovered by Holocene glaciers, the distribution of lakes in formerly glaciated regions is very variable. Because lakes of glacial origins, i.e., Hutchinson's types 23–42, are by far the most numerous lakes

Table 3. Major lakes of tectonic origin[a]

Lake area class (km^2)	Graben lakes (4)			Other lakes (1) (4)			Total	
		A_o (km^2)	V (km^3)		A_o (km^2)	V (km^3)	A_o (km^2)	V (km^3)
>100 000		0	0	Caspian	374 000	78 200	374 000	78 200
100 000–10 000	Tanganyika	32 900	18 900	Victoria	68 460	2 700		
	Baikal	31 500	22 995	Aral (2)	64 100	1 020		
	Malawi	22 490	6 140	Chad	16 600	44		
	Balkhash	18 200	118	Maracaibo	13 010	280		
Total in class		105 100	48 150		162 160	4 044	267 260	52 194
10 000–1000	Turkana	8 860	251	Titicaca	8 030	827		
	Nicaragua	8 150	108	Eyre	7 700	23[b]		
	Issyk-Kul	6 240	1 730	Dong Ting	6 000	18		
	Torrens	5 880	5[b]	Urmia	5 800	45		
	Albert	5 590	151	26 other lakes	63 370	1 010[b]		
	Rukwa	2 716	2[b]					
	Kivu	2 370	569					
	Edward	2 150	117					
	Managua	1 040	33					
	Dead Sea	1 020	188					
Total in class		44 016	3 154		90 900	1 923[b]	134 900	5 077
Total (3)		149 000	51 300		627 000	84 167	776 000	135 000

[a] Small numbers in parentheses: (1) Few lakes ($A_o < 10\,000\,km^2$) may be of graben origin; (2) prior to 1950; (3) all lakes >1000 km^2; (4) mostly based on Herdendorf 1984; 1990.
[b] Values estimated.

Table 4. Lake distribution in deglaciated regions[a]

Lake area class (km^2) Region (area, million km^2)		0.01	0.1	1	10	10^2 (3)	10^3 (3)	10^4 (3)	10^5	Total lake area (km^2)	Limnic ratio (%)
Sweden (1)(2)	d_L										
0.45	A_o		132 000	41 000	8 860	804	42	6.7	0		
	n		1 800	5 000	10 800	8 600	3 640	8 690	0	38 500	8.55
			59 500	19 374	3 990	358	19	3	0		
Finland (1)											
(10)	d_L		118 000	38 500	6 700	820	220	8.8	0		
0.34	A_o		1 050[b]	3 400[b]	6 000[b]	7 250[b]	8 000[b]	6 520	0	32 000	9.4
	n		40 309	13 114	2 283	279	44	3	0		
Norway (1)	d_L	⟵ 650 000 ⟶			6 250	1 400	22	0	0		
0.32	A_o		4 700[b]	5 000[b]	5 200[b]	11 700[b]	18 000[b]	0	0	44 600	13.9
	n	⟵ 208 000 ⟶			200	450	7	0	0		
Kola and Carelia											
(4) 0.25	d_L		120 000[b]	38 000[b]	6 800[b]	800[b]	116	20	4		
	A_o		1 000[b]	2 500[b]	4 400[b]	5 200[b]	7 500	11 950	17 700	50 250[b]	20[b]
	(11)A_o								0	32 550[b]	13[b]
	n		30 000[b]	9 500[b]	1 700[b]	200[b]	29	5	1		

Table 4. (*Contd.*)

Lake area class (km^2) Region (area, million km^2)		0.01	0.1	1	10	10^2 (3)	10^3 (3)	10^4 (3)	10^5	Total lake area (km^2)	Limnic ratio (%)
Scandinavian Shield (5) 1.36	d_L		230 000[b]	45 000[b]	7 300[b]	940[b]	95	8	0.73		
	A_o		8 500[b]	16 000[b]	26 400[b]	33 000[b]	37 000	27 160	17 700	166 000	12.2
	n		320 000[b]	62 000[b]	10 000[b]	1 300[b]	130	11	1		
Saskatchewan (8) 0.65	d_L		100 000[b]	40 000[b]	5 000[b]	642	88	7.7	0		
	A_o		←	27 800	→	11 200	10 330	17 850	0	67 200	10.3
	n		←	93 500	→	415	57	5	0	94 000	
Canadian Shield (9) 8.2	d_L		200 000[b]	50 000[b]	5 000[b]	500[b]	56	3.8	0.85		
	A_o		42 000[b]	107 000[b]	107 000[b]	107 000[b]	120 000	88 000	270 000	841 000	10.3
(12)	A_o						460		84 000	655 000	8.2
	n		1 600 000[b]	410 000[b]	41 000[b]	4 100[b]		31	7		
South Baltic Platform (1) (6) 0.465	d_L		20 000[b]	8 200	1 650	125	11	0.45	0		
	A_o		240[b]	900	2 000	1 500	1 300	4 300	0	10 200	2.2
	n		9 300[b]	3 800	770	58	5	1	0		
Glaciated conterminous USA (7) 0.78	d_L		80 000[b]	18 000[b]	1 800[b]	240	23	2.6	1.3		
	A_o		2 600[b]	3 640[b]	3 640[b]	4 860	4 900	2 270	57 750	79 660	10.2
(13)	A_o								0	21 900	2.8
	n		100 000[b]	14 000[b]	1 400[b]	187	18	2	1		
Patagonia 0.48	d_L		20 000[b]	6 200[b]	1 040[b]	104[b]	21.5	6.1	0		
	A_o		260[b]	800[b]	1 300[b]	1 300[b]	5 279	5 511	0	14 450	3.0
	n		10 000[b]	3 000[b]	500[b]	50[b]	14	4	0		
Alps 0.040	d_L		25 000[b]	6 200[b]	1 750	750	175	0	0		
	A_o		25[b]	65[b]	180	995	2 176	0	0	3 440	8.6
	n		1 000[b]	250[b]	70	30	7	0	0		
Other deglaciated highlands 2.5	d_L		20 000[b]	5 000[b]	1 000[b]	100[b]	20[b]	0.8	0		
	A_o		1 300[b]	3 250[b]	6 500[b]	6 500[b]	13 000[b]	3 780	0	34 300[b]	1.4[b]
	n		50 000[b]	12 500[b]	2 500[b]	250[b]	50[b]	2	0		
Other deglaciated lowlands 4.0	d_L		50 000[b]	10 000[b]	1 700[b]	200[b]	15[b]	0.25	0		
	A_o		5 200[b]	12 500[b]	18 000[b]	20 000[b]	15 600[b]	4 560	0	76 600	1.9
	n		200 000[b]	48 000[b]	6 800[b]	800[b]	60[b]	1	0		
Total deglaciated area 18.0	dL		180 000	30 000	3 500	380	39	2.9	0.5		
	A_o		85 000	144 000	165 000	175 000	197 000	136 000	345 000	1 247 000	6.8
	n		3 250 000	554 000	63 000	6800	710	52	9		

d_L, Lake density (number per Mkm^2); A_o, total lake area (km^2); n, total lake number. Limnic ratios are estimated for lakes >0.1 km^2.

[a] Small numbers in parentheses: (1) EEA (1994); (2) E. Thörneloff personal communication; (3) Major lakes from Herdendorf (1984, 1990); (4) Kola peninsula includes lakes Ladoga and Onega; (5) sum of Sweden, Norway, Finland, and Kola peninsula; (6) sum of Poland, Estonia, Latvia, and Denmark; (7) sum of Vermont, Maine, New Hampshire, New York, Minnesota, Michigan, and Wisconsin extrapolated from Van der Leeden et al. (1989), with lakes Red, Champlain, and Michigan; (8) Hammer (1988); (9) with all Laurentian Great Lakes, Michigan excluded, extrapolated from Gray et al. (1990) and Herdendorf (1984), with similitude to Saskatchewan lakes; (10) Solantie (1973); (11) without Lake Ladoga; (12) without lakes Superior, Huron, Ontario, and Erie; (13) without Lake Michigan.

[b] Estimated values.

presently occurring, it is very important to constrain their global distribution as much as possible. Fortunately, fair lake countings are available for Saskatchewan (Hammer 1988), Wisconsin, Michigan, Minnesota, New Hampshire, Vermont, New York and Maine (Van der Leeden et al. 1989), as well as Sweden (EEA 1994; Thörneloff pers. comm.), Norway (EEA 1994), Finland (Solantie 1973; EEA 1994), and the South Baltic states (EEA 1994). In addition to these data, we have reconstructed lake distribution for two major lake districts in mountainous regions formerly glaciated, the Alps and Patagonia shared by Chile and Argentina, based on Herdendorf (1984), ILEC (1988, 1989, 1990, 1991), and CEC (1994) for the Alps, as well as Herdendorf (1984), Quiros and Drago (1985), Campos et al. (1983), and IARH (1993) for Patagonia.

These basic data are presented in Table 4. Three types of deglaciated areas can be differentiated on the basis of lake densities and distributions:

1. *Shields* as in Saskatchewan and in Scandinavia, i.e., Norway, Sweden, Finland, Kola peninsula, and Carelia in Russia including lakes Ladoga and Onega. Already characterized by the highest LRs, they also have the highest densities, particularly in the 10–100 km^2 area class (from 500 to 940 lakes/million km^2).
2. *Sedimentary platforms* such as the South Baltic and most of the formerly glaciated states in the United States: Vermont, Maine, New Hampshire, New York, Michigan, Wisconsin, and Minnesota. For these states the LR is still very high (10.2%), due to the enormous weight of Lake Michigan alone. When this lake is disregarded, the LR is 2.8%, similar to South Baltic (2.2%), and the densities for the 10–100 km^2 area class lakes are 125 and 240/million km^2, respectively.
3. *Mountainous regions* such as Patagonia and Alps have lake densities closer to those of the sedimentary platforms (100 and 750 for the 10–100 km^2 area class). However, the major difference to previous categories lies in lake depths that are much greater (for a given lake size) for lakes resulting from glacial scour on mountainous regions than for shields and even sedimentary platforms.

When Norway, Sweden, Finland, Kola, and Carelia are taken together, and if lakes Ladoga and Onega are joined to the Carelian lakes, the area referred to here as the Scandinavian Shield, has an average LR of 12.2%. A similar ratio can be obtained for the whole Canadian Shield based on the Herdendorf census for lakes exceeding 500 km^2 and on limited Canadian statistics for lakes exceeding 100 km^2 (Gray et al. 1990). For smaller lakes the distribution has been estimated to be similar to the one found for Saskatchewan and reported by Hammer (1988). With the four Laurentian Great Lakes shared by Canada and the United States (Michigan excluded), the Canadian Shield has a limnic ratio of 12%, and, without them, 9.3%. These figures correspond to 8.2 million km^2 of formerly glaciated area in Canadian lowlands and excludes the glaciated Cordillera, but may include a small area of glaciated sedimentary rocks such as in the Mackenzie river basin. When adding the glaciated lowlands in the United States, the total North American ice cap is 9 million km^2.

5.2 Global Deglaciated Area

The global budget of glacial lakes is highly dependent on the distribution of glaciated area in past geological times, particularly for the last glaciation, which culminated at 18000 B.P. The most detailed account of global glaciation has been made by Flint (1971), where an estimated total area (formerly glaciated) of 28.3 million km^2 is given as: 13.4 million km^2 for the Laurentide Ice Sheet; 2.6 million km^2 for Alaska, Cordilleran, Canada, and the (mainland) United States; 7.2 million km^2 for Europe; 2.7 million km^2 for the Ural-Siberian Ice Sheet; 1.25 million km^2 for central Asian mountains and the Himalayas; 0.7 million km^2 for Patagonia; and 0.45 million km^2 for miscellaneous regions in Central and South America, Africa, and Oceania. In addition, Flint lists Greenland (2.3 million km^2) and Antarctica (13.8 million km^2), which are still glaciated.

Flint's estimate cannot be directly used for the glacial lakes distribution for two reasons: Firstly, he included the area of the glaciated continental shelf when seawater was more than 100 m lower, which corresponds to vast areas, such as Hudson Bay, channels between Canadian Northern Archipelago, parts of the Arctic Ocean north of Siberia, the Baltic and North Seas, etc. Secondly, these figures represent the maximum ice extension that ever occurred during the Pleistocene, whereas the last glacial stage was somewhat less extended.

On the basis of various data, found particularly in Denton and Hughes (1981), the following deglaciated land areas have been taken into account for the reconstruction of the glacial lakes resulting from the last Wisconsin–Weichselian glaciation: North American Shield and platform, 9 million km^2; North American Cordillera from Alaska to the (mainland) United States, 1.75 million km^2; Scandinavian Shield, 1.4 million km^2; Alps, 0.04 million km^2; South Baltic platform and Russian platform, 2.4 million km^2; Ural-Siberian platform, 2.0 million km^2; central Asian and Himalaya mountains, 0.8 million km^2; Patagonia, 0.65 million km^2. The total area is 18 million km^2.

5.3 Total Number of Glacial Lakes

It is assumed that the great majority of lakes encountered in deglaciated regions result from various glacial activities. Fluvial lakes in these regions are therefore counted as glacial lakes. Few lakes of mixed origin may also be found, as in the great lakes categories for Lake Champlain (Canada/USA) and Lake Taymir (Russia), which have been considered as glacial.

The remaining undocumented deglaciated area (Table 4) consists of: 2.5 million km^2 in the highlands (Alaska, Himalaya, and Siberia) assumed to be similar to Patagonia and the Alps, and 4 million km^2 for lowlands (North Siberia, Russia) assumed to be essentially on soft sedimentary rocks with lake densities close to the South Baltic platform and to the deglaciated northern United States. For lakes exceeding 1000 km^2, Herdendorf's census provides the exact figure for these undocumented regions, i.e., lakes Becharoff and Iliamna in Alaska, and Taymir in North Siberia.

The total area of glacial lakes presently in existence (Table 4) is thus estimated around 1 250 000 km^2, for approximately 3 250 000 lakes exceeding 0.01 km^2 (1 ha). It corresponds to a LR of 6.9% for a total territory of 18 million km^2. The accuracy of these estimates depends mostly on Canada, and is probably around 15% for the total area. Lake density below 1 km^2 lake area is accurately known only in Scandinavia. If the estimated average lake density for the 0.01–0.1 km^2 area class is doubled, the corresponding total glacial lake area is only increased by 7%, but the total number of glacial lakes is 7.5 million.

Even considered on a global scale, the North American Great Lakes, from Lake Great Bear to Lake Ontario, do not follow the general distribution of glacial lakes. They correspond to 25% of the global glacial lake area (328 000 km^2 for eight lakes). Projection of the distribution of lakes smaller than 10 000 km^2 would allocate a total number of only four or five for the greatest glacial lakes exceeding 10 000 km^2, and a total area around 100 000 km^2. This figure is only met when lakes Superior (82 100 km^2), Huron (59 500 km^2), and Michigan (57 750 km^2) are withdrawn. These three lakes can be regarded as "outliers" in the global lake distribution.

6 Fluvial Lakes

Fluvial lakes are linked to river erosion and sedimentation processes, and are found in floodplains and deltas. They correspond to Hutchinson's types 49–59. Very few lake censuses exist for this type of lake, which is probably the second in terms of frequency at a global scale, particularly for medium and small sizes ($A_o <$ 10 km^2).

Total floodplain area is estimated to be around 4.46 million km^2 (Bazilevich et al. 1970), of which 1.08 million km^2 can be considered as deltas (Coleman and Wright 1975), leaving 3.38 million km^2 for floodplains along river main stems and tributaries. The proportion of floodplains in a given river system is highly variable. In China a total of 108 000 km^2 is estimated for the combined floodplain of Hai He and Chiang Jiang (or Yang Tze), corresponding to a total basin area of 2.1 million km^2 (Tu and Pu 1991). In this floodplain, some of the world's largest fluvial lakes are found: Poyang, Dong Ting, Hong Ze, Tai, and Chao. In the South American rivers the total floodplain area is estimated to 0.4 million km^2 for the four major river basins (Amazon, Orinoco, Parana, and Paraguay; Hamilton and Lewis 1990), i.e., 4% of total river basin area (9.8 million km^2), a figure similar to the one found for China (5%).

The proportion of lake area in river floodplain is still poorly known, except for a few noted rivers. In the eastern China floodplain the total lake area of 20 800 km^2 is estimated, corresponding to 19% of this area (Tu and Pu 1991). For the Orinoco it is estimated to be 7% by Hamilton and Lewis (1990; 480 km^2 of lake area for 2294 lakes). The most extended lake census is probably the one reported by Sippel et al. (1993) for the Brazilian Amazon floodplain. These authors have

counted 6500 lakes over a floodplain area of 92 000 km^2. The LR for this area is estimated to be around 11.2%, an intermediate value between eastern China and the Orinoco. The lake distribution derived from quartiles given by Sippel et al. is the following (for 92 000 km^2): <0.09 km^2, 1630 lakes; 0.09–0.2 km^2, 1630 lakes; 0.2–0.64 km^2, 970 lakes; >2 km^2, 650 lakes.

The greatest floodplain lakes according to Herdendorf (1984) are: Dong Ting (6000 km^2, China), Poyang (3350 km^2, China), Hung Ze (2700 km^2, China), Tonle Sap or Grand Lac (2450 km^2, Cambodia), Mai Ndombe (2325 km^2, Zaire), Tai (2210 km^2, China), Hulun (1590 km^2, China), and Weishan (1000 km^2, China). The Chinese and Amazonian LR in floodplains are probably high, and an overall ratio of 7.5% is chosen here for the global scale. The following statistical distribution takes into account Herdendorf's census of the great lakes and Sippel et al.'s (1993) population structure of fluvial lakes (Table 5). The total area of floodplain lakes is thus estimated to be 200 000 km^2 for a total floodplain area of 3.4 million km^2 (Table 5).

Lakes in deltas are not well known. Total delta area is estimated to be around 1.08 million km^2 (Coleman and Wright 1975), and only two major lakes exceeding 1000 km^2 are found in this position: Ponchartrain (1620 km^2) in the Mississippi Valley and Manzala (1360 km^2) on the Nile. A census of Louisiana lakes (Van der Leeden et al. 1989) can be used here as a surrogate for a real delta census. A much lower LR (2%) is found for this state than for river floodplains mentioned previously. With five major lakes from 270 km^2 (Edku) to 1360 km^2 (Manzalah), the LR of the Nile delta is much greater (approximately 13% for 23 900 km^2). However, most of these lakes are more the result of coastal transport of sand than of fluvial action. Therefore, as a first estimate the Louisiana figures, lake densities, and LR have been chosen as representative on a global scale (Table 5). Fluvial lakes thus have a total area estimated to be around 315 000 km^2.

7 Global Distribution of Crater Lakes

Although not frequent, volcanic crater lakes are very interesting features in terms of limnology. They have a very low ratio of drainage basin/lake area, generally below 3 they are sometimes very steep, very deep, and are often found in pristine conditions (Meybeck 1995). For these reasons an attempt to set up their global distribution has been made here. Crater lakes are distributed on all continents, generally clustered by provinces: Eifel, Auvergne, and central Italy; Kamchatka, Japan, Philippines, and Indonesia; New Guinea and Australia; Cameroon and East African Rift; Ecuador, Central America; Oregon, Alaska, and the Aleutian islands.

Table 5. Global distribution of lakes of fluvial origin[a]

Lake are class (km^2)	0.01	0.1	1	10	10^2	10^3 (3)	10^4 (2)	10^5	Total lake area	Limnic ratio (%)
A. Lakes in floodplain (1)										
	d_L	100 000	44 000	6 000	600	30	2	0		
	A_o	8 800	39 000	52 000	52 000	26 500	22 560	0	200 000	5.9
	n	340 000	150 000	20 000	2 000	102	8	0		
B. Lakes in deltas (4)										
	d_L (3)	9 000	7 400	900	140	23	2	0		
	A_o	260	2 000	2 600	3 900	6 500	2 980	0	18 200	1.7
	n	10 000	8 000	1 000	150	25	2	0		
C. All lakes of fluvial origins										
	A_o	9 000	41 000	54 600	55 900	33 000	24 600	0	218 000	
	n	350 000	158 000	21 000	2 150	127	10			

A_o, Total lake area (km^2); d_L, lake density (number/Mkm^2); n, total lake number.
[a] Small numbers is parentheses: (1) For a global floodplain area of 3.4 × 10^6 km^2; (2) from Herdendorf (1984); (3) as in Louisiana (from Van der Leeden et al. 1989); (4) for a global delta area of 1.08 × 10^6 km^2. Limnic ratio refers to global floodplain and delta areas.

Table 6. Global distribution of crater lakes

Area classes (km^2)	0.1	1	10	100	1000		Total
n	500	500	150	30	4	1	1200
Total lake area (km^2)	130	130	390	800	607	1100	3150

Limnological curiousities are those exceptional crater lakes created by meteoric impact such as the Botsumvi lake in Ghana, and Crater Lake in northern Quebec (Ouellet and Pagé 1990). They are very unique, and due to their very restricted watershed, their sedimentation rate is very low, explaining why they still have not been filled in since the impact, estimated to be 1.3 million years for both (see Sect. 10.1).

No global census of crater lakes has been done thus far. The greatest one, Lake Toba (A_o = 1100 km^2), in Sumatra, is of mixed origin, giant caldera and tectonic movement. Other big crater lakes are much smaller: Taal (140 km^2, Philippines), Atitlan (130 km^2, Guatemala), Trasimeno (124 km^2), and Bolsena (113.6 km^2), both in Italy. Then there are those crater lakes between 10 and 100 km^2: Wisdom (Papua New Guinea), Kucharo (Japan), Rotorua (New Zealand), Shikotsu, Towada, and Toya (Japan), Bracciano (Italy), Dakataua (Papua New Guinea), Crater (Oregon, USA), Tazawa and Mashu (Japan), Ossa (Cameroon), Vico (Italy), and Ikeda (Japan). However, this list is probably not complete. Kling et al. (1991) have registered all crater lakes in Cameroon. Taking into account the pattern of statistical distribution per lake area classes for that country and the census of major crater lakes exceeding 10 km^2 presented here, the proposed global distribution is shown in Table 6.

The total area of volcanic crater lakes would be around 3150 km^2. When this figure is compared with the global extent of regions underlaid by volcanic rocks, the LR is actually very low: around 0.03%.

8 Global Distribution of Saline Lakes

Saline lakes are conventionally defined as lakes where total dissolved solids (TDS) exceed 3 g/l (Williams 1964; Hammer 1986). The maximum salinities recorded exceed 300 g/l (Urmia in Iran, Dead Sea, Great Salt in Utah, etc.). Regarding lake area, volume, and total mass of salt, the global distribution of saline lakes is much biased by the enormous weight of the Caspian Sea, the salinity of which is close to 13 g/l (Table 7). There are two major origins of saline lakes: (1) lakes having some connection with ocean waters, and (2) lakes for which the evaporation process exceeds external water inputs, particularly terminal lakes without outlets.

The Caspian is not completely a terminal lake, because there is an outlet to the Kara Bogaz Gulf located on its eastern shore. This outlet is 10 km long, 300 m wide, and the water velocity is from 1 to 4 m/s until it reaches the Kara Bogaz through the Karakum waterfalls. The present very high salinity of Kara Bogaz (TDS = 350 g/l) causes massive fish kills of Caspian fishes when they reach the Gulf (in Fairbridge 1968a, p. 579). The Kara Bogaz has thus been differentiated from the Caspian as a separate lake in a position similar to Lake Poopo with regard to Lake Titicaca. A recently built dam now completely isolates the Gulf from the Sea. In the past 25 years, the Kara Bogaz has lost considerable area, due to changes in its water balance (Terziev et al. 1986). The origin of Caspian dissolved salt is multiple: The lake is a remnant of the Parathetys Sea, and a small part of its salt content could be of oceanic origin, although most of it has been probably brought in by the tributaries, Volga, Ural, Terek, and Kura.

8.1 Coastal Lagoons

Coastal lagoons generally result from the movement of sand bars and dunes along the shore line (Hutchinson's types 64 and 65). When separated from the ocean they may be fed by rivers and/or groundwaters, and these coastal lagoons are generally brackish, such as the Chilka Lake, India (TDS = 9.95 g/l), and Luang Lake, Thailand (TDS = 3.7 g/l; Herdendorf 1984). Based on Herdendorf's census of brackish coastal lagoons exceeding 500 km^2 (n = 14), the total area of this type of saline lake is estimated to be 40 000 km^2 over a total area of coastal lagoons of 60 000 km^2. If an average salinity of 5 g/l is attributed to these waters, their total salt mass is limited (M_{salt} = 0.64 10^{15} g). Lake Maracaibo is also linked to the ocean, but is of tectonic origin and much deeper

Table 7. Present distribution of major saline lakes exceeding 500 km^2 ranked in decreasing order of dissolved salt mass

Lake type	A_O (10^3 km^2)	V (km^3)	TDS (kg/m^3)	M_{salt} (10^{15} g)	Reference[a]
Endorheic					
Caspian[b]	374	78 200	13	1016	(1)
Dead Sea	1.02	188	298	56	(1)
Aral	64.1	1 020	10.5	10.7	(1)[d]
Urmia	5.8	45	230	10.35	1
Issyk-Kul	6.24	1 730	5.8	10.0	(1,2)
Kara Bogaz[e]	10.5	20	350	7.0	(2,3)
Great Salt[e]	4.36	19	285	5.4	(1)
Van	3.74	206	22.4	4.6	(1)
Eyre[e]	7.7	23	100	2.3	(1)
Σ Others[c]	101	915	29.5	27	(1–3)
Total with Caspian	578	82 360	13.9	1149	
Total without Caspian	204	4 160	31.9	133	
Exorheic					
Σ Coastal lagoons	40.0	128	5	0.64	This work

Saline lakes are those where TDS ≥ 3 g/l (Williams 1964).
TDS, Total dissolved solids; M_{salt}, total dissolved salt mass.
[a] (1) Herdendorf (1984); (2) Hammer (1986); (3) Fairbridge (1968a).
[b] Without Kara Bogaz.
[c] 42 lakes exceeding 500 km^2, including Turkana and Balkhash.
[d] In the 1950s.
[e] Size variation with hydrological balance.

than the coastal lagoons (Z_{max} = 35 m). Until the dredging of its outlet to the Atlantic Ocean, its chlorinity was only 750 mg/l; thus, it cannot be considered as a natural salt lake; its present chlorinity is around 2000 mg/l (Fairbridge 1968b).

8.2 Salinized Lakes due to Evaporation

Saline lakes of this type are due to the evaporation of freshwaters and/or to the dissolution of pre-existing surface-salt deposits or saline soils found in arid regions. However, Lake Asal (Djibouti) is a noted exception: seawater seeping into this cryptodepression is directly evaporated, thus leading to a TDS record of 304 g/kg (Fontes et al. 1979).

Herdendorf's census is used once more to list the world's major saline lakes. When in terminal position all lakes located in endorheic regions are saline, with very few noted exceptions, such as Lake Chad, in which the major salt regulation occurs in dune depressions fed by lake seepage (Carmouze et al. 1983). Therefore, when no salinity level could be found in Herdendorf's census for those lake types, particularly in central Asia, we attributed an average salinity of 30 g/l, close to the global average calculated for the world's biggest known salt masses in continental waters: Dead, Aral, Issyk Kul, Urmia, Kara Bogaz, Great Salt, Van, and Eyre (Table 7; Caspian excluded for its unique situation). The total area of major saline lakes resulting from evaporation is approximately 600 000 km^2 with the Caspian Sea and 200 000 km^2 without it. This figure is only a rough estimate, because many shallow saline lakes are characterized by marked natural variations in size (Lake Eyre, Lake Poopo, Great Salt Lake, etc.).

9 Global Lake Distribution

Three different estimates of global lake distribution have been made to extrapolate the comprehensive data bank built up by Herdendorf (1984, 1990) to lakes of smaller sizes (<500 km^2). In addition, the global distribution of lakes in exorheic and endorheic regions has also been considered as well as the global distribution of dissolved salts in lakes.

Table 8. Global lake distribution by the extrapolation approach

Lake area class (km^2)		0.01	0.1	1	10	100	1000	10 000	100 000	Total lake area
A. Regional census (58.2 million km^2)[a]										
	d_L		15 000	1 600	153	16.6	1.2	0.2	0.0064	
	A_o	150 000[e]	220 000	245 000	231 000	252 000	200 000	461 000	374 000	2 133 000
	n	5 700 000[e]	850 000	97 000	8 940	968	72	12	1	
B. World great lakes in regions without census (74.8 million km^2)[b]										
	d_L						0.69	0.08		
	A_o						127 000	162 000		289 000
	n						52	6		
C. Extrapolation in regions without census (74.8 million km^2)										
	d_L		3 500	400	45	5.5				
	A_o	40 000	68 000	78 000	88 000	107 000				381 000
	n	1 500 000[e]	260 000	30 000	3 400	410				
D. Global distribution (133 million km^2)[c]										
This work	d_L		8 350	950	93	10.4	0.93	0.13	0.007	
	A_o	190 000[e]	288 000[e]	323 000	319 000	359 000	327 000	623 000	374 000	2 803 000
	n	7 200 000[e]	1 110 000[e]	127 000	12 300	1 380	124	18	1	
Tamrazyan[d]	A_o									2 700 000

d_L, Lake density (number per million km^2); A_o, total lake area (km^2); n, total lake number.
[a] Documented area (see Table 1), Caspian has been added to former USSR.
[b] Values calculated from Herdendorf's census.
[c] Total continental area presently not glaciated.
[d] Tamrazyan (1974).
[e] Estimated values with low accuracy.

9.1 Extrapolation Approach

The present documented area (Table 1) is 58.2 million km^2, or approximately 44% of the world's continent, ice caps excluded. It also includes approximately 64% of the formerly glaciated regions. For the remaining area (74.8 million km^2), the great lakes distribution is accurately known from Herdendorf (1984). Therefore, the remaining lake area to be estimated concerns the smaller lakes ($A_o < 1000\,km^2$), occurring on 44% of the world's continent where nonglaciated area and semiarid regions are important, as in Africa and Australia. This undocumented lake area is limited, probably less than 15% of the total lake area! For this extrapolation, we have considered, as a model of lake densities, the average densities resulting from the grouping of the former Soviet Union, China, Argentina, India, and the United States, which were thought to be representative of the undocumented area. The resulting densities from lake area 0.01–1000 km^2 were somewhat overestimated, due to the underconsideration of desert area mainly found in Africa and Australia. This has been checked on the great lakes (1000–10 000 km^2): average densities derived from Herdendorf for the "undocumented" countries not listed in Table 1 are actually 0.7 lower than those found from the five major countries listed above.

The global distribution by extrapolation of known censuses is made here in three steps; (Table 8): (1) global census of lakes >1000 km^2 from Herdendorf (1984, 1990; Table 8B), (2) regional census for lakes smaller than 1000 km^2 from major documented censuses in all countries and regions listed in Table 1, i.e., for an area of 58.2 million km^2 (Table 8A), and (3) for the smaller lakes (<500 km^2) occurring in the remaining 74.8 million km^2 not documented (Table 8C) the extrapolation has been carried as such: the global extrapolated densities are first determined from Herdendorf's census, i.e., 0.69 lake million km^2 for 1000 to 10 000 km^2 and 0.08/million km^2 lake for 10 000 to 100 000 km^2. For the smaller classes (<1000 km^2), the densities used here are those of the less and/or nonglaciated regions (as for the former USSR, China, USA, India, and Argentina) multiplied by a 0.7 coefficient.

The global distribution with the extrapolation approach corresponds to a total lake area of 2.80 million km^2 for 133 million km^2 or a LR of 2.10% for lakes exceeding 0.01 km^2. With this method, approximately 44% of the global census (in terms of global lake area) is very well documented from Herdendorf's work, 42% is the result of accurate and/or reconstructed regional census, and 14% is extrapolated. It is therefore believed that the accuracy of this global figure is probably better than 10%. The worst estimates are of course those for the smallest lake size (<10 km^2), i.e., about 30% of total lake area. The total number and total area of smaller lakes (0.01–0.1 km^2) are probably not known to better than 50%.

In his work Tamrazyan (1974) does not provide detailed accounts of his global distribution estimated to be 2.7 million km^2, a value very close to the one presented here. It is probably based on the distribution of the 20 or 50 major world lakes, then on an extrapolation of the lake densities found in the former Soviet Union. The good fit between the two estimates is probably due to the excellent representativity of the former Soviet Union territory on a global scale: its densities (Table 1) are very close to the global ones for each lake size, although we have observed that, due to regional differences, lake densities may vary over two orders of magnitude (from 12 to 1400 lakes/million km^2 in the 10–100 km^2 class for India and Norway, respectively).

9.2 Lake Type Approach

This approach is presented in Table 9. It differentiates lakes into six main categories based on lake origins: tectonic, glacial, fluvial, crater, coastal, plus a miscellaneous category including all remaining categories grouped together such as solution lakes, wind deflation, landslide lakes, volcanic dams, etc. As for the previous approach, the distributions for the first three area classes of lakes with regard to lake area (>100 000 km^2, 100 000 to 10 000 km^2, and 10 000 to 1000 km^2) are constrained by Herdendorf's census. The extrapolation to smaller lakes is thus necessary for the smaller lakes only, i.e., approximately 53% of total lake area.

Distribution for tectonic, glacial, fluvial, and crater lakes has already been detailed in Sections 4, 5, 6, and 8. The coastal lagoon distribution is only a rough estimate extrapolated from Herdendorf's census. The miscellaneous lake distribution is also roughly estimated on the basis of 11 lakes in the 1000–10 000 km^2 class that did not belong to any of the previous categories. A dis-

Table 9. Global lake distribution per major origin

Origin		Lake area class (km^2) 0.01	0.1	1	10	100	1000[a]	10 000[a]	100 000[a]	Total lake area (km^2)
Tectonic[b]	A_0	5 000	10 000	20 000	30 000	52 000	134 900	267 300	374 000	893 000
	n	200 000	40 000	8 000	1100	200	40	8	1	
Glacial	A_o	85 000	144 000	165 000	175 000	197 000	136 000	345 000	0	1 247 000
	n	3 250 000	554 000	63 000	6 800	710	52	9		
Fluvial	A_o	9 000	41 000	54 600	55 900	33 000	24 600	0	0	218 000
	n	350 000	158 000	21 000	2 150	127	10	0		
Crater[c]	A_o	130	130	390	800	610	1 100	0	0	3 150
	n	500	500	150	30	4	1			
Coastal lagoons	A_o	700[f]	3 400[f]	5 700[f]	9 400[f]	15 600[f]	15 060	10 140	0	60 000
	n	25 000	13 000	2 200	360	60	10	1		
Miscella-neous	A_o	13 000[f]	15 000[f]	15 000[f]	15 000[f]	15 000[f]	15 000	0	0	88 000
	n	500 000	60 000	6 000	600	60	11	0	0	
	d_L	32 000	6 200	750	80	8.6	0.93	0.13	0.0075	
Total	A_o	113 000	213 000	261 000	286 000	313 000	327 000	623 000	374 000	2 510 000
	n	4 300 000	825 000	100 000	10 600	1 150	124	18	1	4 400 000

d_L, Lake density (number per Mkm^2); A_o, total lake area (km^2); n, total lake number.
[a] From Herdendorf's census (1984, 1990), for lakes >500 km^2
[b] See Table 3.
[c] See Table 4.
[d] See Table 5.
[e] See Table 6.
[f] Estimated values.

tribution law for the smaller lakes has therefore been estimated (Table 9).

When all these lake distributions are added, the total lake area (lakes exceeding 0.01 km^2) found by this method is around 2.5 million km^2 compared with 2.85 Mkm^2 with the extrapolation method. According to this method, the tectonic lakes would represent 35.6% of the present global lake area; glacial lakes, 49.7%; fluvial lakes, 8.7%; coastal lagoons, 2.4%; and all other lake types, only 3.6%. A great discrepancy is noted for the lake number in the smallest area class (0.01–0.1 km^2): 4.3 million compared with 7.2 million by the extrapolation method, which is probably more exact.

9.3 Climatic Typology Approach

This approach aims to link lake distributions with major climatic biomes. Five major biomes are considered here: deglaciated regions, temperate regions, dry and arid regions, deserts, and wet tropics. These subdivisions combine both temperature and surface-water runoff, which are both key factors in lake distribution. These biomes are a combination of 14 major climatic types set up to estimate river inputs to oceans by a typology approach, and for which a global map has been published (Meybeck 1979; Table 10).

The deglaciated land after the last Glacial Maximum, previously estimated to be around 18 million km^2 (Sect. 5.2), actually covers most present-day tundra and taiga. The remaining 5 million km^2 of taiga, thought to be nonglaciated, has been combined with temperate, humid temperate, and wet temperate regions of Meybeck (1979) to form the "temperate biome" where surface runoff exceeds 4 $l s^{-1} km^{-2}$. Former dry temperate regions are combined here with arid regions and savanna to form the "dry and arid biome" (runoff between 0.1 and 4 $l s^{-1} km^{-2}$). "Desert regions" correspond to very low, nonperennial runoff (<0.1 $l s^{-1} km^{-2}$). "Wet tropics" are characterized by runoff exceeding 9 $l s^{-1} km^{-2}$.

The construction of global lake distribution by the climatic approach has been realized in three steps (Table 1): (1) the distribution of deglaciated regions is the one previously estimated (Table 4), (2) for all lakes exceeding 1000 km^2, the 143 lakes listed by Herdendorf with their exact location have been allocated one by one to the five climatic categories, and (3) for smaller lakes (1000 km^2), extrapolations have been made using as much as possible the lake censuses already published (Table 11) as explained below.

The dry and arid distribution starts with Herdendorf's census extrapolated toward smaller lakes combining the present distributions in regions where runoff is between 1 and 4 $l s^{-1} km^2$ such as in Victoria province (Australia), the nonglaciated United States (without Louisiana

Table 10. Climatic divisions chosen for global lake distribution and river load typology

Lake distribution		River load typology[a]			
Climatic division	Total area (million km^2)	Morphoclimatic type[a]	Average air temperature (°C)	Surface runoff ($l s^{-1} km^{-2}$)	Total area (million km^2)
Deglaciated	18	Tundra and taiga	<4	4–9	23.2
		Humid taiga	<4	9–20	
Temperate		Wet taiga	<4	>20	
	26	Temperate	4–15	4–9	20.6
		Humid temperate	4–15	9–20	
		Wet temperate	4–15	>20	
Dry and arid		Dry temperate	4–15	1–4	
	42	Arid	15–25	0.1–1	41.95
		Savanna	>20	1–4	
Desert	23	Desert	15–25	<0.1	23.1
Wet tropics		Humid tropics	>20	9–20	24.05
	24	Wet tropics	>20	>20	
Permanent ice	16				16

[a] According to Meybeck (1979).

Table 11. Global lake distribution by climatic typology approach[a]

Lake area class (km^2) 0.01 0.1 1 10 10^2 10^3 (10) 10^4 (10) 10^5 (10)										Total lake area (million km^2)	Limnic ratio (%)
Climatic zone											
Deglaciated											
(18 million km^2)	d_L	180 000	30 000	3 500	380	39	2.9	0.5			
(5)	A_o	85 000	144 000	165 000	175 000	197 000	136 000	345 000		1.247	6.9
	n	3 250 000	555 000	63 000	6 800	710	52	9			
Dry and arid											
(42 million km^2)	d_L	6 000	800	100	15	2.8	0.64	0.12			
(6)											
	A_o	6 500	8 500	10 500	17 000	28 000	57 000	101 000	374 000	0.602	1.4 (1)
	n	250 000	33 000	4 000	650	120	27	5	1		0.54 (2)
Temperate											
(26 million km^2)	d_L	10 000	2 000	200	30	6	0.73	0.04			
(7)	A_o	7 000	13 000	13 000	21 000	40 000	63 000	31 500		0.188	0.7
	n	260 000	50 000	5 000	800	155	19	1			
Wet tropics											
(24 million km^2)	d_L	20 000	4 000	400	40	4.2	0.42	0.08			
(8)	A_o	13 000	26 000	26 000	26 000	26 000	24 000	81 470		0.223	0.9
	n	500 000	100 000	10 000	1 000	100	10	2			
Desert											
(23 million km^2)	d_L			33	8	1.4	0.69	0.04			
(9)											
	A_o			2 000	5 000	8 600	47 000	64 000		0.127	0.55 (3)
	n			770	190	33	16	1			0.27 (4)
Present ice caps											
(16 million km^2)											
			Very few lakes								
Global											
(133 million km^2)	d_L	32 000	5 550	620	71	8.4	0.93	0.135	0.007		
(11)	A_o	111 000	192 000	216 000	244 000	300 000	327 000	623 000	374 000	2.387	
	n	4 260 000	738 000	83 000	9 440	1 118	124	18	1		

d_L, Lake density (number per million km^2); A_o, total lake area (km^2); n, total lake number.

[a] Small numbers in parentheses:

(1) With Caspian; (2) without Caspian; (3) with Aral; (4) without Aral; (5) see Table 4; (6) Victoria, dry USA, India, and Argentina without Patagonia; (7) southern Europe and China; (8) estimate based mostly on Amazon basin distribution for lakes $<100\,km^2$; (9) Aral Sea accounts for 50% of total lake area; (10) Herdendorf's census is used in all climatic types for lakes $>1000\,km^2$; (11) ice caps excluded.

and Florida), and India and Argentina, without the deglaciated Patagonia (Tables 1 and 2). It must be noted that numerous great lakes (i.e., $A_o > 500\,km^2$) found in these regions are of tectonic origin, such as Caspian, Balkhash, Tanganyika, Malawi, and Chad. All these lakes are presently located in dry regions, but receive their major water inputs from wetter upstream parts of their basins.

The distribution of lakes in deserts is actually dominated by few lakes that are either fed by headwaters such as the Aral Sea and the Great Salt Lake, by coastal lagoons in desert regions (Manzalah in Egypt), and by very shallow or intermittent saline lakes such as Lake Eyre, Torrens, Frome, and Gairdner in Australia, as well as Ebi, Baghrash, and Helmand in Asia. It is assumed here that lake density in this region remains very low for smaller lake sizes. Thus, approximately 90% of total "desert lakes" area is accounted for by few lakes (50% for the Aral Sea at its pre-1950 stage alone).

Lake distribution of the temperate regions also starts with Herdendorf's census extrapolated toward smaller lakes on the basis of various censuses in southern Europe and China (Table 2), where average runoff is between 4 and 20 $l\,s^{-1}\,km^2$.

No local censuses were found for lakes located in the humid and wet tropics. Therefore, we have considered first Herdendorf's census for lakes $>1000\,km^2$, then the distribution of fluvial lakes established in the Amazon floodplain were supposed to be a possible guide in this extrapolation, particularly for its great density of lakes smaller than $100\,km^2$.

Over the total lake area thus reconstructed, approximately 50% is very well documented by Herdendorf, approximately 35% is estimated on a sound bases from known censuses (lakes smaller than $1000\,km^2$ in deglaciated area and in temperate regions), whereas for 15% of the lake area, the uncertainty is still very high (dry and arid regions, wet tropics, and deserts). With these hypotheses global lake area is estimated to be around 2.4 million km^2, a figure slightly lower than the previous figures. It must be remembered here that censuses for lakes exceeding $1000\,km^2$ and the deglaciated regions – a key factor in global lake distribution – are both common to the three estimates; therefore, these extrapolations concern only 45% of the global lake area (lakes smaller than $1000\,km^2$ and not resulting from glacial activity). The global lake distribution in the $100-1000\,km^2$ area class is also constrained by Herdendorf's data on lakes between 500 and $1000\,km^2$.

The distributions of lakes per climatic biomes at present geological time are: 52% for the deglaciated regions and 25% for the dry and arid regions. The limnic ratios are estimated to 6.9, 1.4, 0.7, 0.9, and 0.55% for the deglaciated, dry and arid, temperate, wet tropics, and desert biomes, respectively. These figures are highly influenced by the distribution of tectonic lakes, barely related to climatic influences: if the Caspian and Aral seas are set aside, the LR drops to 0.54% for the dry and arid biome, and to 0.27% for the desert biome, i.e., a 20-fold drop between deglaciated zones and present deserts (Table 11).

9.4 Lake Distribution in Endorheic Areas

Endorheic drainage, i.e., not connected to world oceans, and arheic area (without any organized drainage) represent 33.2 million km^2 over a total continental area of 133.1 million km^2, excluding Antarctica and Greenland (Baumgartner and Reichel 1975). Some of the biggest lakes occur in these regions such as Caspian, Aral, Chad, Eyre, Titicaca, and Balkhash. Exorheic areas are found in all continents and are characterized generally by arid conditions where potential evapotranspiration by far exceeds precipitation as in central Australia, Sahara, Arabia, most parts of central Asia, the North American Great Basin, and the Altiplano.

The determination of the global distribution of lakes in internal areas also takes into account Herdendorf's (1984, 1990) census of great lakes, i.e., lakes exceeding $500\,km^2$. Of 50 endorheic great lakes, only very few are not characterized by saline waters: They are upstream in hydrological systems while salinization takes place in the terminal lake. This is the case for Lake Tahoe (fresh) and Pyramid (salty) in the North American Great Basin (Cohenour 1968), and Lake Titicaca (fresh) and Poopo (salty) in the Bolivian Altiplano (Dejoux 1992), whereas for Lake Chad the salt regulation is not within the lake itself, but through groundwater seepage followed by evaporation (Carmouze et al. 1983). When salinities given by Herdendorf are considered (a few lakes in Tibet are still poorly known), it is observed that all other endorheic lakes were found to be oligo

saline ($3 < TDS < 20$ g/l), mesosaline ($20 < TDS < 40$ g/l), or hypersaline (40 g/l $> TDS$). They represent approximately 75% of the total number of saline great lakes, with other salt lakes being linked to coastal location, mostly coastal lagoons, and exposed to seawater intrusion. There are no saline great lakes apart from coastal lagoons and endorheic basins.

When the distribution of endorheic lakes per area classes is considered, the greatest lakes ($A_O > 10\,000$ km^2, Caspian, Aral, Balkhash, and Chad) carry an important weight compared with smaller lakes ($500 < A_O < 10\,000$ km^2). Therefore, it is believed that lakes exceeding 100 km^2 can provide an accepted estimate of endorheic LR. Herdendorf's number of lakes between 500 and 1000 km^2 has been multiplied by a factor of eight to estimate the total number in class 100–1000 km^2. Only lakes Chad (16 600 km^2) and Titicaca (8030 km^2) cannot be regarded as saline, although already much concentrated by evaporation. All 50 endorheic lakes found in Herdendorf's list have been individually attributed to each continent (Table 12), and Lake Sary-Kamysh has been added. Because the Caspian Sea is shared by Europe and Asia, these two continents have been combined.

Eurasia has by far the greatest number of lakes in an endorheic area, and the LR with the Caspian Sea is approximately 4.3% for an estimated total lake area of 613 000 km^2. This proportion is very high and mostly due to the presence of the Caspian Sea: without it, the LR drops to 1.0%, a proportion closer to that found for Africa (0.8%), Australia (0.8%), and South America (0.8%). The LR for the North American endorheic region is approximately 2.2%. The reliability of these numbers is questionable. Many lakes in internal regions are very shallow and are subject to enormous changes in lake area, such as Lake Eyre in central Australia, which can nearly dry out while at its maximum filling period, such as in the 1949–1950 flood stage, when its area was 9400 km^2 (Flint 1971). The Makarikari salt pan (Botswana) has not been counted by Herdendorf as a permanent water body; its inclusion here would increase Africa's LR to 1%. If the Caspian Sea is disregarded, the global LR for endorheic regions is 0.63%, compared with 1.65% for exorheic regions.

Table 12. Distribution of great lakes in endorheic or arheic regions at present geological time

Lake area class (km^2)		100[a]	1000[b]	10 000[b]	100 000[b]		Total lake area[c]	Total endorheic area	Limnic ratio[c] (%)
Eurasia	A_o	0.077[k]		0.080	0.082 (Aral, Balkhash)	0.374 (Caspian)	0.613[d] 0.13[e]	14.1	4.3[d] 1.0[e]
	n			15[f]	2	1			
Africa	A_o	0.065[k]		0.0126	0.0166 (Chad)	0	0.094	12.2	0.77
	n			3	1	0			
South America	A_o			0.011	0	0	0.012	1.5	0.80
	n			3	0	0			
North America	ΣA_o	0.016[k]		0.0044	0	0	0.020	0.9	2.2
	n	3		1	0	0			
Australia	A_o	0.014[k]		0.021	0	0	0.035	4.2	0.83
	n			4	0	0			
Global	A_o	0.172[k]		0.129	0.099	0.374	0.774[d] 0.2[e]	33.2	2.3[d] 0.63[e]
	n			25	3	1			

A_o, total lake area (million km^2) in each class; n, total lake number.
[a] Eight times the lake number in the 500–1000 km^2 class from Herdendorf (1984).
[b] Herdendorf (1984).
[c] Calculated for lakes exceeding 100 km^2 only.
[d] With Caspian Sea.
[e] Without Caspian Sea.
[f] Including the Lake Sarykamish.
[k] Values estimated.

9.5 Global Dissolved Salt Distribution in Lakes

The global distribution of dissolved salts in lakes is presented for both saline and nonsaline lakes (Table 13). Total volumes for each lake type are also given (Meybeck, in prep.) based on Herdendorf's census and the area–volume relationship for each type. Saline lakes have been grouped into three types: Caspian Sea (88.5% of total salt mass), other endorheic lakes (11.5%), and coastal lakes (0.06%), excluding Maracaibo. It is assumed here that only two-thirds of coastal lakes are saline (i.e., total area of 40 000 km^2). This total salt content is estimated to 1150 × 10^{15} g. Their total volume is 82.5 km^3, a figure very comparable to the total volume of freshwater lakes (93.5 km^3), whereas the total salt mass of the freshwater lakes is only 20.3 × 10^{15} g or 1.6% of the world total of dissolved salts in lakes.

Without the Caspian, the total salt mass in saline endorheic lakes is estimated to be around 133 × 10^{15} g for a total lake area around 204 000 km^2 and a volume of 4160 km^3. This salt budget is a combination of 80% known sample and 20% estimated: This proportion is worse for lake volumes, due to unknown figures for numerous "smaller" central Asia lakes. Numerous small saline lakes of less than 500 km^2 (African Rift, Australia, and central Asia), although generally documented (Hammer 1986; Williams 1981), have a very minor contribution to the global budget and have not been taken into account in the total area or volume. Lakes Turkana and Balkhash, both endorheic, although slightly less saline than the conventional limit (TDS > 3 g/l), have been included here. Lake Sarykamish (1500 km^2), located south of the Aral Sea and omitted by Herdendorf, has a TDS of 15 g/l and is included here. When the Caspian Sea is included, these figures jump dramatically: 1150 × 10^{15} g of salt for 578 000 km^2 and 82 360 km^3 (Table 13). Saline lagoon connected to oceans, although they correspond to approximately 40 000 km^2, hold only 0.64 × 10^{15} g of salt.

The average TDS in freshwater lakes is slightly different for the principal lake categories (Table 13). The weight of African Great Lakes, such as Tanganyika and Malawi, is such that the average tectonic freshwater lakes are nearly three times more mineralized than glacial lakes, mostly located on crystalline shields. This ratio is probably caused by climatic and lithological differences: higher evapotranspiration in East Africa and the impact of hydrothermal inputs. Fluvial lakes have been characterized by TDS as equal to the weighted average river according to Meybeck (1979). Average TDS for crater lakes chosen here corresponds to average TDS in streams draining volcanic rocks (Meybeck 1987). It must be noted that small acidic crater lakes that can be highly mineralized are not accounted for here. Miscellaneous lakes are all those that do not belong to previous categories, such as solution lakes in carbonate terrains, lakes resulting from daming

Table 13. Global distribution of dissolved salts in lakes

Lake type	A_o (10^3 km^2)	V (10^3 km^3)	TDS (kg/m^3)	Msalt (10^{15} g)
Saline[a]				
Caspian	374	78.2	13.0	1016
Other saline endorheic lakes	204	4.16	32.0	133
Saline coastal lakes	40	0.128	5.0[c]	0.64
Total	618	82.5	13.9	1150
Freshwater[b]				
Tectonic	424	54.6	0.29	16.1
Glacial	1247	38.4	0.10	3.8
Fluvial	218	0.58	0.10[c]	0.058
Crater	3.1	0.58	0.080[c]	0.046
Miscellaneous	88	0.98	0.30[c]	0.33
Total	1980	95.14	0.213	20.3

Msalt, total mass of dissolved salts
[a] Terminal lakes in endorheic regions and most coastal lakes.
[b] Exorheic lakes except coastal lakes, and endorheic lakes not in a terminal position.
[c] Estimated values.

action, etc. They are assumed to be slightly more mineralized than glacial, fluvial, or crater lakes.

It is clear from Table 13 that 98% of dissolved salts found in surface waters are stored in only 24% of lake volume, mostly in the Caspian Sea. These figures refer only to the dissolved salts found in saline lake waters. The evaporation process during millennia and sometimes millions of years has resulted in considerable accumulation of salt deposits of continental origin in present and former lake systems. In the world's biggest salar, presently active, of Uyuni (Bolivian Altiplano), the salt accumulation has been estimated to 68×10^{15} g, including the world's greatest deposit of lithium (9×10^{12} g Li; Risacher 1992).

10 Major Changes in Global Lake Distribution in the Geological Past

10.1 Lake Ages

By nature, lakes are not permanent features in earth's histoy: they develop, gradually fill up, and disappear. Lake life cycles can be very short: a few weeks for lakes caused by landslide dams that eventually break up. Most great lakes of tectonic origin are characterized by much older ages (Table 14), a feature that generally goes along with developed endemism. The oldest lakes are probably the great rift lakes, Baikal and Tanganyika, and the Caspian and Aral seas, which are the relicts of the Parathetis, a huge sea

Table 14. Examples of lake ages in relation to lake origin

Origin	Lake	Age	Reference
Tectonic graben	Baikal	≈20 Ma	
	Issyk-Kul	≈25 Ma	
	Tanganyika	20 Ma	Tiercelin and Mondeguer (1991)
	George	4–8 Ma	Timms (1993)
Miscellaneous tectonic	Caspian[a]	>5 Ma	Stanley and Wezel (1985)
	Aral[a]	>5 Ma	Stanley and Wezel (1985)
	Ohrid[a]	>5 Ma?	Stankovic (1960)
	Prespa[a]	>5 Ma?	Stankovic (1960)
	Maracaibo	>36 Ma	Fairbridge (1968a)
	Biwa	2 Ma	
	Eyre	20–50 Ma	Timms (1993)
	Victoria	≈20 000 B.P.	Adamson and Williams (1980)
	Tahoe	2 Ma	Imboden et al. (1977)
Volcano tectonic	Kivu	1 Ma[b]	Degens et al. (1973)
		10 000 B.P.[c]	Tiercelin and Mondeguer (1991)
	Toba	75 000 B.P.	Dawson (1992)
	Lanao (Philippines)	>2 Ma?	Frey (1969)
Glacial	Laurentian Great Lakes	8 000 B.P.[d]	Dawson (1992)
Fluvial	Mississippi lakes	9 000 B.P.	Dawson (1992)
Landslide	Vallon	Born in 1943	Dussart (1992)
	Sarez (Pamir)	Born Feb. 18, 1911	Hutchinson (1957)
Impact crater	Crater (Quebec)	1.3 Ma	Ouellet and Page (1990)
	Botsumvi (Ghana)	1.3 Ma	Livingstone and Melack (1984)
Volcanic crater	Wisdom	300 B.P.	Ball and Glucksman (1978)
	Crater (Oregon)	6 500 B.P.	Fairbridge (1968a)
	Atitlan (Guatemala)	84 000 B.P.	Dawson (1992)
	Le Bouchet (France)	>250 000 B.P.	Williams et al. (1993)
	Viti (Iceland)	May 17, 1724	Hutchinson (1957)

[a] Relict of Thetis Sea.
[b] Age of tectonic depression.
[c] Cutoff of outlet toward Nile basin and connection to Zaire basin through Tanganyika.
[d] In their present configuration.

found at the middle and upper-Miocene; they already existed in the Messinian age (5–6 Ma ago), when the Mediterranean Sea was nearly evaporated and also split into six relict hypersaline basins (Hsü and Kelts 1978). Lakes Eyre and Maracaibo are also very ancient structures (>10 Ma). For all these lakes the sedimentation rates, of the order of 0.1–1 mm/year, are compensated by subsidence rates; otherwise, they would have been filled up on 0.1–1 Ma.

The greatest proportion of world lakes, however, is actually much younger: most lakes associated with glacial activity were formed during the glacial retreat, between 12 000 and 6000 B.P. Probably the best documented examples are the Laurentian Great Lakes, which present considerable changes during this period (Dawson 1992). Coastal lakes are also a very recent geomorphic structure in their present location. They were formed when the sea level stabilized after the Flandrian transgression caused by glacial melting, Ca. 6000 B.P. Most fluvial lakes found in, the floodplains of major rivers, such as the Amazon, Chiang Jiang, etc., are probably also linked to the Flandrian transgression that filled river channels with sediments.

Volcanic lakes have variable ages. In this category it is very rare to find ages exceeding 0.1 Ma: larger crater lakes commonly have average depths of the order of 100–200 m when they are formed, then they gradually filled up with sediments at low rates similar to those found in the center of large tectonic lakes (0.1–1 mm/year), mostly as a result of their limited drainage basin. The lifetime of smaller crater lakes is generally shorter: many craters in the Eifel, Auvergne or Latium are already filled up. Exceptions are noted, such as in Lake du Bouchet (Velay, France), which is more than 0.25 Ma old and well studied for paleolimnological records (Williams et al. 1993). Crater lake formation has been observed in historical time, e.g., at Lake Viti, on May 17, 1724, in Iceland.

Landslide lakes are probably much less durable. The ratio between basin area/lake area sometimes exceeds 100, although it is commonly from 10 to 30 for most lakes (Meybeck 1995), and they are generally located in steep relief regions. Therefore, the allochthonous sediment inputs are very high, actually similar to those found in reservoirs, leading to average sedimentation rates between 1 and 10 mm/year. Their duration is therefore from a few hundred to a few thousand years. Moreover, these dam lakes are also exposed to regressive erosion from the river outlet, which may eventually lead to a catastrophic breakup before the lake has been filled up, as occurred for a dam lake in Kashmir (Timms 1993): it was 64 km long, took months to fill up with water, then broke out in 24 h! The nature of the dam may also play a role in lake duration. In the French Alps (Chablais), Lake Montriond, a few hundred years old, has little sediment accumulation, due to seepage through the rock landslide, whereas Lake Vallon, a few kilometers away, was formed in 1943 by a mud flow, and has already been half filled up.

10.2 Historical Changes

When considering the past extension of lakes, several time scales must be considered. Historical changes that occurred during the past millennia are evidenced in maps, written records, or archeological diggings. They are mostly due to natural lake filling with sediments, to climatic changes, and to human impacts such as drainage or water diversion, or a combination of these. The Aral Sea is probably the best example known. During the Roman period, and at least until 1559 (Fairbridge 1968a), this lake was greater and directly connected by the Uzboi channel to the Caspian Sea. Its shrinking from 68 000 to 33 600 km^2 since 1950 is purely anthropogenic and mostly due to water diversion and evaporation after irrigation of its tributaries, the Amur Darya and Syr Darya (Létolle and Mainguet 1993). In Turkey the huge Lake Bataklik, which once bordered the city of Çatal Hüyük, a cradle of civilization 6000 B.P., is now completely dried up. When Montezuma received Cortez in Tenochtitlan, the capital city of the Aztec empire was in the middle of a huge lake (more than 1000 km^2), which has since dried up in present-day Mexico City.

10.3 Postglacial Changes

Holocene changes in lake extension have been very carefully studied by paleo-limnologists and paleoclimatologists, particularly in endorheic regions, which are sensitive to climate change. It is not the purpose of this chapter to review this question on each continent, but to focus attention

on the great variability of lake development in internal regions and deglaciated areas, which is intimately linked to major changes in hydrological features of many major rivers, due to lake overflow, ice barriers, etc. In few places (e.g., Lake Asal) recent tectonic changes are an additional factor in lake-level changes (Gasse and Fontes 1989). These changes are summarized in Table 15. Dawson (1992) has given an excellent review of lake variations in deglaciated regions. Comparative studies in other regions (Africa, central Asia, and South America) are very difficult to make without very accurate and dated paleolevel records, because lake levels are likely to change dramatically in less than 1000 years (van Campo and Gasse 1993).

In Africa a major change occurred for Lake Chad at 6000 B.P. (Servant and Servant 1983): its size was approximately 20 times greater than it is presently (350 000 km^2). Its maximum depth was 154 m in the Bodelé depression (compared with 2–4 m today). Another possible paleolevel of Chad is reported at 400 m from 30 000 to 22 000 B.P., compared with 282 ± 1 m presently, by Messerli (1980). It is difficult to give an area of this stage because the present 400-m isoline is wide open toward the Niger basin through the Benue valley, but its extension would probably exceed 500 000 km^2. This paleo-mega-Chad is still debated, because neotectonic movements may have affected the altitude of paleoshorelines, and its maximum size could have been only a few times the present extension (Durand 1982).

In the East African Rift, Lake Tanganyika experienced major droughts at 35 000 and 200 000 B.P. Its level dropped down by 150 and 600 m, respectively, the outlet to the Zaire basin via the Lukuga river was cut off and the lake became more saline. For more details, see the comprehensive review by Tiercelin and Mondeguer (1991). Other changes occurred in the Rift region: Lake Turkana (former Rudolf) was once connected to the Nile basin (8000 to 6000 B.P.) and much more extended (Beadle 1981). Another major change occurred in Lake Kivu with the eruption of Virunga volcanoes that changed the northern overflow to the Nile basin for the Zaire basin through the Ruzizi river. In Botswana the Okawango also discharged downstream to the Makarikari depression, which was filled in during a glacial period (lake level 45 m higher than the present depression corresponding to an area of 34 000 km^2; Flint 1971). In their review, Street-Perrot and Harrison (1984) reported that 6000 B.P. lake levels in West and East Africa north of the Equator were generally much higher than present, particularly in the Sahara, where many extended lakes were occurring at that period.

Probably one of the most documented variations in lake level has been realized on the Awash river basin (Ethiopia and Djibouti), now an endorheic river that was connected to the open ocean at 8600 B.P. by a cascade of lakes: Abhe, Hanle-Dobi, Gaggade-Asal-Sukalol, and finally Lake Ghoubbat, presently a marine bay. The total lake area is estimated at that period to be around 7600 km^2 compared with only 365 km^2 presently (Gasse and Fontes 1989). Another wetter period occurred at 6500 B.P. These two major occurrences of higher lake levels were also recorded in central Tibet and in Lake Chad: they could reflect extended climatic changes (van Campo and Gasse 1993).

In South America the paleolimnology of the Bolivian Altiplano has been extensively studied, and several paleolakes have been evidenced (Servant and Fontes 1978). Lake Minchin reached 60 000 km^2, and Lake Tauca, 43 000 km^2, with level changes +114 m and +67 m, respectively, compared with the present level. Poopo Lake and Coipasa and Uyuni salars (or salt pans) are the remnant of these events. More recently (7700 to 3650 B.P.), the level of Titicaca dropped to 50 m, cutting the communication with Lake Poopo through the Desaguaderro, resulting in a salinization of the lake.

In the endorheic region of the North American Great Basin, paleolakes Lahontan and Bonneville were much greater than their remnant lakes of the present, respectively Pyramid and Walker, and Great Salt Lake (Cohenour 1968; Table 15).

The major lake-distribution change during the Holocene is caused by the deglaciation of Manitoba and Saskatchewan. From 12 000 to 8000 B.P., the huge glacial Lake Agaziz covered approximately up to 500 000 km^2, i.e., twice the present total area of all the Laurentian Great Lakes. Many large lakes, such as Winnipeg and Manitoba, are now the relicts of this paleolake. At its greatest stage (9000 to 8400 B.P.), it was connected with Lake Ojibway, was 3100 km long, and had a volume estimated between 75 and 150 $\times 10^3 km^3$. During its 4000-year duration, Lake Agaziz discharged first into the Mississippi, then into the St. Lawrence, and then into the Hudson

Table 15. Examples of major recent changes in lake extension and hydrology during the Pleistocene

Present lake	Present lake area A_o (km^2)	Past changes		Reference
		Past area (km^2)	Age (years B.P.)	
Poopo (Bolivia)	2300	a) Lake Tauca: 43000 km^2	13000	Servant and Fontes (1978)
Coipasa (Bolivia)[a]	2500	b) Lake Minchin: 60000 km^2	27000	
Uyuni (Bolivia)[a]	10000			
Titicaca		Level drop 50 m, salinization	7700–3650	Servant and Fontes (1978)
Great Salt (Utah)	4360	Lake Bonneville: 51560 km^2	18000–14000	Cohenour (1968), Nilsson (1983)
Pyramid (Nevada)	446	Lake Lahontan: 22300 km^2	18000–11000	Cohenour (1968), Nilsson (1983)
Walker (Nevada)	154			
Winnipeg (Canada)	24500	Lake Agaziz: 350000 km^2 then	12000–9000	
Winnipegosis (Canada)	5375			
Manitoba (Canada)	4625	Lakes Agaziz and Ojibway (>500000 km^2)	9000–8400	Dawson (1992)
Woods (Canada)	4350			
Red (USA)	1170			
Dead Sea	1020	Lake Lisan (high stage)	18000–12000	Dawson (1992)
West Siberia and north-east Europe	<50000	Grosswald proglacial lake: 1500000 km^2; Ob and Yenissei overflow to Aral, then Caspian and Black; Pechora overflow to Caspian	18000	Grosswald (1984)
		West Siberian lake and Pur Mensi lake: 200000–300000 km^2; Yenissei overflow to Arctic Ocean; Ob overflow to Aral, then Caspian and Black; Pechora overflow to Caspian	18000	Velichko (1984)
Caspian Sea	374000	Connected in a huge freshwater lake to Black Sea (≈1000000 km^2), outflow to Mediterranean	17000	Wright (1961), Flint (1971), Dawson (1992)
Black Sea	432000	New Euxine lake	29000–9000	Ivanov and Shmuratko (1982)
Baltic Sea	385000	Freshwater lake: Baltic Ice Lake	12000–10450	Flint (1971), Dawson (1992)

Table 15. (*Contd.*)

Present lake	Present lake area A_o (km^2)	Past changes		Reference
		Past area (km^2)	Age (years B.P.)	
Abhe (Ethiopia)	250	5500 km^2	8600	Gasse and Fontes (1989)
Asal (Djibouti)	115	1000 km^2 Lake Gaggade-Asal-Sakalol	8600	Gasse and Fontes (1989)
Okawango (Botswana)	Internal delta	12000 km^2, overflow to Zambezi		Sawula and Martins (1991)
Turkana (Kenya)		Overflow to Nile Basin	8000	Beadle (1981)
Kivu		Overflow to Nile Basin	>10000	Tiercelin and Mondeguer (1991)
Tanganyika		a) Cutoff from Zaire basin: 150 m level drop, salinization	35000	Tiercelin and Mondeguer (1991)
		b) Same: 600 m level drop, split into three lakes	200000	Tiercelin and Mondeguer (1991)
Chad (Chad)	16600	Mega Chad (350000 km^2?), outlet to Niger Basin?	6000	Servant and Servant (1983)
Gregory (Australia)	387	5492	50000–30000	Bowler (1981)
Woods (Australia)	423	5476	?	
Frome (Australia)	2550	3100		
Eyre (Australia)	7700	Lake Dieri: 100000 km^2, overflow to ocean	?	Flint (1971)

[a] Salar.

Bay, mostly through catastrophic breakup of ice dams or jokulhaups (Dawson 1992).

In Asia major changes in lake area are likely due to climatic variations. An intensified monsoon event has been reported for lakes Sumxi and Longmu (Tibet) near 9000 to 8000 B.P. (Gasse et al. 1991). Flint (1971) reviewed these changes in his chapter on Fluvial Lakes, but does not give precise dates: higher lake levels can either result from glacial or from interglacial stages such as the Holocene. He quotes higher levels for Lakes Burdur (+95 m), Van (+60 m), and Tuz (+75 m) in Turkey, Lop Nor (+180 m) and Shorkul (+100 m) in China, and for Urmia Lake (Iran), which "expanded once to nearly twice its present area." Lake Balkhash (Kazakhstan) was also much greater than present (quoted by Nilsson 1983).

In Europe lake distribution during the Wurm-Valdai glaciation and the Holocene has also been dramatically changed. At 10300 B.P., the Baltic was not yet openly communing with the North Sea, but was a lake of approximately 300000 km^2 (Flint 1971), which was eventually connected to the North Sea at 7700 B.P. The recent evolution of the Black Sea and Caspian Sea is much complexer. During the maximum glacial extension (before 18000 B.P.), the Mediterranean Sea level dropped; as a result, the Black Sea was a lake connected by a cascading Bosphorous (Ivanov and Shmuratko 1982). At the start of the postglacial time, the Caspian Sea level was much higher, due to melting of the North Russia ice cap, and this lake was connected to the Black Sea through the Azov Sea by the Manytch depression. The total size of these lakes was near 1000000 km^2 (Wright 1961; Kaiser 1969; Flint 1971). The lacustrine stage of the Black Sea or Lake New Euxine lasted from 29000 to 9000 B.P. according to Varushchenko (1982).

In central Asia the Aral Sea drainage did not grow larger and it had a low level. During the Valdai glaciation until 18000 B.P., the courses of West Siberian rivers were blocked by ice caps and huge proglacial lakes occurred. The extension of these Siberian lakes and their outlet location are still much debated. According to Dawson's review (1992), two hypotheses have been made:

1. A huge lake, up to 1.5 million km^2, which was the result of a complete damming of all rivers by a continuous ice cap, from the eastern Baltic tributaries to the Yenissei inclusive (Kvasov 1979; Grosswald 1984). This lake overflowed to the Aral, and from there to the Caspian Sea and Black Sea, which were at the same levels. Then, at 14000 B.P. the glacial retreat made the Poland passage to the North Sea available for the main overflow: Baïkal was more or less connected with the North Sea.
2. According to Velichko (1984), the ice cap on the Putorana mountains was not connected to the main ice cap and allowed for a passage of Yenissei to the Arctic Ocean; as a result, the proglacial lakes were much smaller, approximately 200000 km^2 (Arkhipov et al. 1986).

In Australia, the major lakes are located in the vast arheic or endorheic region: lakes Eyre (9400 km^2 when filled in), Torrens (5640 km^2), Gairdner (4520 km^2), and Frome (2550 km^2). At their maximum extension during the Pleistocene, they may have been much greater. Lake Dieri, the former Lake Eyre, is estimated to have been around 100000 km^2 (Flint 1971). Bowler (1981) considered the maximum extension of Australian lakes compared with the present area: the ratio ranges from 1.2 for lakes having a very small drainage area to 14 for Lake Gregory (present area 387 km^2; past maximum area 5500 km^2 for a total watershed of 33160 km^2). The present total area of Australian lakes is estimated to be 23500 km^2 with Lake Eyre at full stage. When applying Bowler's ratio (lake maximum area/present area) proportionally to the ratio drainage basin/lake basin, an estimated total lake area of 125000 km^2 is found for their maximum Pleistocene extension with 100000 km^2 for Lake Eyre alone. According to Bowler (1981), the wetter period was between 50000 and 30000 B.P. The LR for Australia, presently estimated from 0.18 to 0.31%, could have reached 1.6% during this period.

11 Discussion and Conclusions

The distribution of lakes follows the same exponential increase at a global scale, when going from large lakes to smaller ones, than the one noted in regional lake censuses. When compared with Wetzel's graph (1990), there is a great similarity for the first part of the distribution concerning large lakes, but Wetzel's estimate for very small lakes (<0.1 km^2) is much higher than

the one proposed here. At this stage the number of lakes depends very much on their definition. Very small shallow lakes (<0.01 km^2; average depth <1 m), such as arctic ponds, may number tens of millions, and the distinction between lakes and wetlands is not clearcut. In our budgets we have estimated the total area and LRs for lakes exceeding 0.01 km^2.

The Laurentian Great Lakes do not fit the global distribution of glacial lakes determined between 1 and 10 000 km^2: they are responsible for a major overweight of the 10 000–100 000 km^2 class in this type.

The distribution of tectonic lakes should not be considered at local or regional scales, but only at the global scale. A good example is provided by Hungary, where tectonic Lake Balaton (A_o = 590 km^2) is an obvious outlier in the local distribution: it triples the LR, being 0.29% without Balaton and 0.90% with it (Szesztay 1966). At present geological times, the Caspian Sea is unique and approximately fits the global lake distribution observed from lake areas 1–10 000 km^2.

The global lake-area estimates that are found here using three different methods are very similar: 2.4, 2.5, and 2.8 million km^2 for climatic typology, lake typology, and extrapolation methods, respectively. These estimates do not have the same accuracy: the climatic typology distribution is based on only 55% of lake distribution, i.e., all lakes exceeding 1000 km^2 and approximately two-thirds of lakes of glacial origin. The lake typology approach is based on approximately 65% of documented lakes, and the extrapolation method on approximately 70% of documented lakes. It must be remembered that only some censuses with appropriate data for lakes between 1 and 10 km^2 were found, and very few for smaller lakes. The difference between the last two estimates illustrates the importance of the hypothesis retained for the extrapolation. The extrapolation method probably leads to an overestimate of lake area, because estimated lake densities in extended desert regions, such as in Sahara, Kalahari, and Arabia, which are in the extrapolated set, are probably too high. The actual estimate is probably between 2.5 and 2.8 million km^2, a value identical to Tamrazyan's estimates, [2.7 million km^2 (1974)] essentially based on a former Soviet Union census. This census is actually very close to the global census: LR 2.3% for the former Soviet Union compared with 2.1% by the extrapolation method, and lake density for class 10–100 km^2 of 106/million km^2 compared with 93/million km^2. Other past estimates are very rare, poorly documented, and generally within the values presented here: 2.5 million km^2 for Penck (1894), which was later accepted by Halbfass (1933), and even by Hutchinson (1957). The undetailed estimates of Mulholland and Elwood (1982) [2.0 million km^2, and of Soviet IHP (1978), 2.1 million km^2] have probably much underestimated the smallest lakes (A_o <10 km^2).

The global lake area is, of course, highly dependent on the largest lakes conventionally taken as >500 km^2 by Herdendorf, but the very small lakes should not be neglected: lakes less than 1 km^2 still correspond to approximately 13% of the global area, but their ecological and geochemical importance, such as their filter function of terrestrial inputs, may be enormous when considering that their total number possibly reaches 10 million. Global lake volume does not follow this trend. On the basis of known volumes (Unesco 1974; Soviet IHP 1978; Lerman and Hull 1987; ILEC 1988, 1989; Herdendorf 1990), and taking into account specific relationships between the volume and area for the various lake types considered here, (Meybeck, in prep.), the total lake volume can be estimated to be 179 000 km^3 (Table 13). When the most important lakes (in terms of volume) are ranked starting from the Caspian Sea (Fig. 2), and when their cumulated A_o or V are calculated, the following figures are found: the Caspian represents 14.4% of global lake area and 44.7% of global lake volume. The

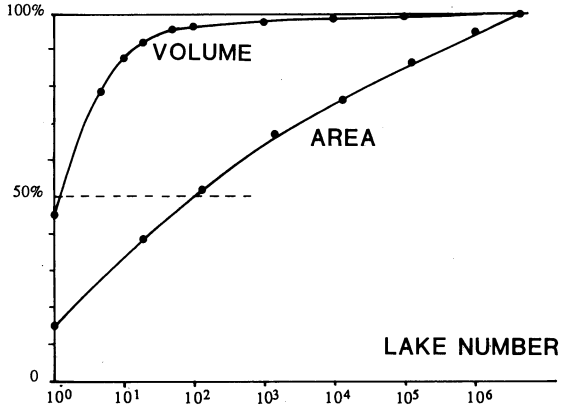


Fig. 2. Cumulated lake area and volumes with increasing lake numbers ranked per area or volume. In both graphs the Caspian Sea is the number one lake

first ten most important lakes correspond to 87.3% of the volume and only 33% of the area.

Another way to present global lake distribution is presented in Fig. 3A, B, and is related to lake area classes. The smallest lakes ($A_o < 1\,km^2$) are estimated to number at least 5 million, but they only contribute to 13% of the total lake area. The medium-sized lakes ($1 < A_o < 100\,km^2$) number around 110000, and correspond to 22% of the total lake area, whereas the biggest lakes ($A_o > 100\,km^2$) estimated to number around 1300 correspond to 65% of the total lake area. The 19 lakes exceeding $10000\,km^2$ cover approximately 40% of the total lake area.

The lake typology approach (Table 9) allows for a graphic decomposition of lake-area distribution per area class (Fig. 3C). Glacial lakes dominate in this model in every class but the last one ($A_o > 100000\,km^2$), where only the Caspian is found. The influence of fluvial lakes is maximum for lake sizes between 0.1 and $100\,km^2$, where it can reach 20%. Other lake categories are thought to be of minor importance in terms of area.

In regions with marked relief, even under humid climates the lithology is probably a limiting factor of lake distribution. When pervious rocks are widely distributed, such as in Japan and in most of the Indonesian archipelago, the LR can be very low: 0.50% for Japan without tectonic Lake Biwa, and 0.26% in Indonesia without volcano-tectonic Lake Toba.

The present lake distribution is therefore greatly affected by the postglacial period and is not at all representative of most of the geological past. Lakes of glacial origin represent approximately 50% of the global figure in terms of area – and much more in terms of number. Tectonic lakes, estimated to a total of $900000\,km^2$, are a more

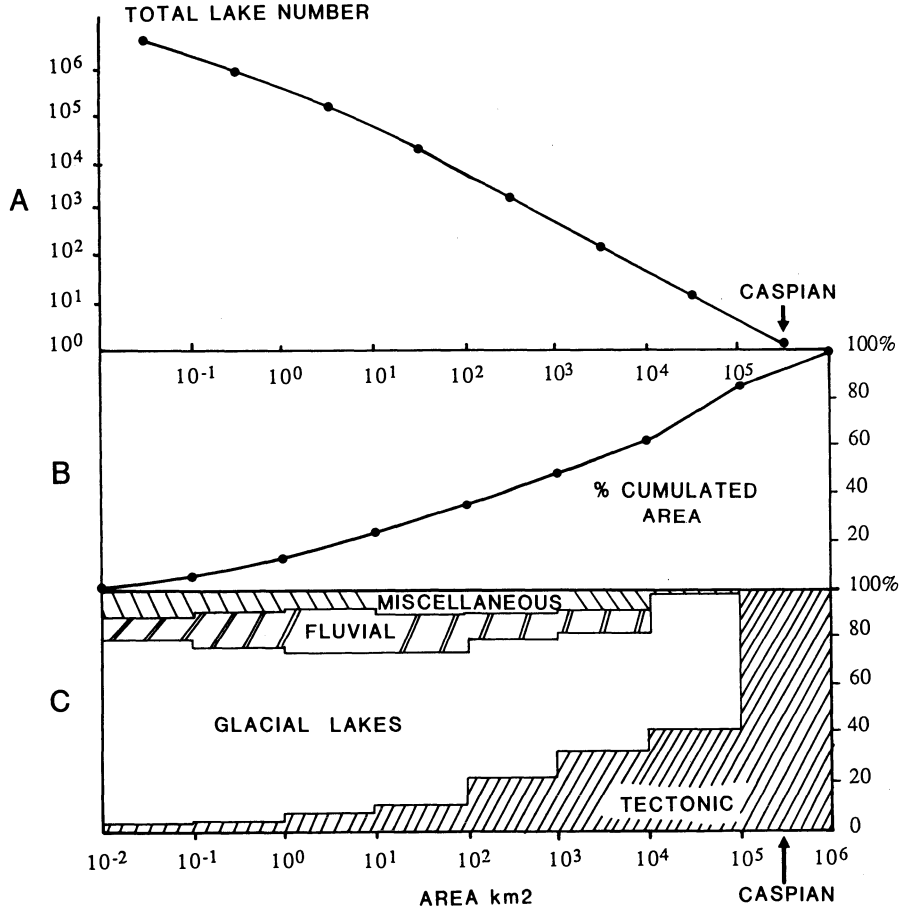


Fig. 3A–C. Lake distribution per lake area classes. **A** Total lake number in each area class; **B** corresponding cumulated area starting from smaller lakes ($> 0.01\,km^2$); **C** proportions of lake types with regards to lake area (tectonic, glacial, fluvial, and all others). The Caspian Sea is the only lake in the 10^5–$10^6\,km^2$ class

permanent feature of lake distribution together with fluvial lakes, coastal lagoons, and volcanic lakes.

In the past 18000 years lake distribution has been profoundly changed, due to (1) deicing and glacial scouring of continents, (2) ice dams, (3) seal-level fluctuations, and (4) marked humidity changes, particularly in endorheic regions presently arid and semiarid. It is still difficult to assess precisely how global lake distribution has varied, but fluctuations from total lake area from 1 to 2 million km^2 are likely from 18000 to 6500 B.P.

The estimates of global distribution presented here are still questionable, particularly due to insufficient information on some lake types (fluvial, coastal lagoons, and craters), or to very poor data on global distribution of smaller tectonic lakes, dissolution lakes, deflation lakes, etc. Herdendorf's exemplary census of large lakes should be extended to lakes between 100 and 500 km^2, which could involve another thousand lakes. Existing census quoted here should be revised order to differentiate, in glaciated regions, the various lake types due to fluvial activity from lakes due to glacial activity, all having been considered here as glacial lakes.

Finally, although it is not the subject of this chapter, it must not be forgotten that human activities have already greatly affected global lake distribution. Avakyan (1987) estimated the total area of reservoirs to be 400000 km^2 for 6000 km^3 in 1986, compared with only 4286 km^3 in 1972 (Soviet IHP 1978). Already 2500 reservoirs exceed a 0.1 km^3 capacity. On the other hand, humans are responsible for intensive wetland filling, which includes the loss of many floodplain lakes in Europe or in the Mississippi Valley. Humans are also responsible for the enhanced evaporation of lake tributaries resulting in shrinking and salinization of lakes, the worst example being the Aral Sea, which decreased from 68000 km^2 in 1960 to 33600 km^2 in 1992, and will probably be reduced to only 23400 km^2 in the year 2000 (Létolle and Mainguet 1993). In addition to these two critical issues, lakes are also facing acidification, contamination with toxic chemicals, eutrophication, enhanced siltation due to accelerated land erosion, and loss of biological diversity (Meybeck et al. 1989; Giussani and Callieri 1993; Kira 1993). For these reasons, it is urgent to improve our knowledge concerning global lake resources.

Acknowledgments. I am thankful to those colleagues who provided precious basic material concerning lake censuses, most of which is still obscure in the literature: Alberto Calcagno (IAHR, Buenos Aires), Sidharth Kaul (Minister of Environment and Forest, New Delhi), Eva Thörneloff (Swedish Environmental Agency, Solna), Hanna Soszka (Institute of Environmental Protection, Warsaw), E. Drago (INL Santo Toma), Akira Kurata (Lake Biwa Research Institute, Otsu), W.D. Williams (University of Adelaide). J. Gat remarks improved this manuscript. The interest of R. Wetzel (University of Alabama) for this work has been greatly appreciated.

References

Adamson D, Williams E (1980) Structural geology, tectonics and the control of drainage in the Nile Basin. In: Williams MAJ, Faure H (eds) The Sahara and the Nile. AA Balkema, Rotterdam, pp 225–252

Anonymous (1990) Wetlands of India, a directory. Ministry of Environment and Forests, Govt of India, New Delhi, 150 pp

Arkhipov SA, Bespaly VG, Faustova MA, Glushkova OY, Isaeva LL, Velichko AA (1986) Ice-sheet reconstruction. In: Sibrava V, Bowen DQ, Richmond GM (eds) Quaternary glaciations of the northern hemisphere. Pergamon Press, Oxford, pp 475–483

Avakyan AB (1987) Reservoirs of the USSR and tasks of their investigation. Water Resour 14:538–549

Ball E, Glucksman J (1978) Limnological studies of Lake Wisdom; a large New Guinea caldera with a simple fauna. Freshwater Biol 8:455–468

Baumgartner A, Reichel E (1975) The world water balance. Elsevier, Amsterdam, 179 pp

Bazilevich NI, Rodin LY, Rozov NN (1970) Geographical aspects of biological productivity. 5th Congr of the Geographical Soc USSR, Soviet Geography, Jan 1971, pp 293–317

Beadle C (1981) Inland waters of tropical Africa: an introduction to tropical limnology. Longman, London, 475 pp

Bowler JM (1981) Australian salt lakes. Hydrobiologia. 82:431–444

Brunskill GJ, Schindler DW (1971) Geography and bathymetry of selected lake basins, experimental lakes area, northwestern Ontario. J Fish Res Board Can 28:139–155

Burgis MJ, Morris P (1987) The natural history of lakes. Univ Press, Cambridge, 218 pp

Campos H, Steffen W, Roman C, Zuniga L, Agüero G (1983) Limnological studies of Lake Villarita, morphometric, physical, chemical, planktonical factors and primary productivity. Arch Hydrobiol (Suppl) 65(4):371–406

Carmouze JP, Durand JR, Lévêque C (eds) (1983) Lake Chad, ecology and productivity of a shallow tropical ecosystem. Junk, Dordrecht, 575 pp
Cleugh TR, Hauser BW (1971) Results of the initial survey of the experimental lakes area, northwestern Ontario. J Fish Res Board Can 28:129–137
Cohenour RE (1968) Great Salt Lake. In: Fairbridge RW (ed) Encyclopedia of geomorphology. Reinhold, New York, pp 506–517
Coleman JM, Wright LD (1975) Modern river deltas. In: Broussard ML (ed) Deltas, models for exploration. Houston Geol Soc, pp 99–150
Coulter G (1991) Lake Tanganyika and its life. Univ Press, Oxford, 354 pp
Dawson A (1992) Ice age earth. Late quaternary geology and climate. Routledge, London, 293 pp
Degens ET, von Herzen RP, Wong HK, Deuser WG, Jannasch HW (1973) Lake Kivu, structure and chemistry of an East African Rift lake. Geol Rdsch 62:245–377
Dejoux C, Iltis A (1992) Lake Titicaca: a synthesis of limnological knowledge. Kluwer, Dordrecht, 573 pp
Delebecque A (1989) Les lacs français. Béranger, Paris, 435 pp
Denton GH, Hughes TJ (eds) (1981) The last great ice sheets. Wiley, New York, 484 pp
Downing JP, Meybeck M, Orr JC, Twilley RR, Scharpenseel HW (1993) Land and water interface zones. Water Air Soil Pollut 70:123–137
Durand A (1982) Oscillations of Lake Chad over the past 50 000 years, new data and new hypothesis. Paleogeogr Paleoclimatol Paleoecol 39:37–53
Dussart B (1992) Limnologie, l'étude des eaux continentales. Boubée, Paris, 680 pp
EEA (1994) European rivers and lakes, Assessment of their environmental state. Kristensen P, 'Hansen HO (eds) European Envir Agency Monogr L', Copenhagen, 122 pp
Egorov AB (1993) Mongolian salt lakes: some features of their geography, thermal patterns, chemistry and biology. Hydrobiologia 267:13–21
Elson JA (1968) Glacial Lake Agassiz. In: Fairbridge RW (ed) Encyclopedia of geomorphology. Reinhold, New York, pp 453–455
Encyclopedia Britannica (1962) William Benton, London, 23 vols
Fairbridge RW (ed) (1968a) Encyclopedia of geomorphology. Reinhold, New York, 1295 pp
Faibridge RW (1968b) Lake Maracaibo. In: Fairbridge RW (ed) Encyclopedia of geomorphology. Reinhold, New York, pp 614–616
Flint RF (1971) Glacial and Quaternary geology. Wiley, Chichester, 892 pp
Fontes JC, Florkowski T, Pouchan P, Zuppi JM (1979) Preliminary isotopic study of Lake Asal system (Republic of Djibouti). In: Isotopes in lake studies. Proc Adv Group Meet, Vienna, 29 Aug–2 Sept 1977, Int Atomic Energy Agency, Vienna, pp 163–174
Frey DG (1969) A limnological reconnaissance of Lake Lanao. Verh Int Ver Limnol 17:1090–1102
Gasse F, Fontes JC (1989) Palaeoenvironments and palaeohydrology of a tropical closed lake (Lake Asal, Djibouti) since 10 000 yrs. Palaeogeogr Palaeoclimatol, Palaeoecol 69:67–102
Gasse F, Arnold M, Fontes JC, Fort M, Gibert E, Huc A, Li Bingyan, Li Yanfang, Liu Qing, Mélières F, van Campo E, Wang Fubao, Zhang Qing Song (1991) A 13 000-year climate record from western Tibet. Nature 353:742–745
Giesen W (1994) Indonesia's major freshwater lakes: a review of current knowledge, development processes and threats. Mitt Int Ver Limnol 24:115–128
Gilliland JA (ed) (1973) Inventory of canadian freshwater lakes. Environment Canada, Inland Water Directorate, Ottawa, 34 pp, 569 maps
Giussani G, Callieri C (eds) (1993) Strategies for lake ecosystems beyond 2 000. 5th Int Conf Conservation and management of lakes, Stresa, May 1993, 598 pp
Gray CB, Dickman M, Krushelnicki B, Cromie V (1990) A survey of canadian lakes. In: Liu Hongliang, Zhang Yutian, Li Haishend (eds) Lake conservation and management. Chin Res Acad Environ Sci, Beijing, pp 41–68
Gray J (ed) (1988) Paleolimnology, aspects of freshwater palaeoecology and biogeography. Elsevier, Amsterdam, 678 pp
Grosswald MG (1984) Glaciation of the continental shelves. Polar Geogr J 8:194–258, 287–351
Halbfass W (1922) Die Seen der Erde. Petermans Mitteil Ergänzungsh 185:169
Halbfass W (1933) Seen. In: Handbuch der Geophysik, 7. Borntraeger, Berlin, pp 122–182
Hamilton SK, Lewis WM (1990) Physical characteristics of the fringing floodplain of the Orinoco river, Venezuela. Interciencia 15:491–500
Hammer UT (1986) Saline ecosystems of the world. Monogr Biol 59, Junk, Dordrecht, 616 pp
Hammer UT (1988) Water resources and their utilization in Saskatchewan, Canada. Verh Int Ver Limnol 23:228–233
Herdendorf CE (1982) Large lakes of the world. J Great Lakes Res 8:379–412
Herdendorf CE (1984) Inventory of the morphometric and limnologic characteristics of the large lakes of the world. Ohio State Univ, Sea Grant Program Tech Bull 17, OHSU, 78 pp
Herdendorf CE (1990) Distribution of the world's large lakes. In: Tilzer MM, Serruya C (eds) Large lakes, ecological structure and function, Springer, Berlin Heidelberg. New York, pp 3–38
Hobbie J (ed) (1980) Limnology of tundra ponds. Dowden Hutchinson & Ross, Stroudsburg, 514 pp
Holling JT, Schilling DH (1981) Late Wisconsin – Weichselian mountain, glaciers and small ice caps. In: Denton GH, Hughes TJ (eds) The last great ice sheets. Wiley, New York, pp 179–206
Hough JL (1968) Great lakes. In: Fairbridge RW (ed) Encyclopedia of geomorphology. Reinhold, New York, pp 499–506
Hsü KJ, Kelts K (1978) Late neogene sedimentation in the Black Sea. In: Matter A, Tucker ME (eds) Modern and ancient lake sediments. Blackwell, Oxford, pp 127–144

Hutchinson GE (1957) A treatise on limnology, vol I. Geography, physics and chemistry. Wiley, New York, 1015 pp

IAHS (Int Assoc Hydrol Sci) (1973) Helsinki Symposium: Hydrology of lakes. Int Assoc Hydrol Sci Publ 109:230 pp

IARH (1993) National data book of Argentine lakes and lagoons and their environment. Istituto Argentino de Recursos Hidrocos, Buenos Aires (preliminary report)

ILEC (1988–1991) Data book of world lake environments, A survey of the state of world lakes. Int Lake Environment Committee and Lake Biwa Research Institute, Otsu, Japan, ≈ p 600 (not numbered)

Imboden D, Weiss RF, Craig H, Michel RL, Goldman CR (1977) Lake Tahoe geochemical study, 1. Lake chemistry and tritium mixing study. Limnol Oceanogr 22:1039–1051

Ivanov GI, Shmuratko VI (1982) Characteristics of variations of the Black Sea level in post-glacial time. Water Resour 9:314–320

Jin Xiangcan, Lu Hongliang, Tu Qingying, Zhang Zonghe, Zhu Xuan (eds) (1990) Hangzhou 90. 4th Int Conf Conservation management of lakes, CRAES-ILEC, Otsu, Japan

Kaiser K (1969) The climate of Europe during the Quaternary ice age. In: Wright WE (ed) Quaternary geology and climate. Natl Acad Sci, Washington, pp 10–37

Kira T (1993) Major environmental problems in lakes. In: Giussani G, Callieri C (eds) Strategies for lake ecosystems beyond 2000. 5th Int Conf Conservation and management of lakes, Stresa, May 1993, 3 pp

Kling GW (1988) Comparative transparency, depth of mixing and stability of stratification in lakes of Cameroon, West Africa. Limnol Ocean 33:27–40

Kling GW, Evans WC, Tattle ML (1991) A comparative view of lakes Nyos and Monoun, Cameroon. Verh Int Ver Limnol 24:1102–1105

Kortelainen P, Mannio J (1988) Natural and anthropogenic acidity sources for Finnish lakes. Water Air Soil Pollut 42:341–352

Kurata A (1990) Natural lakes in Japan. Lake Biwa Res Inst Annu Rep, Otsu, pp 65–73 (in Japanese)

Kvasov DD (1979) The Barentz ice sheet as a relay regulator of the glacial–interglacial alternation. Quat Res 9:288–299

Lerman A (1974) Eutrophication and water quality of lakes: control by water residence time and transport to sediments. Int Assoc Hydrol Sci Bull 19:25–33

Lerman A, Hull AB (1987) Background aspects of lake restauration: water balance, heavy metal contents, phosphorus homeostasis. Schweiz Z Hydrol 49:148–169

Létolle R, Mainguet M (1993) Aral. Springer, Berlin Heidelberg New York, 385 pp

Livingstone DA, Melack JM (1984) Some lakes of subsaharan Africa. In: Taub FB (ed) Lakes and reservoirs, ecosystems of the world 23. Elsevier, Amsterdam, pp 467–497

Löffler H (ed) (1987) Paleolimnology IV. Junk, Dortrecht, 431 pp

Messerli B (1980) Die afrikanischen Hochgebirge und die Klimategeschichte Africas in den letzen 20000 Jahren. In: Oeschger H, Messerli B (eds) Analysen und Modelle. Geschichte und Zukunft, Springer, Berlin, Heidelberg, New York, pp 64–90

Meybeck M (1979) Concentrations des eaux fluviales en éléments majeurs et apports en solution aux océans. Rev Geol Dyn Geogr Phys 21:215–246

Meybeck M (1987) Global chemical weathering of surficial rocks estimated from river dissolved load. Am J Sci, 287:401–428

Meybeck M (1988) How to establish and use world budgets of river material. In: Lerman A, Meybeck M (eds) Physical and chemical weathering in geochemical cycles. Kluwer, Dordrecht, pp 247–272

Meybeck M (1993) Riverine transport of atmospheric carbon: sources, global typology and budget. Water Air Soil Poll 70:443–463

Meybeck M (1995) Les lacs et leur bassin. In: Pourriot R, Meybeck M (eds) Limnologie générale. Masson, Paris, pp 6–59

Meybeck M, Chapman D, Helmer R (eds) (1989) Global freshwater quality: a first assessment. Blackwell, Oxford, 306 pp

Mulholland P, Elwood J (1982) The role of lake and reservoir sediments as sinks in the perturbed carbon cycle. Tellus 34:490–499

Murray J (1910) Characteristics of lakes in general and their distribution over the surface of the globe. In: Bathymetrical survey of the Scottish freshwaters lochs, Edinburgh, 1. Challenger Office, pp 514–658

Nikitin AM (1977) Morphometry and morphology of lakes in central Asia. Tr Sredneaziat Regional Nauk Issled, Gidromet. Inst VA Bugaeva 50(131):4–21 (cited by Savvaitova and Petr 1992) (In Russian)

Nilsson T (1983) The Pleistocene. Reidel Dordrecht, 651 pp

Nontji A (1994) The status of limnology in Indonesia. Mitt Int Ver Limnol 24:95–114

Ouellet M, Page P (1990) Some limnological aspects of Crater Lake, Quebec, Ungawa. Verh Int Ver Limnol 24:348

Penck A (1894) Morphologie der Erdoberfläche, vols I, II. Engelhorn, Stuttgart, pp 471, 696

Qingying TU, Peimin PU (1991) Current situation and changing frequency of water pollution in main lakes of China. Verh Int Ver Limnol 24:1081–1085

Quiros R, Drago E (1985) Relaciones entre variables fisicas, morfometricas y climaticas en lagos patagonicos. Rev Assoc Cienc Nat Litoral 16: 181–199

Risacher F (1992) Géochimie des lacs salés et croûtes de sel de l'Altiplano bolivien. Sci Geol Bull 45:135–198

Romankevich EA, Artemyev VE (1985) Input of organic carbon into seas and oceans bordering the territory of Soviet Union. Mitt Geol Paläont Inst Univ Hamburg 58:459–469

Romanovsky VV (1990) Lake Issyk-Kul – A natural system. Frunze, "Ilim", 168 pp (in Russian)

Savvaitova K, Petr T (1992) Lake Issyk-Kul. Int J Salt Lake Res 1:21–46

Sawula G, Martins E (1991) Major ion chemistry of the low Boro River, Okawango Delta, Botswana. Freshwater Biol 26:481–493

Servant M, Fontes JC (1978) Les lacs quaternaires des hauts plateaux des Andes Boliviennes. Premières interprétations paleoclimatiques. Cah Orstom Sér Geol 10:9–23

Servant M, Servant S (1983) Paleolimnology of an upper Quaternary lake in Chad basin. In: Carmouze JP, Durand JR, Levêque C (eds) Lake Chad. Junk Dordrecht, pp 11–26

Shuncai S (1988) Lakes in China and China lacustrine sedimentology, a brief survey. Mitt Geol Paläont Inst Univ Hamburg 66:165–175

Sippel SJ, Hamilton SK, Melack JM (1993) Inundation area and morphometry of lakes on the Amazon River floodplain, Brazil. Arch Hydrobiol 123: 385–400

Solantie R (1973) Evaporation from the lakes in Finland. Int Assoc Hydrol Sci Publ 109:211–219

Soviet IHP (International Hydrological Programme) Committee (1978) World water balance and water resources of the earth. Unesco, Studies and Report in Hydrology, 663 pp

Stankovic S (1960) The Balkan Lake Ohrid and its living world. Junk, Dordrecht, 357 pp

Stanley DJ, Wezel FC (eds) (1985) Geological evolution of the Mediterranean Basin. Springer, Berlin Heidelberg New York, 650 pp

Street-Perrott FA, Harrison SP (1984) Temporal variations in lake levels since 30 000 yr BP – an index of the global hydrological cycle. In: Hansen J, Takahashi T (eds) Climate processes and climate sensitivity. Geophys Monogr 29(15): 118–129

Szesztay K (1966) Some methodological problems of inventories of lakes. Int Assoc Hydrol Sci Publ 71:894–909

Tamrazyan GP (1974) Total lake water resources of the planet. Bull Geol Soc Finl 46:23–27

Taub FB (1984) Lakes and reservoirs. Ecosystems of the world, vol 23. Elsevier, Amsterdam

Terziev FS, Goptarev NP, Bortnik VN (1986) Problems of the Kara-Bogaz Gulf. Water Resour 13: 167–172

Tiercelin JJ, Mondeguer A (1991) The geology of the Tanganyika trough. In: Coulter G (ed) Lake Tanganyika and its life. Oxford Univ Press, Oxford, 7–48 pp

Timms BV (1993) Lake geomorphology. Gleneagles Adelaide, 180 pp

Tu Qingying, Pu Reimin (1991) Current situation and changing frequency of water pollution in main lakes of China. Verh Int Ver Limnol 24:1081–1085

Unesco (1974) Survey of water balance of lakes and reservoirs of the world, 1 st edn. Water Sci Div, Unesco SC/WS/587, 12 pp

van Campo E, Gasse F (1993) Pollen and diatom inferred climate and hydrological changes in Sumxi Co basin (western Tibet) since 13 000 yr B.P. Quat Res NY 39:300–313

van der Leeden F, Troise FL, Todd DK (1989) Water encyclopedia. Lewis 808 pp

Varushchenko SI (1982) Water balance of the Black Sea in the late Valdai glacial epoch. Water Resour 9:311–319

Velichko AA (ed) (1984) Late Quaternary environment of the Soviet Union. Longman group Ltd, London, 327 pp (cited in Dawson 1992 and Piskhipov et al. 1986)

Wetzel RG (1990) Land-water interfaces: metabolic and limnological regulators. Verh Int Ver Limnol 24:6–24

Williams T, Gier KM, Thouveny N (1993) Preliminary 50 m palaeomagnetic records from Lake du Bouchet, Haute Loire, France. In: Negendank JFW, Zolitschka B (eds) Palaeolimnology of European maar lakes. Springer, Berlin Heidelberg New York, 367–376 pp

Williams WD (1964) A contribution to lake typology in Victoria, Australia. Verh Int Ver Limnol 15:158–168

Williams WD (ed)(1981) Salt lakes. Junk Dordrecht, 444 pp

Wood RB, Talling JF (1988) Chemical and algal relationship in a salinity series of Ethiopian inland waters. In: Melack J (ed) Saline lakes. Junk, Dordrecht, 29–67 pp

Wright HE (1961) Late Pleistocene climate in Europe, a review. Bull Geol Soc Am 72:933–983

2 Hydrological Processes and the Water Budget of Lakes

T.C. WINTER

1 Introduction

Lakes interact with all components of the hydrological system: atmospheric water, surface water, and groundwater. The fluxes of water to and from lakes with regard to each of these components represent the water budget of a lake. Mathematically, the concept of a water budget is deceptively simple: income equals outgo, plus or minus change in storage. In practice, however, measuring the water fluxes to and from lakes accurately is not simple, because understanding of the various hydrological processes and the ability to measure the various hydrological components are limited.

Water budgets are an essential element of many studies that are prompted primarily by chemical or biological interests. Water-flow paths need to be known in order to determine chemical transport; therefore, water budgets are determined for a large number of scientific and management purposes. Determining the water budget of any accounting unit, whether it is a lake, wetland, or drainage basin requires attention to the entire hydrological system; therefore, the expertise of a well-rounded hydrologist or a team of specialists in the various hydrological disciplines is needed. Because such expertise is not available for many studies, water budgets commonly are not of uniform quality from site to site. This uncertainty in the comparability of water budgets limits growth in understanding of lake hydrology as well as the opportunity to make intersite comparisons. Furthermore, most water budgets do not include assessment of the uncertainties in the hydrological values determined (Winter 1981), which also limits their usefulness.

To determine water budgets that can be used with confidence, an awareness of the basic principles, measurement techniques, and uncertainties in values related to the various hydrological components interacting with lakes is necessary. The purpose of this chapter is to provide a foundation from which to develop an understanding of the hydrological processes associated with lakes. This chapter addresses each component of the hydrological system with regard to the basic principles of water movement, underlying assumptions needed to use various measurements or calculations, measurement or calculation alternatives, and uncertainties in values determined by various methods.

US Geological Survey, Water Resources Division, Mail Stop 413, Box 25046, Denver, CO 80225-0046, USA

2 Hydrological System with Regard to Lakes

Considering the lake as the accounting unit of interest, the lake gains water from: (1) the atmosphere by precipitation directly on the surface of the lake, (2) surface water, by streamflow to the lake, and in some settings, by overland runoff, and (3) groundwater, by seepage into the lake. The lake loses water to: (1) the atmosphere, by evaporation directly from the surface, (2) surface water, by streamflow from the lake, and (3) groundwater, by seepage from the lake. For any given time period the imbalance between these gains and losses results in a change in storage that is reflected by the change in lake level.

For some of these components the flux of water can be measured directly and at the lake boundary. For example, streamflow commonly can be gaged at the in- and outflow points of the lake, resulting in highly accurate values for these surface-water components. In addition, reasonably accurate values for atmospheric input can be obtained by using appropriate numbers and spacing of precipitation gages at the lake. For other components the flux values cannot be directly measured accurately. For example, evaporation, overland flow, and groundwater in- and outflow generally need to be calculated from

various types of climatic and hydrogeological data. Although groundwater fluxes can be measured directly by using seepage meters, these devices most commonly are used only for collecting point samples in space and time, not for continuous monitoring. Furthermore, although water fluxes can be measured at the lake boundary for some of the hydrological components, to understand and model the water balance of a lake, especially the interaction with the surface- and groundwater components, an understanding of the flow paths within the surface- and groundwater watersheds associated with the lake is necessary.

2.1 Interaction of Lakes with Atmospheric Water

2.1.1 Precipitation

Movement of water in the atmosphere is complex and highly dynamic, as are the factors that result in precipitation of that water. It has therefore long been a challenge to hydrologists to measure or calculate the depth of precipitation over any given type or size of landscape. Different types of weather patterns result in different types of precipitation patterns. In some areas and in certain seasons, widespread, uniform weather patterns result in uniform precipitation over the landscape; measurement of precipitation under these conditions can be quite accurate. If precipitation is largely from convective thunderstorms accompanied by much wind, however, actual gaging of precipitation is difficult and subject to considerable error. In addition, the pattern and intensity of precipitation from convective storms is highly variable in space, and regionalization of the point data collected at gages can have considerable error. Results of several decades of research on atmospheric dynamics, precipitation-measurement experiments, and regionalization comparisons by the Illinois State Water Survey (e.g., Huff and Neill 1957; Huff and Shipp 1969) have contributed substantially to the understanding of precipitation patterns, which is necessary for accurate determination of the atmospheric-input component of water budgets.

Although uncertainties exist in the actual gaging of precipitation (see Larson 1971 as an example of one of the many literature reviews on this subject), the primary challenge in determining the atmospheric input to a lake is the interpretation or areal distribution of gage data. The common methods of regionalizing point-precipitation data are the isohyetal, Thiessen polygon, and weighted average methods. These methods are described in most hydrology textbooks, but a graphic example of a comparison of the three methods by Linsley et al. (1975) indicates that the volumes of water calculated for a given area using the same measurement numbers at a network of gages differ by 9–18%. This example was of the determination of precipitation on a watershed that had the gages distributed within.

Atmospheric water input directly to a lake seldom is measured over the water body. Because precipitation gages usually must be placed on land, the use of some method of regionalization to determine water depth over the entire lake from the water depths measured at gages is necessary. For small lakes rainfall recorded on land is fairly representative of rainfall over the lake. For large lakes, however, it is usually necessary to use a number of gages around the lake to calculate rainfall on the lake. In some instances even this approach is not satisfactory. For example, large lakes sometimes do not have cloud cover when the surrounding landscape does, and at other times the reverse is true. For large lakes, the uncertainty of the volume of water falling directly on the water body is largely unknown.

The precipitation term of many water budgets commonly is determined from national network data. In the United States the spacing of National Weather Service (NWS) gages is approximately 650 square km per gage. These gages seldom are located in the immediate vicinity of the lake of interest; therefore, one of the methods of regionalization mentioned previously is usually used.

Siegel and Winter (1980) compared regionalization methods at Williams Lake, Minnesota, using precipitation data for the summer of 1978. Precipitation to the lake was calculated using three methods; arithmetic mean, weighted mean, and isohyetal, as well as data from two separate networks, were used. The larger network consisted of three NWS gages located about 40 km in different directions from the lake, and the smaller network consisted of observer-read gages located within approximately 5 km of the lake. The calculated quantities of precipitation were compared with the quantities of precipitation measured by a recording gage at the lake. Within each data network, calculated daily average precipitation over 2-week periods were similar for all three

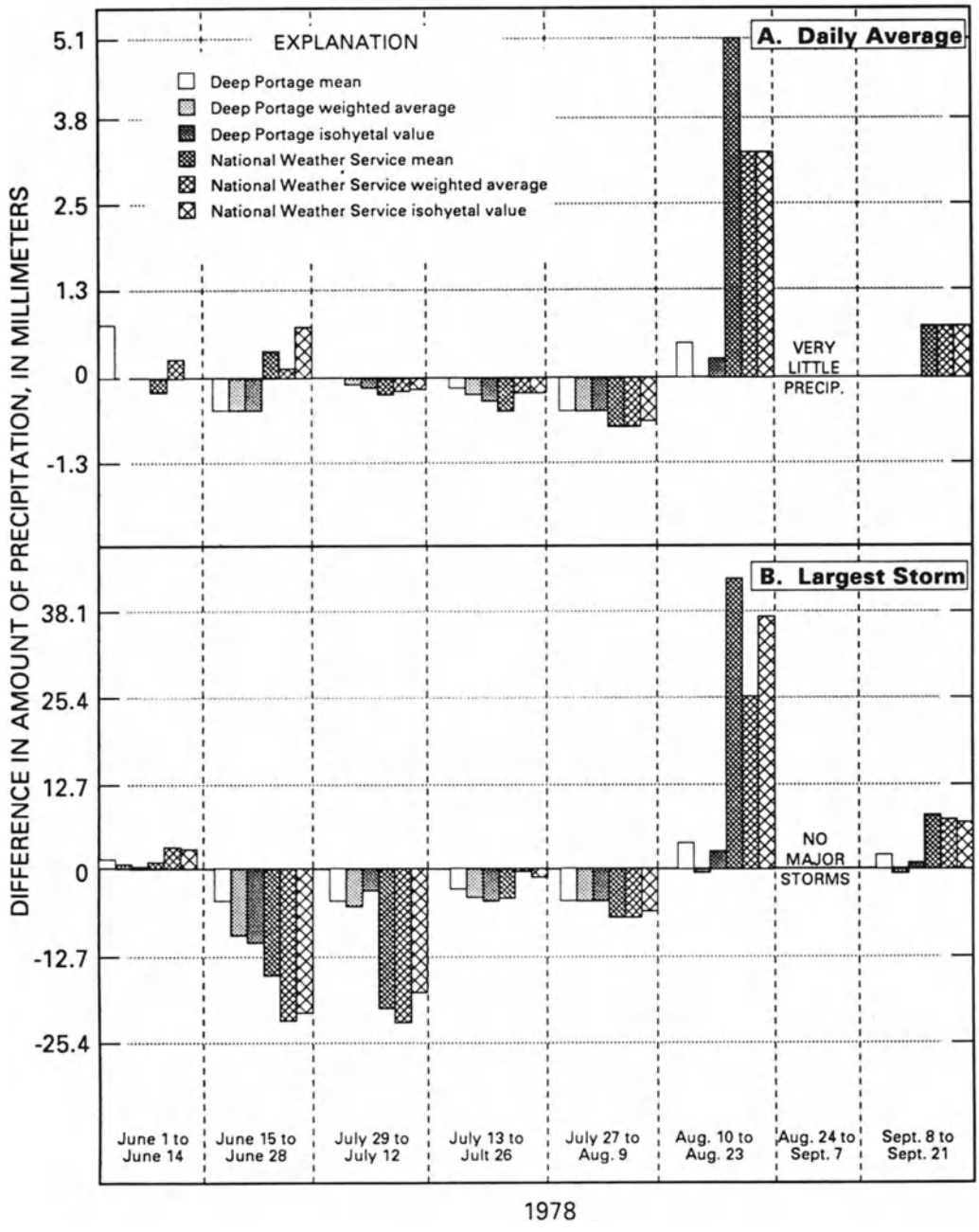


Fig. 1A,B. Difference between precipitation measured by a recording guage at Williams Lake, Minnesota, and that estimated by three regionalization techniques using data from small-scale (Deep Portage) and large-scale (National Weather Service) networks. **A** Average daily precipitation over 2-week periods. **B** Precipitation during largest storm within the 2-week periods. (Modified from Siegel and Winter 1980)

calculation methods (Fig. 1). Estimates from the small-scale network usually were closer to the values recorded at the lake. The greatest difference from values recorded at the lake, when considering the biweekly averages, was for the mid-August period, when NWS data were used. Comparing rainfall data for the largest storm that occurred during each 2-week period indicated that rainfall depths calculated from the small-scale network were nearly always more similar to those recorded at the lake than the rainfall depths calculated from the NWS network. The greatest difference was for a large storm in mid-August when the depths calculated from the NWS net-

work differed by more than 25 mm from depths recorded at the lake or from the small-scale network. These data indicate that precipitation needs to be measured as close to the lake as possible, if not by recording gages at the site, at least by reliable observer-read gages located near the lake.

2.1.2 *Evaporation*

Evaporation is the process by which water at the lake surface is converted from the liquid to the vapor state. The rate of vaporization is directly dependent on the vapor-pressure gradient across the air–water interface. Above the air–water boundary wind and vertical mixing remove the water vapor, thus maintaining the vapor-pressure gradient. Furthermore, because of the great latent heat of vaporization for water, the heat must come from the water itself (Ragotzkie 1978). Therefore, in order to determine evaporation as accurately as possible, radiation, air temperature, vapor-pressure gradient, and temperature of the water need to be measured. Ideally, the total energy balance of the lake (Fig. 2) should be monitored continuously because of the highly dynamic characteristics of climate.

Energy-budget studies of lakes commonly are not done because of the cost and manpower involved. Not only are the instruments expensive, but frequent checks of their calibration with separate sensors are necessary and quality assurance of climate data is time-consuming, resulting in high personnel costs. In addition, temperature profiles at many locations throughout the lake, thermal surveys, need to be made at regular intervals such as weekly, biweekly, or monthly. Nevertheless, the energy-budget method of calculating evaporation generally is considered to be the most accurate for studies covering periods of months, seasons, or years; therefore, it is the standard against which empirical methods commonly are evaluated. A detailed discussion of the energy-budget method of determining evaporation is not presented here, because thermal energy transfer with regard to lakes is discussed by Imboden and Wüest (this Vol.) and by Hostetler (this Vol.), and it is discussed extensively in other books such as that by Brutsaert (1982).

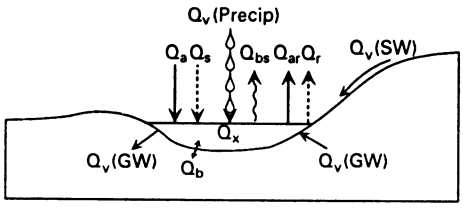


Fig. 2. Energy sources and sinks associated with the energy budget of lakes. Q_s, incoming short-wave solar radiation; Q_r, reflected short-wave radiation; Q_a, incoming long-wave terrestrial radiation; Q_{ar}, reflected long-wave radiation; Q_{bs}, long-wave radiation emitted from the water; Q_b, net energy advected to and from the sediments; Q_v, net energy advected to and from the lake; Q_x, change in heat stored in the lake

One aspect of energy-budget studies that has seldom been considered is the advected energy related to groundwater; most previous studies considered only the advected energy related to precipitation and surface water. Groundwater can be a major component of the water budget of closed lakes. An example of the effect of advected energy related to groundwater on evaporation from a closed lake in a temperate climate was presented by Sturrock et al. (1992). Energy budgets, including the energy flux related to groundwater, were determined for Williams Lake, a small (40 ha) closed lake in north-central Minnesota, for open-water periods of 5 years. Groundwater accounted for greater than 50% of the annual water input to the lake and greater than 50% of the annual water loss from the lake. However, because groundwater in this climate is relatively cold (approximately 7 °C), it contributed minimal thermal-energy input to the lake. Lake water seeping to groundwater was warm only for 1 or 2 months in summer; therefore, minimal thermal energy was lost to groundwater. The overall effect was that less than 1% of the water lost to evaporation at Williams Lake was accounted for by the advected energy related to groundwater.

For most water-budget studies evaporation is determined by an empirical method, because of the costs and expertise involved in determining evaporation by the energy-budget method. At least 30 empirical methods have been used or proposed for determining evapotranspiration, many of which have been used to determine open-water evaporation. The methods have a wide range of data requirements. For example, some methods are modifications of the energy-budget approach, requiring data from many sensors, whereas other methods require data from a single simple sensor such as a temperature probe. Although a number of studies have compared various empirical methods of determining evapotranspiration from

plants (e.g., Tanner 1967; McGuinness and Bordne 1972), fewer studies have compared selected equations for use on open-water surfaces (e.g., Harbeck et al. 1958; Brutsaert 1982; Warnaka and Pochop 1988). The energy-budget study of Williams Lake, Minnesota, required the use of many sensors. Therefore, it was possible to evaluate a number of empirical methods for determining evaporation against the values determined by the energy-budget method.

Eleven empirical methods for determining evaporation were evaluated in the Williams Lake study (Winter et al. 1995). The methods and references to the form of the equations used are listed in Table 1. The comparisons were of monthly values for 22 months of open water over a period of 5 years. Months when the lake was ice covered (6–7 each year), as well as months that did not have a complete data set, were excluded from the comparison. Data from three climate stations were used in the study: a raft in the center of the lake, a land station approximately 100 m from the lake shore, and an agricultural-network station 60 km to the south of the lake. A statistical summary of the comparisons are shown in Table 2.

Based on the average and standard deviation of the monthly differences in evaporation, the Penman, DeBruin-Keijman, and Priestley-Taylor methods compared most favorably with the energy-budget values. The average of the monthly differences was less than 0.5 cm, and the standard deviation of the monthly differences was less than 1.0 cm for all three methods when using data from the raft station. Furthermore, evaporation determined for these three methods using data from the land station also compared favorably with the energy-budget values (Fig. 3a). The common data types that these three methods require are air temperature, net radiation, and change in heat

Table 1. Methods used to compare evaporation determined by empirical methods with evaporation determined by the energy-budget method for Williams Lake, Minnesota

Method	Reference
Brutsaert-Stricker	Brutsaert and Stricker (1979)
DeBruin	DeBruin (1978)
DeBruin-Keijman	DeBruin and Keijman (1979)
Hamon	Hamon (1961)
Jenson and Haise	McGuinness and Bordne (1972)
Makkink	McGuinness and Bordne (1972)
Mass transfer	Harbeck et al. (1958)
Papadakis	McGuinness and Bordne (1972)
Penman	Jensen et al. (1974)
Priestley-Taylor	Stewart and Rouse (1976)
Stephens and Stewart	McGuinness and Bordne (1972)

Table 2. Statistical summary of differences in monthly evaporation for Williams Lake, Minnesota

Method	Raft e_o at T_o[a]		Raft e_o at T_a[b]		Land		Staples	
	Mean	SD	Mean	SD	Mean	SD	Mean	SD
Jenson and Haise	0.00	1.80			−0.33	1.83	0.10	1.95
Penman	−0.03	0.80	−0.79	0.82	−0.87	0.83		
Mass Transfer	−0.10	1.27	−4.64	1.76	−6.26	2.09	−5.20	2.23
DeBruin-Keijman	0.16	0.90			0.08	0.91		
Makkink	−0.35	1.58			−0.46	1.56	−0.14	1.76
Priestley-Taylor	0.42	0.96			0.30	0.96		
Papadakis	−0.43	1.21			2.13	1.35	1.49	1.19
Hamon	0.77	1.65			0.46	1.70	0.85	1.79
DeBruin	0.86	1.78	−4.22	2.05	−5.27	2.28	−4.28	2.22
Stephens and Stewart	−1.30	1.32			−1.57	1.33	−1.10	1.50
Brutsaert-Stricker	2.17	1.27	2.22	1.27	2.09	1.25		

The methods needing net radiation could not be used when using data from Staples.
Only the methods needing saturated vapor pressure (e_o) were recalculated using e_o at T_a in place of e_o at T_o.
Values (in cm) determined by the energy budget and by 11 empirical methods using data from three different climate stations. Data was obtained from a raft station in the center of the lake, a land station 100 m from the lake, and a climate station at Staples, Minnesota, 60 km south of the lake.
e_o, saturated vapor pressure; T_o, temperature of water surface; T_a, temperature of air.
[a] e_o at T_o is the saturated vapor pressure at the temperature of the lake's water surface.
[b] e_o at T_a is the saturated vapor pressure at the temperature of the air.

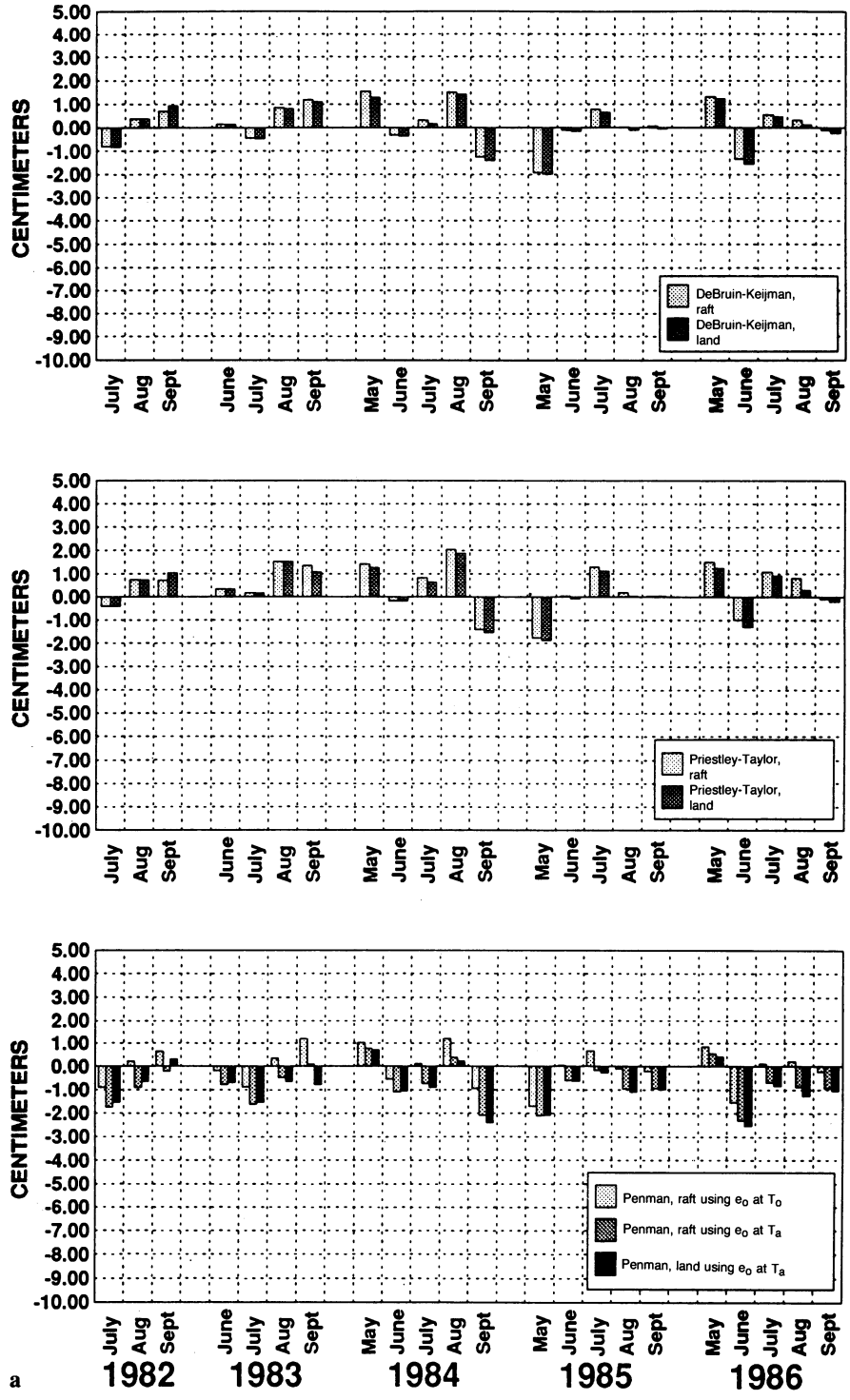


Fig. 3a,b. Difference in calculated evaporation between values determined by the energy-budget method and values determined by selected empirical methods for Williams Lake, Minnesota, 1982–1986. Data were from climate stations based on a raft in the center of the lake, on land 100 m from the lake, and at a climate station at Staples, Minnesota, 60 km south of the lake. Empirical methods that compared most favorably with energy-budget values were **a** DeBruin-Keijman, Priestley-Taylor, and Penman. Those that compared least favorably, especially if data were not from the raft, were **b** mass-transfer and DeBruin. e_o at T_o, saturated vapor pressure at temperature of water surface; e_o at T_a, saturated vapor pressure at temperature of air; raft, data from raft station at center of lake; land, data from land station 100 m from lake; Staples, data from climate station at Staples, Minnesota, 60 km south of lake. (From Winter et al. 1995)

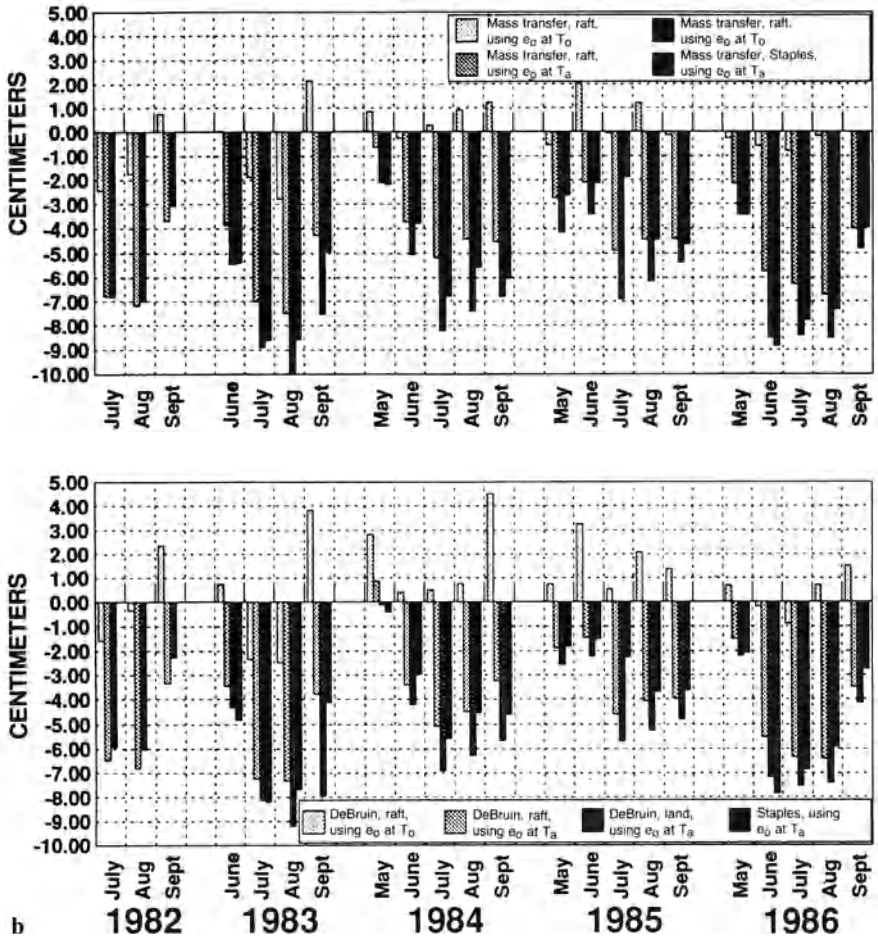


Fig. 3b

stored in the lake from one thermal survey to the next. Therefore, use of these methods requires that instruments be located at the lake, and that site visits be made to check instruments and to do thermal surveys.

The methods that compared least favorably with the energy-budget values when using data from the land station were the mass-transfer and the DeBruin methods (Fig. 3b). Both of these methods have wind speed as a prominent term in the equation. (Although wind speed is used in the Penman method, it is secondary to the more prominent net-radiation term.) The mass-transfer coefficient was calibrated against the energy budget using data from the raft, therefore, the mean difference from energy-budget values when using data from the raft was only −0.10 cm, but the standard deviation was large (1.27 cm). When wind data from the land station were substituted for wind data from the raft station, however, the method proved to be unsatisfactory. Wind-speed data from Williams Lake indicated that wind speed recorded at the land station was commonly 20–40% less than wind speed recorded at the raft station at the center of the lake. These results indicated that empirical methods for determining evaporation that require the use of wind data are satisfactory only if the wind speed is measured at a raft located at the center of the lake.

Despite the interest in the physics of evaporation by climatologists over many years, this component of the water balance of lakes has not received the attention of limnologists in proportion to its importance. Considerably more work is needed in evaluating coefficients, constants, assumptions, instrumentation, and the design of sensor placement for the various methods of determining evaporation. The evaluations need to be done for lakes situated in a wide variety of physiographical and climatic settings.

2.2 Interaction of Lakes with Surface Water

Surface water is the only component of the hydrological system that is generally well defined with regard to its physical dimensions. More than 100 years of research has resulted in an understanding of the physics of water flow in open channels and in the development of gaging structures such as wiers and flumes. When properly built these structures can measure discharge to within approximately 5% of the true value. Therefore, if wiers or flumes can be used to gage streams at the point where they enter or leave a lake, these discharge measurements will be the most accurate values of the water balance. Manuals for selecting and designing wiers and flumes are produced by agencies such as the US Bureau of Reclamation (1975). If streams are large or are not conducive to measurement by wiers or flumes, however, they usually need to be gaged by using a current meter, a recording stage gage, and a stage-discharge rating curve, or by using a dye-tracing method.

To use the current meter, recording stage gage, and stage-discharge relationship, it must be realized that the velocity of water flow in open channels is not uniform. The velocity profile of streams is somewhat parabolic, largely because of friction at the streambed. Discharge is calculated as the product of average velocity times cross-sectional area. Therefore, an accurate discharge measurement requires making many individual velocity measurements throughout the cross section to determine the average velocity, and making an accurate measurement of the cross-sectional profile of the stream bed. Error in discharge measurement associated with the number of individual velocity measurements is discussed by Carter (1973). Technology is available to continuously monitor water-stage accurately. The challenge to obtaining a continuous record of stage is proper maintenance of the gaging system and analysis of factors that affect stage such as ice and other causes of damming. To develop high-quality stage-discharge relationships, measurements made at a wide range of discharges are necessary. The numerous factors that affect flow at the gaging site need to be accounted for such as instability of the streambed or changing slope of the water surface related to rising and falling stages of a flood wave (Dickenson 1967). Methods for measurement and computation of streamflow are given by Rantz et al. (1982).

Where streams are difficult to gage because of site conditions, dye-tracing techniques may be the only alternative for measuring stream discharge. Although stream discharge can be gaged quite accurately by dye-tracing methods, the method is not suitable for continuous monitoring of discharge. The method is based on the principle of travel time, and it is used most effectively on streams that are well mixed such as small mountain streams. The method, its use, and calibration are presented in a manual by Wilson (1968).

Although streamflow to and from lakes can be gaged accurately for purposes of determining a water balance, knowing stream in- and outflow values does not necessarily lead to understanding how the lake interacts with its watershed. To thoroughly understand how a lake functions it is important to understand the runoff characteristics of its watershed. Such understanding is needed particularly for predictive modeling of runoff and solute transport. Many watershed models have been developed, ranging from lumped parameter models (Blackie and Eeles 1985) to distributed parameter models (Beven 1985). Most watershed models are similar in that they attempt to consider all components of the hydrological system interacting within the watershed. Thus, in addition to considering all the hydrological factors that affect the water balance of the lake, evapotranspiration from the upland must also be considered.

A schematic diagram of a watershed model developed by the US Geological Survey (Leavesley et al. 1983) is shown in Fig. 4. As indicated by the diagram a wide variety of information is needed to use the model effectively. The atmospheric component of the model requires data on precipitation, air temperature, and solar radiation. The model can be used for simulation of snowmelt and to calculate evaporation, sublimation, and transpiration. Information is also needed on the partitioning of precipitation between interception and throughfall, as well as on the snowpack and its condition. Surface runoff can be from impervious or pervious surfaces. If infiltration occurs the model has a number of subsurface reservoirs: the soil zone, unsaturated zone, and groundwater zone. Information on the physical characteristics of the watershed is also needed so that the watershed can be subdivided into areas of similar slope and aspect. Additional information includes data on soil types and their infiltration and soil-moisture characteristics.

Mathematical expressions for processes within

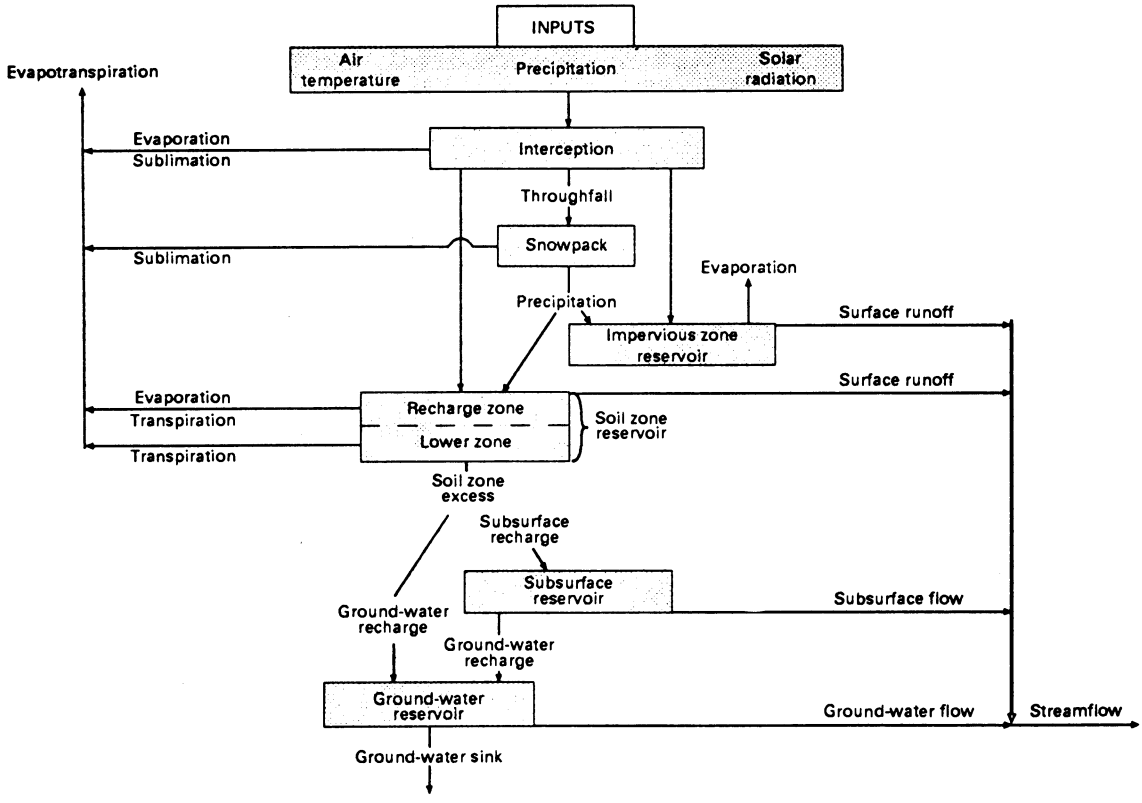


Fig. 4. The U.S. Geological Survey's watershed model. (Modified from Leavesley et al. 1983)

and between all the components of watershed models vary considerably between models. Routing of water can be based on detailed expressions of the physics of flow, or the rates of water movement within a component can be controlled by simple rate-regulation methods. These contrasts are perhaps most evident in the subsurface components of the models (see Sect. 2.3). Although precipitation-runoff models can be very complex and need much information to adequately simulate runoff patterns, these models are used extensively in studies of surface runoff.

Watershed models are also appropriate for use directly on lakes. By using lake stage as the dependent variable, rather than stream discharge, lake-level fluctuations can also be simulated. The model developed by Crowe and Schwartz (1981) has been used to simulate fluctuations of levels of several lakes in the Canadian prairie. The model is somewhat unique in that it emphasizes groundwater, and also because it considers solute transport. In addition, the model has been used to evaluate the effect of climate change on the water level and salinity of a lake in Alberta, Canada (Crowe 1993). Similarly, the watershed model developed for the Integrated Lake-Watershed Acidification Study (ILWAS; Gherini et al. 1985) has been used on lakes in the Adirondack Mountains in New York and glacial-terrane lakes in northern Wisconsin.

2.3 Interaction of Lakes with Subsurface Water

The subsurface component of a water balance is commonly not a dominant term. Most lakes gain more water from and lose more water to atmospheric water and/or surface water. From a chemical-transport perspective, however, subsurface water can be important, because it is a mechanism of transport for chemicals to and from lakes. Chemical transport by way of subsurface water is commonly responsible for the chemical character of closed lakes or lakes that interact with small streams. Studies of lakes in glacial terrane have indicated that the major-ion chemical character of many lakes is related to its position with regard to groundwater flow systems (LaBaugh 1988; Swanson et al. 1988). Krabbenhoft et al. (1990) have indicated the utility of using environ-

mental isotopes of groundwater and lake water to better understand the interaction of lakes and groundwater in glacial terrane.

In most lake-water balance studies that consider groundwater, the groundwater flux is usually determined by direct measurement of seepage. The devices most commonly used to measure seepage directly are seepage meters and minipiezometers. Seepage meters are simple chambers, usually the ends of barrels, that are inserted to enclose a part of the lake bed. The meters have an opening to which a valve and an expandable bag containing a known volume of water are attached. Seepage rate is measured by noting the change in water volume in the bag over the period of time the valve is left open (Lee 1977). Minipiezometers are small diameter piezometers that are inserted into the lake bed. The devices are used to measure the difference in hydraulic head between the groundwater beneath the lake and the lake level by use of a manometer. This is accomplished by attaching a tube from one side of the manometer to the piezometer and letting another tube from the other side of the manometer lay beneath the lake surface. The devices measure hydraulic gradient; they do not measure seepage directly as do seepage meters. Because piezometers measure hydraulic potential and a manometer is an integral part of the device, these devices are more properly termed potentiomanometers (Winter et al. 1988).

A number of researchers have been concerned over the values of seepage determined by seepage meters. For example, Lee (1977), Erickson (1981), and Belanger and Montgomery (1992) experimented with the accuracy of seepage meters in laboratory tanks, where hydraulic gradients and flux rates could be controlled. Belanger and Montgomery used replicate data by having as many as seven meters as well as minipiezometers in a single large experimental tank. Shaw and Prepas (1990a) also evaluated seepage meters in extensive field studies.

In addition to uncertainties associated with the actual measurement of seepage, the distribution of seepage is not uniform in lake beds. Seepage varies spatially in lake beds because of heterogeneous deposits, transpiration from near-shore vegetation, and nonuniform bending of groundwater flow paths where a sloping water table meets the flat lake surface. Nonlinear distribution of seepage across a lake bed, which was indicated from theoretical studies (McBride and Pfannkuch 1975; Pfannkuch and Winter 1984), was first observed using seepage meters at Lake Sallie, Minnesota (Lee 1972). Nonuniform distribution of seepage has since been observed at numerous other lakes in many different climatic and hydrogeological settings such as New England (Asbury 1990), Florida (Fellows and Brezonik 1980), Minnesota (Erickson 1981), Nevada (Woessner and Sullivan 1984), Alberta (Shaw and Prepas 1990b), Ontario (Lee et al. 1980), New Zealand (John and Lock 1977), Spain (Winter, unpublished data), and even in the Great Lakes (Cherkauer and McBride 1988).

Seepage meters and potentiomanometers are unlike other sensors used to measure a water flux at the lake boundary, such as rain gages and stream gages, because they generally are used to collect only discrete samples in space and time. They have the disadvantage, compared with the other two, in that they are not used for continuous monitoring. Rain gages collect discrete samples in space, but they are commonly connected to recorders so that they can collect continuous samples in time. Stream gages are commonly used to collect continuous records of discharge. As is true of the other direct measurements of flux, direct measurement of seepage does not lead to understanding how the lake interacts with hydrological processes that caused the flux. Therefore, it is useful to examine subsurface hydrological processes related to lakes.

The subsurface component of the hydrological system is commonly treated as two subsystems, the unsaturated zone and the groundwater zone. The unsaturated zone is further subdivided into the soil zone and the unsaturated zone between the soil water and the water table (Fig. 5). A considerable amount of research has been done on soil water by agricultural scientists, and on

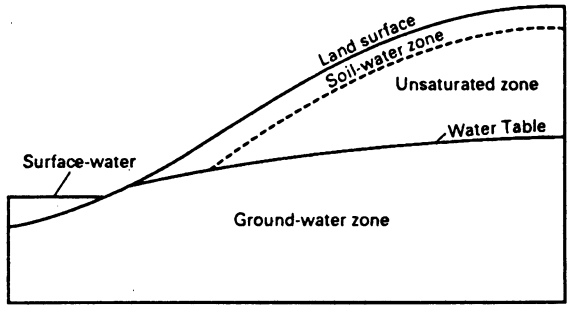


Fig. 5. Subsurface zones of water adjacent to surface water

groundwater by geohydrologists. The understanding of water movement through the complete subsurface continuum, however, and the interaction of subsurface water with surface-water features, such as streams, lakes, and wetlands, is limited. The study of different subsurface zones by scientists from different disciplines has led to a number of concepts concerning the mechanisms of water flow through the subsurface, as indicated in Fig. 6. The primary differences in the concepts are related to the partitioning of water between overland flow, unsaturated-zone flow, and groundwater flow. The concepts and methods of studying the interaction of lakes and groundwater presented here apply equally to any type of surface-water body whether they are streams, lakes, or wetlands.

Studies of the subsurface system with regard to lakes have evolved along two general conceptual frameworks: (1) watershed hydrology, as used in precipitation-runoff studies, and (2) groundwater hydrology. The watershed hydrology concept, sometimes referred to as hill-slope hydrology, has been used with regard to lakes by only a few scientists such as Crowe and Schwartz (1981) and Gherini et al. (1985). As interest in the water and solute linkages between lakes and their watersheds grows, however, models of total watershed processes are likely to be used increasingly as part of lake hydrology studies. Kirkby (1985) provides a useful overview of hill-slope hydrological concepts.

Some watershed hydrologists have indicated that most subsurface water flows through macropores in the unsaturated zone. Much of the acceptance of this concept of preferential flow in the unsaturated zone has been by those working in areas of steep forested hill slopes. Germann and Beven (1985) used kinematic wave theory to mathematically describe the flow of subsurface water through macropores in hill slopes. The most common practice in mathematical treatment of the subsurface part of the hydrology of hill slopes has been as a part of lumped- or distributed-parameter precipitation-runoff models, or a combination of both. Blackie and Eeles (1985) provide an overview of lumped-parameter watershed models, including a history of their development. In the early watershed models, the subsurface components were treated as single lumped units over the entire watershed. In most present studies the watershed is divided into smaller units either as subwatersheds or as small discretized-block units, either horizontally or vertically, or both. These smaller units are then treated in a lumped-parameter manner. An example of a watershed model that treats the subsurface water in this combination manner is that of Leavesley et al. (1983), which was discussed previously (Fig. 4). The following is a brief description of the subsurface components of the model shown in Fig. 4.

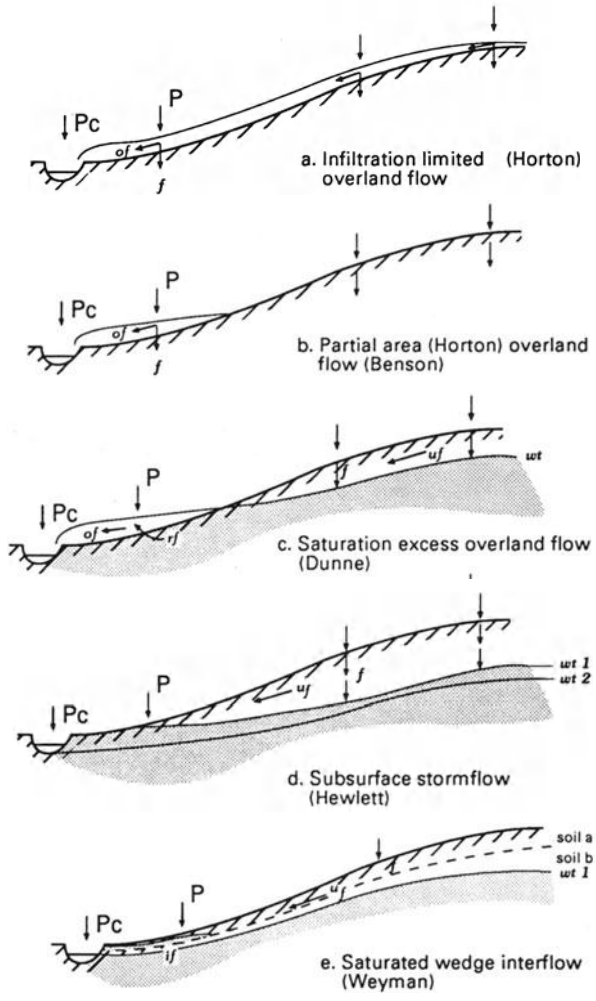


Fig. 6a–e. Concepts of runoff production from hill slopes. The concepts range from **a** overland flow over the entire hillside and the absence of groundwater flow, to **b** overland flow at the base of the hillside and the absence of groundwater flow, to **c** overland flow at the base of the hillside as a result of groundwater reaching the land surface, to **d** subsurface stormflow, to **e** complex flow in the unsaturated zone as a result of different permeabilities of soil horizons and the complete absence of overland flow. P, precipitation; Pc, channel precipitation; *f*, infiltration; *of*, overland flow; *rf*, return flow; *if*, interflow; *uf*, unsaturated-zone flow; *wt*, water table. (Modified from Beven 1986)

Unsaturated-zone flow (referred to as subsurface flow by Leavesley et al. 1983) is considered to be the relatively rapid movement of water from the unsaturated zone to a stream channel. The flow occurs during, and for a period of time, after, rainfall and snowmelt. Inflow to an unsaturated-zone reservoir occurs when the maximum available water-holding capacity of the soil zone is exceeded, and this excess is greater than the recharge rate from the unsaturated zone to the groundwater reservoir, i.e., the difference between soil-water excess and the recharge rate is unsaturated-zone reservoir inflow. Discharge from the subsurface reservoir is either to shallow groundwater zones, or the water moves downslope at shallow depths from the point of infiltration to some point of discharge to the stream above the water table. Initial storage volumes and routing coefficients must be determined for each unsaturated-zone reservoir. The initial estimate of storage is normally zero. Values of routing coefficients are fitted from historical streamflow data. For linear cases the routing coefficient is estimated using a hydrograph separation technique such as that described by Linsley et al. (1975).

The groundwater system is conceptualized as a linear reservoir and is assumed to be the source of all base flow. Water can move to a groundwater reservoir either from the soil zone, the unsaturated-zone reservoir, or both. Recharge to groundwater from a soil zone occurs only when field capacity is exceeded, and is limited by a maximum daily recharge rate. Groundwater recharge from the subsurface reservoir occurs every day there is water available in the subsurface reservoir. Therefore, the use of recharge from the subsurface reservoir preferentially over recharge from the soil zone could decrease subsurface flow and increase groundwater flow contributions to the simulated hydrograph.

An example of another approach for modeling subsurface water flow is the Variable Source Area Simulator (Troendle 1985). The variable-source-area concept (Hewlett and Hibbert 1963) assumes subsurface stormflow is a major source of surface water. The concept states that the largest volume of subsurface water moves through the unsaturated zone, and that groundwater is relatively insignificant. The variable-source-area concept was originally conceived to apply to the forested mountains of the eastern United States, but the concept subsequently has been used to describe subsurface water flow in many other settings. The Variable Source Area Simulator has many characteristics of a complete distributed-parameter variably saturated model. The hill slope is divided into discrete blocks, both horizontally and vertically, and water is moved between blocks by solving Richards' (1931) equation. The variable-source-area model developed by Troendle (1985) has subsequently been modified by P.Y. Bernier (Troendle 1985).

Fully discretized models of subsurface water flow for purposes of watershed hydrology have not been extensively pursued, because of the limitations of understanding and limitations of definition of the subsurface environment of hill slopes. However, the utility of such models was indicated by Freeze (1972) and Stephenson and Freeze (1974), and watershed hydrologists have increasingly pursued development of distributed-parameter models. Beven (1985) discussed the several models under development, with emphasis on the Institute of Hydrology (UK) Distributed Model (IHDM).

The distributed-parameter approach to modeling and studying subsurface water flow from the watershed hydrology perspective leads to the second major conceptual framework for studying the interaction of lakes with subsurface water, which is groundwater. Much of the following discussion of groundwater involves studies of groundwater modeling, because discretized groundwater models have been used most extensively in studying the interaction of lakes with subsurface water. Most surface-water bodies have an areally extensive interface with the groundwater system at their bed. The only other areally extensive interface that surface water has is with the atmosphere. An interface between surface water and the unsaturated zone generally does not exist, because the surface of the groundwater system, the water table, meets the surface water at the shoreline (Fig. 5).

Because groundwater and surface water have such an extensive interface, the interaction of the two has been of interest for more than 100 years (Hall 1968). Since the work of Boussinesq (1877) until recently, the interaction of surface water and groundwater was studied from the perspective of streamflow recession (Barnes 1939; Knisel 1963; Rorabaugh 1964). Recession analysis is still used, as indicated by the precipitation-runoff procedure of Leavesley et al. (1983), the studies of Woods Lake and Panther Lake, New York, by Murdock

et al. (1987), the study of inflow to Mirror Lake, New Hampshire (Winter et al. 1989), and studies of streams in the eastern United States (Rutledge 1993). Recession analysis is based on a one-dimensional flow model that requires the assumption that the stream fully penetrates the groundwater system (Fig. 7). Other assumptions needed to justify use of these highly simplified models include: (1) the porous media must be homogeneous and isotropic, and (2) the aquifer must be of uniform thickness and shape from the surface-water body to the groundwater divide. The only data needed to use recession analysis is a long enough period of continuous streamflow record to determine the correct recession slope.

More realistic treatment of the interaction of surface water and groundwater indicated the need for deterministic analysis of two- and three-dimensional systems. This type of analysis is also needed to evaluate the concepts of subsurface water flow on hill slopes mentioned previously as well as the validity and limitations of recession analysis. The equation commonly used to describe groundwater flow for nonequilibrium conditions in a heterogeneous and anisotropic porous media (McDonald and Harbaugh 1984) is a combination of the continuity equation and Darcy's equation:

$$\frac{\partial}{\partial x}\left(K_{xx}\frac{\partial h}{\partial x}\right)+\frac{\partial}{\partial y}\left(K_{yy}\frac{\partial h}{\partial y}\right)+\frac{\partial}{\partial z}\left(K_{zz}\frac{\partial h}{\partial z}\right)-W=S_s\frac{\partial h}{\partial t}, \quad (1)$$

where x, y, and z = cartesian coordinates aligned along the major axes of hydraulic conductivity K_{xx}, K_{yy}, K_{zz}; h = potentiometric head; W = a volumetric flux per unit volume, representing sources and/or sinks of water; S_s = the specific storage of the porous material; and t = time.

For steady-state conditions, the equation is simplified by not including the flux term, W, and setting the right side of the equation equal to 0.

Toth (1963) solved the steady-state form of Eq. (1) analytically to study two-dimensional vertical sections of groundwater flow. His analysis centered on evaluating flow configurations caused by different water-table configurations. To facilitate the analytical approach, Toth assumed the porous media was isotropic and homogeneous. No-flow boundaries were specified for the sides and base of the sections. The water table was simulated as a sine wave for which different magnitudes and overall slope were varied to produce different regional slopes and local relief of the water table. Results of this study indicated the theoretical presence of flow systems of different magnitude – local, intermediate, and regional (Fig. 8) – and of different sizes, depending on the configuration of the water table. The sections were not intended to study the interaction of groundwater and surface water, but the concepts presented by Toth were the impetus for later studies of this interaction by others.

The numerical solution of Eq. (1) offered greater flexibility than the analytical solution of the groundwater flow equation for studies of groundwater flow systems, because the porous media does not have to be isotropic and homogeneous, and boundary conditions, including the shape of the water table, can be complex (Freeze and Witherspoon 1967). Because of this flexibility, Winter (1976) used numerical analysis to study theoretical groundwater flow systems associated with lakes for several different geometric configurations of lakes and a wide variety of boundary conditions of the groundwater system.

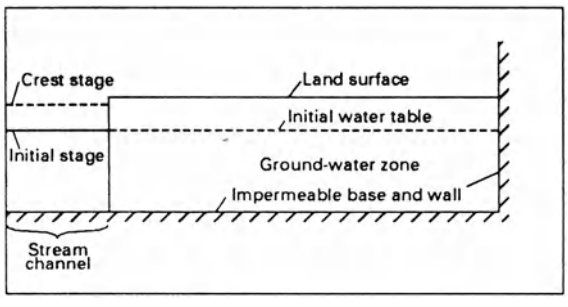


Fig. 7. Surface water fully penetrating the groundwater system

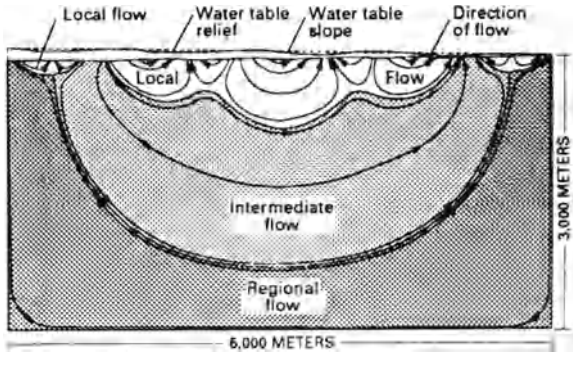


Fig. 8. Hydrological section of a hypothetical two-dimensional setting showing local, intermediate, and regional flow systems in a groundwater reservoir. (Modified from Toth 1963)

The study was designed to define the types of groundwater flow and lake-bed seepage patterns that resulted from different: (1) geometry of the groundwater system, (2) anisotropy, which is the ratio of horizontal to vertical hydraulic conductivity and is a function of grain orientation within rocks, (3) distribution of zones of high hydraulic conductivity, (4) water-table configuration, and (5) lake depth. The analyses were of two-dimensional vertical sections, so they had application only to long linear lakes or streams aligned perpendicular to groundwater flow direction. Furthermore, the simulations were of steady-state conditions, i.e., with a fixed water table. The water table was configured such that mounds were on both sides, with one water-table mound being higher than the other. No simulations were run with the water table lower than the lake, because this would clearly result in seepage out of the lake.

The study indicated that because of the water-table configuration specified, flow in the upper part of the groundwater system was toward the lake for all conditions (Fig. 9). However, seepage was outward from the lake through deeper parts of the lake for some conditions (Fig. 10). The key to understanding why these differences occurred was the continuity of the flow-system boundary that underlies the lake. If the boundary is continuous, as shown in Fig. 9, all hydraulic heads

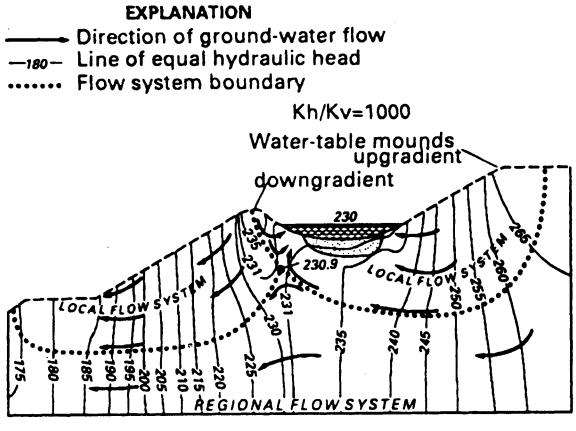


Fig. 9. Hydrological section of a hypothetical two-dimensional setting showing groundwater flow systems associated with a lake that has no seepage from it. The stagnation point along the local flow-system boundary enclosing the lake has a hydraulic head of 230.9 dimensionless units, which is 0.9 greater than the head of 230 represented by lake level. Kh/Kv is the ratio of horizontal-to-vertical hydraulic conductivity

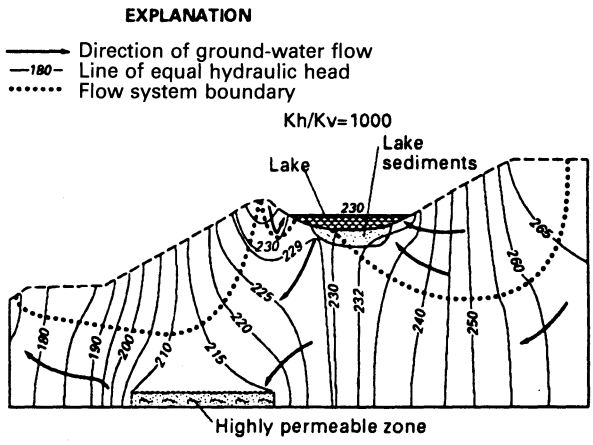


Fig. 10. Hydrological section of a hypothetical two-dimensional setting showing groundwater flow systems associated with a lake that has seepage from it through one-third of its bed, because the local flow-system boundary is discontinuous. Kh/Kv is the ratio of horizontal-to-vertical hydraulic conductivity

within it are greater than the lake and water cannot seep from the lake. If the boundary is not continuous, seepage from the lake can occur. The presence of a stagnation point, the point of least head along the flow-system boundary, indicates that the flow-system boundary is continuous (Winter 1976).

The other general results of the study indicated that the following changes in hydrogeological conditions tended to lessen the difference in head between the lake and the stagnation point, or caused seepage from the lake to occur or increase: (1) lowering the water table, especially on the down-gradient side, (2) increasing the anisotropy (Fig. 11), (3) increasing the hydraulic conductivity of highly permeable zones, (4) increasing lake depth, and (5) moving highly permeable zones that occur beneath and down gradient from the lake from deep to shallower positions within the groundwater system.

Because most lakes are not long, linear, and aligned perpendicular to groundwater flow direction, and because understanding of more realistic lake and groundwater systems was needed, Winter (1978) used a model to evaluate the interaction of lakes and groundwater in three dimensions. The study was designed and conducted much like that described previously, including the dimensions of the lake and groundwater system and steady-state conditions. The principal conclusions of the study indicated that:

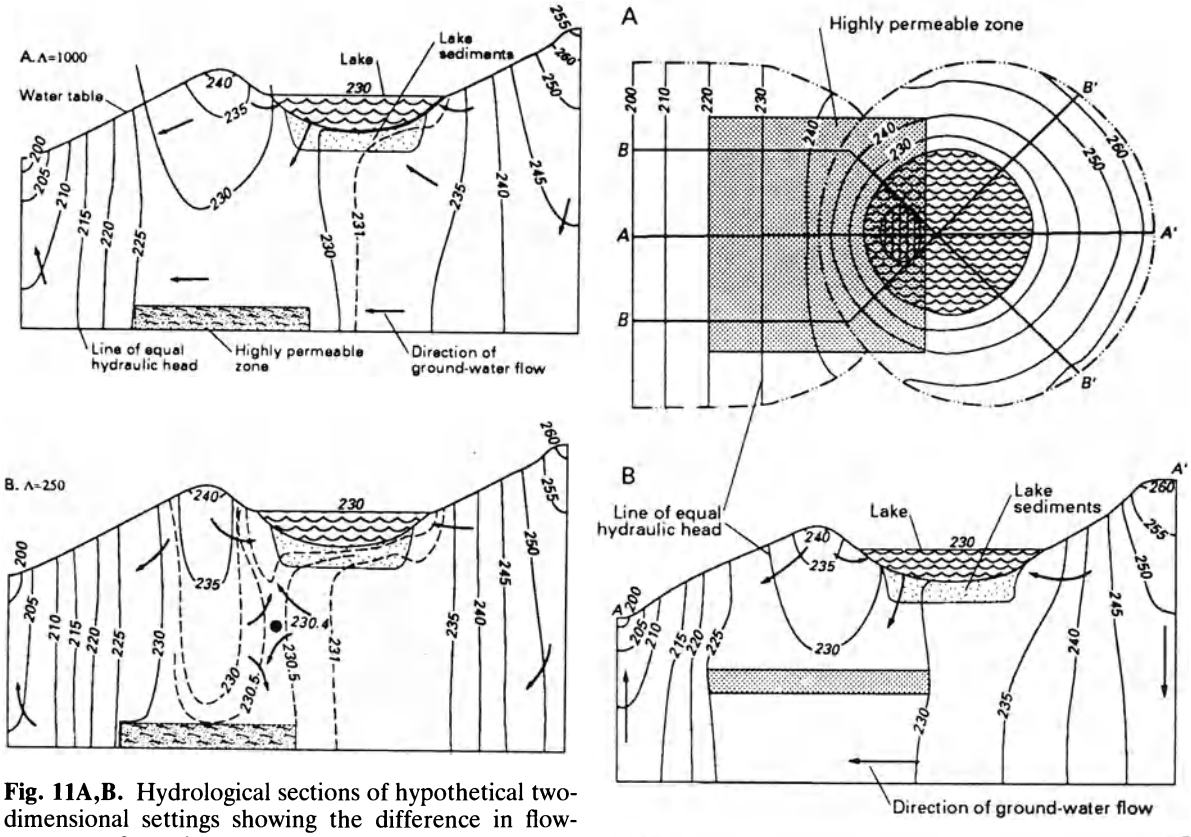


Fig. 11A,B. Hydrological sections of hypothetical two-dimensional settings showing the difference in flow-system configuration and the effect on seepage patterns related to differences in anisotropy, which is the ratio of horizontal-to-vertical hydraulic conductivity. If the porous media has anisotropy of 1000 (**A**), the lake has seepage from it, but if it has anisotropy of 250 (**B**), a stagnation point (*filled circle*) exists, indicating that a closed local flow system encloses the lake, preventing seepage from it. (Modified from Winter and Pfannkuch 1984)

Fig. 12A–C. Hydrological map and sections of a hypothetical three-dimensional setting showing that seepage from a lake can occur even when the gradient of the water table is toward the lake throughout the watershed. (Modified from Winter 1978)

1. A single stagnation point is associated with a closed local groundwater flow system. This point lies along the line of the section that transects the point of minimum head along the groundwater divide enclosing the lake.
2. For lakes enclosed by a groundwater divide, areas of seepage from a lake can occur offshore that would not be detectable with any number of water-table wells placed within the lake's groundwater watershed (Fig. 12).

Although the studies described previously provided insight into groundwater flow processes as they relate to lakes, assuming steady-state conditions imposes severe restrictions on processes that can be very dynamic. Because the configuration of the water table is dynamic, reflecting constantly changing recharge to and discharge from the groundwater system, factors controlling seepage processes needed to be studied using models that permit the water table to move freely. A numerical model that simulates variably saturated (unsaturated and saturated) subsurface flow in vertical section developed by Cooley and Westphal (1974) has the following form:

$$\frac{\partial}{\partial x}\left(K_r K_{xx}\frac{\partial h}{\partial x}\right) + \frac{\partial}{\partial z}\left(K_r K_{zz}\frac{\partial h}{\partial z}\right)$$

$$= \left(S_w S_s + n\frac{dS_w}{dp_h}\right)\frac{\partial h}{\partial t}, \quad (2)$$

where x, z = horizontal and vertical coordinate directions; K_{xx}, K_{zz} = principal components of the hydraulic conductivity tensor, aligned colinear with the x and z directions; K_r = relative hydraulic conductivity, assumed to be a scalar function of water saturation; S_w = water saturation, which varies between zero for dry conditions and 1 for saturated conditions; S_s = specific storage; n = porosity; h = hydraulic head; p_h = pressure head, equal to h–z; and t = time.

This form of the groundwater flow equation differs from Eq. (1) in that the relation between water saturation and pressure head, as well as water saturation and relative hydraulic conductivity, needs to be specified in order to solve the equation for flow in the unsaturated and saturated zones. The relation between water saturation and pressure head is expressed as:

$$S_{wD} = \frac{A}{(-p_h)^c + A}, \quad (3)$$

where $S_{wD} = \frac{S_w - S_{wr}}{1 - S_{wr}}$; S_{wr} = residual water saturation; and A and c = empirical parameters.

The relation between water saturation and relative hydraulic conductivity is expressed as

$$K_r = S_{wD}d, \quad (4)$$

where d is an empirical parameter.

Examples of moisture-characteristic curves of these relations for selected values of A and c for Eq. (3) are shown in Fig. 13A, and for selected values of d for Eq. (4) are shown in Fig. 13B.

The preceding model was used by Winter (1983) to study the interaction of lakes and groundwater when the water table is a dynamic boundary condition. The study was of hypothetical systems that had realistic hydrogeological conditions specified. Two-dimensional vertical sections were used, because the close vertical grid spacing needed to simulate unsaturated flow would result in prohibitively large numbers of nodes if studied in three dimensions. The study involved evaluating groundwater flow-system configuration, and the subsequent effect on seepage through the lake bed, for different initial conditions of the water table. The study then evaluated the effect on these flow characteristics of 15 days of infiltration followed by 7 months of redistribution for two different anisotropies and two different hydraulic conductivities of the porous media.

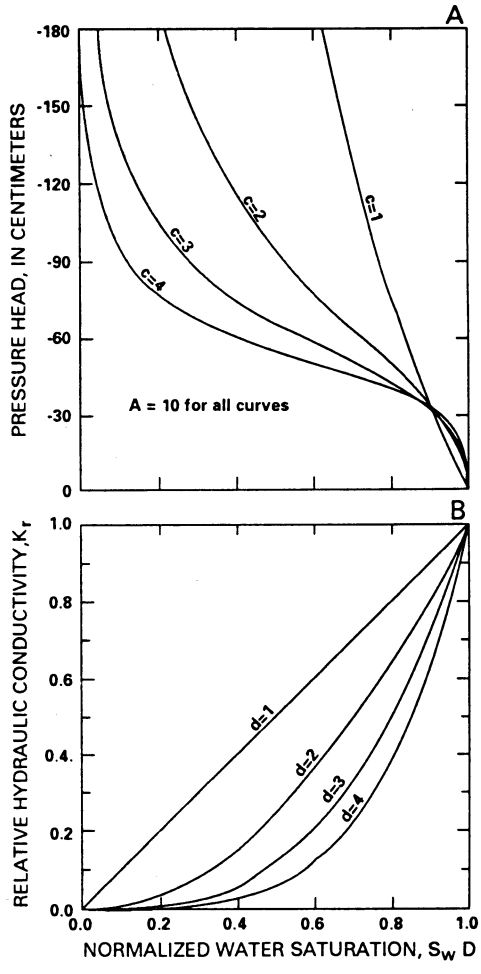
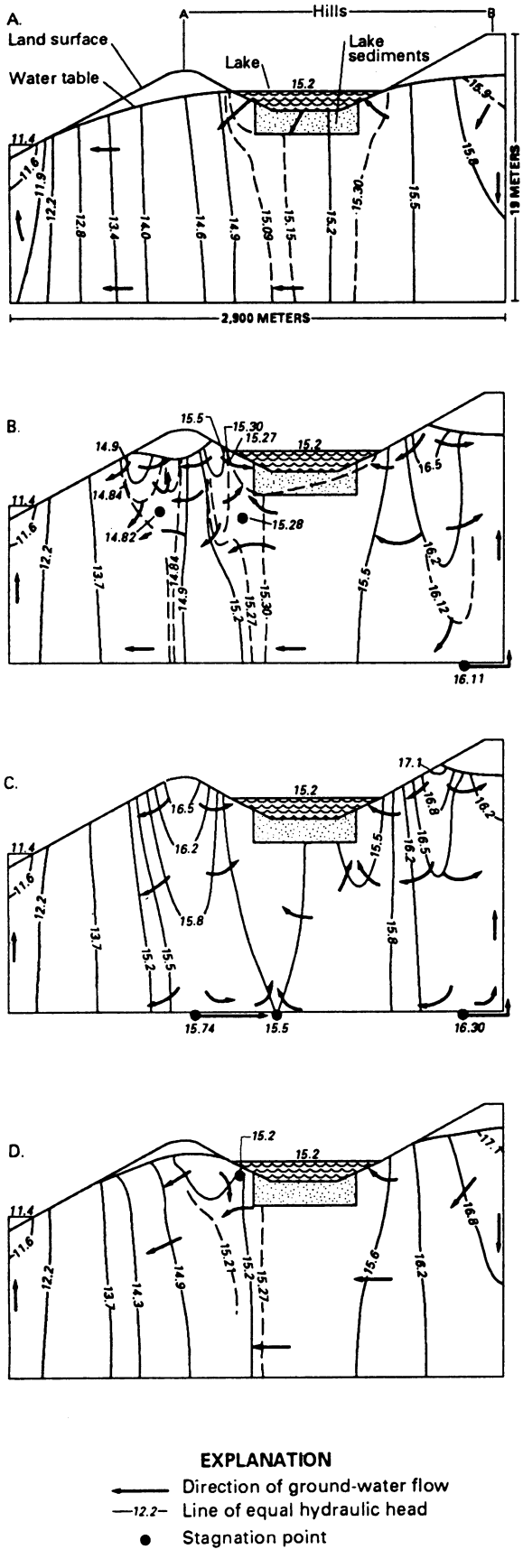


Fig. 13A,B. Relationship of normalized water saturation to pressure head (**A**) and to relative hydraulic conductivity (**B**) for various values of the empirical parameters used to describe flow in the unsaturated zone. (Modified from Winter 1983)

Results of the study indicated that recharge to groundwater is initially focused directly adjacent to the lake. This recharge results in small local flow systems to be established very quickly near the shore, which results in reversal of flow where seepage was previously out of the lake, and increase of seepage into the lake where seepage was already toward it (Fig. 14). In subsequent monthly intervals the groundwater flow systems change substantially in response to the changing configuration of the water table. For example, the series of diagrams in Fig. 14 show the lake fully linked to the regional flow system prior to the 15 days of infiltration (Fig. 14A). After 10 days of



infiltration three local flow systems formed, one of which caused seepage from the lake to cease (Fig. 14B). By the end of the infiltration period 5 days later, the local flow system enclosing the lake extended the full depth of the groundwater system, resulting in no regional flow (Fig. 14C). After 7 months of redistribution the stagnation point was near the lake bed, indicating that a very small closed local flow system enclosed the lake (Fig. 14D). With further decline of the water table seepage from the lake would resume, and most of the groundwater flow would be regional flow.

The results just presented were for a relatively permeable media that had anisotropy of 500. For settings with anisotropy of 100 the local flow systems extended deeper into the groundwater reservoir for equivalent time periods compared to settings with anisotropy of 500. Therefore, regional flow was much less significant for settings having lower anisotropy. This result is consistent with steady-state modeling results (Winter 1976; Winter and Pfannkuch 1984). For settings having relatively low permeability the development of flow systems with changing recharge was very slow; therefore, the flow systems persisted for longer periods of time than was true for more permeable conditions.

Results of these theoretical studies have important implications for understanding groundwater flow and seepage processes related to the interaction of lakes and groundwater. For example, recharge of different magnitude and frequency focused near the edges of lakes result in highly dynamic seepage conditions through lake beds. Furthermore, depression-focused recharge in the uplands away from the lake also affect seepage conditions in the lake (Lissey 1971; Winter 1986).

Fig. 14A–D. Hydrological sections of a hypothetical, two-dimensional, variably saturated setting showing the dynamic flow conditions and seepage patterns related to changing configuration of the water table. The water table reflects the spatial and temporal variation of recharge. Beginning with a water-table configuration resulting from a steady-state recharge rate (**A**), conditions after 10 days of infiltration (**B**) indicate that recharge is focused initially at the lakeshore causing complex flow paths. After 15 days of infiltration (**C**) the local flow system associated with the lake extends to the base of the groundwater system. After 7 months of redistribution (**D**) the stagnation point has risen to a position near the lake bed. If the water table declines further, seepage from the lake will resume. (Modified from Winter 1983)

In addition to focused recharge, bank storage and transpiration add to the complex groundwater flow and seepage conditions near the edge of lakes. Bank storage is water that moves into the groundwater system when the lake has a higher head than the contiguous water table. If the lake then declines more rapidly than the water table, the resulting groundwater mounds result in flow and seepage patterns similar to those resulting from focused recharge (Fig. 15).

Transpiration by near-shore plants cause flow and seepage conditions that are the reverse of those just described. Plants can act as pumps that cause cones of depression on the water table (Meyboom 1966). If these cones of depression extend beneath the lake bed, they can cause or increase seepage out of the lake (Fig. 16). This water loss is not recharge to groundwater; the water is discharged directly to the atmosphere by plants.

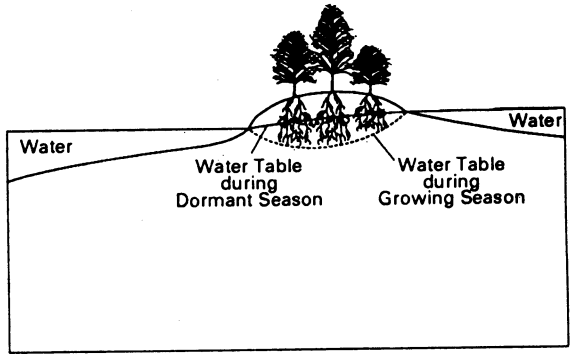


Fig. 16. Effect of transpiration on the water table and on seepage in lake beds. When plants are dormant water flows from the higher lake on the right to the lower lake on the left. During the growing season transpiration by plants causes a cone of depression such that water will seep from both lakes toward the cone of depression

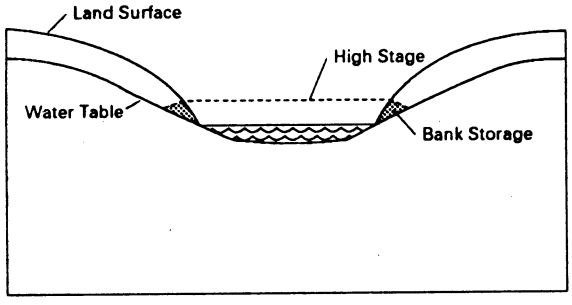


Fig. 15. Diagram of bank storage. At high stage, water flows into the groundwater system. After the surface water declines, the groundwater mounds left behind cause complex flow paths similar to those caused by focused recharge (see Fig. 14B)

Another factor that must be considered in understanding the processes associated with the interaction of lakes and groundwater is the non-linear seepage rate across the lake bed. Theoretical studies of seepage patterns related to the geometric boundaries of lake and groundwater systems indicate that for isotropic and homogeneous porous media seepage decreases exponentially away from the shoreline (McBride and Pfannkuch 1975; Pfannkuch and Winter 1984). This flow pattern is relatively independent of lake

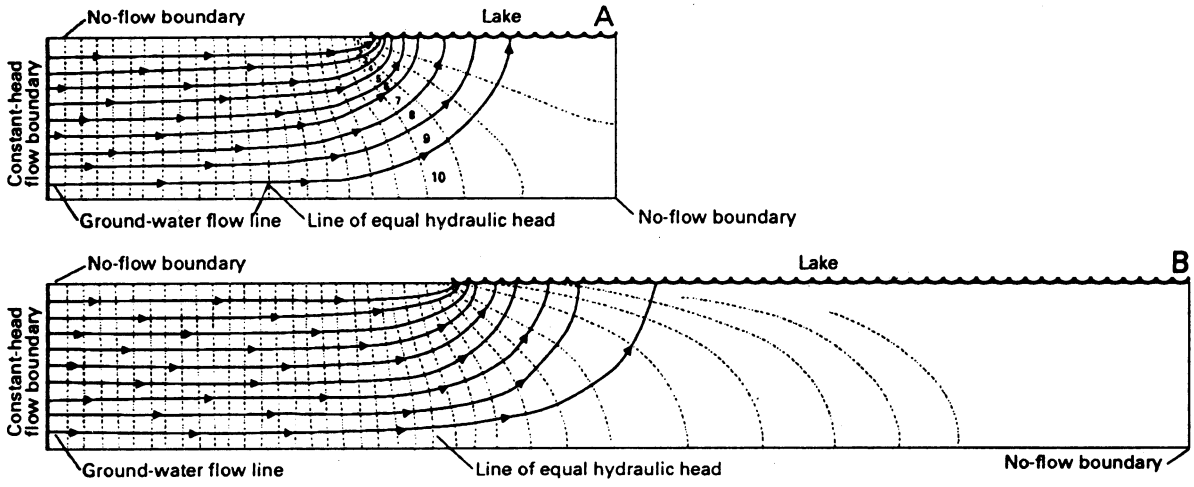


Fig. 17A,B. Hydrological sections of hypothetical two-dimensional settings of nonpenetrating lakes showing seepage is concentrated near the shore, and that seepage patterns are similar, independent of lake size. (Modified from Pfannkuch and Winter 1984)

size (Fig. 17). Even for anisotropic and more complex geological boundaries, the seepage rate is not linear across a lake bed.

The previously mentioned, largely theoretical studies of groundwater flow as it relates to surface water was done because of the need to understand these processes when studying and measuring the groundwater component of lake-water budgets. Field studies to verify configuration of groundwater flow systems, as well as the patterns of seepage in surface-water beds, are time-consuming and expensive. Therefore, the actual data base needed to study and model real-world lake and groundwater linkages, although not extensive, generally verifies results of theoretical studies.

Anderson and Munter (1981) used a two-dimensional, vertical-section model to evaluate the transient interaction of groundwater with Snake Lake, Wisconsin, a lake that had piezometers installed around it earlier by Jaquet (1976). The modeling results revealed the presence of a transient stagnation point on the down-gradient side of the lake, although none of the piezometers located on that side of the lake were completed within the stagnation point (Fig. 18). This result indicates that field study alone generally will not be adequate to fully understand how a lake interacts with groundwater, because it is highly unlikely that a piezometer would be completed directly in a stagnation point, especially when it is apparent that the point moves (Winter 1983).

Other studies that included test drilling, installation of piezometers, and numerical modeling of the interaction of lakes and groundwater generally have been of flow-through lakes, i.e., groundwater seeps into one side of the lake and lake water seeps out the other side (Rinaldo-Lee and Anderson 1980; Karls 1982; Krabbenhoft et al. 1990; Wentz et al. 1990). This approach, with similar results, was also used to study the interaction of groundwater and gravel-pit lakes in Sweden (Landberg 1982). Most of these studies were of entire drainage basins, and the placement of piezometers and grid spacing used in the models were not designed to study the dynamic small-scale, near-shore processes that were discussed previously. These studies are a good example of a common situation in science, i.e., study results reflect, and are constrained by, study design. The studies being conducted at Williams Lake, Minnesota, exemplify this phenomenon.

Williams Lake was established as a site to conduct research on all aspects of lake hydrology,

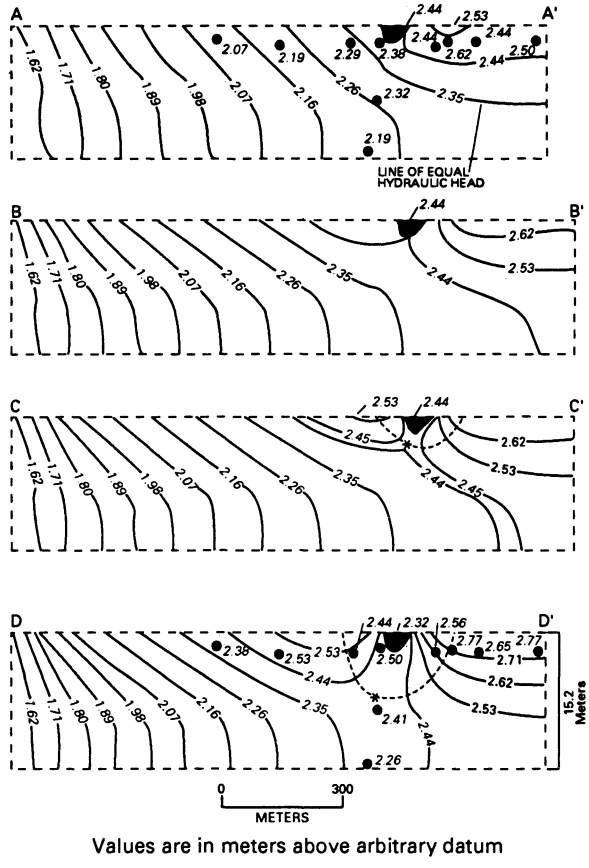


Fig. 18A–D. Hydrological section models of Snake Lake, Wisconsin, showing the formation and growth of a closed local groundwater flow system related to a transient water-table mound down-gradient of the lake. At the initiation of recharge (**A**) the lake had flow-through conditions, i.e., seepage into one side and seepage out of the other side. After 20 days (**B**) the recharge caused a stagnation point to begin to form near the center of the lake bed. After 23 days (**C**) the stagnation point (*asterisk*) was beneath the lake and a small local flow system enclosed the lake, and after 36 days (**D**) the local flow system was even larger. (Modified from Anderson and Munter 1981)

with emphasis on the interaction of the lake with groundwater (Siegel and Winter 1980). Accordingly, wells and piezometers were constructed and placed to evaluate many of the processes indicated by the theoretical studies discussed previously. Water-level data from the large-scale well network and a two-dimensional, vertical-section, steady-state model (Fig. 19) of the Williams Lake drainage basin indicated that groundwater seeped into the lake on one side and the lake lost water to groundwater on the other side (Siegel and Winter 1980). Subsequently, a two-dimensional, transient, areal model of the area indicated similar

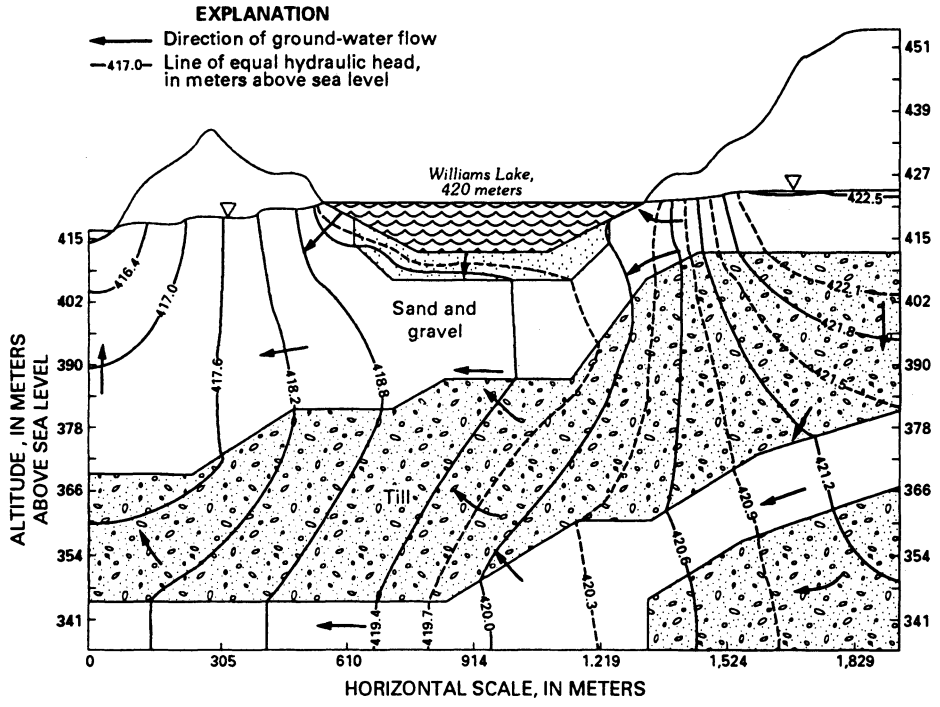


Fig. 19. Hydrological section model of Williams Lake, Minnesota, showing groundwater flow conditions in a complex geological setting. The low hydraulic conductivity of the till prevents flow in the deep sand from having a significant affect on flow in the surficial sand. Furthermore, within the surficial sand a groundwater divide beneath the shoreline on the right side of the lake separates flow such that groundwater in the upper half of the surficial aquifer enters the lake and groundwater in the lower-half passes at depth beneath the lake. (Modified from Siegel and Winter 1980)

lake and groundwater interaction (Karls 1982). However, extensive seepage measurements in the lake bed (Erickson 1981), and detailed studies of the near-shore environment using closely spaced wells, indicated that flow reversals followed periods of heavy rainfall on the side of the lake that usually had seepage from it (Fig. 20). The flow reversals were caused by transient water-table mounds related to focused recharge as described previously. In-lake seepage measurements also revealed reversals of flow from the lake to groundwater during some periods of summer on the side of the lake that generally has seepage into it. These flow reversals were probably caused by transpiration by near-shore vegetation, because data from the well network higher in the watershed indicated that flow was toward the lake. These results indicate that small-scale flow phenomena are commonly not observed if well placement is not designed to observe them.

The increase in seepage or the reversal of seepage caused by recharge focused near shore has been reported for lakes in glacial terrane (Downing and Paterka 1978; Anderson and Munter 1981; Mills and Zwarich 1986; Cherkauer and Zager 1989; Rosenberry and Winter, unpublished data), coastal terrane (Phillips and Shedlock 1993; Shedlock et al. 1993), and karst terrane (Lee and Swancar 1994). Chemical studies of small streams in headwater areas (Sklash and Farvolden 1979) have indicated that streams quickly acquire the chemical characteristics of groundwater during or shortly after storms. The cause is generally attributed to nearby recharge that creates a very short flow path of groundwater to the stream, which is the process discussed previously under focused recharge.

Reversal of seepage direction in lake beds caused by transpiration was described by Meyboom (1966) for small lakes and wetlands in the Canadian prairie. Although believed to be restricted to that region of semiarid climate and geological substrate having low hydraulic conductivity, subsequent studies have indicated that reversal of seepage direction caused by evapotranspiration is much more common than previously believed. Using a potentiomanometer or wells closely spaced near lake shores, flow rever-

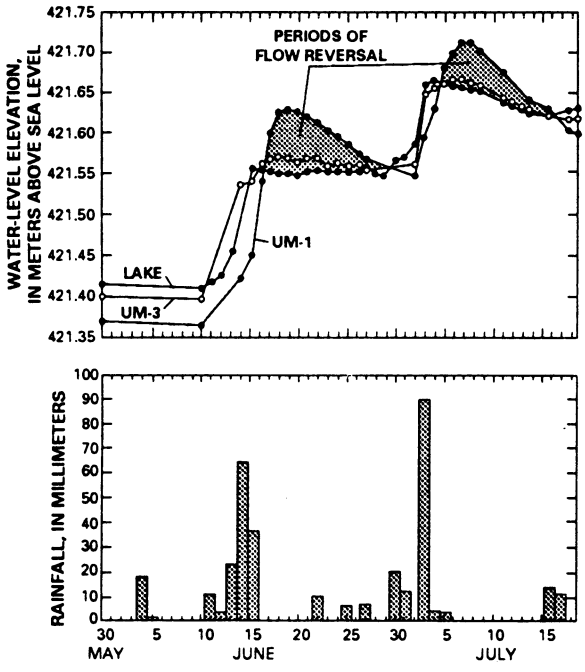


Fig. 20. Periods of focused recharge caused by two periods of heavy rainfall resulted in reversal of groundwater flow on the side of Williams Lake, Minnesota, that normally has seepage to groundwater. The lines designated as *UM-1* and *UM-3* are hydrographs of water levels in wells down-gradient of the lake. (Modified from Rosenberry 1985)

sals related to transpiration have been measured in a wide variety of climatic and geological settings.

The theoretical and field studies discussed previously have important implications for determining the subsurface component of water balances of lakes. If studies are designed to evaluate groundwater flow systems as they interact with lakes, the studies commonly do not include detailed study of the transient near-shore flow processes. Conversely, if studies are designed primarily to measure seepage directly, a basic understanding of the flow processes that cause the seepage patterns is not achieved. Furthermore, continuous direct seepage measurements are generally not made; most are discrete in space and time, which prohibits observance of transient flow and seepage processes.

The various concepts, models, and field studies of the subsurface component of a lake water balance need to be put into perspective with regard to uncertainty, field effort, and adequacy of models. A major advantage of the watershed approach is that the linkage with other components of the hydrological system, and the constraints imposed by them, are part of the study process. A disadvantage of this approach is that the subsurface term is commonly treated such that many simplifying assumptions must be made. Furthermore, few study areas are instrumented thoroughly enough to adequately define small- and large-scale processes of the entire continuum from infiltration to movement through the soil, unsaturated, and groundwater zones to movement to and from a surface-water body. Therefore, largely unquantified uncertainty is generally associated with the subsurface component of watershed models.

The two groundwater approaches, direct measurement of seepage and analysis of groundwater flow systems, each have advantages and disadvantages. Direct measurement of seepage, which consists of discrete measurements in space and time, have the advantage of minimal cost of materials and simple methodology whether using seepage meters or potentiomanometers (Rosenberry 1989). Disadvantages of this approach are:

1. Continuous monitoring is generally not done; therefore, it is unlikely that any of the transient-flow phenomena described previously would be observed, except by chance.
2. Because of the heterogeneous geology of lake beds and the nonlinear seepage patterns across a lake bed, a large number of measurements need to be made so that the data can be analyzed statistically and estimates of error determined.
3. Making the discrete measurements is very time-consuming and therefore manpower-intensive.
4. The study does not result in understanding of processes.

The principal advantage of groundwater flow-system analysis is that understanding of flow systems and lake-bed seepage patterns is achieved, and the interaction of lakes and groundwater can be modeled and predicted. Furthermore, by having wells and piezometers installed throughout the watershed and near the lakeshore, continuous monitoring of head changes throughout the system, including the transient near-shore phenomena, is possible. Disadvantages of this approach are:

1. Construction of a network of wells is expensive.
2. To model groundwater flow systems it is necessary to determine the boundary conditions of the flow field. This requires extensive test

drilling as well as measuring the rates and distribution of recharge and discharge, which, like the watershed approach, requires data on other components of the hydrological system that interact directly with groundwater such as evaporation, transpiration, and movement of water through the unsaturated zone.

3. Because of the heterogeneity of most geological frameworks, determining the hydraulic conductivity distribution within the groundwater system is difficult. For this reason the parameter-estimation approach to modeling these systems is probably the most realistic approach, because the approach leads to estimates of error in the modeling results (Hill 1992).

2.4 Change in Lake Volume

Knowing the volume of a lake is a critically important piece of information in water-balance studies. A change in volume integrates the gains and losses of water from the lake; therefore, it offers an important constraint on the values determined for the other components of the water balance. Fortunately, accurate determination of the volume is possible, provided an accurate bathymetric map is used and a lake-stage recorder is used to monitor changes in stage. The accuracy of bathymetric maps can vary considerably depending on the density of control points or bathmetric traverses. For example, Hakanson (1978) indicated that by decreasing the number of traverses by 50%, the error in a bathymetric map of Lake Ekoln, Sweden, increased by 10% (Fig. 21). Accurate determination of volume changes that occur within the range of stage fluctuations is especially important. As indicated in the discussion of surface water the technology is available to accurately measure lake stage on a continuous basis.

3 Summary

The concept of a water budget is simple, but understanding a water budget requires an understanding of the entire hydrological system. Obtaining values for each of the hydrological

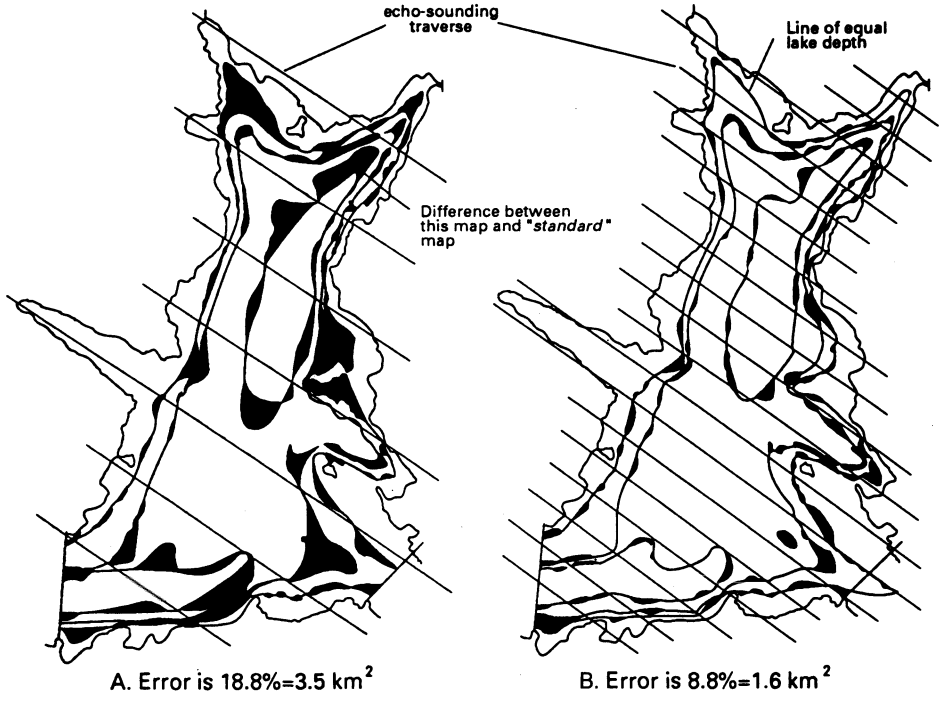


Fig. 21A,B. Bathymetric maps of Lake Ekoln, Sweden, showing total empirically determined error in calculation of the area of the lake bed at three depths. The *shaded areas* show the differences in the shape of the contours between depths determined from echo-sounding traverses and depths that had previously been determined very accurately. Two different densities of echo-sounding traverses are compared. Twice as many data-collection traverses were made for map **B** than for map **A**. (Modified from Hakanson 1978)

components interacting with a lake can be relatively simple. Methods are available to measure inexpensively the atmospheric-water, surface-water, and groundwater components of a water budget. However, the direct measurement approach commonly results in little understanding of hydrological processes, and limits the opportunity to develop predictive models and evaluate the uncertainty of the measured values. For example, gages are available to measure precipitation very accurately, but the gage covers only a very small area. To know precipitation values over an entire area requires a proper number and placement of gages as well as proper interpretation of point values. This basic requirement of gaging and interpreting data applies to all of the hydrological components comprising a water budget. In addition, because the hydrological system is dynamic, continuously recording gages are necessary.

The atmospheric components of a water budget are controlled by circulation of the atmosphere. Therefore, although precipitation is easily gaged, design of the gaging network needs to reflect the types of precipitation patterns common to the area of interest. For example, gage density needs to be greater in mountainous terrane than in areas of more uniform precipitation patterns. Most importantly, the uncertainty in precipitation values needs to be determined for whatever the intensity of the study.

Evaporation, the loss of water vapor from a water body, is controlled by the wind and vapor fluxes over the water body. Reliable methods for continuous direct measurement of evaporation have not been developed. The most accurate method of determining evaporation over periods of months or more is by the energy-budget method. This method is expensive in terms of instruments and manpower, because it involves measuring the gains and losses of heat from all sources: radiation fluxes, latent heat, sensible heat, precipitation, surface water, and groundwater. Because of the magnitude of the commitment to energy-budget studies, evaporation is usually determined by an empirical method. Even in these less intense approaches, however, the instruments to measure wind speed, vapor pressure, and radiation in some instances, need to be located at the study site to minimize error in calculated evaporaton.

Surface water is the easiest component of a water budget to measure accurately, because it can be measured directly and usually at or near the physical boundaries of the lake. However, to understand surface runoff from the watershed of the lake, which is necessary to model and predict surface-water interaction with the lake, hydrological studies of the entire hydrological system operating within that watershed are needed. These types of studies are generally accomplished in a unified way with the aid of watershed models. Although it is difficult to obtain adequate data and estimate parameters for many of the processes considered in watershed models, they have an advantage in that the various components serve as "checks and balances" on the values calculated for contiguous components. In these models the subsurface component is one of the most difficult to deal with, because of limited understanding of subsurface-flow processes and of limited data.

The subsurface consists of the unsaturated zone and the groundwater zone. The unsaturated zone generally has no direct interface with surface water, because the water table, the upper surface of the groundwater zone, meets the surface water at the shoreline. The groundwater zone has the largest interface with surface water. Because of the curvature of lake beds, the interface is even larger than the air–water interface.

The groundwater component of water budgets can be measured directly using seepage meters and hydraulic potentiomanometers. These devices sample seepage discretely in time and space, however, and are generally not used for continuous monitoring. Therefore, this approach does not lend itself to: (1) understanding the flow systems that cause the seepage patterns, (2) realistically addressing the errors in calculated values, and (3) observing and measuring the highly dynamic flow reversals that commonly occur in the near-shore environment. Without understanding groundwater flow systems, modeling and predicting the distribution of seepage within lakes is impossible.

Understanding of groundwater flow systems as they relate to lakes has evolved through numerical experiments of hypothetical settings using two- and three-dimensional models of steady-state and transient conditions. Subsequently, field studies, including modeling, have confirmed the presence of a wide variety of flow conditions. Lakes can interact with local flow systems only, which continuously change over time, or with a combination of local and regional flow systems. Furthermore, near-shore processes, such as focused recharge, bank storage, and transpiration by near-shore plants, can cause seepage conditions to vary signi-

ficantly, including reverse direction, over various periods of time. High cost is a major disadvantage of the flow-system approach to determining the groundwater component of water budgets. Therefore, field data to calibrate and verify models of groundwater flow systems related to lakes are limited.

Change in lake volume is crucial information to have in lake water budgets, because this value integrates all the fluxes to and from the water body, thereby serving as an important check on the values determined for the other components of the water balance. Fortunately, the two pieces of information needed to determine lake volume, bathymetry and stage of the lake surface, can both be measured accurately.

References

Anderson MP, Munter JA (1981) Seasonal reversals of groundwater flow around lakes and the relevance to stagnation points and lake budgets. Water Resour Res 17:1139–1150

Asbury C (1990) Seepage and geochemical processes at the bed of Mirror Lake, New Hampshire. PhD Dissertation, Cornell University, Ithaca, New York, 250 pp

Barnes BS (1939) The structure of discharge recession curves. Trans Am Geophys Union 20:721–725

Belanger TV, Montgomery ME (1992) Seepage meter errors. Limnol Oceanogr 37:1787–1795

Beven KJ (1985) Distributed models. In: Anderson MG, Burt TP (eds) Hydrological forecasting. Wiley, Chichester, pp 405–435

Beven KJ (1986) Runoff production and flood frequency in catchments of order n: an alternative approach. In: Gupta VK, Rodriguez-Iturbe I, Wood EF (eds) Scale problems in hydrology. Reidel, Hingham, pp 107–131

Blackie JR, Eeles CWO (1985) Lumped catchment models. In: Anderson MG, Burt TP (eds) Hydrological forecasting. Wiley, Chichester, pp 311–345

Boussinesq J (1877) Essai sur la theories des eaux courantes. Memoires presentes par divers savants a l'Academic des Sciences de l'Institut National de France, Tome XXIII, No 1

Brutsaert WH (1982) Evaporation into the atmosphere. Reidel, Dordrecht

Brutsaert WH, Stricker H (1979) An advection-aridity approach to estimate actual regional evapotranspiration. Water Resour Res 15:443–450

Carter RW (1973) Accuracy of current meter measurements. Proc Koblenz Symp, 1970, Int Assoc Hydrol Sci 1:86–98

Cherkauer DA, McBride JM (1988) A remotely operated seepage meter for use in large lakes and rivers. Ground Water 26:165–171

Cherkauer DA, Zager JP (1989) Groundwater interaction with a kettle-hole lake: relation of observations to digital simulations. J Hydrol 109:167–184

Cooley RA, Westphal JA (1974) An evaluation of the theory of groundwater and river-water interchange, Winnemucca reach of the Humboldt River, Nevada. University of Nevada, Reno, Hydrol Water Res 19

Crowe AS (1993) The application of a coupled water-balance-salinity model to evaluate the sensitivity of a lake dominated by groundwater to climatic variability. J Hydrol 141:33–73

Crowe AS, Schwartz FW (1981) Simulation of lake-watershed systems I. Description and sensitivity of the model. J Hydrol 52:71–105

DeBruin HAR (1978) A simple model for shallow lake evaporation. J App Meteorol 17:1132–1134

DeBruin HAR, Keijman JQ (1979) The Priestley-Taylor evaporation model applied to a large, shallow lake in the Netherlands. J App Meteorol 18: 898–903

Dickenson WT (1967) Accuracy discharge measurements. Colorado State University, Hydrol Pap 20

Downing JA, Paterka JJ (1978) Relationship of rainfall and lake ground-water seepage. Limnol Oceanogr 23:821–825

Erickson DR (1981) A study of littoral groundwater seepage at Williams Lake, Minnesota, using seepage meters and wells. MS Thesis, University of Minnesota, Minneapolis

Fellows CR, Brezonik PL (1980) Seepage flow into Florida lakes. Water Res Bull 16:635–641

Freeze RA (1972) Role of subsurface flow in generating surface runoff 2. Upstream source areas. Water Resour Res 8:1272–1283

Freeze RA, Witherspoon PA (1967) Theoretical analysis of regional groundwater flow 2. The effect of water-table configuration and subsurface permeability variation. Water Resour Res 3:623–634

Germann PF, Beven KJ (1985) Kinematic wave approximation to infiltration into soils with sorbing macropores. Water Resour Res 21:990–996

Gherini SA, Mok L, Hudson RJM, Davis GF, Chen CW, Goldstein RA (1985) The ILWAS model: formulation and application. Water Air Soil Pollut 26:425–459

Hakanson L (1978) Optimization of lake hydrographic surveys. Water Resour Res 14:545–560

Hall FR (1968) Base-flow recessions, a review. Water Resour Res 4:973–983

Hamon WR (1961) Estimating potential evapotranspiration. Am Soc Civil Engin Proc (HY3) 87: 107–120

Harbeck GE Jr, Kohler MA, Koberg GE et al. (1958) Water-loss investigations: Lake Mead studies. US Geol Surv Prof Pap 298

Hewlett JD, Hibbert AR (1963) Moisture and energy conditions within a sloping soil mass during drainage. J Geophys Res 68:1081–1087

Hill MC (1992) A computer program (MODFLOWP) for estimating parameters of a transient, three-dimensional, groundwater flow model using nonlinear regression. US Geol Surv Open-File Rep 91–484

Huff FA, Neill JC (1957) Rainfall relations on small

areas in Illinois. Ill State Water Surv Bull 46:43–50
Huff FA, Shipp WL (1969) Spatial correlations of storm, monthly, and seasonal precipitation. J App Meteorol 8:542–550
Jaquet NG (1976) Ground-water and surface-water relationships in the glacial province of northern Wisconsin–Snake Lake. Ground Water 14:194–199
Jensen ME (ed) (1974) Consumptive use of water and irrigation requirements. Am Soc Civil Engin, New York
John PH, Lock MA (1977) The spacial distribution of ground-water discharge into the littoral zone of a New Zealand lake. J Hydrol 33:391–395
Karls RM (1982) A ground-water model of the Williams Lake watershed, Hubbard County, Minnesota. MS Thesis, University of Arizona, Tucson
Kirkby MJ (1985) Hillslope hydrology. In: Anderson MG, Burt TP (eds) Hydrological forecasting. Wiley, Chichester, pp 37–75
Knisel WG Jr (1963) Baseflow recession analysis for comparison of drainage basins and geology. J Geophys Res 68:3649–3653
Krabbenhoft DP, Anderson MP, Bowser CJ (1990) Estimating ground-water exchange with lakes, 2. Calibration of a three-dimensional solute transport model to a stable-isotope plume. Water Resour Res 26:2455–2462
LaBaugh JW (1988) Relation of hydrogeologic setting to chemical characteristics of selected lakes and wetlands within a climate gradient in the north-central United States. Verh Int Verein Limnol 23: 131–137
Landberg J (1982) Hydrogeological consequences of excavating gravelpits below the water table in glaciofluvial deposits. University of Gothenburg, Geol Inst Publ A39, Gothenburg, Sweden
Larson LW (1971) Precipitation and its measurement, a state of the art. University of Wyoming, Water Resour Res Inst, Water Resour Ser 24
Leavesley GH, Lichty RW, Troutman BM, Saindon LG (1983) Precipitation-runoff modeling system: users manual. US Geol Survey Water-Resour Invest 83:4238
Lee DR (1972) Septic tank nutrients in groundwater entering Lake Sallie, Minnesota. MS Thesis, University of North Dakota, Grand Forks
Lee DR (1977) A device for measuring seepage flux in lakes and estuaries. Limnol Oceanogr 22:155–163
Lee DR, Cherry JA, Pickens JF (1980) Ground water transport of a salt tracer through a sandy lakebed. Limnol Oceanogr 25:45–61
Lee TM, Swancar A (1994) The influence of evaporation, groundwater, and uncertainty in the hydrologic budget of Lake Lucerne, a seepage lake in Polk County, Florida. US Geol Survey Open-File Rep 93:26
Linsley RK Jr, Kohler MA, Paulhus JLH (1975) Hydrology for engineers, 2nd edn. McGraw-Hill, New York
Lissey A (1971) Depression-focused transient groundwater flow patterns in Manitoba. Geol Assoc Can Spec Pap 9:333–341
McBride MS, Pfannkuch HO (1975) The distribution of seepage within lakes. US Geol Surv J Res 3: 595–612
McDonald MG, Harbaugh AW (1984) A modular three-dimensional finite difference ground-water flow model. US Geol Surv Open-File Rep 83–875
McGuinness JL, Bordne EF (1972) A comparison of lysimeter-derived potential evapotranspiration with computed values. US Agricul Res Serv Tech Bull 1452
Meyboom P (1966) Unsteady groundwater flow near a willow ring in hummocky moraine. J Hydrol 4: 38–62
Mills JG, Zwarich MA (1986) Transient groundwater flow surrounding a recharge slough in a till plain. Can J Soil Sci 66:121–134
Murdock PS, Peters NE, Newton RM (1987) Hydrologic analysis of two headwater lake basins of differing lake pH in the west-central Adirondack Mountains of New York. US Geol Survey Water Resour Invest 84:4313
Pfannkuch HO, Winter TC (1984) Effect of anisotropy and ground-water system geometry on seepage through lakebeds 1. Analog and dimensional analysis. J Hydrol 75:213–237
Phillips PJ, Shedlock RJ (1993) Hydrology and chemistry of groundwater and seasonal ponds in the Atlantic coastal plain in Delaware, USA. J Hydrol 141:157–178
Ragotzkie RA (1978) Heat budgets of lakes. In: Lerman A (ed) Lakes chemistry, geology, physics, Springer Berlin, Heidelberg, New York
Rantz SE et al. (1982) Measurement and computation of streamflow, 2 vols. US Geol Survey Water-Supp Pap 2175
Richards LA (1931) Capillary conduction of liquids through porous mediums. Physics 1:318–333
Rinaldo-Lee MB, Anderson MP (1980) High water levels in ground-water dominant lakes – A case study from northwestern Wisconsin. Ground Water 18:334–339
Rorabaugh MI (1964) Estimating changes in bank storage and groundwater contributions to streamflow. Int Assoc Sci Hydrol 63:432–441
Rosenberry DO (1985) Factors contributing to the formation of transient water-table mounds on the outflow side of a seepage lake, Williams lake, central Minnesota. MS Thesis, University of Minnesota, Minneapolis
Rosenberry DO (1989) Inexpensive ground-water monitoring methods for determining hydrologic budgets of lakes and wetlands. North American Lake Management Society, Chicago
Rutledge AT (1993) Computer programs for describing the recession of groundwater discharge and for estimating mean groundwater recharge and discharge from streamflow records. US Geol Survey Water-Resour Invest Rep 93:4121
Shaw RD, Prepas EE (1990a) Groundwater-lake interactions 1. Accuracy of seepage meter estimates of lake seepage. J Hydrol 119:105–120
Shaw RD, Prepas EE (1990b) Groundwater-lake interactions 2. Nearshore seepage patterns and the con-

tribution of groundwater to lakes in central Alberta. J Hydrol 119:121–136

Shedlock RJ, Wilcox DA, Thompson TA, Cohen DA (1993) Interactions between groundwater and wetlands, southern shore of Lake Michigan, USA. J Hydrol 141:127–155

Siegel DI, Winter TC (1980) Hydrologic setting of Williams Lake, Minnesota. US Geol Survey Open-File Rep 80–403

Sklash MG, Farvolden RN (1979) The role of ground water in storm runoff. In: Back W, Stephenson DA (eds) Contemporary hydrogeology. Elsevier, New York, pp 45–65

Stephenson GR, Freeze RA (1974) Mathematical simulations of subsurface flow contributions to snowmelt runoff – Reynolds Creek Watershed Idaho. Water Resour Res 10:284–298

Stewart RB, Rouse WR (1976) A simple method for determining the evaporation from shallow lakes and ponds. Water Resour Res 12:623–628

Sturrock AM, Winter TC, Rosenberry DO (1992) Energy budget evaporation from Williams Lake: a closed lake in north central Minnesota. Water Resour Res 28:1605–1617

Swanson GA, Winter TC, Adomaitis VA, LaBaugh JW (1988) Chemical characteristics of prairie lakes in south-central North Dakota, their potential for impacting fish and wildlife. US Fish Wildl Serv Tech Rep 18

Tanner CB (1967) Measurement of evaporation. In: Hagan RM, Haise HR, Edminster TW (eds) Irrigation of agricultural lands. Agronomy Monogr No 11, American Society of Agronomy, Madison, Wisconsin, pp 534–574

Toth J (1963) A theory of groundwater motion in small drainage basins in central Alberta, Canada. J Geophys Res 67:4375–4387

Troendle CA (1985) Variable source area models. In: Anderson MG, Burt TP (eds) Hydrological forecasting. Wiley, Chichester, pp 347–403

US Bureau of Reclamation (1975) Water measurement manual. US Government Printing Office, Washington, DC

Warnaka K, Pochop L (1988) Analyses of equations for free water evaporation estimates. Water Resour Res 24:979–984

Wentz DA, Krohelski JT, Rose WJ (1990) Hydrologic component. In: The Wisconsin regional integrated lake-watershed acidification study (RILWAS), 1981–1986. Electric Power Research Institute, Palo Alto, California

Wilson JF Jr (1968) Fluorometric procedures for dye tracing. Techniques of Water-Resources Investigations of the United States Geological Survey, Book 3, Chap A12

Winter TC (1976) Numerical simulation analysis of the interaction of lakes and groundwater. US Geol Surv Prof Pap 1001

Winter TC (1978) Numerical simulation of steady-state three dimensional groundwater flow near lakes. Water Resour Res 14:245–254

Winter TC (1981) Uncertainties in estimating the water balance of lakes. Water Resour Bull 17:82–115

Winter TC (1983) The interaction of lakes with variably saturated porous media. Water Resour Res 19: 1203–1218

Winter TC (1986) Effect of groundwater recharge on configuration of the water table beneath sand dunes and on seepage in lakes in the sandhills of Nebraska. J Hydrol 86:221–237

Winter TC, Pfannkuch HO (1984) Effect of anisotropy and ground-water system geometry on seepage through lakebeds 2. Analog and dimensional analysis. J Hydrol 75:239–253

Winter TC, LaBaugh JW, Rosenberry DO (1988) The design and use of a hydraulic potentiomanometer for direct measurement of differences in hydraulic head between ground water and surface water. Limnol Oceanogr 33:1209–1214

Winter TC, Eaton JS, Likens GE (1989) Evaluation of inflow to Mirror Lake, New Hampshire. Water Resour Bull 25:991–1008

Winter TC, Rosenberry DO, Sturrock AM (1995) Evaluation of eleven equations for determining evaporation for a small lake in the north central United States. Water Resour Res (in press)

Woessner WW, Sullivan KE (1984) Results of seepage meter and minipiezometer study, Lake Mead, Nevada. Ground Water 22:561–568

3 Hydrological and Thermal Response of Lakes to Climate: Description and Modeling

S.W. HOSTETLER

1 Introduction

Lake systems continually respond to climatic conditions that vary over broad scales of space and time. The spatial distribution of lakes on the Earth's surface is indicative of long-term patterns of atmospheric circulation, and the annual cycle of climate over lake basins is reflected in seasonal change in the size and temperature of lakes. Lake size is determined by the balance of water inputs and outputs, and lake temperature is governed by the balance of heat inputs and outputs. The lake hydrological and energy balances are coupled to the atmosphere. In response to the inputs of mass, energy, and momentum (precipitation, radiation, and wind stress), lakes return heat and moisture to the atmosphere through conduction and evaporation. Global, regional, or local change in the hydrological or thermal states of lakes thus represent interactive responses to climatic variation in the supply of water and energy.

Most lacustrine biological, chemical, and physical processes are affected directly by lake hydrological (e.g., lake depth) and thermal changes (e.g., seasonal stratification), and are thus indirectly affected by climate variation. Understanding lake-climate system interactions is therefore of fundamental importance in understanding the effects of climate change on limnological processes. There exist relatively simple numerical models of lake size and temperature that are run using as inputs climatic and hydrological data. These models can be applied to assess the effects of climate change on lacustrine processes, to reconstruct historical changes in lake size, and to link paleoclimate with past lake size.

In this chapter the global distribution of lakes is compared with the global surface hydrological budget. Examples of lake-level fluctuations that have occurred over the past $10-10^4$ years are discussed. Fluctuation in the size of lakes is discussed in terms of the hydrological budget and other nonclimatic factors, and models of lake level are presented. The thermal response of lakes is associated with climatic and meteorological conditions that cause and effect seasonal cycles of the energy budget, and thus of lake-surface temperature and subsurface thermal stratification. An overview of lake models that can be used to simulate lake temperature and evaporation is presented, and applications of lake models to climate-change studies are illustrated.

2 Hydrological Response

The global occurrence of lakes corresponds broadly to basin runoff, which, on long-term average, is equivalent to effective moisture, the difference between total basin precipitation and total basin evaporation and evapotranspiration (Fig. 1, *P-E*). Within the equatorial region (~10°S to 10°N latitude), approximately 1.5% of the Earth's surface is covered by lakes. Here precipitation generally exceeds evaporation, surface runoff is maximized, and lakes primarily are hydrologically open, i.e., water exits the lakes through surface or subsurface outlets. Few lakes are found in the subequatorial high pressure zones (~25°N to 25°S latitude) where evaporation far exceeds precipitation, and a permanent runoff deficit exists. The greatest surface coverage by lakes occurs in the mid-latitude zones (~25° to 60° north and south latitude). The apparent latitudinal anomaly in Fig. 1 between lake distribution and runoff at 45°N is attributed to the large areal extent of the Caspian and Aral Seas (Hutchinson 1957), and to the large number of lakes that were carved out by the northern hemisphere ice sheets. In both hemispheres maxima in the occurrence of hydrologically closed lakes [i.e., lakes within endoreic regions (internally drained basins) that

US Geological Survey, ERL-C, 200 SW 35th, Corvallis, OR 97333, USA

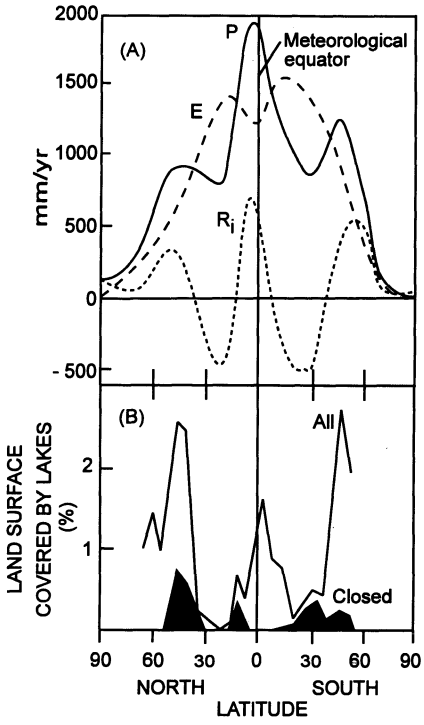


Fig. 1. **A** Zonally averaged rates of precipitation (P), evaporation (E), and runoff (R_i). **B** Latitudinal occurrence of lakes as percent of land surface. (Hydrological data **A** from Budyko 1977, and lake occurrence data **B** modified after Street-Perrott and Roberts 1983)

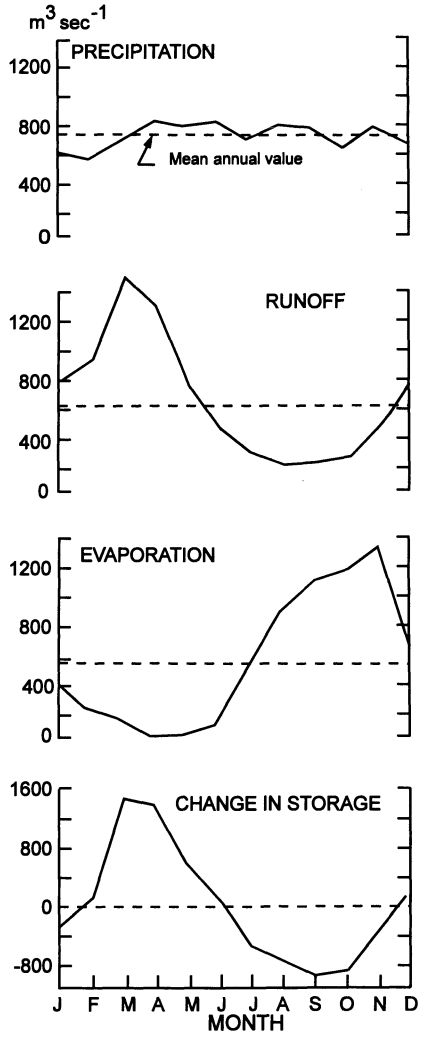


Fig. 2. Long-term average seasonal variation of precipitation, runoff, evaporation, and change in lake storage of Lake Erie. (Modified after Quinn and Guerra 1986)

have no path for water loss except through evaporation] correspond to latitudes at which precipitation is approximately balanced by evaporation ($R_i \approx 0$). The dependence of closed lakes on the near-balance of precipitation and evaporation causes lakes to be very sensitive to hydrological fluctuations, and thus to climate change. Poleward from the mid-latitude zones runoff increases causing a corresponding decrease in the occurrence of closed lakes.

Some lakes fluctuate in size from storm-derived increases in water inputs. Most lakes, however, are relatively insensitive to all but the largest of storms, and short-term fluctuations in size are minor. Lakes usually exhibit seasonal fluctuations in size corresponding to seasonal cycles in the components of the hydrological budget. The average seasonal fluctuation in the size (storage) of Lake Erie, for example, is governed by the magnitude and phase of precipitation, evaporation, and runoff (Fig. 2).

From $10-10^2$ years higher magnitude and longer duration variations in precipitation, evaporation, and runoff combine to cause larger fluctuations in lake size (Fig. 3). Hydrological variations over these time scales are usually the result of continental and regional shifts in atmospheric circulation that can persist for several years (e.g., Andreeva 1974). During the 1980s, for example, wet conditions over North America (Karl and Young 1986; Changnon 1987) produced historical high levels in the Laurentide Great Lakes and the Great Salt Lake, Utah, and other lakes in the Great Basin. This wet period may be associated with continental-scale atmospheric circulation patterns that were set up by an *El Niño Southern Oscillation*, which is a combination of anomalies of sea surface temperatures and atmospheric-pressure patterns in the eastern and

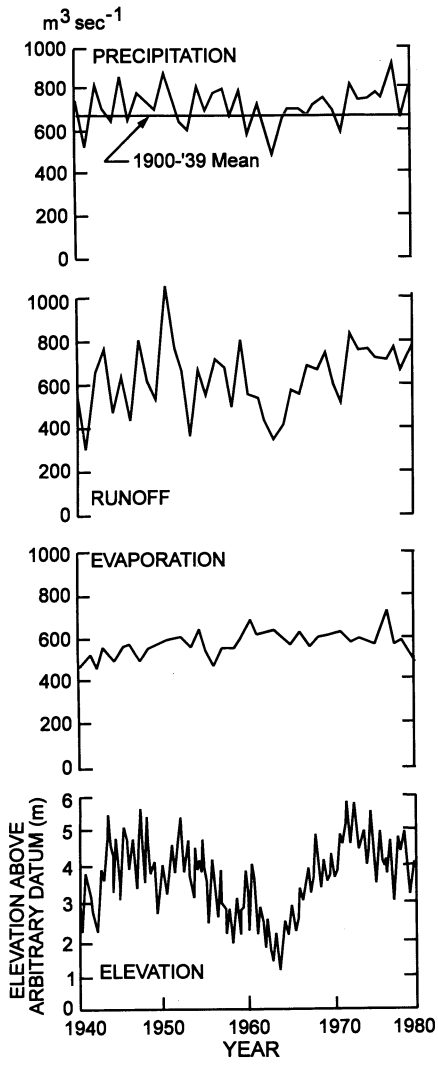


Fig. 3. Long-term variability of the annual hydrological budget of Lake Erie. Precipitation, runoff, and evaporation modified after Quinn and Guerra (1986), and lake-level data from Winter and Woo (1990)

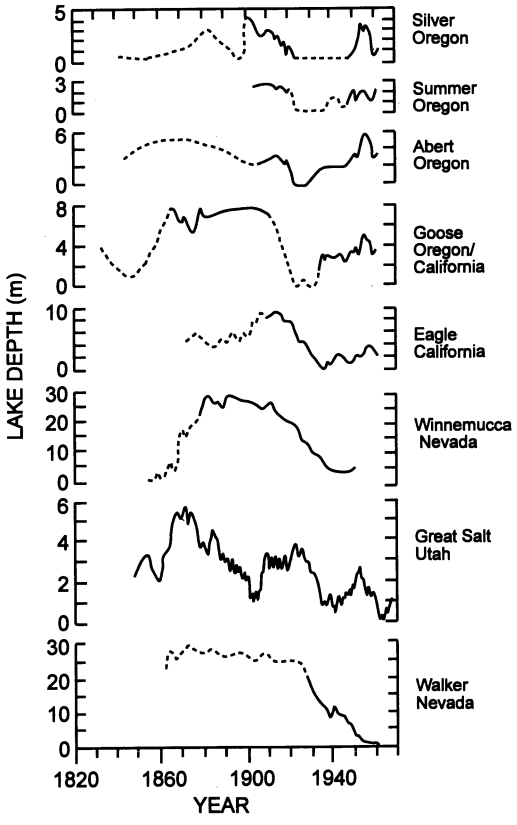


Fig. 4. Long-term trends and variations of lake levels in the Great Basin of the western United States (*dotted line*: historical records; *solid line*: measured). Lake levels are not for pristine (reconstructed) conditions, and therefore reflect the effects of river-water withdrawals for irrigation and other consumptive uses, particularly in the latter periods of the records. (Street-Perrott and Harrison 1985)

southern Pacific Ocean. Over 10^2 years the persistence of climatic shifts are illustrated in the historical records of the levels of the Great Lakes (Fig. 3) and lakes in the Great Basin (Fig. 4).

Large fluctuations in lake size have occurred globally during the past 10^3–10^5 years. The spatial and temporal patterns of these relatively high amplitude, low frequency fluctuations correspond to global climate changes associated, for example, with the advance and retreat of continental ice sheets (e.g., Smith and Street-Perrott 1983; Harrison and Metcalfe 1985; Kutzbach and Street-Perrott 1985; Harrison 1989; Benson et al. 1989). These millennial-scale fluctuations are recorded in many lakes, and much work has been done to establish chronological records of level by reconciling analyses of the chemical, biological, and physical makeup of lake sediments, geomorphic, and geological features, and, sometimes, archeological evidence (e.g., Bradley 1985; Street-Perrott and Harrison 1985; Benson and Thompson 1987a,b; Benson et al. 1989; Gasse and Fontes 1989; COHMAP Members 1989; Benson 1994; Thompson et al. 1994). For example, a chronology of Lake Lahontan, reconstructed from radiocarbon dating of a diverse set of proxy indicators (e.g., tufa, packrat middens), indicates that large late Pleistocene fluctuations in the size of the lake occurred over the past 35 000 years in general correspondence with the timing of the last glacial maximum (18 000 years ago), and subsequent transition to the current interglacial (Fig. 5).

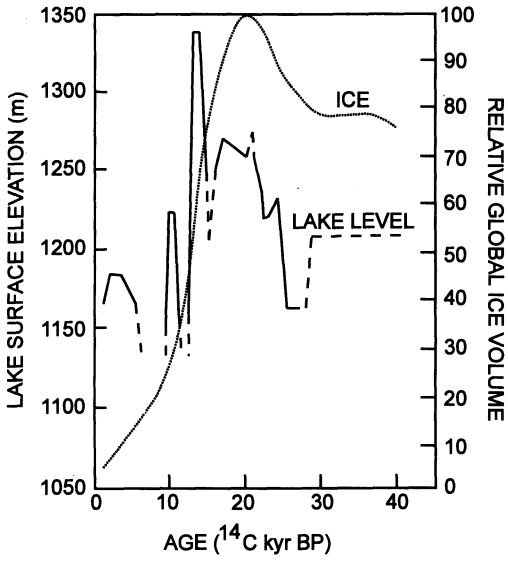


Fig. 5. Late-Pleistocene level chronology of Lake Lahontan (*solid line*) compared with the global volume of ice (*broken line*) estimated from radioisotope analyses of deep-sea cores. Lake level data from Benson (unpubl.) and ice-volume data from Imbrie et al. (1984)

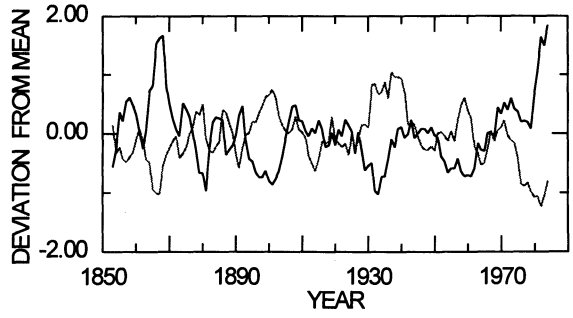


Fig. 6. Departures from the 130-year mean of precipitation (*solid line*) and evaporation (*broken line*) for the Great Salt Lake, Utah. The normalized raw data have been smoothed with a 5-term, moving-average filter. (James 1985; Morrisette 1988; NOAA Climatological Data Summaries)

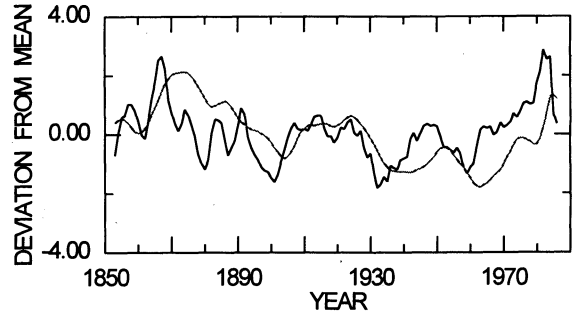


Fig. 7. Departures from the 130-year mean of P-E (*solid line*) and lake level (*broken line*) of Great Salt Lake, Utah. The normalized raw data have been smoothed with a 5-term, moving-average filter. (James 1985; Morrisette 1988; NOAA Climatological Data Summaries)

These chronologies yield valuable information about the relative size and timing of past fluctuations, and can be used together with hydrological and thermal models to infer past paleoclimate.

In the absence of tectonic activity and human influences lakes tend toward a size or level that is in equilibrium or at steady state with the average hydrological balance. If a climate change occurs and persists, the lake will expand or contract to achieve a new steady state. If the lake has insufficient time to reach equilibrium with its new hydrological balance before another climate change occurs, it will be forced toward yet another steady-state size. The history of lake size is thus composed of time-dependent fluctuations that exhibit a broad range of amplitude and frequency. The response of a lake to climate change is determined by a wide variety of factors such as bathymetry and the topography, soils, and vegetation of the catchment.

Climatically induced change in basin-wide precipitation and evaporation induce fluctuations in the size of a lake. Historical data from the Great Salt Lake, Utah (Fig. 6), for example, display a general, inverse covariation between precipitation and evaporation. Periods of extreme variation in precipitation also were periods of extreme variation in evaporation. The reason for this apparent covariance, which tends to maximize hydrologically induced change in lake level, is that atmospheric conditions that favor precipitation (cloudy sky, high humidity) also tend to suppress evaporation and thereby increase effective wetness.

Relative change in effective wetness is often used to associate lake-level fluctuations with climate, especially in studies of paleohydrology. Over sufficiently long averaging periods this association is usually valid. If the climate is in transition, however, change in P-E can occur before associated change in lake level (Fig. 7). Under transient climatic conditions, therefore, the assumption that P-E and lake level increase or decrease together is usually valid for basins where the surface area of a lake is large compared with the total catchment area, for basins with limited

in-basin storage (in soils and glaciers) and for basins uniformly affected by climate.

3 The Hydrological Budget

Changes in lake size can be calculated from known or estimated hydrological budgets. A general equation for the time rate of change of lake volume can be written symbolically as

$$\frac{dV}{dt} = (P_L - E_L)A_L(z) + (P_B - E_B)A_B(z) - R_O + (G_I - G_O), \quad (1)$$

where V is lake volume; P_L is precipitation over lake surface [L/T]; E_L is evaporation from lake surface [L/T]; $A_L(z)$ is surface area of lake at elevation z [L^2]; P_B is precipitation over lake catchment [L/T]; E_B is evapotranspiration from lake catchment [L/T]; $A_B(z)$ is surface area of catchment, excluding the lake, at elevation z [L^2]; R_O is outflow from lake [L^3/T]; G_I is groundwater flow into lake [L^3/T]; and, G_O is groundwater flow from lake [L^3/T].

Depth-area data, A(z), are readily obtained from contour maps, or can be approximated geometrically by cones, trapezoids, or parabolic curves. Equation (1) is applicable to both open and closed lakes. It is important to recognize that the processes represented by the components of the hydrological budget can exhibit very different response times to climatic change. [See, for example, Szestay (1974) and Street-Perrott and Harrison (1985) for classification of lakes with regard to their sensitivities to the components of the hydrological budget.]

Although some of the following discussion is applicable to open lakes, the focus of the rest of this chapter is on closed lakes because they are more widely studied as indicators of climate change. For closed lakes in which the net flux of groundwater can be considered zero for the time scale of interest, Eq. (1) reduces to

$$\frac{dV}{dt} = (P_L - E_L)A_L(z) + (P_B - E_B)A_B(z). \quad (2)$$

Following Eq. (2), the time rate of change of the level of a closed lake is determined by

$$\frac{dz}{dt} = (P_L - E_L) + \frac{A_B(z)}{A_L(z)}(P_B - E_B). \quad (3)$$

Upon making the substitutions $R = R_i = (P_B - E_B)A_B(z)$ and $A = A_L(z)$, the discrete form of Eq. (3) can be written as

$$\Delta z = \left[(P_L - E_L) + \frac{R}{A}\right]\Delta t. \quad (4)$$

The general response of lake level to change in the hydrological balance can be discussed using Eq. (4). For simplicity, we will assume that $P_L - E_L$ is constant, and the lake is at steady state with its initial hydrological budget. At time t_0 with the lake at elevation z_0 and surface area A_0, a climate change occurs such that $R_1 > R_0$, where R_1 indicates the changed runoff value and R_0 the initial runoff value. Because $P_L - E_L$ is a constant (per unit surface area), the new steady-state surface area A_1 will be greater than A_0. Depending on the size of the change in runoff, and on the morphometry of the basin (i.e., the relation of surface area to elevation), the change in level Δz will be larger with each time step Δt immediately following the climate change, and then will increase at a decreasing rate as the surface area of the lake slowly approaches a new steady-state surface area A_1 and the algebraic difference between (R/A_1) and $(P_L - E_L)$ approaches zero (for closed lakes in general $P_L < E_L$). Conversely, if $R_1 < R_0$, then $A_1 < A_0$, and the lake will fall to its steady-state surface area with a trajectory having characteristics similar to those of the rising lake. The nature of these responses to hydrological change suggests that the level trajectories of closed lakes to steady state are asymptotic (Fig. 8).

This asymptotic response is quantified by a more rigorous mathematical treatment of the hydrological budget equations. Such a quantification can be obtained by integrating the differential Eq. (3), which, after algebraic manipulations, yields the solution

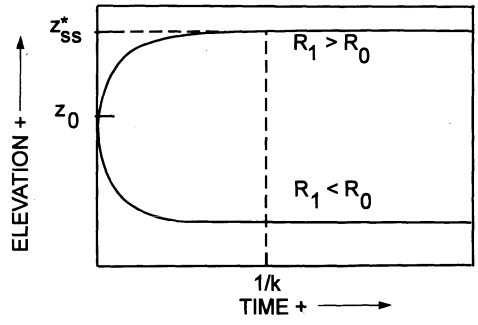


Fig. 8. Example of steady-state trajectories of lake level. (See text for notation)

$$z^*(t) = z^*_{ss}(t)(1 - e^{-kt}), \quad (5)$$

where $z^*(t) = z(t) - z(t_0)$ is the change in level relative to the initial steady-state level $z(t_0)$ at t_0 (Fig. 8). The initial steady state is determined by $Q_0A_L(z_0) = R_oA_B(z_0)$, where $Q_0 = E_L - P_L$ and $R_0 = P_B - E_B$. The new steady-state change in level z^*_{ss} is computed by

$$z^*_{ss} = \frac{A_B(z_0)\Delta R - A_L(z_0)\Delta Q}{\alpha(Q_1 + R_1)}, \quad (6)$$

where ΔQ and ΔR are the hydrological changes at t_0, $Q_1 = Q_0 + \Delta Q$, $R_1 = R_0 + \Delta R$, and $\alpha = dA(z)/dz$ at $z = z_0$. The rate of change of level k in Eq. (5) is computed by

$$k = \frac{\alpha}{A_L(z_0)}(Q_1 + R_1). \quad (7)$$

From Eq. (6) it is clear that whether a lake rises or falls toward a new equilibrium is determined by the sign of the numerator. If $\Delta R > 0$ and $\Delta Q < 0$ (i.e., wetter conditions from higher precipitation or reduced evaporation, or both) then the numerator is positive (rising level). If $\Delta R < 0$ and $\Delta Q > 0$ (i.e., drier conditions from reduced precipitation or increased evaporation or both) the denominator is negative (falling level). The time required for the lake to achieve steady state is given by the value of 1/k (Fig. 8). The rate of change of lake level k in response to a hydrological change is a function of the hydrological budget and of the bathymetry of the lake. From Eqs. (6) and (7) it can be generalized that steep-sided lakes (α small) will respond to a given hydrological change slower than lakes occupying broad, gently sloped basins (α large), with the rate of response depending on the initial level (area) of the lake. All other factors being equal, broad, gently sloped basins (α large) are thus better recorders of rapid, low-amplitude climate changes, whereas deep lakes in narrow basins (α small) are usually better recorders of high-amplitude, low-frequency changes.

4 Hydrological Models

Numerical models of lake level are physically based (i.e., incorporate the hydrological budget equations), statistical (i.e., make use only of the statistical properties of lake-level records), or some combination thereof. A simple model that is useful for investigating lake level response to changes in P, E, and inflow can be obtained by incorporating Eq. (4) into a computer program. Such a program can be used to reconstruct past lake levels, and provides useful insights into the dynamics of lake level change (e.g., Hostetler and Benson 1990). More complex, lake-specific models are built by incorporating more detailed representations of the hydrological budget (e.g., Stauffer 1985). Instead of using observed data, or simply varying model inputs and outputs, other physically based models can be used to simulate the components of the hydrological budget, such as ground-water flow (Winter, this Vol.), surface runoff (Crowley 1990), and, as is discussed in the following sections, evaporation (e.g., Adams et al. 1986; Crowley 1989; Hostetler and Bartlein 1990; Hostetler and Benson 1990). By modeling these hydrological components consistent, interactive responses of lake systems to prescribed climatic and hydrological conditions are obtained, although some degree of uncertainty is associated with the modeled values. Statistical (time-series) models are useful for identifying underlying characteristics (e.g., periodicities) in historical lake-level records (e.g., Küzel and Kesslar 1986), and, with limitations, for making future projections of lake level (e.g., Privalsky 1989; Woodbury and Padmanabhan 1989). Applications of lake-level models is discussed later in this chapter.

5 Thermal Response

All lakes exhibit some degree of regular variation in water temperature that corresponds to seasonal cycles of the prevailing climate. The primary control of the seasonal cycle of water temperature at a given latitude (Fig. 9) is the seasonal cycle of insolation (short-wave or solar radiation) received at that latitude (Fig. 10). Lakes in the equatorial belt stay warm year round and display relatively low-amplitude temperature cycles. From the mid-latitudes poleward, mean annual lake temperature decreases, but the amplitude of the temperature cycle increases in correspondence with that of insolation. Superimposed on the seasonal cycle of temperature are shorter-term (one to several days or more), irregular variations that occur in response to macro- and meso-scale atmospheric disturbances such as the passage of cold fronts (Fig. 11). Diurnal variations of water temperature result from the day–night contrast in

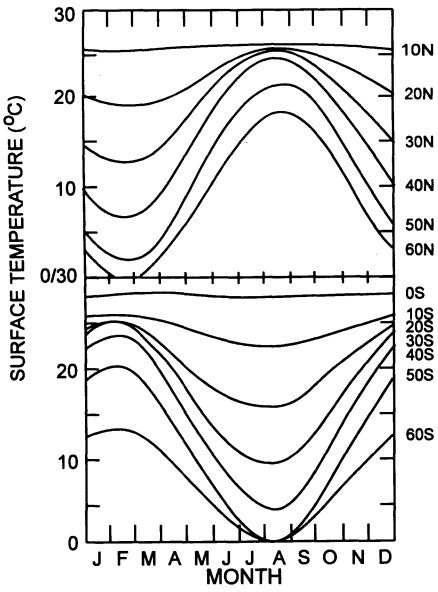


Fig. 9. Annual variation of lake-surface temperature by latitude as estimated by empirical equations. (Modified from Staskraba 1980)

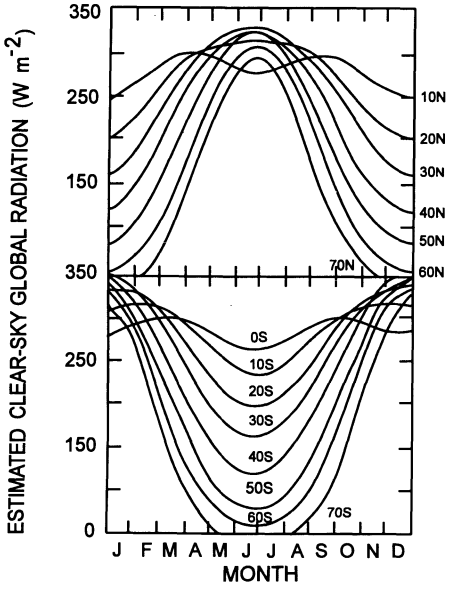


Fig. 10. Estimated annual variation in the latitudinal distribution of clear-sky, global short-wave radiation at the ground. (Modified from Straskraba 1980)

solar insolation and local weather conditions such as gusty winds or cloud cover.

Associated with the latitudinal contrast in temperatures is a similar contrast in the stability of lakes (resistance to wind-driven mixing; Hutchinson 1957; Straškraba 1980; Wetzel 1983). In freshwater lakes this stability is a function of density contrasts in the water column that to a first-order approximation are determined by temperature. [Other physical properties, such as the effects of water chemistry on density, can also be as or more important in determining stratification characteristics of some lakes (e.g., Imboden and Wüest, this Vol.)]. As a result of resistance to mixing, the predominant feature of the annual cycle of lake temperature is the pattern of vertical temperature stratification.

5.1 Energy Budget and Energy Budget Models

The heating of a lake is governed by the partitioning of energy (heat) at the lake surface. If negligible heat transfer occurs between the water in a lake and the underlying sediments, and the lake is unfrozen, the surface energy balance (SEB) is

$$\frac{dq_s}{dt} = (1 - \alpha_{sw})\phi_{sw} + (1 - \alpha_{lw})\phi_{lw} - \phi_{lu} - q_{le} - q_h, \quad (8)$$

where $\frac{dq_s}{dt}$ is the change in lake heat storage in in the surface layer [W/m^2]. α_{sw} is short-wave albedo (reflectivity) of lake surface [dimensionless]; ϕ_{sw} is global short-wave (direct + diffuse) radiation [W/m^2]; α_{lw} is long-wave albedo of lake surface [dimensionless]; ϕ_{lw} is atmospheric long-wave radiation [W/m^2]; ϕ_{lu} is long-wave radiation from lake surface [W/m^2]; q_{le} is latent heat flux, positive if directed away from lake [W/m^2]; and, q_h is sensible heat flux, positive if directed away from lake [W/m^2].

Lake temperature is a measure of the heat stored in a lake. Rearranging Eq. (8) to equate discrete changes in the heat storage in the surface layer to the remaining components of the SEB, and converting change in heat storage to change in temperature per unit time yields

$$\frac{\Delta T}{\Delta t} = \frac{1}{\rho c \Delta z}[(1 - \alpha_{sw})\phi_{sw} + (1 - \alpha_{lw})\phi_{lw} - \phi_{lu} \pm q_{le} \pm q_h], \quad (9)$$

where ΔT is the change in temperature, Δt the time increment, ρ the density of the water, c specific heat of water, and Δz the thickness of the surface layer. Roughly 40% of the net solar radiation passes through the surface layer and is

absorbed at depth in accordance with Beer's law of light transmission in water:

$$\Phi(z) = (1 - \beta)(1 - \alpha_{sw})\phi_{sw}e^{-\eta(z-\Delta z)}, \quad (10)$$

where Φ is energy absorption at depth z (z = 0 at the lake surface), β is the percentage of the solar radiation absorbed in the surface layer (Δz m), and η is the light extinction coefficient. The rate of absorption is determined by the value of the light-extinction coefficient, which varies from greater than one in turbid water to 0.02 in very clear water. Equations (8–10) provide the basis for thermal models that are discussed later in this section.

The components of the energy budget are either measured or computed from expressions that incorporate relevant meteorological parameters (e.g., Henderson-Sellers 1986; US Army Corps of Engineers 1986; Oke 1987; Tennessee Valley Authority 1972). Solar radiation and atmospheric long-wave radiation can be computed, but because these radiation inputs drive the SEB, when possible, it is better that they are measured directly with radiometers. Back radiation from the lake surface is computed as

$$\phi_{lw} = \varepsilon\sigma(T_w + 273.15)^4, \quad (11)$$

where ε is emissivity ($\equiv$0.97), σ is the Stefan-Boltzmann constant ($5.67 \times 10^{-8}\,W\,m^{-2}\,K^{-4}$), and T_w is the temperature of the surface (°C).

The average daily flux of latent heat (evaporation) can be computed from an empirical mass-transfer equation (Brutsaert 1982):

$$q_{le} = L_v N_{mt} U_2 (e_o - e_a), \quad (12)$$

in which L_v is the latent heat of vaporization, N_{mt} is the mass-transfer coefficient, U_2 is the wind speed at 2 m, e_o is the saturated vapor pressure at the temperature of the lake surface, and e_a is the air-vapor pressure of the atmosphere. The mass-transfer coefficient is determined as a function of the surface area of the lake (Brutsaert 1982):

$$N_{mt} = 3.367 \times 10^{-9} A^{-0.05}. \quad (13)$$

Saturated vapor pressure is computed using the equation of Richards (1971):

$$e_o = 101.325 \exp(13.3185t_k - 1.976t_k^2 - 0.6445t_k^3 - 0.1229t_k^4), \quad (14)$$

with $t_k = 1 - [373.15/(T_w + 273.15)]$. Air-vapor pressure can be computed by substituting air temperature for T_w in Eq. (14), and multiplying the result by the decimal-equivalent of relative humidity.

Diurnal variations in the stability of the atmospheric boundary layer can strongly affect the flux of latent heat (evaporation rate). When the boundary layer is unstable (lake warmer than air) the flux of latent heat is enhanced relative to that under stable conditions. A mass-transfer formula (Ryan et al. 1974; Weisman, 1975) that accounts for stability conditions is

$$q_{le} = [b_0(T_{sv} - T_{av})^{1/3} + N_{mt}U_2](e_o - e_a), \quad (15)$$

where b_0 is a constant, T_{sv} is the virtual temperature of the water surface, and T_{av} is the virtual temperature of the atmosphere. If $T_{sv} > T_{av}$, the flux of latent heat is enhanced. If $T_{sv} \leq T_{av}$, the atmosphere is stable and the term involving the temperatures is set equal to zero, reducing Eq. (15) to Eq. (12).

The flux of sensible heat can be computed using a Bowen ratio approach:

$$q_h = Rq_{le}, \quad (16)$$

where the Bowen ratio R is determined by

$$R = \gamma(T_w - T_a)/(e_o - e_a) \quad (17)$$

and γ is the psychrometric constant.

A 3-year time series of meteorological variables for Pyramid Lake, Nevada, resulting from a high-resolution model of regional climate (RCM) simulation, are presented in Fig. 11. Corresponding time series of surface water temperature and the components of the SEB computed from the meteorological data are presented in Fig. 12. Because the energy balance is modulated by solar radiation, over periods of several years the components of the SEB display periodic or quasiperiodic behavior with substantial intraannual variability.

Comparison of the computed annual time series of surface temperature with the meteorological data and the components of the SEB illustrate: (1) that the high-frequency, low-amplitude variability in the meteorological data and the components of the SEB is attenuated in the water-temperature time series, (2) that there is a slight phase shift between net radiation r_n [$(1 - \alpha_{sw})\phi_{sw} + (1 - \alpha_{lw})\phi_{lw} - \phi_{lu}$] and surface temperature, i.e., maxima in lake temperature occur slightly later in the year than do the peaks in r_n, and (3) that the maxima in the flux of latent heat (evaporation) occur later in summer and fall

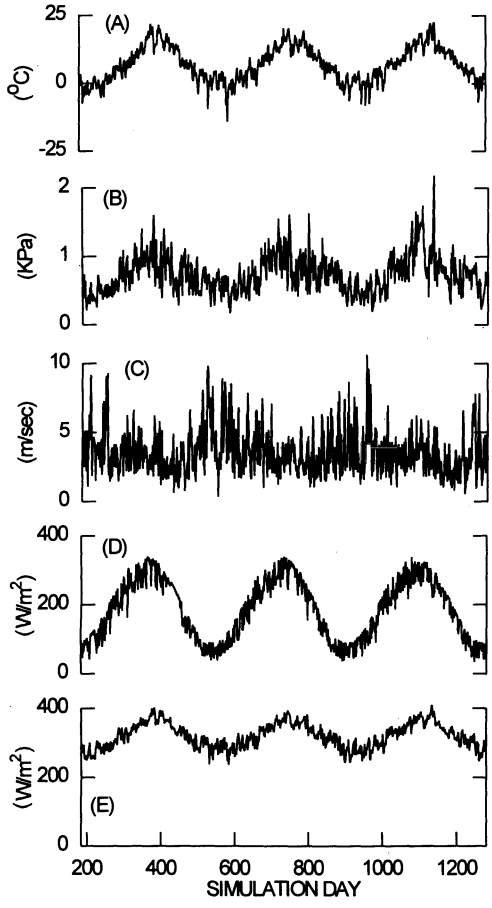


Fig. 11A–E. Three years of daily average meteorological data for Pyramid Lake, Nevada, obtained from a high-resolution climate model. **A** Air temperature; **B** air-vapor pressure; **C** wind speed at 2 m; **D** global short-wave (solar) radiation; **E** atmospheric long-wave radiation

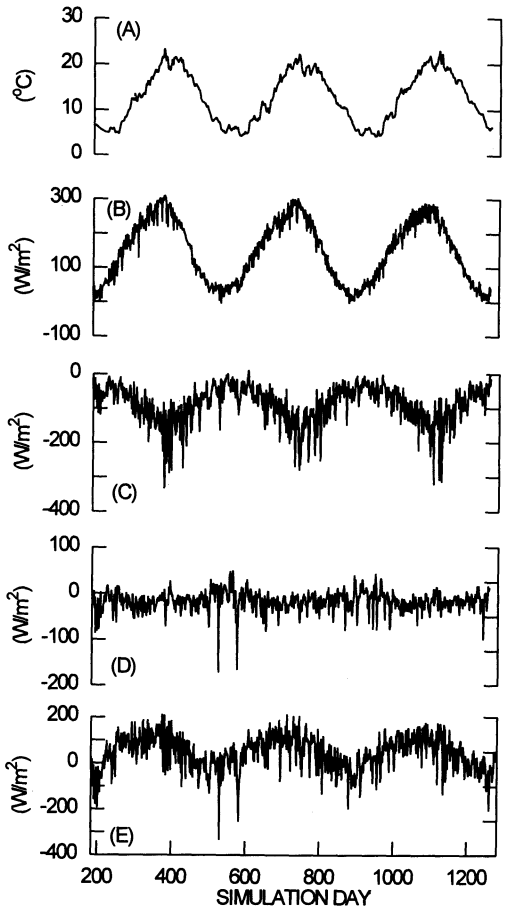


Fig. 12A–E. Three years of daily average temperature and components of the heat budget for Pyramid Lake, Nevada, as simulated by the model described in Eqs (20)–(21). **A** Surface temperature; **B** net radiation; **C** latent heat flux; **D** sensible heat flux; **E** change in heat storage

than the maxima in water temperature and r_n. These three characteristics are effects of thermal inertia, which is associated with the high heat capacity of water (at 4 °C, 4.18 MJ of heat are required to raise the temperature of 1 m^3 of freshwater by 1 °C). In temperate climates evaporation from lakes that store substantial heat peaks during the late summer, fall, and even early winter while the lake surface is warmer than the overlying air and atmospheric moisture levels tend to be lower.

Although the SEB and subsurface absorption of solar radiation adequately account for the heating of most lakes, there are settings in which other sources and sinks of heat are important components of the annual heat budget. In some lake basins large volumes (relative to lake volume) of warm or cold inflow (outflow) advect heat into (out of) the lake and thus must be considered in the heat budget. An additional component of the heat budget also must be considered in shallow lakes wherein heat is transferred between the water and underlying sediments by conduction. In clear lakes the sediments can be heated directly by penetrating solar radiation. [Solar radiation can also be reflected back (upwell) into the water if the albedo of the sediments is high.] The annual flux of heat across the bottom is roughly sinusoidal in form, and is determined by the annual cycle of water temperature and by properties of the sediments. The sediments are generally a sink to heat during spring and summer warming, and a source of heat during fall and winter (Hutchinson 1957; Dutton and Bryson 1962; Hughes 1967).

For lakes that develop winter ice cover, additional terms must be included in the SEB to account for the energetics of ice accretion and ablation (and snow cover). The formation, growth, and melting of ice is governed by the SEB, penetration of solar radiation, and by heat supplied from the underlying water (Ragotzkie 1978; de Bruin and Wessels 1988; Patterson and Hamblin 1988). Of these factors, the SEB dominates, and ice morphology can be predicted (Patterson and Hamblin 1988; Hostetler 1991):

$$-q_i = (1 - \alpha_{sw})\phi_{sw} + \phi_{lw} - \phi_{lu} - q_{le} - q_h \quad (T_s < T_f) \tag{18a}$$

$$-q_i = (1 - \alpha_{sw})\phi_{sw} + \phi_{lw} - \phi_{lu} - q_{le} - q_h + \rho L\frac{dh}{dt} \quad (T_s = T_f), \tag{18b}$$

where q_i is the upward heat flux just below the ice (snow) surface, T_s the surface temperature, T_f the freezing-point temperature, ρ the density of the ice (snow), L the latent heat of the ice (snow), and dh/dt the time rate of change of ice thickness. Equation (18a) is associated with ice formation, and Eq. (18b) with ablation of ice (snow) at the surface. Ice formation and ablation at the water–ice interface is determined by

$$\rho L\frac{dh}{dt} = -q_i + \phi_{pen} + q_w, \tag{19}$$

where ϕ_{pen} is the solar radiation penetrating the ice and snow, and q_w is the flux of heat from the underlying water to the ice.

Thermal stratification and lake mixing are affected by nonclimatic factors such as basin morphometry (surface area and depth), the geostrophic Coriolis force that arises from the rotation of the Earth, and the physical (e.g., turbidity) and chemical (e.g., salinity) properties of lake water (Hutchinson 1957; Straškraba 1980; Wetzel 1983; Henderson-Sellers 1984; Kirk 1988; Imboden and Wüest, this Vol.). Shallow lakes often do not exhibit persistent temperature stratification because it is effectively suppressed by full-depth solar heating and wind-driven mixing, which result in isothermal conditions. Stratification and vertical-temperature contrasts in shallow lakes therefore frequently follow the diurnal patterns of solar radiation and winds. In turbid or eutrophic lakes penetrating short-wave radiation is absorbed and scattered near the surface, resulting in generally shallower thermoclines than are found in clear (oligotrophic) lakes where subsurface heating is distributed to greater depths (Henderson-Sellers 1984, 1988).

5.2 Models and Modeling

The importance of lake thermal cycles in influencing a broad spectrum of limnological processes has motivated the development of empirical and physically based models that calculate lake temperature. Empirical methods for estimating lake surface temperature as a function of latitude have been derived (e.g., Straškraba 1980), and many empirical relations have been used to estimate summer stratification as a function of basin morphometry and wind fetch (the unobstructed water surface exposed to the wind; see Ragotzkie 1978; Arai 1981; Melack 1984; Patalas 1984). Empirical methods can yield useful first-order approximations of lake temperature or mean thermocline depth, however, these methods are not suited for assessing the effect of climatic change on the thermal behavior of a lake, nor can they be used to investigate the dynamics of limnological processes.

The climatic forcing of the thermal behavior of lakes can be simulated by physically based numerical models. For very shallow lakes in which heat storage is relatively minor and therefore the annual cycle of lake temperature is more or less in phase with that of the overlying air, a "zero-dimensional" (0D) model based only on the SEB (Eq. 7) may provide adequate simulations of surface temperature and evaporation (Keijman 1974; Eggers and Tetzlaff 1978). In deeper lakes the seasonal storage and loss of heat is a substantial component of the energy budget that must be addressed in models of water temperature. Two- and three-dimensional models have been developed for this purpose, but one-dimensional (1D) models that resolve only vertical changes in temperature are more widely used. One-dimensional models incorporate the physics of the processes that are most important in governing lake temperature (imbalance in the SEB, absorption of penetrating solar radiation, turbulent mixing, and convection). Two- and three-dimensional mixing mechanisms (e.g., Imboden and Wüest, this Vol.) are not treated in 1D models.

One-dimensional models calculate lake temperature as a function of the vertical transport

and generation of heat. Originally developed for oceanic applications, these models can be broadly classified as energy-balance models, because the SEB and subsurface absorption of solar radiation provide the primary forcing of model response. There are two general categories of 1D thermocline models, mixed layer models (MLMs) and eddy diffusion models (EDMs), that are differentiated with regard to how turbulence (e.g., Imboden and Wüest, this Vol.) is represented. In both types of models turbulence is parameterized, i.e., derived coefficients or relationships are used to represent the physical process. Parameterizations are used in MLMs to account for the budget of total kinetic energy (TKE) in the mixed layer or epilimnion (Niiler and Kraus 1977; Henderson-Sellers and Davies 1989). Turbulent mixing also can be parameterized as eddy diffusion (e.g., Munk and Anderson 1948; Henderson-Sellers 1976, 1982, 1985; Lewis 1982; Pond and Pickard 1983; Powell et al. 1984; Hearn 1988).

Eddy diffusion was first used by atmospheric scientists to approximate atmospheric turbulence. It was developed from Prandtl's mixing-length theory (e.g., Hutchinson 1957), in which turbulent mixing is characterized by analogy to molecular diffusion, and turbulent velocities are represented by an average velocity term. As with all parameterizations there remain questions about the theoretical basis of the eddy diffusion parameterization, particularly with regard to representing turbulence by an average velocity (e.g., Harleman 1982; Pond and Pickard 1983; Kraus 1988; McCormick and Meadows 1988), but the parameterization is widely used in both atmospheric and lake models.

The EDMs are conceptually and computationally the simplest of the physically based thermal models. The models have been demonstrated to be adequate for simulating surface temperature, evaporation, and the seasonal pattern of thermal stratification in lakes and oceans (e.g., Dake and Harleman 1969; Holland 1976; McCormick and Scavia 1981; Martin 1985; Babajimopoulos and Papadapoulos 1986; McCormick and Meadows 1988; Hostetler and Bartlein 1990; Hostetler and Benson 1990; Vassiljev et al. 1994).

A submodel for simulating the formation and melting of ice cover is needed in addition to a water-temperature model for modeling lakes that develop ice cover. Like water-temperature models, the most widely used type of model for simulating ice and snow cover of lakes are 1D models that are driven by the SEB (Eqs. 18 and 19; e.g., Chen and Orlob 1972; Pivovarov 1973; Semtner 1976; Matthews and Heany 1987; de Bruin and Wessels 1988; Patterson and Hamblin 1988; Hostetler 1991; Croley and Assel 1994). In application, a thermal model is used to calculate water temperature until the surface waters are cold enough to freeze, and then an ice model is used to simulate the growth and melting of ice. The thermal model is employed again after the ice melts.

The minimum set of input data for 1D thermal and ice models includes short- and long-wave radiation, wind speed, air vapor pressure or relative humidity, air temperature, (Fig. 11), and an estimate of the turbidity of the water. Most models also incorporate bathymetric data to account for the effects of lake morphometry on mixing and stratification (e.g., Ford and Stefan 1980).

The numerical model of Hostetler and Bartlein (1990) provides an example of a 1D EDM that includes features that are common to most EDMs: a parameterization of eddy diffusion (Henderson-Sellers 1985) and subsurface absorption of solar radiation (Fig. 13). Following Eq. (7), the model is written symbolically as

$$\frac{\partial T}{\partial t} = \frac{1}{A(z)}\frac{\partial}{\partial z}\left\{A(z)[k_m + K(z,t)]\frac{\partial T}{\partial z}\right\} + \frac{1}{A(z)}\frac{(\partial A(z)\Phi)/\partial z}{\rho c_p}, \quad (20)$$

where $A(z)$ is lake area at depth z; k_m is molecular diffusivity of heat; $K(z,t)$ is eddy diffusivity of

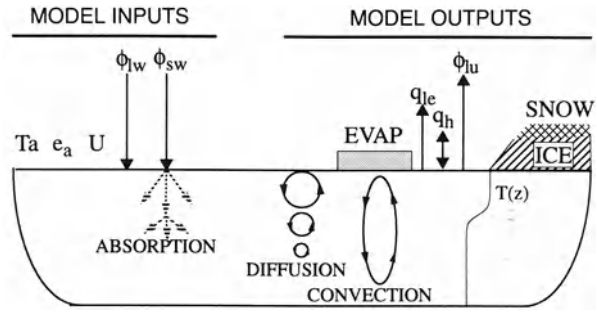


Fig. 13. Portrayal of the input and output of the eddy diffusion model. Radiation and flux terms are defined in Eq.(8). e_a Air-vapor pressure; T_a air temperature; U wind speed, saturated air-vapor pressure at the lake surface; $T(z)$ temperature/depth profile

heat; and Φ is the short-wave radiation absorption term.

The SEB is incorporated into Eq. (20) through the surface boundary conditions

$$-[k_m + K(z,t)]\frac{\partial T}{\partial z} = (1 - \alpha_{sw})\phi_{sw} + (1 - \alpha_{lw})\phi_{lw} - \phi_{lu} - q_{le} - q_h, \quad (21)$$

where z is positive downward (into the lake). A specified temperature-depth profile provides initial conditions, and an insulated bottom is assumed ($\partial T/\partial z = 0$). The equations used to compute the components of the SEB are those given in Eqs. (11–17).

On the right side of Eq. (20), the first term represents the transfer of heat by molecular diffusion and eddies, and the second term represents sub surface heating by penetrating short-wave radiation. A simple, density-driven convective mixing scheme is included in the model, as are variable bathymetry and an ice submodel (Hostetler 1991). An explicit, finite-difference numerical technique [forward time centered space (FTCS), e.g., Noye 1984] is employed using an hourly or daily time step to implement the model on a computer.

Thermal models also can be used to simulate the behavior and distribution of nutrients, biomass (e.g., Imberger and Patterson 1981; Harleman 1982; Henderson-Sellers 1984; US Army Corps of Engineers 1986; Riley and Stefan 1988) and stable isotopes in lakes (Hostetler and Benson 1994). Many nutrients and chemical species are not uniformly distributed with temperature in the water column, and are better modeled by MLMs, because they are able to account for the high-frequency variability of turbulent mixing. Stable isotopes, for example, are uniformly distributed with temperature in the water column, and therefore can be modeled by an EDM.

6 Use of Models to Link Lakes with Climate Change

The models discussed previously are well suited for assessing the effect of climate change on the thermal and hydrological states of lakes. Thermal models can provide insights into how temperature and evaporation may have changed in the past, or what their sensitivities might be under the influence of possible future climates. Lake-level models can be used to evaluate the effects of climatically induced changes in the hydrological budget. Because evaporation is common to both the energy and hydrological budgets, thermal and lake-level models can also be linked.

In this section selected applications of lake models are presented to demonstrate some of the possible ways the models can be used in climate-change studies. One application focuses on assessing the possible response of Yellowstone Lake, Wyoming, to warmer climatic conditions, and three applications demonstrate how thermal and lake-level models can be combined to reconstruct historical and paleolake levels.

7 Input Data Sets

Assessments of past or future lake temperature, evaporation, and level require input data sets both for present and changed climates. Present-day or control data are used to validate a model and to provide baseline or control data that can be modified to reflect changed climate. Validating a model provides an evaluation of the ability of the model to reproduce observed conditions, and an indication of the sensitivity of the model to its parameters and to meteorological forcing (e.g., Tucker 1982; Henderson-Sellers 1988; Vassiljev et al. 1994).

Input data representing changed climates can be derived in several ways. For thermal modeling a straightforward approach that provides insight into the possible range of responses of a lake to past or future climates is to modify a control data set by applying a range of perturbations to the various meteorological parameters (e.g., ±2, 4, and 6 °C changes in mean annual air temperature). Meteorological data sets representing changed climate can also be derived by modifying control data to reflect changes in climatic conditions simulated by numerical climate models. Most lake studies that have employed this approach have made use of output from general circulation models (GCMs). The GCMs produce climate output (e.g., air temperature, humidity, wind velocities, and radiation) on the order of several degrees in latitude by several degrees in longitude. At this rather coarse resolution the accuracy of the simulated climate variables can be poor at a regional or local scale (Grotch 1988; Mearns et al. 1990; Grotch and MacCracken 1991). To

minimize errors associated with GCM simulations, output from the models is not used directly, but rather is used to derive model input by adjusting control data with relative differences or anomalies between simulated present and changed climates. This approach has been applied in lake-modeling studies to assess possible changes in lake temperature and mixing (e.g., McCormick 1990; Hondzo and Stefan 1993), and evaporation (Croley 1990) for warmer climatic conditions.

A new type of atmospheric model, a model of regional climate (RCM), appears to hold promise for providing climatic variables for lake models. The RCMs are run over a limited area or region at much finer resolutions (tens of kilometers in latitude and longitude) than GCMs, and therefore can provide better detail of meteorology that begins to reflect, for example, the influence of mountain ranges on the climate of the region. Hostetler and Giorgi (1993, 1994) have demonstrated that it is possible to use output from an RCM directly in thermal models, which allows simulation of temperature and evaporation for present and changed climates without the need for applying relative anomalies to control data. In addition, the fine resolution of RCMs is amenable to coupling of the models with lake models to enable simulations of lake-atmosphere interactions (Bates et al. 1993; Hostetler et al. 1993, 1994). As is the case with GCM output, estimates of lake temperature and evaporation derived from RCM output are consistent with modeled climates, but are subject to the uncertainties associated with using output from atmospheric models (Hostetler and Giorgi 1993, 1994).

Statistical models can be used to generate (synthetic) time series of meteorological variables for input to thermal models. Because these methods rely on the statistical properties (mean, variance) of past meteorological conditions, however, they are applicable only under the assumption of a stationary climate, i.e., no change in average conditions. Statistical models can be used to generate probability distributions of future lake levels (e.g., Privlasky 1989; Woodbury and Padmanabhan 1989), but these models also are restricted to stationary climate conditions, and therefore are not suitable for climate-change studies.

A variety of methods must be used to derive data sets for the application of lake models in a paleoclimatic context. Analyses of biological geological, and geochemical indicators provide broad indications of past climates such as large changes in mean annual air temperature and effective wetness. These proxy indicators can be combined with results from GCM simulations of paleoclimate (e.g., Saltzman 1990, and citations therein), and, along with the method of specifying ranges to changes, can yield quantitative estimates of climatic and hydrological parameters for lake modeling. Although the relative changes between modern and paleoclimates are often large, there is a great deal of uncertainty associated with quantitative inferences of paleoclimate.

8 Sample Applications

An assessment of the potential effects of global warming on the thermal regime of Yellowstone Lake, Wyoming, was made by Hostetler and Giorgi (1994) using a model similar to that of Eqs. (20) and (21). Hourly meteorological data, obtained from the output of climate simulations conducted with an RCM (Giorgi et al. 1994), were used as input to the model. The thermal model was run for 3 years, both for present and projected future climate under a doubling of atmospheric carbon dioxide concentrations ($2 \times CO_2$). The RCM output, which are from the last 3 years of a 20-year simulation, represent stationary, but different, climatic conditions. Relative to the present climate of Yellowstone Lake, the $2 \times CO_2$ climate is characterized by an increase in mean annual air temperature (from 1.0 to 4.4 °C) and a corresponding increase in the mean annual flux of atmospheric long-wave radiation (from 287 to 305 $W m^{-2}$). Mean annual surface temperatures for the open-water periods

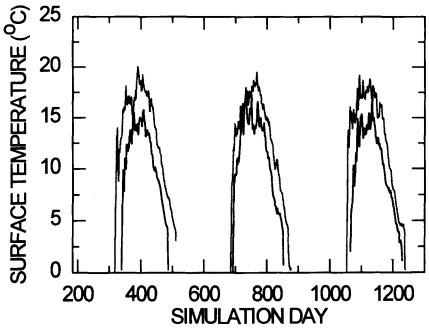


Fig. 14. Three years of simulated surface temperature of Yellowstone Lake, Wyoming, for the open-water periods; present (*solid line*) and for a case of climatic warming (*broken line*). (Hostetler and Giorgi 1994)

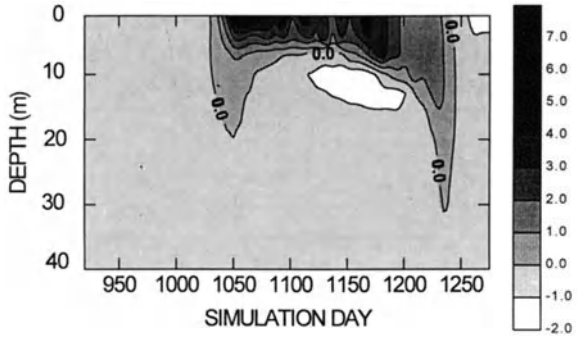


Fig. 15. Present water temperatures minus 2 × CO_2 water temperatures for Yellowstone Lake, Wyoming. Differences are for the last year of 3-year simulations. Scale temperatures in °C, and contour interval of 1 °C. (Hostetler and Giorgi 1994)

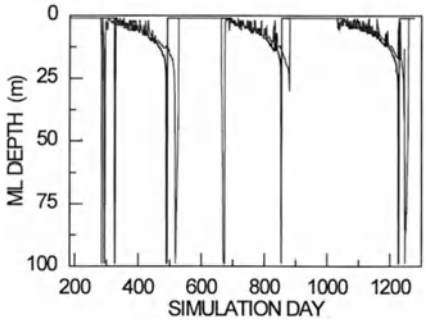


Fig. 16. Three years of the simulated depth of the mixed layer of Yellowstone Lake, Wyoming, for the present (*solid line*) and for 2 × CO_2 (*broken line*). (Hostetler and Giorgi 1994)

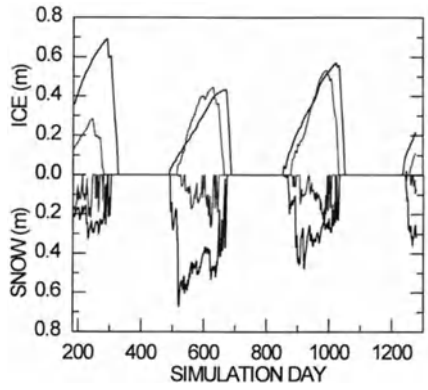


Fig. 17. Three years of simulated ice thickness and snow depth for Yellowstone Lake, Wyoming, for the present (*solid lines*) and 2 × CO_2 (*broken lines*). (Hostetler and Giorgi 1994)

of the lake increased from 11.6 °C for the present to 13.2 °C for the 2 × CO_2 climate (Fig. 14), with the warming mostly confined to the near-surface waters (Fig. 15). Relative to the present, turnover of the lake was simulated to occur earlier in the spring and later in the fall for the warmer climate (Fig. 16), and the mean annual duration of winter ice cover was reduced from approximately 196 days to approximately 153 days (Fig. 17). Computed mean annual evaporation rates increased from 544 mm for the present to 600 mm for the 2 × CO_2 climate. Although it is not definitive, this application demonstrates the use of RCM output in a thermal model and suggests the magnitude of changes that could occur in this large, high-altitude lake from global warming. The output from the lake model could be used further to assess the effects of warmer water conditions on the habitat of the Yellowstone cutthroat trout if the appropriate models were available (e.g., Christie and Regier 1988; Magnuson et al. 1990).

Historical lake-level fluctuations can be reconstructed with numerical models using a combination of measured and modeled input. These reconstructions provide a method for testing lake models, and can be used to investigate the sensitivity of a lake to climate change. Fluctuations of Harney-Malheur Lake, Oregon, that occurred before, during, and after a climatic shift that began in 1982 were reconstructed by Hostetler and Bartlein (1990) using simulated evaporation rates and measured inflows and precipitation. The daily input data (Fig. 18) for the thermal model were assembled from measurements made at nearby weather and solar radiation monitoring stations, and from computed estimates made using the measured data. Simulated daily evaporation rates were accumulated into monthly totals, and monthly lake levels were computed using measured river discharge and precipitation as well as estimated ground-water discharge (Fig. 19). This application demonstrates how climatically determined fluctuations of lake-level can be simulated using coupled thermal and hydrological models and a combination of measured and estimated of meteorological and hydrological input data.

A similar approach was used by Hostetler and Benson (1994) to reproduce the multiyear evolution of the stable isotope of oxygen $\delta^{18}O$ in Pyramid Lake, Nevada. The seasonal behavior of $\delta^{18}O$ during 1987–1989 (Fig. 20) was simulated by coupling the equations of isotopic transport (including inflows) with the EDM of Eq. [20]. A

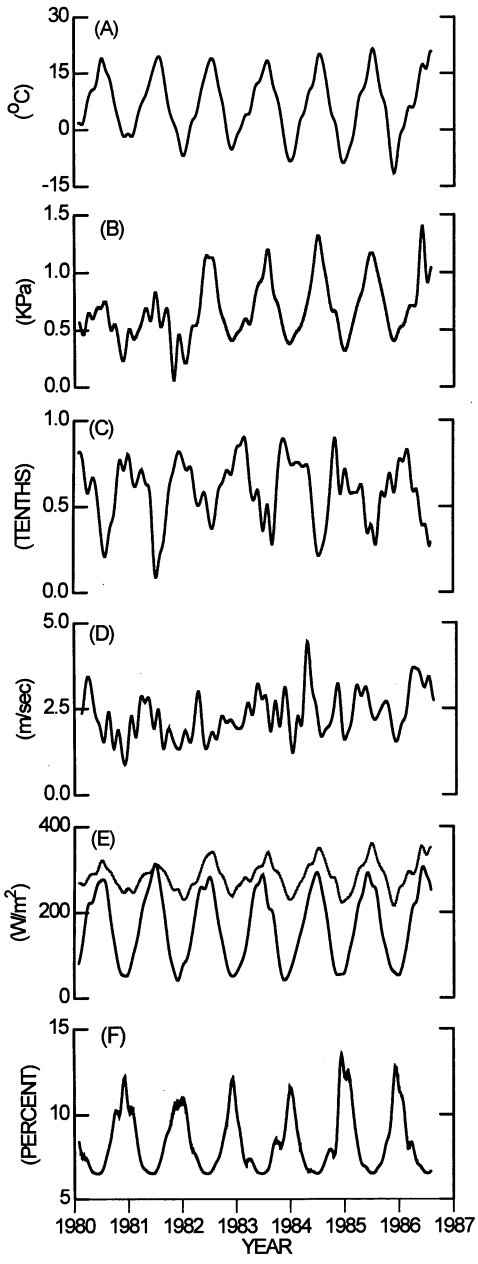


Fig. 18A–F. Daily meteorological data for Harney-Malheur Lake, Oregon, for the period 1980–1986. **A** Air temperature; **B** air-vapor pressure; **C** cloud cover; **D** wind speed; **E** solar radiation (*solid line*) and atmospheric radiation (*broken line*); **F** short-wave albedo of the lake surface. (Hostetler and Bartlein 1990)

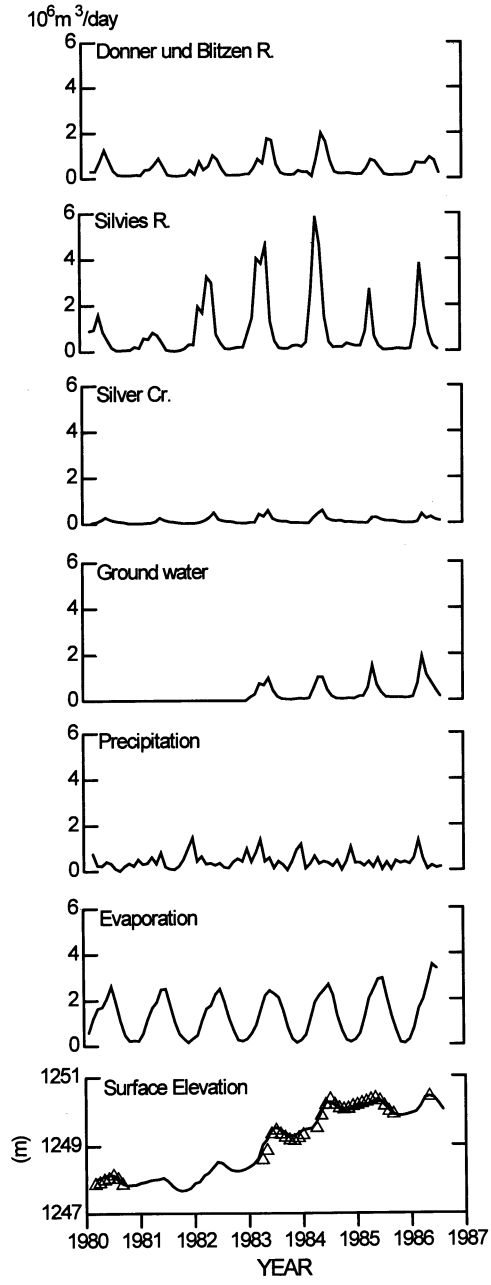


Fig. 19. Monthly water inputs to Harney-Malheur Lake, Oregon, for the period 1980–1986 and simulated (*solid line*) versus measured (*triangles*) lake level for the same period. (Hostetler and Bartlein 1990)

longer-term reconstruction of level and $\delta^{18}O$ (Fig. 21) was achieved using monthly average values of evaporation, epilimnion temperature, and mixed-layer depth from the 1987–1989 simulation, along with measured inflow and precipitation in the lake-level model. Stable isotopes play a key role in studies of the hydrological budget of lakes (Benson 1994; Gat, this Vol.) and in climate reconstruction (Lister et al. 1991).

In paleoclimate reconstructions lake-level fluctuations are generally of comparatively high amplitude and low frequency, and so can be thought of as being determined by long-term

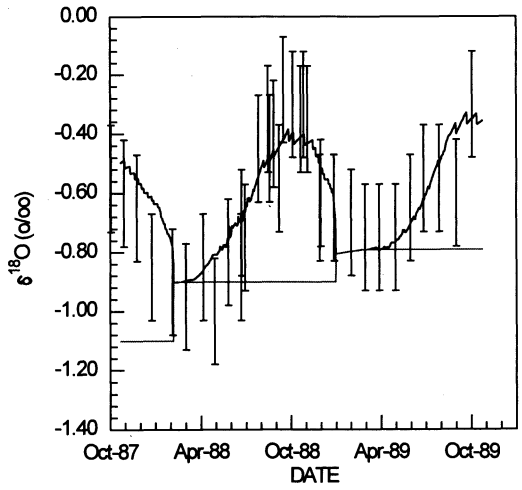


Fig. 20. Simulated epilimnetic (*solid line*) and hypolimnetic (*broken line*) values of δ18O compared with measured 1987–1989 values of the epilimnion of Pyramid Lake, Nevada. Measured values are plotted with 0.2‰ error bars. (Hostetler and Benson 1994)

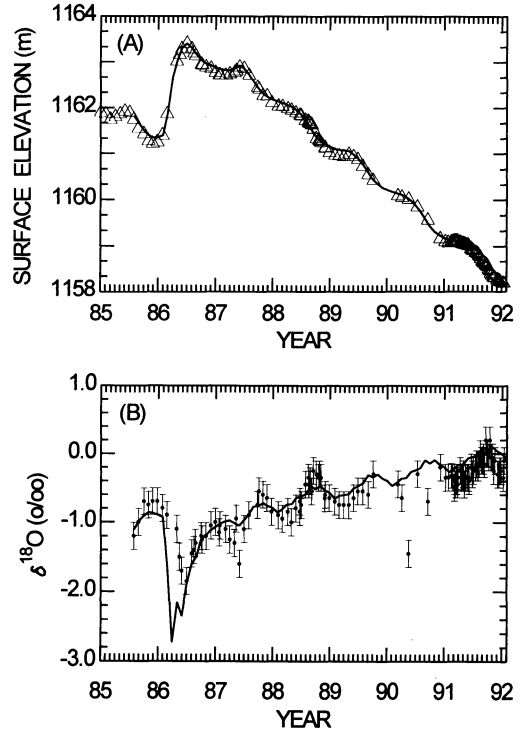


Fig. 21. **(A)** Simulated (*solid line*) versus measured (*triangles*) surface elevation of Pyramid Lake, Nevada. **(B)** Simulated (*solid line*) versus measured epilimnetic δ^{18}O values of Pyramid Lake, Nevada. Measured values plotted with 0.2‰ error bars

change of the effective wetness of a lake basin. Various combinations of precipitation and evaporation, however, can yield the same wetness and thus lake level. If either precipitation or evaporation can be bounded, then so can the range of the complementary component of effective wetness. Paleoprecipitation rates at the spatial scale of a lake basin are difficult to estimate, particularly for basins where orographical effects are strong and the water-producing portion of the basin can be effected by a climate different from that of the lake. A possible approach to modeling paleolake level is to employ some method for assessing paleoevaporation rates, which, in turn, can be used to limit the possible range of paleoprecipitation (and thus runoff). Benson (1981, 1986) demonstrated the use of an energy-budget approach (Eq. 8, without a heat storage term Δq_s) to estimate the sensitivity of paleoevaporation rates of Lake Lahontan. Kutzbach (1980) and Hanstenrath and Kutzbach (1983, 1985) applied a combined energy- and hydrological balance model to estimate the size of African paleolakes, and Adams and Tetzlaff (1984) evaluated evaporation rates and levels of paleolake Chad, Africa, with the 0D thermal model of Eggers and Tetzlaff (1978).

Hostetler and Benson (1990) combined thermal and lake-level models to reconstruct levels of Lake Lahontan (of which Pyramid Lake, Nevada, is a remnant) 18000–12000 years ago (Fig. 5). The GCM simulations (e.g., Manabe and Broccoli 1985; Kutzbach and Guetter 1986; Rind 1987) indicate that relative to today the presence of the Laurentide ice sheet caused a southward displacement of the polar jet stream over western North America during the period. A cloud climatology for Prince George, British Columbia, which is today affected by the polar jet stream in a manner similar to that hypothesized for Lake Lahontan 18000–12000 years ago, was used as an analog for computing solar radiation values, which were found to be 43% less than present on a mean annual basis. The reduced solar radiation values were combined with evidence of a 7 °C air temperature depression (indicated by nivation features) to modify a modern meteorological data set (Hostetler and Benson 1993) that reflected the paleoclimate of the Lake Lahontan. For the hypothesized paleoclimatology simulated mean annual surface temperatures of the lake were 7 °C colder than present (8 °C), and annual lake

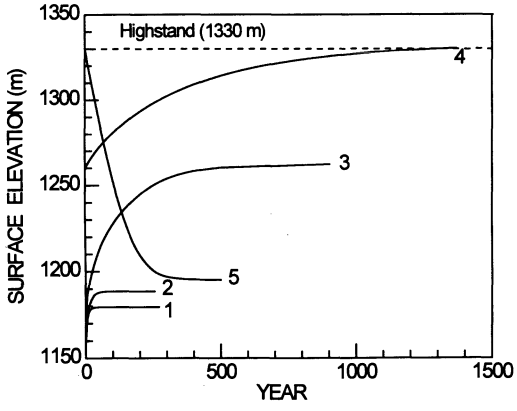


Fig. 22. Simulated level of Lake Lahontan using different hydrological balances expressed as percent change in present mean annual rates of evaporation, precipitation, and runoff, e.g., (E:10, P:10, R:10) reflects increases of 10% in mean annual evaporation, precipitation, and runoff. Trajectory T1 (E:0, P:0, R:0); T2 (E:−42, P:0, R:0); T3 (E:−42, P:76, R:140); T4 (E:−42, P:76, R:280); T5 (E:0, P:76, R:140). (Hostetler and Benson 1990)

evaporation was reduced from a modern value of 1311 to 758 mm.

A series of lake levels were simulated with these evaporation rates and assumed rates of precipitation and inflow to reproduce steady-state target levels (Fig. 22) in the level chronology (Fig. 5). These sensitivity tests indicated that the reduced evaporation rate, the mean annual observed precipitation rate over the basin, and a 3.8-fold increase in mean annual river discharge of the basin could have produced the last highstand of the lake. If winter ice cover formed on Lake Lahontan (ice cover on Pyramid Lake has not been observed) the annual evaporation rate would have been reduced even further (to 527 mm), and a 2.6-fold increase in mean annual discharge, which is within the range of the historical record, would have been sufficient to achieve the highstand (Hostetler 1991). This application demonstrates how lake models can be used to link geological records of lake level with climate and provide a plausible range of past hydrological conditions that correspond to large lake-level fluctuations.

9 Summary

The sensitivity of lake systems to climate is evident in the distribution, size, and thermal structure of lakes throughout the world. The global distribution of lakes reflects global climatic patterns while regional patterns of lake size indicate regional variability of global climate. The thermal structure of lakes is strongly dependent on climatic setting, and thus provides unique and contrasting response to climatic conditions. Changes in both the size and thermal structure of lakes recorded indirectly in lake sediments and by geological features indicate past changes in climate, rendering lakes excellent systems within which to study climate change.

Numerical models of lake size and temperature provide tools that link the physical limnology of lakes directly with the climate system. Application of these models is relatively straightforward and requires minimal computer resources. The models can be used to assess the effect of past, present, and future climates on lake size and thermal structure, and thus on lacustrine biological and chemical processes.

Acknowledgments. I thank L.V. Benson and D.L. Zahnle for their insights and support that led to the final form of this manuscript. I also thank D. Imboden for a careful critique of an earlier manuscript, and for suggestions regarding the mathematical solution of Eq. (3).

References

Adams EE, Bras RL, Harleman DRF, Puente C, Bischoff CM (1986) Short-term lake level predictions for the Great Salt Lake. In: Kay PK, Diaz HF (eds) Problems and prospects for predicting Great Salt Lake levels. Center for Public Affairs and Administration, University of Utah, Provo, Utah, pp 205–217

Adams LJ, Tetzlaff G (1984) Did Lake Chad exist around 18000 yr BP? Arch Meteorol Geophys Bioclimatol 34:299–308

Andreeva MA (1973) The long-term pattern in the level fluctuation of the Ural lakes and its relationship with atmospheric circulation. Hydrology of lakes. IAHS-AISH 109 Adlard and Son, Dorking, pp 177–181

Arai T (1981) Climatic and geomorphological influences on lake temperature. Verh Int Ver Limnol 21:130–134

Babajimopoulos C, Papadapoulos F (1986) Mathematical prediction of thermal stratification of Lake Ostrovo (Vegoritis), Greece. Water Resour Res 22(11):1590–1596

Bates GT, Giorgi F, Hostetler SW (1993) Towards the

simulation of the effects of the Great Lakes on climate. Mon Wea Rev 121:1373–1387
Benson LV (1981) Paleoclimatic significance of lake-level fluctuations in the Lahontan Basin. Quat Res 16:390–403
Benson LV (1986) The sensitivity of evaporation rate to climate change – results of an energy-balance approach. US Geol Surv Water-Res Invest Rep 86:4148
Benson LV (1994) Behavior of the stable isotopes of oxygen and hydrogen in the Truckee River-Pyramid Lake surface-water system 1: data analysis and extraction of paleoclimate information. Limnol Oceanogr 39:344–355
Benson LV, Thompson RS (1987a) The physical record of lakes in the Great Basin In: Ruddiman WF, Wright HE, Jr (eds) North America and adjacent oceans during the last deglaciation. Geol Soc Am K-3, Boulder, CO, pp 241–260
Benson LV, Thompson RS (1987b) Lake-level variation in the Lahontan Basin for the past 50 000 years. Quat Res 28:69–85
Benson LV, Curry DR, Dorn RI, Lajoie KR, Oviatt CG, Robinson SW, Smith GI, Stine S,. Thompson RS (1989) Variation in sizes of four Great Basin lake systems during the past 35 000 years. Paleogeogr Paleoclimatol Paleoecol 78:241–268
Bradley RS (1985) Quaternary paleoclimatology. Allen and Unwin, Boston, 472 pp
Brutsaert W (1982) Evaporation into the atmosphere. Reidel, Dordrecht, 299 pp
Budyko WI (1977) Climatic change. Waverly Press, Baltimore, 261 pp
Changnon SA (1987) Climate fluctuations and record-high levels of Lake Michigan. Bull Am Meteorol Soc 68(11):1394–1402
Chen CW, Orlob GT (1972) Ecological simulation of aquatic environments. Rep 11720, Water Res Eng Inc, Walnut Creek, CA, 156 pp
Christie GC, Regier HA (1988) Measures of optimal thermal habitat and their relationship to yields for four commercial fish species. Can J Fish Aquat Sci 45:301–314
COHMAP Members (1988) Climatic changes of the last 18 000 years: observations and model simulations. Science 241:1043–1052
Croley TE (1989) Verifiable evaporation modeling on the Laurentian Great Lakes. Water Resour Res 25:781–792
Croley TE (1990) Laurentian Great Lakes double CO_2 climate change hydrological impacts. Clim Change 17:27–47
Croley TE, Assel R (1994) One dimensional ice thermodynamics model for the Laurentian Great Lakes. Water Resour Res 30:625–639
Dake JMK, Harleman DRF (1969) Thermal stratification in lakes: analytical and laboratory studies Water Resour Res 5:484–495
De Bruin HAR, Wessels HRA (1988) A model for the formation and melting of ice on surface waters. J Appl Meteorol 27:164–173
Dutton JA, Bryson RA (1962) Heat flux in Lake Mendota. Limnol Oceanogr 7:80–97
Eggers KA, Tetzlaff G (1978) A simple model for describing the heat balance of a shallow lake with application to Lake Chad. Boundary-Layer Meteorol 15:204–214
Ford DE, Stefan H (1980) Stratification variability in three morphometrically different basins under identical meteorological forcing. Water Resour Bull 16:243–247
Gasse F, Fontes JC (1989) Paleoenvironments and paleohydrology of a tropical closed lake (Lake Asal, Djibouti) since 10 000 yr B.P. Paleogeogr Paleoclimatol Paleoecol 69:67–102
Giorgi F, Shields Brodeur C, Bates GT (1994) Regional climate change scenarios over the United States produced with a nested regional climate model: spatial and seasonal characteristics. J Climate 7: 375–399
Grotch SL (1988) Regional intercomparisons of general circulation model predictions and historical climate data. US Department of Energy Report TR041, Washington, DC
Grotch SL, MacCracken MC (1991) The use of general circulation models to predict regional climate change. J Climate 4:286–303
Hanstenrath S, Kutzbach JE (1983) Paleoclimatic estimates from water and energy budgets of East African Lakes. Quat Res 19:141–153
Hanstenrath S, Kutzbach JE (1985) Late Pleistocene climate and water budget of the South American Altiplano. Quat Res 24:249–256
Harleman DRF (1982) Hydrothermal analysis of lakes and reservoirs. Proc ASCE, J Hyd Div 108(HY3): 302–325
Harrison SP (1989) Lake levels and climatic change in eastern North America. Clim Dynamics 3:157–167
Harrison SP, Metcalfe SE (1985) Variations in lake levels during the Holocene in North America: an indicator of changes in atmospheric general circulation patterns. Geógr Phys Quat 39:141–150
Hearn CJ (1988) On the Munk-Anderson equations and the formation of the thermocline. Appl Math Modelling 12:450–456
Henderson-Sellers B (1976) The role of eddy diffusivity in thermocline formation. J Environ Eng Div ASCE 102(EE3):517–531
Henderson-Sellers B (1982) A simple formula for vertical eddy diffusion coefficients under conditions of nonneutral stability. J Geopys Res 87(C8):5860–5864
Henderson-Sellers B (1984) Engineering limnology. Pitman, London, 356 pp
Henderson-Sellers B (1985) New formulation of eddy diffusion thermocline models. Appl Math Modelling 9:441–446
Henderson-Sellers B (1986) Calculating the surface energy balance for lake and reservoir modeling: a review. Rev Geophys 24(3):625–649
Henderson-Sellers B (1988) Sensitivity of thermal stratification models to changing boundary conditions. Appl Math Modelling 12:31–43
Henderson-Sellers B, Davies AM (1989) Thermal stratification modelling for oceans and lakes. Annu Rev Num Fluid Dyn Heat Trans vol 2, pp 86–156

Holland WR (1976) The role of the upper ocean as a boundary layer in models of the oceanic general circulation In: Kraus EB (ed) Modeling and prediction of the upper layers of the ocean. Pergamon Press, New York, pp 7–30

Hondzo M, Stefan HG (1993) Regional water temperature characteristics of lakes subjected to climate change. Clim Change 24:187–311

Hostetler SW (1991) Simulation of lake ice and its effect on the late-Pleistocene evaporation rate of Lake Lahontan. Clim Dyn 6:43–48

Hostetler S, Bartlein PJ (1990) Simulation of lake evaporation using an energy balance/eddy diffusion model of lake temperature: application to modeling lake-level variations of Harney-Malheur Lake, Oregon. Water Resour Res 26:2603–2612

Hostetler S, Benson LV (1990) Climatic implications of highstand Lake Lahontan derived from models of evaporation and lake level. Clim Dynamics 4:207–217

Hostetler SW Benson LV (1993) Meteorological and lake temperature data for Pyramid Lake, Nevada 1987–89. US Geol Sur Open File Rep 92–159, 15 pp

Hostetler SW, Benson LV (1994) Behavior of the stable isotopes of oxygen and hydrogen in the Truckee River–Pyramid Lake surface-water system 2: a predictive model of $\delta^{18}O$ and $\delta^{2}H$ in Pyramid Lake. Limnol Oceanogr 39:356–364

Hostetler SW, Giorgi F (1993) Use of output from high-resolution atmospheric models in landscape-scale hydrologic models: an assessment. Water Resour Res 29:1685–1695

Hostetler SW, Giorgi F (1994) Effects of 2 × CO_2 climate on two large lake systems: Pyramid Lake, Nevada and Yellowstone Lake, Wyoming, global and planetary Change (in press)

Hostetler SW, Bates GT, Giorgi F (1993) Interactive coupling of a lake thermal model with a regional climate model. J Geophys Res 98:5045–5057

Hostetler SW, Giorgi F, Bates GT, Bartlein PJ (1994) Role of lake-atmosphere feedbacks in sustaining lakes Bonneville and Lahontan 18000 years ago. Science 263:665–668

Hughes GE (1967) Analysis of techniques used to measure evaporation from Salton Sea, California. US Geol Surv Prof Pap 272-H

Hutchinson GE (1957) A Treatise on limnology. Wiley, New York, 1015 pp

Imberger J, Patterson J (1981) A dynamic reservoir simulation model: DYRSEM5. In: Fischer HB (ed) Transport models for inland and coastal waters. Academic Press, New York, pp 310–361

Imbrie J, Hayes JD, Martinson DG, McIntyre A, Mix AC, Morley JJ, Pisias NG, Prell WL, Shackleton NJ (1984) The orbital theory of Pleistocene climate: support from a revised chronology of the marine record. In: Berger A, Imbrie J, Hays J, Kukla G, Saltzman B, (eds) Milankovitch and climate, part 1. NATO ASI Series, Series C, vol 126. Reidel, Dordrecht, pp 269–305

James LD (1985) Methodology report: updating the estimation of water surface elevation probabilities and associated damages for the Great Salt Lake. Utah Water Res Lab, Logan

Karl TR, Young PJ (1986) Recent heavy precipitation in the vicinity of Great Salt Lake: just how unusual? J Clim Appl Meteor 25:353–363

Keijman, JQ (1974) The estimation of the energy balance of a lake from simple weather data. Boundary-Layer Meteorol 7:399–407

Kirk JTO (1988) Solar heating of water bodies as influenced by their inherent optical properties. J Geophys Res 93(D9):10897–10908

Kraus EB (1988) Merits and defects of different approaches to mixed layer modeling. In: Nihoul JCL Jamart BM (eds) Small-scale turbulence and mixing in the ocean. Elsevier Oceanogr Ser 46. Elsevier, Amsterdam, pp 37–50

Küzel F, Kesslar A (1986) Investigation of level changes of Lake Titicaca by maximum entropy spectral analysis. Arch Meteorol Geophys Bioclimatol, Ser B36:219–227

Kutzbach JE (1980) Estimates of past climate at paleolake Chad, North Africa, based on a hydrological and energy-balance model. Quat Res 14: 210–223

Kutzbach JE, Street-Perrott FA (1985) Milankovitch forcing of fluctuations in the level of tropical lakes from 18 to 0 kyr BP. Nature 317:130–134

Kutzbach JE, Guetter PJ (1986) The influences of changing orbital parameters and surface boundary conditions on climate simulations for the past 18000 years. J Atmos Sci 43:1726–1759

Lewis WM, Jr (1982) Vertical eddy diffusivities in a large tropical lake. Limnol Oceanogr 27(1):161–163

Lister GS, Kelts K, Zao CK, Yu JQ, Niessen F (1991) Lake Qinghai, China: closed-basin lake levels and oxygen isotope record for Ostracoda since the late Pleistocene. Paleogeogr Paleoclimatol Paleoecol 84:141–162

Magnuson JJ, Meisner JD, Hill DK, (1990) Potential changes in the thermal habitat of Great Lakes fish after global climate warming. Trans Am Fish Soc 119:254–264

Manabe S, Broccoli AJ (1985) The influence of continental ice sheets on the climate of an ice age. Ann Glaciol 5:2167–2190

Martin PJ (1985) Simulation of the mixed layer at OWS N and P several models. J Geophys Res 90:903–916

Matthews PC, Heany SI (1987) Solar heating and its influence on mixing in ice-covered lakes. Freshwater Biol 18:135–149

McCormick MJ (1990) Potential changes in thermal structure and cycle of Lake Michigan due to global warming. Trans Am Fish Soc 119:183–194

McCormick MJ, Scavia D (1981) Calculation of vertical profiles of lake-averaged temperature and diffusivity in Lakes Ontario and Washington. Water Resour Res 17:305–310

McCormick MJ, Meadows GA (1988) An intercomparison of four mixed layer models in a shallow inland sea. J Geophys Res 93(C6):6774–6788

Mearns LO, Schneider SH, Thompson SL, McDaniel LR (1990) Analysis of climate variability in general circulation models: comparison with observations

and changes in variability in 2 × CO_2 experiments. J Geophys Res 95:20, 496–20, 490
Melack JM (1984) Amazon floodplain lakes: shape, fetch, and stratification. Ver Int Ver Limnol 22: 1278–1282
Morrisette PM (1988) The rising level of the Great Salt Lake: impacts and adjustments. Bull Am Meteorol Soc 69(9):1034–1040
Munk WH, ER Anderson (1948) Notes on the theory of the thermocline. J Mar Res 7:276–295
Niiler PP, Kraus EB (1977) One-dimensional models of the upper ocean. In: Krans EB (ed) Modelling and prediction of the upper layers of the ocean. Pergamon Press, New York, pp 143–172
Noye J (1984) Finite difference techniques for partial differential equations. In: Noye J (ed) Computational techniques for differential equations. Mathematics Studies 83. North-Holland, Amsterdam, pp 98–354
Oke TR (1987) Boundary layer climates, 2nd edn. Methuen, London, 435 pp
Patalas K (1984) Mid-summer mixing depths of lakes of different latitudes. Ver Int Ver Limmol 22:97–102
Patterson JC, Hamblin PF (1988) Thermal simulation of a lake with winter ice cover. Limnol Oceanogr 33(3):323–338
Pivovarov AA (1973) Thermal conditions in freezing lakes and rivers. Wiley, New York, 136 pp
Pond S, Pickard GL (1983) Introductory dynamical oceanography, 2nd edn. Pergamon Press, New York, 329 pp
Powell T, Kirkish MH, Neale PJ, Richerson PJ (1984) The diurnal cycle of stratification in Lake Titicaca: eddy diffusion. Ver Int Ver Limnol 22:1237–1243
Privlasky VE (1989) Modeling long term lake variations by physically based stochastic dynamic models. Stochastic Hydrol Hydraul 2:303–315
Quinn FH, Guerra B (1986) Current perspectives on the Lake Erie water balance. J Great Lakes Res 12(2):109–116
Ragotzkie RA (1978) Heat budgets of lakes. In: Lerman A (ed) Lakes: chemistry, geology, and physics. Springer, Berlin Heidelberg New York, pp 1–18
Richards JM (1971) Simple expression for the saturation vapor pressure of water in the range −50 °C to 140 °C. Br J Appl Phys 4:L15–L18
Riley MJ, Stefan HG (1988) MINLAKE: A dynamic lake water quality simulation model. Ecol Model 43:155–182
Rind D (1987) Components of Ice Age circulation. J Geophys Res 92(D4):4241–4281
Ryan PJ, Harleman DRF, Stolzenbach KD (1974) Surface heat loss from cooling ponds. Water Resour Res 10:930–938
Saltzman B (1990) Three basic problems of paleoclimatic modeling: a personal perspective and review. Clim Dynamics 5:67–78
Semtner AJ, Jr (1976). A model of the thermodynamic growth of sea ice in numerical investigations of climate. J Phys Ocean 6:379–389
Smith GI, Street-Perrott FA (1983) Pluvial lakes. In: Porter SC Late Quaternary environments of the United States, vol 1. Univ of Minn Press, Minneapolis, pp 259–253
Stauffer NE (1985) Great Lake water balance model. In: Kay PK, Diaz HF (eds) Problems and prospects for predicting Great Salt Lake levels. Center for Public Affairs and Administration, University of Utah, Provo, Utah, pp 168–178
Straškraba M (1980) The effects of physical variables on freshwater production: analyses based on models. The functioning of freshwater ecosystems. Cambridge University Press, Cambridge, pp 13–84
Street-Perrott FA, Roberts N (1983) Fluctuations in closed-basin lakes as an indicator of past atmospheric circulation patterns. In: Street-Perrott A, Beran M, Ratchiffe R (eds). Variations in the global water budget. Reidel, Dordrecht, pp 331–345
Street-Perrott FA, Harrison SP (1985) Lake levels and climate reconstruction. In: Hecht AD (ed) Paleoclimate analysis and modeling. Wiley, New York, pp 291–340, 445 pp
Szesztay K (1974) Water balance and water level fluctuations of lakes. Hydrol Sci Bull 29(1):73–84
Tennessee Valley Authority (1972) Heat and mass transfer between a water surface and the atmosphere. TVA Lab Rep 14, 0-6803
Thompson RS, Whitlock C, Bartlein PJ, Harrison SP, Spaulding WG (1994) Climatic changes in the western United States since 18 000 yr. BP. In: Wright HE, Kutzbach JE, Webb T, Ruddiman WF, Street-Perrott FA, Bartlein PJ (eds) Global climates since the last glacial maximum. University of Minnesota Press, Minneapolis, pp 468–513
Tucker WA (1982) Surface heat fluxes from Lake Ontario: further verification of lake thermal model. Water Resourc Res 18(1):77–82
US Army Corps of Engineers (1986) CE-QUAL-R1: a numerical one-dimensional model of reservoir eater quality; user's manual, Instruction Report E-82-1, 427 pp
Vassiljev J, Harrison SP, Hostetler SW, Bartlein PJ (1994) Modelling the thermal behavior of three Estonian Lakes: Karujärv, Viljandi, and Kirjaku. J Hydrol 163:107–123
Weisman RN (1975) Comparison of warm water evaporation equations. ASCE Hydr Div 101:1303–1313
Wetzel RG (1983) Limnology. CBS College, New York, 850 pp
Winter TC, Woo M-K (1990) Hydrology of lakes and wetlands In: Moss ME, Wolman MG, Riggs HC (eds) Surface water hydrology, vol O-1. Geol Soc Am Boulder CO, pp 158–187
Woodbury LH, Padmanabhan G (1989) Estimating terminal lake level frequencies. ASCE J Water Resourc Plan Manag 115:321–337

4 Mixing Mechanisms in Lakes

D.M. Imboden and A. Wüest

1 Transport and Mixing

Transport phenomena are among the most important processes in natural systems. Chemical compounds, the constituents of biogeochemical systems, are in continual motion in all parts of the earth. The thermal motion of atoms and molecules is perceived on the macroscopic level as *molecular diffusion*, i.e., as the slow but persistent movement "down along the concentration gradient." Although the average speed of the atoms is on the order of tens to hundreds of meters per second, the net transport is small, because the molecules do not maintain the same direction long enough. Thus, typical molecular diffusion coefficients of solutes in water are approximately $10^{-9}\,m^2s^{-1}$, corresponding to characteristic annual transport distances of approximately 20 cm. In solids the diffusion coefficients even drop to values as low as $10^{-14}\,m^2s^{-1}$ or less.

Obviously, motion at the molecular level can only be a significant source of macroscopic transport, either over very short distances or over very long time scales. Indeed, transport through interfaces is controlled by molecular diffusion, and the kinetics of certain chemical transformations is influenced by the molecular motion of the reagents. Furthermore, geochemical processes in the lithosphere mostly occur at time scales on which molecular processes begin to become important.

However, a major part of the environment (the atmosphere and the hydrosphere) is fluid in nature. Because internal friction in air and water is small, even minor external forces can cause macroscale motion. It is true that the energy of such motion is small compared with that stored in thermal motion, but the flow patterns are structured and long lasting, thus giving rise to a kind of transport called *advection*, which in many cases is much more efficient than molecular diffusion.

Diffusive and advective transport is expressed in terms of the flux vector F describing the net flow of mass along a certain axis per unit area perpendicular to this axis per unit time. In the case of diffusive transport, F is given by the well-known first Fickian Law. Thus, transport is clearly defined; but what is mixing? In his classical study, Eckart (1948) distinguishes between *stirring* and *mixing* by defining the former as a process resulting in an increase in spatial gradients, whereas the latter results in decreasing spatial gradients. Following Eckart, stirring is due to advection: It occurs even during nonturbulent fluid motion when different advection velocities acting on different portions of the volume cause distortion of the fluid. In contrast, the sharp gradients between fluid parcels that are generated by stirring are smoothed out by mixing, a process that can only occur as a result of molecular diffusion as the final step. This distinction, although conceptually correct, is not satisfactory from an intuitive viewpoint. Because molecular diffusion acts on small structures more efficiently than on large ones, some kind of "fine" stirring in combination with molecular diffusion results in the complete "disintegration" of the structure. Thus, advective transport leading to spatial-concentration structures of "subcritical" size can be defined as mixing as well. This kind of advection is, of course, linked to the turbulent nature of the flow. We use the term turbulent mixing in order to distinguish it from purely molecular mixing. The distance over which molecular diffusion becomes effective is proportional to the square root of elapsed time. Thus, the typical spatial scale separating stirring from mixing is not fixed, but increases with observation time.

Transport, stirring, and mixing are of tremendous importance for the pace at which chemical and biological processes develop. The aim of this chapter is to derive the time and space scales

Environmental Physics, EAWAG/ETH, 8600 Dübendorf, Switzerland

resulting from the physics of fluid motion, and to combine them with the scales of the transformation processes. Depending on the nature of these transformations each compound will "feel" its own physical scenery and its individual "view" of movement, either as transport, stirring, or mixing. It is the combination of physical characteristics with the chemical and biological processes that makes the various aquatic systems so varied in appearance.

2 Lakes as Physical Systems

Lakes are complicated and diverse physical systems. One reason for this is the complexity of fluid motion – a property lakes share with other environmental systems such as the ocean and the atmosphere – and another is the large variety in lake size and shape, which results in different boundary effects. We discuss the hydrodynamic aspects first.

The motion of mass is determined by Newton's momentum equation, which states that the acceleration of a body is proportional to the force applied. It is valid for solid as well as fluid systems, but the resulting equations are much more complicated for the latter than for the former. Whereas a solid element of mass keeps its identity while moving across space, a fluid element continually changes its shape and interacts strongly with other fluid elements such that no "empty" space is left behind. Thus, the momentum equation combined with the so-called continuity equation (the equation expressing the conservation of mass of the fluid) results in a complex system of nonlinear differential equations containing the three components of flow velocity as well as the pressure and density of water. Water density, in turn, depends on temperature, pressure, and the chemical composition of the water as described by the so-called *equation of state*.

Two peculiarities arise from the special form of the basic equations of fluid dynamics. First, empirical concepts such as the physicochemical properties of water are essential for describing the macroscopic properties of fluid motion. In fact, the set of equations describing fluid motion includes the equation of state, but also equations describing the friction between fluid elements of different velocity in terms of the fluid viscosity, another material-specific physicochemical property of the fluid.

As a second peculiarity of fluid dynamics we note the much stronger influence of nonlinear effects, which are responsible for turbulence phenomena. In principle there is no way of separating large-from small-scale motion: Large-scale energy of motion is eventually lost to turbulence, and turbulence, in turn, influences large-scale motion. In order to derive a set of equations that solely describe the large-scale motion of the fluid, it is necessary to introduce new empirical macroscopic variables such as Reynolds' stress and turbulent diffusivity.

The large variability in topography and external forcing (Table 1) is responsible for the wide variety in physical appearance exhibited by lakes. Imagine, on one end of the spectrum, a small shallow pond exposed to the wind. We expect to find a well-mixed water body with little or no density stratification and a simple mixing pattern. If we now turn to deeper and larger lakes new phenomena become important. The vertical density structure separates the wind-mixed surface layer from the deep water in which mixing is driven by indirect forcing. Size introduces the effect of the earth's rotation through the Coriolis acceleration, leading to the so-called inertial motions, and, in combination with gravity, to Rossby waves (see Sect. 6.1). Furthermore, size also brings about an increasing sensitivity to meteorological or even climatic gradients: For instance, a small lake tends to react to a passing low-pressure zone instantaneously and as a whole, whereas an air-pressure gradient moving across a large lake may give rise to specific waves and frontal motions.

In most cases mixing is highly variable in both time and space. This variability results mainly from the temporal and spatial structure of the principal driving forces, weather and climate. The topography of the lake and its surroundings may also be responsible for heterogeneous mixing. For instance, the so-called thermal bar, a peculiar mixing phenomenon (Fig. 19), which is frequently observed in large lakes during the initial phase of thermal stratification, is caused by the fact that close to the shore the water column heats up faster than in the middle of the lake. Yet even in smaller lakes differences in the exposure of different parts of the lake to the wind may cause very special mixing patterns (Fig. 22).

As a consequence it is more difficult to account for the size effect when dealing with heterogeneous mixing. It is true that large-scale mixing

Table 1. The variability of lacustrine systems

Shape[a]		
Volume	max. ≈ 23 000 km^3	(Baikal)
Area	max. ≈ 374 000 km^2	(Caspian Sea)
Maximum depth	max. 1637 m	(Baikal)
Mean depth	max. 730 m	(Baikal)
Topography		
Aspect ratio (maximum depth divided by square root of surface area)[b]		
Large	0.084[c]	(Tazawa, Japan)
	0.082[c]	(Crater Lake, USA)
Typical	10^{-3}	
Hydrology		
Hydraulic loading (water input per unit surface area)		
Large	200 m yr^{-1}	(Lake Bienne,
Typical	1–20 m yr^{-1}	Switzerland)
Chemistry		
Concentration of	max. ≈ 280 g kg^{-1}	(Dead Sea)
total dissolved	35 g kg^{-1}	(average seawater)
solids (salinity S)	0.1–0.3 g kg^{-1}	(typical freshwater)
Climate		
Maximum water temperature		>30 °C
Stratification (T_{max}/T_{min} within water column)		≈25 °C/4 °C
Annual variation of heat content per unit area[c]		
Typical (temperate lakes)	1.0 × 10^9 J m^{-2}	
Extreme values	2.7 × 10^9 J m^{-2}	(Baikal)
	2.2 × 10^9 J m^{-2}	(Michigan)
Average absolute heat flux[d]		
Typical	65 W m^{-2}	
Extreme value	170 W m^{-2}	(Baikal)

[a] From Herdendorf (1990).
[b] From Imboden et al. (1988). Hutchinson (1957), based on an expression of Delebecque's, uses the so-called relative depth, which is 89 times the aspect ratio.
[c] From Hutchinson (1957).
[d] Calculated from the annual variation of heat content, assuming two equal periods of half a year each, during which the lake is either gaining or loosing heat at a constant rate.

in the world ocean is driven mainly by persistent wind patterns and the gradient in the heat flux from low-to-high latitudes. Therefore, in the ocean we find typical current systems like the Gulf Stream and Kuroshio Current, or the thermohaline circulation for which no permanent analog exists in lakes. Based on new and better data on water temperature and currents in lakes, however, a picture is evolving according to which horizontal mixing may often be caused by horizontal density currents, which, in turn, are the result of heterogeneous vertical mixing. Thus, the main difference between lacustrine and oceanic systems is the temporal persistence of currents, rather than their existence. Whereas the oceanic circulation pattern is quasi-permanent, its lacustrine counterpart, depending on the weather conditions, may be switched on and off within minutes or hours.

Because of its influence on density, the chemical composition of lake water represents another key variable, which, independently of lake size, determines the lacustrine environment. In lakes the concentration of total dissolved solids, which, even for pure (or fresh) water is often called *salinity*, ranges from virtually zero to saturation. The upper limit is roughly ten times greater than the average salinity of sea water (Table 1). Most

lakes are horizontally stratified, at least temporarily. Chemically induced vertical gradients may strongly influence the vertical mixing regime. This applies also to lakes with extremely low salinity, provided that the water temperature is close to 4 °C, where the thermal expansion coefficient of water approaches zero.

The density stratification is of great importance for the pattern of mixing in lakes. Although the horizontal extension of a lake is usually much larger than its vertical extension, mixing is commonly faster horizontally than vertically. In fact, stratification not only slows down vertical mixing, it also enhances horizontal mixing by channeling the mechanical energy along horizontal surfaces. Furthermore, for increasing stratification the influence of the earth's rotation on currents becomes more pronounced even at small horizontal scales.

In connection with mixing, terms such as horizontal and vertical need some clarification: Because the surfaces of constant density, the so-called *isopycnals*, are hardly ever quiescent, but are rather dynamically distorted by internal waves and external forces, mixing cannot simply be characterized by horizontal and vertical currents. If we need to be more precise, the terms *isopycnal* and *diapycnal* mixing are employed to distinguish the fast transport along the isopycnals from the slower transport across them.

In summary, we find lake size, external forcing, and stratification to be the major factors that select the physical processes relevant in any given lake. The temporal evolution of thermally induced stratification has been used by early limnologists to classify lakes in terms of their mixing regime (e.g., see Hutchinson 1957). With better physical instrumentation it has been found that lakes are too complex to be typified in such a way. In this chapter the reader will thus not find terms such as holomictic or dimictic.

3 Fluid Dynamics: Mathematical Description of Advection and Diffusion

3.1 Equations of Fluid Motion

There are two ways to describe the motion of a fluid. In the first method, the *Lagrangian* representation, the temporal variation of the relevant variables (velocity, pressure, density, etc.) is described for a "moving fluid element." In the second method, the *Eulerian* representation, the dynamic equations for the variables are formulated at "fixed points" (e.g., in a Cartesian coordinate system). For any scalar property f, the two descriptions are related by

$$\left(\frac{df}{dt}\right)_{\text{Lagrange}} = \frac{\partial f}{\partial t} + U_1\frac{\partial f}{\partial x_1} + U_2\frac{\partial f}{\partial x_2} + U_3\frac{\partial f}{\partial x_3}, \tag{1}$$

where $\partial f/\partial t$ is the Eulerian derivative, x_i ($i = 1-3$) are the three Cartesian coordinates with the x_3 coordinate chosen as positive upward, and U_i are the corresponding components of the velocity vector $\mathbf{U}$.

The dynamics of the Lagrangian element is determined by the following processes: (a) gravity (acting only along vertical axis x_3), (b) pressure gradients, and (c) internal friction (viscosity). Because of the rotation of the earth, the chosen Cartesian reference system is not inertial. Therefore, an additional (pseudo) acceleration, the Coriolis acceleration (d), appears in the equations of motion. From Eq. (1) with f as one of the velocity components U_i ($i = 1-3$), we obtain:

$$\left(\frac{dU_i}{dt}\right)_{\text{Lagrange}} = \underbrace{-\delta_{i3}g}_{(a)} \underbrace{-\frac{1}{\rho}\frac{\partial p}{\partial x_i}}_{(b)} \underbrace{+\Psi_i}_{(c)} \underbrace{-\Gamma_i}_{(d)} \tag{2}$$

(acceleration of gravity $g = 9.81\,\text{m s}^{-2}$; $\delta_{i3} = 1$ for $i = 3$, and 0 otherwise; ρ = density of water; p = pressure, Ψ_i = effect of internal friction; Γ_i = Coriolis acceleration). At the boundaries additional terms appear in Eq. (2) that describe the external forces such as wind stress (see Sect. 5.3). For a detailed discussion of the last two terms of the momentum equation, Eq. (2), the reader is referred to the numerous textbooks that exist on fluid mechanics and physical oceanography (e.g., Gill 1982). For small-scale motions relevant to mixing processes, the Coriolis term can be neglected. In addition, incompressible flow can be assumed. Under these conditions the *continuity equation* can be written

$$\sum_i \frac{\partial U_i}{\partial x_i} = 0. \tag{3}$$

(Note: If not otherwise stated in this and the following equations, the summation is always over all three Cartesian coordinates, i.e., $i = 1-3$.)

Neglecting the spatial variability of the viscosity of water, the frictional term for incompressible flow can be written as

$$\Psi_i = \nu \sum_j \frac{\partial^2 U_i}{\partial x_j^2}, \tag{4}$$

where ν is kinematic viscosity. Finally, expressed in Eulerian form, we arrive at the three equations:

$$\underset{(e)}{\frac{\partial U_i}{\partial t} + \sum_j U_j \frac{\partial U_i}{\partial x_j}} = \underset{(a)}{-\delta_{i3} g} \underset{(b)}{- \frac{1}{\rho}\frac{\partial p}{\partial x_i}} + \underset{(c)}{\nu \sum_j \frac{\partial^2 U_i}{\partial x_j^2}}, \quad i = 1\text{–}3, \tag{5}$$

where term (e) describes the acceleration due to velocity gradients relative to the spatially fixed Eulerian system. Equation (5) is called the *Navier-Stokes Equation* for viscous, incompressible flow on a nonrotating earth.

For a scalar quantity, such as concentration C or water temperature T, a similar approach can be adopted by substituting the appropriate expressions on the right side of Eq. (5). The sum of the terms (a) and (b) is replaced by an *in situ* production/consumption rate, which for concentration is S_C and for temperature is $\frac{S_T}{c_p \rho}$, where S_T is the *in situ* production/consumption of heat, and c_p is specific heat of water at constant pressure. Term (c) is substituted by the molecular diffusivity of concentration, D^C, and of temperature, D^T, respectively, and combined with the corresponding second spatial derivatives. Thus, for concentration we get

$$\underset{(e)}{\frac{\partial C}{\partial t} + \sum_j U_j \frac{\partial C}{\partial x_j}} = \underset{(b)}{S_C} + \underset{(c)}{D^C \sum_j \frac{\partial^2 C}{\partial x_j^2}}, \tag{6}$$

and for temperature

$$\underset{(e)}{\frac{\partial T}{\partial t} + \sum_j U_j \frac{\partial T}{\partial x_j}} = \underset{(b)}{\frac{S_T}{c_p \rho}} + \underset{(c)}{D^T \sum_j \frac{\partial^2 T}{\partial x_j^2}}. \tag{7}$$

3.2 Turbulence, Reynolds' Stress, and Eddy Diffusion

We are still one important step away from our general goal of describing transport and mixing. Two kinds of motion appear in Eqs. (5–7), viz. advection (term e) and molecular diffusion (term c). As mentioned in Section 1 turbulent mixing is usually faster than molecular diffusion. This fast mixing is linked to the fine structure of the flow (turbulence) still hidden in the advective term (e).

The usual way to separate (large-scale) advective from (small-scale) turbulent flow is by splitting variables f, such as velocity u_i, temperature T, and concentration C, into two parts, a temporal mean $\bar{f}$ and a fluctuation f' about the mean:

$$f = \bar{f} + f', \quad \text{where } \bar{f}(t) = \frac{1}{T}\int_{t-T/2}^{t+T/2} f(t')\,dt'. \tag{8}$$

Note that a certain degree of ambiguity is inherent in this procedure (often called Reynolds' decomposition), because the length of the time interval T over which the mean is calculated determines to a certain extent the size of $\bar{f}$ and thus of f'. The dynamics of the atmosphere commonly exhibit a so-called spectral gap at time scales of approximately 1 h, within which little variation of wind speed occurs (Van der Hoven 1957). At time scales longer than those of the spectral gap we find synoptic processes, and at shorter time scales we find turbulent fluctuations. Thus, for the atmosphere a scale of approximately 1 h is a natural choice for Eq. (8). Aquatic systems usually do not have such a natural gap separating the time scales of important processes. Nevertheless, Reynolds' decomposition is used for aquatic systems as well, although its scale-dependence often requires special consideration, e.g., by using different intervals T for different purposes.

Let us apply Reynolds' decomposition to the product of two variables, f_1 and f_2:

$$\begin{aligned} f_1 f_2 &= (\bar{f}_1 + f_1')(\bar{f}_2 + f_2') \\ &= \bar{f}_1\bar{f}_2 + \bar{f}_1 f_2' + f_1'\bar{f}_2 + f_1' f_2'. \end{aligned} \tag{9}$$

Taking a time average over both sides of Eq. (9) we obtain

$$\overline{f_1 f_2} = \bar{f}_1\bar{f}_2 + \overline{f_1' f_2'}. \tag{10}$$

In Eq. (10) we have used the rules $\bar{\bar{f}} = \bar{f}$ and $\bar{f'} = 0$. For details the reader is referred to standard textbooks (e.g., Stull 1988). The essential point of the decomposition procedure expressed in Eq. (10) is the following: Calculation of the time average of the product of two variables results in two terms, viz. the product of the means $(\bar{f}_1\bar{f}_2)$ and the mean of the product of the fluctuations $\overline{f_1' f_2'}$. The latter, the so-called covariance of the two variables f_1 and f_2, vanishes if the two vari-

ables f_1 and f_2 are statistically mutually independent. This is obviously not the case if f_1 and f_2 refer to velocity, temperature, pressure, etc. In other words, whenever the equations contain nonlinear terms (e.g., products of variables), Reynolds' decomposition introduces new terms, the physical meaning of which will soon become clear.

We will not go through the algebra of the Reynolds' decomposition of Eqs. (5–7) step by step. An excellent treatment can be found, for example, in Stull (1988). Let us look at the results. Defining

$$U_i = \bar{U}_i + u_i', \quad i = 1\text{–}3, \tag{11}$$

Eq. (5) becomes

$$\underset{(e)}{\frac{\partial \bar{U}_i}{\partial t} + \sum_j \bar{U}_j \frac{\partial \bar{U}_i}{\partial x_j}} = \underset{(a)}{-\delta_{i3} g} \underset{(b)}{- \frac{1}{\rho}\frac{\partial p}{\partial x_i}} + \underset{(c)}{\nu \sum_j \frac{\partial^2 \bar{U}_i}{\partial x_j^2}} \underset{(f)}{- \sum_j \frac{\partial (\overline{u_i' u_j'})}{\partial x_j}}. \tag{12}$$

As a consequence of Reynolds' decomposition, a new term (f) emerges from the nonlinear advection term (e). Using Eq. (3), this term has been transformed into a symmetrical form and moved to the right side of Eq. (12). Term (f) describes the influence of turbulence on the mean motion $\bar{U}_i$. The covariances are usually expressed in terms of the so-called Reynolds' stress:

$$\tau_{ij} = -\bar{\rho}(\overline{u_i' u_j'}). \quad [\mathrm{N\,m^{-2}}] \tag{13}$$

In the same way, Reynolds' decomposition transforms Eqs. (6) and (7) into the equations for mean scalar properties (e.g., $\bar{C} = C - C'$; $\bar{T} = T - T'$):

$$\underset{(e)}{\frac{\partial \bar{C}}{\partial t} + \sum_j \bar{U}_j \frac{\partial \bar{C}}{\partial x_j}} = \underset{(a)}{S_C} + \underset{(c)}{D^C \sum_j \frac{\partial^2 \bar{C}}{\partial x_j^2}} \underset{(f)}{- \sum_j \frac{\partial (\overline{u_j' c'})}{\partial x_j}} \tag{14}$$

and

$$\underset{(e)}{\frac{\partial \bar{T}}{\partial t} + \sum_j \bar{U}_j \frac{\partial \bar{T}}{\partial x_j}} = \underset{(a)}{\frac{S_T}{c_p \bar{\rho}}} + \underset{(c)}{D^T \sum_j \frac{\partial^2 \bar{T}}{\partial x_j^2}} \underset{(f)}{- \sum_j \frac{\partial (\overline{u_j' T'})}{\partial x_j}}. \tag{15}$$

The last terms (f) in each equation, the divergence of the turbulent fluxes,

$$F_j^C = \overline{u_j' c'} \quad \text{and} \quad F_j^T = \overline{u_j' T'}, \tag{16}$$

express the additional transport due to turbulent fluctuations of u_i, C, and T. These terms are much larger than the molecular terms (c), so that the latter are usually omitted.

This new set of equations has introduced several new unknowns, i.e., the covariances (such as the Reynolds' stress terms and the turbulent fluxes). It is possible to derive new dynamic equations for the description of the double correlations, but unfortunately these equations contain triple correlations, e.g., expressions such as $\overline{T' u_i' u_j'}$. Thus, any attempt to derive enough equations to solve for all the unknowns leads to an even larger number of unknowns. There is no way out, unless we find some approximation that expresses the higher-order correlations using lower-order terms (and not the other way around). This procedure is called *closure approximation* (e.g., see Stull 1988).

There are closure schemes of various order. In the simplest of these, the first-order closure scheme, terms including means (such as $\bar{f}$) are retained while all covariances of the form $\overline{f_1' f_2'}$ are parameterized. Analogously, a second-order procedure retains the expressions up to the second order, while the covariances of the third order appearing in the dynamic equation of the second order, such as $\partial(\overline{f_1' f_2'})/\partial t$, are parameterized. Two methods of parameterization can be distinguished, known as *local* and *nonlocal* approximations. In the former an unknown at any given point in space is expressed in terms of certain variables solely at this point; in the latter, the unknown quantity is approximated by values of known quantities within some spatial environment of the point. We first deal with the more common local closure models and restrict our discussion to the first order. Nonlocal schemes are explored in Section 3.4.

In the first-order local closure approximation, the second-order covariance is expressed by

derivatives of the mean quantities. If f is a scalar, then the turbulent flux of the scalar property along the j axis, F_j^f, is approximated by

$$F_j^f = \overline{u_j' f'} = -K_j^f \frac{\partial \bar{f}}{\partial x_j}, \tag{17}$$

where K_j^f is a positive coefficient with dimensions $[L^2T^{-1}]$. [Note that in Eq. (17) it is assumed that the coordinates x_i are principal axes; otherwise, additional terms would appear containing the derivatives with regard to the other axes.] Thus, the scalar f flows in the direction of its negative gradient, i.e., "it flows down the local gradient". Equation (17) is called the *gradient-transport* (or eddy) *formulation* (Fig. 1a). For f we can insert temperature, concentration, or one of the three velocity components U_i, and apply Eq. (17) to Eqs. (12), (14), and (15). If f stands for concentration C, the theory is identical to *Fick's First Law*. If f stands for the velocity component U_i, we can relate the eddy formulation to the Reynolds' stress introduced in Eq. (13):

$$\overline{u_i' u_j'} = -K_{ij}^m \frac{\partial \bar{U}_i}{\partial x_j}, \tag{18}$$

where K_{ij}^m is the turbulent or eddy diffusion coefficient for momentum (also called eddy viscosity) and K_j^T and K_j^C are the eddy diffusion coefficients of temperature and of mass for substance of concentration C, respectively.

By neglecting molecular viscosity and diffusion relative to the turbulent flux terms one obtains:

$$\frac{\partial \bar{U}_i}{\partial t} + \sum_j \bar{U}_j \frac{\partial \bar{U}_i}{\partial x_j} = -\delta_{i3} g - \frac{1}{\rho} \frac{\partial p}{\partial x_i} + \sum_j \frac{\partial}{\partial x_j} \left(K_{ij}^m \frac{\partial \bar{U}_i}{\partial x_j} \right), \quad i = 1\text{–}3; \tag{19}$$

$$\frac{\partial \bar{C}}{\partial t} + \sum_j \bar{U}_j \frac{\partial \bar{C}}{\partial x_j} = S_C + \sum_j \frac{\partial}{\partial x_j} \left(K_j^C \frac{\partial \bar{C}}{\partial x_j} \right); \tag{20}$$

$$\frac{\partial \bar{T}}{\partial t} + \sum_j \bar{U}_j \frac{\partial \bar{T}}{\partial x_j} = \frac{S_T}{c_p \bar{\rho}} + \sum_j \frac{\partial}{\partial x_j} \left(K_j^T \frac{\partial \bar{T}}{\partial x_j} \right). \tag{21}$$

The subscript j refers to the direction of the eddy flux. For stratified fluids the eddy diffusivity along the horizontal axis is usually much larger than along the vertical axis (e.g., $K_z^C \ll K_x^C, K_y^C$).

3.3 Vertical Momentum Equation

The vertical component (i = 3) of the momentum equation (Eq. 19), at steady state and in the absence of spatial velocity gradients, yields the simple *hydrostatic equation*

$$\frac{\partial p}{\partial x_3} = -g\rho. \tag{22}$$

In turn, if Eq. (22) is inserted into the general vertical momentum equation, the first and second term on the right side of Eq. (19) cancel out. The resulting equation is called the *hydrostatic approximation*.

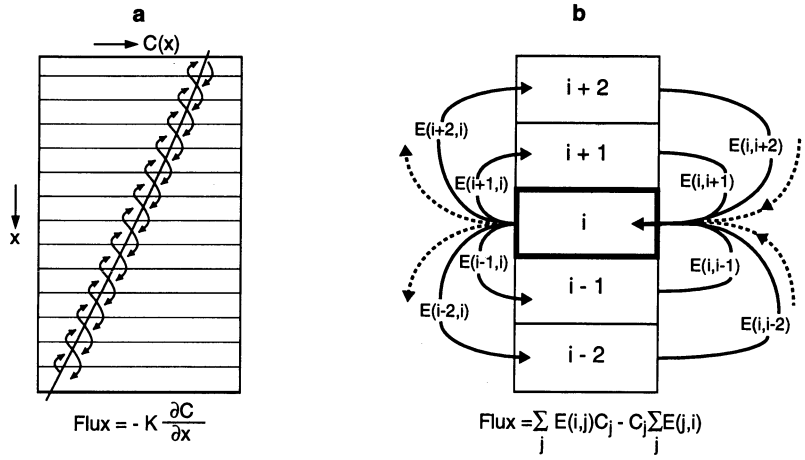


Fig. 1. a The local exchange model leads to the gradientflux model (Eq. 20) as exemplified, for the case of mass fluxes, by Fick's First Law: $F_i = -K \cdot \partial C/\partial x_i$. **b** In contrast, the nonlocal exchange model (Imboden 1981), also named Transilient Turbulence Theory (Stull 1984, 1986), describes the mass flux from box i into box j by the matrix E(j,i). The two boxes do not have to be neighbors. See Eq. (28) for the continuous formulation of the model

A special kind of motion evolves from Eq. (5) if we concentrate our discussion on the vertical direction by assuming horizontal current velocities to be zero, and by neglecting (molecular and turbulent) friction. After performing the Reynolds' decomposition, and in the absence of a mean vertical flow ($\bar{U}_3 = 0$), the only remaining term on the left side of Eq. (12) is the Lagrangian acceleration of the velocity fluctuation u_3'. It is equal to the sum of the two remaining terms on the right side, i.e., the acceleration due to gravity (term a) and the vertical pressure gradient (term b). Multiplying both sides by ρ yields

$$\rho\left(\frac{du_3'}{dt}\right)_{\text{Lagrange}} = -g\rho - \frac{\partial p}{\partial x_3}. \tag{23}$$

This is the equation of motion of a water parcel moving vertically within the water column. At an equilibrium depth z_o, its density is equal to the mean (depth-dependent) density of the surrounding water. If the vertical displacement from the equilibrium depth is small and of short duration, the effect of pressure and of the exchange of heat or salt between the water parcel and its surroundings can be neglected. This means that the density ρ of the water parcel is constant. However, by changing its depth the water parcel is exposed to a different pressure gradient than that prevailing at its equilibrium depth:

$$\left.\frac{\partial p}{\partial x_3}\right|_{z_o+\zeta} = \left.\frac{\partial p}{\partial x_3}\right|_{z_o} + g\frac{d\bar{\rho}}{dz}\zeta = -g\bar{\rho} + g\frac{d\bar{\rho}}{dz}\zeta \tag{24}$$

where ζ is the vertical displacement of the parcel from its equilibrium depth. Replacing this expression for the pressure gradient in Eq. (23), and using $\bar{\rho} = \rho$, yields

$$\left(\frac{du_3'}{dt}\right)_{\text{Lagrange}} = \frac{\partial^2\zeta}{\partial t^2} = \frac{g}{\bar{\rho}}\frac{d\bar{\rho}}{dz}\zeta = -N^2\zeta. \tag{25}$$

This is the equation of motion of a linear oscillator with eigenfrequency

$$N = \left(-\frac{g}{\bar{\rho}}\frac{d\bar{\rho}}{dz}\right)^{1/2}. \quad [s^{-1}] \tag{26}$$

N is called the *stability frequency* or *Brunt-Väisälä frequency*, and is defined for $\frac{d\bar{\rho}}{dz} < 0$ (Table 5). N is often used to quantify the strength of the density stratification. A more exact definition of N is given by Eq. (41).

3.4 Nonlocal Diffusion and Transilient Mixing

The eddy formulation of Eq. (16) is based on the assumption that turbulent motion (expressed by u_j') occurs over small distances, so that the resulting flux F_j^f can be parameterized by the gradient of the mean value of property f "at this very location." Mathematicians call such a relationship *local*, in contrast to an expression in which F_j^f depends on values of $\bar{f}$ at other locations as well, which can be named a *nonlocal* theory (Imboden 1981; Stull 1984; Boudreau and Imboden 1987). The existence of large eddies that can transport fluid across finite distances before they lose their identity due to the action of small-scale eddy mixing may invalidate concepts of local diffusion such as those embodied in Fick's First Law. The natural nonlocal extension of this law is to replace Eq. (24) by the following expression (Imboden 1981):

$$F_j^f(x_j) = -\int_a^b k_j^f(x_j, \tilde{x}_j)\left.\frac{\partial \bar{f}}{\partial x_j}\right|_{\tilde{x}_j} d\tilde{x}_j, \tag{27}$$

where $k_j^f(x_j, \tilde{x}_j)$ is a generalized eddy diffusivity (dimensions LT^{-1}) for property f along the x_j direction, measuring the influence of the $\bar{f}$ gradient at $\tilde{x}_j$ on the turbulent flux at x_j. Parameters a and b are either the boundaries of the system along the x_j axis or the limits beyond which $\bar{f}$ no longer has an effect on the flux at x_j. Equation (27) includes the Fickian expression as the special case $k_j^f(x_j, \tilde{x}_j) = K_j^f\delta(x_j - \tilde{x}_j)$, where $\delta(x) = \infty$ for $x = 0$, and $\delta(x) = 0$ otherwise.

An alternative nonlocal concept is the *exchange model* (Imboden 1981), called *Transilient Turbulence Theory* by Stull (1984, 1986). In its discrete form the model is formulated in terms of a matrix (the transilient matrix), which expresses the probability of fluid exchange between any two finite spatial boxes (Fig. 1b). In its continuous form the last term on the right side of Eqs. (20) or (21) is replaced by the integral

$$\int_a^b E_j^f(x_j, \tilde{x}_j)\bar{f}(\tilde{x}_j)d\tilde{x}_j - \bar{f}(x_j)\int_a^b E_j^f(\tilde{x}_j, x_j)d\tilde{x}_j, \tag{28}$$

where $\bar{f}$ stands for $\bar{C}$ or $\bar{T}$. $E_j^f(x_j, \tilde{x}_j)$ is the exchange probability along the j axis from location $\tilde{x}_j$ to x_j.

A more detailed exposition of nonlocal theories would go beyond the scope of this chapter. Nonlocal theories are more complex than local

theories and require a considerable quantity of field data for their application. This may explain why there have been few applications such as mixing within sediments (Boudreau and Imboden 1987) or mixing in the atmospheric boundary layer (Stull 1988). Still, nonlocal transport models offer a way to overcome some of the problems of the eddy formulation, which are apparent in many situations where transport does not occur in the direction of the local negative gradient.

4 Density and Stability of Water Column

4.1 Equation of State of Water

The density of water, defined as the ratio of mass to volume, depends on temperature, pressure, and the physicochemical properties of the water. In order to calculate the density of distilled water exactly, even the exact isotopic composition [e.g., the abundance of the heavy isotopes ^2H (deuterium) and ^{18}O] and the concentration of dissolved gases (e.g., air) has to be known. Rather detailed expressions for the thermodynamic properties of natural waters covering the limnological range are given by Chen and Millero (1986). They approximate $\rho_o(T)$ for pure water in equilibrium with air at p = 1013 mbar (mean pressure at sea level) by a sixth-order polynomial. A simpler expression is given by Bührer and Ambühl (1975; T in °C):

$$\rho_o(T) = 999.84298 + 10^{-3}(65.4891 \cdot T - 8.56272 \cdot T^2 + 0.059385 \cdot T^3). \quad [kg \cdot m^{-3}] \qquad (29)$$

This equation is valid for temperatures between 1 and 20 °C with a relative deviation from measured values, $\delta\rho/\rho$, of less than 2×10^{-6}.

The thermal expansivity of water, α, is defined by

$$\alpha = -\frac{1}{\rho}\left(\frac{\partial\rho}{\partial T}\right)_{C_n,p}, \quad [K^{-1}] \qquad (30)$$

where the subscripts indicate that the derivative is calculated by keeping pressure p and concentration C_n of every solute n constant. Because the process of thermal expansion is accompanied by a volume change, the C_n values have to be expressed in terms of the mass of dissolved substance n per total mass of solution.

For pure water at p = 1013 mbar, α changes sign at the temperature of maximum density $T_{\rho max}$ = 3.9839 °C, where ρ_o reaches its maximum value of $\rho_{max} = 999.972\,kg\,m^{-3}$ (Chen and Millero 1986). (Note that the approximation Eq. (29), gives slightly different values.) For temperatures $T > T_{\rho max}$, density decreases with increasing temperature and $\alpha > 0$; at $T = T_{\rho max}$, $\alpha = 0$; and for $T < T_{\rho max}$, $\alpha < 0$.

Although the "direct" effect of pressure p on density ρ (the compressibility of water) is not relevant for the stability of the water column (see Sect. 4.2), pressure plays an important "indirect" role through its influence on α and $T_{\rho max}$. In fact, $T_{\rho max}$ decreases with increasing pressure and thus with increasing depth (Chen and Millero 1986):

$$T_{\rho max} = 3.9839 - 1.9911 \times 10^{-2}\,p - 5.822 \times 10^{-6}\,p^2, \quad [°C] \qquad (31)$$

where p is in bar. Note that in fresh water the hydrostatic pressure increases by approximately 0.0981 bar per meter. Thus, $T_{\rho max}$ decreases roughly by 0.2 °C for every 100 m of depth. The influence of pressure on α (*thermobaric effect*) and temperature (*cabbeling*), can affect the sinking and rising of water masses in the ocean and in deep lakes (McDougall 1987a; see also Sect. 6.6). Selected values of $\rho_o(T)$ and $\alpha(T, p)$ are given in Table 2.

A further influence on ρ, α, $T_{\rho max}$, and other physical properties originates from the chemical composition of the water. At sufficiently large dilution the effect of solute n = 1,2, . . . (with concentration C_n) on ρ can be expressed by the linear superposition

$$\rho(T,C_1,C_2,\ldots) = \rho_o(T)[1 + \beta_1 C_1 + \beta_2 C_2 + \ldots], \qquad (32)$$

where

$$\beta_n = \frac{1}{\rho}\left(\frac{\partial\rho}{\partial C_n}\right)_{T,p,C_m}, \quad m = 1,2,\ldots \text{ but } m \neq n \qquad (33)$$

is the specific expansion coefficient of water due to solute n. The coefficient β_n is temperature-dependent; values for various solutes at T = 25 °C are given in Table 3. For dissolved gases β_n can be negative, which means that the density of the water decreases with increasing gas concentration. Equation (33) can also be applied to describe the influence of suspended solids on the density of water.

Table 2. Physical properties of pure water as a function of temperature and pressure[a]

T [°C]	Density $\rho(T)$[b] [kg m^{-3}]	Thermal expansivity $\alpha(T,p)$ [10^{-6} K^{-1}]				
	p = 0	p = 0	p = 20	p = 50	p = 100	p = 180
0	999.839	−68.00	−60.64	−49.59	−31.18	−1.72
1	999.898	−50.09	−43.03	−32.43	−14.78	13.48
2	999.940	−32.77	−26.00	−15.85	1.08	28.17
3	999.964	−16.01	−9.53	0.20	16.42	42.37
4	999.972	0.22	6.43	15.75	31.27	56.11
5	999.964	15.96	21.90	30.81	45.66	69.42
10	999.700	87.99	92.70	99.76	111.52	130.35
15	999.100	150.89	154.55	160.05	169.21	183.86
20	998.204	206.76	209.58	213.79	220.82	232.07
25	997.045	257.17	259.33	262.55	267.93	276.54

[a] The hydrostatic pressure p [bar] is 0 at the water surface.
[b] Density at atmospheric pressure of 1013 mbar.

Table 3. Influence of dissolved or suspended substances on the density of water

Substance	β_n [(g/kg)$^{-1}$][a]
$Ca(HCO_3)_2$	0.807×10^{-3}
$Mg(HCO_3)_2$	0.861×10^{-3}
$Na(HCO_3)$	0.727×10^{-3}
$K(HCO_3)$	0.669×10^{-3}
$Fe(HCO_3)_2$	0.838×10^{-3}
$NH_4(HCO_3)$	0.462×10^{-3}
CO_2	0.273×10^{-3}
CH_4	-1.250×10^{-3}
Air	-0.090×10^{-3}
Suspended solids[b] with $\rho_S = 2.65\,g\,cm^{-3}$	0.623×10^{-3}
with $\rho_S = 1.1\,g\,cm^{-3}$	0.091×10^{-3}
Electrical conductivity (β_κ) due to $Ca(HCO_3)_2$	0.705×10^{-6} (μS/cm)$^{-1}$

[a] β_n values for T = 25 °C as defined in Eqs. (33–35).
[b] ρ_S is dry density of suspended solids.

If the relative chemical composition of the water is constant (as is nearly the case for seawater), the influence of the different components can be represented by a single parameter such as the concentration of total dissolved solids S (salinity), which is expressed as the total mass of dissolved solids (in g) per unit total mass of (salt) water (in kg). The influence of S on ρ is described by β_S, often called the *coefficient of haline contraction*, as follows:

$$\rho(T,S) = \rho_o(T)[1 + \beta_S S],$$
$$\text{with} \quad \beta_S = \frac{1}{\rho}\left(\frac{\partial \rho}{\partial S}\right)_{T,p}. \tag{34}$$

Unlike seawater, the relative chemical composition of lake water is not constant. Not only does the concentration of total dissolved solids vary considerably from lake to lake, from the nearly pure water of alpine lakes to the nearly saturated salt water of the Dead Sea (Table 1), but the chemical composition of the total dissolved solids also varies. In some cases the chemistry of lake water is dominated by a single anion/cation pair, e.g., by calcium and bicarbonate. The electrical conductivity κ_{20} (the subscript refers to the reference temperature of 20 °C) can then serve as a direct measure of the total concentration of these ions. Given their specific electrical conductivity and ionic volumes, we can obtain an

expression for the dependence of ρ on κ_{20}. For the case of calcium carbonate the following relationship is obtained:

$$\rho(T,\kappa_{20}) = \rho_0(T)[1 + \beta_\kappa \kappa_{20}],$$

$$\beta_\kappa = \frac{1}{\rho}\frac{\partial \rho}{\partial \kappa_{20}} = 0.705 \times 10^{-6}(\mu S/cm)^{-1}, \qquad (35)$$

with κ_{20} as the electrical conductivity of water at 20 °C (in μS/cm). Similar relationships can be obtained for other ionic water compositions as long as the concentrations of nonionic species (which have no effect on κ_{20}) are negligible.

Both the temperature of maximum density $T_{\rho max}$ and the thermal expansivity α change with salinity. In fact, at a salinity of 24.8 g/kg, $T_{\rho max}$ sinks below the freezing temperature, which, at this salinity, is T = −1.34 °C. Seawater (with a typical salinity of 35 g/kg) does not exhibit such a density anomaly; α is always positive, i.e., density always increases with decreasing temperature.

4.2 Potential Temperature and Local Vertical Stability

To discuss the concept of local vertical stability two water parcels that are separated by a very small vertical distance are considered. Imagine that the upper parcel is displaced isentropically (i.e., without exchange of heat and salt with the surrounding water) to the depth of the lower one where the densities of the two parcels are then compared. If the density of the water parcel originating from the upper position is smaller than the density of the water parcel from the lower position, the water is said to be locally stable. Because of the buoyancy force, the displaced water parcel is pushed back to the depth from where it originated, i.e., the displacement is reversible. If the density difference is zero, the water column is referred to as neutrally stable. The two water parcels could exchange their positions without altering the potential energy of the water column. Finally, if the water parcel displaced from above has a greater *in situ* density than the water parcel at the deeper position, the water is referred to as locally unstable. In the latter case exchanging the positions of the two water parcels results in a decrease of the potential energy of the water column. Spontaneous convection is initiated, which continues until the density instability has vanished.

Because the displacement of the water parcels are infinitesimally small, the stability depends on the "local" density gradient; hence, the expression *local stability*. The vertical movement of a displaced water parcel close to its equilibrium depth is described by Eq. (25), i.e., by the stability frequency N. In contrast, the concept of *global stability* of a water mass addresses the question of how the total potential energy of the water masses changes if the water is completely mixed adiabatically. Given the very special properties of the density of water as a function of temperature, salt, and pressure it is possible that a water mass is globally unstable despite being locally stable everywhere. The problem of global stability is beyond the scope of this chapter.

Note that local stability does not depend directly on the compressibility of the water, because the densities are compared at the same depth. In other words, an increase in *in situ* density with depth is not sufficient to guarantee local stability. The indirect effect of pressure on stability still has to be taken into account, however. The decompression of a water parcel that is being moved upwards isentropically leads to a small temperature decrease, which is accompanied by a slight density increase if $T > T_{\rho max}$ (and a small density decrease if $T < T_{\rho max}$).

The so-called *adiabatic temperature gradient*,

$$\left(\frac{dT}{dz}\right)_{ad} = -\frac{g\alpha(T + 273.15)}{c_p}, \qquad (36)$$

given by (Kelvin 1875) (the vertical coordinate z is chosen as positive upward), corresponds to the change in *in situ* temperature in a neutrally stable water column. Thus, for $\alpha > 0$ (i.e., $T > T_{\rho max}$) the *in situ* temperature increases with depth at neutral stability. In the deep parts of cold freshwater lakes, $\left(\frac{dT}{dz}\right)_{ad}$ is usually very small, because water temperatures are close to the temperature $T_{\rho max}$ at which α approaches zero. For instance, at a temperature T = 4 °C and a hydrostatic pressure p = 20 bar (corresponding to a depth of approximately 200 m), $\left(\frac{dT}{dz}\right)_{ad}$ is approximately $-4.2 \times 10^{-6}\,K\,m^{-1}$.

The condition for local stability can be expressed as follows:

$$\alpha\left[\frac{dT}{dz} - \left(\frac{dT}{dz}\right)_{ad}\right] > 0. \qquad (37)$$

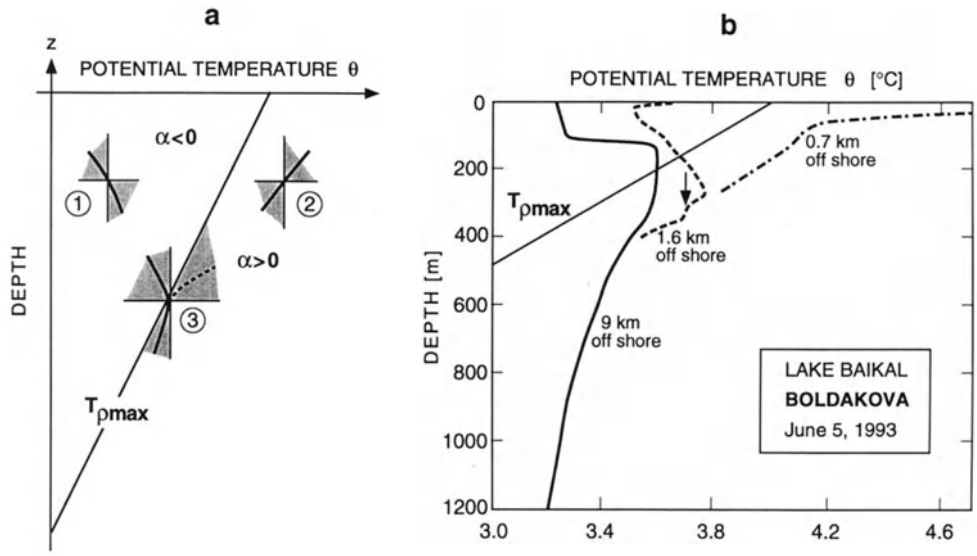


Fig. 2. a Conditions for local stability derived from Eqs. (37) and (38). Stable temperature profiles characterized by $\alpha \cdot \frac{d\theta}{dz} > 0$ lie in the *shaded segments*. ① For $T < T_{\rho max}$, $\alpha < 0$; hence, local stability implies $\frac{d\theta}{dz} < 0$. ② For $T > T_{\rho max}$, $\alpha > 0$; hence, local stability implies $\frac{d\theta}{dz} > 0$. ③ The temperature profile cannot cross the $T_{\rho max}$ line from right to left while depth is increasing. Note that the effect of salinity gradients on stability is not considered here. **b** Vertical temperature profiles from Lake Baikal demonstrate the effect of the pressure dependence of the temperature of maximum density, $T_{\rho max}$. Except for the top 200 m, the temperature decreases with depth, but always remains above the *in situ* $T_{\rho max}$

The consequences of this inequality are illustrated schematically in Fig. 2a. Temperature profiles from Lake Baikal (Siberia) shown in Fig. 2b demonstrate the effect of the pressure dependence of $T_{\rho max}$ on the vertical stability of the water column.

It is often convenient to replace the *in situ* temperature by the so-called potential temperature θ, defined by the differential equation

$$\frac{d\theta}{dz} = \frac{dT}{dz} - \left(\frac{dT}{dz}\right)_{ad}. \tag{38}$$

For an absolute definition of θ a reference depth z_o has to be selected at which T and θ are taken to be equal. In the ocean, z_o is often chosen to lie at 4 km depth, but for lakes it is more appropriate to choose z_o at the surface. Thus,

$$\theta(z) = T(z) - \int_z^{z_o} \left(\frac{dT}{dz}\right)_{ad} dz'. \tag{39}$$

Because $\left(\frac{dT}{dz}\right)_{ad}$ depends on depth, temperature, and salinity, and may even change sign over the integration interval, the evaluation of Eq. (39) is not always trivial.

To include the effect of salt on the stability condition Eq. (37) has to be completed by a term that contains the *in situ* salt gradient and the corresponding expansion coefficient for salt:

$$\left(\alpha\frac{d\theta}{dz} - \beta_S\frac{dS}{dz}\right) = \left(\alpha\left[\frac{dT}{dz} - \left(\frac{dT}{dz}\right)_{ad}\right] - \beta_S\frac{dS}{dz}\right) > 0. \tag{40}$$

We can now define the stability frequency introduced in Eq. (17) more exactly (for the sake of simplicity $\bar{\rho}$ is replaced by ρ):

$$N = \left[\frac{g}{\rho}\left(\alpha\frac{d\theta}{dz} - \beta_S\frac{dS}{dz}\right)\right]^{1/2}. \tag{41}$$

5 Energy Fluxes: Driving Forces Behind Transport and Mixing

All mixing and transport phenomena in the aquatic environment, with the exception of molecular diffusion, are driven by external forces. The mixing patterns that evolve are the result of both external forces and internal properties of the

system such as the morphometry of the water body or the stability of the water column. In fact, the external forces are built into the boundary conditions of the equations of motion derived in Sect. 3. Rather than deal with the mathematical solutions of these equations, however, in this section the various energy fluxes and the way they become apparent in lakes are discussed. Following physical tradition a distinction is made between *thermal* and *mechanical* energy; the latter is further subdivided into *potential* and *kinetic* energy. Thermal energy is stored in the random-velocity distribution of atoms and molecules. Its direct influence on mixing, as manifested in molecular diffusion, is small. Indirectly, however, thermal energy affects mixing very strongly through its influence on water density (Sects. 4 and 6). Compared with thermal energy mechanical energy is highly ordered, and, although its flux is relatively small, it plays a crucial role for mixing in lakes.

Figure 3 illustrates typical orders of magnitude for energy fluxes (energy per unit area per unit time, in $W m^{-2}$) and energy content (energy per unit area, in $J m^{-2}$) for lakes. The reason that these values are normalized by dividing by the surface area is that most exchange of momentum and energy is at the water surface (e.g., heat exchange and wind energy). We first briefly explain how energy is stored in a lake. The largest storage term, ΔE_{heat}, is related to thermal energy. Because there is no meaningful way to define absolute thermal energy content, we use the energy amplitude that is the difference between the maximum and minimum thermal energy content of the water column. ΔE_{heat} is usually approximately $10^9 J m^{-2}$, but may exceed $2.7 \times 10^9 J m^{-2}$ (e.g., Lake Baikal; Table 1). It is by far the largest term in the total energy balance. Next in size is the potential energy term ΔE_{pot} (typically $\approx 10^3 J m^{-2}$), which depends on the vertical-density stratification of the water column. In saline lakes, where the density of water depends not only on temperature but also on salinity, ΔE_{pot} may be much larger. In the Dead Sea, for instance, the potential energy associated with the stratification of the highly saline water reached a value of $4 \times 10^5 J m^{-2}$ in early 1980 (Anati et al. 1987). The smallest storage term (although the most spectacular one if we consider the often devastating power of surface waves!) is given by the kinetic energy of the water, E_{kin}, contained in currents, waves, and turbulent motion. The kinetic energy brought into the lake by inlets (shown on the left side of Fig. 3) varies by several orders of magnitude depending on water-renewal rate. A value of $10^{-4} W m^{-2}$ for E_{kin} is typical for lakes with mean water residence times between 0.5 and 5 years.

The second law of thermodynamics gives a clear meaning to the classification of the different energy terms: Although mechanical energy can be fully transformed into thermal energy, the reverse is not possible. The kinetic energy of water currents is eventually transformed into heat by internal friction. It is possible to drive currents simply by cooling, but only a small fraction of the thermal-energy flux is actually retrieved by the

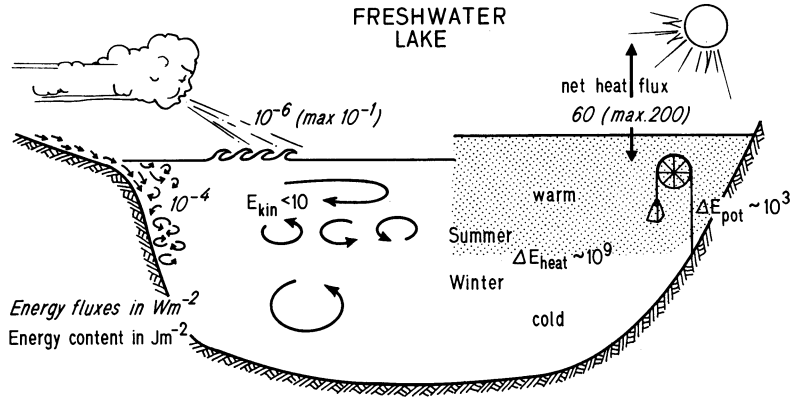


Fig. 3. Typical magnitudes of the energy contents and energy fluxes in a freshwater lake. The thermal energy amplitude, ΔE_{heat}, corresponds to the annual variation between winter and summer. Potential energy, ΔE_{pot}, describes the effect of density stratification. In saline lakes ΔE_{pot} can attain values 2 to 3 orders of magnitude greater than in freshwater lakes

kinetic energy of the flow. Energy transformations are directional and to a large extent irreversible, and therefore a simple comparison of the numbers alone does not reveal the roles played by different energy terms. We now discuss various energy fluxes in greater detail.

5.1 Thermal Energy

The net heat exchange H_{net} between atmosphere and water consists of seven main components (Fig. 4):

$$H_{net} = H_S + H_A + H_W + H_E + H_C + H_P + H_I. \quad [W\,m^{-2}] \tag{42}$$

These terms are defined as positive when directed into the water. They describe the radiative heat fluxes due to solar radiation (H_S) and to the infrared radiation emitted from the sky (H_A) and from the surface of the water (H_W), the nonradiative heat fluxes due to evaporation/condensation (H_E) and convection (H_C), precipitation onto the water surface (H_P), and the effect of the throughflow of water by inlets and outlets (H_I).

The three radiative heat-flux terms are the largest. Two well-separated wavelength domains can be distinguished here: the visible range (wavelength ≈ 0.4–$0.7\,\mu m$), to which the solar radiation H_S belongs, and the infrared range (a wavelength of approximately $10\,\mu m$) of the radiation from sky and water surface (H_A and H_W). The radiative fluxes can be understood on the basis of the physical principles that describe the energy and wavelength distribution of radiation from a surface of (absolute) temperature T. The law discovered by Josef Stefan and Ludwig Boltzmann relates the total amount of energy H_{rad} radiated by a so-called black body per unit surface per unit time to its absolute surface temperature T as follows:

$$H_{rad} = E\sigma T^4, \quad [W\,m^{-2}] \tag{43}$$

where $\sigma = 5.67 \times 10^{-8}\,W\,m^{-2}\,K^{-4}$ is known as the Stefan-Boltzmann constant. The emissivity E of a body is unity in the case of a black body and less than unity for natural surfaces.

Empirical expressions for flux terms are summarized in Table 4. The infrared terms H_A and H_W are formulated according to the Stefan-Boltzmann law (Eq. 43). Water is nearly a black body (emissivity $E_W \approx 0.97$), but E_A is more variable, because the atmosphere is not a homogeneous body. E_A increases with air temperature, moisture content, and cloud cover. Empirical relationships are given by Swinbank (1963) and Brutsaert (1975).

In order to demonstrate the relative importance of the different terms, the mean seasonal variation of the various fluxes is plotted in Fig. 5 for the average meteorological conditions calculated for Lake Zurich (Switzerland) by Kuhn (1979). If real meteorological data from a specific year are used instead, the terms H_S, H_E, H_C, and H_P fluctuate greatly about their means, whereas H_A

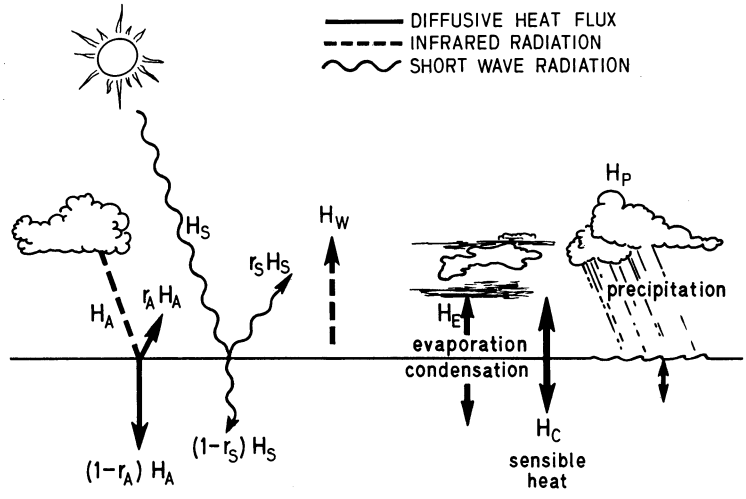


Fig. 4. Heat exchange processes between water and atmosphere (see Eq. 42 and Table 4 for definitions). Not shown here is the term H_I, which describes the influence of inflows and outflows on the heat balance

Table 4. Thermal energy fluxes at water surface

Shortwave radiation from sky (direct and diffuse) $H_S = (1 - r_S)\, H_S^O\, f_S\,(C)$	
$H_S^O\ [Wm^{-2}]$	Clear-sky solar radiation
$r_S\,(C)\ [-]$	Reflection of shortwave radiation from water surface. Typical values lie between 0.04 (June) and 0.20 (December)
$f_S\,(C) = 1 - 0.65\,C^2$	Shading by clouds; empirical relationship of Barry and Chorley (1976)
C	Relative cloud cover of sky
Infrared radiation from sky $H_A = (1\text{-}r_A)\, E_A \sigma T_A^4$	
$r_A\ [-]$	Reflection of infrared radiation from water surface; typical value 0.03
$E_A\ [-]$	Emissivity of atmosphere; empirical relations by Swinbank (1963) and Brutsaert (1975); typical values between 0.6 and 0.9
$\sigma = 5.67 \times 10^{-8}\,W\,m^{-2}\,K^{-4}$	Stefan-Boltzmann constant
T_A [K]	Absolute temperature of the atmosphere
Infrared radiation from the water surface $H_W = -E_W \sigma\, T_W^4$	
$E_W\ [-]$	Emissivity of water, approximately 0.97
$T_W\ [-]$	Absolute temperature of water surface
Flux of sensible heat (convection) $H_C = -f(u, \ldots)\,(T_W - T_A)$	
$f(u, \ldots)\ [W\,m^{-2}\,K^{-1}]$	Transfer function depending on wind velocity u and other meteorological parameters; typical values lie between $3\,W\,m^{-2}K^{-1}$ ($u \approx 0$) and $15\,Wm^{-2}K^{-1}$ ($u \approx 10\,m\,s^{-1}$)
Flux of latent heat (evaporation, condensation) $H_E = -f^*(u, \ldots)\,(e_W - e_A)$	
e_W [mbar]	Water vapor saturation pressure at temperature of water T_W; value reduced in saline waters
e_A [mbar]	Atmospheric water-vapor pressure
$f^*(u, \ldots)\ [W\,m^{-2}\,mbar^{-1}]$	Transfer function Note: f/f* (Bowen coefficient) is roughly constant ($\approx 0.61\,mbar\,K^{-1}$)

Heat fluxes directed from air to water are defined as positive.

and H_W are more stable (Marti and Imboden 1986). In addition, superimposed on the meteorologically induced variations are the diurnal cycles, which, obviously, are especially pronounced in the case of the solar shortwave radiation H_S.

It should also be mentioned that the influence on H_{net} of precipitation onto the lake surface (H_P) is only rarely significant. Changes in surface temperature T_W during rainy weather are usually the result of changes in the flux terms H_W, H_C, and H_E. Also, the heat imported into the water body by inflows and exported via the outlet (H_I) are only of importance in lakes with very high flushing rates.

The geothermal heat flux represents another source of thermally driven mixing. Although usually very small (typically $\approx 0.1\,W\,m^{-2}$), it influences water temperature in those deep zones that are often only slightly, or not at all, affected by the surface heat flux H_{net}. As shown in Sections 6.4 and 6.5, the stratification and mixing of hypolimnetic water can be dominated by exceptionally strong geothermal heat fluxes.

5.2 Potential Energy

As in the case of thermal energy there is no absolute definition of potential energy; we deal rather with changes in energy. The potential energy contained in a stratified water column can be defined as the potential energy difference relative to the situation in which the same water is homogeneously mixed. To characterize changes in potential energy two kinds of quantities are defined, viz., the buoyancy flux J_b (a local quan-

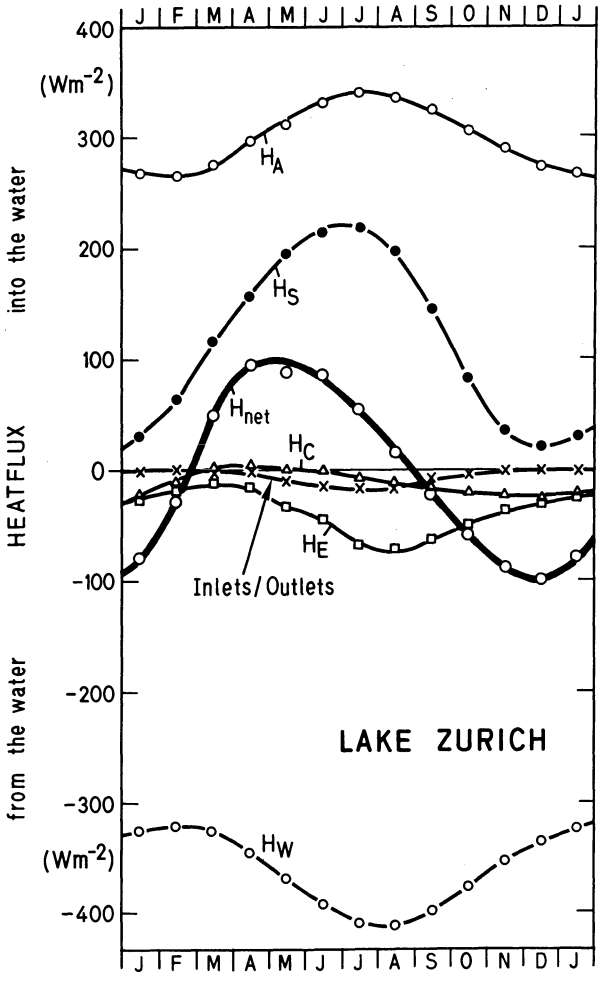


Fig. 5. Monthly mean heat fluxes [$W m^{-2}$] between water and atmosphere calculated for Lake Zurich (Switzerland) from average meteorological conditions. See Table 4 for definitions of the terms. H_I is given by the curve marked *Inlets/Outlets*. (Redrawn from Kuhn 1979)

tity) and the mixed-layer buoyancy fluxes J_b^o and J_b^b (bulk quantities). J_b^o is defined for the surface layer and J_b^b for the benthic boundary layer.

The *buoyancy flux* J_b quantifies the production of potential energy, due to density changes within the water column. It is related to the local vertical exchange of water masses of different density, which, in turn, can be expressed in terms of the local vertical turbulent diffusivity K_z^ρ and the local stability frequency N (Table 5). A negative J_b increases the potential energy of the water column by extracting energy from turbulent currents. Therefore, turbulent mixing in a stably stratified water column always produces a negative buoyancy flux. In contrast, if heavier water is transported downward (convective mixing), J_b is positive, and turbulent kinetic energy is produced.

The *surface buoyancy flux* J_b^o is due to the rate of change of density, $d\rho/dt$, of a well-mixed surface layer of depth h_{mix} (Table 5). It is defined as positive if the surface water is contracting, i.e., if ρ is increasing. Again, a positive J_b^o feeds energy into the water currents and increases mixing. A density change $d\rho$ causes a corresponding change in the mixed layer depth of $dh = -(h_{mix}/\rho)d\rho$. As a result the center of gravity of the mixed-water column is displaced vertically by an amount dh/2. Thus, the change in potential energy per unit area per unit time, P_{pot}, is related to J_b^o by

$$P_{pot} = \frac{dE_{pot}}{dt} = -\frac{1}{2} g h_{mix}^2 \frac{d\rho}{dt}$$

$$= -\frac{1}{2}\rho h_{mix} J_b^o. \qquad [W m^{-2}] \quad (44)$$

The following processes result in a positive buoyancy flux: cooling of the surface water if $T > T_{\rho max}$, warming of the surface water if $T < T_{\rho max}$, evaporation from a salt lake, freezing at the surface of a salt lake, and the inflow of river water with a density exceeding that of the surface water (note that the density of the river water can be high because of low temperature, high salinity, high concentration of suspended particles, or a combination of these factors).

The "inverse" processes will obviously result in negative buoyancy fluxes. Specifically, the addition of fresh water to the surface of a salt lake, e.g., by precipitation, river input, or melting of ice at the surface of salty water, will give rise to a negative buoyancy flux.

The *bottom buoyancy flux* J_b^b, referring to the well-mixed layer that is frequently observed at the bottom of a lake (the benthic boundary layer; see Sect. 6.4), can be defined analogously (Table 5). Note that now J_b^b is positive if less dense water is added to the lake bottom, because such water can rise spontaneously, producing turbulence. An example of the production of positive-bottom buoyancy flux is the input of geothermal heat (if $T > T_{\rho max}$), whereas the addition of cold, salty (i.e., denser) spring water at the bottom of a lake results in a negative bottom buoyancy flux.

5.3 Kinetic Energy

Water in a lake is never at rest. Currents are induced by the wind acting at the water surface,

Table 5. Buoyancy flux, Richardson Numbers, and Monin-Obukhov Length

Buoyancy flux J_b

$$J_b = -\overline{uw'\rho'}\frac{g}{\rho} = K_z^\rho \frac{g}{\rho}\frac{d\rho}{dz} = -K_z^\rho N^2 \quad [W\,kg^{-1}]$$

K_z^ρ [$m^2\,s^{-1}$] Vertical turbulent diffusion coefficient for density

$N = \left(-\frac{g}{\rho}\frac{d\rho}{dz}\right)^{1/2}$ [s^{-1}]: Stability (Brunt-Väisälä) frequency [a]

Surface buoyancy flux J_b^o

$$J_b^o = \frac{g h_{mix}}{\rho}\frac{d\rho}{dt} \quad [W\,kg^{-1}]$$

$g = 9.81\,m\,s^{-2}$ Acceleration due to gravity
h_{mix} [m] Depth of (homogeneous) layer at surface with density ρ

If $d\rho$ is due to temperature change dT caused by heat flux at water surface H_{net},

$$J_b^o = -\alpha g h_{mix}\frac{dT}{dt} = -\frac{\alpha g}{c_p \rho} H_{net} \quad [W\,kg^{-1}]$$

α [K^{-1}] Thermal expansion coefficient of water
c_p [$J\,kg^{-1}\,K^{-1}$] Specific heat of water at constant pressure ($4180\,J\,kg^{-1}\,K^{-1}$)
H_{net} [$W\,m^{-2}$] Net heat flux at water surface (positive, if directed into the water)

If $d\rho$ is due to change of salinity S caused by evaporation or precipitation,

$$J_b^o = g h_{mix} \beta_S \frac{dS}{dt} = \frac{g \beta_S S}{\rho} m_E = -\frac{g \beta_S S}{\rho \lambda_e} H_E \text{ [b]} \quad [W\,kg^{-1}]$$

β_S [−] Coefficient of haline contraction
m_E [$kg\,m^{-2}\,s^{-1}$] Evaporation rate (or precipitation onto lake surface if $m_E < 0$)
H_E [$W\,m^{-2}$] Heat flux due to evaporation (H_E negative for positive m_E)
λ_e [$J\,kg^{-1}$] Latent heat of evaporation of water

Flux Richardson Number R_f (used for $J_b < 0$)

$R_f = -J_b/J_R$ [−]

$J_R = -\overline{u'w'}\frac{\partial u}{\partial z}$ [$W\,kg^{-1}$] Rate of production of turbulent kinetic energy due to Reynolds' stress (see Eqs. 50 and 51)

Monin-Obukhov Length L_M [c]

$L_M = -\frac{u_*^3}{k J_b^o}$ [m]

u_* [$m\,s^{-1}$] Friction velocity (see Eq. 62)
$k = 0.41$ von Kàrmàn constant

Gradient Richardson Number R_i

$R_i = \frac{N^2}{(\partial u/\partial z)^2}$ [−]

u [$m\,s^{-1}$] Horizontal current velocity

All definitions are made for a Cartesian coordinate system with its vertical axis z defined as positive upward.

[a] N is defined for stable stratification only, i.e., for $\frac{d\rho}{dz} < 0$.

[b] Replace $S\beta S$ by $\kappa_{20}\beta_\kappa$ if salinity is expressed by electrical conductivity κ_{20} (Eq. 35).

[c] Note that for *positive* J_b^o (condition of convection), L_M is negative and defines a depth at which the buoyancy flux and wind shear are of equal importance for the production of turbulent kinetic energy (TKE). Below this depth buoyancy is the dominant source of TKE. For *negative* J_b^o (stabilizing conditions), L_M is positive and defines the depth to which the wind shear can mix the water column against the stabilizing effect of the density stratification, which is produced either by warming or by input of less saline water.

by inflows, by density gradients caused by differential heating and cooling, or by varying concentrations of dissolved substances (see Sect. 4.1). Strong winds during storm events are often the largest source of kinetic energy (Fig. 3).

The wind force creates a stress τ_o at the lake surface that is assumed to be constant within a certain layer extending from the air into the water (constant stress layer). It is difficult to measure τ_o directly; therefore, it is commonly parameterized by the square of the wind speed, W_{10}, measured at a standard height of 10 m above the water surface:

$$\tau_o = \rho_{air} C_{10} W_{10}^2, \quad [N\,m^{-2}] \tag{45}$$

where ρ_{air} is the density of air ($\approx 1.2\,kg\,m^{-3}$ at 20 °C) and C_{10} is the so-called drag (or wind stress) coefficient, which has been the subject of a great number of experimental investigations. Not very surprisingly, it appears that C_{10} is not really a constant, because the coupling between air and water depends on the roughness of the interface, i.e., on the wave field. In the ocean or in large lakes, C_{10} is expected to be larger than in a small lake. Also, because wave heights increase with increasing wind speed, C_{10} should be larger for large W_{10}. Based on data from numerous investigators Amorocho and deVries (1980) identified three wind-speed regimes for C_{10}. For $W_{10} \leqslant 7\,m\,s^{-1}$, where the wind waves do not break, C_{10} is approximately 0.001; in an intermediate regime, characterized by the onset of breaking waves, C_{10} increases steadily up to a value of 0.0025 at $W_{10} = 17$ to $20\,m\,s^{-1}$; and at higher wind speeds breaker saturation is attained and C_{10} becomes constant.

Connected with the stress τ_o acting on the lake surface is an energy flux from the atmosphere down to the air–water interface. At a height of 10 m above the water surface the energy flux, P_{10}, is given by

$$P_{10} = \tau_o W_{10} = \rho_{air} C_{10} W_{10}^3. \quad [W\,m^{-2}] \tag{46}$$

It is generally found that a small fraction χ of approximately 1–2% of P_{10} is transferred to the water and is available for mixing in the surface layer (Denman and Miyake 1973). Thus, the kinetic energy flux from the wind field into the lake is

$$P_{kin,W} = \chi \rho_{air} C_{10} W_{10}^3 = \eta W_{10}^3, \quad [W\,m^{-2}] \tag{47}$$

where $\eta = \chi \rho_{air} C_{10}$ typically lies between 1 and $5 \times 10^{-5}\,kg\,m^{-3}$. (Note that when η is expressed in $kg\,m^{-3}$ and W_{10} in $m\,s^{-1}$, $P_{kin,W}$ will be expressed in $W\,m^{-2}$.)

The vertical structure of mixing, characterized by the production of turbulent kinetic energy, is related to the vertical-shear profile, which is the result of the wind-induced energy flux. The dependence of mixing in the surface layer on the wind stress is discussed in Section 6.2.

Rivers entering a lake are another external source of kinetic energy, which, if normalized by the lake surface area, can be expressed as

$$P_{kin,R} = \frac{1}{2} \rho\, q\, \overline{u_R^2}, \quad [W\,m^{-2}] \tag{48}$$

where $q[m\,s^{-1}]$ is the inflow of water per unit lake area (hydraulic loading) and $\overline{u_R^2}$ is the mean square water velocity at the river mouth. In order for $P_{kin,R}$ to reach a size comparable to the effect of a continuous wind speed of, say, $W_{10} = 1\,m\,s^{-1}$ (say, 1% of $P_{10} = 1.2 \times 10^{-5}\,W\,m^{-2}$), assuming a typical $\overline{u_R^2} = 0.25\,m^2\,s^{-2}$, the hydraulic loading q has to be on the order of $12\,m\,yr^{-1}$, a value attained by an appreciable number of freshwater lakes (Table 1). Thus, from a purely energetic point of view inflows are important; however, their kinetic energy undergoes a great degree of local dissipation, and so inflows affect lake dynamics differently than does the wind, which acts on the whole lake surface.

5.4 Turbulent Kinetic Energy Balance in Stratified Water

As stated in the introduction, mixing results from the turbulent part of the advective motion. In contrast to the mean flow, turbulence is nondirectional, although it may be anisotropic. Thus, the turbulent kinetic energy (TKE), defined by

$$TKE = \frac{1}{2} \sum_i \overline{u_i'^2}, \tag{49}$$

is the relevant property to describe turbulent mixing. As discussed in Section 3.2 the separation of mean flow from turbulent velocity fluctuations (Eq. 11) is arbitrary to a certain extent, and inherently selects some time and space scale, which, in turn, depends on the system and process under consideration. Such scales are discussed in Section 7.1.

Let us assume that the appropriate scale can be chosen. The momentum equation can then be

used to derive a dynamic equation for TKE similarly to the way the expression for the mean flow (Eq. 12) was derived by Reynolds' decomposition (e.g., see Stull 1988 for details). For homogeneous conditions (no spatial gradients of TKE), one obtains the following expression (i,j = Cartesian coordinates x,y,z; z positive upward, ν: viscosity):

$$\frac{\partial}{\partial t}(\mathrm{TKE}) = \underbrace{-\sum_{ij} \overline{u_i' u_j'} \frac{\partial \bar{U}_i}{\partial x_j}}_{(1)} \underbrace{- \overline{\rho' u_3'} \frac{g}{\rho}}_{(2)}$$

$$\underbrace{-\nu \sum_{ij} \overline{\left(\frac{\partial u_i'}{\partial x_j} + \frac{\partial u_j'}{\partial x_i}\right) \frac{\partial u_i'}{\partial x_j}}}_{(3)}. \quad [\mathrm{W\,kg^{-1}}] \qquad (50)$$

The terms on the right side describe the sources and sinks of the turbulent kinetic energy (see also Table 5). For horizontal mean flow along the x axis ($\bar{U}_1 \equiv U$, $\bar{U}_2 = \bar{U}_3 = 0$, and $u_3' \equiv w'$), and for homogeneous and isotropic turbulence, the three terms take on the following simple forms:

1. Rate of production of TKE (J_R) due to the Reynolds' stress:

$$J_R = -\overline{u'w'} \frac{\partial U}{\partial z} \qquad (51)$$

2. Buoyancy flux (J_b; change of potential energy of the water column):

$$J_b = -\overline{\rho' w'} \frac{g}{\rho} = K_z \frac{\partial \rho}{\partial z} \frac{g}{\rho} = -K_z N^2 \qquad (52)$$

3. Rate of dissipation of TKE (ε) by viscous (internal) friction:

$$\varepsilon = 7.5 \nu \overline{\left(\frac{\partial u'}{\partial z}\right)^2} \qquad (53)$$

(The factor 7.5 applies to the special situation, which is assumed here.) Thus, for homogeneous turbulence the temporal change in TKE is due to the balance of TKE production from the mean flow J_R (through the Reynolds' stress), the buoyancy flux J_b, and the TKE dissipation ε by viscous forces:

$$\frac{\partial}{\partial t}(\mathrm{TKE}) = J_R + J_b - \varepsilon. \qquad (54)$$

Note that J_R and ε are always positive, whereas J_b can take on either sign. For $J_b < 0$, mixing is "against the density gradient," and the potential energy of the water column is increased, whereas for $J_b > 0$, TKE is produced by the sinking of heavier or rising of lighter water parcels (convective turbulence). For turbulence produced by Reynolds' stress it is common to define a ratio expressing the consumption of TKE by the storage of potential energy, J_b, relative to the production of TKE. Two quantities are defined to describe the efficiency of the transfer to buoyancy flux, the Flux Richardson Number (Table 5)

$$R_f = -J_b/J_R, \qquad (55)$$

and the *mixing efficiency*

$$\gamma_{mix} = -J_b/\varepsilon = K_d N^2/\varepsilon. \qquad (56)$$

For stationary conditions Eq. (54) can be written as $\varepsilon = J_R + J_b$. Thus, the mixing efficiency can be expressed as $\gamma_{mix} = R_f/(1 - R_f)$.

Only a small fraction of the available kinetic energy is used for mixing against the density gradient and is transferred into potential energy, because turbulent motion cannot efficiently generate low-entropy potential energy. Furthermore, viscous dissipation occurs in each velocity component, whereas the production of negative buoyancy occurs only via the diapycnal component. Experimentally, γ_{mix} has been found to lie within the range 0.05–0.25 depending on the mixing regime (Sect. 6.3).

This concept has also occasionally been used for negative buoyancy flux produced by the increase in stability resulting from heating of the water column (Sect. 6.2). In this case R_f is the ratio of the TKE suppressed by the negative buoyancy flux, due to heating to the TKE production J_R. In the well-mixed surface layer this approach serves to calculate the dynamics of the depth of the mixed layer (Sect. 6.2).

5.5 Internal Turbulent Energy Fluxes: Turbulence Cascade

Equation (50) expresses the TKE balance regardless of the spatial and temporal scales among which it is distributed. In order to understand the consequences of the Reynolds' decomposition (Eq. 11), we should also address the question of how the TKE is typically distributed in space and time. Energy is brought into lakes at different length scales. Major turbulent production by Reynolds' stress occurs at large scales, termed the *energy-containing range*, where a significant part of the energy input also occurs. Energy is generally

transferred from low to high frequencies and from large to small scales. This flow, called the *turbulence cascade*, is generated by nonlinear interactions originating in the nonlinear term of the momentum Eq. (5). At the smallest scales, given by the Kolmogorov Scale $L_K = (\nu^3/\varepsilon)^{1/4}$, the turbulent kinetic energy is converted into heat by molecular viscosity ν. According to L_K the size of the smallest existing eddies depends only on the level of turbulence (and the viscosity): A higher level of turbulence is able to produce smaller scales before the energy dissipates. In summary, isopycnal eddy sizes cover a range extending from the size of the lake itself down to a few millimeters. A summary of the various relevant scales describing turbulence is given in Table 6.

Under isotropic, homogeneous, and stationary conditions a range of eddy size develops in which the spectrum of turbulent kinetic energy is independent of both the production of TKE and the energy dissipation due to viscosity. If energy is neither added by the mean flow nor removed by viscous dissipation, the energy flux across the so-called *inertial subrange* is constant and equal to the energy dissipation rate at the small-scale end of the spectrum. The spectrum of turbulent kinetic energy E(k) depends only on the dissipation rate ε. E(k)dk is the energy of eddies with wave numbers between k and k + dk (k = 2π/length of eddy). Dimensional analysis yields

$$E(k) = \alpha\varepsilon^{2/3}k^{-5/3}. \quad [W\,kg^{-1}\,m\,s = m^3\,s^{-2}] \tag{57}$$

Experimental determination put the value of the nondimensional constant α at approximately 1.56 (Wyngaard and Cote 1971). Because of the re-

Table 6. Tubulence length scales

Length scale	Definition	Typical range	Significance
Energy-containing	L_i	1 to 10^3 m	Scale at which energy is brought into system, e.g., length scale of lake for seiches, mixed-layer depth for surface mixing
Kolmogorov	$L_K = (\nu^3/\varepsilon)^{1/4}$	10^{-3} to 10^{-2} m	Viscous force equals inertial force: lower end of TKE and dissipation spectra, i.e., velocity fluctuations (gradients) disappear for smaller scales
Batchelor	$L_B = (\nu D^2/\varepsilon)^{1/4}$	$\approx 10^{-4}$ (salt) to $\approx 10^{-3}$ m (temperature)	Lower end of dissipation spectrum of a passive scalar (temperature, salt, etc.): fluctuations (gradients) of the scalar disappear for smaller scales
Ozmidov	$L_O = (\varepsilon/N^3)^{1/2}$	10^{-2} to 1 m	Buoyancy force equals inertial force: maximum vertical scale of eddies; larger eddies are suppressed by buoyancy
Thorpe-displacement	Δ_T		Absolute vertical displacement of a water parcel from its "equilibrium position" in the corresponding smooth and stable (reordered) profile
Thorpe	$L_T = (\overline{\Delta_T^2})^{1/2}$		Root mean square of Thorpe displacements Δ_T within a water column: L_T is a statistical measure for the vertical size of the overturning eddies
Monin-Obukhov length	$L_M = -\frac{u_*^3}{kJ_b^o} =$	1 to 10^2 m	Depth (height) where production of TKE by shear is equal to production of TKE by buoyancy flux

Definitions and typical sizes of relevant parameters:
ν, kinematic viscosity, 1 to $2 \cdot 10^{-6}\,m^2\,s^{-1}$; ε, rate of dissipation of TKE, 10^{-10} to $10^{-7}\,m^2\,s^{-3}$ ($W\,kg^{-1}$); N, stability frequency, 10^{-3} to $10^{-2}\,s^{-1}$ (deep hypolimnion down to $10^{-4}\,s^{-1}$); D, molecular-diffusion coefficient of scalar property (temperature, salt, etc.), 10^{-10} to $10^{-9}\,m^2\,s^{-1}$ for salt and $\approx 1.4 \cdot 10^{-7}\,m^2\,s^{-1}$ for temperature.

quired isotropy, the inertial subranges are restricted to nonstratified water layers such as the well-mixed boundary layers (the epilimnion and the bottom boundary layer), and consequently extend only over a range of several meters to decimeters. In Fig. 6 an example is given for Lake Tahoe (Dillon and Powell 1979).

A conservative scalar property (salt, temperature, etc.) mixed by a turbulent flow produces a fluctuation spectrum that again covers the range from the energy-containing eddies to the smallest scales limited by molecular properties. The smallest scales not only depend on ε and ν (as does L_K), but also on the molecular diffusivity D of the scalar. The corresponding scale, often called the *Batchelor Scale*, $L_B = (\nu D^2/\varepsilon)^{1/4}$, is smaller than L_K, because the molecular diffusivities, D^T and D^C, are always smaller than ν. For wave numbers k well below L_B^{-1}, the molecular diffusivity of heat or salt does not influence the spectrum very much; therefore, the spectra are similar to the velocity spectrum E(k), which falls off proportional to $k^{-5/3}$ (inertial-convective subrange). For smaller scales, velocity fluctuations are reduced progressively by viscosity, but the diffusivity of heat or salt is not yet effective (viscous-convective subrange). This part of the spectrum, also called the *Batchelor Spectrum* (Batchelor 1959), is depicted in Fig. 6 as the range in which E(k) falls off proportional to k^{-1}. Its upper limit is determined by $k = L_B^{-1}$.

Large eddies tend to be anisotropic, because their structure is related to the energy input. Successive interaction between the three space components redistributes the turbulent kinetic energy equally among the components, leading to progressive isotropy at smaller scales. Because of stratification, however, complete isotropy is seldom attained, not even at the smallest scales. For the dissipation range ($k \sim L_K^{-1}$) to be isotropic, Gargett et al. (1984) found that the turbulence level ε has to obey the condition $\varepsilon > 200\,\nu N^2$. This means that the stronger the stratification (expressed by N) and the higher the viscosity (expressed by ν) of the water, the larger the critical size of ε.

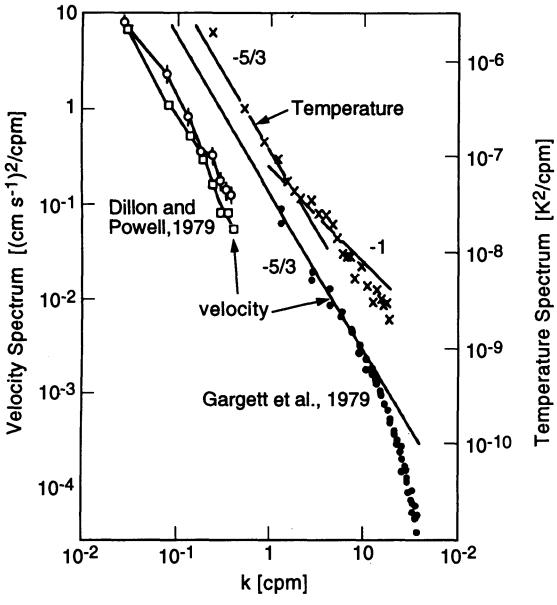


Fig. 6. Velocity and temperature spectra measured in the surface mixed layer of the ocean by Gargett et al. (1979). Because of viscosity, at $k > 10$ cpm (cycles per meter) the velocity spectrum drops below the $k^{-5/3}$ line. The cutoff in the temperature spectrum (Batchelor wave number), located just above the upper end of the plotted points, is not resolved. The two lowest curves represent the velocity spectra observed by Dillon and Powell (1979) in the mixed layer of Lake Tahoe

6 Mixing Processes in Lakes

In density-stratified lakes small-scale turbulence is essential for energy and mass transfer. Although the energy is brought into the system at much larger scales, it is the small-scale turbulent motion that brings different water masses in close enough contact for mixing by viscosity and diffusivity to occur (Eckart 1948). In addition, in density-stratified water only small-scale eddies can exist. Because of space limitations, this section concentrates on these small-scale processes. Descriptions of additional phenomena may be found in other textbooks (e.g., Imberger and Patterson 1990).

In lakes two principal sources of turbulent kinetic energy (TKE) in Eq. (54) have to be considered, viz., Reynolds' stress J_R and buoyancy flux J_b. Because dissipation ε is the main TKE sink, ε is a quantitative measure of the rate of production of TKE, and is therefore characteristic of the level of turbulence. In the absence of stratification ($N = 0$) and for homogeneous and steady conditions, the TKE equation (Eq. 54) states that the rate of production of turbulence is equal to its dissipation rate. Explicitly, this implies that $J_R = \varepsilon$ in the surface and bottom boundary layers, and $J_b^o = \varepsilon$ for convectively driven surface mixing and double diffusion. Usually, however,

most of the water column is stratified to some extent. Because the mixing of stratified water always results in an increase in potential energy, the buoyancy flux also has to be included as a (minor) sink of TKE in Eq. (54).

Because of the large diversity in the characteristic properties of lakes, the basic sources of mixing can lead to very different mixing phenomena in real situations. Some of these are outlined schematically in Fig. 7. In any given lake the relevant mixing processes depend on external forcing (river inflow and outflow, turbidity currents, underwater springs, wind, surface heat flux, geothermal heat flux, etc.) as well as lake morphometry (boundary mixing, differential heating/cooling/mixing, etc.). The goal of this chapter is to describe the most important mixing mechanisms. Specific examples are added for illustration. We start with an overview of the various types of waves occurring in lakes, because waves play a crucial role in energy storage and also act as the link between the input of energy and the production of turbulence.

6.1 Waves and Mixing

6.1.1 "Wave Zoo" in Lakes

Immediately apparent to any observer are lake-surface gravity waves. These are, however, only one of many types of wave existing in lakes, some of which have practically no effect on the water surface. For wave motion to exist two forces are required: one tending to initiate motion and one tending to restore equilibrium. Different equilibria and restoring forces give rise to numerous types of waves (Lighthill 1978). Waves in lakes are excited mostly by wind stress. In larger lakes, however, atmospheric pressure changes and tidal forces can be important as well. Although rare, waves of exceptionally large amplitude can be induced by seismic activity and landslides (Bünti 1914; Siegenthaler and Sturm 1991).

Waves are usually categorized with regard to equilibrium state and restoring force (Table 7). A lake water body can oscillate at its surface and internally about surfaces of equal density. Because in the latter case the surfaces of constant density do not coincide with the surfaces of constant pressure, these internal waves are referred to as *baroclinic*. In contrast, surface waves are referred

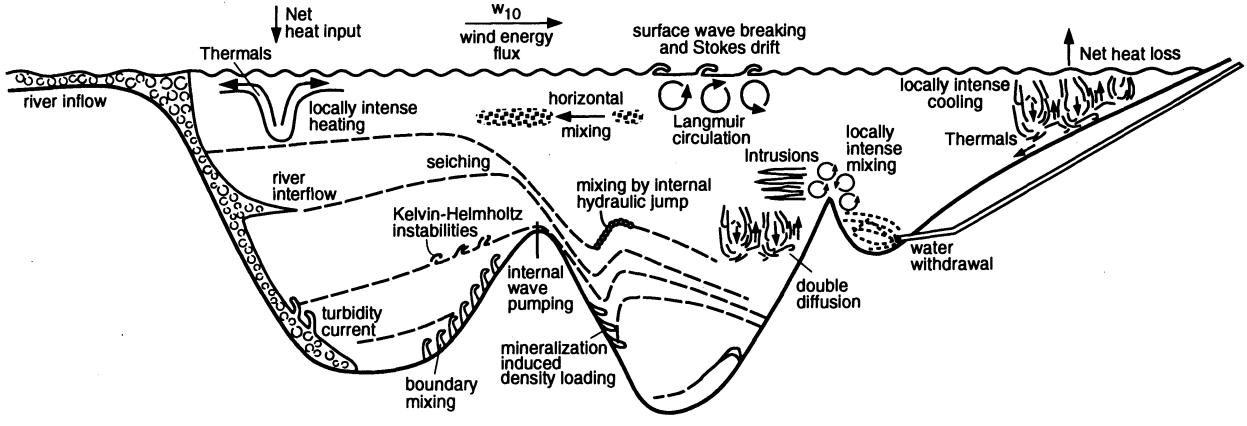


Fig. 7. Schematic overview of mixing processes in lakes. Wind introduces kinetic energy and produces turbulence by means of surface waves and drift-shear (Stokes' drift) in a relatively thin surface layer of typically a few meters of thickness (Fig. 9a). This layer is also subject to vertical Langmuir circulation if the wind speed exceeds approximately $3\,m\,s^{-1}$. Convective mixing, driven by density production (usually cooling), efficiently mixes the surface layer by causing the sinking and rising of water parcels (thermals). A decrease in density (usually brought about by heating) stabilizes the water column and consequently suppresses vertical exchange. Waves (internal seiches; Fig. 8) are activated by the wind and lead to horizontal currents (Fig. 14a), and, therefore, to internal mixing (Fig. 12), and especially to boundary mixing (Fig. 14b). The subsequent small-scale (eddy-type) turbulent diffusion (Fig. 11) recycles nutrients and affects the exchange through the sediment–water interface. Density currents, e.g., turbidity flow from tributaries or currents stimulated by differential mixing (or heating/cooling), transport water masses vertically and horizontally on a basinwide scale (Fig. 22)

Table 7. "Wave zoo" in lakes

Wave	Restoring force	Characteristics of governing wave equation	Dispersion relation
Capillary	Surface tension		$k^3 = \frac{\rho}{\delta}\omega^2$
Surface gravity	Gravity	First class, barotropic	$\tanh(kH) = \omega^2/gk$ long: $k^2 = \omega^2/gH$ short: $k = \omega^2/g$
Internal gravity	Gravity in density-stratified fluid	ρ = variable	$k^2 = \frac{\omega^2 - f^2}{N^2 - \omega^2}m^2$
Inertial	Coriolis force		
Poincaré (or Sverdrup)	Gravity and Coriolis force	First class, long gravity waves affected by Coriolis force $f \neq 0$, ρ = const	$k^2 = \frac{\omega^2 - f^2}{gh}$
Kelvin	Like Poincaré, but with boundary conditions	f = const, depth H = const, $u_{boundary} = 0$	$k = \frac{\omega}{\sqrt{gH}}$
Planetary or Rossby	Gravity, Coriolis force; potential vorticity	Large scale, long period, 2nd class, f linear approximation of ϕ, ρ = const, H = const	$k^2 = -\frac{\beta k}{\omega}$
Topographical Rossby waves	Gravity, Coriolis force; potential vorticity	Similar to Rossby waves, but water depth $H \neq$ const	

Definitions: First class: gravity waves modified by rotation; Second class: variation of potential vorticity; ω, wave frequency; ρ, density of water; k, horizontal wave numbers; m, vertical wave number; N, buoyancy frequency; H, water depth; δ, surface tension; $f = 2\Omega \sin\phi$, inertial frequency ($\Omega = 7.27 \cdot 10^{-5} s^{-1}$); ϕ, geographical latitude; $\beta = (2\Omega/R)\cos\phi$, change of f with latitudinal distance (R = earth radius).

Variables for two-layer Merian Formula (Eq. 58):

$g' = \frac{\Delta\rho}{\rho} g$ Reduced gravity ($\Delta\rho$: density difference between layers).

$h' = h_1 \cdot h_2/(h_1 + h_2) = [(1/h_1) + (1/h_2)]^{-1}$ Reduced depth (h_1, h_2: depth of layers).

to as *barotropic*. They do not require the existence of density gradients in the water for their excitation. The restoring forces are: surface tension (capillary waves), gravity (gravity waves), Coriolis force (inertial waves), and change of potential vorticity (Rossby waves). Change of potential vorticity can be due either to a change in inertial frequency (planetary waves) or to a change in basin depth (topographical Rossby waves). It is obvious that combinations of restoring forces are often present such as, for example, gravity and Coriolis force (Poincaré or Sverdrup waves). For a detailed discussion of waves in lakes the reader is referred to Mortimer (1974), Hutter (1983), Stocker and Hutter (1987), and LeBlond and Mysak (1978).

Capillary waves, with wavelengths on the order of 1 cm, are the shortest waves present at the lake surface. Surface gravity waves are omnipresent in lakes: both short gravity waves (with wavelengths less than water depth) and long gravity waves (with wavelengths greater than water depth) are excited simultaneously. The longest surface waves are the long basin standing waves (*seiches*) first observed by Forel (1876) in Lake Geneva. This barotropic seiching motion can easily be observed with a limnigraph (water-level recorder) especially at the end of a lake, but its observation

is possible even in deep water using high-sensitivity current meters.

A water parcel moving with velocity u, assumed to be subject only to the Coriolis force, follows a circle with radius R = u/f, the so-called inertial circle ($f = 1.46 \times 10^{-4} \sin\phi$ [s^{-1}] is the inertial frequency and ϕ [°] is the geographical latitude). Gravity waves in lakes with dimensions greater than R are affected by Coriolis forces. Poincaré waves can be observed especially in the central part of such lakes. A good example of this is given by Mortimer (1974) for Lake Michigan. Near the shore of the water basin the Coriolis force leads to another kind of wave called Kelvin waves. The amplitudes of Kelvin waves are largest at the lake shore, decaying exponentially with distance from the shore. In the northern hemisphere their direction of propagation is such that with the shore on the right, they move anticlockwise around the basin. An impressive illustration of Kelvin waves is given by Mortimer (1975).

Potential vorticity depends on both inertial frequency and total water depth. Because of the limited north–south extent of lakes, the latitude ϕ, and thus the inertial frequency f, does not change much within any one lake. However, lake topography does change much more than f; therefore, Rossby waves, also known as topographical (Rossby) waves, can exist in lakes. In the simplest case the whole basin oscillation consists of parallel currents on opposite sides of the basin with a jet across the lake center. These low-frequency oscillations have been observed in lakes by Saylor et al. (1980) and Mysak et al. (1983; see also Fig. 8).

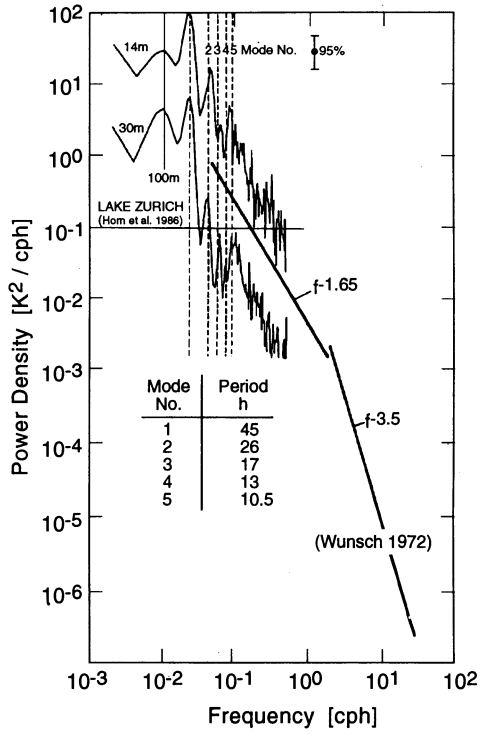


Fig. 8. Spectra of temperature fluctuations $(T')^2$ in Lake Zurich (Switzerland) by Horn et al. (1986) reveal the "red" nature of internal waves (energy drops at high frequencies). Long-term fluctuations are due principally to internal seiches. Note that the basin modes of the first vertical seiche mode (indicated by the numbers *1–5*) are not harmonics in the strict sense, i.e., their periods are not whole fractions of 45 h. The maximum at 100 h may be due to topographical Rossby waves. The *straight lines* summarize the spectrum from temperature fluctuations measured in the thermocline of the Atlantic Ocean near Bermuda (Wunsch 1972). The internal-wave spectra from both the lake and the ocean fall off proportionally to $f^{-5/3}$. *cph*: Cycles per hour

6.1.2 Surface-Wave Mixing

With regard to mixing (both internal and surficial), gravity waves are the most important type of wave. A glance at the surface of a lake demonstrates how surface waves cause mixing. During strong winds, breaking surface waves lead to an efficient mixing of surface water. During most of the time, however, surface waves have small amplitudes and their motions are almost reversible. In this case only little energy is lost by turbulence at the open lake surface, but some surface mixing still occurs along the shoreline. Stokes' drift is then the dominant irreversible component of wave motion, causing a horizontal net transport. Stokes' drift results from the fact that the orbits of the water parcels are not properly closed, because the horizontal velocity component of the orbits decreases with depth. During calm and sunny days strong temperature gradients at the very top of the water column demonstrate the absence of surface-wave mixing.

Another minor contribution to mixing comes from the internal currents associated with surface waves. Those currents, which can be observed even at the deep sediment boundary, are, however, of less importance for boundary mixing than the currents originating from internal waves. Boundary mixing generated by internal waves is discussed in Section 6.4.

6.1.3 *Internal-Wave Mixing*

Internal waves are crucial for mixing in the stratified water column below the energetic surface layer. They induce shear in the interior of the water column (especially in the zone between hypolimnion and epilimnion) as well as at the sediment boundary.

Internal gravity waves are mostly generated by wind. The wind stress piles up surface water at the leeward end of the lake. At the same time water from greater depth rises closer to the surface at the windward end. When the wind relaxes the tilted interface starts to oscillate. Because the solid barrier of the lake boundary reflects internal waves, the superposition of the original and reflected waves gives rise to standing internal waves called *internal seiches*. These are a prominent feature of closed basins and can be found in nearly all internal-wave spectra (Figs. 8 and 14). In addition, the internal-wave field contains a large variety of other modes with frequencies ranging from the inertial frequency f to the stability frequency N.

In a stratified fluid an infinite number of eigenvalues exists with periods $T_{n,m}$, which can be labeled with two "quantum numbers" associated with the horizontal mode (n) and the vertical mode (m). In the simplest case of the first vertical mode (m = 1), corresponding to a two-layer system, longitudinal oscillation periods $T_{n,1}$ and wavelength $\lambda_{n,1}$ for a basin of length L can be approximated by the generalized Merian Formula

$$T_{n,1} = \frac{2L}{n}(g'h')^{-1/2}; \quad \lambda_{n,1} = \frac{2L}{n}, \tag{58}$$

where n is the number of nodal lines and g′ and h′ are reduced gravity and depth, respectively, as defined in Table 7. An example of an internal-temperature spectrum that clearly shows higher horizontal modes up to n = 5 of the first vertical mode (m = 1) is given in Fig. 8. A better approximation is given by the extended Defant procedure (Mortimer 1979). Examples are given by Lemmin and Mortimer (1986). These examples (Fig. 8) show that frequencies of higher horizontal modes are not harmonics in the strict sense, as is the case in acoustics.

In order to describe higher vertical modes, a finer vertical grid is needed. An impressive example of a second vertical seiche mode (m = 2) (Fig. 14) has been described by Münnich et al. (1992) using both three-layer and continuous-stratification models. An even more detailed description is given by a two-dimensional model that includes lake topography as well as a continuous stratification. Münnich (1993) has shown that several modes with similar periods and spatial scales, but differing spatial structures, become possible if both these factors are taken into account.

Internal waves produce horizontal currents in the hypolimnion that may lead to turbulent mixing provided they are strong enough to overcome the density stratification. As long as the Gradient Richardson Number R_i, which expresses the ratio of the vertical shear $\partial u/\partial z$ to the vertical density stability N (Table 5), remains much greater than approximately 0.25, turbulence, and thus mixing, is suppressed (Fig. 12). The thermocline then acts as a slippery surface permitting relative motions of the surface layer with regard to the hypolimnion. Under such conditions internal waves have relatively small amplitudes and are well within the linear range. When turbulence is nearly absent energy dissipation is low and internal waves can persist for weeks (Lemmin 1987). Internal seiches of higher vertical mode (m > 1) correspond to the oscillation of an (m + 1)-layer system. Their amplitudes are generally smaller, but the induced horizontal currents change sign over smaller vertical scales giving rise to larger shear (Münnich et al. 1992).

For $R_i < 0.25$, streamlines become increasingly disturbed until they turn over and irreversibly mix adjacent layers (Fig. 11). In this case the energy dissipation is large and the internal-wave field decays quickly (Fig. 21). The wave-induced growth of the so-called Kelvin-Helmholtz billows, and their subsequent breakdown has been beautifully documented in natural waters with dye experiments in the Mediterranean thermocline by Woods (1968). The corresponding irreversible mixing across density interfaces is discussed in Section 6.3.

6.2 Mixing in the Surface Layer

Wind stress, surface buoyancy flux, and river inflows supply the energy required for turbulent mixing in the surface layer of a lake. Although wind stress is usually responsible for mixing in the uppermost part, the sharp density interface com-

monly found at the end of the stratification period results from the positive buoyancy flux produced by surface cooling and subsequent convection in the mixed layer. Whereas wind and convective turbulence are discussed in this section, mixing due to river inflows is not considered further, because this complicated process is beyond the scope of this chapter.

6.2.1 *Wind-Driven Turbulence*

As shown in Section 5.3 wind introduces turbulent kinetic energy to the lake by creating a stress τ_o acting on the lake surface (Eq. 45). This wind stress, which is usually assumed to be constant within a layer extending from the air into the water (constant-stress layer), can be expressed as

$$\tau_o = \rho_{air}\overline{u'_{air}w'_{air}} = \rho\overline{u'w'}, \quad [N\,m^{-2}] \qquad (59)$$

where u′ and w′ are the horizontal- and vertical-velocity fluctuations, respectively, and the variables without indices refer to the water column. In contrast to the definition introduced in Eq. (13), the sign of τ_o is chosen in order to indicate a stress acting from the atmosphere to the water.

Based on dimensional arguments it can be shown that in the constant-stress layer at steady state, the functional dependence of the horizontal velocity u on depth h (positive downward, h = −z) is given by the "law of the wall":

$$\frac{\partial u}{\partial h} = -\frac{(\tau_o/\rho)^{1/2}}{kh}, \quad [s^{-1}] \qquad (60)$$

where k = 0.41 is the von Kàrmàn constant. Integration yields the well-known logarithmic profile

$$u(h) = -\frac{u_*}{k}\ln\left(\frac{h}{h_o}\right), \qquad (61)$$

with the following definition for the friction velocity:

$$u_* = (\tau_o/\rho)^{1/2}. \qquad (62)$$

According to *Fick's Second Law*, the rate of production of turbulent kinetic energy per unit mass J_R is proportional to the vertical gradient of the energy flux, $\partial(\tau_o \cdot u)/\partial z$. Within the constant-stress layer ($\partial\tau_o/\partial z = 0$), J_R is then given simply by

$$J_R = -\tau_o/\rho\frac{\partial u}{\partial h} = -\overline{u'w'}\frac{\partial u}{\partial h}. \quad [W\,kg^{-1}] \qquad (63)$$

Inserting Eqs. (60) and (62) into Eq. (63) yields the following expression for the rate of production of TKE:

$$J_R = \frac{(\tau_o/\rho)^{3/2}}{kh} = \frac{u_*^3}{kh}, \quad [W\,kg^{-1}] \qquad (64)$$

which is specific to the logarithmic boundary layer. For homogeneous and stationary conditions TKE production J_R and dissipation ε are in balance. In the nonstratified surface water (where buoyancy flux $J_b = 0$), production must be equal to dissipation, i.e.,

$$\varepsilon = J_R = \frac{u_*^3}{kh} = \left(\frac{\rho_{air}C_{10}}{\rho}\right)^{3/2}\frac{W_{10}^3}{kh}, \quad [W\,kg^{-1}] \qquad (65)$$

and consequently we can estimate the level of wind-induced turbulence within the mixed layer from the wind velocity W_{10} alone.

Experimental verification of Eq. (65) is sparse. Temperature microstructure measurements in lakes carried out by Dillon et al. (1981), Imberger (1985), and Piepke et al. (unpubl.) support a relationship of the form ε = constant/h (Fig. 9a). Turbulence measurements made by Oakey and Elliott (1982) using the *dissipation method* (Table 8) in an ocean mixed layer are consistent with $\varepsilon = \text{const}\ W_{10}^3$. Measurements carried out by Lombardo and Gregg (1989) in an ocean-surface boundary layer show that dissipation rates match both the vertical decay of ε proportional to h^{-1} and the magnitude of the scaling for wind-driven turbulence. They found that the relationship

$$\varepsilon_{exp} = 1.8 \cdot \left(\frac{\rho_{air}C_{10}}{\rho}\right)^{3/2}\frac{W_{10}^3}{kh} \quad [W\,kg^{-1}] \qquad (66)$$

gave the best fit to data measured during periods of wind-dominated turbulence. Measurements in lakes yield a coefficient somewhat smaller than 1.8 (Piepke et al. unpubl.). Although this factor (for several reasons) is not well established experimentally, the overall level of turbulence in a well-mixed and stationary surface layer can be predicted relatively well.

An epilimnion subjected to wind-stress forcing is, however, not always well mixed with regard to density. If some stability (N^2) remains the buoyancy term cannot be omitted from Eq. (50). In such cases mixing can be described by a process analogous to diffusion. The corresponding vertical eddy diffusion coefficient K_z can be estimated by assuming that at every depth a constant fraction

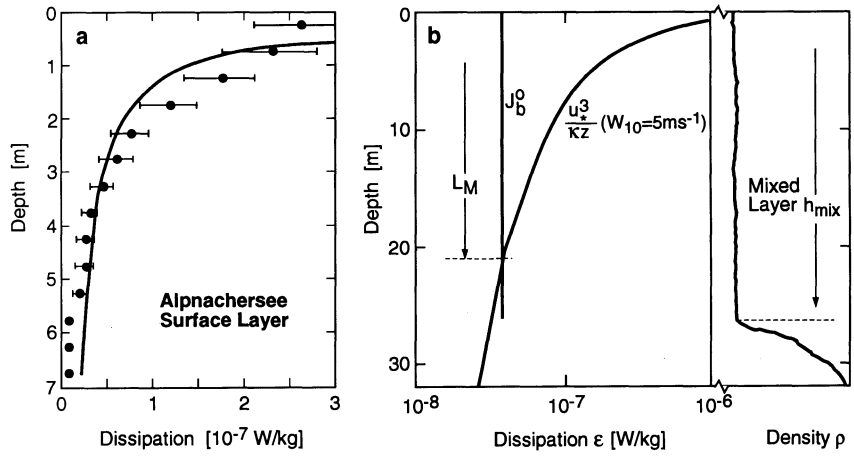


Fig. 9. **a** Rate of dissipation of turbulent kinetic energy ε as a function of depth as measured in Alpnachersee (Switzerland). Within the well-mixed surface boundary layer (the uppermost 5 m), dissipation follows similarity scaling within the 63% confidence level and decreases as h^{-1} (Eq. 65). In the stratified water column (below 5 m) the production of turbulent kinetic energy collapses rapidly due to decreasing shear stress τ and suppression by the stratification N^2. (Data by Piepke et al., unpubl.) **b** Definition of the Monin-Obukhov Length L_M for positive surface buoyancy flux J_b^o (due to net heat loss at the water surface) and wind-induced turbulence ε. L_M is the depth at which the contribution to mixing from J_b^o (constant with depth) and from the wind friction ($u_*^3/k \cdot h$; decreasing with depth) are equal. As a typical example, values for J_b^o and ε were calculated from T = 15 °C, $H_{net} = -100\,W\,m^{-2}$, and a wind speed of $5\,m\,s^{-1}$. In this case L_M is smaller than h_{mix}, and thus entrainment at the base of the mixed layer occurs due to convection. (See text for symbols)

Table 8. Methods for estimating diapycnal eddy diffusivity

Method	Assumptions	Equation[a]	References
Budget-gradient	Rate of change of property C below z solely by local diapycnal flux (C can be replaced by T)	$K_d(z) = \frac{\int_{Sed}^{z} A(z')\frac{\partial C}{\partial t}(z')\,dz'}{A(z)\frac{\partial C}{\partial z}(z)}$	Powell and Jassby (1974)
Tracer[b]	Broadening of a tracer distribution; the vertical variance (σ^2) depends on K_d only	$K_d = \sigma^2/2t$	Numerous
Cox Number	Rate of production of temperature variance (fluctuations) by turbulence equals rate of diffusive smoothing	$K_d = 3 \cdot D^T \frac{(\partial T'/\partial z)^2}{(\partial T/\partial z)^2}$	Osborn and Cox (1972)
Dissipation	A fraction γ_{mix} of the dissipated turbulent kinetic energy ε is transformed to potential energy (buoyancy flux)	$K_d = \gamma_{mix}\,\varepsilon/N^2$	Osborn (1980) Oakey (1982) Gregg (1987)
Ozmidov or fine scale	Thorpe scale equals Ozmidov scale and same assumptions as dissipation method[c]	$K_d = \gamma_{mix} L_T^2 N$	Thorpe (1977) Dillon (1982) Peters et al. (1988)

[a] Note that the vertical coordinate z is positive upward.
[b] This method is not applicable when a nonconservative tracer (e.g., radon-222) is used in nonstationary turbulence.
[c] For definition of L_T see Table 6.

γ_{mix} (Eq. 56) of the wind-produced TKE, J_R (Eq. 64), is fed into the buoyancy flux $J_b = -K_z N^2$. Thus, the dependence of K_z on wind forcing is given by

$$K_z = \gamma_{mix} \left(\frac{\rho_{air} C_{10}}{\rho} \right)^{3/2} \frac{W_{10}^3}{N^2 kh}. \quad (67)$$

Kullenberg et al. (1973) have demonstrated that the vertical dispersion of dye did indeed follow this relationship over several orders of magnitude. If no specific data are available, we can consider Eq. (67) as a realistic estimate (or perhaps a good guess) for diapycnal diffusivity in the epilimnion.

6.2.2 *Convective Mixing*

Another source of TKE for mixing in the surface boundary layer is the positive surface buoyancy flux J_b^o. As described in Section 5.2, J_b^o can result from cooling (or heating for $\alpha < 0$), from an increase in salinity due to evaporation of saline water, or from a combination of both processes. As summarized in Table 5, J_b^o for these two processes is quantified by

$$J_b^o = -\frac{\alpha g}{c_p \rho} H_{net} + \frac{g \beta_s S}{\rho} m_E. \quad (68)$$

The two terms on the right side describe the effects of heat loss ($H_{net} < 0$) and evaporation ($m_E > 0$), respectively. In fresh water ($S = 0$), evaporation produces no buoyancy flux. Because the thermal expansion coefficient α is negative below $T = 4\,°C$, J_b^o also becomes negative if the water is undergoing warming ($H_{net} > 0$). The temperature range over which α is negative exists only for salinities S smaller than approximately 24.7‰ (see Sect. 4.1).

It is usually assumed that the convection process is initiated by the sinking of heavier water parcels from the lake surface after a certain degree of instability is exceeded. Because of the continuity of mass, these sinking plumes (Fig. 7) imply the existence of simultaneous rising plumes, and thus the surface layer is subject to intense stirring. For this reason it is intuitively plausible that the relevant physical parameter describing the TKE balance is the surface buoyancy flux J_b^o. Energy dissipation ε is therefore usually scaled by the surface buoyancy flux J_b^o once stationary conditions have been reached:

$$\varepsilon = a\, J_b^o. \quad (69)$$

The relatively rare experimental studies of convection in the mixed layer show a gradual decrease of $a = \varepsilon(z)/J_b^o$ with depth (Lombardo and Gregg 1989), indicating a slightly nonuniform loss of energy of the sinking plumes. It is fascinating to note that the factor a, if plotted as a function of the nondimensional depth z/D (D: depth of the mixed layer), i.e., $a = a(z/D)$, follows a universal curve for atmospheric and for different oceanic regimes (Shay and Gregg 1986). However, turbulence measurements reveal that $\varepsilon(z)/J_b^o$ also depends on the state of convection, i.e., on whether J_b^o and the depth of the mixed layer are in steady state or changing (see Sect. 7.1).

The detailed structure of convection in the surface layer is poorly resolved, especially in the horizontal. Recent measurements (Soloviev 1990) indicate that sinking and rising plumes show similar spatially coherent, organized structures (on scales of tens of meters) as observed in the atmosphere, but not much more insight is available. Despite this insufficiency, for this regime a parametrization also exists that is a good enough approximation for practical purposes, i.e., $\varepsilon = 0.5\, J_b^o$.

6.2.3 *Mixed-Layer Dynamics and the Monin-Obukhov Length*

As demonstrated in laboratory experiments by Deardorff et al. (1969), sinking thermals still have part of their kinetic energy when they reach the bottom of the mixed layer. Consequently, the sinking water parcels can overshoot the density surface at the base of the mixed layer and partly penetrate through the pycnocline into the hypolimnion below (penetrative convection). A fraction of that energy is available for the entrainment of heavier water from below into the mixed layer, leading to *mixed-layer deepening*. Finally, a minor part of the energy from the sinking plumes may be transferred to the hypolimnion by internal waves. The example given in Fig. 10 (*inset*) agrees with the assumption that 30% of the production of potential energy by surface cooling (P_{pot} in Eq. 44) goes into increasing the potential energy of the mixed layer. This fraction is related to the mixing efficiency, defined as the ratio of potential energy production to disspation, $\gamma_{mix} = J_b/\varepsilon$ (Eq. 56). Because the energy of sinking plumes is more directed than that of shear turbulence, plumes generally have a greater mixing efficiency ($\gamma_{mix} \approx$

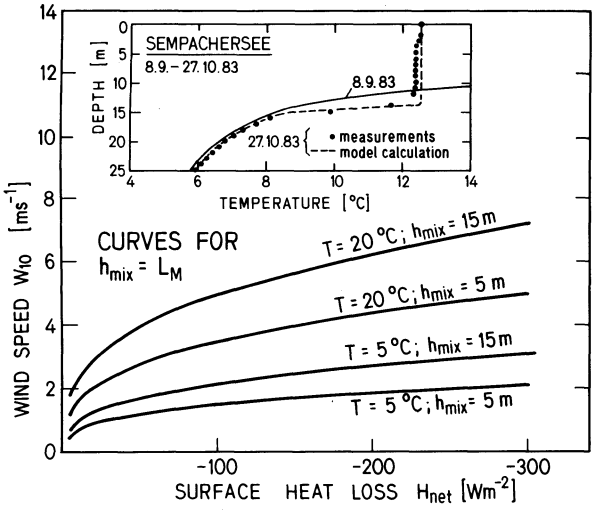


Fig. 10. Relationship between surface heat loss H_{net} and wind speed W_{10} for which the Monin-Obukhov Length L_M and the mixing depth h_{mix} (chosen as 5 and 15 m) are equal. The curves show that the influence of the wind on entrainment increases with decreasing mixed layer depth h_{mix} and decreasing water temperature T. Calculated from Eqs. (68) and (70) with $m_E = 0$ and $C_{10} = 1.5 \times 10^{-3}$. *Inset* Comparison between measured temperature profiles and model calculations during convective mixing due to surface heat loss (in Sempachersee). The measurements agree with the assumption that 70% of the energy is dissipated within the mixed layer and 30% is used for entrainment at the base of the mixed layer. (Redrawn from Wüest 1987)

0.20–0.25) than turbulence produced by Reynolds' stress (see Sect. 6.3).

Convective turbulence is not the only agent for the entrainment of thermocline water into the surface mixed layer; another source is provided by wind stirring (Eq. 47). The relative importance of these two agents changes with depth h: the effect of the wind is inversely proportional to h, whereas the effect of convection (a in Eq. 69) decrease more gradually with depth. For the sake of simplicity it is assumed that the turbulence level for convective mixing is constant with depth and that a = 1 (in Eq. 69). The *Monin-Obukhov Length* L_M (Table 5) is defined as the depth h = L_M at which the two quantities $\varepsilon = J_R$ (Eq. 65) and $\varepsilon = J_b^o$ (Eq. 68) are equal:

$$L_M = -\frac{u_*^3}{kJ_b^o} = -\left(\frac{\rho_{air} C_{10}}{\rho}\right)^{3/2} \frac{W_{10}^3}{kJ_b^o}. \qquad (70)$$

The negative sign is chosen by convention in order to distinguish this situation from the case with negative buoyancy flux J_b^o (e.g., warming of the water column). Note that the major contribution to entrainment is convection if $L_M < h_{mix}$ and wind if $L_M > h_{mix}$. A schematic diagram of all the quantities discussed is provided in Fig. 9.

In Fig. 10 the effect of the two mixing processes is compared quantitatively. The relationship between surface heat loss H_{net} and wind speed W_{10} is plotted for two different mixing depths with $h_{mix} = L_M$ (equal contributions to entrainment, i.e., equal levels of turbulence at the base of the mixed layer). Because L_M decreases with increasing α (Eq. 70 and Table 5), and thus with water temperature T, entrainment in temperate lakes is usually controlled by cooling. However, when the surface temperature approaches 4 °C, L_M becomes large and wind remains as the only stirring agent.

6.2.4 *Langmuir Circulation*

In addition to wind-induced small-scale turbulence, an organized vertical motion of the scale of the epilimnion depth also evolves under the action of surface wind stress. The hydrodynamics of these vortices, termed Langmuir cells, is not simple; the reader is referred to Leibovich (1983) for an overview of the relevant theories.

When the wind speed exceeds a certain threshold speed of roughly 3 m s^{-1}, within a few minutes streaks, aligned approximately parallel to the wind direction and composed of floating objects such as bubbles and leaves, can appear on the lake surface. As Langmuir (1938) showed, these streaks, which are obvious even to the non-limnologist, result from the convergence of two counter-rotating vortices at the top of the epilimnion with axes nearly parallel to the wind. Hence, surface water is transported downward at the streaks and upwelling occurs in between.

This circulation pattern establishes itself independently of surface heating or cooling. A destabilizing surface heat flux may lower the threshold for the onset of these convective rolls. At wind speeds exceeding 3 m s^{-1}, however, the strength and form of the circulation are apparently not much altered even under conditions of negative surface buoyancy flux (i.e., stabilizing conditions due to heating).

The form of the rolls is asymmetrical, but the lateral width (approximately half of the streak spacing L) and the vertical penetration depth of the rolls are observed to be approximately equal.

The spacing L of the streaks generally increases with wind speed W_{10} and can be approximated by

$$L \approx (2 \text{ to } 5\,s)\, W_{10} \quad [m] \tag{71}$$

(Leibovich 1983). However, the vertical size of the circulation is obviously limited by the base of the mixed layer, where strong density gradients inhibit vertical motion. Thus, Eq. (71) can only hold as long as L/2 is smaller than the epilimnion depth. Hence, the wind threshold and the epilimnion depth put lower and upper limits on the size of the Langmuir vortices. In fact, the size of the cells in lakes is mostly on the order of 10 m.

Downwelling at the convergence streaks can be very vigorous. Observed maximum vertical velocities attain 1% of the wind speed. The structure of the rolls is asymmetrical, with the downwelling currents being of higher velocity than the upwelling currents. Downwelling velocities generally increase with wind speed and are comparable to wind-induced surface drift.

High downwelling velocities suggest that Langmuir circulation may represent an important epilimnion mixing mechanism. Although observations led Langmuir (1938) to believe that the vortices are largely responsible for the formation and maintenance of the mixed layer, presently it is not certain whether Langmuir circulation is resonsible for a significant part of the stirring. Turbulence measurements by Lombardo and Gregg (1989) indicate that Langmuir circulation does not invalidate the similarity scaling of the rate of dissipation of TKE (Eq. 65). Langmuir cells can possibly be considered as just a component of the largest-scale motion related to the dynamics of the surface boundary layer, implying that it is not necessary to add an additional term to the TKE budget (Eq. 54) to account for it.

Langmuir cells are nevertheless important for the ecology of lakes, because the environment to which an algal cell is exposed – especially light intensity – may depend critically on whether it is undergoing vertical transport by such vortices.

6.3 Diapycnal Mixing

6.3.1 Kelvin-Helmholtz Instabilities

Diapycnal mixing (mixing across surfaces of equal density) is a complex process, and much less is known about the properties of turbulence in stratified fluids than in fluids of uniform density. This complexity is due to intermittance in the production of turbulence, to its spatial heterogeneity, and to the fact that it is generally anisotropic as a result of density stratification. In large water bodies, such as ocean basins, an additional complication arises, due to the fact that the vertical direction is not necessarily identical to the diapycnal coordinate axis (Gregg 1987).

If no energy is applied to a stratified water body, the streamlines will remain laminar and heat and mass transfer will be molecular. Diapycnal shear, however, can generate turbulence when the stratification (quantified by N) is small relative to the vertical gradient of the horizontal current ($\partial u/\partial z$). This comparison is usually expressed by the *Gradient Richardson Number* $R_i = N^2/(\partial u/\partial z)^2$. If R_i is small, e.g., below 1/4, so-called Kelvin-Helmholtz instabilities can occur. Fluid from adjacent layers is then wrapped around like a cinnamon roll, with a highly organized substructure. The billows thicken, become statically unstable, and collapse, leaving a small turbulent patch. The development of a Kelvin-Helmholtz billow is illustrated in Fig. 11a. The mixing of two fluids of different density increases the potential energy of the water column, as described by the buoyancy flux $J_b = -K_d N^2$. In the TKE equation (Eq. 54) the buoyancy flux is negative and thus represents a further sink for TKE (in addition to viscous dissipation).

6.3.2 Diapycnal Diffusivity

As explained in Section 5.4 only a small fraction of the kinetic energy is transformed to potential energy during the diapycnal mixing process, and therefore the mixing efficiency $\gamma_{mix} = -J_b/\varepsilon = K_d N^2/\varepsilon$ (Eq. 56) is significantly smaller than 1. Peters and Gregg (1987) estimated the mixing efficiency in a strong shear zone of the Equatorial Countercurrent to be $\gamma_{mix} = 0.12$, a value that also seems to be typical for shear-induced mixing in lake hypolimnia (Ivey and Imberger 1991).

The practical importance of γ_{mix} is its applicability to turbulence measurements. Equation (56) can be used to relate dissipation to diapycnal diffusivity in a steady shear zone (Table 8):

$$K_d = \gamma_{mix}\, \varepsilon/N^2. \quad [m^2 s^{-1}] \tag{72}$$

Dissipation measurements are carried out with lift probes (Osborn 1974), which sense one com-

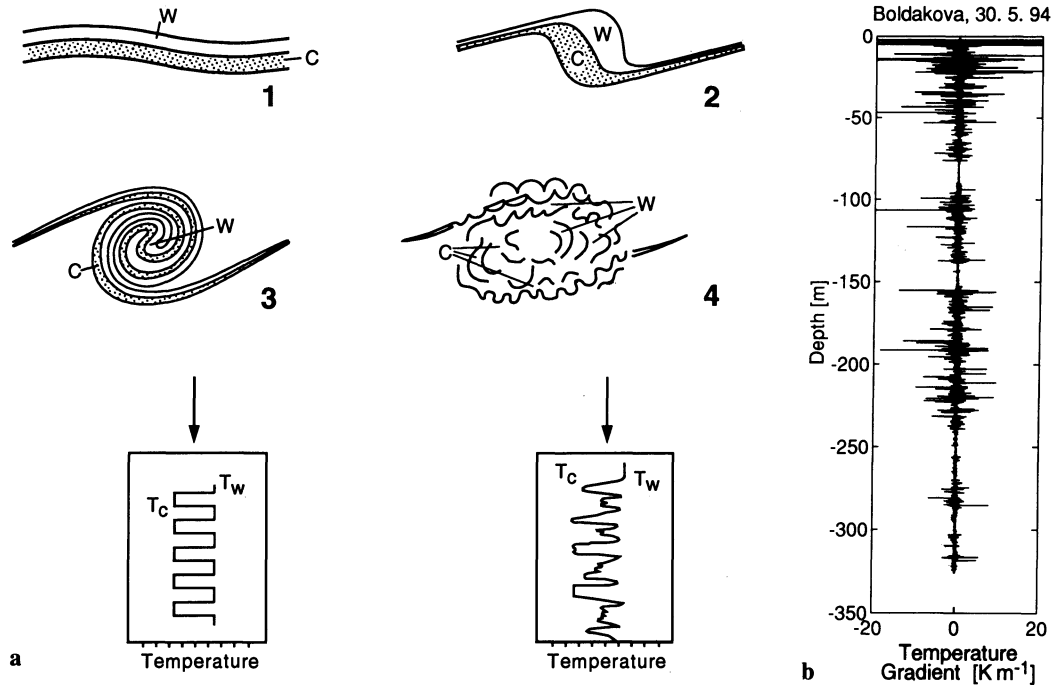


Fig. 11. a Schematic diagram of the mixing of two water masses *C* (cold) and *W* (warm) due to a Kelvin-Helmholtz instability in the stratified shear flow occurring for $R_i < 0.25$ (R_i = Gradient Richardson Number; see Table 5; modified from Thorpe 1969). **b** Vertical profile of temperature microstructure gradients [K m^{-1}] measured in the top 325 m near Boldakova at the southern shore of Lake Baikal. The profile indicates large sections of vigorous mixing (large two-sided fluctuations) and sections of complete inactivity (e.g., from 80–90 m depth)

ponent of the shear with a spatial resolution of approximately 2 cm (Oakey 1982). Equation (53) is then employed to determine ε.

Another approach to diapycnal diffusivity is based on temperature fluctuations. Turbulent overturns in a well-defined mean temperature gradient $\partial T/\partial z$ produce fluctuations T′, because distorted water parcels retain their temperature during the turbulent event and for some time afterward (Fig. 11b). The steady-state balance equation for T'^2 in homogeneous turbulence states that the production due to overturns is equal to the rate of diffusive smoothing, i.e.,

$$-\overline{w'T'}\,(\partial T/\partial z) = 3\,D^T\,\overline{(\partial T'/\partial z)^2}. \qquad (73)$$

If the term $-\overline{w'T'}$ is replaced by a Fickian flux (Eq. 17), the diapycnal eddy diffusion coefficient for heat (Table 8) becomes

$$K_d^T = CD^T; \qquad (74)$$

with the so-called Cox Number, C, given by $C = 3\,\overline{(\partial T'/\partial z)^2}\,/(\partial T/\partial z)^2$ (Osborn and Cox 1972). Measurements of C are made with *fast-response thermistors* (Fozdar et al. 1985; Dillon and Caldwell 1980), which can resolve spatial gradients down to a scale of less than 1 cm (Fig. 11b).

Depending on the available energy and on stratification, the maximum size of overturning eddies provides a further way of estimating diapycnal diffusivity (Table 8). The length scale at which buoyancy is suppressed by stratification is given by the *Ozmidov Scale*:

$$L_O = (\varepsilon/N^3)^{1/2}. \quad [m] \qquad (75)$$

As mentioned previovsly, turbulence produces temperature fluctuations. The vertical displacement of an individual water parcel can be calculated by rearranging the discrete temperature values within a vertical profile such that the temperatures decrease monotonically with depth. The root mean square of all the displacements within a certain layer, termed the *Thorpe Scale* L_T (Thorpe 1977), provides a scale for the vertical extension of the overturning eddies. Measurements in lakes (Dillon 1982) and in the ocean (Peters et al. 1988) have shown that in well-defined temperature gradients, the Ozmidov and Thorpe Scales are nearly equal, i.e., $L_T \approx L_O$. By combin-

ing Eqs. (72) and (75) a link between the Thorpe Scale and the diapycnal eddy diffusivity can be derived:

$$K_d = \gamma_{mix} L_T^2 N. \quad (76)$$

A summary of the various mixing scales and the methods for estimating diapycnal diffusivity are given in Tables 6 and 8, respectively.

6.3.3 *Experimental Observations*

In order to describe aquatic systems quantitatively, it is often desirable to determine the rate of vertical exchange, which can be described by diapycnal diffusivity (Eq. 17). Attempts have therefore been made to find a parameterization for K_d in terms of easily measurable quantities. Peters et al. (1988) have systematically investigated the dependence of K_d on R_i as qualitatively postulated by the Kelvin-Helmholtz instability model illustrated in Fig. 11a. Among other parameters, they measured vertical shear $\partial u/\partial z$, temperature gradient $\partial T/\partial z$, stability frequency N, and dissipation rate ε, across the Equatorial Undercurrent in the Pacific Ocean. The coefficient of diapycnal diffusivity does indeed show a dramatic increase below $R_i = 0.3$ (Fig. 12) As their entire data set demonstrates, however, the parameterization is not at all simple.

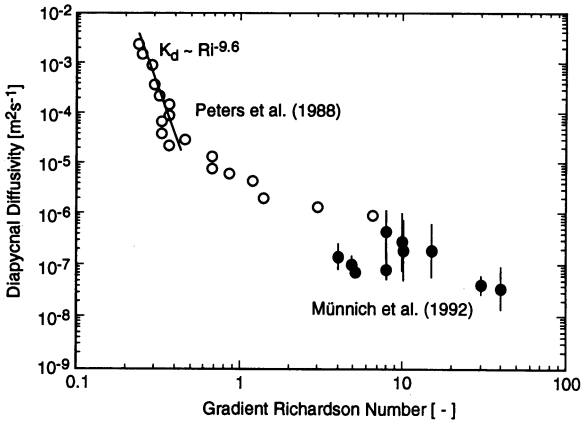


Fig. 12. Relationship between Gradient Richardson Number R_i and diapycnal eddy diffusivity of heat, K_d, measured in the Equatorial Undercurrent in the Pacific Ocean by Peters et al. (1988) (*open circles*) and in a small lake by Münnich et al. (1992) (*filled circles*). Whereas the diapycnal diffusivity increases only gradually with decreasing R_i for $R_i > 0.3$, it rises dramatically for $R_i < 0.3$

As discussed in Sect. 6.1 internal seiches are often the main source of diapycnal shear in lake hypolimnia. The corresponding R_i values, however, are considerably in excess of 0.25. For example, for the intense seiching motion shown in (Fig. 14), the Gradient Richardson Numbers R_i at the center of the lake, calculated from the modal structure, lie between two and several hundred (Münnich et al. 1992), a range which seems to leave little chance for the development of turbulent overturn events. The diapycnal diffusivity measured by the temperature microstructure method (Table 8) in the interior of the hypolimnion of Alpnachersee is low, but still clearly above the molecular level (Fig. 12). Values of K_d are approximately the same as the molecular diffusivity of heat ($1.4 \cdot 10^{-7}\,m^2 s^{-1}$ at 4 °C), which is still two orders of magnitude above the molecular diffusivity of dissolved matter ($\approx 10^{-9}\,m^2 s^{-1}$). The low but still present turbulence may be due to local regions of high shear produced by the superposition of different internal seiches and waves. The Gradient Richardson Number R_i calculated from one single internal mode (even if it is the dominant one) must be regarded as a baseline from which smaller-scale fluctuations produce locally intermittent low R_i values and turbulent patches. The monotonic decrease in mixing as a function of R_i, as shown in Fig. 12, also supports this assumption for $0.3 < R_i < 10$.

Figure 13 demonstrates another feature of diapycnal diffusivity in lakes. In contrast to the situation in the ocean, where internal wave energy has a residence time of months (Gregg and Sanford 1988), internal seiches in lakes, which are responsible for most of the diapycnal mixing, are often excited sporadically by storm events (Fig. 21; Sect. 7). As a result mixing in lakes has a much more intermittent character than it does in the ocean. Figure 13 shows an example of the enormous difference in K_d (nearly three orders of magnitude) between the typical long-term mean K_d (July to October) in Urnersee and the mean K_d in Zugersee during a storm event lasting a few days in November 1982. This is due to the enormous variation in TKE input from the wind, which varies with W_{10}^3 (Eq. 46). On November 7 and 8, 1982, Zugersee was hit by the strongest *föhn* storm this century (Fig. 21).

As clearly shown in Fig. 9a, turbulence in the hypolimnion is much weaker than in the mixed layer. Except after strong forcing, only a small fraction of the hypolimnion contains turbulent

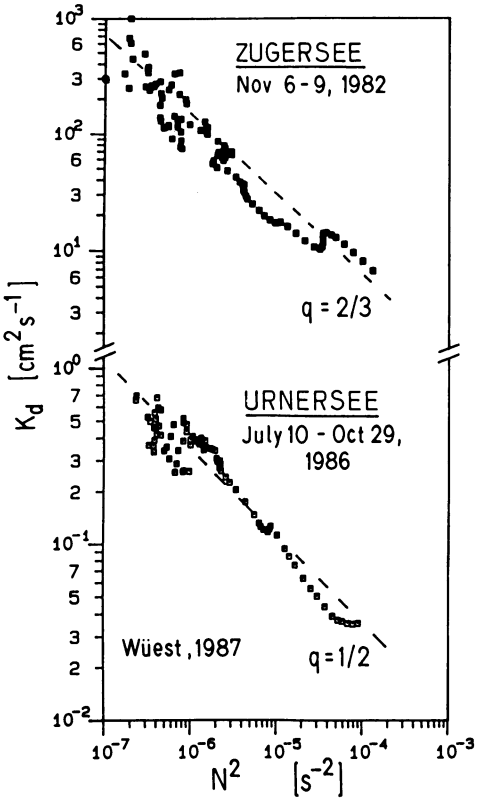


Fig. 13. Relation between diapycnal eddy diffusivity K_d and stability frequency N^2 from two neighboring lakes in central Switzerland. The data conform fairly well to the Welander (1968) parameterization K_d = const $(N^2)^{-q}$, which has a rational physical interpretation only in the upper thermocline. In deep-water layers (low N^2) diapycnal diffusivity is generally governed by other parameters (see Sect. 6.4). The large difference between long-term mean K_d values and those from November 1982 demonstrates the intermittent character of diapycnal mixing. On November 7/8, 1982, Zugersee was hit by an extremely strong storm (see also Fig. 21; redrawn from Wüest 1987)

patches: The pycnocline is an effective barrier against the transmission of epilimnetic turbulence. As a rule we can say that the rate of change of potential energy in the hypolimnion (buoyancy flux) is approximately 1% of the energy entering the epilimnion (Wüest 1987), which, in turn, is on the order of 1% of the energy flux P_{10} at a height of 10 m above the water surface (Eq. 46).

Typical long-term diapycnal eddy diffusion coefficients in medium-sized temperate lakes during strong stratification (determined indirectly from long-term tracer-diffusion studies) are on the order of 0.01–0.1 cm^2 s^{-1}. These values are much larger than the diapycnal diffusivities induced by internal seiches at high Gradient Richardson Numbers (Fig. 12) observed in the interior of the water column. This comparison allows us to conclude that boundary mixing has to be responsible for the discrepancy between interior and total diapycnal diffusivity. Internal seiches are accompanied by horizontal currents in the hypolimnion (Fig. 14), which do indeed generate boundary mixing above the lake sediment. It seems that the shearing induced by the vertical mode produces significantly more mixing at the sediment boundary than in the interior of the hypolimnion. This question is addressed in more detail in the following section.

6.4 Boundry Mixing

In lakes and oceans physical processes occurring at the sediment-water interface are of paramount importnace, because they control the fluxes of chemical elements and compounds across the boundary. In addition, most diapycnal mixing occurs here. The energy for mixing at the boundary is provided by currents caused by internal and surface waves, by density currents (e.g., turbidity currents), and by inflowing rivers. In contrast to the boundary at the water surface, the sediment is rigid. Consequently, currents must fall to zero at the interface, where the fluid is in contact with the sediment. These currents at the sediment surface create a bottom stress τ_o. The boundary layer is defined as the region where the currents are affected by the presence of the boundary.

The theory of the bottom-boundary layer (BBL) is nevertheless closely related to the theory of wind shear as expressed in Section 6.2. A summary of the relevant equations and parameters is given in Table 9. For recent reviews on the dynamics of ocean boundary layers the reader is referred to Thorpe (1988), Garret (1991), and Woods (1991).

6.4.1 Velocity Structure of the Bottom-Boundary Layer

The main velocity gradient is localized in the viscous layer (Caldwell and Chriss 1979) and is strongly affected by viscosity. Its thickness δ_v (typically mm to cm) scales with ν/u_* and is found experimentally to be aproximately $\delta_v \approx 10\,\nu/u^*$ (Hinze 1975), where u^* is the friction velocity

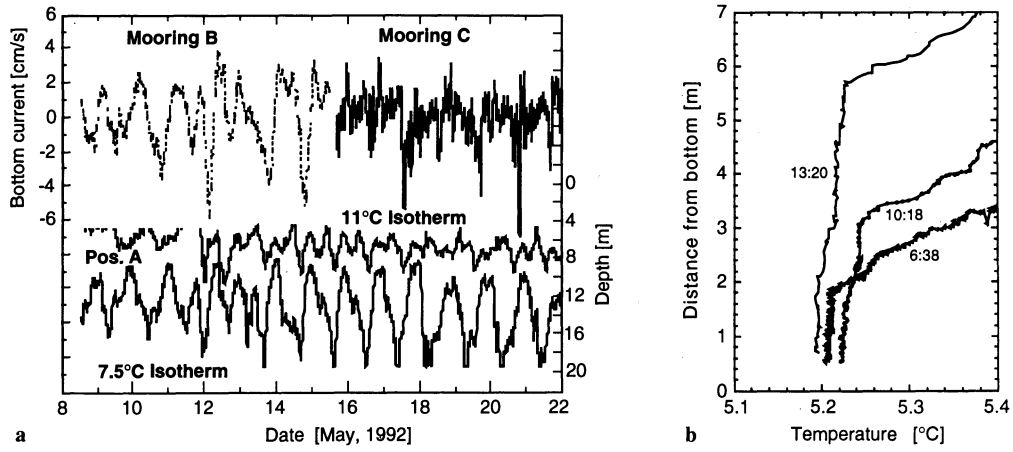


Fig. 14. **a** *Above* The component of the bottom current (driven by internal seiches) along the major axis of Alpnachersee lake at two sampling stations at the eastern end (*station C*) and in the middle (*station B*) of the lake. Note that velocities are approximately three times smaller than in the example given in Table 9. *Below* Time series of the depths of two selected isotherms recorded at the western end of the lake basin (*station A*). Coherence and phase spectra of bottom current and isotherm depth reveal that seiching and currents were coherent with a phase lag of 90°, which is exactly the value expected for first horizontal seiche modes. (Redrawn from Gloor et al. 1994.) **b** Three examples of temperature profiles in the benthic boundary layer, generated by the bottom currents shown in **a**, indicating the layer to be well mixed. The numbers give the sampling time (h:m) on May 12, 1992. (Redrawn from Gloor et al. 1994)

(Table 9) defined as for the surface-boundary layer (Eq. 62). Within the viscous sublayer turbulent eddies are virtually absent. The *Reynolds Number* $\mathrm{Re} = u\delta_v/\nu$ is on the order of 100 or smaller, and consequently the flow is likely to be laminar. Similar to Eq. (45), bottom stress τ_o, and thus friction velocity u^*, are related to the horizontal current velocity U_z measured at a height z above the sediment (Table 9).

Above the viscous layer turbulent eddies can exist with scales that increase with distance from the boundary. Within certain limits the stress τ_o can be assumed to be constant (constant-stress layer). As in Eq. (61) the "law of the wall" leads to a logarithmic velocity distribution with the *roughness length* z_o related to the topographical bottom structure of the sediment boundary. If the length scales z_s of the sediment structure is on the order of the viscous layer δ_v or less, the logarithmic velocity distribution does not depend on the bottom structure z_s. This case, called the *smooth flow regime*, applies when $z_s \lesssim \nu/u_*$; the roughness length is then $z_o \approx 0.1\,\nu/u^*$ and much smaller than δ_v. For a coarser topography, i.e., $z_s \gtrsim 3\,\nu/u^*$, the roughness length is given by $z_o = z_s/30$ (*rough flow; see Chriss and Caldwell 1982).*

6.4.2 *Energy Fluxes in Bottom-Boundary Layer*

The agent for boundary-layer mixing is bottom friction. The total energy flux into the bottom layer of thickness z is given by

$$P_{diss} = \tau_o U_z = \rho C_z U_z^3 = \frac{\rho}{C_z^{1/2}} u_*^3, \quad [\mathrm{Wm^{-2}}] \quad (77)$$

where z (often chosen as 1 m) lies within the constant-stress layer ($\tau(z) = \tau_o$). An appreciable amount of the energy is dissipated within the viscous sublayer on a molecular level determined by the viscous stress (Table 9):

$$\varepsilon_v = \frac{\tau_o}{\rho}\frac{\partial u}{\partial z} = u_*^4/\nu \quad [\mathrm{W\,kg^{-1}}] \quad (78)$$

Hence, the total dissipation in the viscous sublayer is given by

$$P_{diss}^{v} = \rho\varepsilon_v\delta_v = \frac{\rho}{\nu}u_*^4\delta_v \approx 10\,\rho u_*^3. \quad [\mathrm{W\,m^{-2}}] \quad (79)$$

Comparing Eqs. (77) and (79) shows that $P_{diss}^{v}/P_{diss} = 10\,C_{1m}^{1/2} \sim 0.4$. Thus, approximately 40% of the total energy entering the bottom layer is dissipated within the viscous sublayer, with the remainder being dissipated within the logarithmic layer. If no stratification is present, production due to Reynolds' stress is equal to dissipation:

Table 9. Characteristic equations and values for sediment-boundary-layer dynamics

Parameter	Equation	Value (for $U_{z=1\,m} = U_{1\,m} = 0.1\,ms^{-1}$)[a]	
Bottom stress	$\tau_o = \rho C_{1m} U_{1m}^2$	$\tau_o = 1.5 \cdot 10^{-2}$	$[N\,m^{-2}]$
Friction velocity	$u_* = (\tau_o/\rho)^{1/2} = C_{1m}^{1/2} U_{1m}$	$u_* = 4 \cdot 10^{-3}$	$[m\,s^{-1}]$
Total energy dissipation by friction below 1 m	$P_{diss} = \tau_o U_{1m} = \rho C_{1m} U_{1m}^3$	$P_{diss} = 1.5 \cdot 10^{-3}$	$[W\,m^{-2}]$
Viscous sublayer			
Thickness of viscous sublayer	$\delta_v \approx 10\,\nu/u_*$	$3 \cdot 10^{-3}$	[m]
Thickness of diffusive sublayer for heat	$\delta_T \approx \left(\frac{D^T}{\nu}\right)^{1/3} \delta_v$	$1.5 \cdot 10^{-3}$	[m]
Thickness of diffusive sublayer for salt	$\delta_s \approx \left(\frac{D^S}{\nu}\right)^{1/3} \delta_v$	$3 \cdot 10^{-4}$	[m]
Velocity gradient	$\partial u/\partial z = \frac{u_*^2}{\nu}$	12	$[s^{-1}]$
Rate of viscous dissipation	$\varepsilon_v = \frac{\tau_o}{\rho} \partial u/\partial z = u_*^4/\nu$	$1.8 \cdot 10^{-4}$	$[W\,kg^{-1}]$
Logarithmic layer			
Velocity distribution	$u(z) = \frac{u_*}{k} \ln (z/z_o)$		$[m\,s^{-1}]$
Velocity gradient	$\partial u/\partial z(z) = u_*/kz$		$[s^{-1}]$
Eddy coefficient for momentum	$K^m(z) = \frac{\tau_o}{\rho \partial u/\partial z} = k u_* z$		$[m^2\,s^{-1}]$
Rate of dissipation of TKE	$\varepsilon(z) = \frac{\tau_o}{\rho} \frac{\partial u}{\partial z} = \frac{u_*^3}{kz}$		$[W\,kg^{-1}]$

[a] Bottom friction coefficient $C_{1m} = 1.5 \times 10^{-3}$ (Elliott 1984).

$$\varepsilon = \frac{\tau_o \partial u}{\rho\, \partial z} = \frac{u_*^3}{k\,z} \quad [W\,kg^{-1}] \tag{80}$$

Thus, as in the surface layer turbulence decreases with increasing distance from the boundary (Fig. 9a).

Within the boundary layer the flux of heat and solutes also drops toward molecular levels. Because molecular diffusion is smaller than viscosity, the zone of pure molecular transport is confined to the so-called *diffusive sublayer*, which is thinner than the *viscous sublayer* (Table 9). The magnitude of the molecular diffusivity of heat results in the thickness of the *thermal diffusive sublayer* lying between those of the diffusive and viscous sublayers. The eddy diffusivities of both heat and salt increase rapidly with distance above their respective diffusive sublayers.

As long as the constant-stress-layer assumption applies, the eddy coefficient for momentum K^m is given by

$$K^m = \frac{\tau_o}{\rho\, \partial u/\partial z} = k u_* z. \quad [m^2\,s^{-1}] \tag{81}$$

The dependence of K^m on height z is related to the fact that eddy size increases with distance from the sediment surface. The dependence on u_* implies that the transfer rate increases with horizontal current velocity U_z. In Table 9 all properties discussed are listed for the example of a smooth flow regime with $U_{1m} = 0.1\,m\,s^{-1}$, an upper limit for typical current speeds in the hypolimnion.

The effects of boundary mixing induced by bottom currents are often observed in aquatic systems. The most prominent feature is a well-mixed layer (BBL) above the sediment–water interface. Whereas the existence of a well-mixed

BBL in the ocean is due to geostrophic or thermohaline circulation, seiching motions and the associated hypolimnetic bottom currents are responsible for intense mixing in the zone of high shear above the sediment in lakes. Because hypolimnetic currents are generally less energetic than deep-water currents in the ocean, the well-mixed BBLs in lakes are typically an order of magnitude thinner.

Figure 14a shows an example of internal seiching motion and the corresponding bottom currents, which are typically $\sim 3\,cm\,s^{-1}$ and peak around $7\,cm\,s^{-1}$. The bottom currents have established a distinct and relatively well-mixed BBL with a temporally varying thickness of 2–6 m (Fig. 14b). The temperature gradients within this layer are an order of magnitude smaller than those just above it. The time required to build up a mixed bottom layer of this thickness by continuous erosion of a background density stratification would be more than a month (see Sect. 7). It can therefore be concluded that the changing thickness is associated only with the seiching motion and not with erosion of the density gradient by intermittent boundary mixing (Gloor et al. 1994).

As mentioned in Sect. 6.3, diapycnal diffusivity in the hypolimnia of small to mediumsized lakes can be dominated by mixing within the BBL, where the main source of turbulent kinetic energy is located (Wüest et al. 1994). The vertical modal structure (see Sect. 6.1) and amplitudes of the internal seiches, as well as the lake topography (mainly the surface-to-volume ratio), are the main factors determining whether overall diapycnal exchange is dominated by internal or boundary mixing.

We have not tested thus far whether the bottom buoyancy flux J_b^b has to be taken into account. In the same way as surface cooling generates a surface buoyancy flux J_b^o, the heat flux H from the sediments (of geothermal or other origin) releases potential energy and induces convection. Analogous to Table 4, the bottom buoyancy flux is given by

$$J_b^b = \frac{g\alpha}{\rho c} H. \quad [W\,kg^{-1}] \tag{82}$$

In mid-latitude lakes the geothermal heat flux leads to a typical value for J_b^b of $4 \times 10^{-12}\,W\,kg^{-1}$ ($T_b = 5\,°C$, $H = 0.1\,W\,m^{-2}$), which is much lower than friction-induced turbulence (Table 9). Consequently, free convection influences the boundary dynamics in rare cases only. For lakes with extensive geothermal springs, however, convectively induced mixing at the lake bottom can become the dominant mixing process. For example, in Lake Kivu (Fig. 16) a heat flux of approximately $1\,W\,m^{-2}$ at $T \approx 26\,°C$ gives rise to a bottom buoyancy flux of approximately $7 \times 10^{-10}\,W\,kg^{-1}$, and to mixing by double diffusion (see Sect. 6.5).

Determination of boundary-layer characteristics in lakes or oceans is not simple. Methods that have been applied in natural waters (Table 10) all suffer from some drawback. For example, the inertial-dissipation-rate technique is applicable only to isotropic turbulence, a condition that is not always fulfilled in lakes, due to chemical stratification near the sediment boundary (Wehrli

Table 10. Methods to quantify macroscopic boundary layer characteristics

Method	Measured parameter	Derived parameters	Reference
Stress measurement	u_* (or τ)	K^m, ε, z_o (for smooth regime only)	Gust and Weatherly (1985) Soulsby (1983)
Velocity measurement	u (z)	U_* (or τ_o), z_o, K^m	Weatherly (1972) Chriss and Caldwell (1982, 1984)
Dissipation rate technique	ε (z)	u_*, K^m	Dewey et al. (1987) Dewey and Crawford (1988)
Inertial-dissipation rate technique	E (k, z)	$\varepsilon = \left(\frac{E(k)^3 k^5}{\alpha^3}\right)^{1/2}$	Grant et al. (1984)
		$u_* = \left(\frac{E(k)\,k^{5/3}}{\alpha}\right)^{1/2} (kz)^{1/3}$	Wimbush and Munk (1970) Dimai et al. (1994)

1993). This may lead to suppression of the diapycnal exchange. Direct estimation of skin friction (τ_o) measured with flush-mounted hot-film sensors (Gust 1982) requires great care to avoid additional drag from the sensors. Finally, if τ_o is inferred from current measurements made well above the sediment surface, the unknown influence of the sediment structure is a further source of uncertainty, as discussed in Sect. 6.4.3.

6.4.3 *Interaction of Currents with the Sediment*

In addition to the force exerted on the particles at the sediment surface, known as *skin friction*, bottom irregularities experience a force analogous to the drag of a body in a stream. This force is known as *form drag*, because it depends on the shape and orientation of large-scale topographical features of the sediment surface. It is important to distinguish between the contribution of skin friction, which refers to the shear stress averaged over several grain diameters, and that of form drag, which is related to the length scale of the large-scale topographical features. The flow in the upper part of the boundary (the logarithmic layer) is influenced by the total stress, but erosion and near-bed sediment transport are related to skin friction alone. When form drag is significant the layer above the viscous sublayer may accordingly consist of more than one logarithmic layer. If the friction velocity u_* is determined from current measurements made a few tens of centimeters above the bottom, the values obtained are much larger than those due to skin friction alone (Chriss and Caldwell 1982, 1984; Dimai et al. 1994), resulting in an overestimate of the force exerted on the particles at the lake bottom.

In shear-generated turbulence close to the sediment boundary, the vertical-velocity fluctuations are asymmetrical, resulting in a vertical net momentum directed away from the sediment, which can hold sediment particles in the flow in equilibrium with gravity (Leeder 1983). Consequently, suspension or resuspension of sediment particles occurs when u_* (or U_{1m}) exceeds a threshold value that depends on the density, size, and degree of cohesion of the particles (Shields 1936; Miller et al. 1977). Note that algal and bacterial growth at the sediment–water interface can significantly alter particle cohesion, and thus the tendency for resuspension to occur.

The resuspension-settling cycles increase the size of the zone of contact between particle surfaces and the water column, and thus enhance the fluxes from and to the particles. This exchange may be appreciable compared with molecular diffusion into the sediment. For example, the large specific surface area of small sediment particles emphasizes the importance of resuspension for the mineralization process.

6.4.4 *Relevance of Bottom-Boundary Mixing for the Whole Lake*

Recent experimental results indicate that mixing in the bottom-boundary layer may be important for the whole lake. In fact, for approximately the past 20 years the quantification of diapycnal diffusion near the bottom of the ocean and of lakes has been based on measurements of the diffusion of the naturally occurring radioisotope Rn-222 (with a half-life of 3.8 days) out of the sediments (Chung and Kim 1980). Imboden and Joller (1984) observed near-bottom diffusivities of 0.1–1 $cm^2 s^{-1}$ in the small Baldeggersee, and concluded that mixing is more intense near the boundary than in the interior of the water column. This observation is supported by recent microstructure measurements that show a strong increase in turbulence toward the sediment (Wüest et al. 1994). The contribution to the overall diapycnal fluxes in the hypolimnion of processes occurring at the bottom boundary may therefore be significant, especially in small to medium-sized lakes. This possibility, which was earlier evaluated for the ocean by Armi (1978, 1979), is supported by recent measurements conducted by Ledwell (1993) and Toole et al. (1994). Although not yet universally accepted, the importance of the contribution made by bottom-boundary mixing to overall mixing in all density-stratified natural water bodies must be taken into account (Garrett 1990).

Another important aspect is the mass flux between the sediment and the lake water through the diffusive sublayer. This flux is proportional to the vertial concentration gradient between sediment-pore water and the overlying water. However, it is not simple to relate the proportionality factor to the flow regime in the water column, because several factors complicate the picture. Firstly, as explained in this section the methods of characterizing the bottom-boundary layer (Table 10) are complex. Secondly, because of the episodic forcing, the parameters of the boundary layer are

extremely variable. In fact, the quantities developed for smooth flow using classical boundary-layer theory (Table 9) are only partially valid, and then only for mean values. Thirdly, there exists a feedback mechanism between physical and biogeochemical processes that can lead to so-called biogenic stratification, which is difficult to predict quantitatively. Mineralization and dissolution processes at the sediment surface fuel the fluxes of solutes into the deep water. If the energy input (and thus the mixing rate) is small, the solutes accumulate above the sediment (Wehrli 1993). Consequently, the density stratification becomes stronger, which slows down diapycnal mixing in the bottom-boundary layer even further. Vice versa, a larger energy input may prevent the build-up of a chemically induced density gradient, and may thus tend to maintain mixing. Both extremes, the well-mixed (Fig. 14b) and the highly stratified bottom-boundary layer, can be observed in nature, and the switch from one to the other may be triggered by small, difficult-to-predict changes in the production of TKE.

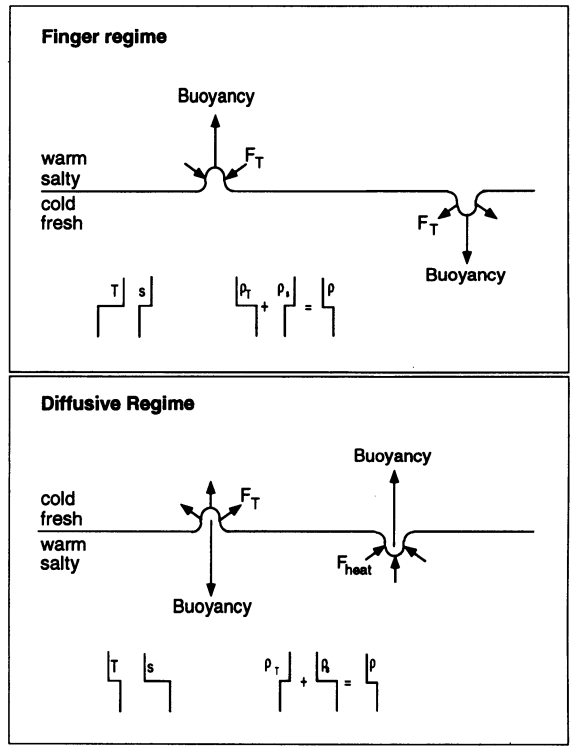


Fig. 15. Double diffusion occurs if the vertical distribution of salt and temperature is such that one component tends to stabilize the water column, while the other tends to destabilize it, leaving an overall stable stratification. In the finger regime (temperature stabilizing), a distorted water parcel exchanges heat approximately $D^T/D^s \sim 70$ times faster than salt, thus creating salt fingers, which move into the adjacent layers. In the diffusive regime (salt-stabilizing), the faster rate of heat exchange causes an enhanced rejection of the distorted water parcel, giving rise to strong mixing within a certain layer. An example of the layering created by the diffusive regime is given in Fig. 16

6.5 Double Diffusion

6.5.1 The Phenomenon

A temperature profile from Lake Kivu taken by Newman (1976; Fig. 16) shows fascinating step-like structures. Such phenomena are also observed in the ocean. They are related to double diffusion, a process based on the large difference between the molecular diffusivity of temperature and of salts. Because double diffusion can be the major process resulting in vertical mixing under certain conditions, this phenomenon deserves to be mentioned here.

Because the density of water depends on temperature and salinity, local stability (see Sect. 4) can be attained in different ways. In most temperate lakes temperature decreases and salinity increases with depth. Consequently, both temperature and salinity have a stabilizing influence on the water column. This diffusively stable situation is not discussed here further.

Double diffusion occurs when temperature (salinity) tends to stabilize the water column, whereas salinity (temperature) tends to destabilize it, but in such a way that the resulting density profile is stable. If the temperature is stabilizing a finger regime results, whereas if salinity is stabilizing a diffusive regime results (Fig. 15). Because the stabilizing contribution has to be larger than the destabilizing one, the *stability ratio* (often but not accurately called the density ratio) R_ρ, defined as

$$R_\rho = \frac{\text{stability due to the stabilizing component}}{\text{instability due to the destabilizing component}} \tag{83}$$

exceeds unity for both regimes. The relative density gradients due to temperature and salinity are given by $\alpha\ \partial T/\partial z$ and $\beta_s\ \partial S/\partial z$, respectively (see Eq. 40). Thus,

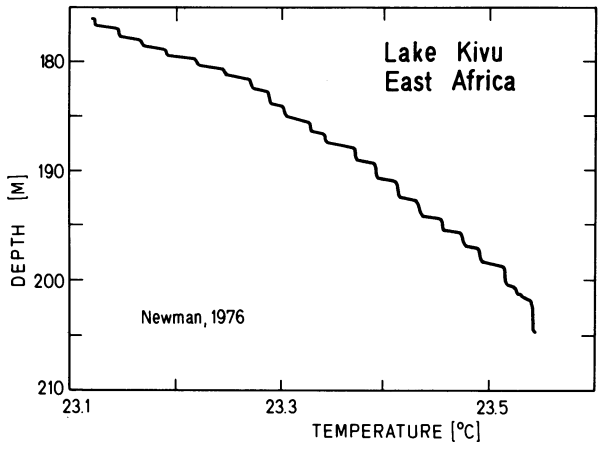


Fig. 16. Step-like temperature structure in Lake Kivu (East Africa) resulting from double diffusion (diffusive regime). In 1976, temperature increased from a minimum of 22.5 °C at a depth of 50 m to 26 °C near the bottom. The figure shows approximately 20 steps out of a total of approximately 150 (typically, $\Delta z = 0.1$ m, $\Delta T = 0.01$ to 0.03 K, and $\Delta S = 10^{-2}$ g/kg). The regime is sustained by geothermal springs that release warm, salty water into the deep part of the lake. R_ρ is between 1.3 and 2.1. Using an empirical relationship (Table 11), the vertical heat flux was calculated to lie between 0.7 and 1.6 W m^{-2}. (Redrawn from Newman 1976)

$$R_\rho = \left(\frac{\alpha \partial T/\partial z}{\beta_s \partial S/\partial z}\right)^{\pm 1}, \qquad (84)$$

with +1 (−1) for the finger (diffusive) regime.

The mixing conditions in the water column are determined by two parameters, i.e., by the absolute stability, quantified by N^2, and by the stability ratio R_ρ. If $R_\rho \gg 1$, the destabilizing factor can be ignored, and we would simply expect the vertical mixing intensity to be somehow related to N^2, but not to R_ρ. If R_ρ is only slightly larger than 1, however, the water column can become locally unstable, despite its absolute stability. This is due to the fact that the molecular diffusion of heat occurs approximately two orders of magnitude faster than the molecular diffusion of salt.

6.5.2 *Fluxes*

The local instability can be understood by considering a cold freshwater layer lying on top of a warm salty layer (diffusive regime; Fig. 15). A water parcel displaced upward slightly from its equilibrium position loses heat to its surroundings, but hardly any salt. As a result, the water parcel is forced back downward beyond its former equilibrium position. In turn, if the water parcel is moving downward it gains heat, but nearly no salt. Thus, buoyancy forces it back upward beyond its former position. In other words, unlike the classical stability oscillation (frequency N), double-diffusive regimes are characterized by a situation where the amplitude of a vertical displacement continually increases, leading to enhanced vertical mixing.

In the finger regime (Fig. 15), the downward movement of warm salty water across the density interface is accelerated, because the water loses heat faster than salt, and thus increases in density. As a result fingers of salty water (salt fingers) penetrate from above into the lower layer and enhance vertical mixing. Note that in both cases the accelerated water parcel gets its energy from the potential energy of the water column: Potential energy (buoyancy flux) is released from the stratification by the upward flux of heat in the diffusive regime and the downward flux of salt in the finger regime.

Theoretically, double diffusion comes into play when $1 < R_\rho < (D_T/D_s) \approx 70$, and is expected to become stronger when R_ρ approaches unity. Indeed, both laboratory measurements (Turner 1967; McDougall and Taylor 1984) and theory (Stern 1976) show that the flux of salt, heat, and buoyancy due to salt fingers depends only on the stability ratio R_ρ and the salinity difference ΔS. A similar dependence on R_ρ and ΔT was found by Turner (1965) for the diffusive regime. It is intuitively clear that for low R_ρ the fluxes depend on the difference across the interface of either salinity or temperature, whichever is responsible for the destabilizing tendency. This is simply because the convective plumes (thermals or fingers) have roughly the salinity or temperature (whichever is destabilizing) of the adjacent layer. The drastic increase in the fluxes when R_ρ approaches unity is also evident as the density profile becomes neutral ($N^2 = 0$). The empirical equations summarized in Table 11 allow the calculation of fluxes in double diffusive regimes based on high-resolution conductivity/temperature/depth (CTD) measurements.

It is interesting to note that in both regimes the buoyancy flux J_b follows a 4/3-power law, viz. proportional to $(\Delta S)^{4/3}$ for the figer regime, and to $(\Delta T)^{4/3}$ for the diffusive regime, where ΔS and ΔT are the concentration and temperature differences, respectively, across the interface (Table 11). Surprisingly, J_b seems to be independent of

Table 11. Definitions and flux laws for the two double-diffusive regimes

Definitions

F_T: Vertical temperature flux
F_s: Vertical salt flux
αF_T, $\beta_s F_s$: Vertical density flux due to temperature and salt flux, respectively
$g\alpha F_T$, $g\beta_s F_s$: Buoyancy flux due to temperature and salt flux, respectively

Density (or stability) ratio[a]: $R_\rho = \left(\frac{\alpha \partial T/\partial z}{\beta_s \partial S/\partial z}\right)^{\pm 1}$

Density flux ratio[a]: $R_f^* = (\alpha F_T/\beta_s F_s)^{\pm 1}$

Finger regime

$$g\beta_s F_s = -\frac{0.19}{(R_\rho - 0.5)} g\,(gD^T)^{1/3} (\beta_s \Delta S)^{4/3}$$

for $1.2 < R_\rho < 2$: $R_f^* = \frac{0.44}{(R_\rho - 0.6)^{1/2}}$ (McDougall and Taylor 1984)

for $R_\rho > 2$: $R_f^* = 0.56$ (Turner 1967)
$R_f^* \approx 0.5$ (Schmitt 1979)

Total buoyancy flux: $J_b = g(\alpha F_T - \beta_s F_s) = g\beta_s F_s (R_f^* - 1)$

Note: ΔS is the (positive) difference between upper and lower layer

Diffusive regime (Turner 1965, 1968, 1973)

$$\alpha g F_T = \frac{0.32}{R_\rho^2} \left(\frac{g}{K^T \nu}\right)^{1/3} K^T g (\alpha \Delta T)^{4/3}$$

For $1 < R_\rho < 2$: $R_f^* = 1.85 - 0.85 R_\rho$
$R_\rho > 2$: $R_f^* = 0.15$

Total buoyancy flux: $J_b = g(\alpha F_T - \beta_s F_s) = g\alpha F_T (1 - R_f^*)$

Note: ΔT is the (positive) difference between lower and upper layer

[a] Finger regime: exponent +1; diffusive regime: exponent −1

the thickness of the interface. Based on stability theory, however, Kunze (1987) showed that for the finger regime the flux laws listed in Table 11 are only valid for interfaces thinner than approximately 30 cm. At thicker interfaces the fluxes are reduced. In contrast, the diffusive regime, which is more common in lakes, tends to sharpen the interfaces, due to the eroding effect of the convecting thermals. The application of laboratory results to natural conditions is thus less problematic in the diffusive regime than in the finger regime (e.g., see Huppert and Turner 1972).

Double diffusion causes diapycnal mixing that can be compared with shear-induced mixing. In a double-diffusive homogeneous-mixed layer the TKE balance equation (Eq. 54) states that dissipation is equal to buoyancy flux, which is given by the empirical formula in Table 11. We thus obtain

$$\varepsilon = J_b = g\alpha F_T (1 - R_f^*) \quad (85).$$

(for symbols see Table 11). The mean vertical temperature gradient is related to the stability N^2 by the expression

$$N^2 = -\frac{g}{\rho}\frac{\partial \rho}{\partial z} = -g\left(-\alpha \frac{\partial T}{\partial z} + \beta_s \frac{\partial S}{\partial z}\right)$$
$$= -g\alpha \frac{\partial T}{\partial z}(R_\rho - 1). \quad (86)$$

Thus, by using the heat-flux formula from Table 11 the apparent diapycnal heat diffusivity becomes

$$K_d^T = \frac{-F_T}{\partial T/\partial z} = \frac{(R_\rho - 1)}{(1 - R_f^*)} \frac{\varepsilon}{N^2} \approx 1.2\varepsilon/N^2 \quad (87)$$

for an arbitrarily chosen $R_\rho = 2$. (Note that from Table 11 we get $R_f^* = 0.15$.) In contrast, given a

typical mixing efficiency γ_{mix} of 0.1 for shear-induced diapycnal mixing (Eq. 56 and Sect. 6.3), $-J_b = K_d^T N^2 = 0.1\varepsilon$. The apparent diffusivity is accordingly given by

$$K_d^T = 0.1\varepsilon/N^2. \quad (88)$$

There is thus a difference of one order of magnitude between the diapycnal diffusivity expressions depending on whether dissipation originates from double diffusion or shear. This demonstrates the different character of the two mixing mechanisms as well as the potential importance of double diffusion for diapycnal mixing.

6.5.3 Layering

Laboratory experiments show that in both regimes double diffusion causes layering (finger regime: Stern and Turner 1969; diffusive regime: Turner 1973). According to observations in natural waters layering occurs only if R_ρ is smaller than 2–4. The layer-generating mechanism is not properly understood. In the diffusive regime, when the water is heated from below, instabilities drive convection, creating a homogeneous bottom layer of increasing thickness. When the heat flux through the top interface and the flux from below become equal, the layer ceases to grow. Then the next layer develops above the first layer at the bottom, and so on (Turner 1973).

For the finger case, the temporal development of the layers is more complicated (Stern and Turner 1969). Observations in the ocean show that in some cases the layers can extend coherently over hundreds of kilometers (Schmitt et al. 1987). In other cases the lateral structure is less than several hundred meters in extent (Padman and Dillon 1987).

6.5.4 Occurrence of Double Diffusion

Double diffusion in lakes occurs in the stratified hypolimnion when sources are available to produce gradients of temperature and dissolved solids that are of equal sign. For the diffusive regime geothermal heat flux, geothermal springs, and the decomposition of organic material (Wüest et al. 1992) provide the necessary heat and salt sources. In Lake Kivu (Fig. 16) it is the geothermal heat flux that keeps the double-diffusive buoyancy flux alive (Newman 1976). Intrusions produced by river discharge, differential mixing, or the flow over a sill separating two basins (Figs. 7 and 22) can also create double-diffusive conditions. For example, river interflow (Fig. 7) usually favors a diffusive regime at the upper boundary and a salt-finger regime at the lower boundary of the merging river water. Diffusive regimes have also been found in meromictic lakes that have developed from former fjords containing trapped seawater subject to geothermal heating (Sanderson et al. 1986).

6.6 Isopycnal Mixing

6.6.1 Scale Dependence of Isopycnal Mixing

Only little energy is necessary for a water parcel to move adiabatically along a surface of constant density. Thus, isopycnal transport is several orders of magnitude faster than diapycnal transport. As described in Section 3, the distinction between advective and turbulent mass flux is arbitrary in the sense that it depends on the scales that are considered. This is especially true for isopycnal transport, because the eddy size covers the entire range from the length of the lake down to the dissipation scale (mm).

Isopycnal currents have complex spatial and temporal structures, and exhibit fluctuations with various periods. In lakes velocities averaged over long time intervals are usually very small. Over short time scales, however, horizontal velocities can cause significant advection. Thus, a tracer cloud is primarily moved around advectively by eddies that are significantly larger than the size of the tracer patch. In contrast, eddies that are smaller than the tracer distribution generate mixing within the patch, a process that is usually interpreted as turbulent diffusion. Intermediate eddies of a size comparable to that of the tracer cloud cause distortion and stretching of the cloud, due to the shear of the velocity field. In combination with small-scale mixing this leads to an efficient growth of the tracer cloud. Figure 17 shows an example of the horizontal extension of the fluorescent dye uranin 30 h after it was artificially added to Lake Lucerne as a small, roughly circular patch.

In order to separate advective from diffusive transport it is necessary to characterize a tracer cloud by distinguishing the movement of its *center of mass* (x_s,y_s) from the temporal development of

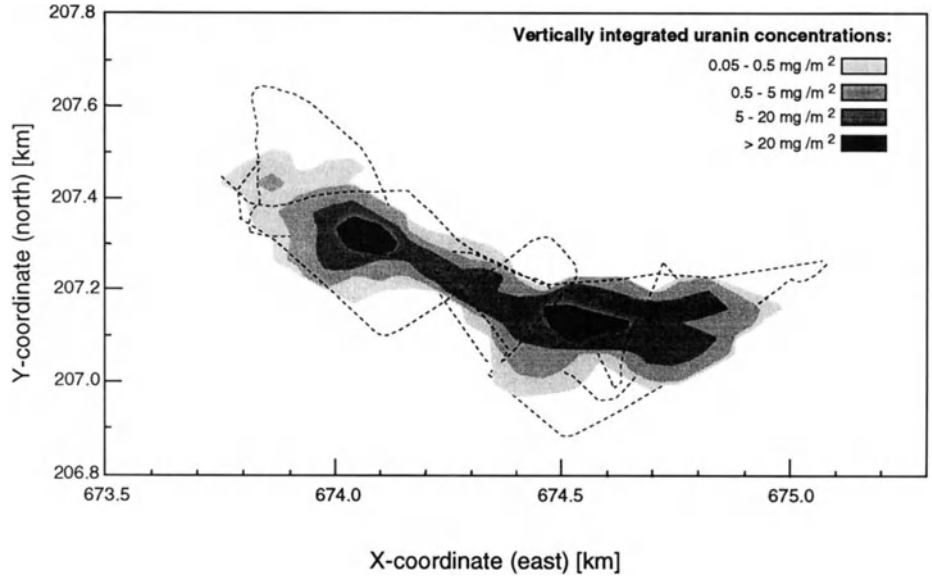


Fig. 17. Radially asymmetrical horizontal concentration distribution of uranin, 30 h after release as a point source into a basin of Lake Lucerne. The *shading* indicates the vertically integrated concentration of the tracer. The *dashed line* represents the path of the ship during the survey of the tracer cloud. This particular tracer distribution represents one point of Fig. 18 (*open circles*), showing the temporal growth of tracer clouds. (Redrawn from Peeters et al. 1993)

its shape relative to the center of mass. The following considerations focus on isopycnal (horizontal) mixing. The influence of vertical mixing is compensated for by using the vertically integrated concentration C(x,y). The center of mass is given by the coordinates

$$x_s = \frac{1}{M}\iint x\, C(x,y)\,dx\,dy;$$

$$y_s = \frac{1}{M}\iint y\, C(x,y)\,dx\,dy, \tag{89}$$

where M is the total mass of the tracer cloud, given by

$$M = \iint C(x,y)\,dx\,dy. \tag{90}$$

The shape of the tracer cloud can be described by its statistical characteristics, e.g., by its moments of order n about the center of mass. Often, only the second moments (the variances σ_x^2 and σ_y^2 and the covariance σ_{xy}) are considered. These are defined by

$$\sigma_x^2 = \frac{1}{M}\iint (x - x_s)^2\, C(x,y)\,dx\,dy;$$

$$\sigma_y^2 = \frac{1}{M}\iint (y - y_s)^2\, C(x,y)\,dx\,dy;$$

$$\sigma_{xy} = \frac{1}{M}\iint (x - x_s)(y - y_s)C(x,y)\,dx\,dy. \tag{91}$$

As demonstrated in Fig. 17, the spreading of a tracer cloud is often highly anisotropic. By rotation of the coordinate system, the x and y axes can be made to coincide with the major and minor principal axes, respectively (Peeters 1994). The corresponding variances are σ_{ma}^2 and σ_{mi}^2, whereas the covariance is zero. (In fact, the variances along the principal axes are the eigenvalues of the matrix σ_{ij} as calculated from Eq. 91 for an arbitrary coordinate system.) The size of a tracer cloud is somewhat arbitrarily defined (Okubo 1971) as

$$\sigma^2 = 2\sigma_{ma}\,\sigma_{mi}. \tag{92}$$

This choice is reasonable insofar as in the case of a two-dimensional Gaussian distribution, the area of a circle with radius σ contains 63% of the total tracer mass. (Furthermore, if a radially symmetrical distribution is constructed from a tracer cloud, as is often the case, the corresponding variance σ_r^2 is equal to σ^2, provided that the cloud can be viewed as an isotropic Gaussian distribution.)

Isopycnal mixing rates are quantified by the growth of the size of tracer clouds. Figure 18 shows a few examples of the temporal increase of σ^2 as a function of the diffusion time t. A common

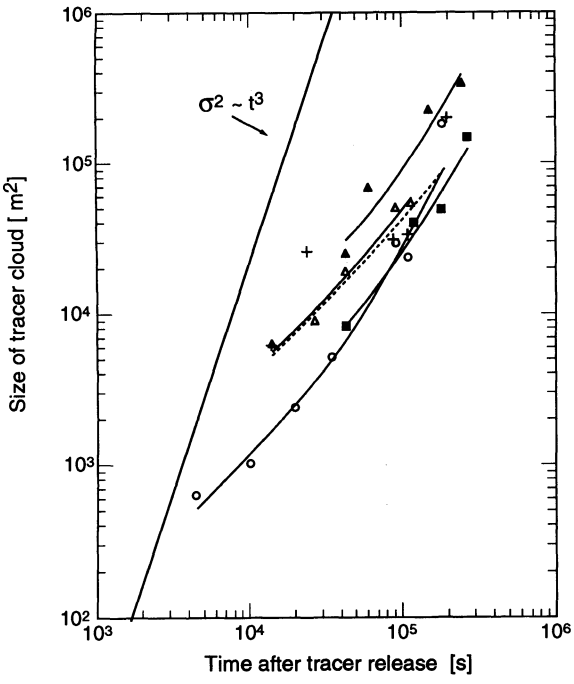


Fig. 18. Size of tracer clouds as a function of time for experiments in Lake Ontario (Murthy 1976; *filled symbols*), Lake Lucerne (Peeters 1994; *open circles*) and the ocean (Okubo 1971; *crosses*). The *thin lines* represent the fits of the shear-diffusion model (Eq. 98) to data from experimental tracer clouds such as those shown in Fig. 17. The *thick solid line* represents the fit to the inertial-subrange model (Eq. 96) of data from several dye experiments in ocean surface waters summarized by Okubo (1971). This comparison supports the superiority of the shear-diffusion model to describe the long-term spreading of a tracer. (Redrawn from Peeters et al. 1993)

approach to characterizing the growth rate is by approximating the size σ^2 using the simple power-law relation

$$\sigma^2(t) = at^m. \tag{93}$$

As a first step we can try to interpret observations of isopycnal spreading in terms of an isotropic first-order local closure scheme (Fickian diffusion; Eq. 17). The apparent diffusivity K_i would then be related to $\sigma^2(t)$ by

$$K_i = \frac{1}{4}\frac{d\sigma^2(t)}{dt}. \tag{94}$$

In order for K_i to be constant with time, m = 1 would be needed. In fact, measurements in lakes (Murthy 1976; Peeters et al. 1993), fjords and coastal waters (Kullenberg 1972), and oceanic surface waters (Okubo 1971) show that irrespective of macroscopic conditions the growth of tracer clouds is neither isotropic (Fig. 17) nor linear with time (Fig. 18), because nearly all observations yield values of m larger than 1. This implies that isopycnal diffusion is dependent on length scale and is non-Fickian. Combining Eqs. (93) and (94) yields an expression relating the apparent diffusivity K_i to the length scale σ of the tracer distribution:

$$K_i = A\sigma^{[2(m-1)/m]} \quad \left(A = \frac{m}{4}a^{1/m}\right). \tag{95}$$

The anisotropic character of isopycnal mixing is addressed in the following brief discussion on diffusion models.

6.6.2 *Diffusion Models*

There is no well-founded theory on isopycnal diffusion in lakes. In fact, almost all of the models listed in Table 12 are of empirical origin, rather than being based on a deeper understanding of the physics behind the mixing processes.

The simplest model, corresponding to Fickian diffusion, is parameterized by a constant diffusivity K_i. As discussed previously (Eq. 94), cloud size, according to this model, should grow linearly with elapsed diffusion time t. In contrast to small-scale diapycnal diffusion, isopycnal transport also occurs over large scales. We therefore expect to find Fickian-type isopycnal mixing only for very small patches. In fact, isopycnal Fickian diffusion has never been observed in field studies.

A particularly popular diffusion model is based on the assumption that the turbulent regime falls into the inertial subrange. As can be recalled from Section 5.5, this means that energy enters at scales larger than the spatial scale under consideration and dissipates at smaller scales, and also that turbulence is steady, homogeneous, and isotropic. For such a situation the similarity theory (Kolmogorov 1941) predicts that the cloud size σ^2 will grow proportional to t^3 if the initial patch is small (Richardson 1926; Batchelor 1950). Furthermore, the spreading of the cloud should depend on the intensity of the turbulence as measured by the rate of dissipation ε of TKE. Dimensional analysis leads to the expression

$$\sigma^2 = \text{const}\,\varepsilon t^3. \tag{96}$$

Table 12. Isopycnal diffusion models

Diffusion model	Physical basis and parameter	Power law for $\sigma^2(t)$ (Eq. 93)	Diffusion law for K_i (Eq. 95)	References
Fickian	Constant diffusivity in analogy to molecular diffusion	m = 1	K_i = constant	
Diffusion velocity (or Joseph-Sendner)	Diffusion due to relative velocity v; velocity v and length scale L	m = 2	$K_i = vL$	Joseph and Sendner (1958)
Inertial subrange	Similarity in the inertial subrange; energy dissipation ε and length scale L	m = 3	$K_i = c\varepsilon^{1/3}L^{4/3}$	Okubo and Ozmidov (1970)
Shear diffusion	Interaction of horizontal and vertical shear ($\partial u/\partial y$ and $\partial u/\partial z$, respectively) with small-scale horizontal and vertical diffusion (K_h and K_d, respectively)	m = 1–2	$K_i = f\left(\frac{\partial u}{\partial y}, \frac{\partial u}{\partial z}, K_h, K_d\right)$ See Eq. (98)	Young et al. (1982) Taylor (1953) Kullenberg (1972) Carter and Okubo (1965) Peeters (1994)
"Half-past-one-in-the-morning"	No physical basis	m = 1.5	K_i = const $L^{2/3}$	Ewart and Bendiner (1981)

The apparent isopycnal diffusivity is calculated from Eq. (94):

$$K_i = \text{const}\,\varepsilon^{1/3}\sigma^{4/3}. \tag{97}$$

This specific scale dependence of K_i is well known from the work of Okubo (1971), who compiled the most reliable data from many different dye experiments in ocean surface waters and demonstrated a surprisingly good agreement with the 4/3-power law over distances from 100 m to 1000 km. However, this agreement has often led to serious misinterpretations. Because the diagram represents an ensemble of experiments with different initial sizes and different environmental conditions, it does not necessarily describe the temporal development of an individual tracer distribution. In fact, as shown by Peeters (1994), individual clouds, even the original clouds of Okubo (1971; Fig. 18), grow more slowly with time (or with size) than predicted by Eq. (96).

There is an even more severe reservation with regard to the inertial subrange mixing model, viz. the obvious anisotropic spreading of tracer clouds. Because natural waters are always stratified to some extent, it does not come as a surprise that turbulence in the vertical is suppressed. It is more difficult to understand why isotropy does not hold, at least in the horizontal direction. A relevant argument is introduced by the *shear-diffusion model* (Okubo 1967; Kullenberg 1972; Young et al. 1982; Peeters 1994) in which a non-turbulent shearing-velocity field is combined with small-scale (Fickian) turbulence, expressed by the small-scale horizontal and diapycnal diffusivity, K_h and K_d, respectively. In this model it is assumed that the small-scale horizontal turbulent diffusivities are spatially homogeneous ($K_x = K_y = K_h$), and that the nonturbulent velocity field is along the x axis and has the simple form $u = a \cdot y + b \cdot z$. Then the variances in the lengths of the major and minor principal axes of an evolving tracer cloud are given by the following expressions (Peeters 1994):

$$\begin{aligned}
\sigma_{ma}^2 &= 2K_h t + \tfrac{1}{3}(a^2K_h + b^2K_d)t^3 + \sqrt{K_h^2 a^2 t^4 + [\tfrac{1}{3}(a^2K_h + b^2K_d)t^3]^2};\\
\sigma_{mi}^2 &= 2K_h t + \tfrac{1}{3}(a^2K_h + b^2K_d)t^3 - \sqrt{K_h^2 a^2 t^4 + [\tfrac{1}{3}(a^2K_h + b^2K_d)t^3]^2};\\
\sigma^2 &= 2\sigma_{ma}\sigma_{mi}\\
&= 2\sqrt{4K_h^2 t^2 + \tfrac{1}{3}K_h(a^2K_h + 4b^2K_d)t^4}.
\end{aligned} \tag{98}$$

In rivers and streams the combined action of lateral and vertical shear ($a = \partial u/\partial y$ and $b = \partial u/\partial z$, respectively), as well as horizontal and

vertical small-scale diffusion (K_h and K_d, respectively), produces stretching and thus growth of the patch along the major principal axis, because the tracer is distributed by diffusion among layers of different horizontal velocities. As long as the vertical and horizontal extension, and thus the velocity shear, can be assumed to be unbounded relative to the actual size of the tracer cloud, the growth in the variance of the tracer distribution with time (second term in Eq. 98) increases progressively with larger shear (a and b) and larger diffusivity (K_h, K_d).

Note that for short times t the growth in cloud size σ^2 is proportional to the elapsed diffusion time t (m = 1, as for the Fickian model), whereas for long time intervals the growth of σ^2 is proportional to the square of elapsed time (m = 2), and the variance along the major principal axis σ_{ma} can even increase proportionally to t^3 (see second and last terms in Eq. 98) as follows:

$$\sigma_{ma}^2 \sim \frac{2}{3}(a^2K_h + b^2K_d)t^3 \qquad (99)$$

if t is very large. Hence, the inertial subrange model is not the only one that implies a 4/3-power law for the apparent isopycnal diffusivity K_i, at least along the major axis.

6.6.3 *Experimental Observations*

Among the models presented previously, only the shear-diffusion model is able to explain the two most important experimental findings on isopycnal diffusion in lakes, which are: (1) the tracer distributions are not radially symmetrical, but are stretched out along the direction of the main current (Fig. 17), and (2) the growth rate of the cloud sizes is less than predicted by the inertial subrange model, but increases with increasing elapsed diffusion time t (Fig. 18). The anisotropic spreading of individual dye clouds has been observed by Murthy (1976) in Lake Ontario. The variance along the length of the cloud exceeded that along its breadth by a factor of 5–10. Comparable anisotropy has been found in experiments carried out in several medium-sized Swiss lakes (Peeters et al. 1993; Fig. 17).

If the inertial subrange model provides the right qualitative dependence on ε (Eq. 97), the apparent isopycnal diffusion below the pycnocline of a stratified lake should be much smaller than in surface waters. Values of K_i observed by Murthy (1976) in the hypolimnion of Lake Ontario were indeed one to two orders of magnitude smaller than those found in the epilimnion. A well-sampled dye experiment in the stratified water column of the Pacific (Ewart and Bendiner 1981) demonstrated that diffusivity decreased with depth at depths less than 500 m. Both experiments support the explanation that a decrease in TKE is responsible for the decrease in the apparent isopycnal diffusivity K_i.

It is less clear how shear-induced horizontal diffusion varies within the hypolimnion. As shown in Fig. 13, the diapycnal diffusivity is inversely related to the density stratification N, and thus commonly increases with depth below the pycnocline. In contrast, vertical shear usually has its maximum in the upper thermocline, where stratification is largest (see Sect. 6.1). In the density-stratified hypolimnion the vertical shear usually oscillates with time (see Sect. 6.1), e.g., $\partial u/\partial z \approx \sin(\omega t)$. The corresponding variance then increases only linearly with time (Kullenberg 1972):

$$\sigma^2 = \text{const}\, K_d\left(\frac{\partial u}{\partial z}\right)^2 t. \qquad (100)$$

Isopycnal diffusion in lakes is generally smaller than in oceans (Fig. 18) and in fjords (Kullenberg 1972), and depends strongly on external forcing, i.e., on storm events (see Sect. 7.1). Diffusivities measured by Murthy (1976) and Peeters (1994) in the hypolimnion of various lakes range from $0.02\,m^2s^{-1}$ to less than $0.3\,m^2s^{-1}$, i.e., about five times smaller than in oceans. Under special conditions, e.g., below ice (Colman and Armstrong 1987), they may reach extremely low values. Because the two shear components ($\partial u/\partial z$ and $\partial u/\partial y$) are difficult to predict, since they depend on the local forcing, the parameterization of scale-dependent isopycnal mixing is generally difficult as well.

6.6.4 *Intrusions*

At lake surfaces wind is the main driving force for the currents that are responsible for velocity shear, and thus for isopycnal diffusion. In contrast, in the density-stratified hypolimnion, currents are also driven by intrusion, i.e., by isopycnal pressure forces resulting from horizontal-density gradients between adjacent water columns and from lateral water input. Intrusions

can have several origins (Fig. 7) including plunging rivers, subsurface springs, the subsurface withdrawal of water, differential mixing at the sediment surface and at topographical features such as sills and narrows, differential deepening of the pycnocline due to spatial heterogeneity of the surface wind stress, and large-scale exchange between basins with different mixing characteristics (Fig. 22). In the epilimnion, intrusions also result from differential cooling and heating, especially in the shallow parts of a lake. Because of the limited depth, the daily variation of the surface temperature is larger in shallow side arms than, for instance, in the open lake. Consequently, during the heating period the surface water from the side arms floods the open lake (Patterson 1987). In contrast, during cooling, surface water sinks to the bottom of the side arms, creeps down the slope, and merges into the lake interior (Horsch and Stefan 1988). There is no general theory for describing the vertical mixing due to horizontal density currents and intrusions, although their significance has become more apparent during the past few years. Because intrusions are directed, a diffusion scheme is hardly adequate for their description.

6.6.5 *Diapycnal Effects of Isopycnal Mixing*

Surfaces along which water moves without experiencing a restoring buoyancy force are termed *neutral surfaces* (McDougall 1987b). Neutral surfaces are nearly identical to isopycnal surfaces. Temperature and salinity changes along neutral surfaces are related by $\alpha d\theta = \beta_S dS$, where θ is potential temperature (Eq. 39). If water moving along a neutral surface mixes laterally with surrounding water, water with a new temperature and salinity is created. Because the equation of state of water is nonlinear (Eq. 29), the modified water has a density that is larger than the density corresponding to the particular neutral surface. The parcel thus experiences a force perpendicular to the neutral (or isopycnal) surface. As mentioned in Section 4.1, the two largest contributions to the nonlinear effect are *thermobaricity* (caused by the pressure dependence of α) and *cabbeling* (caused by the temperature dependence of α) (McDougall 1987a).

Cabbeling is well known in lakes. For example, when equal volumes of water of 3 °C from the open lake and 5 °C from near the shore merge, the mixed water of 4 °C is heavier and sinks. This effect leads to the well-known thermal bar phenomenon. Figure 19 shows a thermal bar observed in Lake Baikal in early summer. The lines of constant salinity indicate the strong vertical exchange near the thermal bar, approximately 1.5 km offshore. Because the shape of the $\rho(T)$ function is such that mixed water is always heavier than the original waters, cabbeling not only occurs at temperatures near 4 °C; yet, it always causes downwelling of fluid through

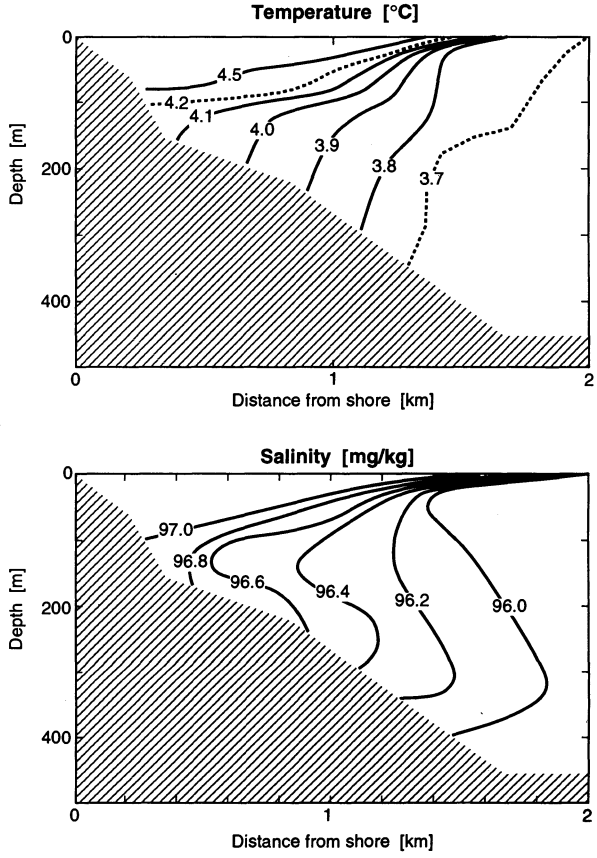


Fig. 19. Formation of the thermal bar in Lake Baikal as observed on 7 June 1993 at the eastern shore of the middle basin near Boldakova. In spring, the nearshore waters warm up faster than the waters of the central part of the lake. The mechanisms for this differential heating are not yet fully understood, but it seems that at least part of the warming is due to relatively warm water from the Selenga River, the major inflow to Lake Baikal, flowing north along the eastern shore. The *upper figure* shows the isotherms (temperatures in °C) in an east/west section perpendicular to the shore. At the surface, the thermal bar, determined by the temperature of maximum density (4 °C), lies approximately 1.5 km offshore. As shown in the *lower figure*, the lines of constant salinity indicate fast vertical mixing in this zone

neutral surfaces. In contrast, thermobaricity, depending on the slope of the neutral surface, can lead to either upwelling or downwelling.

7 Mixing and Its Ecological Relevance

7.1 Time Scales of Mixing

Mixing phenomena in lakes cover a wide range of time scales, from hundreds to thousands of years in the case of permanent stratification to seconds for surface waves and turbulent eddies (Table 13). On one hand, this enormous range reflects the spectrum of external forces extending from individual wind gusts up to climate changes; on the other hand, the time scales are also determined by the characteristics of the various physical phenomena that occur internally in lakes, which are discussed in the following sections.

7.1.1 Seconds and Minutes

The processes at one end of the mixing hierarchy, the short- and small-scale events, bridge the gap from stirring to mixing and are thus the essential elements for mixing. Here, we find the surface waves and the turbulent overturns depicted in Fig. 11a. However, because these features (Fig. 11b) are small they do not survive long, unless they are continually fed with energy from the large-scale processes.

7.1.2 Hours

This is the most typical time scale for epilimnetic processes, although the development of some hypolimnetic processes, e.g., storm-induced turbidity currents and standing internal waves, also occur on the same time scale. In contrast to the internal-wave field, which is important for hypolimnetic mixing, the energy that drives mixing in the epilimnion cannot easily be stored in a non-turbulent way. The response of the epilimnion to wind stress and surface buoyancy flux is therefore immediate and fast. The typical response time of a nonstratified epilimnion is given by a characteristic turbulent velocity u_{turb} and the depth of the mixed layer h_{mix}:

$$t_{resp} = \frac{h_{mix}}{u_{turb}}. \tag{101}$$

The characteristic turbulent velocity u_{turb} is defined as the friction velocity, $u_* = (\tau_o/\rho)^{1/2}$, if wind-driven turbulence dominates, and as $u_b = (h_{mix}\, J_b^o)^{1/3}$ for convectively driven mixing (Deardorff 1970). This scale represents the time lag between the onset of the forcing and the time

Table 13. Characteristic time scales of mixing processes in lakes

Time scale	Process	Examples
Seconds and minutes	Surface waves	
	Turbulent overturns	Thorpe (1977) and Dillon (1982)
	Stability oscillation in stratified water	
	Langmuir circulation	Leibovich (1983)
Hours	Wind setup	Spigel and Imberger (1980)
	Internal waves	
	Diurnal mixed layer	Imberger (1985)
	Lateral convection due to differential heating/cooling	Horsch and Stefan (1988)
	Convective turbulence	Lombardo and Gregg (1989)
	Turbidity currents	Lambert (1988)
	Inertial modes	
Days	Mixing due to storms	Imboden et al. (1988)
	Basin modes (topographical waves)	Saylor et al. (1980)
Weeks and months	Annual stratification cycles	
	Basin-wide exchange due to horizontal density gradients	Wüest et al. (1988)
	Internal-wave damping in regularly shaped basing	Mortimer (1974), Csanady (1974)
	Thermal bar	
Years	Meromixis	Sanderson et al. (1986), Steinhorn (1985)

when turbulence in the mixed layer becomes stationary and pycnocline erosion starts. The following example yields typical values for t_{resp}: For a wind speed $W_{10} = 5\,m\,s^{-1}$, the friction velocity u_*, and thus u_{turb}, is roughly 5×10^{-3} $m\,s^{-1}$, yielding $t_{resp} \sim 0.5$ h for $h_{mix} = 10$ m. In the case of a positive surface buoyancy flux J_b^o, caused for instance by surface cooling, we obtain a value u_b of the same magnitude as u_* if $J_b^o = 10^{-8}$ $W\,kg^{-1}$. This buoyancy flux would result, for example, from a net heat loss $H_{net} = -60\,W\,m^{-2}$ from a water body at 10 °C.

Buoyancy flux and wind shear are hardly ever in balance in the epilimnion. Thus, during the day a weak stratification, the *diurnal pycnocline*, is usually formed. An increase in the production of TKE causes the turbulence front to move downward from the surface, resulting in erosion of the diurnal pycnocline. Associated with the mixing of a layer of depth h_{mix} with stratification N is a change in potential energy of $\frac{1}{12}\rho N^2 h_{mix}^3$ $[J\,m^{-2}]$, provided that the density of the mixed water can be approximated by a linear function of the properties of the water that determine its density (usually temperature and salinity). The change in potential energy is fueled by the buoyancy flux J_b, which, as discussed in Section 5.4, is roughly 10% of the total dissipation (Eq. 56). Given this mixing efficiency and the vertical profiles of dissipation for wind and convectively driven surface turbulence (Fig. 10), i.e., $\varepsilon_w(z) = \frac{u_*^3}{kz}$ and $\varepsilon_c(z) = J_b^o$, we can estimate the mixing time scales simply by integration. The resulting time scale is

$$t \approx \frac{5}{3} N^2 h_{mix}^3 k/u_*^3 \tag{102}$$

for wind-driven turbulence and

$$t \approx \frac{5}{2} N^2 h_{mix}^2 / J_b^o \tag{103}$$

for convectively driven mixing. The difference in the form of the dependence of t on layer depth h_{mix} again reflects the high deepening efficiency of the wind in shallow water and the dominance of convection at greater depth. An example for the diurnal energetics of the epilimnion under different forcing was given by Imberger (1985).

Mixing events in the hypolimnion generally have time scales on the order of days. In Fig. 20, however, a fascinating example is shown where photo-autotrophic bacteria are able to produce convective mixing in the hypolimnion on time scales of hours to days.

7.1.3 Days

Internal waves in lakes have time periods of hours to days. Forcing is applied at the same time scales, because wind-speed spectra have a synoptic scale maximum (i.e., 1 to several days). If a wind event lasts longer than roughly a quarter of the seiche period of the first internal horizontal mode, first-mode seiching is the dominant response to the

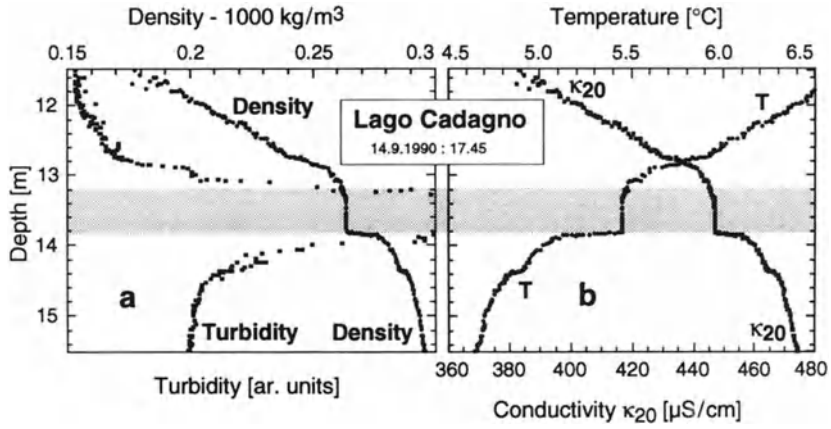


Fig. 20. Turbidity and density (**a**) as well as temperature and the ionic concentration (**b**) in Lago Cadagno reveal a homogeneous layer (indicated by the *gray shading*) of 0.8 m thickness in a depth of approximately 13.5 m. The well-mixed layer coincides with a dense population of photo-autotrophic sulfur bacteria growing in the oxic–anoxic transition zone. Based on turbulent kinetic energy arguments, it can be shown that the microorganisms are able to mix this layer convectively within a few hours by means of swimming. (Redrawn from Wüest 1994)

wind. An exceptional situation occurs if a lake that is predominantly driven by diurnal winds has an internal mode of higher order with a period close to 24 h. This is the case in Alpnachersee, a small basin of Lake Lucerne (Switzerland). Münnich et al. (1992) found the *first horizontal/second vertical* mode to be the dominant internal mode during most of the time (see Sect. 6.1 and Fig. 14a).

Further development of the internal-wave motion is complex. The first mode generally decays into modes of higher horizontal and vertical order (Wiegand and Chamberlain 1987). The time scale for the decay of the internal-wave field is strongly dependent on mixing. If nonlinearities occur, damping is strong and intense mixing occurs even within one seiche period. An example from Zugersee (Switzerland) is given in Fig. 21. In contrast, small internal amplitudes in regularly shaped basins are only moderately damped and can last for weeks (Lemmin 1987).

7.1.4 Weeks and Months

The annual stratification of a lake is the most prominent feature occurring on a time scale of weeks and months. The seasonal pycnocline represents an integral response to heating, wind stress, convectively driven turbulence, and river inflows. However, the temporal evolution of the vertical density stratification may vary slightly over the lake surface. This is especially the case during the initial phase of the seasonal temperature stratification when the density gradients are still small, and slight differences in the wind-shear stress, for example, may result in significant variations in pycnocline depth. Such horizontal density gradients, coupled to the stratification cycle, may cause long-lasting basinwide currents.

Another source of horizontal density gradients is given by river inflows of different thermal or chemical characteristics. The induced basinwide exchanges may be long-lasting or even permanent, especially if the density difference among the inflows is due to different geochemical composition. An example from Lake Lucerne (Switzerland), where both thermal and geochemical effects are important, is given in Fig. 22.

In large lakes in which the surface temperature has dropped below 4 °C during the winter, a thermally driven circulation pattern may occur in spring, when the water in the zones near the shore

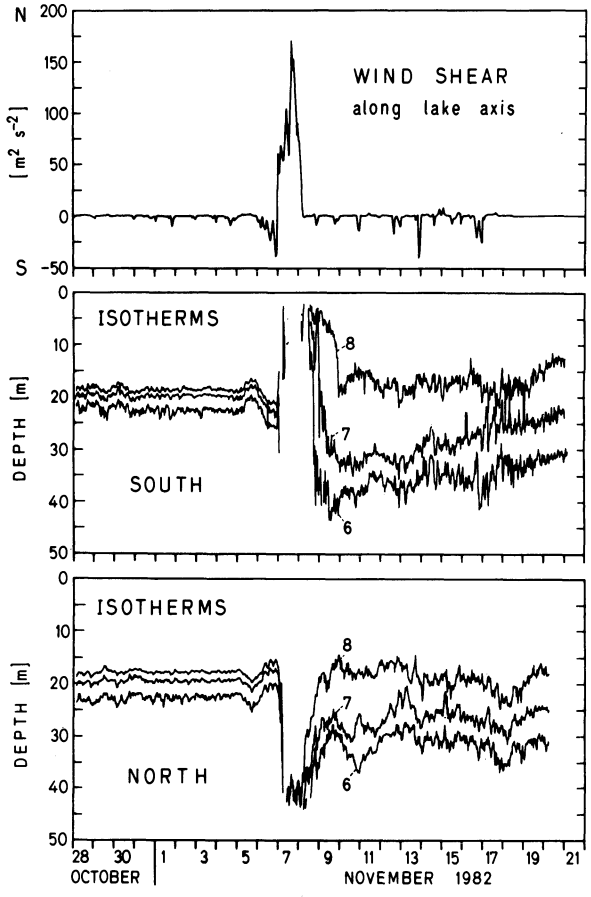


Fig. 21. Wind stress (*upper panel*) along the main axis of Zugersee (Switzerland) and corresponding isotherm depths during a vigorous föhn storm with wind speeds measured at a nearby weather station exceeding 45 m s^{-1}. The storm blowing from the south began on 7 November 1982, after a short period during which the wind blew from the north. At the southern end of the lake cold water was brought to the surface (*middle panel*), while at the northern end (*lower panel*) the warm surface water was pushed down below 45 m, the lower end of the thermistor string. After the storm large-amplitude internal waves, generated by nonlinear interactions, remained in the lake for more than 10 days. The first mode of the internal seiche, however, was strongly damped, due to shear instabilities (Fig. 11) leading to an increase in short-term diapycnal eddy diffusion of nearly three orders of magnitude compared with the preceding 6 months (see also Fig. 13). (Redrawn from Imboden et al. 1988)

warms up faster than in the middle of the lake. This difference may be caused by warm river water, by reduced vertical wind mixing, or by a combination of both. Thus, during the onset of stratification a situation occurs in which part of the lake surface is occupied by water that is warmer than 4 °C, while the rest of the surface

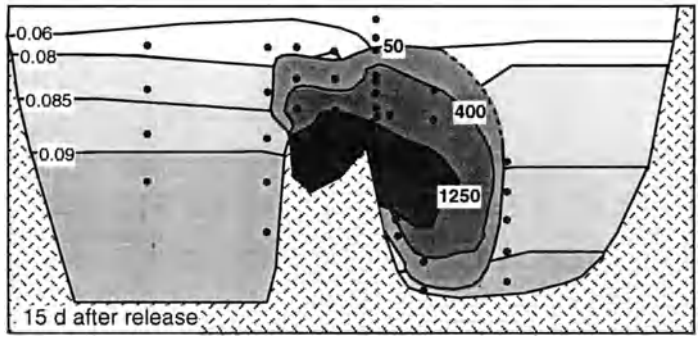


Fig. 22. Urnersee (*right*) and Gersauersee (*left*), spearated by two sills, are adjacent deep basins of Lake Lucerne (Switzerland), with similar topography but remarkably different wind exposure. Urnersee experiences diurnal winds and occasional strong storms from the south (*right*), whereas the wind over the sheltered Gersauersee is usually weak. In spring, large-scale wind mixing results in the subsurface water of the wind-exposed Urnersee becoming warmer and lighter. This differential mixing generates a weak horizontal density gradient between the two basins, demonstrated by the change of depths of the isopycnals between the basins. As a consequence, nearly the whole of the deep water of Urnersee is replaced by a slow but long-lasting exchange flow of approximately $10^7\,m^3\,d^{-1}$ of water (Wüest et al. 1988). The figure shows the effect of this exchange via the distribution of SF_6, 15 days after its release into the intermediate basin (redrawn from Schlatter 1991). Once the horizontal-density gradient has vanished, water from below the sill can still undergo exchange by a process termed seiche pumping, in which heavier water can flow over the sill during the maximum rise of the isotherms and merge into the deep part of Urnersee. (Van Senden and Imboden 1989)

water is still colder than 4 °C. The two water masses are separated by a transition zone (thermal bar) where water sinks to the deeper part of the lake, due to cabbeling. As the heating continues the thermal bar moves offshore until the temperature of the entire surface exceeds 4 °C. Because of the Coriolis effect, specific thermally driven coastal currents are induced by the thermal bar (Csanady 1974; Mortimer 1974). Figure 19 shows a thermal bar in Lake Baikal, Siberia.

7.1.5 Years

During periods of lowest stability, if convective mixing due to heat loss and wind shear is too weak to destroy the density stratification, part of the lake may remain permanently stratified. This is called *meromixis*. Mixing rates in the deep layers of meromictic lakes are extremely slow, approaching rates of molecular diffusion. In such a situation differences in the molecular-diffusion coefficients of ions may become relevant. An instructive example of *differential diffusion* occurring over a time scale of 10 000 years is given by Sanderson et al. (1986) for the case of seawater trapped in a deep fjord lake.

Another interesting example of meromixis was found in the Dead Sea, a deep ($\approx$ 320 m), warm (minimum temperature $\approx$ 18 °C), and hypersaline ($S = 280\,g/kg^{-1}$) lake (Steinhorn 1985). The meromixis originates from the freshwater input to the lake from the rivers, which creates a strong pycnocline. During the past 300 years winter cooling was not able to overcome this strong stratification. In the past few decades, however, and especially since 1964, an increasing fraction of the water from the Jordan and Yarmuk rivers has been diverted for irrigation purposes, resulting in a decrease in the amount of fresh water flowing into the Dead Sea. Consequently, because of evaporation, the thickness of the less-saline surface layer decreased and the water level of the lake dropped. Furthermore, the salinity differences between surface and deep waters were reduced from 50‰ in 1864 to <0.1‰ in 1978. The final consequence of this was that the long period of strong meromixis ended in early 1979. Since then the meromictic structure has been variable. The Dead Sea can now turn over during winter depending on the strength, timing, and duration of river inflow, evaporation, and cooling (Anati et al. 1987).

7.2 Reactive Species and Patchiness

The distribution of a chemical or biological species in a lake is determined by the ratio of two kinds of time scales, the reaction and input time scales on

one hand, and the mixing time scales on the other. The latter have already been discussed extensively in the preceding sections and are summarized in Table 13. We now add a few remarks on reaction rates.

The time scales of reactions range from milliseconds (or less) to millions of years. Examples for the former are fast equilibrium reactions (e.g., hydrolysis), and for the latter the slow diagenetic transformations occurring in ocean and lake sediments or the radioactive decay of long-living isotopes such as ^{238}U. Although reactions exhibit a great variety of kinetics (zero, first, and higher orders), the instantaneous rate of change can be characterized by the relative rate λ_r (or the reaction time τ_r)

$$\lambda_r = \tau_r^{-1} = \frac{1}{C}\left|\frac{dC}{dt}\right|_{reaction}. \quad [s^{-1}] \tag{104}$$

For a first-order reaction, such as radioactive decay, λ_r is constant; otherwise, λ_r represents an instantaneous pseudo-first-order rate that changes its size with changing concentrations of the reaction partners.

A simple way to deal with the simultaneous action of mixing and reaction is to compare the relative size of mixing and reaction times, τ_{mix} and τ_r (Imboden and Lerman 1978). As demonstrated previously, because mixing in aquatic systems usually consists of a whole set of simultaneous processes occurring on different time scales, it is appropriate to consider the effect of a reaction (characterized by τ_r) on a whole spectrum of mixing processes such as the turbulent velocity spectrum in the inertial subrange, E(k), defined in Eq. (57).

Corrsin (1961) calculated the spatial spectrum of a reactive species, $E_c(k)$, undergoing a first-order reaction in an isotropic, stationary turbulent field. He found that there exists a critical wave number k_r, given by

$$k_r = |\lambda_r|^{3/2}\varepsilon^{-1/2}, \quad [m^{-1}] \tag{105}$$

below which the velocity and concentration spectra diverge. If k_r lies in the inertial-convective subrange (see Sect. 5.5), we expect to find a k range of large (and thus slow) modes where E(k) and $E_C(k)$ are different and therefore reveal the non-conservative nature of the reactive species. In contrast, for short wavelengths (large k), the two spectra would be identical. The critical-length scale k_r^{-1}, above which tracer-specific patterns are to be expected, lies between approximately 10^3 m at large turbulence intensity for species reacting within hours and 10^5 m at high intensity for species reacting within months. (Species with much shorter or longer reaction times are not relevant to the above!) Strictly speaking, these length scales are much larger than the Kolmogorov Scale (Table 6). Therefore, it is not clear how Corrsin's theory can be applied to the conditions existing in lakes.

Denman et al. (1977) showed that for a tracer with positive reaction (e.g., phytoplankton growth), the spectrum $E_C(k)$ should reach a maximum at $1.3\,k_r$. Powell et al. (1975) measured the velocity and chlorophyll spectra in Lake Tahoe (California/Nevada). In the chlorophyll spectrum they found a peak at $k = 10^{-2}\,m^{-1}$, which was not present in the velocity spectrum, and which they attributed to Langmuir circulation. In light of the theory of Denman et al. (1977), the peak could also be the result of phytoplankton growth (see Imboden 1990, for details).

The interplay of turbulence and reactivity produces a pattern in the spatial concentration distribution, which, for certain wave numbers, bears the imprint of the reaction. This is equivalent to saying that reaction creates patchiness. In fact, patchiness is a special property of biological species. Yet, turbulence is not the only explanation for the occurrence of patchiness; another source of patchiness is related to the nonlinear nature of biological processes such as the predator–prey interaction described, for example, by the Lotka-Volterra model. Steele (1974) was the first to draw attention to the special phenomena that appear if the nonlinear Lotka-Volterra interaction is combined with a spatial diffusion term. We first discuss the equation for a prey (e.g., a phytoplankton species, described by its concentration P) during exponential growth (growth rate α) under the influence of Fickian (turbulent) diffusion (diffusivity K):

$$\frac{\partial P}{\partial t} = \alpha P + K\frac{\partial^2 P}{\partial x^2}. \tag{106}$$

(For simplicity, only one dimension is considered here!) Assume that at some initial time t, P(x) has an arbitrary spatial variance expressed by the Fourier-transform function $\hat{P}(k)$. Its time rate of change is

$$\frac{\partial \hat{P}}{\partial t} = (\alpha - k^2 K)\,\hat{P}. \tag{107}$$

Thus, the mode $\hat{P}(k)$ can only grow provided that

$$k < \left(\frac{\alpha}{K}\right)^{1/2}. \tag{108}$$

This is equivalent to saying that a species patch can only grow in size provided that its length scale L is larger than a critical size L_{crit}:

$$L > L_{crit} = 2\pi\left(\frac{K}{\alpha}\right)^{1/2}. \tag{109}$$

L_{crit} is the well-known critical-length scale first introduced by Kierstead and Slobodkin (1953). Because the growth rate α decreases at higher trophic levels (zooplankton, fish, etc.), the minimum stable patch size L_{crit} becomes larger with higher trophic level. Steele (1978) developed this model further to explain the patchiness of biomass in the ocean (Fig. 23).

The terms involving interactions between different species, such as the predator–prey interaction appearing in the Lotka-Volterra model, mix the different k modes, modify the stability criterion, and create new spatial structure in the ecosystem such as "prey–predator waves" (Dubois 1975).

Further discussion of the problem of spatial variability in ecological systems is beyond the scope of this chapter. The interested reader is referred to Platt and Denman (1975) as well as Wroblewski and O'Brien (1976), in which the role of mixing in the evolution and stability of ecosystems is treated.

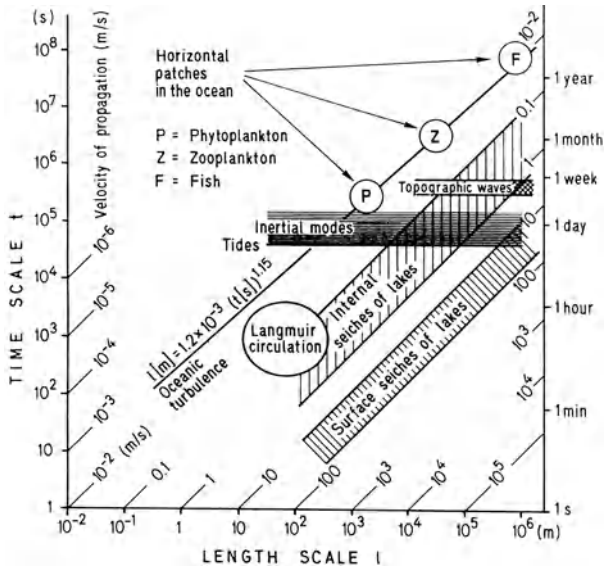


Fig. 23. Typical length and time scales of mixing modes in lakes: The diagonals of *gradient 1* represent lines of constant velocity of propagation (e.g., surface seiches move with velocities between approximately 10 and 100 m s^{-1}). Included is Okubo's (1971) fit between length and time scales for oceanic turbulence. Typical scales of biological patchiness (phytoplankton, zooplankton, and fish) taken from Steele (1978) can be interpreted as the direct consequence of the influence of the isopycnal turbulent scales on species with different growth rates. (Imboden 1990)

7.3 Mixing and Growth: The Search for an Ecological Steering Factor

The problem of influence of turbulence on phytoplanktic species selection and photosynthesis is as yet unsolved. The literature on the subject is contradictory. For instance, Lewis et al. (1984a) concluded for the upper mixed layer in Bedford Basin (Nova Scotia) that "dissipation of turbulent kinetic energy was a strong determinant of algal photosynthetic rate." In contrast, Gallegos and Platt (1982) found in the eastern Canadian Arctic that mixing had only little effect on primary production in the water column.

In the meantime, new insight has been gained by combining measurements of physical and biological parameters with computer models of photosynthesis. Lewis et al. (1984b) developed a theory that characterizes the mixing/production relationship by two nondimensional numbers. The first of these is the mixing–photoadaptation ratio, which is large if the time taken by the plankton to move through different light zones is short compared with the typical photoadaptation time. The second number measures the degree of homogeneity of light intensities within the mixed layer. To summarize the ideas of Lewis et al. (1984b), fast mixing and small light gradients in the mixing layer favor the appearance of a homogeneous planktonic community, whereas low turbulence and large light gradients lead to the establishment of distinct communities that differ with regard to their light-adaptation characteristics.

There are as yet no comparable studies on lakes. In fact, the many factors that influence the dynamics of a lake (Table 1 and Fig. 7) make it more difficult to separate the effect of mixing from other effects. Based on a dynamic model for photosynthesis, however, Pahl-Wostl and

Imboden (1990) gave some theoretical arguments supporting the idea that the mixing regime of a lake could play a role not only in the spatial distribution of abiotic components, but also in the competition between biological species. Building and strengthening a bridge to link the various limnological disciplines will certainly be among the most urgent and exciting tasks to be tackled in lake research in the future.

References

Amorocho J, deVries JJ (1980) A new evaluation of the wind stress coefficient over water surfaces. J Geophys Res 85:433–442

Anati DA, Stiller M, Shasha S, Gat JR (1987) Changes in the thermohaline structure of the Dead Sea: 1979–1984. Earth Planet Sci Lett 84:109–121

Armi L (1978) Some evidence for boundary mixing in the deep ocean. J Geophys Res 83:1971–1979

Armi L (1979) Effects of variation in eddy diffusivity on property distributions in the ocean. J Mar Res 37:515–530

Barry RG, Chorley RJ (1976) Atmosphere, weather and climate. Methnen, London

Batchelor GK (1950) The application of the similarity theory of turbulence to atmospheric diffusion. Q J R Meteorol Soc 76:133–146

Batchelor GK (1959) Small-scale variation of convected quantities like temperature in turbulent fluid. J Fluid Mech 5:113–139

Boudreau BP, Imboden DM (1987) Mathematics of tracer mixing in sediments: III. The theory of non-local mixing within sediments. Am J Sci 287: 693–719

Brutsaert W (1975) On a derivable formula for long-wave radiation from clear skies. Water Resour Res 11:742–744

Bührer H, Ambühl H (1975) Die Einleitung von gereinigtem Abwasser in Seen. Schweiz Z Hydrol 37:347–369

Bünti JL (1914) Chronicle. Neujahrsbl Uri, Altdorf 20:8–9

Caldwell DR, Chriss TM (1979) The viscous sublayer at the sea floor. Science 205:1131–1132

Carter HH, Okubo A (1965) A study of the physical processes of the movement and dispersion in the Cape Kennedy area. Final Rep under US Atomic Energy Comm, Chesapeake Bay Inst, John Hopkins Univ, Rep No NYO-2973-1, 164 pp

Chen CTA, Millero FJ (1986) Precise thermodynamic properties for natural waters covering only the limnological range. Limnol Oceanogr 31:657–662

Chriss TM, Caldwell DR (1982) Evidence for the influence of form drag on bottom boundary layer flow. J Geophys Res 87:4148–4154

Chriss TM, Caldwell DR (1984) Universal similarity and the thickness of the viscous sublayer at the ocean floor. J Geophys Res 89:6403–6414

Chung Y, Kim K (1980) Excess ^{222}Rn and the benthic layer in the western and southern Indian ocean. Earth Planet Sci Lett 49:351–359

Colman JA, Armstrong DE (1987) Vertical eddy diffusivity determined with Radon-222 in the benthic boundary layer of ice covered lakes. Limnol Oceanogr 32:577–590

Corrsin S (1961) The reactant concentration spectrum in turbulent mixing with a first-order reaction. J Fluid Mech 11:407–416

Csanady GT (1974) Spring thermocline behavior in Lake Ontario during IFYGL. J Phys Oceanogr 4:425–445

Deardorff JW (1970) Convective velocity and temperature scales for unstable planetary boundary layer and for Rayleigh convection. J Atmos Sci 27:1211–1213

Deardorff JW, Willis CE, Lilly DK (1969) Laboratory investigation of non-steady penetrative convection. J Fluid Mech 28:675–704

Denman KL, Miyake M (1973) Upper layer modification at Ocean Station Papa: observations and simulations. J Phys Oceanogr 3:185–196

Denman KL, Okubo A, Platt T (1977) The chlorophyll fluctuation spectrum in the sea. Limnol Oceanogr 22:1033–1038

Dewey RK, Crawford WR (1988) Bottom stress estimates from vertical dissipation rate profiles on the continental shelf. J Phys Oceanogr 87:1167–1177

Dewey RK, Crawford WR, Gargett AE, Oakey NS (1987) A microstructure instrument for profiling oceanic turbulence in coastal bottom boundary layers. J Atmos Oceanic Technol 4:288–297

Dillon TM (1982) Vertical overturns: a comparison of Thorpe and Ozmidov length scales. J Geophys Res 87:9601–9613

Dillon TM, Caldwell DR (1980) The Batchelor spectrum and dissipation in the upper ocean. J Geophys Res 85:1910–1916

Dillon TM, Powell TM (1979) Observations of a surface mixed layer. Deep-Sea Res 26(A):915–932

Dillon TM, Richman JG, Hansen CG, Pearson MD (1981) Near-surface turbulence measurements in a lake. Nature 290:390–392

Dimai A, Gloor M, Wüest A (1994) Bestimmung der Intensität von Turbulenz in der Bodengrenzschicht von Seen. Limnologica 24:339–350

Dubois DM (1975) A model of patchiness for prey-predator plankton populations. Ecol Modelling 1:67–80

Eckart C (1948) An analysis of the stirring and mixing processes in incompressible fluids. J Mar Res 7: 265–275

Elliott AJ (1984) Measurements of the turbulence in an abyssal boundary layer. J Phys Oceanogr 14:1778–1786

Ewart TE, Bendiner WP (1981) An observation of the horizontal and vertical diffusion of a passive tracer in the deep ocean. J Geophys Res 86:10974–10982

Forel FA (1876) La formule des seiches. C R Acad Sci Paris 83:712–714

Fozdar FM, Parker GJ, Imberger J (1985) Matching temperature and conductivity sensor response

characteristics. J Phys Oceanogr 15:1557–1569
Gallegos CL, Platt T (1982) Phytoplankton production and water motion in surface mixed layers. Deep-Sea Res 29:65–76
Gargett AE, Sanford TS, Osborn TR (1979) Surface mixing layers in the Sargasso Sea. J Phys Oceanogr 9:1090–1111
Gargett AE, Osborn TR, Nasmyth PW (1984) Local isotropy and the decay of turbulence in a stratified fluid. J Fluid Mech 144:231–280
Garrett C (1990) The role of secondary circulation in boundary mixing. J Geophys Res 95:3181–3188
Garrett C (1991) Marginal mixing theories. Atmos Ocean 29:313–331
Gill AE (1982) Ocean atmosphere dynamics. Academic Press, New York
Gloor M, Wüest A, Münnich M (1994) Benthic boundary mixing and resuspension induced by internal seiches. Hydrobiologia 284:59–68
Grant WD, Williams III AJ, Glenn SM (1984) Bottom stress estimates and their prediction on the northern California continental shelf during CODE-1: the importance of wave-current interaction. J Phys Oceanogr 14:506–527
Gregg MC (1987) Diapycnal mixing in the thermocline: a review. J Geophys Res 92:5249–5286
Gregg MC, Sanford TB (1988) The dependence of turbulent dissipation on stratification in a diffusively stable thermocline. J Geophys Res 93:12381–12392
Gust G (1982) Tools for oceanic small-scale, high-frequency flows: metal-clad hot wires. J Geophys Res 87:447–455
Gust G, Weatherly GL (1985) Velocities, turbulence and skin friction in a deep-sea logarithmic layer. J Geophys Res 90:4779–4792
Herdendorf CE (1990) Distribution of the world's large lakes. In: Tilzer M, Serruya C (eds) Large lakes: ecological structure and function. Springer, Berlin, Heidelberg, New York, pp 3–38
Hinze JO (1975) Turbulence, 2nd edn. McGraw-Hill, New York, 618 pp
Horn W, Mortimer CH, Schwab DJ (1986) Wind-induced internal seiches in Lake Zurich observed and modeled. Limnol Oceanogr 31:1232–1254
Horsch GM, Stefan HG (1988) Convective circulation in littoral water due to surface cooling. Limnol Oceanogr 33:1068–1083
Huppert HE, Turner JS (1972) Double-diffusive convection and its implications for the temperature and salinity structure of the ocean and Lake Vanda. J Phys Oceanogr 2:456–461
Hutchinson GE (1957) A treatise on limnology. Wiley, New York
Hutter K (1983) Hydrodynamics of lakes. Springer, Berlin, Heidelberg, New York
Imberger J (1985) The diurnal mixed layer. Limnol Oceanogr 30:737–770
Imberger J, Patterson JC (1990) Physical Limnology. Advances in applied mechanics. Academic Press, Cambridge, pp 303–475
Imboden DM (1981) Tracer and mixing in the aquatic environment. Swiss Federal Institute of Technology, Zürich
Imboden DM (1990) Mixing and transport in lakes: mechanisms and ecological relevance. In: Tilzer M, Serruya C (eds) Large lakes: ecological structure and function. Springer, Berlin, Heidelberg, New York, pp 47–80
Imboden DM, Lerman A (1978) Chemical models of lakes. In: Lerman A (ed) Lakes – chemistry, geology, physics. Springer, Berlin, Heidelberg, New York, pp 341–356
Imboden DM, Joller T (1984) Turbulent mixing in the hypolimnion of Baldeggersee (Switzerland) traced by natural radon-222. Limnol Oceanogr 29:831–844
Imboden DM, Stotz B, Wüest A (1988) Hypolimnic mixing in a deep alpine lake and the role of a storm event. Verh Int Verein Limnol 23:67–73
Ivey CN, Imberger J (1991) On the nature of turbulence in a stratified fluid. Part I. The energetics of mixing. J Phys Oceanogr 21:650–659
Joseph J, Sendner H (1958) Über die horizontale Diffusion im Meer. Dtsch Hydrogr Z 11:49–77
Kelvin L, Thomson SW (1875) On an alleged error in Laplace's theory of the tides. Philes Mag 4:227–242
Kierstead H, Slobodkin LB (1953) The size of water masses containing plankton blooms. J Mar Res 12:141–147
Kolmogorov AN (1941) The local structure of turbulence in an incompressible viscous fluid for very large Reynolds numbers. Dokl Akad Nauk USSR 30:299–303
Kuhn W (1979) Aus Wärmehaushalt und Klimadaten berechnete Verdunstung des Zürichsees. Vierteljahresschr Naturforsch Ges Zür 123:261–283
Kullenberg G (1972) Apparent horizontal diffusion in stratified vertical shear flow. Tellus 24:17–28
Kullenberg G, Murthy CR, Westerberg H (1973) An experimental study of diffusion characteristics in the thermocline and hypolimnion regions of Lake Ontario. Proc 16th Conf Great Lakes Res, pp 774–790
Kunze E (1987) Limits on growing, finite length salt fingers: a Richardson number constraint. J Mar Res 45:533–556
Lambert A (1988) Records of riverborne turbidity currents and indications of slope failure in the Rhone delta of Lake Geneva. Limnol Oceanogr 33: 458–468
Langmuir I (1938) Surface motion of water induced by wind. Science 87:119–123
LeBlond PH, Mysak LA (1978) Waves in the ocean. Elsevier, Amsterdam
Ledwell JR, Watson AJ, Law CS (1993) Evidence for slow mixing across the pycnocline from an open-ocean tracer-release experiment. Nature 364: 701–703
Leeder MR (1983) On the dynamics of sediment suspension by residual Reynolds stresses – confirmation of Bagnold's theory. Sedimentology 30:485–491
Leibovich S (1983) The form and dynamics of Langmuir circulations. Annu Rev Fluid Mech 15:391–427
Lemmin U (1987) The structure and dynamics of internal waves in Baldeggersee. Limnol Oceanogr 32:43–61
Lemmin U, Mortimer CH (1986) Tests of an extension to internal seiches of Defant's procedure for determination of seiche characteristics in real lakes.

Limnol Oceanogr 31:1207–1231
Lewis MR, Horue EPW, Cullen JJ, Oakey NS, Platt T (1984a) Turbulent motions may control phytoplankton photosynthesis in the upper ocean. Nature 311:49–50
Lewis MR, Cullen JJ, Platt T (1984b) Relationship between vertical mixing and photoadaptation of phytoplankton: similarity criteria. Mar Ecol Prog Ser 15:141–149
Lighthill J (1978) Waves in fluids. Cambridge Univ Press, Cambridge
Lombardo CP, Gregg MC (1989) Similarity scaling of ε and χ in a convecting surface boundary layer. J Geophys Res 94:6273–6284
Marti DE, Imboden DM (1986) Thermische Energieflüsse an der Wasseroberfläche: Beispiel Sempachersee. Schweiz Z Hydrol 48:196–229
McDougall TJ (1987a) Thermobaricity, cabbeling and water mass conversion. J Geophys Res 92: 5448–5464
McDougall TJ (1987b) Neutral surfaces. J Phys Oceanogr 17:1950–1964
McDougall TJ, Taylor JR (1984) Flux measurements across a finger interface at low values of the stability ratio. J Mar Res 42:1–14
Miller MC, McCave IN, Komar PD (1977) Threshold of sediment motion under unidirectional currents. Sedimentology 24:507–527
Mortimer CH (1974) Lake hydrodynamics. Verh Int Verein Limnol 20:124–197
Mortimer CH (1975) Substantive corrections to SIL communications (IVL Mitteilungen) Numbers 6 and 20. Verh Int Verein Limnol 19:60–72
Mortimer CH (1979) Strategies for coupling data collection and analysis with dynamic modelling of lake motion. In: Graf WH, Mortimer CH (eds) Hydrodynamics of lakes. Elsevier, Amsterdam, pp 183–222
Münnich M (1993) On the influence of bottom topography on the vertical structure of internal seiches. Diss No 10434, ETH Zürich
Münnich M, Wüest A, Imboden DM (1992) Observations of the second vertical mode of the internal seiche in an alpine lake. Limnol Oceanogr 37: 1705–1719
Murthy CR (1976) Horizontal diffusion characteristics in Lake Ontario. J Phys Oceanogr 6:76–84
Mysak LA, Salvadè G, Hutter K, Scheiwiler T (1983) Lake of Lugano and topographic waves. Nature 306:46–48
Newman FC (1976) Temperature steps in Lake Kivu: a bottom heated saline lake. J Phys Oceanogr 6: 157–163
Oakey NS (1982) Determination of the rate of dissipation of turbulent energy from simultaneous temperature and velocity shear microstructure measurements. J Phys Oceanogr 12:256–271
Oakey NS, Elliott JA (1982) Dissipation within the surface mixed layer. J Phys Oceanogr 12:171–185
Okubo A (1967) The effect of shear in an oscillatory current on horizontal diffusion from an instantaneous source. Limnol Oceanogr 1:194–204
Okubo A (1971) Oceanic diffusion diagrams. Deep-Sea Res 18:789–802
Okubo A, Ozmidov RV (1970) Empirical dependence of the coefficient of horizontal turbulent diffusion in the ocean on the scale of the phenomenon in question. Izv Atm Oc Phys 6:534–536
Osborn TR (1974) Vertical profiling of velocity microstructure. J Phys Oceanogr 4:109–115
Osborn TR (1980) Estimates of the local rate of vertical diffusion from dissipation measurements. J Phys Oceanogr 10:83–89
Osborn TR, Cox CS (1972) Oceanic fine structure. Geophys Fluid Dyn 3:321–345
Padman L, Dillon TM (1987) Vertical heat fluxes through the Beaufort Sea thermohaline staircase. J Geophys Res 92:10799–10806
Pahl-Wostl C, Imboden D (1990) DYPHORA – A dynamic model for the rate of photosynthesis of algae. J Plankton Res 12:1207–1221
Patterson JC (1987) A model for convective motions in reservoir side arm. Proc XXII, IAHR Congr Lausanne 1987, pp 68–73
Peeters F (1994) Horizontale Mischung in Seen. Diss No 10476 ETH Zürich, p 147
Peeters F, Wüest A, Imboden DM (1993) Comparison of the results of tracer experiments in lakes with predictions based on horizontal mixing models. Verh Int Verein Limnol 25:67–74
Peters H, Gregg MC (1987) Some dynamical and statistical properties of equatorial turbulence. In: Nihoul J (ed) Small-scale turbulence and mixing in the ocean, Proc of the 19th Int Liège Colloq on Ocean hydrodynamics. Elsevier, Amsterdam
Peters H, Gregg MC, Toole JM (1988) On the parametrization of equatorial turbulence. J Geophys Res 93:1199–1218
Platt T, Denman KL (1975) Spectral analysis in ecology. Annu Rev Ecol Syst 6:189–210
Powell T, Jassby A (1974) The estimation of vertical eddy diffusivities below the thermocline in lakes. Water Resour Res 10:191–198
Powell TM, Richerson PJ, Dillon TM, Agee BA, Dozier BJ, Godden DA, Myrup LO (1975) Spatial scales of current speed and phytoplankton biomass fluctuations in Lake Tahoe. Science 189:1088–1090
Quay PD, Broecker WS, Hesslein RH, Schindler DW (1980) Vertical diffusion rates determined by tritium tracer experiments in the thermocline and hypolimnion of two lakes. Limnol Oceanogr 25:201–218
Richardson LF (1926) Atmospheric diffusion on a distance-neighbour graph. Proc R Soc A 110: 709–737
Sanderson B, Perry K, Pederson T (1986) Vertical diffusion in meromictic Powell Lake, British Columbia. J Geophys Res 91:7647–7655
Saylor JH, Huang JCK, Reid RO (1980) Vortex modes in southern Lake Michigan. J Phys Oceanogr 10: 1814–1823
Schlatter JW (1991) Schwefelhexafluorid als Tracer zum Studium von Mischungsprozessen in Seen. Diss No 9596, ETH Zürich
Schmitt RW (1979) Flux measurements on salt fingers at an interface. J Mar Res 37:419–436
Schmitt RW, Perkins H, Boyd JD, Stalcup MC (1987) C-salt: an investigation of the thermohaline staircase in the western tropical North Atlantic. Deep-Sea

Res 34:1655–1665
Shay TJ, Gregg MC (1986) Convectively driven turbulent mixing in the upper ocean. J Phys Oceanogr 16:1777–1798
Shields A (1936) Anwendung der Aehnlichkeitsmechanik und der Turbulenzforschung auf die Geschiebebewegung. Mitt Preuss Versuchsanst Wasserbau Schiffbau 26, Berlin. pp 1–26
Siegenthaler C, Sturm M (1991) Slump induced surges and sediment transport in Lake Uri, Switzerland. Verh Int Verein Limnol 24:955–958
Soloviev AV (1990) Coherent structures at the ocean surface in convectively unstable conditions. Nature 346:157–160
Soulsby RL (1983) The bottom boundary layer of shelf seas. In: Johns B (ed) Physical oceanography of coastal and shelf seas. Elsevier, Amsterdam, pp 189–266
Spigel RH, Imberger J (1980) The classification of mixed-layer dynamics in lakes of small to medium size. J Phys Oceanogr 10:1104–1121
Steele JH (1974) Spatial heterogeneity and population stability. Nature 248:83
Steele JH (1978) Some comments on plankton patches. In: Steele JH (ed) Spatial pattern in plankton communities. Nato Conf Ser IV. Plenum, New York, pp 1–20
Steinhorn I (1985) The disappearance of the long term meromictic stratification of the Dead Sea. Limnol Oceanogr 30:451–462
Stern ME (1976) Maximum buoyancy flux across a salt finger interface. J Mar Res 34:95–110
Stern ME, Turner JS (1969) Salt fingers and convecting layers. Deep-Sea Res 16:497–511
Stocker T, Hutter K (1987) Topographic waves in channels and lakes on the f-plane. Springer, Berlin, Heidelberg, New York
Stull RB (1984) Transilient turbulence theory. Part 1. The concept of eddy mixing across finite distances. J Atmos Sci 41:3351–3367
Stull RB (1986) Transilient turbulence theory. Part 3. Bulk dispersion rate and numerical stability. J Atmos Sci 43:50–57
Stull RB (1988) An introduction to boundary layer meteorology. Kluwer, Dordrecht
Swinbank WC (1963) Long-wave radiation from clear skies. Q J R Meteorol Soc 89:339–348
Taylor GI (1953) Dispersion of soluble matter in solvent flowing slowly through a tube. Proc R Soc Lond A 219:186–203
Thorpe SA (1969) Experiments on the stability of stratified shear flows. Radio Sci 4:1327–1332
Thorpe SA (1977) Turbulence and mixing in a Scottish loch. Philos Trans R Soc Lond Ser A 286:125–181
Thorpe SA (1988) The dynamics of the boundary layers of the deep ocean. Sci Prog 72:189–206
Toole JM, Polzin KL, Schmitt RW (1994) Estimates of diapycnal mixing in the abyssal ocean. Science 264:1120–1123
Turner JS (1965) The coupled turbulent transports of salt and heat across a sharp density interface. Int J Heat Mass Transfer 8:759–767
Turner JS (1967) Salt fingers across a density interface. Deep-Sea Res 14:599–611
Turner JS (1968) The behavior of a stable salinity gradient heated from below. J Fluid Mech 33: 183–200
Turner JS (1973) Buoyancy effects in fluids. Cambridge Univ Press, Cambridge
Van der Hoven I (1957) Power spectrum of horizontal wind speed in the frequency range from 0.0007 to 900 cycles per hour. J Meteorol 14:160
Van Senden DC, Imboden DM (1989) Internal seiche pumping between sill-separated basins. Geophys Astrophys Fluid Dyn 48:135–150
Weatherly GL (1972) A study of the bottom boundary layer of the Florida current. J Phys Oceanogr 2: 54–72
Wehrli B (1993) Chemie am Seegrund. Vierteljahresschr Naturforsch Ges Zürich 138:1–11
Welander P (1968) Theoretical forms for the vertical exchange coefficients in a stratified fluid with application to lakes and seas. Geophys Gothenburg 1:1–27
Wiegand RC, Chamberlain V (1987) Internal waves of the second vertical mode in a stratified lake. Limnol Oceanogr 32:29–42
Wimbush M, Munk W (1970) The benthic boundary layer. In: Maxwell AE (ed) The sea, vol 4. Interscience, New York, pp 731–758
Woods JD (1968) Wave-induced shear instability in the summer thermocline. J Fluid Mech 32:791–800
Woods AW (1991) Boundary-driven mixing. J Fluid Mech 226:625–654
Wroblewski JS, O'Brien JJ (1976) A spatial model of phytoplankton patchiness. Mar Biol 35:161–175
Wüest A (1987) Ursprung und Grösse von Mischungsprozessen im Hypolimnion natürlicher Seen. Diss No 8350, ETH Zürich
Wüest A (1994) Interaktionen in Seen: Die Biologie als Quelle dominanter physikalischer Kräfte. Limnologica 24:93–104
Wüest A, Imboden DM, Schurter M (1988) Origin and size of hypolimnic mixing in Urnersee, the southern basin of Vierwaldstättersee (Lake Lucerne). Schweiz Z Hydrol 50:40–70
Wüest A, Aeschbach-Hertig W, Baur H, Hofer M, Kipfer R, Schurter M (1992) Density structure and tritium-helium age of deep hypolimnetic water in the northern basin of Lake Lugano. Aquat Sci 54:205–218
Wüest A, van Senden DC, Imberger J, Piepke G, Gloor M (1994) Diapycnal diffusivity measured by microstructure and tracer techniques: a comparison. Symp on Turbulent flow, Grenoble, 8 pp
Wunsch C (1972) The spectrum from two years to two minutes of temperature fluctuations in the main thermocline at Bermuda. Deep-Sea Res 19:577–593
Wyngaard JC, Cote OR (1971) The budget of turbulent kinetic energy and temperature variance in the atmosphere surface layer. J Atmos Sci 28:190–201
Young WR, Rhines PB, Garrett CJR (1982) Shear-flow dispersion, internal waves and horizontal mixing in the ocean. J Phys Oceanogr 12:515–527

5 Stable Isotopes of Fresh and Saline Lakes

J.R. GAT

1 Introduction

The enrichment of the heavy isotopic species ($H_2{}^{18}O$ and HDO) in surface waters and lakes was already observed during the early surveys of stable isotope variations in the hydrological cycle (Rankama 1954). Craig (1961a) noted that the isotope compositions of waters from African lakes were displaced in δ-D vs δ-^{18}O space relative to other freshwaters whose composition follows the meteoric water line (MWL).

This enrichment in the heavy isotopic species has been widely utilized as a "fingerprint" for identifying lake water contribution to groundwaters (Payne 1981; Darling et al. 1990; Krabbenhoft et al. 1990), and, moreover, also as a measure of the water balance of a lake, especially of the component of evaporation. Previous reviews by Dincer (1968), Gat et al. (1968), Pearson and Coplen (1978), Moser and Rauert (1980), Gat (1981), Zuber (1983), Gonfiantini (1986), and others summarized the state of the art in this regard.

The basis for the "evaporative isotopic signature" in surface waters exposed to the atmosphere is the isotopic fractionation that occurs at the air–water interface in accompaniment of the evaporation process. According to Craig and Gordon (1965; see also Merlivat and Coantic 1975), this fractionation is made up of two components: one due to the fact that the lighter isotopes are favored in the liquid-to-vapor transition, because of vapor-pressure differences between the isotopic species (the so-called equilibrium isotope effect), and an additional effect (often called the kinetic or transport isotope effect) that results from the different rates of diffusion of the isotopic water molecules through the air-boundary layer.

Department of Environmental Sciences and Energy Research, Weizmann Institute of Science, 76100 Rehovot, Israel

Figure 1 shows schematically a lake in relation to its environment. The change of the isotopic composition in such a surface-water body that is exposed to the atmosphere can be formulated as

$$\frac{d(V \cdot \delta_L)}{dt} = F(in) \cdot \delta_{in} - F(out) \cdot \delta_L - E \cdot \delta_e, \quad (1)$$

where V is the volume of the system; F(in) is the sum of inflows such as precipitation, surface runoff, and groundwater discharges; F(out) is the total outflow including both groundwater leakages and river outflows; E is the evaporation flux; δ_L, δ_{in}, and δ_e are the isotopic compositions of the lake water, of the amount-weighted inflows, and of the evaporative flux, respectively.

In Section 1.1, the methodology for solving this balance equation is given. Table 1 gives the solutions of Eq. (1) for the isotopic buildup in lakes under a steady-state regime and for a desiccating pool of water. In practical situations, however, one rarely encounters such simple steady-state situations. Not only are surface-water systems notoriously changeable, due to random processes, but there are inherent seasonal changes in both the isotopic composition of the influx and the atmospheric moisture, in the hydrological balance and in the relationship between inflows and evaporation rates, as well as in the mixing regime in the lakes. The isotopic composition of a lake reflects such changes; its modeling is thus rather complex. Most present studies have avoided this issue, trying to extract hydrological information from the isotope composition of a lake based on steady-state solutions. The variability in the data, seasonal or other, was then usually incorporated into the error analysis, and is responsible for some of the pessimistic assessments of the isotope-balance method in lake studies (Lewis 1979; Zimmerman and Ehhalt 1970). However, the very sensitivity of a lake's isotopic composition to environmental changes

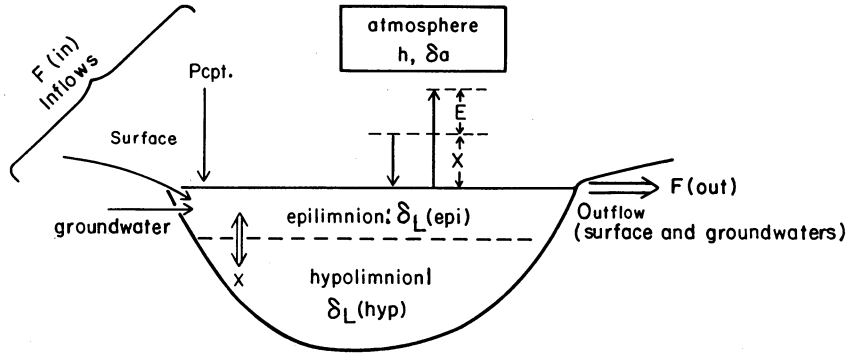


Fig. 1. Representation of the hydrological interrelationship between a lake and its environment. *X* signifies the exchange flux between the surface waters and the atmospheric moisture, and the double arrows the exchange between the mixed upper layer and the hypolimnion

Table 1. Enrichment in heavy isotopic species in various lake systems at steady state

Case 1 A desiccating pond at isotopic steady state
(there is no hydrological steady state in this case):

$$\Delta\delta = \delta_{ss} - \delta_0 = \delta_a + \frac{\varepsilon}{h} - \delta_0 = (\delta_a - \delta_0) + \frac{\varepsilon}{h}\frac{(1-h)}{h}C_k$$

when $\delta_a - \delta_0 = -\varepsilon^*$:

$$\Delta\delta = \frac{(1-h)\cdot(\varepsilon^* + C_k)}{h}$$

Case 2 A terminal lake at hydrological and isotopic steady state:

$$\Delta\delta = \delta_{ss} - \delta_{in} = h\cdot(\delta_a - \delta_{in}) + \varepsilon = h\cdot(\delta_a - \delta_{in}) + \varepsilon^* + (1-h)C_k$$

when $\delta_a - \delta_{in} = -\varepsilon^*$:

$$\Delta\delta = (1-h)(\varepsilon^* + C_k)$$

Case 3 A through-flow lake at hydrological and isotopic steady state:

$$\Delta\delta = \delta_{ss} - \delta_{in} = \frac{\left(\delta_a - \delta_{in} + \frac{\varepsilon}{h}\right)}{\left\{1 + \frac{F(in)}{E}\cdot\frac{(1-h)}{h}\right\}} = \frac{\left(\delta_a - \delta_{in} + \frac{\varepsilon}{h} + \frac{(1-h)}{h}C_k\right)}{\left[1 + \frac{F(in)}{E}\cdot\frac{(1-h)}{h}\right]}$$

when $\delta_a - \delta_{in} = -\varepsilon^*$:

$$\Delta\delta = \frac{(1-h)\cdot(\varepsilon^* + C_k)}{\left[h + (1-h)\cdot\frac{F(in)}{E}\right]}$$

h, ambient humidity, normalized to the saturated vapor pressure at the liquid surface; δ_a, isotopic composition of atmospheric moisture; δ_0, initial isotope composition of the waters that evaporate; δ_{in}, isotope composition of inflow waters; δ_{ss}, steady-state isotopic composition of lake waters; ε^*, C_k, equilibrium isotope separation factor and kinetic constant.

and to variations in the hydrological regime enables one to use the measurement of the δ-values as a valuable tool, both for monitoring immediate environmental and hydrological changes and as a long-range paleoclimatic indicator, using appropriate proxy materials such as limnic carbonate deposits (Stuiver 1970; Lemeille et al. 1983; Talbot 1990).

In later sections of this chapter, the isotopic enrichment in different lakes is discussed, based on the methodological background presented in Section 1.1. The information concerning the water budget and dynamics in a lake system that can be inferred from the isotopic data is pointed out. The principles are first applied to rather simple and homogenous systems. We then move on to lakes of increasing complexity, with either a vertically stratified structure, a large geographical extent, or high salinities.

Whenever available, examples of studies are given that make use of the isotopic data for obtaining information on the lake's hydrology, water balance, or interaction with its environment. Unfortunately, in many cases it is only possible to show the potential of the isotope studies theoretically, with a view of encouraging such applications in the future.

1.1 Isotope Separation During Evaporation

The solution of Eq. (1) requires a value for the isotope composition of the evaporative flux, δ_e, which is not amenable to direct measurement. We can know its value only in exceptional circumstances, e.g., when the evaporation is non-fractionating (which seems to be case for transpired water from plants), or in the case of a terminal lake at steady state, when material-balance considerations require the evaporation flux to equal the inflowing waters, i.e., $\delta_{in} = \delta_e$. In other cases one has to resort to a theoretical approach based on models of the evaporative transport of water from the surface into the atmosphere.

Following Craig and Gordon's formulation (1965) δ_e is given by the relationship

$$\delta_e = \frac{(\alpha^* \cdot \delta_L - h \cdot \delta_a - \varepsilon)}{\{(1 - h) + \Delta\varepsilon\}}, \tag{2}$$

which often can be approximated to

$$\delta_e = \frac{(\delta_L - h \cdot \delta_a - \varepsilon)}{(1 - h)}, \tag{2a}$$

where h is the relative humidity, normalized to the saturated vapor concentration at the liquid surface; δ_a is the isotopic content of the atmospheric moisture in the ambient air; α^*, α are the equilibrium and total unit fractionation factors, respectively; and ε^* and ε are then defined as follows: $\varepsilon^* = (1 - \alpha^*)$ and $\varepsilon = (1 - \alpha)$. These are related to each other by the relationship $\Delta\varepsilon = \varepsilon - \varepsilon^*$.

In this formulation the fractionation, due to the diffusive transport of water molecules through the air-boundary layer, is expressed as $\Delta\varepsilon$, which, based on a Langmuir-type resistance model, has been shown by Craig and Gordon (1965) to have the following form:

$$\begin{aligned}\Delta\varepsilon &= (1 - h)\left[\frac{\rho_A}{\Sigma\rho}\left(\frac{\rho_{i,A}}{\rho_A} - 1\right) + \frac{\rho_B}{\Sigma\rho}\left(\frac{\rho_{i,B}}{\rho_B} - 1\right)\right] \\ &= (1 - h)\frac{\rho_A}{\Delta\rho}\left(\frac{\rho_{i,A}}{\rho_A} - 1\right) \\ &\equiv (1 - h)\,\theta \cdot C_k,\end{aligned} \tag{3}$$

where ρ, ρ_i are transport resistances with subscript i standing for the isotopic species, and subscripts A and B, respectively, standing for the diffusive layer(s) near the interface and the turbulent region above it. The RHS of this equation is written in recognition of the nonfractionating nature of turbulent transport in the atmosphere, so that the term $\left(\frac{\rho_{i,B}}{\rho_B} - 1\right)_{n \neq A} = 0$, and $\theta = \rho_A/\Sigma_\rho$. The term $\left(\frac{\rho_{i,A}}{\rho_A} - 1\right) \equiv C_k$ was shown to be approximately 13‰ for the case of the deuterated water molecule and 15‰ for the O-18 labeled molecule under moderate wind conditions for evaporation from an open water body (Merlivat 1970).

Usually the ambient parameters δ_a and h are measured or estimated close enough to the diffusive sublayer so that ρ_B is negligibly small compared with ρ_A, and the weighting term in Eq. (3) can then be neglected writing $\Delta\varepsilon$ simply as

$$\Delta\varepsilon = (1 - h) \cdot C_k. \tag{3a}$$

This expression for $\Delta\varepsilon$ can be applied while using values for the ambient parameters h and δ_a as measured throughout the air column, whenever there is no significant source of sink of water in the air column, so that h and δ_a are invariant with height. As is discussed below, however, this may not be the case over a large lake whose evaporative flux is an important component of the atmospheric water balance, or under conditions of poor mixing (stagnancy) within the air column.

One should note that the formulation of the isotopic composition of the evaporation flux in

Eq. (2) contains the notion of an exchange of moisture between the lake surface and the atmosphere. The backflow of air moisture becomes especially pronounced at high ambient humidity. It is to be further noted that we neglect any resistance to vertical mixing within the liquid. This assumption may not always be justified, especially under still-wind conditions (Gat 1970; Siegenthaler 1975).

With δ_e given by Eq. (2a), and because the hydrological balance equation is

$$\frac{dV}{dt} = F(in) - F(out) - E, \tag{4}$$

then Eq. (1) can be rewritten as follows:

$$\frac{d\delta_L}{dt} = \frac{F(in)}{V} \cdot (\delta_{in} - \delta_L) - \frac{E}{V}\left\{\frac{h(\delta_L - \delta_a) - \varepsilon}{(1-h)}\right\}. \tag{5}$$

This equation is the basis for calculating the isotopic buildup in surface-water bodies.

Relatively simple solutions can be given for well-mixed systems under hydrological steady state, both for a through-flow lake and a terminal one, and also for a system without inflow as it dries up. These solutions are shown in Table 1 in an abbreviated fashion and are discussed in Section 2.

On comparing the relative changes of the two isotopic species ^2H and ^{18}O [whose abundances are expressed as δ_D and δ_{18}, respectively, relative to the SMOW standard (standard mean ocean water) [Craig 1961b] it is seen that these differ from an equilibrium relationship where the slope $S = \frac{\Delta\delta_D}{\Delta\delta_{18}}$ (in δ_D vs δ_{18} space) is given by the ratio of the equilibrium fractionation factors $\frac{\varepsilon^*_D}{\varepsilon^*_{18}}$. This ratio varies between 7.54 and 8.64 for the temperature range of 0–35 °C (Majoube 1971). It is close to the value of 8 at a temperature of 20 °C, and thus defines the slopes of the meteoric water line (Craig 1961a). On the other hand, the slope of the evaporation lines that describe the change in the δ values as evaporation proceeds, as derived from Eq. (5), is

$$S = \frac{[h(\delta_a - \delta_{in}) + \varepsilon]_D}{[h(\delta_a - \delta_{in}) + \varepsilon]_{18}}. \tag{6}$$

Because the magnitude of C_k for both isotopic species is similar (13 and 15‰, respectively, for D and O-18), it follows that the slope of the evaporation line is considerably lower than the slope of the "equilibrium line." The slope of the evaporation line according to Eq. (6) depends on ambient (atmospheric) parameters, namely the humidity and isotopic composition of the atmospheric moisture, and on the isotope fractionation factor.

Figure 2 gives the value of the slope for the evaporation lines in δ_D vs δ_{18} space as a function of $(\delta_a - \delta_{in})_{18}$ for various humidity values and for different values of $\Delta d = d_a - d_{in}$, where d_a and $d_{(in)}$ are the "d-excess" values of the atmospheric moisture and the inflow waters, respectively; the "d-excess" was defined by Dansgaard (1964) as $d = 8 \cdot \delta_{18} - \delta_D$. A similar figure was shown by Gat (1971), but for different values of C_k, namely 32 and 16‰, respectively, for ^{18}O and D. The presently adopted values of 15 and 13‰ appear to be more realistic. It is to be noted that for the case where the moisture and the input waters are in isotopic equilibrium with each another, i.e., where $\delta_a - \delta_{in} = -\varepsilon^*$ and $\Delta d \sim 0$, then the value of S is independent of the humidity and given by the ratio of $(\varepsilon^* + C_k)_D/(\varepsilon^* + C_k)_{18} \sim 3.55$. This is usually the case in a midcontinental location (Craig and Horibe 1967). It is to be further noted

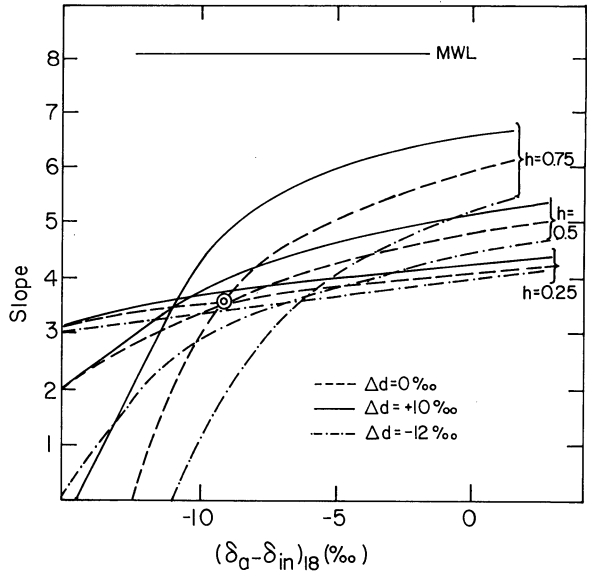


Fig. 2. The slope of the evaporating line as a function of the parameters of Eq. (6), for the three cases of $\Delta d = (d_a - d_{in}) = -12$, 0, and +10‰, respectively. *MWL* Meteoric water line

that beyond this singular point, the dependence of the slope on the humidity is reversed. The actual degree of enrichment (relative to the initial value of δ_{in}), which will be reached in a surface water body by the process of evaporation and vapor exchange, for either ^{18}O or deuterium, depends on all the parameters of Eq. (5), including hydrological parameters such as the through-flow rate, the mixing volume, etc. Obviously by following the degree of isotopic buildup in a lake, one obtains a measure of the hydrological balance and of its changes in time, as exemplified in Section 2.

2 Small-Area Lakes

In this section an idealized lake is discussed. For this purpose the following characteristics are assumed:

1. A mixed volume with no marked horizontal or vertical inhomogeneities in isotopic composition (the effect of vertical stratification is taken up in Sect. 2.2)
2. A limited geographical extent, so that it can be assumed that the environment (and especially the ambient moisture) is not perturbed by the evaporative flux from the lake

The steady-state solutions for the isotopic balance of such an ideal lake under the assumption of time-invariant parameters, given in Table 1, is

$$\Delta = \delta_{L,SS} - \delta_{in} = \frac{\left(\delta_a + \frac{\varepsilon}{h} - \delta_{in}\right)}{\left[1 + \frac{F_{in}}{E} \cdot \frac{(1-h)}{h}\right]} \qquad (7)$$

This value is seen to depend on the parameters h and δ_a, and on a hydrological characteristic of the lake, namely the ratio of the through-flow fluxes: F(in)/E. Temperature, the most prominent of environmental parameters, is expressed in a hidden way, affecting both the humidity term (through the dependence on the saturated vapor pressure of the water surface) and the equilibrium isotope fractionation factor, ε^* (Majoube 1971). As shown in Fig. 3, the degree of the isotope enrichment in the lake is very sensitive to the hydrological model. If one compares the three model systems that are summarized in Table 1, the "evaporating pan," a terminal lake, and a through-flow system, then evidently the isotopic composition in the terminal lake is shifted toward the isotope composition of the inflow waters (which are usually more depleted in the heavy isotopic species) compared with the highly enriched waters of the evaporation pan. The through-flow lake's isotope composition is even closer to the value of the inflowing waters the larger the value of the parameter F(in)/E. Not too surprisingly, sensitivity to changes in the through-flow ratio is highest under those conditions where evaporation is the dominant factor in the water balance of the system, i.e., at relatively low humidities and when the ratio F(in)/E approaches a value of unity.

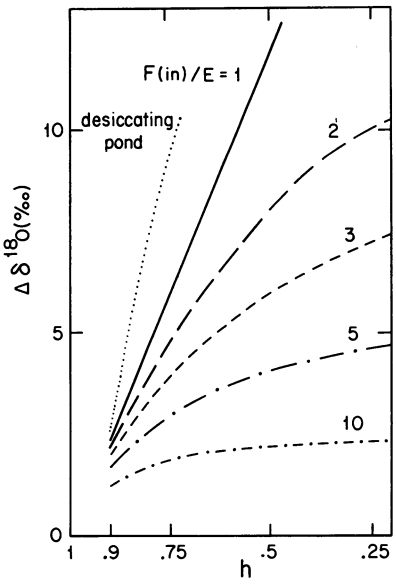


Fig. 3. The isotopic buildup ($\Delta = \delta_{ss} - \delta_{in}$) in through-flow lakes at steady state as a function of humidity (h) and the throughflow ratio ($F(in)/E$; obviously F(in)/E = 1 corresponds to a terminal lake without outflow. The values for a desiccating pond (the so-called evaporation pan) are given for comparison. It is assumed that the inflow waters and the atmospheric moisture are in isotopic equilibrium with each other, so that $\delta_a - \delta_{in} = -\varepsilon^*$

The practical application of the isotopic water balance equations to the determination of components of the hydrological balance, be it the value of E or of leakage rates from the lake or reservoir, requires a value for δ_e, which, as discussed previously, is very difficult to obtain because it is not directly amenable to measurement. To derive δ_e based on Eq. (2) requires that the values of δ_a, h, and the fractionation factors be properly averaged to account for the process over as long a period as the water-residence time in the lake. This often presents almost insurmountable

problems because of the variability of these parameters, and is responsible for a relatively uncertainty of this method. Welhan and Fritz (1977) discussed attempts to measure these parameters by using evaporation pans as model lakes. It was shown by Allison et al. (1979), however, that such a method is not too successful, because of the short integration time of these pans when compared with the natural systems. Indeed, a more promising alternative was proposed by Dincer (1968), namely, the use of an "index lake" of known hydrology and which is situated in the same area, from whose isotope values the properly weighted values of δ_a and h can be inferred. A homogeneous, terminal lake would serve this function best. The usefulness of this approach was demonstrated for a group of Turkish lakes by Merlivat (1970), and in a saline setting by Gat and Levy (1978).

Additional components of the water-balance equation can be determined if a third balance equation is introduced in addition to those for the water and isotopes. A combined solution of the three balance equations for water, isotopes, and salt, respectively, in those system where salinity is a conservative tracer and where there are no extraneous sources of salinity other than those brought into the lake by the major tributaries, can be used to advantage. As an example, Dincer et al. (1979) distinguished between the water losses by evaporation and by transpiration of the aquatic plants in the Okavango swamp. This was done simply by comparing the buildup of the heavy isotopes (by E only) to that of the salinity (Cs), which is increased by the combined evapotranspiration flux (E+T). On neglecting the inflow term, one then finds that

$$\frac{dC}{d\delta} = \frac{(1 - h) \cdot \left\{\frac{(E + T)}{E}\right\} \cdot Cs}{\{h(\delta_a - \delta_L) + \varepsilon\}}. \quad (8)$$

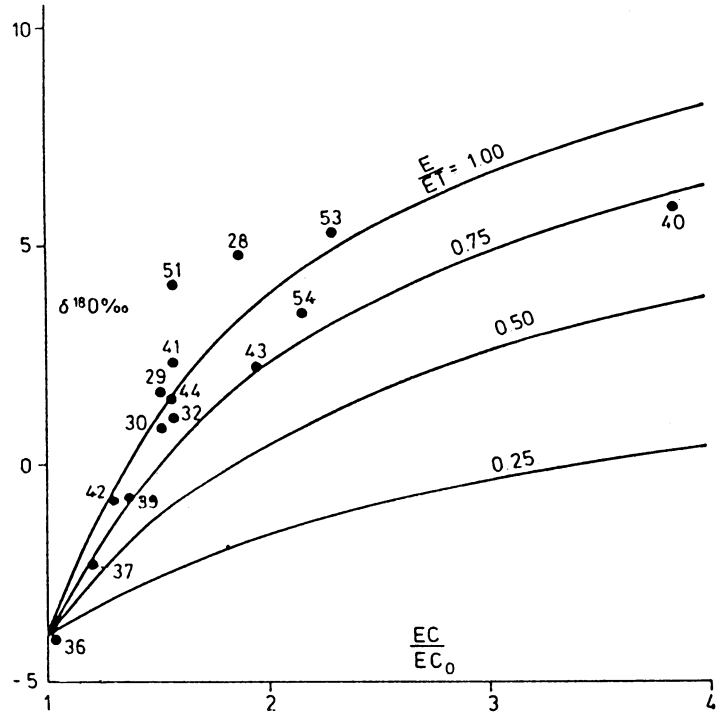
From the results of Dincer, shown in Fig. 4, one observes that the contribution of transpiration to water loss was highest (approximately 71%) during the summer low-water stand, but almost negligible during winter.

2.1 Seasonal and Annual Changes

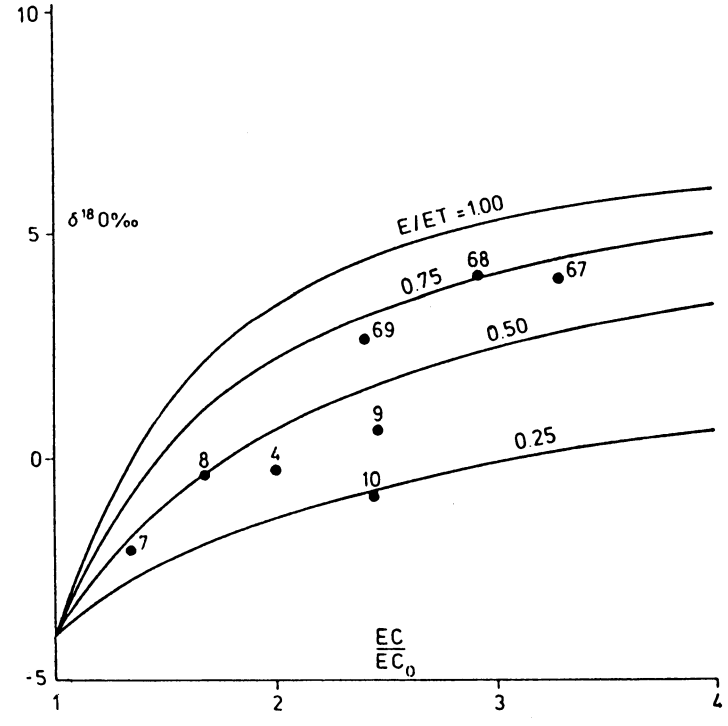
In most cases the parameters that govern a lake's isotopic composition undergo seasonal changes that affect the enrichment of the heavy isotopic species in the lake. Thus, evaporation rates often peak during summer and the isotopic composition of precipitation goes through an annual cycle (Yurtsever and Gat 1981). The latter affects that part of the term δ_{in}, which results from the direct contribution of precipitation and surface runoff to the lake's inflows. Any groundwater contributions to the lake's water sources can be expected to be more stable in its isotopic composition throughout a year, a was indeed found to be the case (Stichler and Moser 1979; Krabbenhoft et al. 1990). The seasonality in δ_{in} thus depends on the lake's hydrological setting. At most continental locations the isotopic composition of the atmospheric moisture closely tracks that of the precipitation, so that the difference between the isotopic composition of the atmospheric vapor (δ_a) and of precipitation (δ_p) remains close to the equilibrium relationship $\delta_a - \delta_p = -\varepsilon^*$. Other parameters, however, do not necessarily change in concert, and depending on climate, on the one hand, and the hydrological and geographical setting, on the other, a variety of circumstances are encountered.

From Eq. (5) it is evident that the response of a lake's isotopic composition to changing input parameters depends on the size of the reservoir, more precisely on the residence time of water in the lake. For a very shallow lake, the water will at any time be close to the steady isotope composition for the momentary set of parameters, and the isotope composition of the lake will vary in an extreme manner as these parameters change. On the other hand, the larger the mixing volume, the more restrained the response in the isotopic composition of the lake water for any given environmental change. In most lakes whose water-residence time is of the order of a year and longer, the stable isotope composition of the lake water just fluctuates around the mean steady-state isotopic composition. Indeed, the magnitude of the isotopic response in the lake water to a given change in input parameters can be used as a sensitive measure of the hydrological variables F(in)/V or F(in)/E.

Zimmermann et al. (1976) took advantage of such a situation in an elegant study of the mixing and through-flow characteristics of the River Niger through Kainji reservoir. By comparing the change in the isotopic composition of the outflow from the reservoir with the seasonally changing isotope composition of the Niger River, it was possible to determine the ratio of the effective mixing volume to the volume of the reservoir as a



Equal evaporation/evapotranspiration ratio curves for winter with data points.



Equal evaporation/evapotranspiration ratio curves for summer with data points.

Fig. 4. The buildup of isotopic enrichment in the Okavango swamp, Botswana, as a function of the salinity increase for different ratios of the evaporation to the total evapotranspiration flux. (Dincer et al. 1979)

whole. This ratio varied from approximately 10% at low-water stand (signifying that the river bypassed most of the lake's volume at that time) to a value of 60–80% during the flood stage period.

Figure 5 simulates the response of the isotope composition of an idealized temperate-zone lake to seasonal changes in the external parameters, based on the data for Lake Tiberias, a warm lake situated in a semiarid Mediterranean climate in the upper Jordan Valley (Israel). In this case changes in the isotopic composition of the inflowing waters throughout the year are found to be limited, because the inflows are predominantly from groundwater-fed river systems; these change from winter to spring and into summer merely from a value of $\delta_{18} = -6.9‰$ to $\delta_{18} = -6.3‰$ and finally to $\delta_{18} = -5.9‰$. The admixture of the local winter precipitation, having δ_{18} values between -3 to $-5‰$, makes the isotopic values of the inflow term even less variable. Moreover, the influence of the yearly cycle of the isotopic composition of the atmospheric moisture [$\delta_a(^{18}O)$ values range from approximately -12 to $-15‰$ (Tzur 1971)] is restrained by the low humidity that prevails over most of the year, averaging around 50%. The changes in the hydrological parameters [e.g., F(in)/E], and, to a more limited extent, humidity, are evidently most influential.

In contrast, it has been found that long-term change in the hydrological balance overrides the effects of seasonal changes. The volume of the annual inflow varied over the years of the study (1950–1970) by more than a factor of two, due to drought conditions and (as shown in Fig. 6) the isotopic response of the lake water's isotopic composition to these changes in through-flow rates in the lake, amounting to more than 2‰ in δ_{18}, by far outweighing the seasonal amplitude of approximately 0.5‰ (Gat 1970). Indeed, the effects of variation in the through-flow rates dominate that of all other environmental parameters. The lake's isotopic composition thus serves as a hydrological monitor for this region, much more than the isotopic composition of the precipitation, which is not correlated too well with seasonal rain amounts.

2.2 Deep Freshwater Lakes

Most deeper lakes develop a vertical-density stratification during part of the yearly cycle, whereas very deep lakes and especially saline lakes may show long-term stratification. To recall some limnological terms used in this chapter, it is to be remembered that in a lake that is stratified

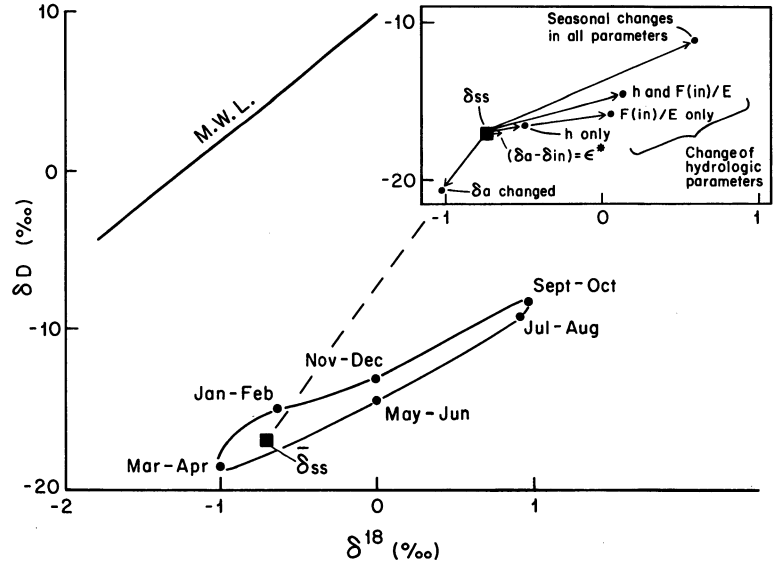


Fig. 5. Seasonal change in the isotope composition of a temperate zone lake based on parameters given by Gat (1970) for Lake Tiberias. The steady-state value (δ_{ss} is given for the following mean values of the parameters: $h = 0.683 \frac{V}{E} = 30.4$; $\frac{F(in)}{E} = 2.71$; $\delta_{in} = (-5.4;-33)$; $\delta_a = (-14.4;-105)$. Values in parentheses are those for δ_{18} and δ_D in permil, respectively. The effect of the seasonal variability in these parameters on steady-state isotopic build-up is shown in the *inset*

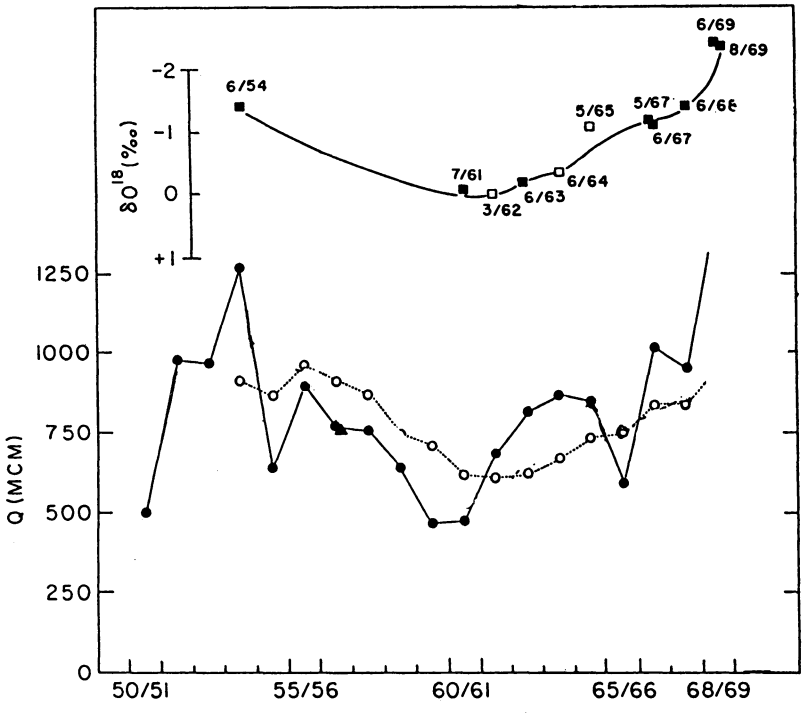


Fig. 6. Comparison between long-term changes in δ_{18} (*upper curve*) of Lake Tiberias waters and the 5-year average of the amount of inflow (*lower curve*). Full circles show the annual inflow during the preceding hydrological year (October–September). (Taken from Fig. 7 of Gat 1970)

(due to a vertical temperature and/or salinity profile), the upper less-dense region is called the epilimnion, with the denser deeper layer being the hypolimnion. Lakes that undergo one yearly cycle of overturn, due to a seasonal temperature buildup in summer, are called monomictic. Lakes with two yearly overturns, such as would typically occur in cold regions, are dimictic. Lakes that do not regularly undergo the annual mixing cycle, and which are more permanently stratified, are named meromictic lakes (Hutchinson 1957). In the latter case a strong density gradient can prevent the exchange of matter between the mixed upper layer and the deeper waters for all practical purposes (Lerman 1971), and the epilimnion can then be treated as a separate "floating" system with a fixed volume above a virtual bottom. However, in most other circumstances, e.g., in the case of a thermal stratification, one has to take into account an exchange of matter across the thermocline. Moreover, the effective mixing volume changes over a yearly cycle. As the thermocline builds up and dissipates, deeper water layers are incorporated into the epilimnion. At the time of the overturn of a lake's water masses this effect is extreme.

In order to account for this exchange of matter across the thermocline, additional terms have to be added to the RHS of Eq. (5). If δ(hyp) represents the isotope content of the deeper layer below the thermocline, then these additional terms can be written as

$$\frac{+\,\mathrm{X(epi-hyp)}}{\mathrm{V}}\cdot[\delta(\mathrm{hyp})-\delta_{\mathrm{L}}] + \frac{\Delta \mathrm{V}}{\mathrm{V}}\cdot[\delta(\mathrm{hyp})-\delta_{\mathrm{L}}],$$

where the first term accounts for the exchange of matter between the epilimnion and the hypolimnion at constant volume of the mixed layer, and the second term describes the incorporation of a volume ΔV of hypolimnic waters into the mixed layer by a descending thermocline. The exchange term is not usually very significant [its magnitude can be measured by the changes in the value of δ(hyp)], provided that the exchange is the only process that causes an isotopic change in the hypolimnion. Although the value of [δ(hyp) $-\ \delta_{\mathrm{L}}$] is typically not very large (of the order of 1‰ in δ_{18}), the whole term of $\Delta\mathrm{V}/\mathrm{V}\cdot[\delta(\mathrm{hyp})-\delta_{\mathrm{L}}]$ can be great significance in the isotopic balance,

because of the preponderance of ΔV relative to other hydrological components of the water-balance equation during periods of a rapidly descending pycnocline, as exemplified below. It goes without saying that this opens up the possibilities of detecting any incorporation of water masses from one stratum into another, by following the changes in the isotopic composition during the buildup or dissipation of stratification. A vertical isotope profile is obviously most useful in establishing to what extent the deeper water masses indeed represent a closed system, in which case the isotopic composition of the hypolimnion is expected to be invariant as long as the stratification remains intact.

Consider as a working example the case of Lake Tiberias, a monomictic lake, 40 m deep with a mean water-residence time of the order of 5 years whose surface-water balance was discussed previously. The lake is found to be in a mixed state from about December to March: A thermocline builds up during spring, deepening from a position at −5 m in April to 18–19 m later in the summer until it stabilizes in the fall and early winter at a depth of approximately −25 m. The stratification is terminated by an overturn, which usually takes place during December (Oren 1962).

The isotope measurements reported by Gat (1970; Fig. 7) show the hypolimnic waters to conserve the composition of the lake during March, just as stratification sets in, as expected. During the period of summer thermal stratification, the surface waters are more enriched in the heavy isotopes than the hypolimnion and the thermocline is well delineated by the isotopic profile. The inset of Fig. 7 shows the influence of the stratification and of the changing mixing volume on the evolution of the isotopic composition during the year. One notes in particular the effect of the deepening of the thermocline by approximately 5 m in September, which results in a marked discontinuity in the isotopic curve.

Krabbenhoft et al. (1990) have described a dimictic, ice-covered lake located in north-central Wisconsin: Sparkling Lake, a morphologically simple one-basin kettle lake, 20 m deep, with a water-residence time of approximately 10 years. Having no surface outlets and inlets, it is essentially a groundwater-window lake with the evaporitic signature of the lake's water being well recognized in the downstream part of the aquifer. Figure 8 shows the isotopic profile during winter (ice-covered period) and summer stratification, respectively. An interesting pattern is the relative depletion of the heavy isotopes in the (under ice) surface waters in winter, attributed by the authors to the selective enrichment of the heavy isotopes in ice, leaving the waters more depleted. Indeed Ragotzkie and Friedman (1965) evoked a similar explanation to account for the somewhat lower isotope content of Lake Vanda, Antarctica, compared with the inflow waters from ice melt. During summer, on the other hand, the isotopic profile in Sparkling Lake is normal, with an isotopically enriched epilimnion perched on top of the isotopically more depleted hypolimnic waters.

Isotopic profiles for two deep meromictic lakes, situated in the African Rift Valley, have been reported. Lake Malawi, with a maximum depth of 785 m, and Lake Tanganyika (1470 m deep) both show a thermocline between 100 and 250 m across which an isotopic difference is maintained. A two-step profile was found in Lake Malawi (Gonfiantini et al. 1979) with the δ_{18} values increasing from +1.65‰ in the epilimnion to +1.92‰ in the transition zone, and to +2.08 ± 0.05‰ in the hypolimnion. In Lake Tanganyika, Craig (1974) found a gradual increase in isotopic values across the thermocline, from surface value of +3.4‰ in δ_{18} to a value of +4.19 ± 0.03‰ at depths in excess of 200 m.

In the case of these African lakes the waters are enriched in the heavy isotopic species and their isotopic values displaced relative to the meteoric water line (Craig 1961a). However, under colder and more humid conditions the evaporative signature is less apparent; such is the case of Lake Baikal, where the mean isotopic value of $\delta_D = -117$‰ and $\delta_{18} = -16$‰ lies close to the MWL (Ferronsky and Polyakov 1982).

2.3 Transient Surface-Water Bodies

Figure 9 schematizes some shallow and transient surface-water bodies and follows their hydrological and isotopic evolution from a filling stage into the dry period. In all of these systems the isotope composition approaches that of the diluting meteoric waters during the flushing phases, whereas the heavy isotopic species become enriched during the evaporitic phases at low-water stand. The degree of enrichment is evidently larger the higher the role of the evaporation in

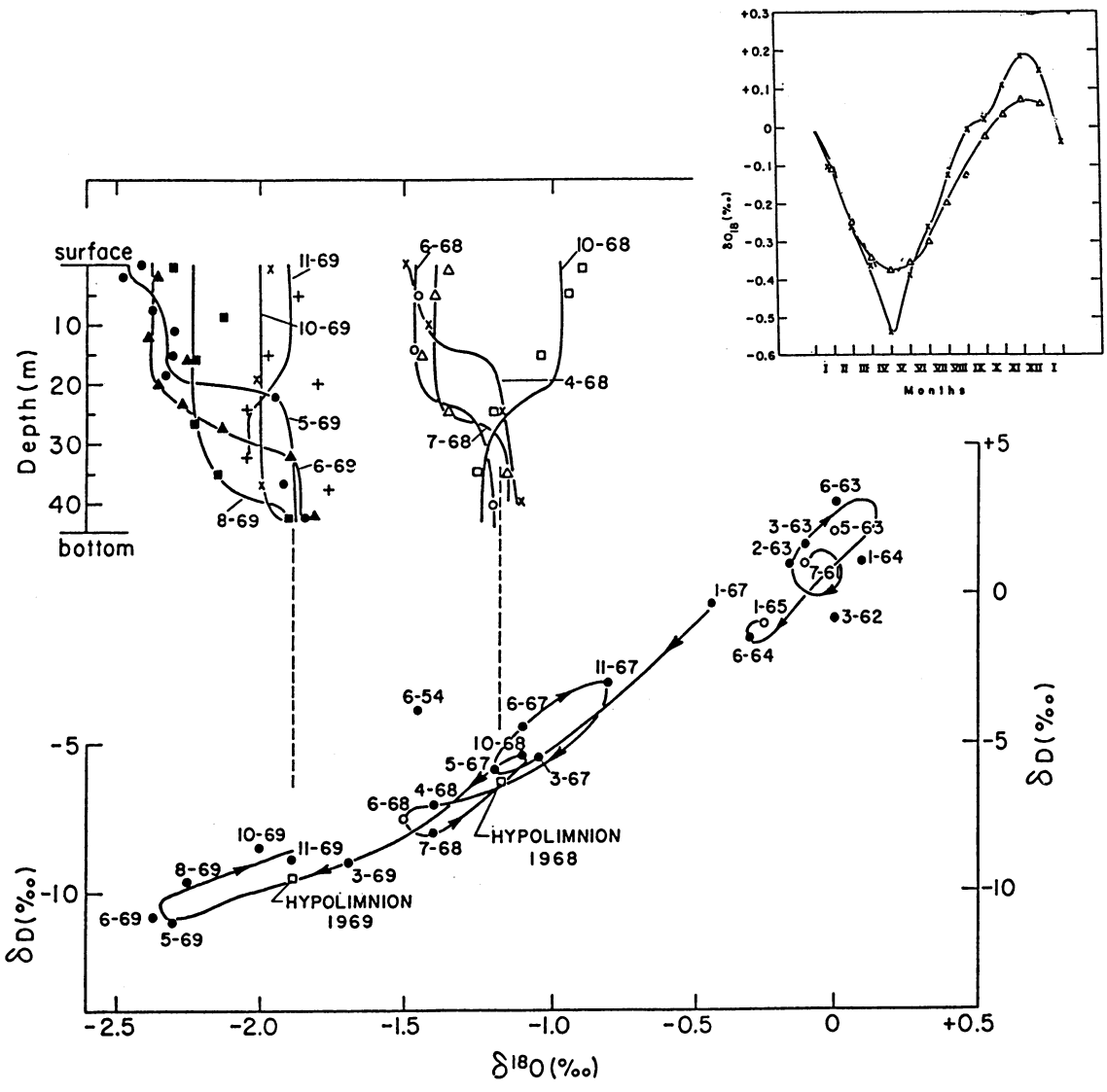


Fig. 7. Stable isotope composition of Lake Tiberias waters during 1963–1969, showing seasonal and long-term variations. The vertical isotopic profiles for 1968–1969 are given on top. The *inset* shows calculated monthly values of δ_{18} of Lake Tiberias surface waters on the assumption of a mixed ($-\Delta-\Delta-$) and stratified system ($-x-x-$), respectively. In the latter case the thermocline depths described by Oren (1962) were assumed. (Adapted from Gat 1970)

the total water balance. This is the basis for the practical applications of the isotopic measurements in order to quantify the hydrological balances in such systems. Because some of the parameters in Eq. (5) change over the life cycle of the transient system, a numerical integration usually has to be performed in order to account for the changing isotopic composition of the lake. Details obviously depend on the particular circumstances. However, one interesting general characteristic of these transient lakes is an accelerated rate of change in the isotopic composition toward the end of the life cycles of these systems, as their volumes shrink.

A special situation is presented by (river-) floodplain lakes, which are inundated by overflowing river waters at high water stage. Lakes that may then be formed in depressions of the plain change in their volume drastically as the rivers recede, and they may eventually dry up or be totally drained. Isotopic studies can be used to differentiate between waters originating from the overflowing river, the local drainage, or residual waters from previous cycles of the lake

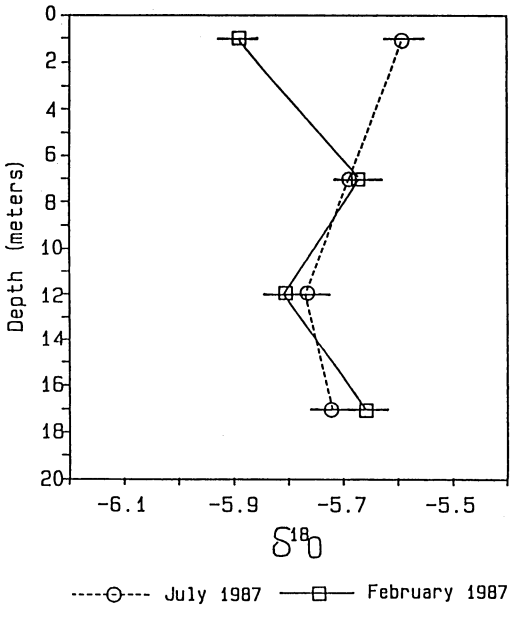


Fig. 8. Winter and summer isotopic profiles in Sparkling Lake, Wisconsin. (Krabbenhoft et al. 1990)

(which usually shows the isotopic signature of the evaporation process).

A study of such a system is that of Martinelli et al. (1989) on lakes in the Amazonian "varzea." The isotopic composition of many of these lakes change from depleted isotopic values characteristic of the mainstream of the Amazonas and its tributaries to more enriched values, due to increasing participation of the waters from the local runoff and precipitation at the particular locality. Because the isotope compositions of both these end members are situated on the MWL, so will be that of the lake water for most of its life cycle, as shown schematically in Fig. 10. Deviations from the MWL in the direction of an evaporation line, however, is then indicative of the loss of water by evaporation in the lake system, the degree of displacement along such an evaporation line being a measure of the relative amount of water loss by this mechanism.

In some of the transient situations there is no net export of liquid water, and the conditions are

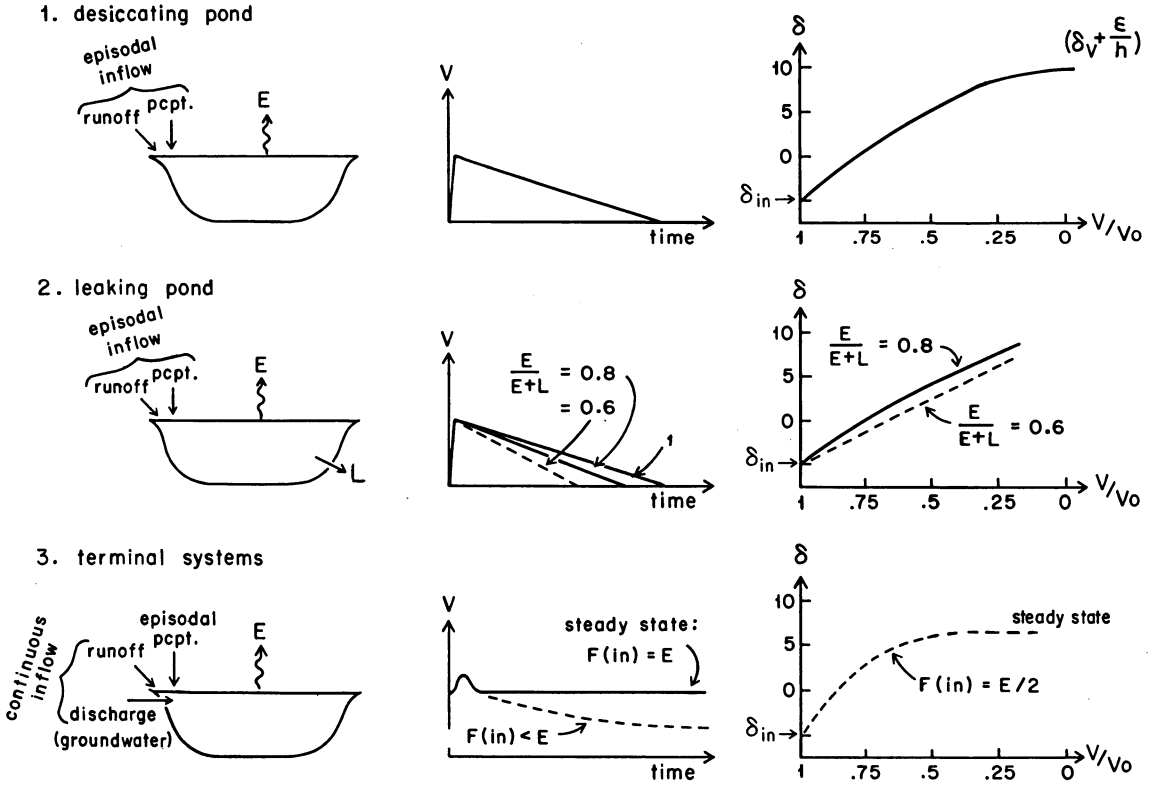


Fig. 9. Three ephemeral lake systems showing the evolution of water depth (volume) vs time, and the buildup of the enrichment in the heavy isotopic species as a function of the decrease in volume (RHS diagram). *E* and *L* stand for the evaporation and leakage fluxes, respectively

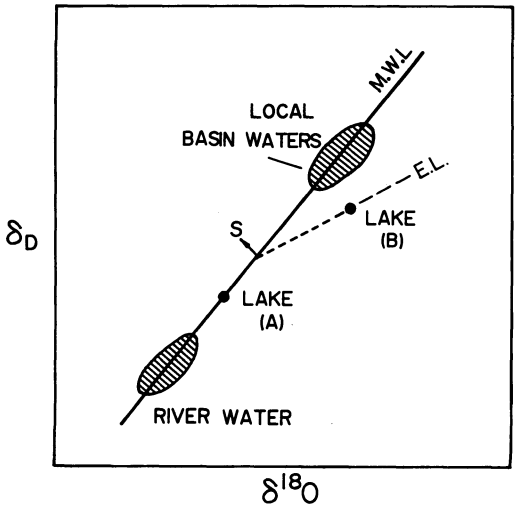


Fig. 10. Isotopic composition of floodplain lakes: Lake *A* is a case where the lake's isotopic composition falls on the MWL, evidently a mixture of river water and local drainage and runoff. Lake *B* is a case where the lake water's isotope composition falls to the right of the MWL, due to evaporation. In this case the source composition (*S*) is calculated by back extrapolation to the MWL along the stippled "evaporation line." (Adapted from Martinelli et al. 1989)

then favorable for the accumulation of salinity. Examples of transient saline systems are discussed in greater detail in Section 5.

3 Interactive and Feedback Systems

In the cases discussed thus far the lake could be viewed as a passive entity in its environmental setting, with a given isotopic composition of both inflow and atmospheric moisture imposed by large-scale processes and not influenced by the local evaporative systems. Such is the situation with regard to a relatively small and isolated lake.

The interactions between the lake and its environment cannot, however, be ignored in the case of either large evaporative systems or a string of lakes where the outflow of one lake, enriched in the heavy isotopic species, serves as part of the hydrological input to other lakes. We now discuss how such interaction may affect the isotopic buildup in the lake's waters and in its atmospheric environment. The equally important interaction between the lake waters and the interstitial waters in the bottom sediments or in the banks of the lake is taken up later in relation to saline lakes, where this type of interaction is most significant.

3.1 Network of Surface-Water Bodies

A commonly encountered situation is that of a string of lakes, along either a surface or groundwater flow path, where the output of an upstream lake contributes to the input into a downstream lake. When this happens there is a further buildup of isotopic enrichment in the secondary lake, so that one can distinguish between a primary lake, fed only by meteoric waters, and a downstream lake based on the relative enrichment of the isotopic species. One example where such an effect was used is given by Friedman and Redfield (1971), who could comment on the hydrological interrelationships of lakes of the Grand Coulee region, based on the degree of enrichment of the heavy isotopic species in the lakes.

One of the largest interactive lake system is that of the Great Lakes in northern America. Isotopic measurements by Brown (1970) show the gradual buildup of heavy isotopic value along the flow path. However, the buildup is perturbed by meteoric water inputs from drainage of the surrounding watersheds, making it difficult to model the system without having a much more detailed set of sampling points, both atmospheric and of the various streams and lakes in the region. The situation is much simpler in more arid regions where little dilution of the surface waters by incoming streams will occur.

A river system from which water is lost by evaporation along its flow path, as reviewed by Fritz (1981), can be considered to be the extreme example of a string of lakes. An "evaporation pond" model is found to be applicable in this case, with a length scale being substituted for the time axis (Fontes and Gonfiantini 1967).

Let us now consider the rules of the isotopic buildup in a string-of-lakes system, based on the discussion in Section 1.1. Assuming for ease in calculation that the local precipitation (δ_p) is in isotopic equilibrium with the atmospheric moisture (δ_a), so that $\delta_a = \delta_p - \varepsilon^*$ [which is a reasonable assumption for a mid-continental, temperate-zone setting (Craig and Horibe 1967; Jacob and Sonntag 1991)], and assuming further that the lakes are in both isotopic and hydrological steady state, then the difference in isotopic buildup between a string of lakes compared with that of a single-lake system stems simply from the fact that the value of the term ($\delta_a - \delta_{in}$) in Eq. (5) is more negative in the case of a secondary lake whose inflow consists in part of waters enriched in

the heavy isotopic species (in the first lake $\delta_{in} = \delta_p$; in the downstream lake $(-\delta_{in}) < (-\delta_p)$ and δ_a is of course a strongly negative number). It can be shown theoretically, however, that there will be an "ultimate" isotopic buildup beyond which no further isotopic enrichment occurs, due to the effect of backflow of the atmospheric moisture (Gat and Bowser 1991). In fact, the limiting value is reached when $\delta_a - \delta_{in} = \varepsilon/h$.

Incidentally, the isotopic concentration of this ultimate lake corresponds to the steady-state solution for isotopic enrichment of a water pool that evaporates to dryness according to the Craig and Gordon model (1965).

Figure 11 shows the isotopic buildup reached in a coupled lake system for a variety of boundary conditions. The enrichment in a multiple-lake system evidently exceeds that of a single lake with comparable hydrological characteristics. It is to be noted that humidity is the major controlling parameter: At high humidities (such as 90%) the enrichment never exceeds approximately 3‰ in δ_{18}, whereas extremely enriched values occur when humidity drops below 50%. It is further evident that the hydrological balance, quantified by the parameter F(in)/E, has a large influence on the isotope content of the evaporating system, and hence it has been proposed to use the isotopic buildup in lakes as a measure for this parameter (McGrath et al. 1989).

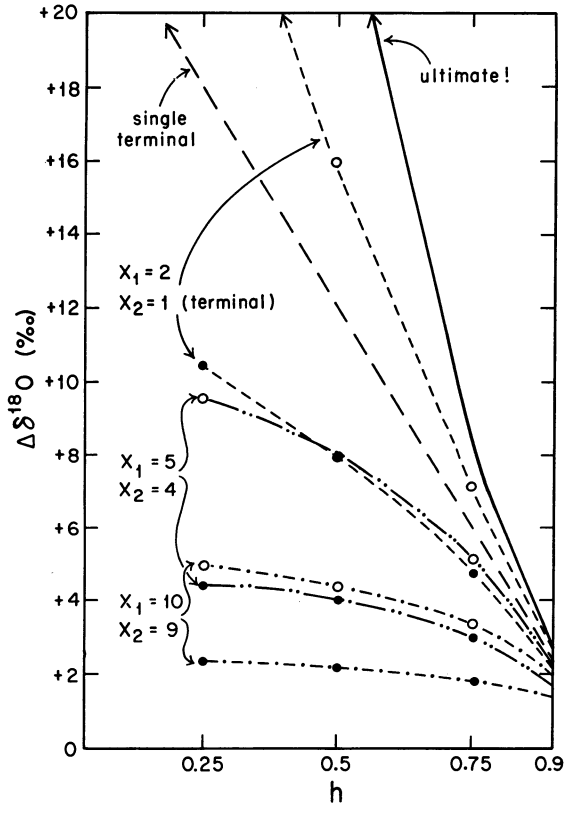


Fig. 11. Isotopic buildup ($\Delta = \delta_{ss} - \delta_{in}$) as a function of the ambient humidity for a two-lake system (*open circles*) compared with a one-lake system having the combined evaporation rate of the two lakes (filled circles).

$X = \frac{F(in)}{E}$ is the through-flow ratio, with X_1 and X_2 referring to the first and second lake, respectively. Isotopic equilibrium between δ_a and δ_{in} is assumed. Data for a terminal lake and a desiccating pond (the ultimate possible enrichment for these environmental parameters) are also shown

3.2 Recycling of Reevaporated Moisture into the Atmosphere

Evapotranspiration returns some of the rained-out moisture to the atmosphere. Over large evaporative systems, such as the tropical rain forests and the lake regions of North America, this becomes a significant factor in the atmospheric water balance.

Transpiration and closed-basin evaporation returns the moisture essentially unfractionated to the atmosphere. In terms of its isotopic composition, this process moves the isotopic vapor's delta value along the MWL toward more positive values (Fig. 12). An extreme example is encountered in the Amazon basin, where during part of the year most of the precipitation falling on the region is recycled, resulting in a negligibly small isotopic gradient from the coast inland into the basin (Salati et al. 1979). To the extent that evaporation from open surface waters contributes to the evapotranspiration flux, however, the reevaporated moisture's isotope content (δ_e) lies way off the MWL (a mirror-image effect of the position of a lake's isotopic composition on a low-slope evaporation line), so that the admixture of the reevaporated moisture into the atmosphere yields atmospheric vapor with an increased deuterium excess value compared with the MWL, as shown in Fig. 12. This effect has been documented in the Amazon basin (Gat and Matsui 1991), tropical Africa (Dansgaard 1964), and the Great Lake region of North America (Gat et al. 1994).

Gat and Bowser (1991) have estimated the effect of this recycled moisture on the evaporative enrichment in (downwind) lakes. Once again the results differ depending on whether the isotopic composition of the inflowing waters changes

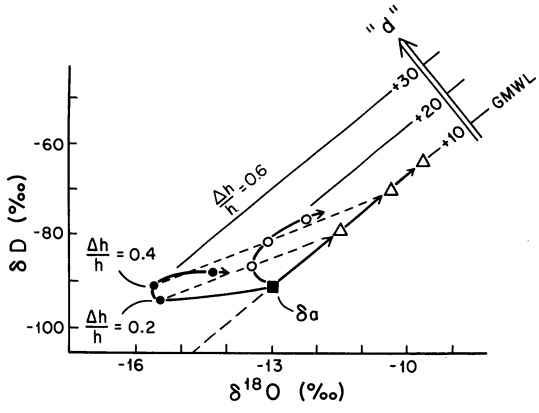


Fig. 12. Changes in the isotopic composition of atmospheric moisture by admixture of the evapotranspiration flux. $\Delta h/h$ gives the ratio of added-to-original atmospheric moisture content; Δ-Δ-Δ transpiration only, which returns the unfractionated waters to the atmosphere and causes the atmospheric vapor's isotopic composition to move upward along the appropriate MWL (the locus line for both δ_a and δ_{in}). -*o*-*o*- shows the result of admixture of evaporate from an open surface water body, and -*o*-*o*- for a 1:1 ratio of the evaporation and transpiration fluxes. In all three cases the successive data points correspond to Δh/h = 0.2, 0.4, and 0.6, respectively. (Adapted from Goodfriend et al. 1989)

along with the buildup of the isotopic signature in the atmospheric moisture. In the first case any change in the value of Δ of Eq. (7) is due only to the changing humidity while $\delta_a - \delta_{in}$ remains invariant. Conditions such as these apply whenever the input to the lake is exclusively from the local precipitation. On the other hand, where the inflow is that of a regional river or groundwater flow system that is not affected by the atmospheric buildup, the value of Δ changes along the flow path, due to the change in both δ_{in} and the humidity. It is evident that the degree of the evaporative enrichment is influenced more by the humidity than by the minor change in the isotopic composition of the atmospheric moisture. Because the humidity profile also determines the evaporation flux itself, the isotopic buildup can be used as a measure for the change in the rate of evaporation as a result of water recycling in such systems.

When one studies large evaporative (continental scale) systems, such feedback effects have to be taken into account. Properly applied, the measurement of the isotopic buildup can be an important tool for studying regional water balances. In studies in the Amazon basin, the increase in the d parameter in the recycled moisture was found to be a very useful tool in this regard (Gat and Matsui 1991). Similar studies have been performed in the western United States (Ingraham and Taylor 1991) and the Great Lakes region (Gat et al. 1994).

3.3 Large Lakes

As wind blows over a large fetch of water, the evaporated moisture blankets the downwind side of the lake, reducing its evaporation rate. The isotopic water–air interaction will obviously be different at the wind side of the lake, where unaltered continental air interacts with the lake waters, and on the downwind side, where both the humidity and isotopic profiles in the air are perturbed. The formulation of the isotopic fractionation during evaporation over the entire lake would be grossly in error if it were to be based on the δ_a value of the incoming air and its humidity. The total evaporation and isotopic change for the lake as a whole must be calculated in a weighted fashion over the entire extent of the lake, taking these differences into account. The moisture buildup over the lake depends critically on the degree of turbulent mixing in the atmosphere above the lake, especially in the lower 100 m.

Because the formulation of the isotopic exchange involves the difference between the values of δ_L and δ_a, any change in either of these quantities has to be considered. Because of the relatively large horizontal eddy diffusivity and rapid mixing in lakes, especially under strong wind conditions, one can usually assume that there will not be a marked isotopic inhomogeneity in the surface waters in the horizontal dimension, just as one does not encounter strong temperature anomalies except for cases where upwelling of cold bottom waters occurs in stratified lakes. However, the humidity increase over the lake in the downwind direction, and the resulting reduction in latent heat flux, is well documented (Holland et al. 1981).

No systematic field study of the effect of this moisture buildup over large bodies of water on the isotopic balance has yet been published, so that the following discussion is based on the general principles introduced in Section 1.1.

The change in the isotopic composition of atmospheric moisture as a result of admixture of the evaporation flux is given by material balance as

$$h \cdot \delta_a + (h' - h) \cdot \bar{\delta}_e = h' \cdot \delta'_a, \qquad (9)$$

where the primed values (′) refer to downwind conditions following moisture buildup. The $\bar{\delta}_e$ is, of course, the averaged value of δ_e over the length of the fetch up to the point considered (where humidity and its isotope composition have the values of h′ and δ'_a, respectively). Using Eq. (2), it should be possible to calculate δ_e at any location in two ways, namely either based on data from above the lake where the atmospheric parameters are δ'_a, and h′, or based on the upwind, unperturbed atmospheric parameters h and δ_a. In the second case, however, $\Delta\varepsilon$ cannot be approximated by Eq. (3a), but proper account has to be given to the transport resistance in the blanketing layer above the lake using the RHS of Eq. (3). The evaluation of the values of the transport resistances necessitates analysis of the vertical humidity profile over the region. In terms of the nondivergent flow model of Craig and Gordon, $\theta = (1 - h')/(1 - h)$ and can be estimated from the measured relative humidity values. As an example the magnitude of this weighting term was estimated for Lake Superior (during summer months) as $\theta = 0.88$ (Gat et al. 1994). In either case, irrespective of whether a reference point close to the surface of the lake or way above it is chosen, the humidity value introduced into the $\Delta\varepsilon$ term must be that of h′. The calculation of the isotopic content of the evaporative flux will then yield the same result in either case, as is to be expected from the linear nature of the resistance model.

To illustrate the potential magnitude of the effect of moisture buildup over a lake on isotope data, we calculate the expected values of δ_e when humidity increases from 60 to 75% over the fetch of a lake. [The following initial isotopic data were assumed in this calculation: $\delta_e(18) = -14‰$; $\delta_L(18) = -2.2‰$.] The calculated values of δ_e for the initial and downwind conditions were, respectively, $\delta_e(18) = -22‰$ and $\delta'_a(18) = -13‰$. The magnitude of the term $E \cdot \bar{\delta}_e$, which is the one to be introduced into the lake's balance equation (taking the arithmetic mean between these two δ_e values) is then $-5.7/\rho$ compared to the value of $-8.8/\rho$ if this correction were to be ignored. Evidently such effects are significant and cannot be ignored in any attempt to formulate an isotopic balance over a large lake.

It is of interest to note that there is also a slight shift in the slope of the evaporation line (in δ_D vs δ_{18} space) along the wind fetch. The more humid, downwind side of the lake is characterized by a steeper slope compared with the wind side.

3.4 Large-Area Lakes with Restricted Circulation

In lakes with a complex morphology, different parts of the lake typically acquire different isotopic compositions, either as a result of a "string-of-lake" effect, or because a separate water-balance equation applies to each of the different branches of the lake. Modeling the lake as a whole, based on equations such as Eq. (5), is impractical. On the other hand, the isotope data can be used to advantage to trace mixing patterns and throughflow currents. One practical and useful application is the identification of stagnant water bodies, which are not flushed effectively and which might be of concern in relation to eutrophication and pollution processes. Fontes et al. (1970) described a lake (Lake Chad), where the inhomogeneity results from an inhibited circulation due to a subsurface ridge.

In the "classical" Dead Sea, i.e., before the falling water levels resulted in the drying up of its southern, shallow basin, the difference in isotopic content between the southern basin and the deep northern part, enabled tracing a backflow of the southern-basin waters and their role in deep-water formation of the meromictic northern basin (Fig. 13; Nissenbaum 1969). In this case the spatial inhomogeneity resulted mainly from a string-of-lakes effect. In many other cases the different isotopic signatures are engendered by variations in the isotopic composition of inflow waters (e.g., a local runoff vs a river with a different isotopic composition or rivers having very different watershed characteristics). As an example one can then take the data of Brown (1970) from the Great Lakes of northern America, which were mentioned previously.

4 Saline Lakes

Many terminal lakes become increasingly saline, sometimes to an extent where evaporitic minerals, such as gypsum and halite, are deposited (Eugster and Hardie 1978). Whereas in fresh or brackish systems the salinity can be used as a measure of the water balance and particularly the degree of evaporation (on the assumption that salts behave as conservative components of the system and that there are no saline inflows), this is no longer possible in the case of brines. Stable isotopes are therefore the preferred tool for quantifying water balance.

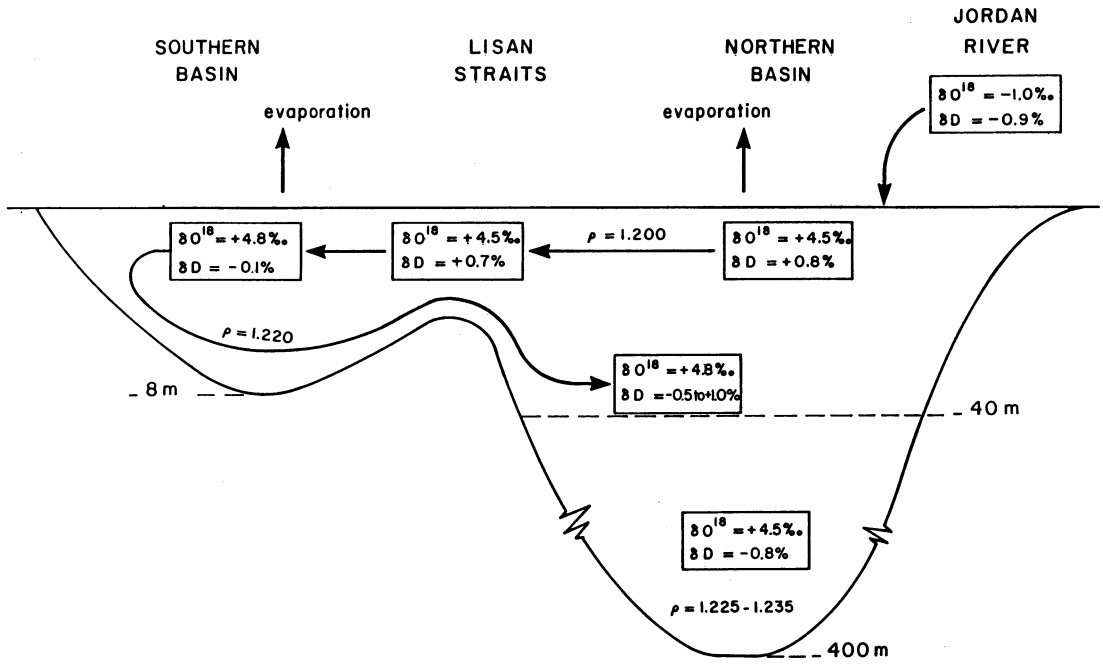


Fig. 13. The circulation of waters from the two basins of the Dead Sea (after Nissenbaum 1969). ρ is the water's density value (a measure primarily of its salinity)

To a first approximation the stable isotope balance and fractionation is not much affected by the salinity in brackish and moderately saline solutions. When concentrations exceed those of seawater appreciably, however, a number of "salinity effects" on the isotopic fractionation assume importance (as reviewed by Gat 1979, 1980, and Horita 1989); foremost is the effect on the humidity term, h, the governing parameter in the exchange process between atmospheric moisture and the lake. Obviously, h will reach higher values over a brine for any given atmospheric vapor pressure, because humidity is normalized relative to the saturated vapor pressure over the solution, and the latter is reduced with increasing salt concentration (Gonfiantini 1965). Furthermore, the salt effect on the equilibrium isotope fractionation factor between solution and vapor has to be considered. This factor is a function of salinity, because of the preferential binding of one or the other isotopic species into the hydration sphere of the ions concerned (Feder and Taube 1952). Finally, salinity may affect the dynamics of water movement and mixing in the lake and result in its stratification, so that different degrees of isotopic buildup may occur in a saline lake compared with a freshwater lake for a given external set of parameters.

The magnitude of the first of these effects on the isotopic buildup in a lake, namely, that on the h term, can be appreciated by considering the evolution of the isotopic composition of a terminal lake in which salinity accumulates for a given set of values of δ_a, δ_{in}, and water vapor concentration in the atmosphere (Fig. 14). It is to be noted that as h increases with increasing salinity the steady-state isotope composition (Eq. 7) is progressively less enriched in the heavy isotopic species, and the isotopic composition of the lake's waters seem to "chase" these steady-state values, which correspond to the lower humidities. This continues until the ambient moisture content equals that of the saturated air layer above the brine at the temperature of the liquid surface. At this point further evaporation ceases. Up to this point the effect of h is the dominant one, but the isotopic composition of the brine lake may well continue to change, even after saturation through an exchange mechanism, until the brine and the ambient moisture are in isotopic equilibrium with each another. At this stage the isotope content of the surface waters is determined by the magnitude of the salt effect on the equilibrium fractionation factor. This effect now assumes dominance, as indicated in Fig. 14.

The relationship of α_b^*, the isotopic fractiona-

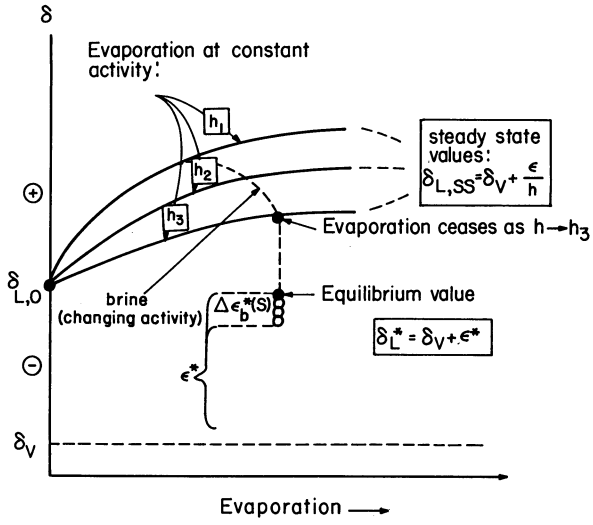


Fig. 14. Salt effect on the buildup of heavy isotopic species in a (saline) terminal lake. δv is the isotopic composition of the equilibrium vapor at the brine/atmosphere interface

tion factor in the vapor-liquid exchange over a brine, is related to the value over freshwater as follows (Sofer and Gat 1972):

$$\alpha_b^*(T, S) = \Gamma(S) \cdot \alpha^*(T).$$

Numerous attempts have been made to determine the magnitude of this equilibrium salt effect, Γ (Sofer and Gat 1972; Truesdell 1974; Sofer and Gat 1975; Stewart and Friedman 1975), and its value was for a long time in disagreement between different sets of measurements, especially with regard to the deuterium salt effect. Lately, however, following the careful work of Kakiuchi et al. (1987), most discrepancies seem to be resolved (Horita 1988). To a first approximation the effect of the different ions in a multicomponent brine are additive (Sofer and Gat 1972, 1975). Some synergistic effects are, however, noted at high ionic strengths (Horita 1988).

The salinity effect on the equilibrium isotope fractionation factor has special relevance to the intercomparison of experimental data sets, because some of the analytical techniques for measuring the isotopic composition yield data on an "activity" scale [δ(act)], whereas others (especially those in which the water is separated from the brine prior to mass-spectrometric analysis) give the data on a "concentration" scale, δ(conc). To intercompare and interpret the data it is obviously necessary to use concordant data and also a proper value for the isotopic fractionation factor. In the case of a lake exposed to evaporation for which a material-balance formulation such as Eq. (1) applies, it was shown by Gat (1984) that the concentration units δ(conc) are the appropriate form of expressing the δ values. For the ^{18}O data, where the common measurement technique yields the δ_{18} values on an activity scale as a result of the use of the exchange reaction between water and CO_2 gas in the measurement process, it is necessary to apply the correction formula described by Sofer and Gat (1972), namely, $\Delta\delta = \Sigma M_i \cdot \alpha_i$ (α_i is the correction term for ion i; Mi is molar concentration of ion i), to those terms that relate to the saline water component of the balance equation. (There is obviously no correction to be applied for freshwater values such as δ_a, and, in most cases, for δ_{in}.) However, in the case of the evaporation flux, δ_e, which, according to Eq. (2), is a mixed term involving saline and nonsaline components as well as the equilibrium fractionation factor, this correction has to be judiciously applied. One can then either introduce into Eq. (2) the value of δ_L on an activity scale and α^* (i.e., the freshwater fractionation factor for that temperature) or the value of α_b^* together with the corrected δ_L(conc) value. In either case the humidity term h must be chosen to take into account the depression of the saturated watervapor concentration above the brine.

Another subtle point to be mentioned relates to the slope of the evaporation line of a saline lake in δ_D vs δ_{18} space. This slope is defined by the relationship $S = (\delta_L - \delta_{in})_D/(\delta_L - \delta_{in})_{18}$. When the slope is derived from the measured isotopic value of the saline lake's water by the conventional analytical method, whereby δ_D is obtained on the concentration scale, then the slope is found to have a very low value compared with that of a freshwater lake at comparable ambient conditions. This value is, however, just an artifact of the salt correction. Expressing δ_D on the activity scale, i.e., making the salt-effect correction $\Delta\delta$ as given above, is the correct procedure, and the value thus derived will match that calculated on the basis of Eq. (6) (Gat 1984).

The steady-state isotopic concentration for a terminal brine lake can be written in the following way:

$$\delta_{L,SS} = (\delta_a - \delta_{in} - C_k) \cdot h + (\varepsilon^* + C_k + \delta_{in}). \quad (10)$$

Both h and ε^* are affected by salinity, but this formulation illustrates the importance of the value of h and that of the thermodyamic activity

of the water (which changes the value of h) in dominating the response of a brine lake's isotopic composition to an increase in salinity. One cannot overemphasize the fact, which is counterintuitive, that those terminal lakes that are in a more evaporative stage and have accumulated a higher salinity are characterized by a lower degree of buildup of the heavy isotopic species at steady state. We will come back to this point in relation to the interpretation of the isotope composition of paleolimnic carbonates.

4.1 Isotope Hydrology of Large Salt Lakes

The Dead Sea, situated at the lowest terrestrial spot on earth at close to −400 m below sea level, is also the saltiest of the large salt lakes of the earth (in terms of the depression of the water-vapor pressure). Until 1979 the Dead Sea was the classical example of a salinity-stratified lake with a pronounced halocline extending between 40 and 75 m below the lake level (Neev and Emery 1967). The lower water mass reached the high salinity of 275.8 g/kg and its isotopic composition, analyzed by Craig during 1959–1960, was shown to be very homogeneous to within ±0.02‰ in δ_{18}, with a mean value of +4.43‰. The surface waters, on the other hand, showed variable enrichments, ranging from values of δ_{18} = +1.60‰ to +5.1‰ (Gat and Dansgaard 1972). The deuterium value was reported to be approximately a value of δ_D = 0‰, but subsequent work by Horita and Gat (1988) indicated that this number was probably too low, due to an artifact of the incomplete separation of the water from the mineral load during the course of the deuterium analysis. A value of δ_D = +9‰ seems more correct for the hypolimnic waters at that time. At these concentrations the salinity-to-activity correction factor appeared to be 17‰ for deuterium, whereas the ^{18}O correction factor was given by Sofer and Gat (1972) to be 2.2‰.

Because of the diversion of its freshwater inflow, the level of the Dead Sea gradually declined, and its salinity increased over the past 30 years, until the salinity gradient disappeared and the lake finally overturned in the beginning of 1979, at a salinity of 276.2 g/kg (Steinhorn et al. 1979). During this period the lake's isotopic composition was exposed to two conflicting trends, namely the non-steady-state effect of an increase in the isotopic composition as a result of the desiccation of the lake (due to the deficient dilution by the inflowing waters) and the converse trend, a decrease in the isotopic enrichment due to the effect of increasing salinity. In a study on the isotopic composition of the lake in the years following the overturn (Gat 1984), it was shown that the surface water's isotope composition closely followed the salinity excursions, so that evidently the short-range fluctuations of the water balance dominate the isotopic evolution of the surface waters during recent years.

A number of additional factors that would change the mean isotope composition (the steady-state value, around which the temporal variations occur) have to be considered in the case of the Dead Sea. These are the result of climatic or human-made shifts in the isotopic composition of the inflow waters. Such changes occurred during the past 30 years or so, mainly as a result of the diversion of Lake Tiberias waters into the irrigation network of the region, thus lowering the value of δ_{in} by at least 2‰ in δ_{18}. The new steady-state composition of the Dead Sea water, which is expected in response to the changed inflow and the increased salinity (shown in Fig. 15) will not be reached, however, until such time when the system stabilizes at a much lower level of the lake and at a much higher salinity. Until that time the unsteady nature of the system, resulting from a continuous excess of E over F(in), pushes up the isotopic composition throughout a yearly cycle by an order of 1‰, as is evident from the results of the model calculations of the isotopic buildup in the Dead Sea (Fig. 16). As is discussed in Section 5, it is important to take such non-steady-state situations into account when interpreting paleolimnological data.

The isotopic buildup in other highly evaporitic salt lakes is comparable to the Dead Sea. For example, in Lake Giuiletti in the Danakil depression (Ethiopia) whose salinity is given as 158 g/l, Gonfiantini et al. (1973) found the lake waters enriched up to +6‰ in δ_{18}. Both the somewhat lower salinity compared with the Dead Sea and the fact that part of the water sources are of marine origin may contribute to the somewhat more enriched isotopic value in this case.

4.2 Ephemeral Salt Lakes and Sabkhas

On the other extreme of the scale from the large and deep saline lakes just described are the salt flats, shallow saline features found in low-lying areas of the arid regions and in groundwater

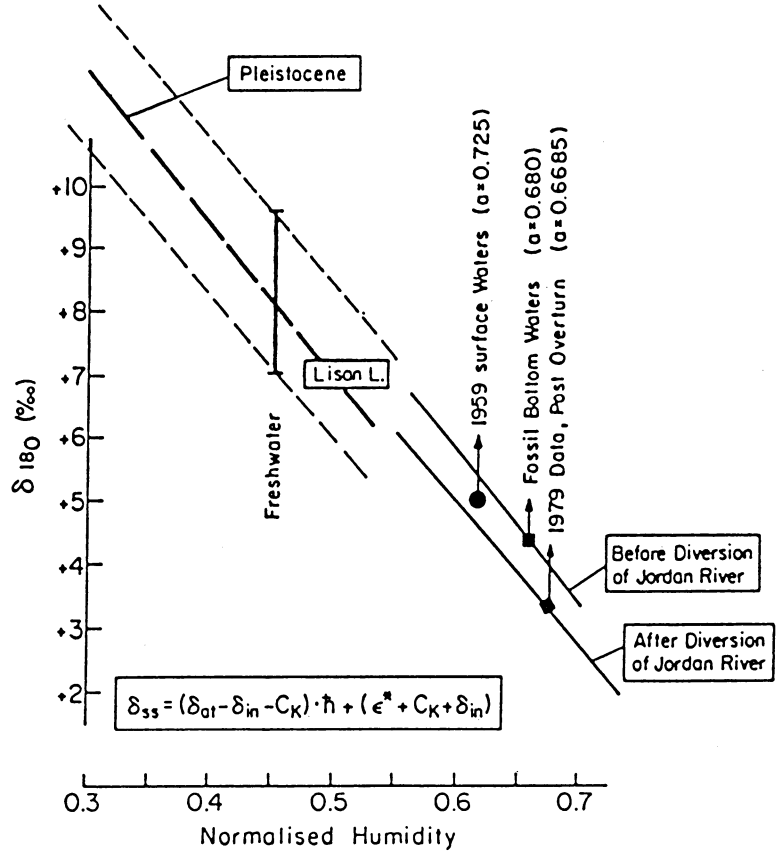


Fig. 15. Isotopic steady-state values in the Dead Sea system for a variety of past and future hydrological scenarios. *a* denotes the thermodynamic activity of water in the brines. Note that the normalized humidity is determined by the salinity of the brine. Over freshwater the value is approximately h = 0.45. (Gat 1984)

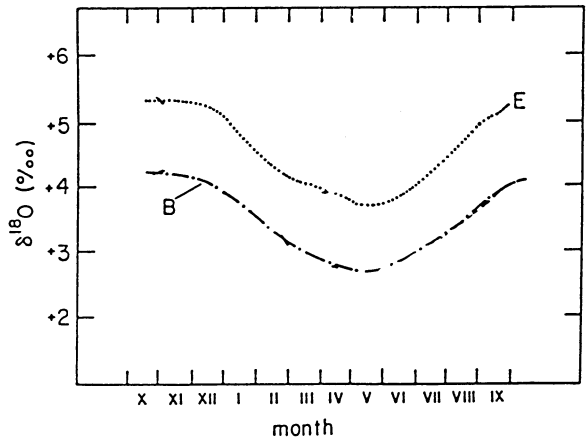


Fig. 16. Model calculations on the seasonal march of the isotopic content of Dead Sea surface waters. Curve *B* refers to a (hypothetical) hydrologically balanced year, whereas curve *E* applies to conditions of a continuous hydrological deficit of 0.5 m y^{-1} in water depth. (Adapted from Gat 1984)

discharge zones. These are inundated periodically following a rain or flood event and then dry up during drier intervals, leaving accumulations of brines and evaporitic minerals. Such transient lakes show a wide range of chemical and isotopic compositions, because they go through the various stages of their life cycle.

The profound effect of the salt load on the isotopic enrichment attained in such salt lakes, when compared with freshwater systems that are exposed to a similar environmental setting, is illustrated by measurements on a series of ephemeral lakes (locally named "dry lakes") in the Raak plains of southern Australia. A large number of pond-like depressions fill up after the rains, displaying a wide range of salinities. In the extreme case one encounters a saturated brine because of the dissolution of NaCl crusts, which cover the valley's floor. The ponds then gradually dry up and their isotope composition changes accordingly. As shown in Fig. 17, which is based

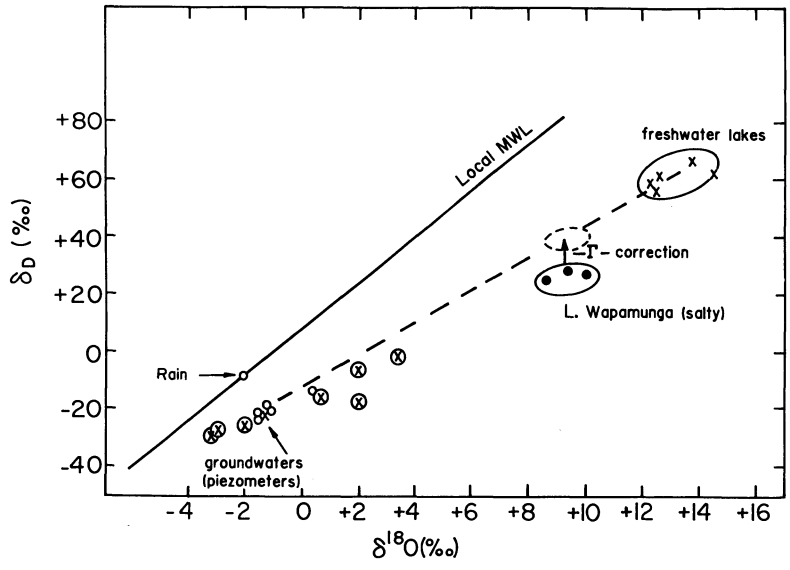


Fig. 17. Isotope composition of a freshwater and saline (NaCl saturated) lake in southern Australia. *o* are data from piezometer bores on the shore of the salt lake; ⊗ corresponds to samples near freshwater lakes; Γ is the δ(conc) to δ(act) correction according to Horita and Gat (1988)

on unpublished data of Allison and Gat, the isotopic enrichment in the salty systems falls short of their fresh-water analog, obviously because of the apparently higher ambient humidity (h) seen by the brines.

In addition to their economic importance as sources for minerals, such systems are of interest in relation to their role in the hydrological cycle, either as an outlet for groundwaters or as sources of salinity. Because of their complexity and the nonconservative behavior of most salts in these systems, researchers have turned increasingly to the isotopic composition of salt lakes and their surroundings in an attempt to decipher their hydrology.

Three basic interrelationships between a saline lake and its (subsurface) environment are considered in Fig. 9:

1. The "evaporative outlet" model. Surface or groundwaters drain into the surface depression. Salinity will obviously accumulate on or near the surface, except for that part lost by eolian transport (Langbein 1961; Gill 1987).
2. Recharge occurs from the salt lake into the subsurface system. This is an equivalent of the seepage reflux model described by Adams and Rhodes (1960) for sabkhas. Groundwater through-flow lakes can be considered in this category, provided evaporation is a dominant factor resulting in an appreciable salinity increase in the lake.
3. The "bank storage" model, where recharge to adjacent aquifers occurs at higher-water stands, to be released later as backflow to the lake once the waters have evaporated and receded. The case of pore waters that are in diffusive exchange with lake waters may be considered to be in this category.

It is very evident that the chemical and isotopic makeup of the (aquifer) waters adjacent to a salt lake, and of the interstitial waters in its sediments, can reveal as much about the hydrology of the system as the analyses of the lake waters proper. Thus, in the first model described, one obviously expects to encounter nonenriched, meteoric, waters throughout the subsurface domain. However, some diffusive exchange between the interstitial pore waters and the saline lake has to be taken into account, which may establish a salinity gradient in the subsurface and in part counteract the effects of the advective water flux, as witnessed by Stiller et al. (1975) in the bottom sediments of Lake Kinneret. (In this case these sediments were actually the source of salinity.)

In the second model, the isotopic composition of groundwaters situated downstream from the lake should represent a weighted mean of the

surface-water composition during the period that recharge takes place. The expected value can be given by the leaking evaporation pond model of Gat and Tzur (1967), which gives the composition of the water leaking from the lake into the subsoil approximately as

$$(\bar{\delta} - \bar{\delta}_0)_{\text{leakage}} \cong \frac{\{\varepsilon^* \cdot h - \varepsilon\}}{\left\{(1-h)\cdot \frac{F(L)}{E} + 1\right\}}, \quad (11)$$

where F(L) is the leakage flux, whose isotopic composition is assumed to be that of the lake water at any time. After such a lake has finally dried up, any further evaporative water loss from within the bottom sediments could result in further enrichment of the heavy isotopic species and of the salinity in the pore waters as described by Barnes and Allison (1988). This enrichment can actually be used to estimate the evaporation loss from within the sediments.

The third model in which a two-way movement of water occurs in the subsurface domain is characterized by great variability in the isotopic composition and the salinity in time and space. An example of such a situation was described in the Arava Valley by Gat and Naor (1979), where the evaporative signature of a sabkha was traced "upstreams" into the aquifer for a couple of kms (possibly aided by increased pumping in that aquifer).

A number of ephemeral salt lakes have been studied in both a coastal and inland setting. Isotopic measurements have enabled researchers to specify the hydrological mechanisms involved in both the flooding and desiccation stages of these systems, as exemplified by the study on salt lakes in the Bardawil area by Gat and Levy (1978). Specifically, that study involved some sabkhas situated among successive 25-m-high sand-dune ridges on a traverse extending approximately 5 km inland from the marine lagoon. Each of these salt lakes is approximately 1–2 km long and 0.5 km wide, with no visible surface connections or inflows. Salts seem of marine origin, but a prolonged evaporitic and diagenetic history resulted in a very varied assembly of NaCl and $CaSO_4$ brines (Levy 1977). Following rain in the region all of these lakes fill up to a level of approximately 10 cm, dissolving some of the accumulated surface salts, with a commensurate change in the isotopic composition. This water depth is in excess by a factor of 3–5 over the direct precipitation, indicating drainage from adjacent sand dunes. Water levels then recede slowly over a couple of months. Most of the lakes dry up in spring and summer, with a concentrated brine hiding just a few centimeters below the salt crust. As shown in Fig. 18, the isotopic composition of the waters at high-water stage was similar in all the sabkhas, but the final enrichment reached during the desiccation cycle differed for the four systems under investigation.

The isotopic composition of possible sources of inflow water are very distinct in this case, being $\delta_{18} = -6.5‰$ for dircect precipitation, $\delta_{18} = -1‰$ for shallow groundwaters and dune waters, and +3‰ for the subsurface brines, which remain after the previous desiccation cycle [in some Persian Gulf sabkhas, Hsu and Schneider (1973) considered such subsurface brines to be the source for rising waters during the flood stage.] Because of these differences, it was possible to specify which of these inflow models applied to the

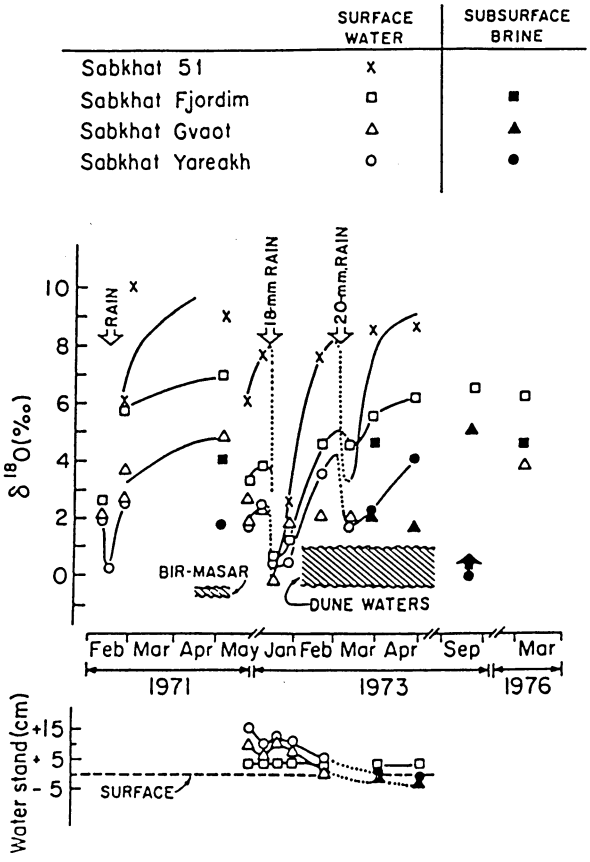


Fig. 18. A flushing and desiccation cycle in the sabkhas of the Bardawil area. *Upper curves* are $\delta^{18}O$ values; *lower curve* is water level. (Adapted from Gat and Levy 1978, and Gat 1980)

Bardawil sabkhas. A value of −0.75, +0.70 and +1.77‰, respectively, was computed by material balance for the composition of the inflow waters into three of the sabkhas considered. This seems to match the isotope composition of the shallow groundwaters in the area.

The slow recession of water levels during the dry period indicates that additional water inflow occurs into those sabkhas over an extended period during the desiccation stage, but that the sabkhas differ from each other in this regard. Only one of the sabkhas (#51) responded like an isolated evaporation pan, and this property was used in order to estimate the value of the atmospheric variables δ_a and h for this region at that time, using this sabkha as an "index lake." These values were then introduced into the balance equations of either a terminal or through-flow system. Upon comparing the measured values in the other three sabkhas with the model calculations, it was possible to establish the hydrological characteristics of these sabkhas based on the degree of isotope enrichment in the various water bodies (Gat and Levy 1978).

Saline systems are evidently ones in which the isotopic data can be used successfully to decipher both the hydrological and geochemical balances, as well as the interrelationships of the lakes with their environment.

5 Isotopic Paleolimnology

The isotopic composition of a lake's waters is conserved in some of the limnic sediments, especially in authogenic carbonates, in the shells of aquatic animals, as well as in the interstitial waters of lake sediments. Except for the latter, the isotopic composition of the oxygen in the minerals concerned will be a function of both temperature and the isotopic composition of the lake (Stuiver 1970); hence, a change in either of these results in a signal in the carbonate record. This has been recently reviewed by Talbot (1990).

On the assumption that the isotopic composition in the sediment is not changed by diagenetic processes (and correcting for possible temperature variations in the lake), the isotopic record of a limnic sediment reflects the changing isotopic values of the lake's waters. These can be reconstructed by taking into account the isotopic fractionation between the water and the mineral concerned. The interpretation in terms of paleolimnic parameters is, however, by no means as straightforward as in the case of a marine sediment. One must consider changes in both climatically controlled parameters (such as δ_p, δ_a, and humidity), hydrological factors and especially the through-flow ratio and evaporation rate, the possible changes in the isotopic signal of the watershed (Gat and Lister 1994), but also the limnological features such as the mixing regime and the vertical stratification. Perhaps the most dramatic change would result from a shift in a lake's situation from that of a terminal lake to an open system (Lister et al. 1991).

Observing an isotopic record in the interstitial waters, rather than in the sediments themselves, has the advantage that one has a record of both water isotopes (^{18}O and D), so that even in the case where the oxygen isotopic composition is changed by diagenetic interactions with the mineral phases, the hydrogen isotopes survive to tell the story. Furthermore, temperature variations in the lake are not a factor in this case. On the other hand, the pore-water system cannot be regarded as a closed system for any length of time, so that the memory of the interstitial waters is limited to a few thousand years at most. One successful application was that of Stiller et al. (1983), who reconstructed the salinity and other properties of the Dead Sea from the record in the interstitial waters of its sediments.

Liquid inclusions in evaporites (particularly halites) can also be utilized in this fashion. Horita (1990) studied the isotopic composition of fluid inclusion from halites of Searles Lake, California, and interpreted the data within the framework of steady-state isotopic composition of either pan, terminal, or flushed lake systems.

Katz et al. (1977) reported ^{18}O profiles in carbonates of the Lisan sediments, Lake Lisan being the Pleistocene precursor of the Dead Sea and believed to have been just half as salty. Even allowing for possible temperature variations, they concluded that Lake Lisan waters reached δ_{18} values of +6–+8‰ compared to δ_{18} = +4–+5‰ in the more saline waters of the present Dead Sea. This result, although surprising at first sight, is indeed to be expected because of the salinity effect on the isotopic buildup in a terminal lake (Gat 1984), which was discussed previously. On the other hand, Spencer et al. (1984) found an opposite effect in carbonates deposited from the precursors of Great Salt Lake (Utah), namely a freshening of approximately 5‰ in δ_{18} in the

Pleistocene lake. It appears that this system changed from a terminal lake into a flushed lake, so that the through-flow pattern overcame the effect of salinity on the isotopic buildup. The hydrological setting of the systems under study must obviously be taken into account in any paleo-limnological interpretation.

6 Conclusions: From Lakes to Oceans

The amount of buildup of heavy isotopes in an evaporative water body has been shown to be a function of its scale, determined by the degree of feedback between the evaporating system and the atmosphere with which it interacts. The larger the lake, the more dominant the role of the evaporation flux in the total moisture balance.

On one extreme of the size scale, one finds small continental lakes whose effects on its atmospheric environment can, on the whole, be ignored. The other extreme is given by the oceanic systems of (essentially) infinite size. If we were to extrapolate considerations such as those expounded in Section 3.3 to this scale, then this would lead to a situation where a saturated air layer, whose isotopic composition is in equilibrium with surface waters, prevents any further evaporation. This is not what happens in reality. The marine air–sea system as described schematically by Craig and Gordon (1965) is a system in which vertical motions (which were ignored in our treatment of lakes) and the resultant rain-out of atmospheric moisture are dominant factors. The marine atmosphere then remains in a state of undersaturation, and the marine atmospheric moisture is depleted, isotopically speaking, relative to the equilibrium vapor or the evaporation flux.

It is evident that as the sizes of the interacting systems increase, the vertical motions and the resultant buildup of clouds and rain-out cannot be further ignored. The stability of the air above the lake, which is dictated by the relative temperature of surface waters and of the air, plays a significant role in the distinction between what we can name the "lake effect" on the air–sea interaction (where the vertical motions are neglected), and the "maritime" regime, on the other hand, where the vertical convection is the dominant factor, as exemplified by the Great Lakes region (Ragotskie and Bratnick 1965) and the Mediterranean Sea (Gat and Carmi 1970). During fall and early winter, when relatively warm water masses underlie the cold continental air that blows over it, the air column is vertically unstable, and buildup of storm systems occurs up to the point of cyclogenesis (Trewartha 1961). During spring and early summer, on the other hand, the opposite situation develops with stable atmospheric layering repressing the vertical motions and minimizing the air–sea interactions under a high-humidity regime.

Whether vertical convective motions take place over the water body is thus not only a function of the size of the water body, but also depends on the air–sea interaction pattern. The isotopic signature, especially the effect on the d-excess in the atmospheric moisture, provides us with a diagnostic tool for judging the situation. A regional buildup of a large deuterium excess will be indicative of a continual large saturation deficit over the evaporating surface, which can, of course, only be achieved in a vertically convective system.

This transition from a process in which the horizontal extent of the wind fetch dictates the degree of interaction, to one in which the vertical dimension assumes dominance, deserves further study. The third dimension will undoubtedly have to be considered, even in the discussion of larger lake systems as well as in the study of oceanic systems on the lee side of the continents.

Acknowledgments. This review was written while the author spent a sabbatical leave at the Department of Geology and Geophysics, University of Wisconsin, Madison, WI. The hospitality of the department is gratefully acknowledged, and, in particular, many constructive discussions with my host, Dr. Carl Bowser. I also acknowledge the capable execution of the graphics by Ms. Susan Werther.

References

Adams JE, Rhodes ML (1960) Dolomitisation by seepage reflux. Bull Am Assoc Petr Geol 44:1912–1920

Allison GB, Brown RM, Fritz P (1979) Evaluation of water balance parameters from isotopic measurements in evaporation pans. In: Isotopes in lake studies, IAEA, Vienna, pp 21–32

Barnes CJ, Allison GB (1988) Tracing of water movement in the unsaturated zone using stable isotopes of hydrogen and oxygen. J Hydrol 100:143–176

Brown RM (1970) Distribution of hydrogen isotopes in

Canadian waters. In: Isotope hydrology 1970, IAEA, Vienna, pp 3–21
Craig H (1961a) Isotopic variations in meteoric waters. Science 133:1702–1703
Craig H (1961b) Standards for reporting concentrations of deuterium and oxygen-18 in natural waters. Science 133:1833
Craig H (1974) Lake Tanganyika geochemical and hydrographic study: 1973 expedition. Scripps Inst Oceanogr Ser 75-5:83
Craig H, Gordon LI (1965) Deuterium and oxygen-18 variations in the ocean and marine atmosphere. In: Stable isotopes in oceanographic studies and paleotemperatures, Pisa, pp 9–130
Craig H, Horibe Y (1967) Isotope characteristics of marine and continental water vapour. Trans Am Geophys U 48:135
Dansgaard W (1964) Stable isotopes in precipitation. Tellus 16:436–468
Darling WG, Allen DJ, Armannson H (1990) Indirect detection of subsurface outflow from a Rift Valley lake. J Hydrol 113:297–305
Dincer T (1968) The use of oxygen-18 and deuterium concentration in the water balance of lakes. Water Resour Res 4:1289–1305
Dincer T, Hutton LG, Kupee BBJ (1979) Study, using stable isotopes, of surface-groundwater relations and evapo-transpiration in the Okavonga Swamp, Botswana. In: Isotope hydrology 1978, IAEA, Vienna, pp 3–26
Eugster HP, Hardie LA (1978) Saline lakes. In: Lerman A (ed) Lakes: chemistry, geology, physics. Springer, Berlin Heidelberg New York, pp 237–294
Feder HM, Taube H (1952) Ionic hydration: an isotopic fractionation technique. J Chem Phys 20:1335
Ferronsky VI, Polyakov VA (1982) Environmental isotopes in the hydrosphere. Wiley, New York, 474 pp
Fontes JC, Gonfiantini R (1967) Comportment isotopique au cours de l'evaporation de deux bassin sahariens. EPSL 3:258–266
Fontes JCh, Gonfiantini R, Roche E (1970) Deuterium et oxygene-18 dans les eaux du Lac Tschad. In: Isotope hydrology 1970, IAEA, Vienna, pp 387–402
Friedman I, Redfield AC (1971) A model of the hydrology of the lakes of the lower Grand Coulee, Washington. Water Resour Res 7:874–898
Fritz P (1981) River waters. In: Gat and Gonfiantini (eds) Stable isotope hydrology; deuterium and oxygen-18 in the water cycle. IAEA, Tech Rep Ser 210:177–202
Gat JR (1968) Evaporation from lakes. In: Guidebook on nuclear techniques in hydrology, IAEA, Tech Rep Ser 91:175–183
Gat JR (1970) Environmental isotope balance of Lake Tiberias. In: Isotope hydrology 1970, IAEA, Vienna, pp 109–127
Gat JR (1971) Comments on the stable isotope method in regional groundwater investigations. Water Resour Res 7:980–993
Gat JR (1979) Isotope hydrology of very saline surface waters. In: Isotopes in lake studies, IAEA, Vienna, pp 151–162
Gat JR (1980) Isotope hydrology of very saline lakes. In: Nissenbaum A (ed) Hypersaline brines and evaporitic environments. Elsevier, Amsterdam, pp 1–8
Gat JR (1981) Lakes. In: Gat JR, Gonfiantini R (eds) Stable isotope hydrology; deuterium and oxygen-18 in the water cycle. IAEA, Tech Rep Ser 210:203–222
Gat JR (1984) The stable isotope composition of Dead Sea waters. EPSL 71:361–376
Gat JR, Bowser C (1991) The heavy isotope enrichment of water in coupled evaporative systems. In: Taylor H, O'Neil J, Kaplan LR (eds) Stable isotope geochemistry: a tribute to Samuel Epstein. Spec Publ 3, The Geochemical Soc, pp 159–168
Gat JR, Carmi I (1970) Evolution of the isotopic composition of atmospheric waters in the Mediterranean Sea area. JGR 75:3039–3048
Gat JR, Dansgaard W (1972) Stable isotope survey of the freshwater occurrences in Israel and the northern Jordan Rift Valley. J Hydrol 16:177–212
Gat JR, Levy Y (1978) Isotope hydrology of inland sabkhas in the Bardawil area, Sinai. Limn Oceanogr 23:841–850
Gat JR, Lister GS (1994) The "catchment effect" on the isotopic composition of lake waters; its importance in palaeo-limnological interpretations. EPC Publications (in press)
Gat JR, Matsui E (1991) Atmospheric water balance in the Amazon Basin: an isotopic evapotranspiration model. JGR 96:13179–13188
Gat JR, Naor H (1979) The relationship between salinity and the recharge/discharge mechanism in arid lowlands. In: Hydrology of areas of low precipitation, IAHS Publ 128:307–312
Gat JR, Tzur Y (1967) Modification of the isotopic composition of rainwater by processes which occur before groundwater recharge. In: Isotopes in hydrology, IAEA, Vienna, pp 49–60
Gat JR et al. (1994) The contribution of evaporation from the Great Lakes to the continental atmosphere: estimate based on stable isotope data. Geophys Res Lett 21:557–560
Gill TE (1987) Particulate episodes at Mono and Owen Lakes. EOS 68:1273
Gonfiantini R (1965) Effeti isotopici nell'evaporazioni di acqua salate. Atti Soc Toscana Sci Nat A72:550
Gonfiantini R (1986) Environmental isotopes in lake studies. In: Fontes JC, Fritz P (eds) Handbook of environmental isotope geochemistry, vol 2. Elsevier, Amsterdam, pp 113–168
Gonfiantini R, Borsi S, Ferrara G, Panichi C (1973) Isotopic composition of waters from the Danakil depression (Ethiopia). EPSL 18:13–21
Gonfiantini R, Zuppi GM, Eccles DH, Ferro W (1979) Isotope investigations of Lake Malawi. In: Isotopes in lake studies, IAEA, Vienna, pp 195–207
Goodfriend GA, Magaritz M, Gat JR (1989) Stable isotope composition of land snail body water and its relation to environmental waters and shell carbonate. Geochim Cosmochim Acta 53:3215–3221
Holland JZ, Chen W, Almazar JA, Elder FC (1981) Atmospheric boundary layer. In: Aubert TJ, Richard TL (eds) IFYGL — The International Field Year

for the Great Lakes. Noaa Great Lakes Env Res Ser, Ann Arbor, pp 109–168
Horita J (1988) Hydrogen isotope analysis of natural waters using an H_2-water equilibration method: a special implication to brines. Chem Geol 72:89–94
Horita J (1989) Analytical aspects of stable isotopes in brines. Chem Geol (Isotope Geoscience Section) 79:107–112
Horita J (1990) Stable isotope paleo-climatology of brine inclusions in halite: modeling and application to Searles Lake, California. Geochim Cosmochim Acta 54:2059–2073
Horita J, Gat JR (1988) Deuterium in the Dead Sea: remeasurement and implications for the isotopic activity correction in brines. Geochim Cosmochim Acta 53:131–133
Hsu KJ, Schneider J (1973) Hydrology of the Abu Dhabi sabkhas, Arabian Gulf. In: Purser BH (ed) The Persian Gulf. Springer, Berlin Heidelberg New York, pp 409–422
Hutchinson GE (1957) A treatise on limnology. John Wiley, New York
Ingraham NL, Taylor BE (1991) Light stable isotopes systematics of large scale hydrologic regimes in California and Nevada. Water Resour Res 27: 77–90
Jacob H, Sonntag C (1991) An 8-year record of the seasonal variation of ^2H and ^{18}O in atmospheric water vapour and precipitation of Heidelberg, Germany. Tellus 43B:291–300
Kakiuchi M, Niki T, Okutsu K (1987) Temperature dependence of hydrogen isotope fractionation in aqueous NaCl solutions. Geochem Soc Jpn, Abstr P, p 33 (in Japanese)
Katz A, Kolodny Y, Nissenbaum A (1977) Geochemical evolution of Pleistocene Lake Lissan – Dead Sea system. Geochim Cosmochim Acta 41:1609–1626
Krabbenhoft DP, Bowser CJ, Anderson MP, Valley J (1990) Estimating groundwater exchange with lakes. 1. The stable isotope mass balance method. Water Resour Res 26:2445–2453
Langbein WB (1961) Salinity and hydrology of closed lakes. USGS PP #412, p 20
Lemeille E, Letolle R, Meliere F, Olive P (1983) Isotope and other physico-chemical parameters of palaeolake carbonates: tools for climatic reconstruction. In: Paleoclimates and paleowaters, IAEA, Vienna, pp 135–150
Lerman A (1971) Time to chemical steady states in lakes and oceans. Adv Chem Ser 106:30–76
Levy Y (1977) The origin and evolution of different types of brines in coastal sabkhas, northern Sinai. J Sedim Petrol 47:451–462
Lewis S (1979) Environmental isotope balance of Lake Kinneret as a tool in evaporation rate estimates. In: Isotopes in lake studies, IAEA, Vienna, pp 33–65
Lister GS, Kelts K, Zao CK, Yu JQ, Niessen F (1991) Lake Quinqhai, China: closed basin lake levels and the oxygen isotope record for ostracoda since the late Pleistocene. Palaeogeogra-Climatol-Ecol 84: 141–162
Majoube M (1971) Fractionement en oxygene-18 et deuterium entre l'eau et sa vapeur. J Chim Phys 68:1423–1436
Martinelli LA, Victoria RL, Matsui E et al. (1989) The use of oxygen isotopic composition to study water dynamics in Amazon floodplain lakes. In: Isotope hydrology investigations in Latin America, IAEA, Vienna, Tecdoc-502, pp 91–101
McGrath R, Krabbenhoft D, Bowser CJ, Gat JR (1989) Stable isotopes in northern Wisconsin lakes: determination of the groundwater component of the lake hydrologic budgets. AWRA symp on the 1988 Drought and global climatic changes: effect on Wisconsin water resources, Abstr Program, p 46
Merlivat L (1970) Quantitative aspects of the study of water balance in lakes using the deuterium and oxygen-18 concentration in the water. In: Isotope hydrology 1970, IAEA, Vienna, pp 89–107
Merlivat L, Coantic M (1975) Study of mass transfer at the air–water interface by an isotopic method. JGR 80:3455–3464
Moser H, Rauert W (1980) Isotopenmethoden in der Hydrologie. Gebr Borntraeger, Stuttgart, pp 116–138
Neev D, Emergy KO (1967) The Dead Sea: depositional processes and environments of evaporites. Geol Surv Isr Bull 41:147
Nissenbaum A (1969) Studies in the geochemistry of the Jordan River–Dead Sea system. PhD Thesis, UCLA, 288 pp
Oren OM (1962) Physical and chemical characteristics of Lake Tiberias. Bull Res Counc Isr 11G:1–33
Payne BR (1981) Practical applications of stable isotopes to hydrological problems. Chapter 13. In: Gat JR, Gonfiantini R (eds) Stable isotope hydrology, IAEA Tech Rep Ser 210:303–334
Pearson FJ, Coplen TB (1978) Stable isotope studies of lakes. In: Lerman A (ed) Lakes: chemistry, geology, physics. Springer, Berlin Heidelberg New York, pp 325–339
Ragotskie RA, Bratnick M (1965) Infrared temperature pattern on Lake Superior and inferred vertical motions. Publ #13, Great Lakes Res Div, Univ of Michigan, pp 349–357
Ragotzkie RA, Friedman I (1965) Low deuterium content of Lake Vanda, Antarctica. Science 148: 1226–1227
Rankama K (1954) Isotope geology. Pergamon Press London, 477 pp
Salati EA, Dal'ollio E, Matsui E, Gat JR (1979) Recycling of water in the Amazon basin: an isotopic study. Water Resourc Res 15:1250–1258
Siegenthaler U (1975) Report to the Swiss National Fund, Univ Bern
Sofer Z, Gat JR (1972) Activities and concentrations of oxygen-18 in concentrated aqueous salt solutions; analytical and geophysical implications. EPSL 15: 232–238
Sofer Z, Gat JR (1975) The isotope composition of evaporating brines: effect on the isotopic activity ratio in saline solutions. EPSL 80:179–186
Spencer RJ et al. (1984) Great Salt Lake and precursors, Utah: the last 30000 years. Contrib Miner Petrol 86:321–334
Steinhorn I, Assaf G, Gat JR et al. (1979) The Dead Sea: deepening of the mixolimnion signifies the

overture to overturn of the water column. Science 206:55–57

Stewart MK, Friedman I (1975) Deuterium fractionation between aqueous salt solutions and water vapour. JGR 80:3812–3818

Stichler W, Moser H (1979) An example of exchange between lake and groundwater. In: Isotopes in lake studies, IAEA, Vienna, pp 115–120

Stiller M, Carmi I, Munnich KO (1975) Water transport through Lake Kinneret sediments traced by tritium. EPSL 25:297–304

Stiller M, Kanshansky P, Carmi I (1983) Recent climate changes recorded by the salinity of pore waters in the Dead Sea sediments. Hydrobiologia 103:75–79

Stuiver M (1970) Oxygen and carbon isotope ratios of freshwater carbonates as climatic indicators. JGR 75:5247–5257

Talbot MR (1990) A review of the paleohydrological interpretation of carbon and oxygen isotopic ratios in primary lacustrine carbonates. Isot Geosci 11: 261–280

Trewartha GT (1961) The earth's problem climates. Univ of Wisconsin Press, p 334

Truesdell AH (1974) Oxygen isotope activities and concentrations in aqueous salt solution at elevated temperatures: consequences for isotopic geochemistry. EPSL 23:387–396

Tzur Y (1971) Isotope effects in the evaporation of water into air. PhD Thesis, Feinberg Graduate School, The Weizmann Institute of Science, p 165

Welhan JA, Fritz P (1977) Evaporation pan isotopic behaviour as an index for isotopic evaporation conditions. Geochim Cosmochim Acta 41:682–686

Yurtsever Y, Gat JR (1981) Atmospheric waters. In: Gat JR, Gonfiantini R (eds) Stable isotope hydrology: deuterium and oxygen-18 in the water cycle, IAEA, Tech Rep Ser 210:103–142

Zimmermann U, Ehhalt D (1970) The use of stable isotopes in the study of the water balance of Lake Neusiedl Austria: investigation of the reliability of the stable isotope method. In: Isotope hydrology 1970, IAEA, Vienna, pp 129–138

Zimmermann U, Baumann U, Imevbore AMA, Henderson F (1976) Study of the mixing pattern of Lake Kainji using stable isotopes. Catena 3: 63–76

Zuber A (1983) On the environmental isotope method for determining the water balance components of some lakes. J Hydrol 61:427

6 Exchange of Chemicals Between the Atmosphere and Lakes

P. VLAHOS[1], D. MACKAY[1], S.J. EISENREICH[2], and K.C. HORNBUCKLE[2]

1 Introduction

The exchange of chemical substances between the atmosphere and lakes can play an important role in determining abiotic and biotic conditions and levels of contamination. Natural substances such as carbon dioxide, oxygen, hydrogen sulfide, and methane migrate between air and water in pristine conditions, whereas contaminants such as polychlorinated biphenyls (PCBs), polycylic aromatic hydrocarbons (PAHs), and lead may enter lakes primarily from the atmosphere. For other contaminants, such as volatile organic chemicals, evaporation is the dominant route of loss from lakes. There is often appreciable cycling of chemicals between air and water with the magnitude and direction of net movement changing with season. It is now recognized that concentrations of chemicals prevailing in even large lakes, such as Lake Superior, can be influenced or even controlled by the presence of these chemicals in the atmosphere (Eisenreich 1987).

Perhaps the most convincing demonstration of the role of the atmosphere is the case of the remote Siskiwit Lake in Isle Royale in Lake Superior (Swain 1978). The water, sediment, and fish of this pristine lake have been observed to contain appreciable quantities of organochlorine compounds, which can only have reached the lake by atmospheric transport. Remote Arctic lakes have shown similar behavior.

In this chapter we describe the phenomena involved in air–water exchange and suggest approaches to quantifying rates of transfer. Whereas experimental measurements can determine the concentrations in air and water, rates of transfer cannot be measured directly, but can only be inferred by calculations. The magnitude and even the direction of transfer may not be obvious. We first address this issue by quantifying chemical equilibrium between air and water in the form of partition coefficients or the Henry's Law Constant, because it is the departure from equilibrium that drives the processes of evaporation and absorption. The rates of these diffusive processes are then considered, first by briefly reviewing the fundamentals of diffusion, then describing the two-resistance approach for estimating air–water transfer rates. Key determinants of exchange rates are mass-transfer coefficients, which essentially control the velocity of diffusion. Methods of estimating values of these coefficients are described. The "availability" of chemicals in dissolved form in water, and gaseous form in air, is also an important consideration that is addressed, and is essentially an assessment of the extent of sorption. The mechanisms and rates of nondiffusive processes of wet and dry deposition are then described. It is by these processes that chemicals that are sorbed to aerosol particles are conveyed to the water by dustfall or rainfall. This is the dominant mechanism of transfer for involatile substances, such as lead, but it is also important for "semivolatile" substances such as PCBs.

The overall picture of these air–water exchange processes, as illustrated in Fig. 1, can thus be very complex with several complementary and competing processes in effect. To assist the reader to appreciate the nature of these processes a specimen calculation is provided for a PCB congener in which the rates of all processes are deduced from specified concentrations in air and water.

Finally, case studies are presented for specific lakes in which the role of air–water exchange has been quantified.

[1] Department of Chemical Engineering and Applied Chemistry, University of Toronto, 200 College St., Toronto, Ontario, M5S 1A4, Canada
[2] Gray Freshwater Institute and Department of Civil Engineering, University of Minnesota, P.O. Box 100, Navarre, MN 55392, USA

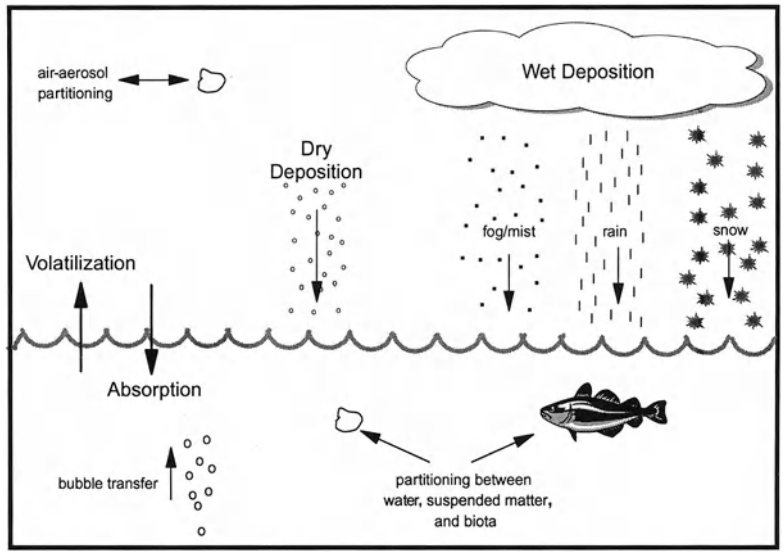


Fig. 1. Air–water exchange processes

2 Air–Water Partitioning Equilibria

Equilibrium between air and water is usually expressed as a dimensionless air–water partition coefficient (K_{AW}), or by a Henry's Law constant H (Pa m^3/mol), which relates equilibrium concentrations of a chemical in the two phases as follows:

$$K_{AW} = C_A/C_W \quad \text{or} \quad P_A = HC_W. \tag{1}$$

Here, C is concentration (mol/m^3), P is partial pressure (Pa), and subscripts A and W refer to air and water phases. Note that C is the concentration of the dissolved chemical and does not include any sorbed material. Other definitions of H are used, for example, to express concentration as a mole fraction.

The relationship between air-phase gaseous concentration and partial pressure can be determined using the ideal gas law ($C_A = n/V = P_A/RT$), where n is the number of moles, V is volume (m^3), R is the gas constant [8.314 Pam^3/(molK)], and T is temperature (K). The equilibrium partition coefficient K_{AW} can thus be shown to be H/RT. If these equations are applied to saturation conditions (designated superscript S) at which a pure chemical phase can coexist with air and water, then

$$K_{AW} = C_A^S/C_W^S = P_A^S/(RTC_W^S) \tag{2}$$

where P_A^S is the chemical's saturation vapor pressure (Pa) in air and C_W^S is its saturation solubility in water (mol/m^3). It follows that H can often be deduced from the vapor pressure and solubility in water as P_A^S/C_W^S. For some chemicals, such as ethanol, no solubility exists, and H or K_{AW} must be determined by direct experimental measurement of C_A and C_W.

It should be noted that when applying physical chemical data, such as H, P_A^S, or C_W^S from handbooks to real lakes, these properties are dependent on temperature, and appropriate corrections must be made. The dependence of H on temperature can be estimated from the expression

$$\ln(H) = A - \Delta h/RT$$
$$\text{or } \ln(H_1/H_2) = -(\Delta h/R)(1/T_1 - 1/T_2), \tag{3}$$

where A is a proportionality constant and Δh is the enthalpy of evaporation (kJ/mol) from solution, and subscripts 1 and 2 refer to two different temperatures. For example, for PCBs Δh is approximately 50 kJ/mol (Hulsher 1992). A general rule is that H doubles for every 10 °C increase in temperature (Mackay and Shiu 1981). For example, in the Great Lakes during the month of August, surface waters reach their highest temperatures; this elevates the Henry's Law constant, facilitating water-to-air exchange (McConnell et al. 1993).

Although lower H values are expected for less volatile chemicals, this is not always the case. For some substances, such as PCBs, although the

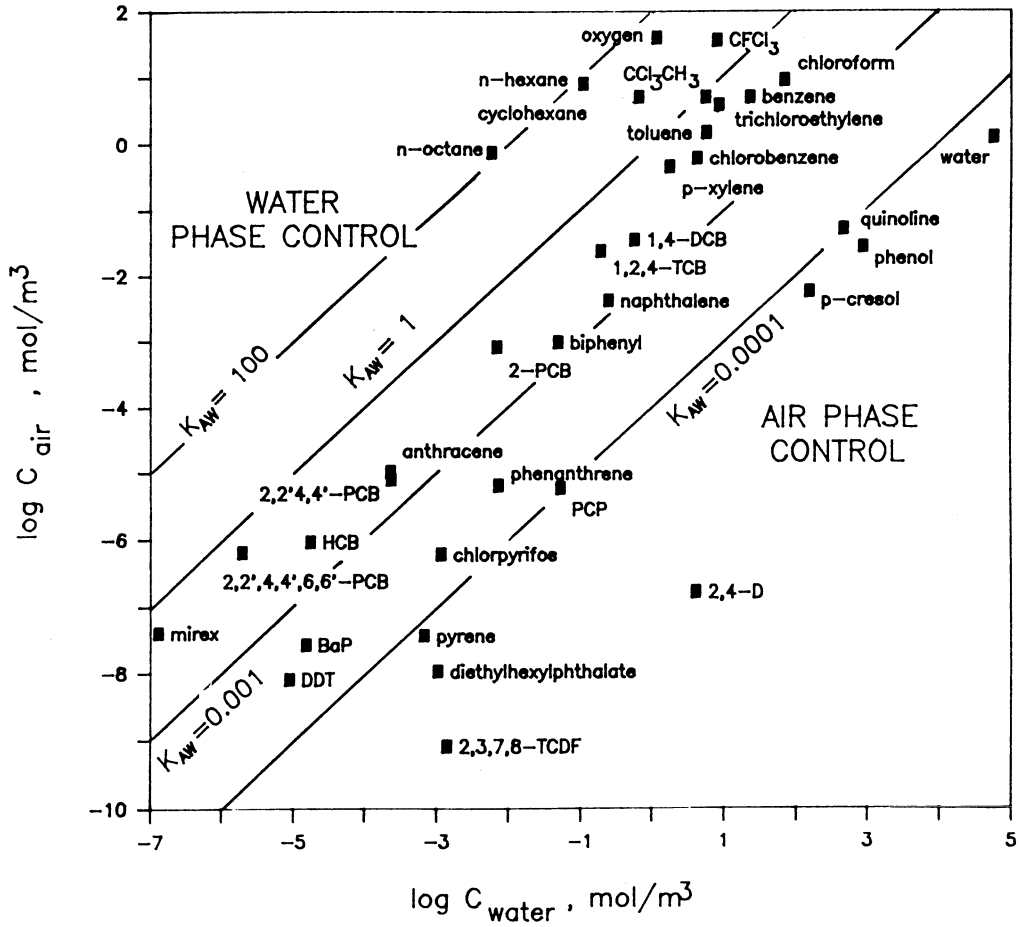


Fig. 2. Plot of log solubility in air (i.e., vapor pressure/RT) vs log solubility in water for selected chemicals. Chemicals of equal H or K_{AW} lie on the same 45° angle. (Reproduced from Mackay 1991, with permission)

vapor pressure is low, the solubility in water is also low (i.e., they are hydrophobic), and the ratio of these quantities can be large, implying significant potential for volatilization (appreciable values of H). Homologous series of chemicals tend to exhibit similar values of K_{AW} and H, even when P^S and C^S vary by orders of magnitude as shown in Fig. 2. For more detailed accounts of air–water partition coefficients, as well as their measurement and correlation, the reader is referred to reports by Shiu and Mackay (1986), Meylan and Howard (1991), Suntio et al. (1988), and Mackay (1991).

3 Diffusion Between Water and Air

Diffusion is a passive process that occurs within and between the air and water phases. Unlike unidirectional atmospheric deposition, diffusion is reversible and contributes to cycling between these phases. As shown in Fig. 3, a molecule moving from water to air must diffuse to the air/water interfacial region through the bulk water, and then through a near-stagnant water film, the thickness of which depends on environmental factors such as turbulence and wind speed. It must then cross the interface and pass through an air-boundary layer into the bulk air region. These boundary layers present the greatest resistance to chemical passage and involve the slowest or rate-limiting steps to transfer.

The rate of transfer, or *flux*, by diffusion in air or water is described by Fick's First Law, which, in its integrated form states that the flux N (mol/h) is inversely proportional to the distance or path length y (m), through which it must diffuse, directly proportional to the area through which it is diffusing, A (m^2), and proportional to the difference in the dissolved concentration ($C_1 - C_2$)

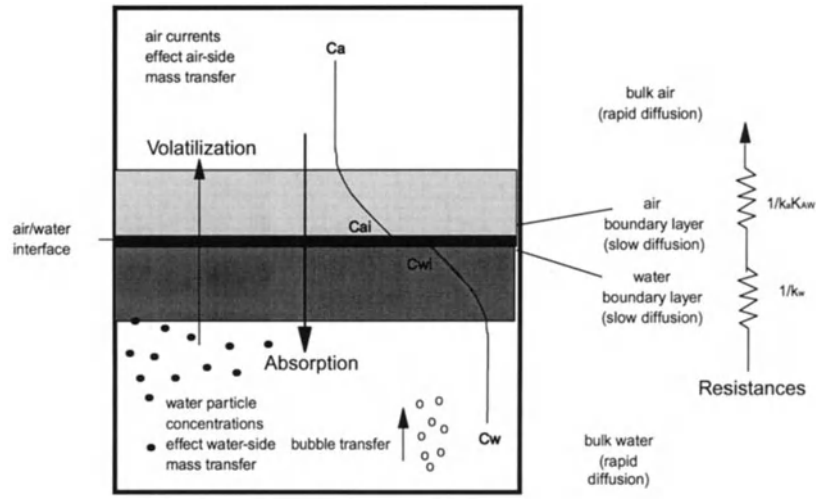


Fig. 3. Mass transfer between water and air illustrating the two-resistance concept

(mol/m^3) applying over the path length. The constant of proportionality is the diffusion coefficient or diffusivity D (m^2/h):

$$N = AD(C_1 - C_2)/y. \quad (4)$$

It should be emphasized here that the diffusing molecules are merely undergoing random motion in all directions, but in the presence of a concentration gradient there will be net transfer in one direction, namely, from high to low concentration. The diffusion coefficients in air and water can be determined from correlations. They depend on the properties of the diffusing species, the phases through which it is diffusing, temperature, and pressure. Detailed derivations and correlations are available in texts on the properties of fluids (e.g., Reid et al. 1987).

Because there may be doubt about the magnitude of D and y, it is convenient to define the group D/y as a single parameter, the mass-transfer coefficient k (m/h), which can be determined experimentally by measuring N, A, and $(C_1 - C_2)$ under controlled conditions. The mass-transfer coefficient has units of velocity, and is therefore an actual velocity of transport or a diffusion velocity. Equation (4) now becomes

$$N = k_i A(C_1 - C_2). \quad (5)$$

4 Volatilization and Absorption: Two-Resistance Approach

As shown in Fig. 3, the chemical diffuses across two boundary layers in series, and thus experiences two diffusive resistances. The flux of chemicals during evaporation through the water-boundary layer to the interface can be expressed as

$$N = k_W A(C_W - C_{Wi}), \quad (6)$$

where C_W is the bulk air concentration, C_{Wi} is the water side interfacial concentration, and k_W is the water-side mass-transfer coefficient. For air the flux is similarly

$$N = k_A A(C_{Ai} - C_A). \quad (7)$$

At steady state both fluxes must be equal, because there is no accumulation of chemicals at the interface. We further assume that C_{Ai} and C_{Wi} are in such intimate contact that they are related by the air–water partition coefficient:

$$C_{Ai}/C_{Wi} = K_{AW} \quad (8)$$

Substitution of this expression into Eqs. (6) and (7) and elimination of C_{Ai} and C_{Wi} gives, after some rearrangement,

$$\begin{aligned} N &= k_{OW} A(C_W - C_A/K_{AW}) \\ &= k_{OA} A(C_W K_{AW} - C_A), \end{aligned} \quad (9)$$

where

$$\begin{aligned} 1/k_{OW} &= 1/k_W + 1/(k_A K_{AW}) \\ \text{and } 1/k_{OA} &= 1/k_A + K_{AW}/k_W \\ &= K_{AW}/k_{OW}. \end{aligned} \quad (10)$$

Here, k_{OW} is the *overall water-side mass-transfer coefficient*. Similarly, k_{OA} is the *overall air-side mass-transfer coefficient*. The equations in k_{OW} and k_{OA} are ultimately identical algebraically.

The term $1/k_{OW}$ can be viewed as the total resistance to transfer, which is the sum of the water resistance ($1/k_W$) and air resistance ($1/k_A K_{AW}$). The analogy to Ohm's Law is obvious. The air resistance is adjusted by the air–water partition coefficient, which dictates the absolute concentration in each phase at equilibrium. When K_{AW} is large, the concentration of the diffusing species in the air is large relative to the concentration in water. Diffusion in the air is thus facilitated; the air-resistance term is small; thus, the water resistance dominates k_{OW}. Such systems are said to be *water-phase-resistance controlled*. When the K_{AW} term is small, the concentration in the water is greater, the resistance in air becomes the limiting factor, and the system is *air-phase-resistance controlled*. Typically, k_A is approximately 100 times larger than k_W, because of the greater diffusivity in air; thus, when K_{AW} is approximately 0.01, or H is approximately 25 Pa m^3/mol, the resistances are approximately equal. A consequence of this two-resistance-in-series behavior is that one resistance is often insignificant and there is little need to know the corresponding mass-transfer coefficient accurately. Although the mass-transfer coefficient k can be regarded as a ratio of diffusivity D to diffusion path length, the reality is more complex. The dependence of k on D is rarely linear, k usually being proportional to D raised to a power ranging from 0.5 to 0.8. The reason for this is that diffusive conditions are partly nonsteady state is nature as eddies of water are exposed to transfer at the interface for periods of seconds giving rise to penetration transfer in which Fick's Second Law, rather than Fick's First Law, applies. It is somewhat misleading to report values of y deduced as D/k, because these path lengths are hypothetical, rather than real.

5 Factors Affecting Mass-Transfer Coefficients

Air-water mass-transfer coefficients depend on a number of factors including molecular properties, temperature, and boundary-layer conditions, which vary with wind conditions and the turbulence of the water surface as induced by current. Several studies of transfer dependence on wind speed have been conducted in tanks with a more limited number in lakes. Wind speeds over bodies of water up to 3 m/s result in near-laminar conditions, in transitional conditions between 3 and 6 m/s, and in turbulent conditions above 6 m/s. Under near-laminar conditions a near-stagnant layer of air exists over the air–water interface, which is on the order of 1 mm in thickness, through which diffusing molecules must pass. The mass-transfer coefficients k_A and k_W are then on the order of 3 and 0.01 m/h, respectively. As wind speeds increase the boundary layer thins and conditions become turbulent. The result is a nonuniform air–water interface that exhibits waves and greater drag forces caused by the friction of the moving wind over the water. The drag force can be related to the air-side friction velocity, which, in turn, determines the magnitude of both mass-transfer coefficients (Mackay and Yeun 1983). Typical ranges at higher wind speeds are 10–30 m/h for k_A and 0.02–0.2 m/h for k_W.

Several correlations describing mass-transfer dependence on wind velocity (U, m/s) have been proposed. Mackay and Yeun (1983) have quantified this dependence for both air and water:

$$k_W(\text{m/s}) = 1.0 \times 10^{-6} + 3.41 \times 10^{-3} U^* Sc_W^{-0.5} \quad (U > 9\,\text{m/s}) \quad (11a)$$

$$= 1.0 \times 10^{-6} + 1.44 \times 10^{-2} U^{*2.2} Sc_W^{-0.5} \quad (U < 9\,\text{m/s}) \quad (11b)$$

$$k_A(\text{m/s}) = 1.0 \times 10^{-3} + 4.62 \times 10^{-2} U^* Sc_A^{-0.67}, \quad (12)$$

where Sc is the dimensionless Schmidt number, which is the ratio of viscosity/(density × diffusivity) and is commonly in the range of 0.5–2.0 for gases (Sc_A) and 500–2000 for water (Sc_W); U* is the friction velocity caused by the wind and can be related to the 10-m wind speed U by

$$U^* = 0.01U(6.1 + 0.63U)^{0.5}. \quad (13)$$

Schwarzenbach et al. (1993) suggest the following simpler correlations for air and water mass-transfer coefficients as a function of wind speed U (m/s):

$$k_A\,(\text{cm/s}) = 0.3 + 0.2U \quad (14)$$

$$k_W\,(\text{cm/s}) = 4 \times 10^{-4} + 4 \times 10^{-5} U^2. \quad (15)$$

Under very turbulent conditions, such as breaking waves, waterfalls, or cascades when air bubbles are propelled into the water column, or when water spray is generated, the area of transfer becomes much larger and uncertain, and Eq. (9) can no longer be applied.

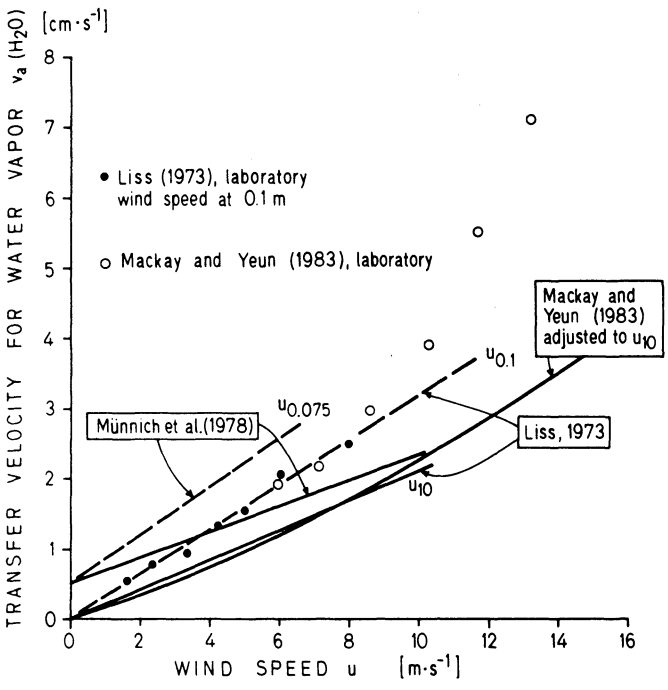


Fig. 4. Correlations showing the dependence of air-phase mass-transfer coefficients k_A on wind speed. (Reproduced from Schwarzenbach et al. 1993, with permission)

Figures 4 and 5 illustrate the dependence of k_A and k_W on wind speed as expressed by several correlations. Temperatures and pressures also affect the magnitude of k_A and k_W. The relationship between these variables can be expressed by extrapolation of the effects of temperature and pressure on the diffusion coefficient:

$$k_{A2} \propto k_{A1}(P_1/P_2)(T_2/T_1)^{3/2}. \quad (16)$$

6 Partitioning of Chemical to Particulate Matter in Air and Water

Not all the chemical in the air and water phases is available to diffuse, adsorb, or evaporate, because some may be sorbed to particles. Essentially, such sorbed chemical does not contribute to the concentrations employed in the Fick's Law equations. It is thus essential to measure or calculate this extent of sorption.

6.1 Air

The extent of sorption onto airborne particulate matter or aerosols can be calculated from measured concentrations of chemicals in the air in vapor form C_V and in the particulate phases C_P both in ng/(m^3 air). It is common to combine these quantities with the total suspended particulate concentration TSP ng/m^3 as the group C_VTSP/C_P. This group is essentially a partition coefficient between gaseous phase and particles. As illustrated later, Mackay et al. (1986) have correlated the partition coefficient directly with the chemical's liquid or subcooled liquid vapor pressure. The extent of sorption, and thus the relative quantities of chemicals associated with particles and in the vapor phase, depends on several properties such as vapor pressure, temperature, relative humidity, and the nature of the particles (Yamasaki et al. 1982; Bildeman and Foreman 1986; Pankow et al. 1993). Metals (with the exception of Hg) in the atmosphere are completely sorbed to particulate matter. As temperature decreases and molecular weight increases the chemical becomes increasingly sorbed.

6.2 Water

Partitioning between chemicals and dissolved particulate matter in lakes is a more complex phenomenon, because of the variety of sorbents present in the water column. For hydrophobic chemicals partitioning depends primarily on the organic carbon content of the particulate matter. Chemicals tend to sorb to these particles to an extent inversely proportional to their solubility in

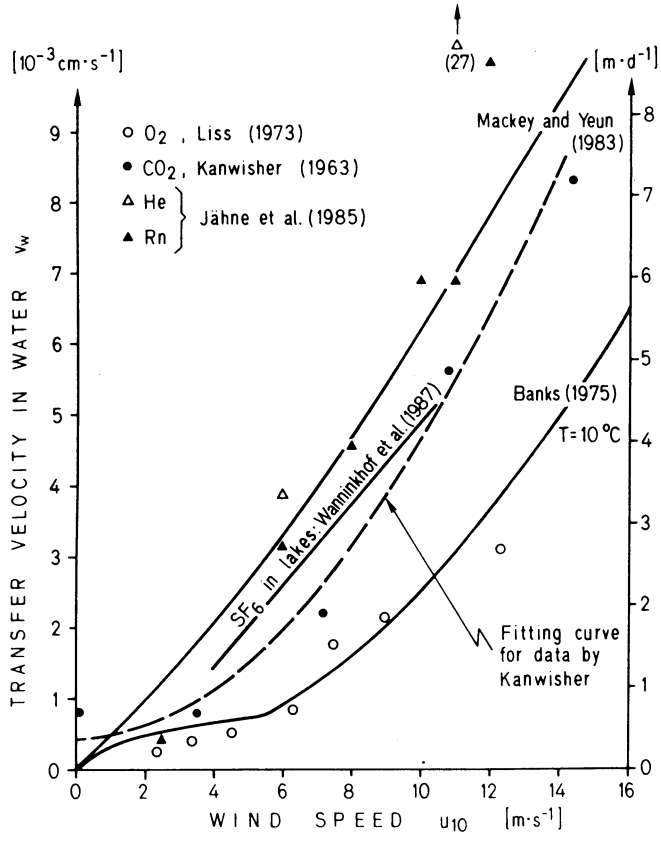


Fig. 5. Correlations showing the dependence of water-phase mass-transfer coefficients k_W on wind speed. (Reproduced from Schwarzenbach et al. 1993, with permission)

water. The most common approach for expressing the hydrophobic nature of a chemical, and thus its sorption to particles from solution, is its octanol–water partition coefficient K_{OW}. This quantity is inversely related to water solubility, and its use in this context implies that a chemical will partition to the organic carbon in particles to a similar extent to which it dissolves in octanol (DiToro 1985). For several chemicals the "equivalent" amount of octanol is obtained by correcting the organic carbon content by a factor of 0.2 to 0.8 (Karickhoff 1981), with 0.4 being a typical value. The value depends on the chemical in question and the nature of the organic matter.

Among the most abundant particulate matter in surface waters are photosynthetic algae, which exist within the first 20 m of the water column where there is sufficient light penetration. There is substantial sorption of hydrophobic contaminants onto this algal matter, which creates a distinct pathway for chemical transport by sedimentation when the algae die and settle. Chemical uptake occurs in a rapid initial adsorption followed by slower diffusion across the cell membrane. Correlations have been sought between the cell-water and the octanol-water partition coefficients, and with the organic carbon content of the algae, but these appear to be nonlinear, and the mechanism is not fully understood.

7 Atmospheric Deposition Processes

7.1 Dry Deposition

Particles or aerosols in the atmosphere result from naturally occuring dust and particulate matter from industrial and other emissions. These particles, and any chemicals sorbed to them, migrate, fall, or diffuse to the lake surface and are captured by water. This provides an important pathway for chemical transport from air to lake.

The amount of chemical delivered to a lake of area A (m^2) can be determined by the product of the dry particle settling rate U_D (m/h), the concentration of chemical on the particles C_P (ng/m^3air), and area A:

$$\text{dry deposition rate of chemical} = D_D\,(\text{ng/h}) = U_D C_P A. \quad (17)$$

Deposition velocities are on the order of 0.3 cm/s or 10 m/h, and particulate concentrations are

usually in the range of 10–100 $\mu g/m^3$. The velocity of depositing particulate matter varies as a function of particulate sizes and shapes, the seasonal properties of the air (density, temperature, etc.), and the stability conditions of the atmosphere; thus, U_D represents an average value.

7.2 Wet Deposition

Wet deposition occurs in the form of rain, snow, and finer droplets of mist. As the droplet of water or the snowflake falls, it scavenges particulate matter and associated chemicals. It has been observed that during its fall a droplet can scavenge chemicals from as much as 200 000 times its volume of air. This quantity, called the scavenging ratio Q, varies depending on the nature of the water droplet, its exposure time in the atmosphere, and its ability to scavenge particles.

Contaminant delivery to a lake surface by wet deposition can be calculated from the rain rate R (m/h, but normally expressed in m/year) per unit area A (m^2), the concentration of the contaminant in the air in particulate form (C_P, ng/m^3), and the dimensionless scavenging ratio Q. The concentration in collected rainfall (C_R, ng/m^3) can also be measured directly by analyzing collected precipitation:

$$\text{chemical wet deposition} = D_W\,(ng/h) = QRAC_P = RAC_R. \quad (18)$$

A "wash-out ratio" is also defined as the ratio of total concentration of contaminant in rain (C_R) to that in air [$(ng/m^3)/(ng/m^3)$]. It may also be expressed in terms of mass ratios [(ng/kg)/(ng/kg)], which lowers the value by a factor of approximately 820, the density ratio of water to air. Snow is another form of wet deposition for which scavenging or washout ratios are less established.

In addition to the capture of particles, a falling water droplet may dissolve chemicals and approach equilibrium with the air. In such cases their chemical concentrations can be estimated from the air-water partition coefficient K_{AW} and the air concentration C_A as C_A/K_{AW}. This usually represents only a small fraction of the concentration in rainfall, most chemicals being particle-associated. The exceptions are chemicals of low K_{AW} or high water solubilities such as alcohols:

$$\text{chemical dissolution in rain} = D_R\,(ng/h) = RAC_A/K_{AW}. \quad (19)$$

8 Specimen Calculation

The nature and magnitudes of these processes are best appreciated by calculating the air–water exchange behavior of a chemical such as PCB congener 169, which is a coplanar hexachlorobiphenyl. It is considered one of the more toxic congeners and is highly bioaccumulative. Its estimated properties at 15 °C are given in Table 1.

We perform calculations for a fictitious lake with a surface area of 10 ha or 100 000 m^2 at a temperature of 15 °C (288 K). The total concentration of PCB in air is assumed to be 0.1 ng/m^3, whereas in water it is 0.5 ng/l. The data in Table 1 are used to deduce the rates of exchange by evaporation, absorption, and wet and dry deposition.

8.1 Step 1: Physicochemical Properties

The first step is to calculate H and K_{AW} using Eqs. (3) and (4). The water solubility is 500×10^{-6} g/m^3 or 1.39×10^{-6} mol/m^3.

$$H = 25 \times 10^{-6}/1.39 \times 10^{-6} = 18\,Pa\,m^3/mol$$

$$K_{AW} = H/RT = (18)/(8.314 \times 288) = 0.0075$$

At equilibrium the concentration of the chemical in water will be 133 times ($1/K_{AW}$) that in the air. Such values are characteristic of the PCB homologous series.

8.2 Step 2: Mass-Transfer Coefficients

From correlations for wind speed and chemical diffusivity it could be estimated that k_W is 0.05 m/h and k_A is 5 m/h. We then use Eq. (11) to determine the overall mass-transfer coefficient k_{OW}: $k_{OW} = (1/k_W + 1/(k_A K_{AW}))^{-1} = (20 + 26.7)^{-1} = 0.0215$ m/h.

The resistance in the water film is thus 20 h/m, whereas that in air is 26.7 h/m, a total of 46.7 h/m. The resistance in the air is 57% of the total; thus, both k_W and k_A must be known accurately.

Table 1. Estimated properties of PCB congener 169 at a temperature of 15 °C (Mackay et al. 1992)

Molecular weight (g/mol)	361
Melting point (°C)	202
Solid vapor pressure (Pa)	25×10^{-6}
Aqueous solubility of the solid (g/m^3)	5×10^{-4}
Log K_{ow}	7.0

8.3 Step 3: Sorption in Air and Water

8.3.1 Air

It is necessary to estimate the fraction of chemical that is dissolved in water or air (i.e., in gaseous form) as distinct from that associated with particles. This is best done experimentally by measuring the total concentration and the concentration after filtering. If only the total concentration is known, the partition coefficient may be estimated as described previously and the dissolved and sorbed concentrations deduced.

Using the correlation suggested by Mackay et al. (1986), the dimensionless aerosol–air partition coefficient is deduced from the subcooled liquid vapor pressure P_L^S. In this case the fugacity ratio or ratio of solid (P_S^S) to liquid (P_L^S) vapor pressures is 0.0122 as estimated from the melting point using the expression

$$P_S^S/P_L^S = \exp[-6.79(T_M/T - 1)] = 0.0122,$$

where T_M is the melting point (475 K) and T is 288 K. The hypothetical liquid vapor pressure is thus 0.00205 Pa and the partition coefficient K_{QA} is

$$K_{QA} = 6 \times 10^6/P_L^S$$
$$= 6 \times 10^6/0.00205 = 2.93 \times 10^9.$$

Assuming an aerosol concentration of $30\,\mu g/m^3$ and a density of $2.0\,g/cm^3$ gives a volume fraction of aerosol of 15×10^{-12}. The fraction in gaseous form is thus

$$1/(1 + K_{QA} \times 15 \times 10^{-12})$$
$$= 1/(1 + 0.044) = 0.958,$$

and the remaining 4.2% is sorbed to aerosols. The gaseous concentration C_V is thus 95.8% of $0.1\,ng/m^3$ or $0.0958\,ng/m^3$. Alternatively, correlation of the group $C_V TSP/C_P$ could have yielded $684\,\mu g/m^3$, from which, inserting $30\,\mu g/m^3$ for TSP (total suspended particles) gives, a ratio of C_V/C_P of 22.8, i.e., 0.0958/0.0042. The concentration in aerosol particles is $K_{QA}C_V$ or $0.28\,g/m^3$ of particulate, which is very much larger than the concentration in air.

8.3.2 Water

Similarly, from the known total concentration in water we can deduce the fractions dissolved and associated with particles. The suspended particle concentration is taken to be $15\,g/m^3$. The sorbed contaminant concentration can be estimated using the organic carbon partition coefficient and an assumed 20% organic carbon in the particles

$$K_{OC} = 0.41K_{OW} = 0.41 \times 10^7;$$

thus,

$$K_P = 0.2K_{OC} = 0.82 \times 10^6\ (L/kg).$$

The fraction in solution can then be deduced from K_P and the suspended particle concentration C_S (kg/L) as

$$1/(1 + C_S K_P) = 1/(1 + 15 \times 10^{-6} \times 0.82 \times 10^6)$$
$$= 1/(1 + 12.3) = 0.075.$$

The dissolved concentration is thus 7.5% of 0.5 ng/l, i.e., 0.0375 ng/l, whereas the sorbed concentration is 0.4625 ng/l.

The actual extent of sorption may differ from region to region within the lake and between lakes depending on the nature of the particles and their organic carbon content.

8.4 Step 4: Equilibrium Status

The concentration of PCB in air at equilibrium with the dissolved concentrations of 0.0375 ng/L is $K_{AW}C_W$ or 0.00028 ng/L or $0.28\,ng/m^3$. This exceeds the actual gaseous concentration of $0.0958\,ng/m^3$ by a factor of 2.9. The system is thus not at equilibrium, the water is *supersaturated* with regard to the air, and there is a net diffusive flux or evaporation from water to air.

8.5 Step 5: Volatilization and Deposition Rates

The rate of net volatilization, i.e., the rate of volatilization V_L minus the rate of absorption A_B, can be calculated using Eq. (10):

$$V_L - A_B = k_{OW}A(C_W - C_A/K_{AW})$$
$$= 0.0215 \times 10^5 \times (0.0375 \times 10^{-6}$$
$$- 0.0958 \times 10^{-9}/0.0075)$$
$$= 53.2 \times 10^{-6}\,g/h = 0.466\,g/year.$$

This is actually the difference between the gross evaporation rate of $80.6\,\mu g/h$ or $0.706\,g/year$, and absorption of $27.4\,\mu g/h$ or $0.240\,g/year$. We also estimate the rates of deposition processes. Assuming a dry deposition velocity of 0.3 cm/s or 10.8 m/h, the rate of particle deposition using Eq. (11) is

$$10.8\,\text{m/h} \times 10^5\,\text{m}^2 \times 15 \times 10^{-12}\,\text{m}^3\,\text{particle/m}^3 \text{ air} = 16.2 \times 10^{-6}\,\text{m}^3\text{/h or } 0.142\,\text{m}^3\text{/year}.$$

Because the concentration on the particles is $0.28\,\text{g/m}^3$ the dry deposition rate D_D is

$$D_D = 0.142 \times 0.28 = 0.0397\,\text{g/year}.$$

Assuming a rain rate of 0.8 m/year and a scavenging coefficient of 200 000, the rate of wet deposition is

$$D_W = 200\,000 \times 0.8\,\text{m/year} \times 10^5\,\text{m}^2 \times 15 \times 10^{-12} \times 0.28\,\text{g/m}^3 = 0.0672\,\text{g/year}.$$

The total rate of transfer from air to water (dry and wet deposition and absorption) is thus 0.347 g/year, which is less than the gross evaporation rate of 0.706 g/year. We thus have a situation in which there is net water-to-air transfer or *net volatilization* of 0.359 g/year. The excess transfer from water to air is presumably accounted for by direct discharges of chemicals to the lake. A computer program that conducts a calculation such as the previous is included in the text by Mackay (1991).

9 Role of Air–Water Exchange in Lake Mass Balances

Having examined in detail the fluxes across the air–water interface, it is then possible to examine the larger picture of the mass balance over the entire lake. This places air–water exchange in perspective along with other processes such as reaction, sedimentation, and outflow, as well as with discharge rates from industrial, municipal, and other sources. In principle, the process rates can be combined to give the rate of change in mass of chemicals in the water of the lake (Mkg) as follows:

$$\begin{aligned} d(M)/dt &= \text{inputs} - \text{outputs} \\ &= (D_W + D_D + A_B + I + E) \\ &\quad - (V_L + R_X + O + S). \end{aligned} \tag{20}$$

Here, the inputs are rates of wet and dry deposition (D_W and D_D), absorption A, inflow to the lake I, and direct discharge E. The output processes include volatilization V_L and losses due to reaction R_X, outflow O, and the net sedimentation S.

The relative importance of all processes becomes clear. It is possible to solve this differential equation numerically or analytically to estimate the historical or future changes in mass of chemicals in the water, and hence concentrations in the water and its resident biota. A critically important quantity obtained from this analysis is the potential rate of recovery of the lake as a result of remedial measures to reduce inputs.

The remainder of this chapter is a series of case studies in which these principles are illustrated by considering whole-lake mass balances and specific cases of air–water exchange.

10 Case Studies

The role of air–water exchange of compounds such as the PCBs, PAHs, and HCHs (hexachlorocyclohexanes) in aquatic contaminant cycles has only recently been studied in a quantitative manner (e.g., Mackay 1979; McVeety and Hites 1988; Achman et al. 1993; McConnell et al. 1993). The strategies applied to air–water exchange include construction of chemical mass balances and calculation of fluxes based on simultaneously determined air and water concentrations and environmental parameters such as wind speed.

10.1 Mass Balance on Siskiwit Lake, Isle Royale

Hites and coworkers (McVeety and Hites 1988; Swackhamer et al. 1988) compiled mass balances for input and output of PAHs and PCBs in Siskiwit Lake, Isle Royale located in the central basin of remote Lake Superior. The location and uses of the lake ensure that chemical input is dominated by the atmosphere.

Measurement of rain and snow, atmospheric gas and aerosol, and water column and outflow concentrations on a seasonal basis, as well as surface-sediment concentrations, permit the calculation or assignment of all parameters of the mass balance Eq. (20), except for the dry deposition velocity U_D and the overall mass-transfer coefficient k_{OW}. Both parameters must be calculated from various correlations (e.g., Mackay and Yuen 1983; Schwarzenbach et al. 1993) or may be surmised from the previous mass-balance expression. By treating certain low molecular weight PAHs and PCBs that are known to exist only in the gas phase (i.e., C_P is negligible), the mass balance yields k_{OW} and air–water exchange fluxes. Considering those compounds known to

exist primarily in the particle phase (high molecular weight species) yields U_D and dry particle deposition fluxes. The overall liquid phase mass-transfer coefficients were estimated to be 0.1 and 0.18 m/day for PCBs and PAHs, respectively. These values are consistent with the approach given previously, and resistance is dominated by transfer across the liquid phase. The estimated annual average dry-deposition velocities were estimated to be 0.16 and 0.99 cm/s for PCBs and PAHs, respectively. The latter differences cannot be easily explained, unless uncertainties in the mass balance and/or real differences in atmospheric chemistry and speciation between the compounds are invoked. At this remote location it is surmised that dry-particle-deposition velocities closer to 0.2 cm/s for submicron aerosols are more likely.

The inputs and outputs for several individual PCBs and PAHs are given in Figs. 6 and 7. The PCB inputs to Siskiwit Lake were dominated by wet deposition in rain and snow with a minor contribution from dry-particle deposition. Outputs from the remote lake were dominated by volatilization, especially for the lower molecular weight congeners. Total PCBs lost by volatilization amounted to 8.5 $\mu g/m^2$ per year in contrast to 5.6 $\mu g/m^2$ per year for sedimentation, the other major loss process. For PAHs inputs were dominated by dry-particle deposition, with rain and snow contributing little to the total loading. Losses of PAHs from Siskiwit Lake were dominated by volatilization for the low molecular weight compounds, especially phenanthrene, fluorene, and pyrene, but represented only minor losses for higher PAHs. In this case the role of volatilization decreased with decreasing vapor pressure, a feature common to most recent studies. This is attributed to the increased sorption of the chemicals to the atmospheric aerosol and water particulate phases.

10.2 Mass Balance on Lake Superior

Another strategy to demonstrate the importance of volatilization compared with other input and loss processes on a whole-lake scale was employed

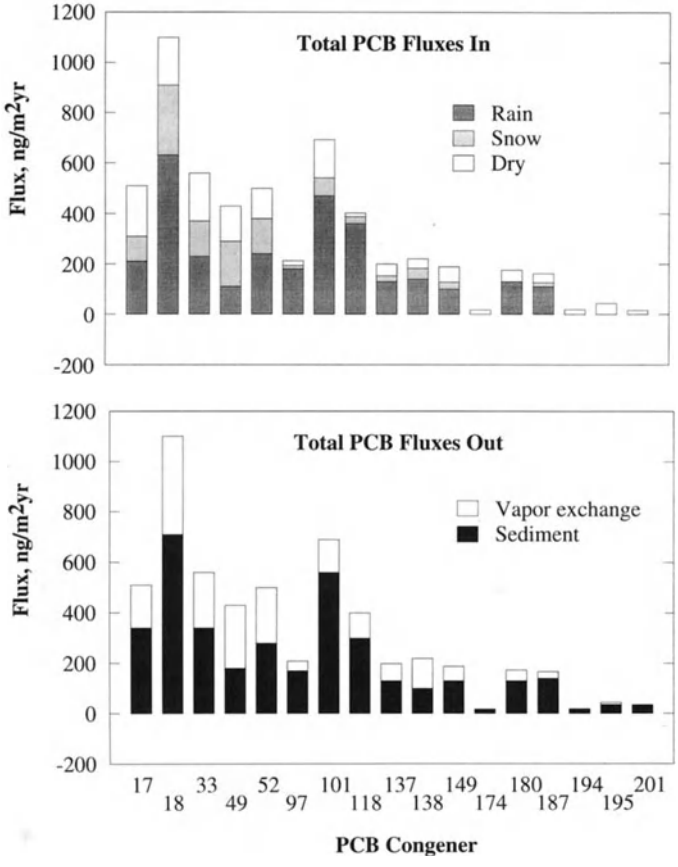


Fig. 6. Estimated fluxes of PCB congeners to and from Siskiwit Lake. Adapted from Swackhamer et al. (1988)

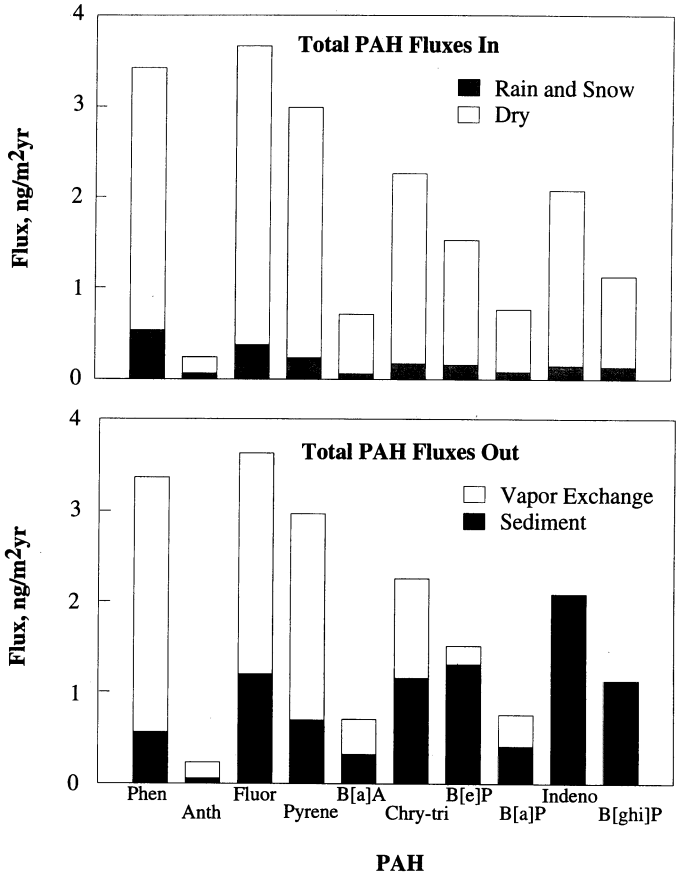


Fig. 7. Estimated fluxes of PAHs to Siskiwit Lake. Adapted from McVeety and Hites (1988)

by Jeremiason et al. (1994). They used the recorded decrease in PCB concentrations in the water column of Lake Superior from 1978–1992 to drive the mass balance of the system. Lake Superior is an atmospherically driven aquatic system, because this large lake has a relatively small basin area and receives more than 60% of its water input by direct precipitation on the lake surface. There are few sources of chemicals, other than atmospheric deposition and air–water exchange. The PCB concentrations in water decreased from ~2.4 ng/l in 1980 to 0.18 ng/l in 1992 corresponding to a loss of ~26 000 kg of PCBs with a first-order rate constant of 0.2/year. A mass balance of PCBs in Lake Superior was then constructed to determine the source of PCB loss in the system. In other words, Where did all the PCBs go? Table 2 shows the inputs and outputs of PCBs in Lake Superior for the comparison year of 1986, in which the net loss of PCB from the water column was calculated to be approximately 1800 kg, which must represent the excess of outputs over inputs.

Table 2. Estimated inputs and outputs of PCBs to Lake Superior in 1986. (Jeremiason et al. 1994)

Inputs	kg/year	Outputs	kg/year
Riverine	110	Outflow	60
Other[a]	41	Sedimentation	110
Dry deposition	32	Volatilization[b]	~1900
Wet deposition	125		
Total	308	Total	~2070

[a] Municipal and industrial discharges.
[b] Net volatilization = volatilization − absorbtion = inputs − outputs + mass lost.

Table 2 indicates that 60 kg is lost to outflow from the lake, and ~100 kg is lost to sedimentation leaving a shortfall of ~1900 kg, which is attributed to volatilization. Given that inputs and outputs of PCBs are highly constrained by known levels of riverine, municipal, and atmospheric wet and dry deposition, as well as the decrease in water-column concentrations, the loss must be attributed to volatilization. It is a remarkable discovery that

volatilization losses exceed sedimentation losses by a factor of 17. Hydrophobic organic chemicals, such as PCBs, have high values of K_{OW} and high affinities for particles rich in organic carbon. Although the delivery of PCBs to the benthic region is very efficient, their incorporation into the sediment is not. It is concluded that the importance of volatilization relative to other losses is attributable in large part to the inefficient burial of PCBs in the sediments of this lake, thereby increasing water-column residence times. In other large lakes in which sediment burial is more efficient as a result of higher sediment loads, a smaller proportion of total losses may be attributed to volatilization. Both examples strongly point to the absolute and relative importance of volatilization in whole-lake contaminant cycles.

10.3 Air–Water Exchange in Green Bay, Lake Michigan

As was outlined previously in the specimen calculation, it is possible to use information on physicochemical properties, concentrations, and environmental conditions to deduce the direction and rate of air–water exchange in specific situations. Achman et al. (1993) examined the air–water exchange of PCBs in Green Bay, Lake Michigan, a large freshwater estuary that is hypereutrophic, relatively shallow, and highly contaminated by historical PCB inputs from the Fox River. The PCB gradient from south (near the river mouth) to north (boundary with Lake Michigan) reveals water and sediment concentrations of PCBs decreasing by a factor of 200. Achman et al. (1993) collected air (gas phase) and water (dissolved phase) samples simultaneously from the bow of a 18-m boat in a south-to-north gradient during several cruises covering the ice-free period. A comparison of atmospheric gas phase and aqueous dissolved-phase concentration (Fig. 8) clearly shows their intimate linkage. Proceeding from the highly contaminated south to the less contaminated north, both air and water concentrations decreased in proportion. Hornbuckle et al. (1993) showed that water controlled the PCB concentrations in air throughout much of the Bay, and over-water concentrations exceeded over-land concentrations determined simultaneously nearby. Calculations showed that the direction of transfer was from water to air (i.e., volatilization) at all sites, during all seasons, and at all locations. In the framework of fugacity or PCB partial pressure differences, the fugacity of PCBs in the water column ranged from 5 to 100 times that of the overlying atmosphere. Volatilization was dominated by the di- through tetrachlorobiphenyls, and decreased with increasing molecular weight. A sensitivity analysis of the system demonstrated that dissolved-phase concentrations of PCBs, water temperature, and

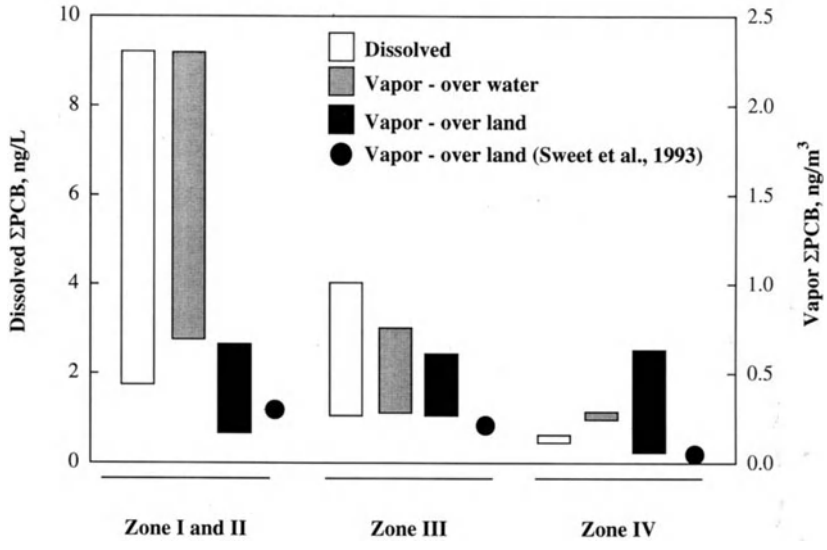


Fig. 8. Relationship between PCB concentrations dissolved in water and in the vapor phase from sample lakes over the water of Green Bay and over land

wind speed drove the fluxes. At low wind speeds of 1–3 m/s, PCB volatilization fluxes were 15–300 ng/m^2 per day. At higher wind speeds, PCB volatilization fluxes were 50–1300 ng/m^2 per day. The total net volatilization of PCBs from Green Bay, Lake Michigan is ~132 kg/year or an average of 314 ng/m^2 per year. This value was obtained by estimating instantaneous volatilization fluxes in several spatially distributed zones and summing over the seasons. This approach fails to recognize that temporally and spatially dependent variations in air and water concentrations add significant uncertainty to the whole-lake flux calculation on an annual basis, especially over the winter and in periods when no samples were taken. In addition, similar variations in wind speed and surface-water temperature over time and space make the estimation of an annual whole-lake calculation problematic. The final case study describes a scenario in which an attempt is made to include such variations.

10.4 Air–Water Exchange in Lake Superior

To determine the annual cycle of air–water exchange in Lake Superior, appropriate water temperature, wind speeds, and dissolved and vapor concentrations must be accurately known for all seasons. Hornbuckle et al. (1994) obtained normal water temperatures based on satellite and airborne surface-temperature imaging collected by government agencies, which provide the means for assessing water temperatures over space and time (seasonally) (Schneider et al. 1993). For calculating PCB air–water exchange, semi-monthly average whole-lake values were used. Seasonal wind speeds were measured at Eagle Harbor, Michigan, on the south shore of the central basin of Lake Superior for 1992. Values of 1.34 m/s for December through February, 2.24 m/s for March through August, and 3.58 m/s for September through November were selected. No report of seasonal variations in dissolved total PCB have been reported for the open waters of Lake Superior or other large lake systems. Because so little information is available, a constant dissolved total PCB concentration of 0.173 ng/l, the 1993 value, was applied to the annual flux calculations.

Vapor-phase PCB concentrations vary significantly throughout the year, as shown in Fig. 9, with higher concentrations in the summer than in the winter (Hoff et al. 1992). These data describe a yearly maximum vapor PCB concentration in July/August, and were modeled as a Lorenzian function:

$$\chi(\tau) = \chi_{\min}\left(1 + \frac{A_m \Gamma^2}{(\tau - \tau_{\max})^2 + \Gamma^2}\right),$$

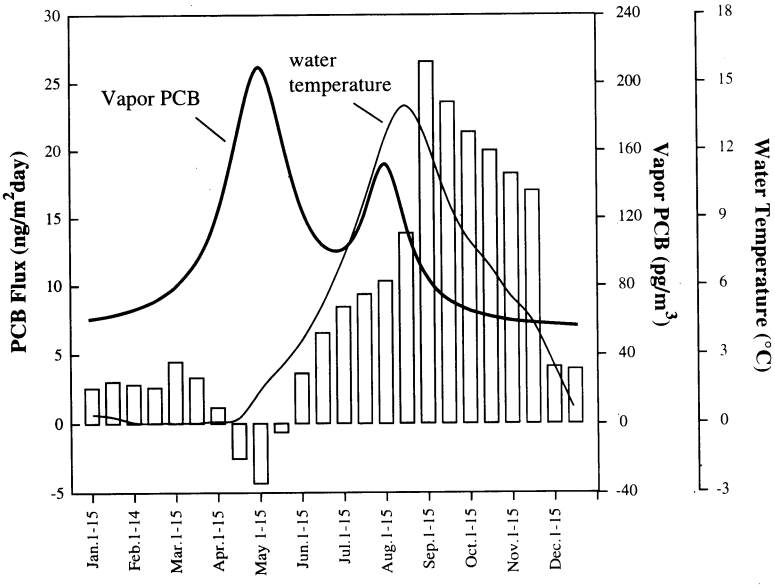


Fig. 9. Annual flux of total PCB (*bars*) plotted as the average daily flux (ng/m^2 per day) for 24 half-month periods. Negative fluxes indicate transport of PCB into Lake Superior. The *line* is the modeled vapor concentrations used for calculating PCB fluxes. The strong seasonal variation is evident. Reproduced from Hornbuckle et al. (1994) with permission

where $\chi(\tau)$ is the compound vapor concentration (ng/m^3), χ_{min} is the minimum average monthly vapor concentration (ng/m^3), A_m is the ratio of highest-to-lowest monthly average vapor-phase concentration, Γ is the width of the peak at half height in months, and τ is the independent variable month. The months are defined from 0 to 12, where 0.5 is mid-January, 1 is the end of January, 1.5 is mid-February, 2 is the end of February, and so forth. For total PCBs χ_{min}, A_m, τ_{max}, and Γ were equal to 0.055 ng/m^3, 14, 6.7, (late July), and 0.67 months, respectively. Total PCB vapor concentrations from samples collected at Eagle Harbor averaged 0.095 ± 0.080 ng/m^3, ranged from 0.013 to 0.390 ng/m^3, and exhibited two maxima: The first and largest monthly average concentration was observed in April/May, whereas a second, smaller peak was observed in July/August.

The cause of the April/May peak in vapor-phase PCBs measured at Eagle Harbor is unclear, but may be related to the spring snow melt. The July/August peak is attributed to volatilization from terrestrial surfaces during periods of warm summer temperatures. A similar model, even if applied to the volatilization of chemicals from water surfaces, cannot explain the trend in the Eagle Harbor data. Melted snow may deliver PCBs to the air by direct volatilization from the melting snow, from the frozen terrestrial surface, or from runoff streams. Because the snow in this region rarely melts between November and April, atmospheric contaminants accumulate. More research into the annual cycle of dissolved PCBs, the impact of snow melt on PCB air and water cycles, and over-water vapor PCBs is clearly needed.

The annual vapor PCB cycle is modeled, therefore, using two Lorentzian functions, which, when summed, describe the annual cycle of atmospheric vapor total PCBs as shown in Fig. 9. The seasonal trend for PCB flux at the air–water interface is determined semimonthly using whole-lake mean water temperatures, 1992 seasonal wind speeds, and the May 1992 dissolved ΣPCB concentration 0.173 ng/L linked to the method outlined previously. All mass-transfer parameters, such as H, k_A, k_{OW}, and K_{OL}, were determined for all 85 PCB congeners in the same manner as for the instantaneous fluxes. The dimensionless Henry's Law Constant, H, the dissolved water concentration, and K_{OW} (m/day) were averaged by homolog group. The PCB homolog fluxes for each semimonthly period were then calculated using the Lorenzian function described previously for air concentrations. The average k_{OW} values for total PCBs is equal to 0.080 m/day, and the annual flux is approximately 250 kg/year. The more volatile (i.e., low molecular weight and chlorine number) congeners exhibited volatilization fluxes throughout the year, and the higher-chlorinated congeners show depositional fluxes at all times of the year, although they represent a very small proportion of the total.

The largest depositional flux of total PCBs was calculated for May, due to higher vapor concentrations. The highest volatilization flux was calculated for September (27 ng/m^2 per day), when water temperatures and seasonal wind speed (3.6 m/s) are highest (Fig. 8). The congeners with less than six chlorines constituted more than 90% of PCB volatilization (June–March) fluxes and ~50% of the deposition (April, May) fluxes. Instantaneous fluxes were frequently greater than the average values calculated by season, because daily wind speeds measured aboard ship were often higher than the 15-day average wind speed used in the annual calculations. (Vapor-phase PCB concentrations measured over water may exceed the modeled values from on-shore sampling, and surface-water temperatures on any given day may be different from semimonthly averages).

The annual flux of total PCB from Lake Superior in 1992 was calculated by multiplying daily average fluxes (ng/m^2 per day) by the appropriate time period. This resulted in average semi-monthly fluxes of −63 ng/m^2 to 404 ng/m^2 for the 24 periods. These fluxes were summed and applied to the surface area of the lake to yield an overall volatilization flux of 249 kg/year or ~8 ng/m^2 per day on an annual basis. Jeremiason et al. (1994) estimated that loss by volatilization was ~400 kg/year in 1992 or ~13 ng/m^2 per day based on decreasing PCB water concentrations and a highly constrained accounting of inputs and outputs. There is thus a satisfying reconciliation between the fluxes calculated by these independent methods.

Results of Hornbuckle et al. (1994) suggest that vapor deposition of PCBs to Lake Superior occurs only briefly in the spring, whereas volatilization occurs throughout the rest of the year. The large autumn volatilization fluxes result from moderate surface-water temperatures and low vapor concentrations. However, the effect of wind speed on air–water exchange may be

Table 3. Estimated air–water fluxes of total PCBs in natural waters (ng/m^2 per day) for a range of contaminated and less-contaminated sites

Location	Total PCB flux	Reference
	Freshwater	
Green Bay	+15 to +300 (1–3 m/s) +50 to +1300 (4–6 m/s)	Achman et al. (1993)
Green Bay	+35	Green Bay Mass Balance (1992)
Lake Superior	+19 (Still Air, 1992) +141 (5 m/s, 1992)	Baker and Eisenreich (1988)
Lake Superior	+63 (1986)	Strachan and Eisenreich (1988)
Lake Superior	+63 (1986) +13 (1992)	Jeremiason et al. (1994)
Lake Superior	+8.3 (1992)	Hornbuckle et al. (1994)
Siskiwit Lake, Lake Superior	+24 (1986)	Swackhamer et al. (1988)
Lake Michigan	0 to +13 000	Doskey and Andren (1981)
Lake Michigan	+240	Strachan and Eisenreich (1988)
Lake Michigan	+15	Swackhamer and Armstrong (1986)
Lake Ontario	+81	Mackay (1989)
River Elm, Sweden	+50	Larsson et al. (1990)
	Seawater	
Oceans	−160 to −450	GESAMP (1988)
Oceans	−4.5	Atlas and Giam (1986)
Oceans	−0.6 to −10	Atlas et al. (1986)
Oceans	−140 to +40	Iwata et al. (1993)

underestimated using this approach. Because k_W has a nonlinear dependence on wind speed, higher-than-average instantaneous winds will produce large fluxes that will not be balanced by wind speeds lower than average. Livingstone and Imboden (1993), using a Weibull probability function for the wind-speed input, suggested that the effect of large instantaneous wind speeds may double the fluxes calculated from average wind speeds.

As shown in Table 3, the magnitude of PCB flux across the air–water interface varies with the climatological and hydrological conditions of each specific location linked to the dynamics of chemical loading and cycling in the air and water. Even so, estimates of the air–water fluxes of PCB in natural waters nearly all show net volatilization with typical values of 10–60 ng/m^2 day in uncontaminated systems, and substantially more in contaminated systems. For chemicals in a homologous series, air–water exchange is likely to be greater for the lower molecular weight species. For chemicals that have lower K_{AW} values, the direction of transfer may be from air to water (i.e., absorption) and represent a net loading to the lake.

11 Conclusions

There is now a satisfactory understanding of the processes by which chemicals cross the air–water interface of lakes. The rates of these processes can be measured directly in some cases (such as wet deposition), but they can only be estimated from mathematical models in other cases, e.g., evaporation. For many chemicals there is active absorption, deposition, and volatilization, and the net direction of transfer may not be obvious. Often there will be strong seasonal variations in transfer rates and even in directions. Much remains to be done to better parameterize the various transfer coefficients and velocities, and to devise better averaging methods. It is hoped that the theoretical treatment and case studies presented in this chapter will encourage further work and a fuller appreciation of the rate of air–water exchange on the chemistry of lakes.

References

Achman DR, Hornbuckle KC, Eisenriech SJ (1993) Volatilization of polychlorinated biphenyls from Green Bay, Lake Michigan. Environ Sci Technol 27:75–87

Atlas E, Giam CS (1986) Sea-air exchange of high molecular weight synthetic organic compounds. In: Buet-Menard P. (ed) The role of air–sea exchange in geochemical cycling, Reidel, Dordrecht, pp. 295–323

Atlas E, Bidleman TF, Giam CS (1986) Atmospheric transport of PCB to the oceans. In: Waid JS (ed) PCBs and the environment, vol 1. CRC Press, Boca Raton, pp 79–100

Baker JE, Eisenreich SJ (1990) Concentrations and fluxes of PAHs and PCBs across the air–water interface of Lake Superior. Environ Sci Technol 24:342–352

Bidleman TF, Billings WN, Foreman WT (1986) Vapor-particle partitioning of semivolatile organic compounds: estimates from field collections. Environ Sci Technol 20:1038–1042

DiToro DM (1985) A particle interaction model of reversible organic chemical sorption. Chemosphere 14:1503–1538

Eisenreich S (1987) Chemical limnology of non-polar organic contaminants: polychlorinated biphenyls in Lake Superior. In: Hites RA, Eisenreich S (eds) Sources and fates of aquatic pollutants. American Chemical Society, Washington DC, 216:319–364

GESAMP, Joint Group of Experts on the Scientific Aspects of Marine Pollution (1989) Atmospheric input of trace species to the world ocean. In: GESAMP Working Group No 14 on the Interchange of pollutants between the atmosphere and oceans. World Meteorological Organization, Athens, March 7, 1989, 85 pp

Hoff RM, Muir DCG, Grit NP (1992) Annual cycle of PCBs and organohalogen pesticides in air in southern Ontario. 1. Air concentration data. Environ Sci Technol 26:266–275

Hornbuckle KC, Achman DR, Eisenreich SJ (1993) Over-water and over-land polychlorinated biphenyls in Green Bay, Lake Michigan. Environ Sci Technol 27:87–98

Hornbuckle KC, Jeremiason JD, Sweet CW, Eisenreich SJ (1994) Seasonal variations in air–water exchange of PCBs in Lake Superior. Environ Sci Technol 28:1491–1501

Hulsher T, Van der Velde LE, Bruggeman WA (1992) Temperature dependence of Henry's Law Constants for selected chlorobenzenes, polychlorinated biphenyls and polycyclic aromatic hydrocarbons. Environ Toxicol Chem 11:1595–1603

Iwata H, Tanabe S, Sakal N, Tatsukawa R (1993) Distribution of persistent organochlorines in the oceanic air and surface seawater and the role of ocean on their global transport and fate. Environ Sci Technol 27:1080–1098

Jeremiason JD, Hornbuckle KC, Eisenreich SJ (1994) PCBs in Lake Superior, 1978–1992: decreases in water concentrations reflect loss by volatilization. Environ Sci Technol 28:903–914

Karickhoff SW (1981) Semiempirical estimation of sorption of hydrophobic pollutants on natural sediments and soils. Chemosphere 10:833–849

Larsson P, Okla L, Ryding S-O, Westoo B (1990) Contaminated sediment as a source of PCBs in a river system. Can J Fish Aqu Sci 47:446–454

Livingstone DM, Imboden DM (1993) The non-linear influence of wind-speed variability on gas transfer in lakes. Tellus 45B:275–295

Mackay D (1991) Mutimedia environmental models: the fugacity approach. Lewis Publishers, Chelsea Michigan

Mackay D, Shiu WY, Ma KC (1981) A critical review of Henry's Law constants for chemicals of environmental interest. J Phys Chem Ref Data 10:1175–1199

Mackay D, Yuen AT (1983) Mass transfer coefficient correlations for volatilization of organic solutes from water. Environ Sic Technol 17:211–217

Mackay D, Shiu WY, Sutherland RP (1979) Determination of air–water Henry's Law constants for hydrophobic pollutants. Environ Sci Technol 15: 333–337

Mackay D, Paterson S, Schroeder WH (1986) Model describing the rates of transfer processes of organic chemicals between atmosphere and water. Environ Sci Technol 20:810–816

Mackay D, Shiu WY, Ma KC (1992) Illustrated handbook of physical chemical properties and environmental fate for organic chemicals, vol I. Lewis Publishers, Chelsea Michigan

McConnell L, Cotham WE, Bidleman TF (1993) Gas exchange of hexachlorocyclohexane in the Great Lakes. Environ Sci Technol 27:1304–1311

McVeety BD, Hites RA (1988) Atmospheric deposition of PAHs to water surfaces: a mass balance approach. Atmos Environ 22:511–536

Meylan WM, Howard PH (1991) Bond contribution method for estimating Henry's Law constants. Environ Toxicol Chem 10:1283–1293

Pankow JF, Storey JM, Yamasaki H (1993) Effects of relative humidity on gas/particle partitioning of semivolatile organic compounds to urban particulate matter. Environ Sci Technol 27:2220–2226

Reid RC, Prausnitz JM, Poling BE (1987) The properties of gases and liquids. McGraw-Hill, New York

Schneider K, Assel RA, Croley TE (1993) Normal water temperature and ice cover of the Laurentian Great Lakes, a computer animation, data base, and analysis tool. National Oceanic and Atmospheric Administration (NOAA), Great Lakes Environmental Research Laboratory, Ann Arbor, MI (GLERL)

Schwarzenbach RP, Gschwend PM, Imboden DM (1993) Environmental organic chemistry. Wiley InterScience, New York

Shiu WY, Mackay D (1986) A critical review of aqueous solubilities, vapor pressure, Henry's Law Constants, and octanol-water partition coefficients of the polychlorinated biphenyls. J Phys Chem Ref Data 15-2:911–929

Strachan WMJ, Eisenreich SJ (1988) Mass balancing of toxic chemicals in the Great Lakes: the role of atmospheric deposition. International Joint Commission, Windsor, Ontario, 161 pp

Suntio LR, Shiu WY, Mackay D, Seiber JN, Golfeity D (1988) Critical review of Henry's Law constants for pesticides. Rev Environ Contam Toxicol 103:1–59

Swackhamer DL, McVeety BD, Hites RA (1988) Deposition and evaporation of PCBs to and from Siskiwit Lake, Isle Royal, Lake Superior. Environ Sci Technol 22:664–672

Swain W (1978) Chlorinated organic residues in fish, water, and precipitation from the vicinity of Isle Royale, Lake Superior. J Great Lakes Res 4:398–407

Sweet CW, Murphy RJ, Bannasch JH, Kelsey CA, Hong J (1993) Atmospheric deposition of PCBs into Green Bay. J Great Lakes Res 19:109–128

Yamasaki H, Kuwata K, Miyamoto H (1982) Effects of ambient temperature on aspects of airborne polycyclic aromatic hydrocarbons. Environ Sci Technol 16:189–194

7 Atmospheric Depositions: Impact of Acids on Lakes

WERNER STUMM[1] and JERALD L. SCHNOOR[2]

Abstract

In this chapter we concentrate on the chemical and biogeochemical processes involved in the anthropogenic generation of acidity and its transfer through the atmosphere to the terrestrial and aquatic environment. Unifying definitions of acid- and base-neutralizing capacity (alkalinity and acidity) are helpful in appreciating the major H^+ yielding and H^+ consuming processes occurring in the atmosphere, in the watersheds, and in the lake. Because the transfer of electrons is coupled with the transfer of protons, oxidation and reduction are accompanied by proton release and proton consumption. Among the redox processes that have a major impact on H^+ balance are the synthesis and mineralization of biomass. Any uncoupling between photosynthesis and respiration affects acidity and alkalinity in terrestrial and aquatic ecosystems. In the watershed, aggrading vegetation (forests and intensive crop production) produces acidity; chemical weathering, on the other hand, neutralizes inputs of acids by atmospheric deposition and internal acidity production. Models to estimate the critical load of acid deposition that can be neutralized by the ecosystem without causing deleterious biological effects are currently under development. Two case studies are reviewed briefly: (1) acid alpine lakes, where acid deposition is neutralized partially by chemical weathering of crystalline rocks, and (2) a large-scale watershed manipulation in which the stream has been acidified by the addition of $(NH_4)_2SO_4$ via uptake of ammonium by vegetation and nitrification with the export of nitrate and sulfate evident in the streamwater. The latter case is an example of a forested catchment exhibiting nitrogen saturation.

1 Introduction: Anthropogenic Generation of Acidity

Acid atmospheric deposition results from the disturbance of cycles that couple atmosphere, land, and water. The surface of our environment is in a global sense on the average with regard to a proton and electron balance in a stationary state. Considering the Goldschmidt reaction in its most simple scheme

$$\text{igneous rock} + \text{volatile substances} \rightleftharpoons \text{air} + \text{seawater} + \text{sediments.} \quad (1)$$

Sillén (1961) gave the picture that volatiles (H_2O, CO_2, HCl, and SO_2), the acids of volcanoes (i.e., the acids that have leaked from the interior of the earth) have reacted in a gigatic acid base reaction with the bases of rocks (silicates, oxides, and carbonates). Similarly, he calculated from a model system the quantities of redox components that have participated in a redox titration. The present day stationary state with regard to H^+ and e^- balance is reflected in an atmosphere with 20.9% O_2, 0.03% CO_2, and 79.1% N_2, as well as a world ocean with pH $\approx$ 8 and p$\varepsilon \approx$ 12.5. This steady state is achieved by a global balance of oxidation and reduction, and H^+ ion production and consumption. Above all, the rate of oxidation of reduced S, Fe, and C occurring during the weathering of continental rocks, is balanced by the rate of reduction of higher valent S, Fe, and C into reduced forms during and after deposition onto land and in the sediments.

Oxidation and reduction are accompanied by proton release and proton consumption, respectively. (In order to maintain charge balance, the production of e^- will eventually be balanced by the production of H^+.) Furthermore, the dissolution of rocks and the precipitation of minerals are

[1] Institute for Water Resources and Water Pollution Control (EAWAG), Swiss Federal Institute of Technology (ETH), Zurich, Switzerland
[2] Department of Civil and Environmental Engineering, University of Iowa, Iowa City, IO, USA

accompanied by H^+ consumption and H^+ release, respectively. Thus, as shown by Broecker (1971), the $p\varepsilon$ and pH of the surface of our global environment reflect the levels where the oxidation states and the H^+ ion reservoirs of the weathering sources equal those of the sedimentary products.

1.1 Genesis of Acid Precipitation

The oxidation of carbon, sulfur, and nitrogen, resulting mostly from fossil-fuel burning, disturbs redox conditions in the atmosphere. The atmosphere is more susceptible to anthropogenic emissions than are the terrestrial or aqueous environments, because, from a quantitative point of view, the atmosphere is much smaller than the other reservoirs. Furthermore, the time constants concerning atmospheric alterations are small in comparison with those of the seas and the lithosphere.

In oxidation-reduction reactions, electron transfers (e^-) are coupled with the transfer of protons (H^+) to maintain a charge balance. A modification of the redox balance corresponds to a modification of the acid–base balance. The net reactions of the oxidation of C, S, and N exceed reduction reactions in these elemental cycles. A net production of H^+ ions in atmospheric precipitation is a necessary consequence. The disturbance is transferred to the terrestrial and aquatic environments, and it can impair terrestrial and aquatic ecosystems.

Figure 1 shows the various reactions that involve atmospheric pollutants and natural components in the atmosphere. The following reactions are of particular importance in the formation of acid precipitation: oxidative reactions, either in the gaseous phase or in the aqueous phase, leading to the formation of oxides of C, S, and N (CO_2, SO_2, SO_3, H_2SO_4, NO, NO_2, HNO_2, and HNO_3), absorption of gases into water (cloud droplets, falling raindrops, or fog) and interaction of the resulting acids ($SO_2 \cdot H_2O$, H_2SO_4, HNO_3) with ammonia (NH_3) and the carbonates of airbore dust, and the scavenging and partial dissolution of aerosols into water. In this case aerosols are produced from the interaction of vapors and airbore (maritime and dust) particles; they often contain $(NH_4)_2SO_4$ and HN_4NO_3.

The products of the various chemical and physical reactions are eventually returned to the earth's surface. Usually, one distinguishes between wet and dry deposition. Wet deposition (rainout and washout) includes the flux of all those components that are carried to the earth's surface by rain or snow, i.e., those dissolved and particulate substances contained in rain or snow. Dry deposition is the flux of particles and gases (especially SO_2, HNO_3, and NH_3) to the receptor surface during the absence of rain or snow. Deposition also can occur through fog aerosols and droplets, which can be deposited on trees, plants, or the ground. With forests, approximately half of the deposition of SO_4^{2-}, NO_3^-, and H^+ occurs as dry deposition (Lindberg et al. 1986).

We concentrate on three elementary chemical concepts that are the prerequisites to understand the genesis and properties of acid deposition. The first of the three concepts is a simple stoichiometric model, which explains on a mass-balance basis that the composition of rain results primerily from a titration of the acids formed from atmospheric pollutants with the bases (NH_3^- and CO_3^{2-}-bearing dust particles) introduced into the atmosphere. Next is an illustration of the absorption equilibria of such gases as SO_2 and NH_3 into water, which represents their interaction with cloud water, raindrops, fog droplets, or surface waters. Finally, a quantitative interpretation of the acid-base balance is presented. This requires a rigorous definition of acid-neutralizing capacity (alkalinity) and base-neutralizing capacity (acidity) to measure the residual acidity of acid precipitation, and to interpret the interaction of acid deposition with the terrestrial and aquatic environment.

1.1.1 Stoichiometric Model

The rainwater shown in Fig. 1 contains an excess of strong acids, most of which originate from the oxidation of sulfur during fossil-fuel combustion, and from the fixation of atmospheric nitrogen to NO and NO_2 (e.g., during combustion of gasoline by motor vehicles). It also should be mentioned that there are natural sources of acidity, resulting from volcanic activity, from H_2S from anaerobic sediments, and from dimethylsulfide and carbonylsulfide that originate in the ocean. The HCl results from the combustion and decomposition of organochlorine compounds such as polyvinylchloride. Bases originate in the atmo-

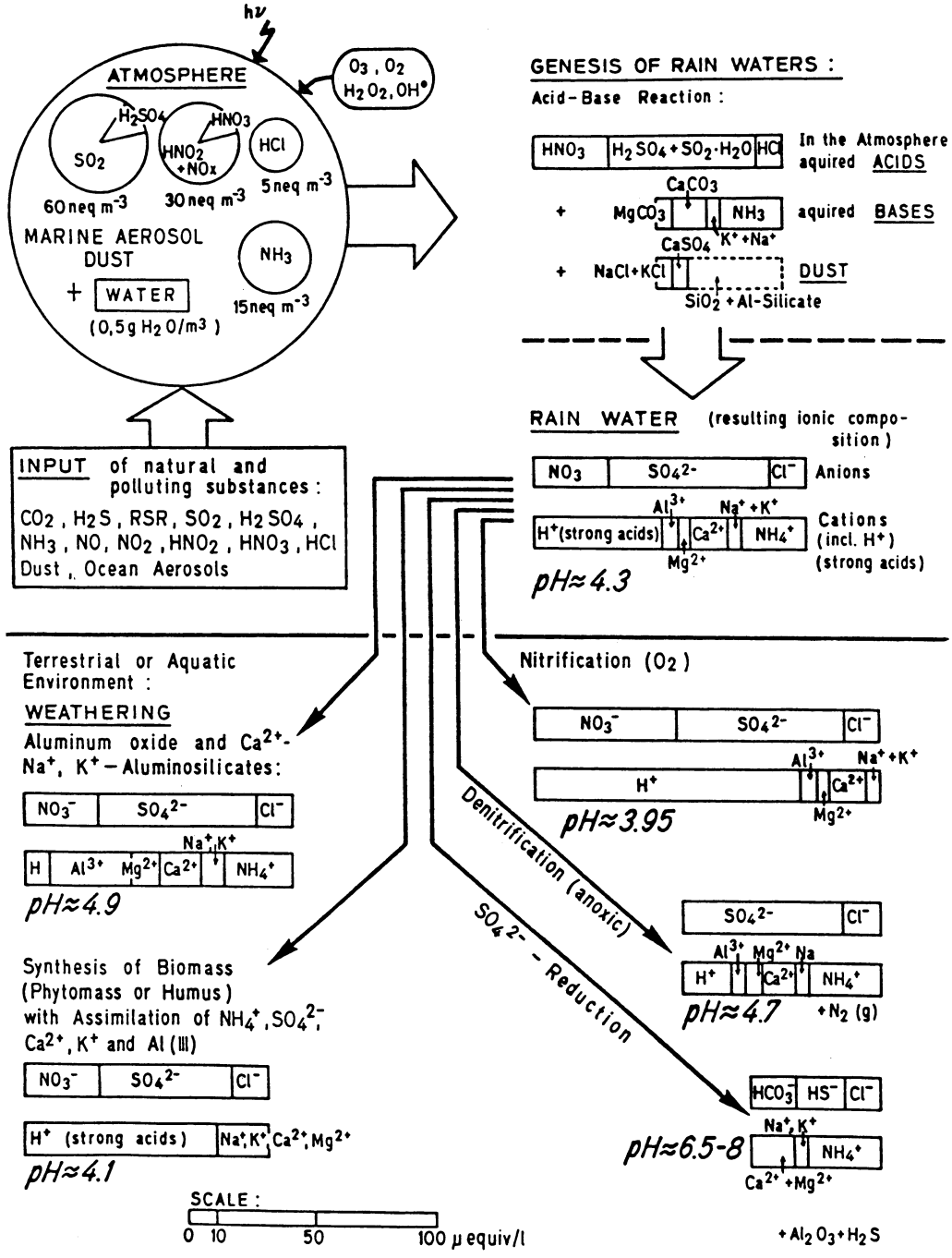


Fig. 1. Genesis of acid rain. From the oxidation of S and N during the combustion of fossil fuels there is a buildup in the atmosphere (in the gas phase, aerosol particles, raindrops, snowflakes, and fog) of CO_2 and the oxides of S and N, which leads to acid–base interaction. The importance of absorption of gases into the various phases of gas, aerosol, and atmospheric water depends on a number of factors. (In this figure, we assume a yield of 50% for SO_4^{2-} and NO_3^-, of 80% for NH_3, and of 100% for HCl.) The genesis of acid rain is shown in the *upper right* as an acid–base titration. The data given are representative of the situation encountered in Zurich, Switzerland. Various interactions with the terrestrial and aquatic environment (see Table 2) are shown in the lower part of the figure. (Schnoor and Stumm 1985)

sphere as the carbonate of wind-blown dust and from NH_3, generally of natural origin. The NH_3 comes from NH_4^+ and from the decomposition of urea in soil and agricultural environments.

The reaction rates for oxidation of atmospheric SO_2 (0.05–0.5 day^{-1}) yield a sulfur residence time of several days at the most; this corresponds to a transport distance of several hundred to 1000 km (Samson and Small 1984). The formation of HNO_3 by oxidation is more rapid, and, compared with H_2SO_4, results in a shorter travel distance from the emission source. The H_2SO_4 also can react with NH_3 to form NH_4HSO_4 or $(NH_4)_2SO_4$ aerosols. In addition, the NH_4NO_3 aerosols are in equilibrium with $NH_3(g)$ and $HNO_3(g)$ (Seinfeld 1986).

The flux of dry deposition is usually assumed to be a product of its concentration adjacent to the surface and the deposition velocity. Deposition velocity depends on the nature of the pollutant (type of gas, particle size), the turbulence of the atmosphere, and the characteristics of the receptor surface (water, ice, snow, vegetation, trees, rocks). Dry deposition is usually collected for study in open buckets during dry periods, but this method underestimates the flux of pollutants, particularly gases (SO_x, NO_x), to a foliar canopy or lake surface (Zobrist et al. 1993). (Fog can be collected with special devices, but it is not measured quantitatively in a wet or dry bucket collector.)

The foliar canopy receives much of its dry deposition in the form of sulfate, nitrate, and hydrogen ion, which occur primarily as SO_2, HNO_3, and NH_3 vapors. Dry deposition of coarse particles has been shown to be an important source of calcium and potassium ions deposition on deciduous forests in the eastern United States (Table 1; Lindberg et al. 1986).

In addition to the acid–base components shown in Fig. 1, various organic acids are often found. Many of these acids are by-products of the atmospheric oxidation of organic matter released into the atmosphere (Galloway et al. 1982; Kavamura and Kaplan 1984; Keene and Galloway 1984). Of special interest are formic, acetic, oxalic, and benzoic acids, which have been found in rain water in concentrations occasionally exceeding a few micromoles per liter. Thus, they must be included in the calculated acidity of rainwater, and their presence in larger concentrations has an influence on the pH of rain and fog samples.

Figure 2 illustrates the inorganic composition of representative rain samples. The ratio of the cations (H^+, NH_4^+, Ca^{2+}, Na^+, and K^+) and the anions (SO_4^{2-}, NO_3^-, and Cl^-) reflects the acid–base titration that occurs in the atmosphere and in rain droplets. Total concentrations (the sum of cations or anions) typically vary from 20 to 500 $\mu eq/\ell$. Dilution effects, such as washout by atmospheric precipitation, can in part explain the

Table 1. Total annual atmospheric deposition of major ions to an oak forest at Walker Branch Watershed

Process	Atmospheric deposition (mEq/m^2 per year)					
	SO_4^{2-}	NO_3^-	H^+	NH_4^+	Ca^{2+}	K^+
Precipitation	70 ± 5	20 ± 2	69 ± 5	12 ± 1	12 ± 2	0.9 ± 0.1
Dry deposition	7 ± 2					
Fine particles	19 ± 2	0.1 ± 0.02	2.0 ± 0.9	3.6 ± 1.3	1.0 ± 0.2	0.1 ± 0.05
Coarse particles	62 ± 7	8.3 ± 0.8	0.5 ± 0.2	0.8 ± 0.3	30 ± 3	1.2 ± 0.2
Vapors[a]	160 ± 9	26 ± 4	85 ± 8	1.3	0	0
Total deposition		54 ± 4	160 ± 9	18 ± 2	43 ± 4	2.2 ± 0.3

Values are mean ± SE for 2 years of data. Numbers of observations range from 15 (HNO_3) to 26 (particles) to 128 (precipitation) to 730 (SO_2). In comparing these deposition rates it must be recalled that any such estimates are subject to considerable uncertainty. The standard errors given provide only a measure of uncertainty in the calculated sample means relative to the population means; hence, additional uncertainties in analytical results, hydrological measurements, scaling factors, and deposition velocities must be included. The overall uncertainty for wet deposition fluxes is approximately 20%, and that for dry deposition fluxes is approximately 50% for SO_4^{2-}, Ca^{2+}, K^+, NH_4^+, and approximately 75% for NO_3^- and H^+ (Lindberg et al. 1986).

[a] Includes SO_2, HNO_3, and NH_3. Complete conversion of deposited SO_2 to H_2SO_4, and of NH_3 to NH_4^+ was assumed in determining the vapor input of H^+. NH_3 deposition was estimated from the literature.

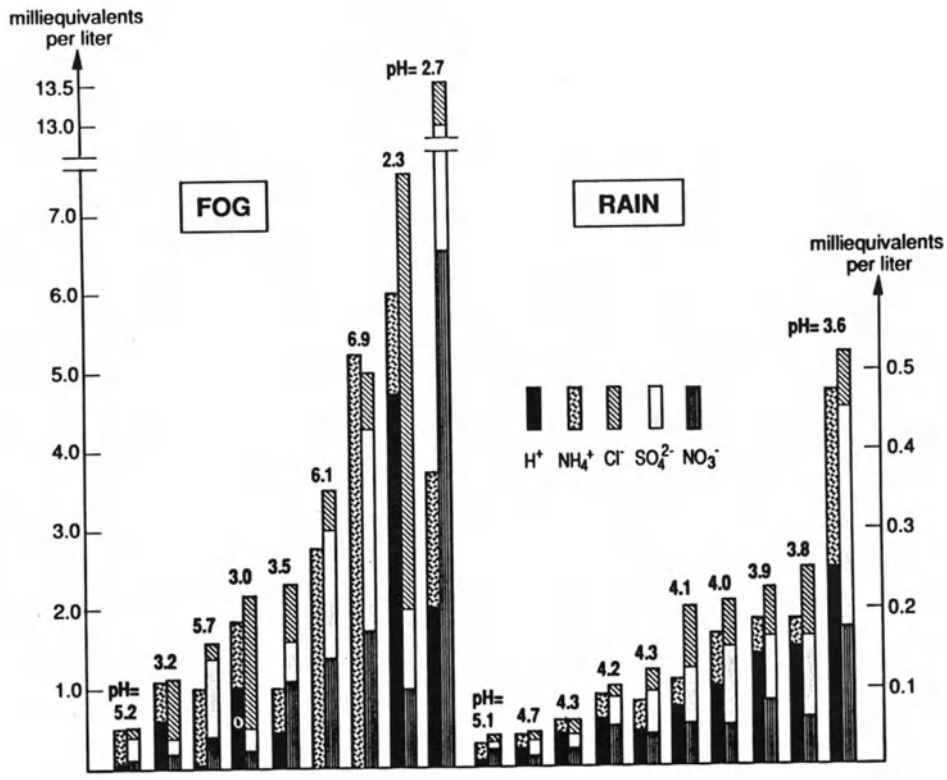


Fig. 2. Composition of fog and rain samples in a highly settled region around Zurich, Switzerland. The composition of fog varies widely and reflects to a larger extent than rain the influence of local emissions close to the ground. The fog concentration increases with decreasing liquid water content. (Stumm et al. 1987)

differences observed. For example, the highest concentrations are observed after long, dry periods; the lowest concentrations are typically recorded at the end of prolonged rain.

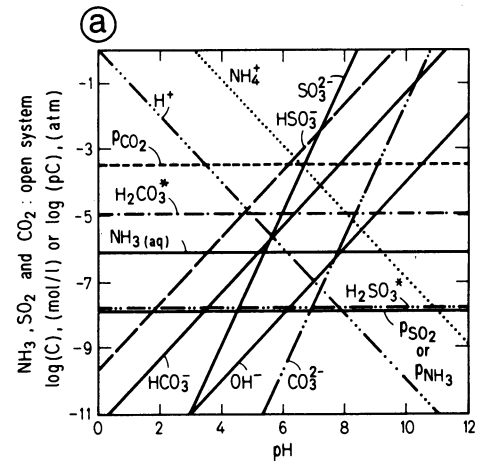
When fog is formed from water-saturated air, water droplets condense on aerosol particles. In addition to components of the aerosols, the fog droplets can absorb such gases as NO_x, SO_2, NH_3, and HCl, which form a favorable milieu for various oxidation processes, especially the formation of H_2SO_4. Fog droplets (10–50 μm in diameter) are much smaller than rain droplets. The liquid water content of fog is often in the range of 1×10^{-4} ℓ/m^3 air, so that acids in fog are typically 10–50 times more concentrated than those found in rain (Fig. 2; Johnson and Sigg 1985).

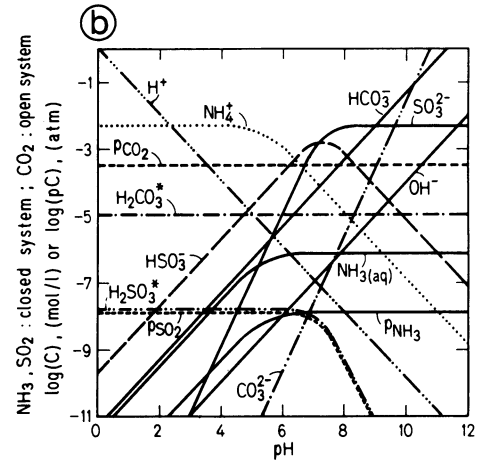
Rain clouds process a considerable volume of air over relatively large distances, and thus are able to absorb gases and aerosols from a large region. Because fog is formed in the lower air masses, fog droplets are efficient collectors of pollutants close to the earth's surface. The influence of local emissions (such as NH_3 in agricultural regions or HCl near refuse incinerators) is reflected in the fog composition. Fog waters typically contain total ionic concentrations of 0.5–15 meq/ℓ, as shown in Fig. 2. Remarkably different pH values can be observed in fog. In addition to neutral fogs (pH 5–7), some of which have very high anion concentrations, we have found, as have others, extreme acidity (pH 1.8; Waldman et al. 1982).

1.1.2 SO_2 and NH_3 Absorption

The distribution of gas molecules between the gas phase and the water phase depends on the Henry's Law equilibrium distribution. In the case of CO_2, SO_2, and NH_3 the dissolution equilibrium is pH-dependent, because the components in the water phase – $CO_2(aq)$, H_2CO_3, $SO_2 \cdot H_2O(aq)$, $NH_3(aq)$ – undergo acid-base reactions.

Two varieties of calculation are possible: In an open-system model, a constant partial pressure of the gas component is maintained. In a closed system, an initial partial pressure of a component





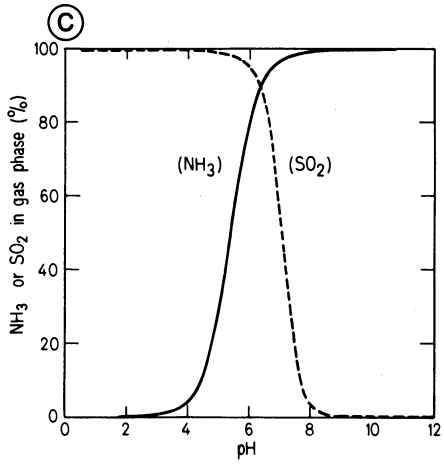


Fig. 3a–c. Equilibria of SO_2, NH_3, CO_2 and H_2O of water and/or gas system as a function of acid and base added. $(p_{SO_2}) = (p_{NH_3}) = 1.22 \times 10^{-8}$ atm or $\{SO_2\} = \{NH_3\} = 5 \times 10^{-7}$ mol m^{-3}; liquid water content (q): 10^{-4} ℓ m^{-3}; temperature 298 K. For the calculation, (**a**) an open system for SO_2 and NH_3, or (**b**) a closed system for SO_2 and NH_3 was assumed; (**c**) the percentage of the total amount of NH_3 and SO_2 present in the system is given as a function of pH

is given, e.g., for a cloud before rain droplets are formed or for a package of air before fog droplets condense. In these cases the system is considered closed; from then on, the total concentration in the gas phase and in the solution phase is constant (Fig. 3).

These examples illustrate the strong pH dependence of the solubility of these atmospheric gases. They relate to the question of linearity of emission controls for SO_2. In some instances other factors may affect the solubility. For example, the presence of formaldehyde can enhance the absorption of (total) SO_2 in water, because CH_2O reacts with HSO_3^- to form $CH_2OHSO_3^-$. Hydroxymethane-sulfonic acid is a very strong acid and oxidation of S(IV) bound to it is inhibited (Hoffmann and Boyce 1984).

2 Acidity and Alkalinity: Neutralizing Capacities

One has to distinguish between the H^+ concentration (or activity) as an intensity factor and the availability of H^+, the H^+ ion reservoir as given by the base-neutralizing capacity (BNC) or the H acidity [H-Acy]. The BNC relates to the alkalinity [Alk] or acid-neutralizing capacity (ANC) by

$$\text{H-Acy} = -[\text{Alk}]$$
$$\text{base-neutralizing capacity} = -\text{acid neutralizing capacity.} \quad (2)$$

The BNC can be defined by a net proton balance with regard to a reference level: the sum of the concentrations of all the species containing protons in excess of the reference level, minus the concentrations of the species containing protons

in deficiency of the proton reference level. For natural waters a convenient reference level (corresponding to an equivalence point in alkalimetric titrations) includes H_2O and H_2CO_3:

$$[\text{H-Acy}] = [H^+] - [HCO_3^-] - 2[CO_3^{2-}] - [OH^-]. \quad (3)$$

The ANC or alkalinity [Alk] is related to [H-Acy] by

$$-[\text{H-Acy}] = [\text{Alk}] = [HCO_3^-] + 2[CO_3^{2-}] + [OH^-] - [H^+]. \quad (4)$$

Considering a charge balance for a typical natural water (Fig. 4), we realize that [Alk] and [H-Acy] can also be expressed by a charge balance: the equivalent sum of conservative cations, minus the sum of conservative anions ([Alk] = a − b). The conservative cations are the base cations of the strong bases $Ca(OH)_2$, KOH, etc. The conservative anions are those that are the conjugate bases of strong acids (SO_4^{2-}, NO_3^-, and Cl^-):

$$[\text{Alk}] = [HCO_3^-] + 2[CO_3^{2-}] + [OH^-] - [H^+] = [Na^+] + [K^+] + 2[Ca^{2+}] + 2[Mg^{2+}] - [Cl^-] - 2[SO_4^{2-}] - [NO_3^-]. \quad (5)$$

The [H-Acy] for this particular water, obviously negative, is defined ([H-Acy] = b − a) as

$$[\text{H-Acy}] = [Cl^-] + 2[SO_4^{2-}] + [NO_3^-] - [Na^+] - [K^+] - 2[Ca^{2+}] - 2[Mg^{2+}]. \quad (6)$$

These definitions can be used to interpret interactions of acid precipitation with the environment. A simple accounting can be made: Every base cationic charge unit (for example, Ca^{2+} or K^+) that is removed from the water by whatever process is equivalent to a proton added to the water, and every conservative anionic charge unit (from anions of strong acids, e.g., NO_3^-, SO_4^{2-}, or Cl^-) removed from the water corresponds to a proton removed from the water, or generally,

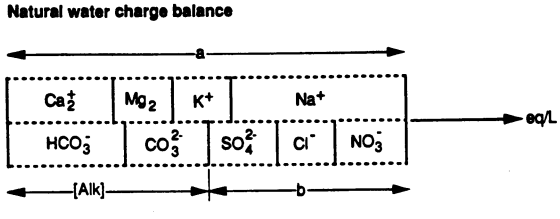


Fig. 4. Natural water charge balance

$$\Sigma\Delta[\text{base cations}] - \Sigma\Delta[\text{conservative anions}] = +\Delta[\text{Alk}] = -\Delta[\text{H-Acy}]. \quad (7)$$

If the water under consideration contains other acid- or base-consuming species, the proton reference level must be extended to the other components. In addition to the species given, if a natural water contains organic molecules, such as a carboxylic acid (H-Org) and ammonium ions, the reference level is extended to these species.

One usually chooses the ammonium species NH_4^+ and H-org as a zero-level reference condition. In operation, we wish to distinguish between the acidity caused by strong acids (mineral acids and organic acids with $pK < 6$), typically called mineral acidity or free acidity, which often is nearly the same as the free-H^+ concentration, and the total acidity given by the BNC of the sum of strong and weak acids. (Johnson and Sigg 1985; Sigg and Stumm 1994).

The distinction is possible by careful alkalimetric titrations of rain and fog samples. Gran titrations have found wide acceptance in this area. The strong acidity, [H-Acy], is expressed with regard to the reference conditions: H_2O, H_2CO_3, SO_4^{2-}, NO_3^-, Cl^-, NO_2^-, F^-, HSO_3^-, NH_4^+, H_4SiO_4, and ΣH_nOrg (organic acids, $pK_a < 10$):

$$[\text{H-Acy}] = [H^+] + [HSO_4^-] + [HNO_2] + [HF] + [H_2SO_3] - [OH^-] - [HCO_3^-] - 2[CO_3^{2-}] - [NH_3] - [H_3SiO_4^-] - \Sigma n[Org^{n-}]. \quad (8)$$

Components such as HSO_4^-, HNO_2, HF, H_2SO_3, CO_3^{2-}, NH_3, and $H_3SiO_3^-$ are in negligible concentrations in typical rain water. Thus, the equation may be simplified to

$$[\text{H-Acy}] = [H^+] - [OH^-] - [HCO_3^-] - \Sigma n[Org^{n-}]. \quad (9)$$

For most rain samples of pH 4–4.5, [H-Acy] is equal to $[H^+]$, but in highly concentrated fog waters (in extreme cases, pH < 2.5) HSO_4^- and $SO_2 \cdot H_2O$ become important species contributing to the strong acidity.

The reference conditions pertaining to the determination of total acidity [Acy_T] are H_2O, CO_3^{2-}, SO_4^{2-}, NO_3^-, Cl^-, NO_2^-, F^-, SO_3^{2-}, NH_3, $H_3SiO_4^-$, ΣOrg^{n-}, and $Al(OH)_3$. (When aluminum is titrated from pH 4 to pH 10, it will hydrolyze from Al^{3+} to $Al(OH)_3$, consuming

three equivalents of base for every molecule of Al^{3+}.)

$$[Acy_T] = [H^+] + 2[H_2CO_3] + [HSO_3^-] + [NH_4^+] + [H_4SiO_4] + 3[Al^{3+}] + 2[Al(OH)^{2+}] + [Al(OH)_2^+] + \Sigma n[H_nOrg] - [OH^-]. \quad (10)$$

For most samples this equation can be simplified as

$$[Acy_T] = [H^+] + [NH_4^+] + 2[H_2CO_3] + n[H_nOrg]. \quad (11)$$

Figure 5 shows a titration curve obtained from the addition of base to a test solution that can be converted to Gran plots to ease determination of equivalent points. This figure is a typical Gran plot of a rainwater titration that contains strong and weak acids. A Gran titration of the strong acidity usually gives a good approximation of the acidity [H-Acy], as defined above, but one must be aware that organic acids with pK_a 3.5–5 are partly included in this titration and may affect the resulting Gran functions. For the determination of total acidity, H_2CO_3 is usually stripped (with N_2) out of the samples, because when H_2CO_3 is present it is more difficult to reach the end point of the titration and to calculate the concentration of the weak acids.

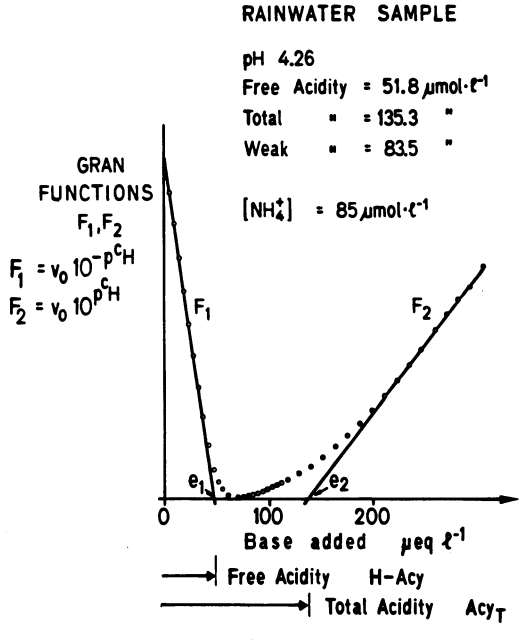


Fig. 5. Gran plot of a typical rainwater sample. Linear extrapolation of the Gran function $F_1 = v_0 10^{-pcH}$ and $F_2 = v_0 10^{pcH}$ to zero gives free (strong) acidity and total acidity, respectively. Weak acidity = 83.5 μmol/ℓ. pcH = $-\log[H^+]$; the glass electrode is calibrated at a given ionic strength (the solutions were made 0.05 M with regard to KCl) in terms of H^+ ion concentration. The CO_2 was removed by stripping with nitrogen gas prior to the titration. (Johnson and Sigg 1985; adapted with permission from Chimia 1985)

2.1 Transfer of Acidity (or Alkalinity) from Pollution Through the Atmosphere to Ecosystems

As we have pointed out, in a (hypothetically closed) large system of the environment consisting of the reservoir's atmosphere, hydrosphere, and lithosphere, a proton and electron balance is maintained. Temporal and spatial inhomogeneties between and within individual reservoirs, cause significant shifts in electron and proton balance, so that subsystems contain differences in acidity or alkalinity. Any transfer of an oxidant or reductant, of an acid or base, or of ions from one system to another – however caused, by transport, chemical reaction, or redox process – causes a corresponding transfer of acidity or alkalinity.

2.1.1 Atmospheric Acidity (Alkalinity)

It is essential to consider the acid–base neutralization process in the entire atmospheric system. Morgan (1982), Liljestrand (1985), and Jacob et al. (1986) introduced the concept of atmospheric acidity and alkalinity to interpret the interactions of NH_3 with strong acids emitted into and/or produced within the atmosphere. A net atmospheric acidity can be defined by summing over all potential acids and bases in the gas, aerosol and liquid phases, using reference conditions for specific redox conditions, and assuming the presence of liquid water.

Figure 6 exemplifies the concept of alklinity, Alk, and acidity, Acy, for a gas–water environment and defines the relevant reference conditions. In Fig. 6a and b, it is shown how the gases NH_3, SO_2, NO_x, HNO_3, HCl, and CO_2 (potential bases or acids, respectively), subsequent to their dissolution in water and the oxidation of SO_2 to H_2SO_4 and NO_x to HNO_3, become alkalinity or acidity components. Thus $\{Alk\}_{(gas)}$ and $\{Acy\}_{(gas)}$, for the gas phase, is defined by the following relation (Behra et al. 1989):

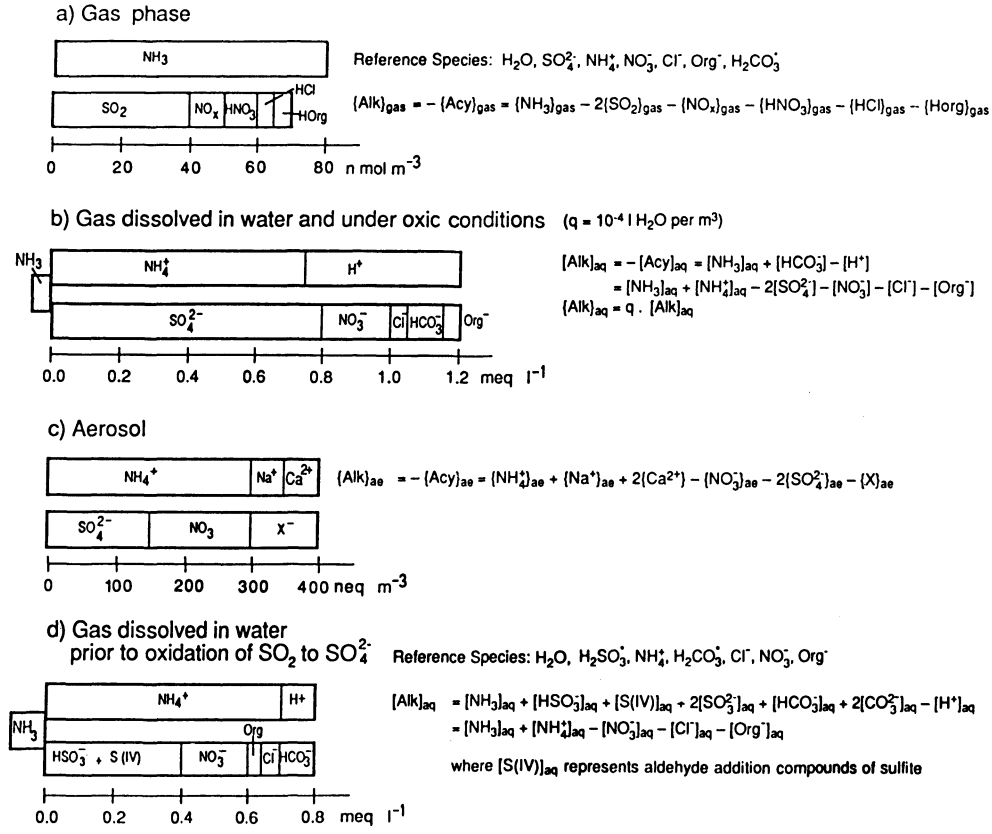


Fig. 6a–d. Alkalinity/acidity in atmosphere, aerosols, and atmospheric water. Alkalinity and acidity can be defined for the atmosphere using a reference state valid for oxic conditions (SO_2 and NO_x oxidized to H_2SO_4 and HNO_3) and in the presence of water. The neutralization of atmospheric acidity by NH_3 is a major driving force in atmospheric deposition (Behra et al. 1989)

$$\{Alk\}_{(gas)} = \{NH_3\}_{(gas)} - 2\{SO_2\}_{(gas)} - \{NO_x\}_{(gas)} - \{HNO_3\}_{(gas)} - \{HCl\}_{(gas)} - \{HOrg\}_{(gas)} \quad (12)$$

and

$$\{Alk\}_{(gas)} = -\{Acy\}_{(gas)}, \quad (13)$$

where { } indicate mol m^{-3} and HOrg is the sum of volatile organic acids. Figure 6b shows that these potential acids and bases subsequent to their dissolution in cloud or fog water with q = 10^{-4} l H_2O per m^3 atmosphere give a water with the equivalent acidity.

In the case of aerosols, we can define the alkalinity by a charge balance of the sum of conservative cations, $\Sigma n\{Cat.^{n+}\}_{(æ)}$, of NH_4^+, $\{NH_4^+\}_{(æ)}$, and of the sum of conservative anions, $\Sigma m\{An.^{m-}\}_{(æ)}$ (Fig. 6c):

$$\{Alk\}_{(æ)} = \Sigma n\{Cat.^{n+}\}_{(æ)} + \{NH_4^+\}_{(æ)} - \Sigma m\{An.^{m-}\}_{(æ)}. \quad (14)$$

2.1.2 *Role of NH_3*

NH_3 essentially "titrates" the inputs of the potential strong acids in the atmosphere (Jacob et al. 1986; Behra et al. 1989). The oxidation of SO_2 in atmospheric water (cloud, rain, liquid aerosol, and fog) is influenced by the presence of NH_3. The enhancing effect of NH_3 is especially pronounced if the oxidation occurs with an oxidant such as O_3, for which the reaction rate increases strongly with increasing pH, because NH_3 (1) codetermines the pH of the water, and thus, in turn, the solubility of SO_2, and (2) provides acid-neutralizing capacity as well as buffer intensity to the heterogeneous atmosphere–water system in counteracting the acidity produced by the oxidation of SO_2. (Behra et al. 1989). At low buffer intensity, e.g., in case of residual atmospheric acidity, i.e., if

$$\{NH_3\}_{(gas)} < 2\{SO_2\}_{(gas)} + \{NO_x\}_{(gas)} + \{HNO_3\}_{(gas)} + \{HCl\}_{(gas)}, \quad (15)$$

the acidity production alleviates further SO_2 oxidation.

Thus, while NH_3 introduced into the atmosphere reduces its acidity, it enhances the oxidation of SO_2 by ozone, participates in the formation of ammonium sulfate and ammonium nitrate aerosols, and accelerates the deposition of SO_4^{2-}. Furthermore, any NH_3 or NH_4^+ that is returned to the earth' surface becomes, as a consequence of microbial nitrification, HNO_3

$$NH_3 + 2O_2 = H^+ + NO_3^- + H_2O$$
$$NH_4^+ + 2O_2 = 2H^+ + NO_3^- + H_2O \qquad (16)$$

and may aggravate the acidification of soils and lakes. This effect is not sufficiently considered in the assessment of NH_3 emissions (e.g., agriculture, feed lots) and the use of excess NH_3 used in technical processes to reduce nitrogen oxides.

3 Acidification of Aquatic and Terrestrial Ecosystems

In order to understand how acid deposition affects the H^+ ion balance in the watersheds we must consider the major H^+-yielding and H^+-consuming processes occurring in these watersheds. Of great significance here, in addition to the H^+ ion consumption by weathering processes (Table 2) and biologically mediated redox processes, are biological assimilation and mineralization.

3.1 Disturbance of H^+ Balance from Temporal or Spatial Decoupling of the Production and Mineralization of the Biomass

In a most general way the synthesis (assimilation) and the decomposition (respiration) of biomass can be written stoichiometrically as

Table 2. Processes that modify the H^+ balance in waters

Processes	Changes in alkalinity $\Delta[Alk] = -\Delta[H\text{-}Acy]$ [equivalents per mol reacted (reactant is italicized)]
1. Weathering reactions:	
$CaCO_3(s) + 2H^+ \rightleftharpoons Ca^{2+} + CO_2 + H_2O$	+2
$CaAl_2Si_2O_8(s) + 2H^+ \rightleftharpoons Ca^{2+} + H_2O + Al_2Si_2O_5(OH)_4(s)$	+2
$KAlSi_3O_8(s) + H^+ + 4\frac{1}{2}H_2O \rightleftharpoons K^+ + 2H_4SiO_4 + \frac{1}{2}Al_2Si_2O_5(OH)_4(s)$	+1
$Al_2O_3 \cdot 3H_2O + 6H^+ \rightleftharpoons 2Al^{3+} + 6H_2O$	+6
2. Ion exchange:	
$2ROH + SO_4^{2-} \rightleftharpoons R_2SO_4 + 2OH^-$	+2
$NaR + H^+ \rightleftharpoons HR + Na^+$	+1
3. Redox processes (microbial mediation):	
Nitrification $HN_4^+ + 2O_2 \rightleftharpoons NO_3^- + H_2O + 2H^+$	−2
Denitrification $1\frac{1}{4}CH_2O + \frac{1}{4}NO_3^- + H^+ \rightarrow \frac{1}{4}CO_2 + \frac{1}{2}N_2 + 1\frac{3}{4}H_2O$	+1
Oxidation of H_2S $H_2S + 2O_2 \rightarrow SO_4^{2-} + 2H^+$	−2
SO_4^{2-} reduction $SO_4^{2-} + 2CH_2O + 2H^+ \rightarrow 2CO_2 + H_2S + H_2O$	+2
Pyrite oxidation $FeS_2(s) + 3\frac{3}{4}O_2 + 3\frac{1}{2}H_2O \rightarrow Fe(OH)_3 + 2SO_4^{2-} + 4H^+$	−4
4. In the buildup (or breakdown) of biomass, the uptake (release) of each equivalent of conservative anion causes an equivalent increase (decrease) in alkalinity, and each equivalent of base cations that is taken up (released) results in an equivalent decrease (increase) of alkalinity. The reduction of Fe(III)(hydr)oxides and of Mn(III,IV)(hydr)oxides by biota is particularly efficient in generating alkalinity in the hypolimnion of lakes.	
$\{(CH_2O)_{106}(NH_3)_{16}(H_3PO_4)\}_{Biota} + 424Fe(OH)_3 + 862H^+ \rightarrow 424Fe^{2+} + 16NH_4^+ + 106CO_2 + HPO_4^{2-} + 1166H_2O$ (a)	
$\{(CH_2O)_{106}(NH_3)_{16}(H_3PO_4)\} + 212MnO_2 + 398H^+ \rightarrow 212Mn^{2+} + 16NH_4^+ + 106CO_2 + HPO_4^{2-} + 298H_2O$ (b)	

$$a\,CO_2(g) + bNO_3^- + cHPO_4^{2-} + dSO_4^{2-} + gCa^{2+} + hMg^{2+} + iK^+ + fNa^+ + xH_2O + (b + 2c + 2d + 2g - 2h - i - f)H^+ \rightleftharpoons \{C_aN_bP_cS_d \ldots Ca_gMg_hK_iNa_fH_2O_m\}_{biomass} + (a + 2b)O_2(g). \quad (17)$$

Using our definition for alkalinity or ANC, whereby any decrease (increase) in concentrations of base cations (e.g., K^+, Ca^{2+}, Fe^{2+}, etc.) or any increase (decrease) in concentrations of "acid anions" e.g., NO_3^-, HPO_4^{2-}, SO_4^{2-}, etc.) is accompanied by a decrease (increase) in alkalinity. Thus, as illustrated in Fig. 7 the net synthesis of terrestrial biomass [e.g., on the forest and forest floor, where more cations than anions are taken up by the plants (trees), is accompanied by a release of H^+ into the environment. The acidification of the environment is accompanied by an increase in base in the aggrading biomass (wood and vegetation)]. The ash of wood and of vegetation is alkaline; one speaks of "potash." Figure 8a illustrates that forest trees act like a base pump. The "export" of alkalinity occurs by the harvesting of the wood and the release of base cations to the aqueous runoff; this is balanced by the production of base cations in the weathering process of minerals. Ion exchange processes of soil minerals and of humus represents an intermediate buffering pool of fast exchangeable bases. The large pool of mineral bases is characterized by relatively slow kinetics of chemical weathering.

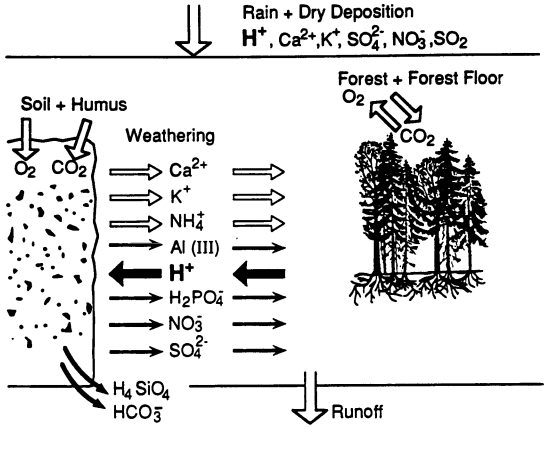


Fig. 7. Process affecting the acid neutralizing capacity of soils (including exchangeable bases, cation exchange, and mineral bases). H^+ from acid precipitation and from the release by the roots react by weathering rocks and by ion exchange on clays and humus. (Stumm and Schnoor 1986)

If chemical weathering did not replace exchangeable bases in acid soils of temporal regions receiving acidic deposition, the base-exchange capacity of the soils would be completely diminished over a period of 50–100 years.

The interaction between acidification by an aggrading forest and the leaching (weathering) of the soil is schematically depicted in Fig. 7. If the weathering rate equals or exceeds the rate of H^+ release by the biota, such as would be the case in a calcareous soil, the soil will maintain a buffer in base cations and residual alkalinity. On the other hand, in noncalcareous "acid" soils, the rate of H^+ release by the biomass may exceed the rate of H^+ consumption by weathering and cause a progressive acidification of the soil. In some instances the acidic atmospheric deposition may be sufficient to disturb an existing H^+ balance between aggrading vegetation and weathering reactions. A quantitative example is provided by the carefully established acidity budget in the Hubbard Brook Ecosystem (Fig. 8b; Driscoll and Likens 1982), where, because of acid deposition, H^+ ion sources nearly balance H^+ ion sinks.

Humus and peat can likewise become very acidic and deliver some humic or fulvic acids to the water. In wetlands certain plants, such as the bog moss Sphagmur avidly taking up base cations and releasing H^+ ions, act like cation exchangers. Note that the release of humic or fulvic material (HOrg, Org^-) to the water is in itself not necessarily the cause of resulting acidity, but rather the consequence of H^+ production and aggrading vegetation humus and net production of BNC.

3.2 In Situ H^+ Ion Neutralization in Lakes

In addition to processes in the terrestrial drainage, in situ biogeochemical processes can be major sources of alkalinity, especially in pool-buffered (noncarbonate) watersheds. The chemistry of this alkalinity generation is well understood (Froelich et al. 1979; Goldman and Brewer, 1980; Stumm and Morgan 1995; Schnoor and Stumm 1985; Cook et al. 1986; Psenner 1988; Lerman and Stumm 1989), and is based on the equations in Table 2. Basically, the interaction of the organic products of photosynthesis (e.g., settling algae and biological debris) as reductants (electron donors) with oxidants such as nitrates, sulfates, or Fe(III)(hydr)oxides and Mn(III,IV)(hydr)oxides, is accompanied by alkalinity generation. One can

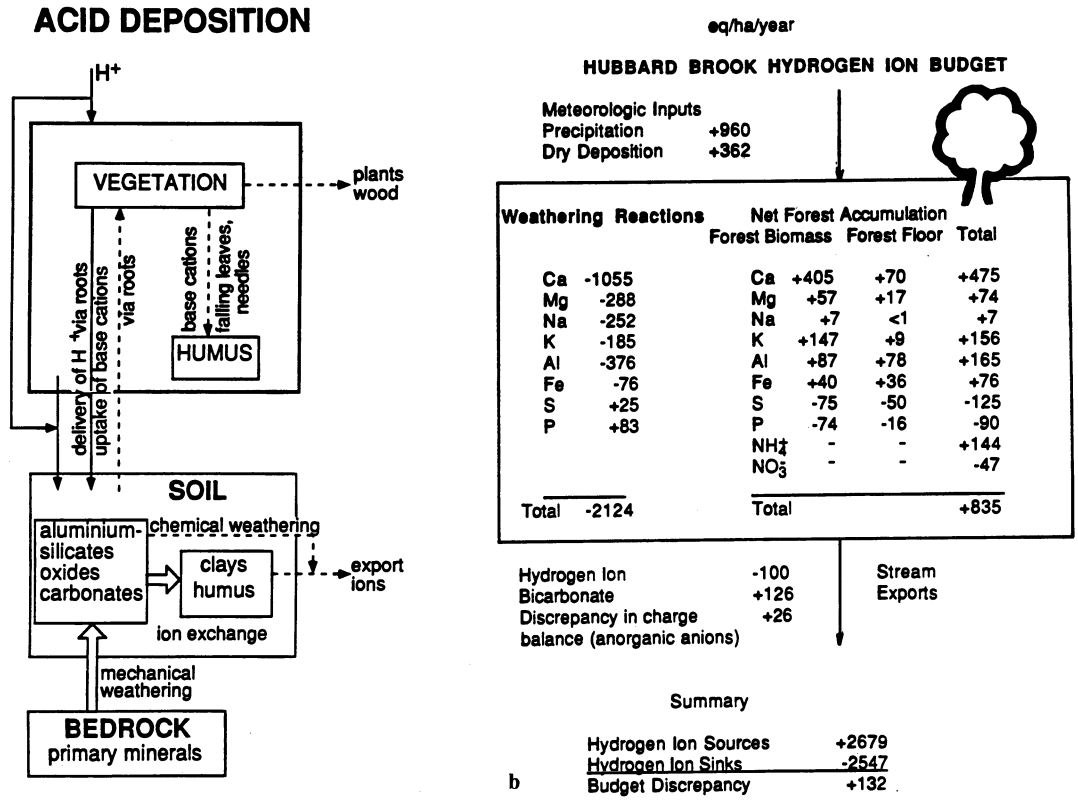


Fig. 8. a Processes affecting the acid-neutralizing capacity (ANC) of soils (including the exchangeable bases, cation exchange, and mineral bases). H^+ ions from acid precipitation and from the release by the roots react by weathering carbonates, aluminum silicates, and oxides, as well as by surface complexation and ion exchange on clays and humus. Mechanical weathering resupplies weatherable minerals. *Solid lines* indicate flux of protons; *dashed lines* show flux of base cations (alkalinity). The trees (plants) act like a base pump (Schnoor and Stumm 1986). **b** Budger of H^+ Sources and H^+ Sinks in Hubbard Brook Ecosystem. H^+ ion released or consumed in eq $ha^{-1} yr^{-1}$ as a consequence of ion uptake by the aggrading forest biomass (+ forest floor) and ion release by weathering reactions, respectively. Because of atmospheric deposition of acid, H^+ sources nearly balance H^+ sinks. (Likens et al. 1977)

illustrate this in terms of stoichiometrically formulated redox processes (Table 2) or the H^+ ion balance accounting can simply be made as suggested in Eq. (5), i.e., by summing up the concentration changes in "base" cations (Ca^{2+}, K^+, Fe^{2+}, Mn^{2+}), and in "acid" anions (NO_3^-, SO_4^-, HPO_4^{2-}, HS^-).

Figure 9a illustrates the relationship between consumed nitrate and alkalinity in Lake 227 as reported by Schindler (1985). A more complete balancing of alkalinity changes in the same lake, as reported by Cook et al. (1986), is given in Fig. 10.

3.2.1 Biomass as a Reductant

In watersheds and lakes the biomass originally produced by photosynthesis (redox disproportionation of water into oxygen and hydrogen that combines with C and other elements to living organic matter) is the most important reductant (electron donor). In the reduction of NO_3^-, SO_4^{2-}, $Fe(OH)_3$, and MnO_2 by the biomass and its debris and decompensation products, protons are consumed (corollary to the electron consumption), i.e., alkalinity is generated (Table 2). In a lake the hypolimnion and the sediment is continuously "titrated" with the settling phytoplankton. Figure 9b illustrates the gradient in H^+ and in HCO_3^- in Clearwater Lake (Canada) in June (Carignan 1985) at the sediment–water interface. Because the sediments are more reducing than the overlying waters, the more intense reduction processes in the sediments consume more H^+ ions than in the overlying waters; the sediments are a sink for H^+ and a source of HCO_3^-. Eutrophication produces more biomass and thus counteracts

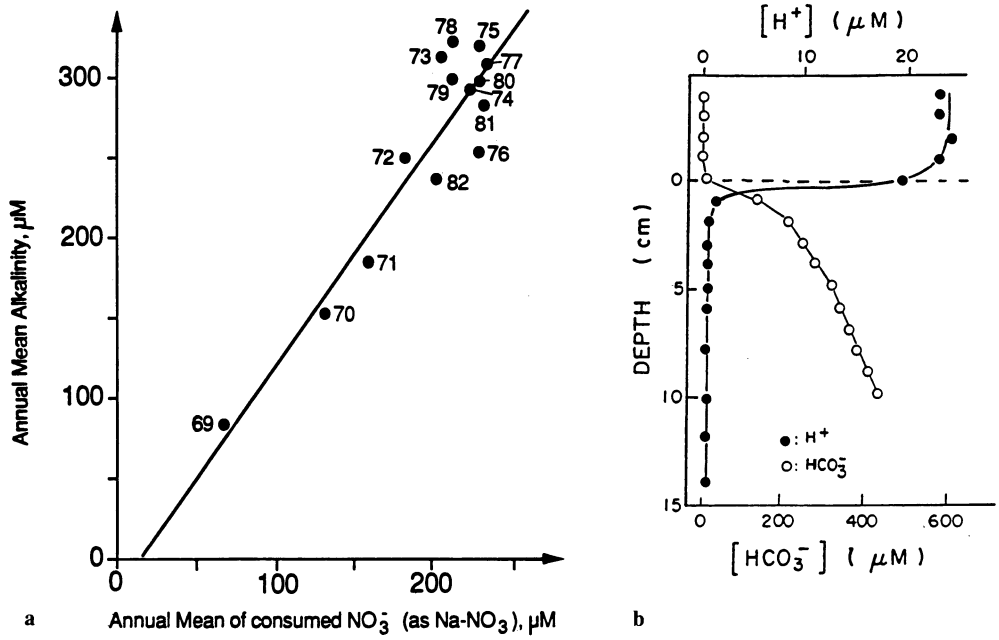


Fig. 9. a Alkalinity production in lakes by redox reactions. The relationship between consumed nitrate (as represented by Na-NO_3) and alkalinity in Lake 227. Na^+ is affected only by water renewal, whereas NO_3 is affected by both biological uptake and water renewal. Points are mean annual averages for the years indicated by the number (Schindler 1985). **b** Pore-water concentration profiles of H^+ and HCO_3^- obtained at a station located in Clearwater Lake. The flux of alkalinity to the overlying water is given by the flux of HCO_3^- minus the flux of H^+. (After Carignan 1985)

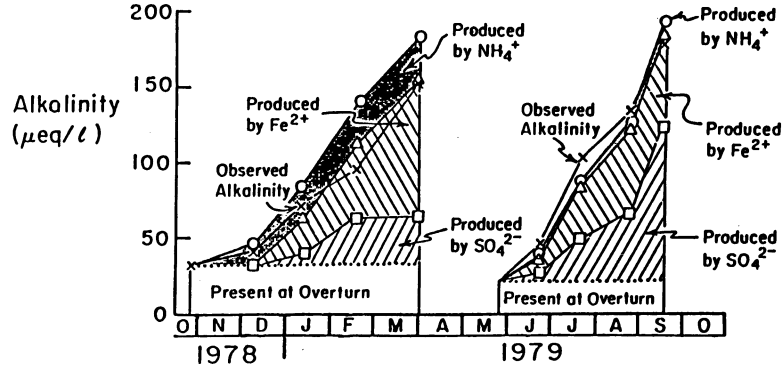


Fig. 10. Observed volume-weighted average alkalinity in the hypolimnion and that predicted from Fe^{2+} production, SO_4^{2-} reduction, and NH_4^+ production. Mn^{2+} also accounts for alkalinity production (9 μeq/ℓ in winter and 7.5 μeq/ℓ in summer), which was not plotted for the sake of clarity. The volume of the 10- to 14-m zone is 2.22×10^3 m^3 and the area of sediment in this zone is 8.25 ha. (Cook et al. 1986)

acidification. Davison (1986) has shown that disposal of sludge to an acidified lake reduces its acidity. Even land eutrophication (excessive production of crops) can cause acidification of soils.

3.3 Krug and Frink Revisited

Krug and Frink (1983) wrote a paper doubting the evidence for the acidification of lakes. Their hypothesis was that most of the lakes in the world that were presently acidic were also rich in organic acids, presently or in the past. Often these lakes are colored waters with dissolved organic carbon concentrations greater than 10 mg/l. The input of strong acids from anthropogenic acidic deposition did little to change the pH of the systems according to Krug and Frink. It simply changed the acid from organic to sulfuric, and coagulated the organics with metal ions, e.g., aluminum.

Aluminum ions are liberated from ion exchange in the organic soil and from dissolution of aluminum oxides in the mineral soil upon addition of acid deposition (H_2SO_4). The waters became less colored during this titration, but they remained acidic with little change in pH.

The argument of Krug and Frink seemed to minimize the importance of acidic deposition and its impacts on lakes. In this regard, it missed several important points:

1. Although the lakes are buffered by aluminum exchange and dissolution, there is a small, but significant, change in pH of the system as it changes from organic acids controlling the pH to dilute strong acids.
2. The liberation of aluminum is toxic to fish, amphibians, and other living organisms. Thus, although the change in pH may be small, the ecological effects can be large. Schnoor et al. (1986a) found several examples in the Upper Peninsula of Michigan of two lakes, side by side, with similar pH values (pH 4.8), one with organic acids and a healthy fish population, and the other with clear water and barren of fish.
3. Buffering of natural waters with alumina is not effective during storm events and winter snowmelt. Thus, acid pulses will result in systems receiving acidic deposition that will affect the chemistry and biology of the streams and lakes.

Krug and Frink (1983) did provide a valuable reminder of the importance of organic acids in poorly drained natural waters. Models that did not fully account for the role of organic acids and aluminum complexation, e.g., the ETD model by Nikolaidis et al. (1988) and the MAGIC model by Cosby et al. (1985), were not able to reproduce this nuance in colored lakes. Nevertheless, the hypothesis of Krug and Frink (1983) does not account for the acidification of a significant number of clear-water systems that were never colored. Diatom-inferred pH studies from paleoecology have demonstrated that these lakes became acidic during the past 50 years (Baker et al. 1991).

4 Brønsted Acids and Lewis Acids: Pollution by Heavy Metals, as Influenced by Acidity

The two major pollution problems in the world today, acid pollution and metal pollution, are both manifestations of acid–base disturbances in the most general sense. As we have seen, deposition of acidity results from intensive oxidative production of Brønsted acids (H_2SO_4, HNO_3) causing increased BNC in ecosystems. Metal pollution introduces excessive quantities of certain Lewis acid metals to ecosystems (Morgan and Stumm 1989). The biological consequences of metal pollution strongly depend on the resulting chemical speciation, which is a function of the kinds and amounts of Lewis bases, the redox intensity ($p\varepsilon$), and the acidity–alkalinity (pH) characteristics of particular environments. In the biota the key Lewis bases include ligands (in solution as well as on particle surfaces) containing oxygen donors (e.g., $-OH$, RCOOH), sulfur donors (e.g., $-SH$), or nitrogen donors (e.g., $-NH$, $-NH_2$), which can become coordinated to *essential trace metals*, e.g., Mg, Mn, Fe, Co, Zn, and Cu.

In biochemistry, geochemistry, environmental chemistry, and in chemistry of metal emission control it is important to recognize and make use of the general pattern of chemical affinities between Lewis acids and bases, i.e., the energetics of equilibria for all reactions of interest of metal coordination

$$M_i + L_j \rightleftharpoons M_iL_j, \tag{18}$$

including aqueous, solid, and surface complex species, and extending to multiple metal (e.g., polynuclear) or multiple ligand (e.g., mixed ligand) forms. The *aqueous proton* is one of the most influential M_i, and the hydroxide ion one of the more influential ligands. Redox state of the electron acceptors, M_i, and of the donors, L_j, *strongly* affect the affinities (e.g., Fe^{3+} vs Fe^{2+} and SO_4^{2-} vs S^{2-}).

The proportion of free metal ions, and thus potential ecologically adverse effects, increases markedly with lower pH, because H^+ ions compete successfully with metal ions for the available ligands:

$$\begin{aligned} CO_3^{2-} + H^+ &= HCO_3^- \\ RCOO^- + H^+ &= RCOOH \\ {=}MeO^- + H^+ &= {=}MeOH \\ Al(OH)_3 + H^+ &= Al(OH)_2^+ \end{aligned} \tag{19}$$

$$CuCO_3(aq) + H^+ = Cu^{2+} + HCO_3^-$$
$$RCOOZn^+ + H^+ = RCOOH + Zn^{2+}$$
$$=MeOPb^+ + H^+ = =MeOH + Pb^{2+} \quad (20)$$

For example, heavy metal concentrations measured in acidic mountain lakes, despite significantly smaller pollutional metal input, are much larger than those measured in lakes in eutrophic-carbonate-bearing watersheds, because metal ion binding by sorption to particle surfaces decrease with decreasing pH (Sigg 1985). As shown by Tessier et al. (1989), the scavenging of metals by sinking particles is less in acid lakes. Thus, the concentration of dissolved metal ions in acid lakes is often larger in the hypolimnetic waters than in the sedimentary pore waters, especially if redox conditions are conducive to metal sulfide formation; steep concentration gradients develop at the sediment–water interface.

A comparison of typical metals essential for life with the potentially *hazardous* metals is of interest (metalloids are italicized): essential metals are Na, K, Mg, Ca, Cr, Mn, Fe, Co, Ni, Cu, Zn, and Mo; hazardous metals are Cr, Cu, Zn, *As*, *Se*, Ag, Cd, In, Sn, *Sb*, Hg, Tl, Pb, and Bi.

4.1 Cycling of Metals

The dispersion of metals into the atmosphere appears to rival and sometimes exceed natural mobilization. Despite many uncertainties, the conclusion emerges from Sposito's review (1986) that the trace metals Cu, Zn, Ag, Sb, Sn, Hg, and Pb are the most potentially hazardous on a global or regional scale. Lead is of acute concern on the global scale, because of its prominent showing in all the enrichment factors and tranfer rates considered. These conclusions are in accord with those of Andreae et al. (1984).

The B metals, i.e., the soft Lewis acids, are not only enriched in the natural environment, but they are also, because of their toxic effect (i.e., their tendency to react with soft bases; e.g., to SH- and NH-groups in enzymes) potentially hazardous to ecology and human health.

Settling particles, especially bioorganic particles, play a dominating role in binding heavy metals and transferring them to the deeper portion of oceans and lakes where they are partially mineralized and transformed into the sediments. Biological surfaces are especially efficient scavengers – probably (for equal specific surface area) better ones than the mineral surfaces – for heavy metals (Morel and Hudson 1985; Sigg 1985, 1987; Whitfield and Turner 1987).

Lakes, despite being polluted with metal ions 10–100 times as much as oceans from riverine and atmospheric inputs, are often nearly as much depleted in these trace metals as are oceans. Therefore, the elimination mechanisms in lakes must be more efficient than those in oceans. Larger productivities and higher sedimentation rates for particles are primarily responsible for the more efficient scavenging in lakes through adsorption of metals on phytoplankton, and to a lesser extent, by other particles. The input of phosphorus into a lake, influencing the production of biogenic particles, is a major factor controlling the sedimentation rate of biogenic particles and in removing "biophile" heavy metals (Sigg et al. 1987). Settle and Patterson (1980) have used data on the memory record of sediments in the Pacific Ocean to compare prehistoric and present-day eolian inputs. These data suggest that the present Pb(II) input is two orders of magnitude larger than that of prehistoric time. What does this mean with regard to ecology? We really do not know.

4.2 Pb in Soils

Acid deposition is accompanied by toxic metals from industrial point sources and mobile sources. One of the most serious metals from a health perspective has been lead, a primary anti-knock compound in gasoline in the United States until 1974. Deposition of acids may affect the fate and transport of metals as they move through soil horizons to groundwater or surface water. In the case of lead, it is important to understand factors controlling the recovery time for ecosystems following a major management action, such as the removal of lead from gasoline. Friedland et al. (1992) reported the rapid decrease of lead in the forest floor of the northeastern United States between 1980 and 1990, a 12–17% change in lead concentrations. The estimated residence time for lead in the organic horizon of forest soils is approximately 150–500 years; therefore, a change of 12–17% in the lead concentration in only 10 years is, indeed, unexpected. The forest floor is defined as the top few centimeters of soil that is

rich in organic carbon (50–75% by mass) and that overlies the mineral soil in forests.

A case study for lead has been conducted in the Hubbard Brook Experimental Forest (HBEF), US Department of Agriculture, in central New Hampshire. Figure 11 summarizes the research of Driscoll et al. (1994) at Hubbard Brook and the Council on Environmental Quality (1990) on the ambient air quality monitoring network in the northeast. Concentrations of lead in ambient air decreased rapidly after 1974, from ~1.2 mg/m^3 to ~0.1 mg/m^3. The dramatic improvement in air quality was corroborated by the decrease of Pb in precipitation samples collected at HBEF between 1976 and 1988. Similar to the report by Friedland et al. (1992), the data of Driscoll et al. (1994) at HBEF demonstrates a dramatic decrease of Pb in the forest floor. Although Pb has been leaving the organic soil horizon, it has not been measured in streams draining the forests, and it would seem that it is adsorbing in the deeper mineral soils. It is likely that there is a large labile pool of Pb in the forest floor that responds to changes in deposition and biomineralization very rapidly, but the exact mechanism of mobilization has yet to be determined (Friedland et al. 1992). Concomitant changes in acid deposition may be responsible for changing the binding constants of Pb-organic complexes in the organic soil and rendering it more mobile than models would predict.

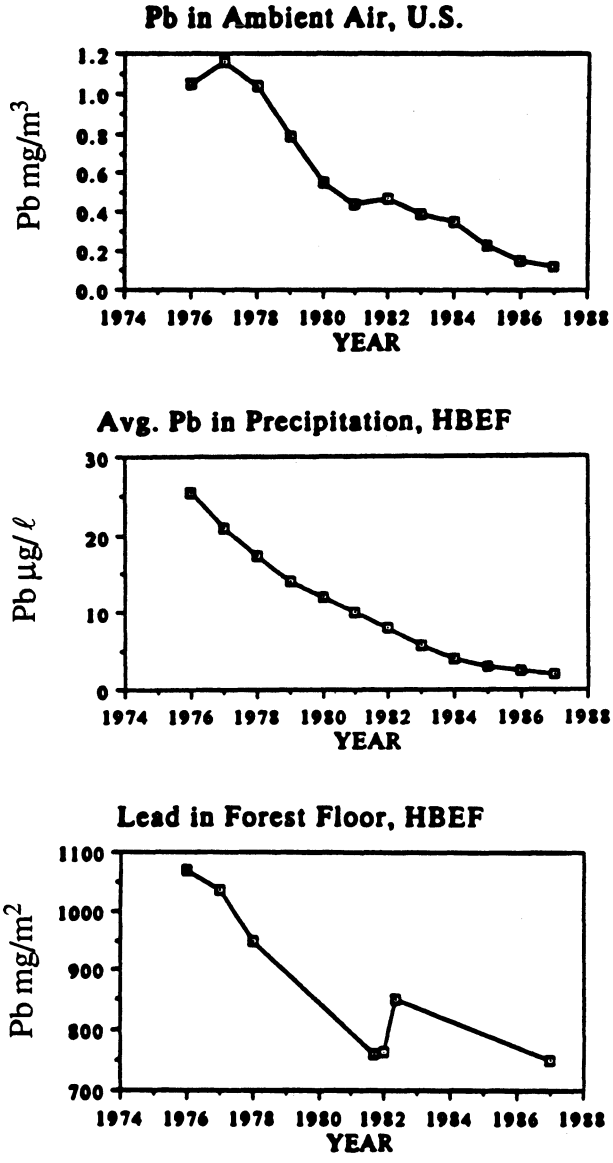


Fig. 11. Lead concentrations in ambient air (CEQ 1990) and in precipitation samples and the forest floor at the Hubbard Brook Experimental Forest, New Hampshire, 1976–1987. (Driscoll et al. 1993)

5 Impact of Acidity on Ecology in Watersheds

5.1 Soils

Although we concentrate on describing the ecological impact of acidity on lakes, a few remarks on the acidification of soils in their watersheds are relevant. The regions where acid deposition has been reported to affect lakes (Adirondacks, New York, southern Norway, and Sweden) also have acid soils. If chemical weathering cannot replace exchangeable bases in soils quickly enough, base cations become depleted from the upper soil profile, and iron and aluminum are mobilized. Such chromatographic effects can lead to podsolic acid soils. Aluminum is not only liberated from the soil in the rooting zone, but it is at high concentrations as Al^{3+} or $AlOH^{2+}$ on the fine roots and mycorrhizal fungal associations. The possible toxic effects of Al^{3+}, its uptake by trees in acid soils, and sorbed Al effects on active and passive transport of nutrients to the tree are the subject of many current debates (Ulrich 1981; Van Breemen et al. 1983). Lower pH values accentuate the potential negative effects of heavy metals.

5.2 Lakes

It is been pointed out by Schindler (1987) that sensitivities of terrestrial and aquatic ecosystems to atmospheric pollutants are remarkably dif-

ferent. Primary production seems to be reduced at a much earlier stage of air pollution stress in terrestrial ecosystem than in aquatic ecosystem. Soils, like lake sediments, tend to be sinks for pollutants; this may protect the pelagic regions of lakes from influxes of toxic substances that would occur if watersheds and sediments were unreactive (Schindler 1987). The careful studies by Schindler et al. (1985) of experimental acidification on a small lake (Lake 223) – over a period of 8 years the pH of the lake was gradually decreased from 6.8 to 5.0 by the addition of H_2SO_4 – have provided invaluable documentation and interpretation of response of a lake to long-term ecosystem stress. The acidification produced dramatic changes in the lake's food web; above all, in phytoplankton species, in the disappearance of benthic crustaceans, and the cessation of fish reproduction. Schindler et al. (1985) report that key organisms in the food web leading to lake trout were eliminated from the lake at pH values as high as 5.8. They interpret this as an indication that irreversible stresses on aquatic ecosystems occur earlier in the acidification process than was heretofore believed. These changes are caused in Lake 223 by H^+ ion alone, and not by the secondary effect of aluminum toxicity.

The humic substances are adsorbed to oxide and other soil minerals; the adsorption is pH-dependent and decreases with increasing pH. Thus, the acidification of soil systems reduces the drainage of humic substances into receiving waters. Furthermore, the increased dissolved Al(III) forms complexes with the residual humic acids. All of these effects, (lowering of pH, increase of Al(III), and decrease in concentration of humic acids) increase the activity of free heavy metals. Increased free metal ion activity can have an impact on ecological structure of phytoplankton. There also can be some speculations on whether toxic algal blooms in the North Sea or in the Adriatic Sea may have been accentuated by these indirect consequences of the increased acid deposition during the past decades.

5.3 Nitrogen Saturation of Forests

Nitrogen in the form of ammonium and nitrate is a fertilizer for forest growth. In most forests of the northern temperate and boreal zones, nitrogen is considered to be the limiting nutrient for forest growth. However, nitric acid deposition and other forms of nitrogen are increasing worldwide. Human capacity to fix nitrogen from the atmosphere in the form of ammonia for fertilizer and NOx from fossil-fuel combustion now rivals the total nitrogen fixed by natural processes such as nitrogen-fixing plants and by lightning. Whereas sulfur deposition has been decreasing over the past 5–10 years in developed countries, nitrogen deposition continues to increase, and it is becoming a larger fraction of total acid deposition. Nitrogen saturation may be defined as a surplus of mineral nitrogen in forests beyond the capacity for plant uptake or soil immobilization. Increasingly saturated with nitrogen, forest growth could become limited by other factors such as phosphate, magnesium, water, light, or temperature.

When forests lie in hydrogeographical settings that are sensitive to acid deposition, the leaching of nitrate from the forest floor during snowmelt or runoff events becomes an acidifying influence on soils, streams, and lakes. Organic nitrogen is mineralized to ammonium in forest soils, and the ammonium undergoes nitrification releasing hydrogen ions. Similarly, hydrogen ion is released from root cells when ammonium is taken up by vegetation; the process is necessary to achieve a charge balance in the plant tissue. Leaching of nitrate from forest soils has been correlated with low ANC and acid pulses in many stream ecosystems in the northeastern and southeastern United States (Murdoch and Stoddard 1992; Herlihy et al. 1993). It has also been linked to liberation of aluminum in soils, root toxicity, and/or forest nutrition problems. Leakage of nitrate can become a significant contribution to eutrophication of lakes and estuaries, particularly if they are nitrogen-limited such as Chesapeake Bay.

Forests in southern Sweden and Denmark are currently receiving more than 20 kg N/ha per year, and nitrogen deposition in the northernmost Scandinavia, which probably reflects background levels, is approximately 5 kg N/ha per year (Rosen et al. 1992). Figure 12 is a schematic of the flow of nitrogen through a forest ecosystem. Typically 30–50 kg N/ha per year is mineralized in the forest floor in Scandinavia, so deposition in excess of these quantities required to sustain vegetation is subject to nitrate export from the watershed, which has been termed *nitrogen saturation*. Rosen et al. (1992) has published critical-load maps for nitrogen deposition in Nordic countries based on a simple mass-balance approach that ranges from 35 kg N/ha per year in the south to 1.3 kg N/ha per year in the north of

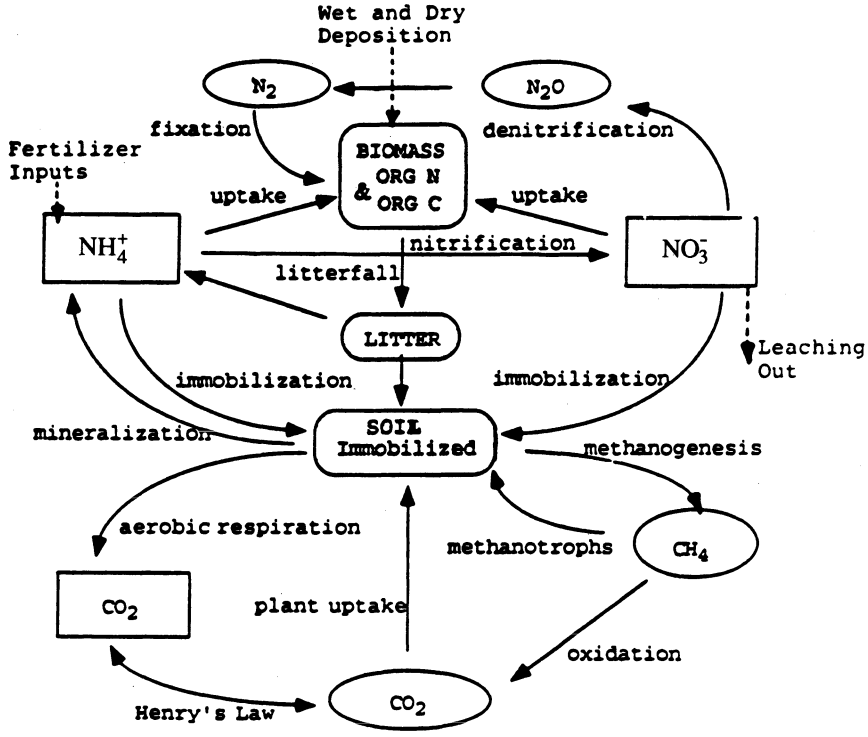


Fig. 12. Schematic of nitrogen and carbon flow through a forested ecosystem showing the immobilization of ammonium and nitrate into the organic soil pool and subsequent mineralization and nitrification of ammonium that results in the leakage of nitrate to drainage waters. (Rees 1992)

the Nordic countries. These levels are exceeded in southern and southwestern parts of the Nordic countries, with little or no excess in the north.

Figure 13 is a hypothetical plot of nitrogen accumulation in forests and export to streams as a function of nitrogen deposition. It is an idealized graph, because it does not take into account the age of the forest nor the time horizon for nitrogen saturation to occur. Low levels of nitrogen deposition (0–25 kg/ha per year), are immobilized into the organic pool and taken up by vegetation, a fertilization effect resulting from increased primary production. In sensitive forested ecosystems, N deposition in the range of 25–50 kg N/ha per year results in initial export of nitrate to drainage water. Generally nitrate-nitrogen concentrations are low (<0.2 mg/ℓ), but as N deposition increases they may increase to 0.3–0.7 mg/ℓ, the first signs of N saturation and possible forest effects at some time in the future. The mass of nitrate exported via the stream is still small compared with the total deposited, but it increases as deposition increases to become >50 kg N/ha per year, and N saturation becomes more serious, as shown in Fig. 13.

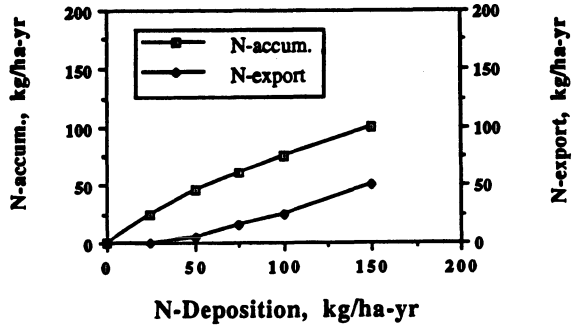


Fig. 13. Hypothetical plot of nitrogen accumulation in an ecosystem (organic N in canopy, bole, roots, and soil) and nitrogen export (nitrate predominantly) from forested catchments as a function of atmospheric deposition in kg N/ha per year

6 Critical Loads

Critical loads have been defined as "a quantitative estimate of an exposure to one or more pollutants below which significant harmful effects on specified sensitive elements of the environment do not occur according to our present knowledge" (see Brodin and Kuylenstierna 1992). The interest in

critical loads has increased over the past 5 years, because of its appeal to both scientists and policy makers. It is appealing to some scientists because the concept of critical loads considers biological effects of pollution in a quantitative framework. Biological effects are really the end point that scientists and the public are seeking, e.g., preservation a fishery rather than placing an arbitrary effluent limit on industry that may or may not produce the desired effect. In practice, the environmental scientist resorts to chemical indicators of biological effects. The concept of critical loads appeals to some policy makers as well, because there is an implicit assumption that the critical load will truly protect the natural resource, and the decision maker can take comfort in that fact with constituencies.

In 1985 the Convention on Long Range Transboundary Air Pollution of the United Nations Economic Commission for Europe was signed and ratified by 21 European countries, the United States, and Canada. It formed the so-called 30% club, countries that pledged to decrease their sulfur emissions by 30% from 1980 levels by 1993. The agreement has been largely successful, but it left people wondering whether 30% was enough. What reduction in emissions would be required to prevent future acidification of lakes or forest decline? Critical loads have been the management tool of choice in Europe ever since. In 1988 the NOx protocol was signed by 25 European countries, the United States, and Canada, promising that NOx emissions should not increase from 1980–1985 levels. It included the use of critical load estimates as the protocol for future pollution control agreements (Brodin and Kuylenstierna 1992).

Estimates of critical loads are fraught with many scientific ambiguities, however. Turning back to the definition, let us examine a few key arguments that point out the difficulties in estimating critical pollutant loads for a given region or country:

1. Pollutants. Which pollutants are the most critical and how do the various pollutants interact to cause biological effects?
2. Harmful effects. Which effects are most harmful?
3. Sensitive elements of the environment. Which elements of the ecosystem are we trying to protect, and which one is the most sensitive on which spatial scale?

It may not be possible to protect the most sensitive lake in a region, so how much of the total resource can be protected? Maintaining pollution levels below the critical load is supposed to ensure that harmful effects do not occur, but what is the appropriate time horizon on which to base an estimate of the critical load? Perhaps the most vexing of problems from an implementation standpoint is the difficulty of defining a sourcereceptor relationship for allocation of transboundary pollutant emissions. It must be both scientifically defensible and politically palatable.

The estimation of critical loads is viewed as a scientific problem. Once the critical loads have been established, it is up to each country to determine *target loads*. Target loads take into account technical, social, economic, and political considerations including what is achievable and what is desirable for the individual country. The relationship between critical loads and target loads is roughly analogous to that of water quality criteria and water quality standards in the United States. Target loads, like water quality standards, would be enforceable by law. Target loads could be set more stringently than critical loads in order to ensure a safety factor and to prevent significant deterioration of resource quality. On the other hand, target loads could be set less stringently than the critical load, thus admitting that some resources would be affected, but, perhaps, allowing for more stringent target loads to be set at some point in the future when the country or countries are better able to respond.

6.1 Critical Load Maps

Pollutants that should be considered for critical loads and target loads to protect lakes and forest soils include sulfur deposition (both wet and dry, $SO_4^=$ and SO_2) for lakes and hydrogen ion deposition for forest soils (because it includes the effects of both sulfuric acid and nitric acid inputs to soils). Smith et al. (1993) have shown that atmospheric deposition of hydrogen and calcium ions to dystrophic peat in Great Britain is capable of producing pH changes in soil solution of 0.2–0.6 units more readily than previously reported. In addition, forests and forest soils may be sensitive to total nitrogen inputs (N saturation), so critical loads for nitrogen are being explored (Kämäri et al. 1993). Sulfate concentration in

lakes has also been utilized to set critical loads in lieu of sulfur deposition (Posch et al. 1993), and ANC have been used as the water quality parameter that protects against effects (fish mortality) in lakes. The ANC values of 20 μeq/ℓ (Henriksen 1992), 25 μeq/ℓ, and 0 μeq/ℓ (Holdren et al. 1993) have been cited for use in critical load assessments. Hydrogen ion deposition to forest soils is a surrogate parameter to estimate the ratio of base cations to aluminum ion in soil moisture. Sverdrup et al. (1992) assumes that the critical molar ratio $(Ca^{2+} + Mg^{2+})/Al$ is 1:1; above this ratio, roots are protected from aluminum toxicity and magnesium deficiency. The critical molar ratio is used together with a gibbsite solubility constant ($[Al^{3+}]/[H^+]^3$) = $10^{8.3}$) to estimate the alkalinity (or base cations) that need to be leached from soils in order to prevent aluminum buildup in soil solution.

Figure 14 is a map of critical loads expressed in terms of acidity (from both wet and try deposition) deposited in Europe (Kämäri et al. 1992). The pollutant designated for control is therefore hydrogen ion deposition and the element of the ecosystem intended for protection is forests. The biological effect in consideration is forest decline stemming from acidification of soil over a decade–centuries time horizon. Only a fraction of the resource can be protected, the most sensitive forest soil cannot; therefore, the decision was made to include 95% of the forest soils on an areal basis (i.e., 5% of the forest soils would require critical load values more stringent than those shown within each grid cell of 150 × 150 km in Fig. 14). The Steady-State Mass Balance Method (SMB) by Hettelingh et al. (1991) was used to make the map in Fig. 14. Considerable concern exists for forest soils, due to the reported die-back in Germany, Poland, and former Czechoslovakia, and because there is evidence that soils have acidified during the twentieth century in southern Sweden (Eriksson et al.

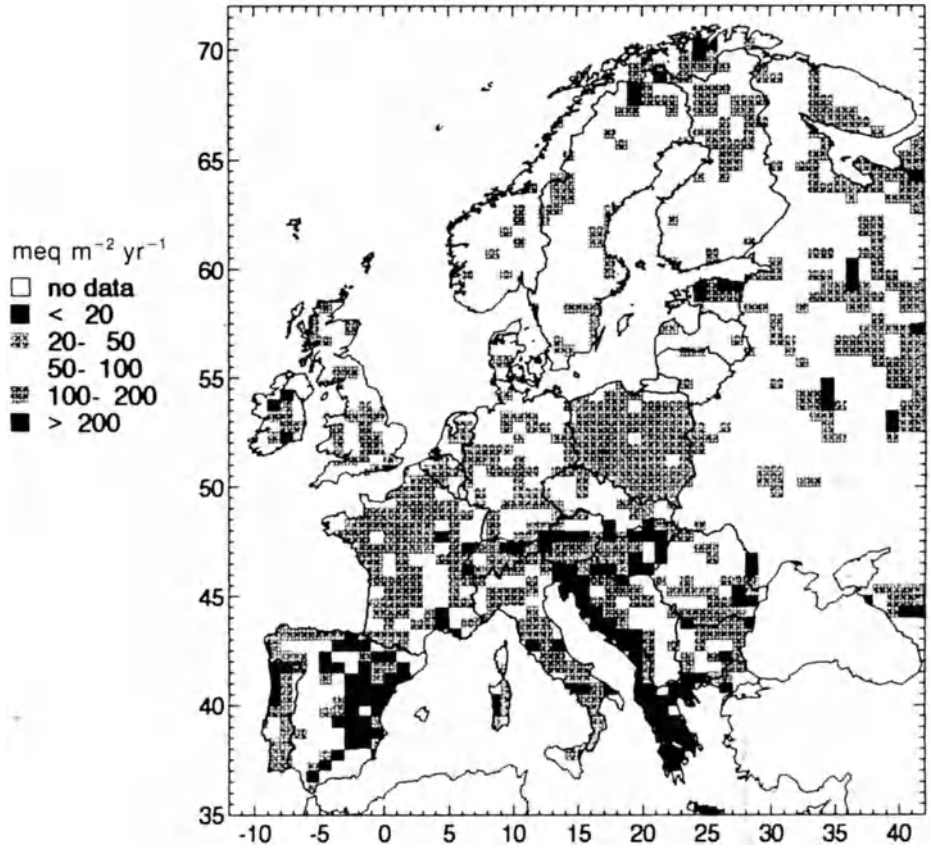


Fig. 14. Critical load map for protection of 95% of forest soils in Europe (within 1° longitude and 0.5° latitude grid cells) using the Steady State Mass Balance model (SMB). Deposition includes total wet and dry acid deposition in units of meq/m^2 per year. (Kamari et al. 1992)

1992). But Henriksen et al. (1992) report that lakes are the most sensitive receptors in Nordic countries. However, 82% of the forest soils in Nordic countries receive deposition exceeding the critical loads shown in Fig. 14; thus, target loads must be set more stringently than critical loads in order to affect recovery (Kämäri et al. 1992; Sverdrup et al. 1992).

Preliminary target loads have been published for the Nordic countries of Sweden, Norway, Finland, and Denmark (Broden and Kuylenstierna 1992). They are 0.5 g S/m^2 per year, except in southern Sweden where the target load has been designated as 0.3 g S/m^2 per year, and in central and northern Finland where the target loads are 0.4 and 0.2 g S/m^2 per year, respectively. These are very stringent targets for enforcement, and most of the area will require further emission reductions to be able to meet the target loads. A European Monitoring Network (EMEP) plot of total sulfur deposition for Europe is given in Fig. 15, demonstrating that most of Europe received deposition greater than 0.5 g/m^2 per year in 1985. Alcamo et al. (1990) have developed a regional assessment model (RAINS) to incorporate transfer functions from the EMEP model to relate emissions of a country to deposition in 150 km-by-150 km grid cells. Models such as RAINS will be needed to arrive at estimates for target loads.

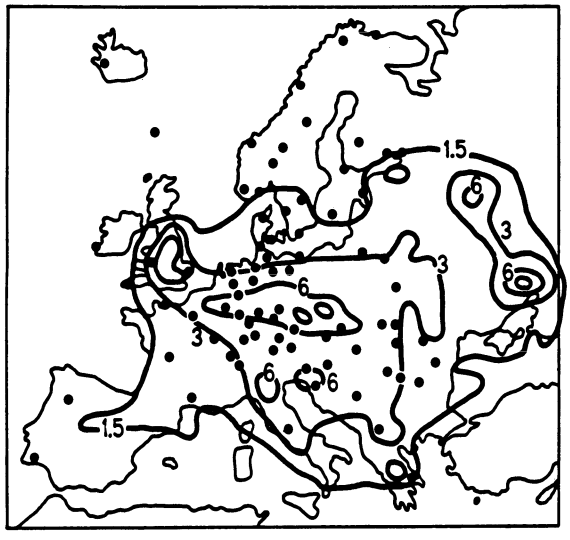


Fig. 15. Monitoring Network (EMEP) map of total sulfur deposition in g S/m^2 per year (1985)

6.2 Model for Critical Load Evaluation

Simple steady-state models have been used to determine critical loads for lakes and forest soils. The basic principle is that primary mineral weathering in the watershed is the ultimate supplier of base cations, which are required elements for vegetation and lake water to ensure adequate ANC (see previous definitions of ANC as the sum of base cations minus acid anions). If more acid is deposited in a watershed than chemical weathering can neutralize, acidification of the soils and water will eventually occur. It may not happen immediately; there could be a delayed response, because ion exchange reactions can supply base cations to vegetation and runoff water for a period, but eventually the exchange capacity of the soil will become depleted and acidification will result. The delay period can be estimated as the base cation exchange capacity (exchangeable Ca, Mg, Na, and K ions) of the soil divided by the cation denudation rate, typically on the order of a few decades in poor, acidic soils. The exchanger (cation exchange complex in soil) is "set up" by the mineralogy and lithology of the parent material, and this determines the base exchange capacity and even the chemistry of the soil.

Sverdrup et al. (1992) have developed the PROFILE model, which is based on the principle of continuity of alkalinity or ANC in soil. The critical load is defined as the allowable acid loading that will not acidify forest soils and cause the release of aluminum and hydrogen ions into soil solution:

$$CL = BC_w - Alk_L, \tag{21}$$

where CL is the critical load, meq/m^2 per year; BC_w is the weathering rate, meq/m^2 per year; and Alk_L is alkalinity leaching, meq/m^2 per year.

The amount of alkalinity that is necessary to leach from the soil can be estimated from the ratio of base cations to aluminum, (Ca + Mg)/Al, assuming a critical threshold value for biological effects at 1:1. Then, based on gibbsite solubility and a minimum required base cation concentration for forest nutrition of 5 meq/m^2 per year, it is possible to estimate the required alkalinity leaching for healthy soils. The SMB model includes a third term on the right side of Eq. (21) for cation uptake required by vegetation, which is another acidifying influence on forest soils that must be subtracted from the weathering rate (Posch et al. 1993). Furrer et al. (1989) have a

more detailed steady-state model than SMB or PROFILE. It includes weathering, ion exchange, base cation uptake by trees, nitrogen tranformation reactions, and equilibrium soil chemistry under steady-state conditions. The model has not been used for critical load assessments, but it represents a more comprehensive approach.

Methods to calculate critical loads from steady-state models do not take time scales for acidification and recovery into account. Detailed non-steady-state models have been used to estimate target loads for three watersheds in Norway and Finland (Warfvinge et al. 1992). Three different models were used in the predictive mode such that deposition was adjusted until the soil-solution chemistry produced the desired 1:1 ratio between base cations and aluminum by the year 2037 (50-year simulations). All three models gave similar results for catchments with shallow soils, but the differences were great when soils were deep and hydrological assumptions in the models varied as to how water should be routed through the soil and into the stream. The Birkenes catchment in southern Norway has become to acidified that the target load must be reduced to less than 0 meq/m^2 per year of S deposition in order for it to recover by the year 2037.

Holdren et al. (1993) found that results of dynamic models gave very different results for target loads in a population of 762 lakes from northeastern Pennsylvania to Maine. This is the population of lakes that was selected for the Eastern Lake Survey (ELS) in a stratified random sample of 7150 lakes in the region. In the Direct Delayed Response Project, three models were used to assess the projected recovery of these lakes under a scenario of a 30% decline in S deposition, as a result of the 1990 Clean Air Act Amendments in the United States. The three models included the ILWAS model by Gherini et al. (1985), the MAGIC model by Cosby et al. (1985), and the Enhanced Trickle-Down (ETD) model by Nikolaidis et al. (1988). The ILWAS model is the most detailed; it includes a lumped-parameter hydrological model and detailed soil-exchange chemistry. The ILWAS requires a tremendous amount of input data, and, thus, it is limited in its application for regional assessments of large populations of lakes. The MAGIC model is a simple soil-equilibrium chemistry model that has been used with success in Europe and the United States. It does not include a hydrological subprogram, but it can be run in conjunction with other hydrological models. The MAGIC model is designed to give annual average predictions over long-time horizons due to its simplicity, but it is not suited for assessing episodic events that may be a threat to biota in lakes with positive, small annual average alkalinity concentrations but are subject to snowmelt or runoff excursions of acidity.

Each data point in Fig. 16 represents a lake selected in the stratified random sample with different weighting factors; each point represents approximately 12–27 lakes in the region of similar hydrogeochemical characteristics. These are among the most sensitive lakes in the region, generally with crystalline bedrock that is slow to weather and flashy hydrographs. Figure 16 shows a correlation suggesting that sulfate is a key variable in the ANC concentration of lakes in the region. In lakes with high sulfate concentrations (in areas receiving greater acid deposition), the ANC concentration generally decreases. This offers some evidence of sulfuric acid deposition as being responsible for acidification of lakes among a class of lakes with the greatest sensitivity in the northeastern United States. The linear least squares regression line through the data in Fig. 16 follows an F factor of 0.8, where the F factor is defined by the change in the sum of base cation concentrations in the lakes divided by the change in the sulfate anion concentration:

$$F = \{\Delta\Sigma\text{Base Cations}\}/\Delta\{SO_4^{2-}\}. \quad (22)$$

Equation (22) gives a measure of the degree of buffering that a watershed can provide to

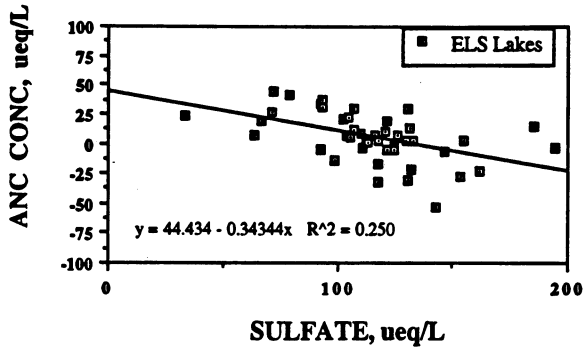


Fig. 16. ANC vs sulfate concentration in μeq/ℓ for 43 lakes in the northeastern United States, part of the Eastern Lakes Survey (ELS) data base. These lakes were the most sensitive lakes of 762 lakes sampled representing the entire data base of 7150 lakes from northeastern Pennsylvania to Maine. (Linthurst et al. 1986)

increased sulfur deposition. For example, if the sulfate anion concentration in a lake increased by $50\,\mu eq/\ell$, due to acid deposition, increased ion exchange and weathering might be able to provide an additional release of $25\,\mu eq/\ell$ of a base cations, resulting in an F factor of 0.5. Alkalinity is a surrogate variable for base cations in Fig. 16, because for every release of base cation from weathering or exchange, an equivalent amount of alkalinity is generated. In the example, the release of $25\,\mu eq/\ell$ of a base cations would provide $25\,\mu eq/\ell$ of alkalinity, and the change in alkalinity in the lake, due to $50\,\mu eq/\ell$ of strong acid, would be $-25\,\mu eq/\ell$. The slope of the regression line in Fig. 16 for lakes in the ELS indicates an F factor of 0.66.

The ETD model was designed as a lumped-parameter watershed model that operated with alkalinity as the master variable. Individual cations and anions were not simulated. This approach has both strengths and weaknesses. It is computationally much simpler to model only alkalinity, and it allows ETD a detailed hydrological model that is capable of simulating events with a variable time step of 10 min to 1 day. However, if forest nutrition questions such as aluminum or magnesium concentrations are desirable, ETD cannot make those predictions directly. Results of the ETD model for 81 lakes in the ELS survey are shown in Fig. 17. A 30% decrease in total S deposition was used as input to the model; the decrease was input as a declining ramp function over a 15-year period, and the results shown in Fig. 17 are the changes in ANC and sulfate ion concentrations in the lake after 50 years (approximate steady state). The surprising result was that the lakes did not respond to the declining deposition to a large extent. The slope of the regression line indicates an F factor of 0.9. The lakes were relatively well buffered, due to a variety of mechanisms including ion exchange, chemical weathering, and sulfate sorption. (It is difficult to change the ANC and pH of the lakes dramatically either via increased or decreased deposition. In this case the prospect for improving the lakes by decreasing emissions was modest.) Six lakes of a stratified random sample of 81 lakes recovered from an ANC of less than zero to a positive ANC. Initially, there were 15 acid lakes with ANC concentrations less than zero. The average lake increased its ANC concentration by approximately $6\,\mu eq/\ell$.

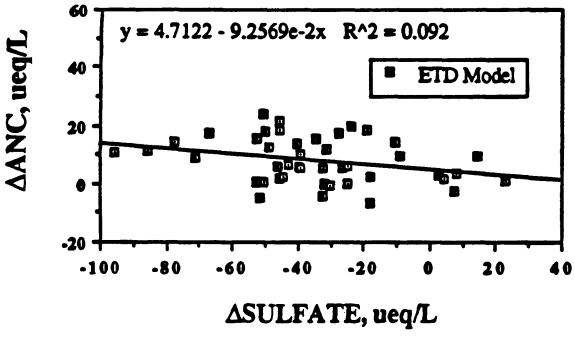


Fig. 17. Change in ANC vs change in sulfate concentration following a 30% ramp function decrease in sulfur deposition, 50-year simulation, using the Enhanced Trickle-Down (ETD) model by Nikolaidis et al. (1988). Lakes were generally well buffered (average F factor approximately 0.8), and the increase in ANC is small relative to the decrease in sulfate concentration

It is apparent that two of the models, MAGIC and ETD, omit another important buffering mechanism in acid lakes, especially colored waters with high dissolved organic carbon (DOC) concentrations. As discussed earlier, acid bog lakes are subject to titration with strong acids, resulting in coagulation of the DOC and a change in the anion concentration from organic to sulfate anions. Presumably, as sulfur emissions are further controlled in developed countries, some lakes will revert to becoming more colored with very little change in pH. These waters should prove less toxic to fish, due to the lower inorganic monomeric aluminum, however.

7 Case Studies

Two case studies are given to illustrate lake and stream acidification. In the first example, acidification of a lake in a sensitive small watershed alpine area with sparse vegetation and thin soils has occurred at relatively low levels of acidic deposition. Here emphasis is on explaining the weathering of crystalline rocks in acidic catchments. The second example gives data from a watershed study in a forested area where a whole catchment of 40 acres has been artificially acidified. The result is consistent with other watershed studies, such as that of Likens et al. (1977), and it illustrates the importance of nitrogen status of a forested ecosystem to increased deposition of nitric acid or ammonium salts. Many stream systems are poised to become

acidic, especially during snowmelt or runoff events if acid deposition increases.

7.1 Chemical Weathering of Crystalline Rocks in the Catchment Area of Acidic Ticino Lakes, Switzerland

Figure 18 gives the water composition of four lakes at the top of the Maggia valley (Giovanoli et al. 1988). Although these lakes are less than 10 km apart, they differ markedly in water composition as influenced by different bedrocks in their catchments. All lakes are at an elevation of 2100–2550 m. The small catchments are characterized by sparse vegetation (no tree), thin soils, and steep slopes.

The composition of Lakes Cristallina and Zota, situated within a drainage area characterized by the preponderance of gneissic rocks and the absence of calcite and dolomite, and Lake Val Sabbia, the catchment area of which contains dolomite, are markedly different. The waters of Lake Cristallina and Lake Zota exhibit mineral acidity (i.e., caused by mineral acids and HNO_3), their calcium concentrations are 10–15 μmol/l, and their pH is <5.3. On the other hand, the water of Lake Val Sabbia is characterized by an alkalinity of 130 μmol/l and a calcium concentration of 85 μmol/l. The water of Lake Piccolo Naret is intermediate; its alkalinity is <50 μmol/l and appears to have been influenced by the presence of some calcite or dolomite in its catchment area.

Weathering Processes Regulating Chemical Water Composition

On the basis of simple mass-balance considerations plausible reconstructions reactions were attempted for the contribution of the various weathering processes responsible for the residual water composition of the acidic Lake Cristallina. Stoichiometric reactions are presented in Table 3 for the interaction of acidic deposition (snowmelt) with weatherable minerals in the drainage area. The composition of atmospheric deposition results

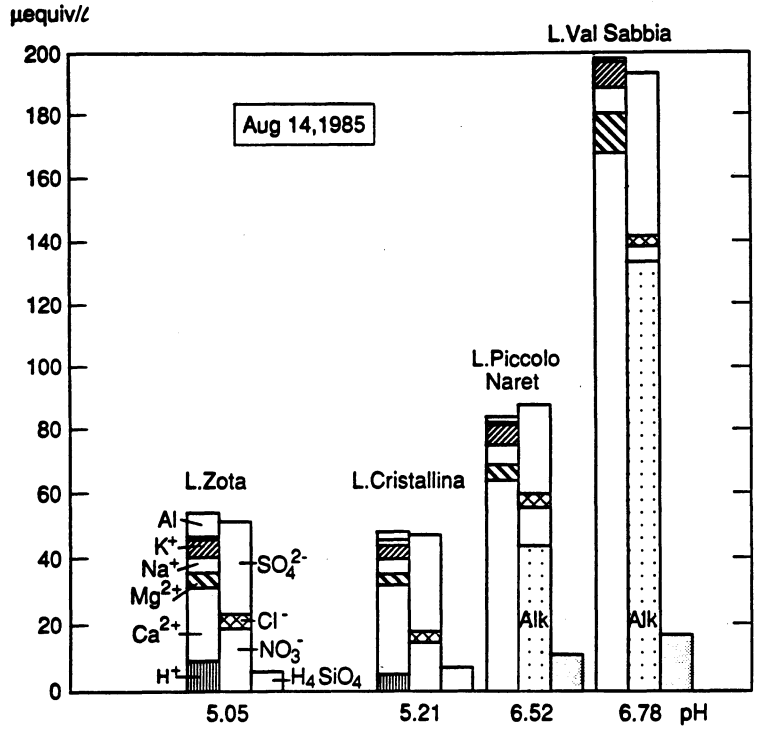


Fig. 18. Comparison of water composition of four lakes influenced by different bedrocks in their catchments. Drainage areas of Lake Zota and Lake Cristallina contain only gneiss and granitic gneiss; that of Lake Piccolo Naret contains small amounts of calcareous schist; that of Lake Val Sabbia exhibits a higher proportion of schist. (Giovanoli et al. 1988)

Table 3. Weathering of crystalline rocks in the catchment area of Lake Cristallina

Reactants	Substances produced or consumed (−)											
Genesis of precipitation (wet and dry deposition)	H^+	Na^+	K^+	Ca^{2+}	Mg^{2+}	NH_4^+	$Al(OH)_{3-v}^{y}$	SO_4^{2-}	NO_3^-	Cl^w	H_4SiO_4	$\{Al(OH)_3\}_s$
	μeq/liter										μmol/liter	
31 μeq H_2SO_4 } acids	31							31				
11 μeq HNO_3 } acids	11								11			
3 μeq NaCl } "dust"			3							3		
2 μeq KCl } "dust"				2						2		
19 μeq $CaCO_3$ } bases	−19			19								
2 μeq $MgCO_3$ } bases	−2				2							
10 μeq NH_3 } bases	−10					10						
Resulting composition	11	3	2	19	2	10	<1	31	11	5	<1	<1
After evaporation[a]	16	4	3	27	3	14	<1	44	16	7	<1	<1
Lake Cristallina												
– Weathering reactions												
1 μmol calcite	−2			2								
4 μmol plagioclase (x = 0.25)	−5	3		2							13	5
2 μmol epidote (x = 0.5)	−8			8							6	5
1 μmol biotite (x = 0.5)	−2		1		1						3	1
1 μmol K-feldspar	−1		1								3	1
– Additional reactions												
NH_4 assimilation[b]	−13					−13						
Dissolution of $\{Al(OH)_3\}_s$[c]	−6						6					
Final composition												
Calculated	5	7	5	39	4	1	6	44	16	7	25[d]	8
Measured September 1985	4	6	5	40	4	1	6	42	16	8	15	–

Possible reaction sequences coupled with stoichiometric calculations for establishing chemical composition of lake water (Giovanoli et al. 1988).

[a] Evapoconcentration factor = $\frac{\text{precipitation}}{\text{runoff}} = \frac{1.7\,\text{m}}{1.2\,\text{m}} = 1.42$.

[b] NH_4 assimilation: $NH_4^+ \rightarrow (NH_3)org + H^+$.

[c] $\{Al(OH)_3\}_s + vH^+ \rightarrow Al(OH)_{3-v}^{y}$, v depends on the pH of the lake water.

[d] Loss of H_4SiO_4 due to incorporation in diatoms and adsorption on noncrystalline $Al(OH)_3$ not included.

generally from the interactions of strong acids (H_2SO_4, HNO_3), bases (NH_3), and wind-blown dust and aerosols ($CaCO_3$, $MgCO_3$, NH_4NO_3, NaCl, and KCl).

In Table 3 the contributions of the individual weathering reactions were assigned and combined in such a way as to yield the concentrations of Ca^{2+}, Mg^{2+}, Na^+, K^+, and H^+ measured in these lakes. The amounts of silicic acid and aluminum hydroxide produced and the hydrogen ions consumed were calculated stoichiometrically from the quantity of minerals assumed to have reacted. Corrections must be made for biological processes (Schnoor and Stumm 1985) such as ammonium assimilation and nitrification as well as the uptake of silicic acid by diatoms. Some of the H_4SiO_4 was apparently lost by adsorption on aluminum hydroxide and Fe(III)(hydr)oxides, but the extent of these reactions was difficult to assess.

Although an unequivocal quantitative mass balance could not be obtained, a plausible reaction sequence was deduced that accounts reasonably well for the residual chemical–water composition. The amount of $CaCO_3$ that had to be dissolved to establish the residual water composition is approximately the same as what can be accounted for by wind-blown calcite dust. The neutralization of the acidic precipitation by NH_3 was, subsequent to its deposition, largely annulled by the H^+ ions produced by nitrification and NH_4^+ assimilation.

According to Table 3, in the drainage area of Lake Cristallina, approximately 4 μmol of plagioclase, 2 μmol epidote, 1 μmol biotite, and 1 μmol K feldspar per liter of runoff water are weathered per year. This amounts to 19 meq of cations per m^2/year. The situation is similar for Lake Zota (16 meq of cations per m^2/year).

7.2 Watershed Manipulation Project at Bear Brooks, Maine

The site of Bear Brooks Watershed at Lead Mountain, Maine (latitude 44°51′75″; longitude 68°6′25″) contains two almost identical streams, each draining 15 ha, with a southern exposure from the top of Lead Mountain, 450 m above mean sea level. It is a part of the United States Environmental Protection Agency's (EPA's) Watershed Manipulation Project, a long-term experimental manipulation in which the western catchment has been artificially acidified with applications of ammonium sulfate, and the eastern catchment has remained as a reference.

Bedrock at the site consists of metamorphosed quartz sandstones with granitic sills and dikes, overlain by a glacial till 4–5 m thick at the lower elevations. Exposed bedrock is visible at the summit of Lead Mountain. Mineralogy by X-ray diffraction of the soils (B and C horizons) consists of quartz as the major mineral, followed by feldspar as a significant mineral [$X(Si,Al)_4O_8$, X = Na, K, Ca, Ba], and minor minerals muscovite $KAl_3Si_3O_{10}(OH)_2$, chlorite $(Mg,Fe,Al)_6(Si,Al)_4O_{10}(OH)_8$, and hornblende $X_2Y_5(Si,Al)_8O_{22}(OH)_2$, X = Na, K, Ca, Mn, Fe, and Y = Mg, Al, Ti, Mn, Fe. The parent material and soils are very deficient in calcium (0.8–1.3% by weight as oxide equivalents). In the fine size fractions of the upper B-horizon soil, there is considerable iron oxide (4.1% by mass) and organic carbon (15% as measured by loss on ignition at 1050 °C). Little chemical differences exist among the various size fractions otherwise. The B-horizon soils have more Fe and Al than C-horizon soils, as expected for acidic, podzolic soils.

Manipulation at Bear Brook forested catchment using stable isotopic $(^{15}NH_4)_2SO_4$ applications have allowed a tracer experiment to document the fertilization effect of ammonium ion and the degree of nitrogen saturation. Steve Norton at the University of Maine, in cooperation with Aber and Nadelhofer (1993) applied approximately 16.8 kg N/ha per year of dry ammonium sulfate to a 15 ha catchment, West Bear Brook. It was expected that most of the ammonium would be taken up by the mixed hardwood forest in the middle of succession and/or immobilized into the forest floor in a stable organic-humate phase. The forest is owned by a paper company that allowed the experiment to be performed. It was clear cut less than 40 years ago; therefore, the system was thought to be in a rather immature state of succession, and it was not expected that it would leak much nitrogen.

Most of the sulfate applied was adsorbed in the first year after treatment, but SO_4^{2-} has been increasingly mobile in subsequent years, as shown in Fig. 19. Treatment of ammonium sulfate began as quarterly applications in November 1989 (approximately day 730 in Fig. 19). The reference catchment (West Bear Brook) did not demonstrate an increase in sulfate concentration in the Brook, but the treated catchment (East Bear Brook)

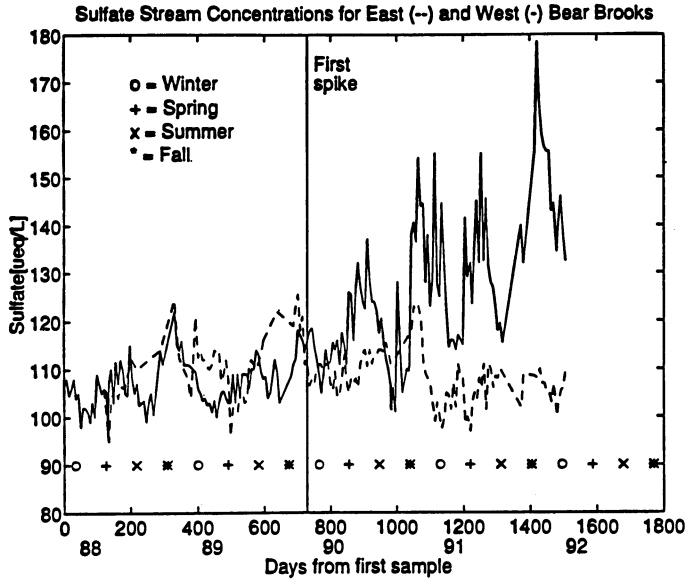


Fig. 19. Sulfate concentration in East Bear Brook (the reference catchment) and West Bear Brook (receiving 19.2 kg S/ha per year in the form of ammonium sulfate additions). Ammonium sulfate additions began on day 730 in November 1989. The sulfate concentration in West Bear Brook (*solid line*) has increased significantly compared with the reference (*dashed line*)

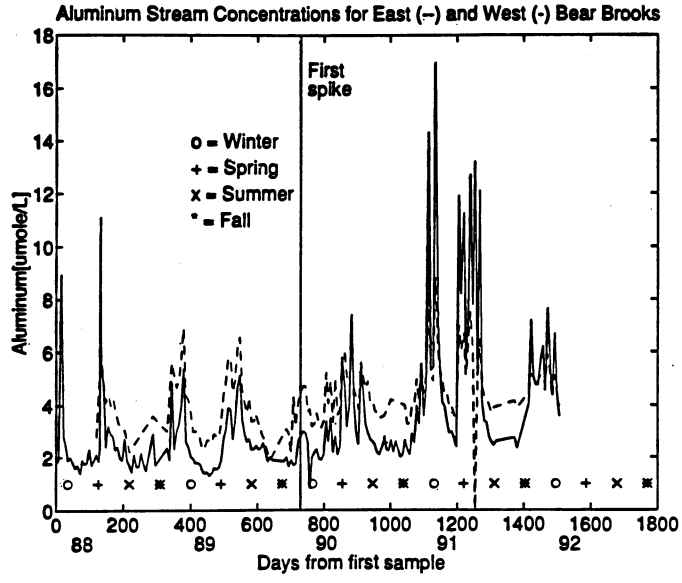


Fig. 20. Total aluminum concentration in stream samples at East Bear Brook (reference) compared with West Bear Brook, which was acidified via the addition of ammonium sulfate, Total aluminum concentrations in West Bear Brook (*solid line*) have increased since the manipulation began on day 730

showed an increase from an average concentration of 105 to 135 μeq/ℓ. In the third year of applications, approximately one-third of the applied sulfate was exported from the catchment in West Bear Brook. In effect, the uptake of ammonium by vegetation caused a small release of sulfuric acid into Bear Brook, acidifying the soil and the Brook and releasing inorganic monomeric aluminum (Fig. 20). Total aluminum concentrations doubled from the preapplication period, and high concentrations of inorganic monomeric aluminum were evident during spring snowmelt and runoff events.

A significant increase in the export of nitrate-

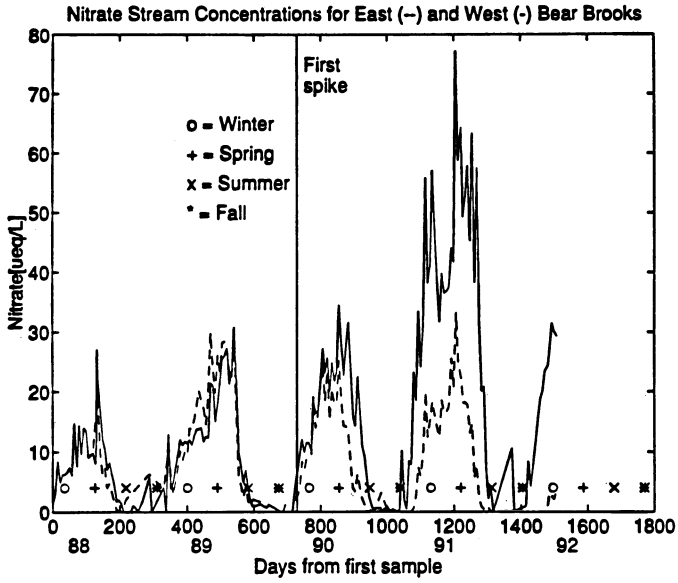


Fig. 21. Nitrate concentration in stream samples from East Bear Brook (reference) and West Bear Brook, amended with 16.8 kg N/ha per year beginning on day 730 (November 1989). Nitrate concentrations in West Bear Brook (*solid line*) increased steadily since the applications began, and the export of nitrate-nitrogen amounts to approximately 15% of the ammonium sulfate additions

nitrogen entering Bear Brook was observed after applications of ammonium sulfate began (Fig. 21), indicating that excess nitrogen had been nitrified and that the soils were somewhat nitrogen-saturated. Approximately 2.5 kg N/ha per year (15% of the application rate) was measured in West Bear Brook in 1991–1992 (Fig. 21). Vegetation could not take up all of the applied nitrogen, and most of it was incorporated into the immobilized organic fraction of the soil, approximately 12–13 kg N/ha per year. The chemistry and the fate of this immobilized organic nitrogen in the upper soil are not very well understood, yet, it accounts for a very large pool that could supply ammonium (via mineralization) for the annual increment of the forest for many years. Uptake by vegetation only accounted for 1–2 kg ^{15}N/ha per year of the 16.8 kg N/ha per year applied, so the forest was fertilized, but not as much as might have been expected. The organic immobile pool in the soil is large, 350–800 kg N/ha, and it represents approximately 20 years of nitrogen application.

The manipulation at West Bear Brook testifies to the importance of long-term, large scale field experiments to test models and hypotheses. It appears that the forest is leaking nitrogen more readily than had been expected, although it is a small fraction of the total amount that was applied. It points out research needs: A better understanding is needed of the large immobile organic pool that accumulates in forests and the effects of excess nitrate on ecosystems. The application rate of 16.8 kg N/ha per year is not a large loading, and critical load estimates for the region would probably range approximately 20–30 kg N/ha per year. Because the background levels of nitrogen and acid deposition to West Bear Brook are approximately 10–12 kg N/ha per year, the total nitrogen deposition to West Bear Brook is in the range of the critical loading, making the manipulation a particularly pertinent experiment. The experiment is continuing, and thus far, long-term harmful effects on the forest have not been observed.

8 Summary

Atmospheric deposition can affect the chemical and biological characteristics of lakes. Biogeochemical reactions in forested watersheds include the transfer of electrons coupled with the transfer of protons, so changes in deposition may alter the acid–base balance of terrestrial and aquatic ecosystems. Critical loads have been developed to protect lakes, soils, and forests from effects due to acid deposition, and target loads are under consideration by governments to manage emissions of transboundary pollutants. Research at the

catchment scale, including watershed manipulations, are indispensable to test models and to gain an understanding of the protection and management of ecosystems.

Acknowledgments. The ideas presented here have been influenced by stimulating collaboration with James J. Morgan and Laura Sigg. Collaborators in the Watershed Manipulation Project who provided advice and correspondence of data include Steve Norton, Steve Kahl, Charles Driscoll, John Aber, Myron Mitchell, and James Szydlik. Partial funding for research came from the U.S. EPA Corvallis Environmental Research Laboratory and from a subcontract with State University of New York, Syracuse. No endorsement by granting agencies should be inferred.

References

Alcamo J, Shaw R, Hordijk L (1990) The RAINS model of acidification: science and strategies in Europe. Kluwer, Dordrecht

Andreae MO, Byrd JT (1984) Determination of tin and methyltin species by hydride generation and detection with graphite-furnace atomic absorption or flame emission spectrometry. Anal Chim Acta 156:147–157

Baker LA, Herlihy AT, Kaufman PR, Eilers JM (1991) Acidic lakes and streams in the United States: the role of acid deposition. Science 252:1151–1154

Behra P, Sigg L, Stumm W (1989) Dominating influence of NH_3 on the oxidation of aqueous SO_2: the coupling of NH_3 and SO_2 in atmospheric deposition. Atmos Environ 23:2691–2707

Blum AE, Lasaga AC (1987) Monte Carlo simulations of surface reaction rate laws. In: Stumm W (ed) Aquatic surface chemistry. Wiley-Interscience, New York, pp 255–292

Brodin YW, Kuylenstierna JCI (1992) Acidification and critical loads in Nordic countries: a background. Ambio 21:332–339

Broecker WS (1971) A kinetic model for the chemical composition of sea water. Quart Res 1:188

Carignan R (1985) Quantitative importance of alkalinity flux from the sediments of acid lakes. Nature 317: 158–160

Christopherson N, Wright F (1981) Sulfate budget and a model for sulfate concentrations in streamwater at Birkenes, Norway. Water Resour Res 17:377–389

Christophersen N, Seip HM, Wright RF (1982) A model for streamwater chemistry at Birkenes, Norway. Water Resour Res 18:977–996

Cook RB, Kelly CA, Schindler DW, Turner MA (1986) Mechanisms of hydrogen ion neutralization in an experimentally acidified lake. Limnol Oceanogr 31(1):134–148

Cosby BJ, Hornberger GM, Galloway JN, Wright RF (1985) Modeling the effects of acid deposition: assessment of a lumped parameter model of soil water and streamwater chemistry. Water Resour Res 21:51–63

Council on Environmental Quality (1990) Environmental quality – twentieth annual report, US Government Printing Office, Washington, DC, 494 pp

Davison W (1986) Sewage sludge as an acidity filter for groundwater-fed lakes. Nature 22:820–822

Driscoll CT, Likens GE (1982) Hydrogen ion budget of an aggrading forested ecosystem. Tellus 34:283–292

Driscoll CT, Iverfeldt A, Otton JK (1994) Trace metals speciation and cycling. In: Cerny J, Moldan B (eds) Biogeochemistry of small catchments, SCOPE series, John Wiley and Sons, New York (in press)

Eriksson E, Karitun E, Lundmark JE (1992) Acidification of forest soils in Sweden. Ambio 21:150–156

Eshleman KN, Hemond HF (1988) Alkalinity and major ion budgets for a Massachusetts reservoir and watershed. Limnol Oceanogr 33(2):174–185

Friedland AJ, Craig BW, Miller EK, Herrick GT, Siccama TG, Johnson AH (1992) Decreasing lead levels in the forest floor of the northeastern USA. Ambio 21:400–403

Froelich PN, Klinkhammer GP, Bender ML, Luedtke NA, Heath GR, Cullen D, Dauphin P, Hammond D, Hartman B, Maynard V (1979) Early oxidation of organic matter in pelagic sediments of the eastern equatorial Atlantic: suboxic diagenesis. Geochim Cosmochim Acta 43:1075–1090

Furrer G, Westall I, Sollins P (1989, 1990) The study of soil chemistry through quasi-steady state models; I. Mathematical definition of the problem. Geochim Cosmochim Acta 53:595–601 (1989); II. Soil solution acidity

Galloway JN, Likens GE, Keene WC, Miller JM (1982) The composition of precipitation in remote areas of the world. Geophys Res C87:8771–8786

Gherini SA, Mok L, Hudson RJM, Davis GF, Chen CW, Goldstein RA (1985) The ILWAS model: formulation and application. Water Air Soil Pollut 26(4):425–460

Giovanoli R, Schnoor JL, Sigg L, Stumm W, Zobrist J (1988) Chemical weathering of crystalline rocks in the catchment area of acidic Ticino lakes, Switzerland. Clay and Clay Minerals 36/6:521–529

Goldman JC, Brewer PG (1980) Effects of nitrogen source and growth rate on phytoplankton mediated changes in alkalinity. Limnol Oceanogr 25:352–357

Henriksen A (1979) Regional survey of lakewater chemistry of large lakes in south Norway, winter 1979. TN 50/79, SNSF-Proj., Oslo

Henriksen A, Kamari J, Posch M, Wilander A (1992) Critical loads of acidity: Nordic surface waters. Ambio 21:356–363

Herlihy AT, Kaufmann PR, Church MR, Wigington PJ Jr., Webb JR, Sale MJ (1993) The effects of acidic deposition on streams in the Appalachian Mountain and Piedmont region of the mid-Atlantic United States. Water Resour Res 29:2687–2703

Hettelingh JP, Downing RJ, de Smet PAM (eds)

(1991) Mapping critical loads for Europe. CCE technical report no. 1, National Institute of Public Health and Environmental Protection, Bilthoven, The Netherlands

Hoffmann MR, Boyce SD (1984) Kinetics and mechanism of the formation of hydroxymethanesulfonic acid at low pH. J Physical Chem 88:4740

Holdren GR Jr., Strickland TC, Shaffer PW, Ryan PF, Ringold PL, Turner RS (1993) Sensitivity of critical load estimates for surface waters to model selection and regionalization schemes. J Environ Qual 22: 279–289

Jacob DJ, Munger JW, Waldman JM, Hoffmann MR (1986) The H_2SO_4-HNO_3-NH_3 system at high humidities and in fogs. J Geophys Res 91:1073–1096

Johnson CA, Sigg L (1985) Acidity of rain and fog: conceptual definitions and practical measurements of acidity. Chimia 39:59–61

Kämäri J, Amann M, Brodin YW, Chadwick MJ, Henriksen A, Hettlingh JP, Kuylenstierna J, Posch M, Sverdrup H (1992) The use of critical loads for the assessment of future alternatives to acidification. Ambio 21:377–387

Kämäri J, Forsius M, Posch M (1993) Critical loads of sulfur and nitrogen for lakes II: regional extent and variability in Finland. Water Air Soil Pollut 66:77–96

Kavamura K, Kaplan IR (1984) Capillary gas chromatography determination of volatile organic acids in rain and fog samples. Anal Chem 56:1616–1620

Keene WC, Galloway JN (1984) Atmos Environ 18:2491

Krug EC, Frink CR (1983) Acid ran and acid soil: a new perspective. Science 221:520–525

Lerman A, Stumm W (1989) CO_2 storage and alkalinity trends in lakes. Water Res 23:139–146

Likens GE, Bormann FH, Pierce RS, Eaton JS, Johnson NM (1977) Biogeochemistry of a forested ecosystem. Springer, Berlin Heidelberg New York, 146 pp

Liljestrand HM (1985) Average rainwater pH. Concepts of atmospheric acidity and buffering in open systems. Atmos Environ 19:487–499

Lindberg SE, Lovett GM, Richter DD, Johnson DW (1986) Atmospheric deposition and canopy interactions of major ions in a forest. Science 231:141–145

Linthurst RA, Landers DH, Eilers JM, Brakke DF, Overton WJ, Meier EP, Crowe RE (1986) Characteristics of lakes in the eastern United States, vol 1. US EPA-600-4-86-007a, Environmental Protection Agency, Washington, DC

Morel FMM, Hudson RJM (1985) The geobiological cycle of trace elements in aquatic systems: Redfield revisited. In: Stumm W (ed) Chemical processes in lakes, John Wiley, New York, pp 251–281

Morgan JJ (1982) In: Goldberg ED (ed) Atmospheric chemistry. Springer, Berlin Heidelberg New York, pp 17–39

Morgan JJ, Stumm W (1989) Chemical processes in the environment, relevance of chemical speciation. In: Merian E (ed) Metals and their compounds in the environment, VCH Verlagsges, Weinheim, FRG

Murdoch PS, Stoddard JL (1992) The role of nitrate in the acidification of streams in the Catskill Mountains of New York. Water Resour Res 28:2707–2720

Nikolaidis NP, Rajaram H, Schnoor JE, Georgakakos KP (1988) A generalized soft water acidification model. Water Resour Res 24:1983–1996

Posch M, Forsius M, Kämäri J (1993) Critical loads of sulfur and nitrogen for lakes I: model description and estimation of uncertainty. Water Air Soil Pollut 66:173–192

Psenner R (1988) Alkalinity generation in soft-water lake: watershed and in-lake processes. Limnol Oceanogr 33:1463–1475

Rees T (1992) PhD Diss, The University of Iowa, Iowa City, Iowa

Reuss JO (1978) Simulation of nutrient loss from soils due to rainfall acidity. Environ Prot Agency, Rep EPA-660/3-78-053, Corvallis, Oregon

Reuss JO (1980) Simulation of soil nutrient losses resulting from rainfall acidity. Ecol Model 11:15–38

Reuss JO, Christophersen N, Seip HM (1986) A critique of models for freshwater and soil acidification. Water Air Soil Pollut 30:909–930

Rosen K, Gundersen P, Tegnhammar L, Johansson M, Frogner T (1992) Nitrogen enrichment of Nordic forest ecosystems – the concept of critical loads. Ambio 21:364–369

Samson PJ, Small MJ (1984) In: Schnoor JL (ed) Modeling of total acid precipitation impacts. Butterworth, Boston, pp 1–24

Schindler DW (1985) The coupling of elemental cycles by organisms: evidence from whole lake chemical perturbations. In: Stumm W (ed) Chemical processes in lakes. Wiley-Interscience, New York, pp 225–250

Schindler DW (1987) Detecting ecosystem responses to anthropogenic stress. Can J Fish Aquat Sci 44:6–25

Schindler DW, Mills KH, Malley DF, Findlay DL, Shearer JA, Davies IJ, Turner MA, Lindsey GA, Cruikshank DR (1985) Long-term ecosystem stress: the effects of years of experimental acidification on a small lake. Science 228:1395–1401

Schnoor JL, Stumm W (1985) Acidification of aquatic and terrestrial ecosystems. In: Stumm W (ed) Chemical processes in lakes. Wiley-Interscience, New York, pp 311–338

Schnoor JL, Palmer WD Jr., Glass GE (1984) In: Schnoor JL (ed) Modeling of total acid precipitation impacts. Butterworth Publishers, Boston

Schnoor JL, Nikolaidis NP, Glass GE (1986a) Lake resources at risk to acid deposition in the upper Midwest. J Water Pollut Control Fed 58(2):139–148

Schnoor JL, Lee SJ, Nikolaidis NP, Nair DR (1986b) Lake resources at risk to acidic deposition in eastern United. Water Air Soil pollut 31:1091–1107

Schnoor JL, Lee SJ, Georgakakos KP (1989) Longterm response of lakes to acidic deposition. Proc Environ Eng Specialty Conf, EE Div/ASCE, Austin, Texas, pp 584–591

Seinfeld JH (1986) Atmospheric chemistry and physics of air pollution. Wiley, New York

Settle DM, Patterson CC (1980) Lead in albacore: guide to lead pollution in Americans. Science 207: 1167–1176

Sigg L (1985) Metal transfer mechanisms in lakes, the role of settling particles. In: Stumm W (ed) Chemical processes in lakes. Wiley-Interscience, New York, pp 283–310

Sigg L (1987) Surface chemical aspects of the distribu-

tion and fate of metal ions in lakes. In: Stumm W (ed) Aquatic surface chemistry. Wiley- Interscience, New York, pp 319–349

Sigg L, Stumm W (1994) Aquatische Chemie. Teubner-Verlag, Stuttgart, 498 pp

Sigg L, Stumm W, Zobrist J, Zürcher F (1987) The chemistry of fog: factors regulating its composition. Chimia 41:159–165

Sillén LG (1961) The physical chemistry of sea water. In: Sears M (ed) Oceanography. AAAS, Washington, DC

Smith CMS, Cresser MS, Mitchell RDJ (1993) Sensitivity to acid deposition of dystrophic peat in Great Britain. Ambio 22:22–27

Sposito G (1986) Sorption of trace metals by humic materials in soils and natural waters. CRC Crit Rev Environ Control 16:193–229

Stumm W, Morgan JJ (1995) Aquatic chemistry, 3rd edn. John Wiley & Sons, New York

Stumm W, Schnoor JL (1983) Acid rain – a result of disruptions in hydrogeochemical processes. Naturwissenschaften 70:216

Stumm W, Furrer G, Kunz B (1983) The role of surface coordination in precipitation and dissolution of mineral phases. Croat Chem Acta 56:585–611

Stumm W, Sigg L, Schnoor JL (1987) Aquatic chemistry of acid deposition. Env Sci and Technol 21:8–13

Sverdrup H, Warfvinge P, Frogner T, Haoya AO, Johansson M, Andersen B (1992) Critical loads for forest soils in the Nordic countries. Ambio 21:348–355

Tessier A, Carignan R, Dubreul B, Rapin F (1989) Partitioning of zinc between the water column and the sediments in lakes. Geochim Cosmochim Acta 53:1511–1522

Ulrich B (1981) Eine ökosystemare Hypothese über die Ursachen des Tannen-sterbens (*Abies alba* Mill.). Forstwiss Centralbl 100:228

Van Breemen N, Driscoll CT, Mulder T (1983) Acid deposition and internal proton sources in acidification of soils and waters. Nature 307:599

Waldman JM, Munger JW, Jacob DJ, Flagan RC, Jorgan JJ, Hoffmann MR (1982) Chemical composition of acid fog. Science 218:677–680

Warfvinge P, Holmberg M, Posch M, Wright RF (1992) The use of dynamic models to set target loads. Ambio 21:369–376

Westall J (1980) Chemical equilibrium including adsorption on charged surfaces. In: Kavanaugh MC, Leckie JO (eds) Particulates in Water. Advances in chemistry series 189. Am Chem Soc

Whitfield M, Turner DR (1987) The role of particles in regulating the composition of natural waters. In: Stumm W (ed) Aquatic surface chemistry, Wiley-Interscience, New York, pp 457–493

Zobrist J, Wersin P, Jacques C, Sigg L, Stumm W (1993) Dry deposition measurements using water as a receptor: a chemical approach. Water Air Soil Pollut 71:111–130

8 Redox-Driven Cycling of Trace Elements in Lakes

J. HAMILTON-TAYLOR and W. DAVISON

1 Introduction

This chapter encompasses the transformation and movement of selected trace metals, metalloids, and radionuclides between phases and/or compartments in lakes, arising from biologically and chemically mediated redox reactions. Thus, it is concerned with the spatial and temporal distributions and speciation of trace elements in solution, in suspended particles, and in sediments. It updates and complements an earlier overview (Sholkovitz 1985), which considered the redox-related behavior of alkaline earth elements and ^{137}Cs.

As previously recognized (Sholkovitz 1985; Murray 1987), the same basic biogeochemical processes operate in lakes as in oceans, but, unlike oceans, simple patterns of trace element distributions and behavior are rarely seen in lakes. This has been attributed to the highly dynamic nature of lakes, where inputs, mixing, and removal processes can vary substantially on a variety of time scales, such that non-steady-state conditions may be regarded as the norm. Other important factors are the greater availability of competing scavenging phases (e.g., detrital particles, phytoplankton, and authigenic precipitates), the variation in the chemical composition of lake waters, and the compressed depth scales. An illustration of the latter is the virtual absence of a suboxic zone in many lake systems, where the transition from the oxic zone to the zone of sulfide precipitation is often abrupt.

It is in fact variety that seems to characterize trace element distributions and behavior in lakes, although doubts have been expressed as to the validity of at least some published freshwater trace element data. These doubts stem from the development in recent years of "clean techniques" in equivalent oceanographic studies and the consequent decrease in reported trace element concentrations (Johnson et al. 1992a). Furthermore, the application of clean techniques to freshwater systems have provided direct evidence of inaccuracy for some previously reported concentrations (e.g., Windom et al. 1991). Another factor contributing to the reported variation in trace element behavior in lakes may have been the diversity in methods of study. These include laboratory studies, ranging from sequential extractions to incubation experiments, field experiments involving enclosed mesocosms or whole lakes in which elements or radiotracers are added and conditions artificially manipulated, and synoptic field observations usually involving the measurement of one or more of the following: vertical profiles (i.e., concentration gradients) through the water column and sediments, depositional fluxes by sediment trapping, and sediment–water diffusive fluxes using benthic chambers.

It is likely that most elements are involved to some degree in redox cycling in lakes. In his earlier overview Sholkovitz (1985) emphasised the relation between redox reactions and the mobility of elements. He particularly used the increased concentrations of certain elements that develop in the anoxic hypolimnia of productive lakes as a paradigm for illustrating the effects of redox behavior. This chapter, on the other hand, takes a broader view of redox cycling in lakes and shows that the effects on element distributions are highly diverse.

The first part of the chapter includes sections on several key topics: the main processes causing the redox-driven cycling of elements, the special role played by Fe and Mn, and the redox-driven fluxes of elements across the sediment–water interface. The following two sections provide case studies of selected elements, which highlight the biogeochemical pathways directly or indirectly involving redox transformations. Direct involvement is used here to mean that the element itself

Institute of Environmental and Biological Sciences, Lancaster University, Lancaster LA1 4YQ, UK

undergoes a redox reaction [e.g., As(V)–As(III)], whereas indirect involvement means that the distribution of the element is affected by redox-driven cycling, but apparently does not itself undergo a redox transformation (e.g., Zn). For more detailed information on particular aspects of the subject, the reader is referred to the following: main carrier phases for trace metals (Forstner 1982; Hart 1982; Sigg 1985; Tessier 1992), chemical processes at the sediment–water interface (Santschi et al. 1990), and the use of radionuclides in understanding biogeochemical cycling in lakes (Santschi 1988, 1989).

2 Major Biogeochemical Cycles and Pathways

The predominant mechanisms driving the redox cycling of elements in lakes are plankton synthesis in surface waters and the bacterial degradation of organic matter in subsurface waters and sediments. Organic matter degradation proceeds through a series of redox reactions in which oxidants (including Mn(IV) and Fe(III)) are consumed theoretically in order of decreasing free energy yield. In practice, the reaction sequence is subject to oxidant availability and kinetic constraints, including the dominance of particular microbial populations. These reactions are responsible for regulating the redox potential of the local environment. Elements may be affected by these processes in a variety of different ways. They may be adsorbed or assimilated by plankton in surface waters and released back into solution at depth, possibly in a different redox state. Alternatively, the elements may act directly as terminal electron acceptors in the microbial degradation of organic matter or the redox state of elements may be chemically mediated by reaction with excess concentrations of inorganic oxidizing or reducing agents [e.g., O_2 or S(-II)]. At least some of the redox reactions previously attributed to chemical mediation are now thought to be the result of dissimilatory microbial activity, e.g., as with the reduction of U(VI) (Lovley et al. 1991). The actions of chemoautotrophic bacteria, which obtain energy from the oxidation of reduced inorganic species, e.g., Mn^{2+} and Fe^{2+}, can also have a significant effect on element behavior in lakes.

The redox-driven cycling of elements additionally occurs through more obscure pathways. The most important result from a chemical association (i.e., sorption and/or coprecipitation) between elements and redox-sensitive carrier phases, e.g., Fe and Mn oxides and sulfides. Thus, elements hypothetically may be mobilized through the reductive dissolution of oxides or the oxidation of sulfides. Additionally, the iron cycle is capable of markedly influencing the concentration of humic substances, which sometimes increase in the anoxic waters of a seasonally stratified lake, apparently due to release from dissolving Fe oxides (see Davison 1993). Because humic substances are well known for their metal complexing ability, metal mobility may be increased. Other pathways are associated with pH variations and with the increased concentrations of metabolites (e.g., NH_4^+ and HCO_3^-/CO_3^{2-}), resulting from the anaerobic degradation of organic matter (e.g., Sigg et al. 1991). The pH can vary, temporally and vertically, by more than 3 pH units in productive, poorly buffered lakes, due to the effects of photosynthesis and respiration (Talling 1976). Thus, the sorption of elements by, for example, Fe and Mn oxides, may vary substantially due to such pH changes. Increases in cation and inorganic ligand concentrations may similarly influence metal mobility. For example, the effects of NH_4^+ in displacing $^{137}Cs^+$ from surface and interlayer sites of illite grains are well established for lake systems (see Sect. 6.1), and CO_3^{2-} complexation has been invoked to explain the unusually high actinide concentrations in a saline, alkaline lake in California (Anderson et al. 1982; Simpson et al. 1982).

Redox boundaries, where distinct changes in chemical concentrations and redox potential are observed, are rarely simple or well-defined examples of chemical equilibrium. Kinetic constraints may lead to chemically incompatible forms such as O_2 and S(-II) coexisting in water columns and Fe oxide and Fe sulfide particles coexisting in both water columns and sediments. Pore waters and their surrounding solid phases may appear to be out of balance, due to non-steady-state behavior associated with seasonal developments. For example, the pore waters of surface sediments in early spring may contain exclusively reduced forms, but the sediment material may still have a red-brown appearance characteristic of Fe oxides. This heterogeneity of the redox boundary and its tendency to migrate seasonally complicate the interpretation of the mechanisms of redox transformations.

Direct photochemical oxidation and reduction of elements may occur in lakes. A number of such reactions have been reported for Fe and Mn, although the data for freshwater systems are relatively scarce with regard to Mn (Davison 1993). The authors know of little direct evidence for photochemical reactions affecting other elements in lake waters, although such reactions have been postulated or observed in estuarine and sea waters in the case of Cu, Co, Cr, V, Se, U (Waite 1988), and Pu (Mudge et al. 1988). Photochemically induced redox reactions appear to be particularly important in the dynamic redox cycle of Cu(II)–Cu(I) in near-surface sea waters, but probably have little effect in freshwater systems (Moffett and Zike 1983; Moffett and Zika 1987). The photochemical reduction of Cr(VI) to Cr(III) has recently been reported in a series of surface waters, including two freshwater lakes (Kaczynski and Kieber 1993).

3 Iron and Manganese

3.1 Transformations and Cycling

The redox behavior of Fe and Mn in lakes has been very well studied and comprehensively reviewed (Davison 1993). Other recent reviews have addressed the role of Fe (Davison and De Vitre 1992) and Mn (De Vitre and Davison 1993) particles in freshwaters, whereas Stumm and Sulzberger (1992) have considered current knowledge and understanding of the mechanisms of redox transformations of Fe.

In well-oxygenated waters the stable forms of Fe and Mn are their higher oxidation states [Fe(III) and Mn(III/IV)], which are completely hydrolyzed oxides present as colloids or particles. Where oxygen is absent the lower redox states, Fe(II) and Mn(II), are favored. These divalent ions are very soluble in the pH range of 4–8. As a consequence of these properties Fe and Mn are mainly present in well mixed, fully oxygenated lake water as particles at typical concentrations of $0.4–2\,\mu mol\,l^{-1}$. In seasonal or permanently stratified lakes where the bottom waters become anoxic, Fe(II) and Mn(II) can accumulate to high concentrations, sometimes approaching $100\,\mu mol\,l^{-1}$. The reduced metal ions are supplied by reductive dissolution of oxide present in surface sediments and in particles sinking through the water column. The relative dominance of these two supply terms often changes as the season progresses with release from the sediment being initially important. As the sediment supply becomes progressively exhausted, which occurs particularly for Mn, release from particles becomes more important.

At the oxic/anoxic boundary in the water column the upwardly diffusing Fe(II) and Mn(II) may be oxidized to form oxides that may then be present at a localized high concentration. In neutral lake waters the oxidation of Fe(II) is believed to proceed chemically, although its removal below the oxycline indicates that oxidants other than oxygen, such as nitrate and Mn(II), may be involved (De Vitre et al. 1988). In a well-oxygenated soft water (pH 7) at 10 °C, the half-life of Fe(II) is approximately 4 h (Davison and Seed 1983). By contrast, Mn(II) has a typical half-life for the same conditions of between 1 and 100 days (Tipping et al. 1984). These lower rates of removal for Mn are dependent on microbial mediation, because the purely chemical reaction, involving heterogeneous catalysis by Fe and Mn oxides, would take approximately 300 years (Diem and Stumm 1984). A consequence of the slower oxidation of Mn(II) than Fe(II) is that the resulting particulate Mn tends to be more diffusely spread throughout the lake water. The slower oxidation is also responsible, along with the thermodynamic consideration of Mn(II) being more stable than Fe(II), for the maximum concentration of Mn particles occurring above that for iron particles.

The above account is a simplified version of Fe and Mn cycling. Details now emerging show several complications (Davison 1993). Electrochemical procedures (De Vitre et al. 1988) and ultrafiltration (Yagi 1988) have shown that up to 50% of the $0.45\,\mu m$ filterable Mn(II) and Fe(II) in anoxic lake waters may be present as small colloids, perhaps due to organic interactions. Large particles that occur near to the oxic–anoxic boundary are found to embrace a range of oxidation states ($MnO_{1.64–1.99}$; Tipping et al. 1984). Iron oxide particles may comprise 50% Fe(II) (Buffle et al. 1989) and contain appreciable concentrations of Ca, P, N, Mn, Si, S, and Mg (Tipping et al. 1981; Buffle et al. 1989). The surface characteristics of Fe, and to a lesser extent Mn oxides, are determined by adsorbed humic substances (Tipping and Heaton 1983; Tipping and Ohnstad 1984).

When anoxic conditions are well advanced,

dissolved sulfide can accumulate in the anoxic hypolimnia of lakes, leading to the precipitation of FeS (Davison 1991). These highly reducing FeS particles can coexist with iron oxides (Davison and De Vitre 1992) and indeed amorphous iron oxides are present in organic-rich reducing sediments (Hilton et al. 1986).

The redox cycling of Fe and Mn is not restricted to anoxic water columns. When sinking particles encounter the sediment of well-oxygenated water columns, reductive dissolution may occur and both Mn(II) and Fe(II) can be released to the overlying water column. Release of Fe(II) is less marked, but occurs in productive systems where Fe(II) is produced near the surface of the sediment. However, Fe(II) is quickly oxidized in the overlying water and returned to the sediment so that it is effectively trapped. The greater release of Mn(II) and its slower rate of oxidation allows it to be distributed throughout the water column (Davison 1993). However, because vertical dispersion is pronounced during periods of complete mixing, it is difficult to detect the release until the onset of stratification when mixing is greatly reduced.

Organic material, particularly in the presence of sunlight, can reduce oxides of Fe and Mn in surface waters (Collienne 1983). Such effects are most easily observed in acidic waters where Fe(II) in particular has a much longer half-life and diurnal cycles can be observed (Sulzberger et al. 1990).

Whereas redox transformations tend to dominate the behavior of Mn in lakes, such processes usually only affect less than 10% of the Fe that enters. A large fraction of the Fe is present in clay minerals and as relatively unreactive oxides that are not reduced. However, there is usually a plentiful supply of readily reducible Fe oxides, whereas the supply of the less abundant Mn oxide can become exhausted.

3.2 Iron and Manganese Compounds as Carrier Phases

3.2.1 Oxides

Under oxic conditions Fe and Mn oxides, together with organic matter, are generally regarded as the most important scavenging or carrier phases for the labile trace element fraction in aquatic environments (Hart 1982; Forstner 1982; Sigg 1985; Tessier 1992). Our understanding of element adsorption by Fe and Mn oxides under model laboratory conditions is sufficiently well developed for it to be modeled quantitatively by surface complexation theory (e.g., Dzombak and Morel 1990). The picture for real lake systems is less clear. The following account is intended to demonstrate the wide variety of evidence indicating a significant role for Fe and Mn oxides in the cycling of trace elements in lakes. It does not follow, however, that trace element mobility is necessarily enhanced by the reductive dissolution of the oxides, because the element may be rescavenged by other phases e.g., sulfide precipitation.

Laxen (1984, 1985) and Laxen and Sholkovitz (1981) carried out a series of laboratory sorption experiments with Fe oxide, employing natural materials under realistic lacustrine conditions. The oxide was produced by slow oxidation of natural anoxic lake waters. Substantial amounts of Pb, Cu, Cd, and to a lesser extent Ni, were sorbed under most conditions. The amounts of metals bound through coprecipitation (i.e., oxidation and sorption occurring simultaneously) were generally greater than through adsorption alone (i.e., sorption onto preformed Fe oxide). Sorption was modified substantially in the presence of humic substances, with Cd and Ni sorption being enhanced and Cu sorption being decreased. This was attributed, respectively, to strong binding of Cd and Ni to sorbed humics (i.e., "ligand-like behavior") and the greater affinity of Cu to the dissolved humic fraction. The Cd sorption was also highly sensitive to competition from Ca^{2+}.

Information on element binding by Fe and Mn oxides is also available from various laboratory leaching/dissolution studies of lake particles and sediments. Sequential leaching of sediment trap material, netted plankton samples, surface sediment floc, and sediments indicated that in Lake Michigan Pu isotopes and ^{241}Am are associated primarily with hydrous oxide coatings (Alberts et al. 1989). Statistical analysis of 1 M HCl extractable metal concentrations indicated that the mobility of Cd, Zn, Co, Pb, Cr, and Ni are controlled by Fe oxides in Lake Erie and Detroit River sediments (Lum and Gammon 1985). Sequential leaching of contaminated reservoir sediments (Schintu et al. 1991) indicated that Fe and Mn oxides were the dominant sorbent for Pb, and, together with the carbonate fraction, for Cd. Copper, on the other hand, although present in

the oxide fraction, was bound mainly by organic matter. Aggett and Roberts (1986) used the rates of element dissolution in ethylenediaminetetraacetate (EDTA) solutions to show that As is bound by Fe oxide in Lake Ohakuri sediments (New Zealand). The authors interpreted the constancy of the Fe: As ratio during dissolution as being indicative of coprecipitation of As at the time of oxide formation.

Lacustrine ferromanganese concretions contain significant amounts of trace metals, although they are impoverished relative to their marine counterparts (Harriss and Troup 1970; Calvert and Price 1977). Trace elements are also associated with the enhanced Fe and Mn oxide concentrations commonly observed in surface lake sediments (i.e., above the O_2-H_2S redox front; e.g., Lovell and Farmer 1983; Kepkay 1985; Cornwell 1986; Williams 1992). Supporting pore-water data are scarce. One of the most convincing data sets is that for a Scottish lake, in which the sediment and pore-water profiles of Co, Zn, and, to a lesser extent, Cu, closely follow those of Mn (Fig. 1). Williams (1992) attributed a causal link to these observations and suggested that trace metal distributions are controlled by the redox cycling of Mn. The association between trace elements and Fe and Mn oxides may be more complicated, however, and probably is not the overriding factor with regard to trace element distributions in most situations. In a recent study of Lake Superior sediments (McKee et al. 1989a,b), the observed sediment profile included the following zones at increasing depths: unconsolidated interfacial (~1 cm) material ("fluff"), an oxidized zone with intermediate total Fe and Mn concentrations, and an oxidation zone with maximal Fe and Mn concentrations, due to local oxidative precipitation following classic redox recycling from a deeper zone of reduction, containing the lowest total Fe and Mn concentrations. The fluff layer contained the highest concentrations of Zn, Cu, Pb, and organic carbon, but was not elevated in Fe and Mn. The oxidized zone also contained high trace metal concentrations, attributed previously to enhanced anthropogenic metal inputs. The Zn was bound dominantly by the oxide fraction, less so Pb, and Cu was associated mainly with the oxidizable (i.e., organic and sulfide) fraction. By comparison the Mn and Fe oxides formed diagenetically lower down the profile in the oxidation zone did not accumulate significant amounts of Zn, Pb, and Cu. Although the data do not exclude an anthropogenic effect, the trace metals appear to be undergoing significant diagenetic transformations, to some extent independent of the recycling of Fe and Mn. McKee et al. (1989a,b) came to the overall conclusion that the decay of organic matter near the sediment surface provides the main supply of available trace metals, and these can become bound to the oxides in the oxidized zone, but not to those at depth. Thus, the low trace metal content of the Fe and Mn oxides forming at depth in the oxidation zone is due to a decreased availability of the trace metals. These studies suggest that trace metal profiles in lake sediments can be significantly affected by chemical diagenesis, so that such profiles may not always provide a reliable historical record of anthropogenic metal inputs.

A novel approach to studying the Fe oxide–trace element association in surface sediments has been developed by Tessier et al. (1985, 1989). This work is important, because it establishes a link between theoretical surface complexation modeling, model laboratory experiments (i.e., with well-defined synthetic phases), and the far more complex environmental systems. It combines sediment and pore-water sampling, a modified Tessier sequential leaching scheme, and a simplified surface complexation model. Partitioning of Cd, Cu, Ni, Pb, and Zn between the Fe-oxide-bound fraction, defined by sequential leaching, and the pore waters in lakes of varying pH, was generally consistent with surface complexation theory (Tessier et al. 1985). Furthermore, at high pH the partitioning of Cd, Ni, and Zn was similar to that reported in the literature for adsorption by amorphous Fe oxyhydroxide in $NaNO_3$ solution. The Cu and Pb binding at high pH was less than that observed in model laboratory systems, which was attributed to the competitive action of dissolved ligands. At low pH sorption was greater than that reported for model Fe oxide for all the metals, and this was attributed to formation of ternary complexes between the oxide and some metal-ligand complex. This is the same explanation, i.e., ligand-like behavior of trace metals, as that invoked by Laxen in his sorption experiments with natural lake materials. Tessier's combined approach has also been used to show that As binding by Fe oxides in lakes of pH 4.0–8.4 agrees well with that observed for amorphous Fe oxyhydroxide in model laboratory experiments (Belzile and Tessier 1990).

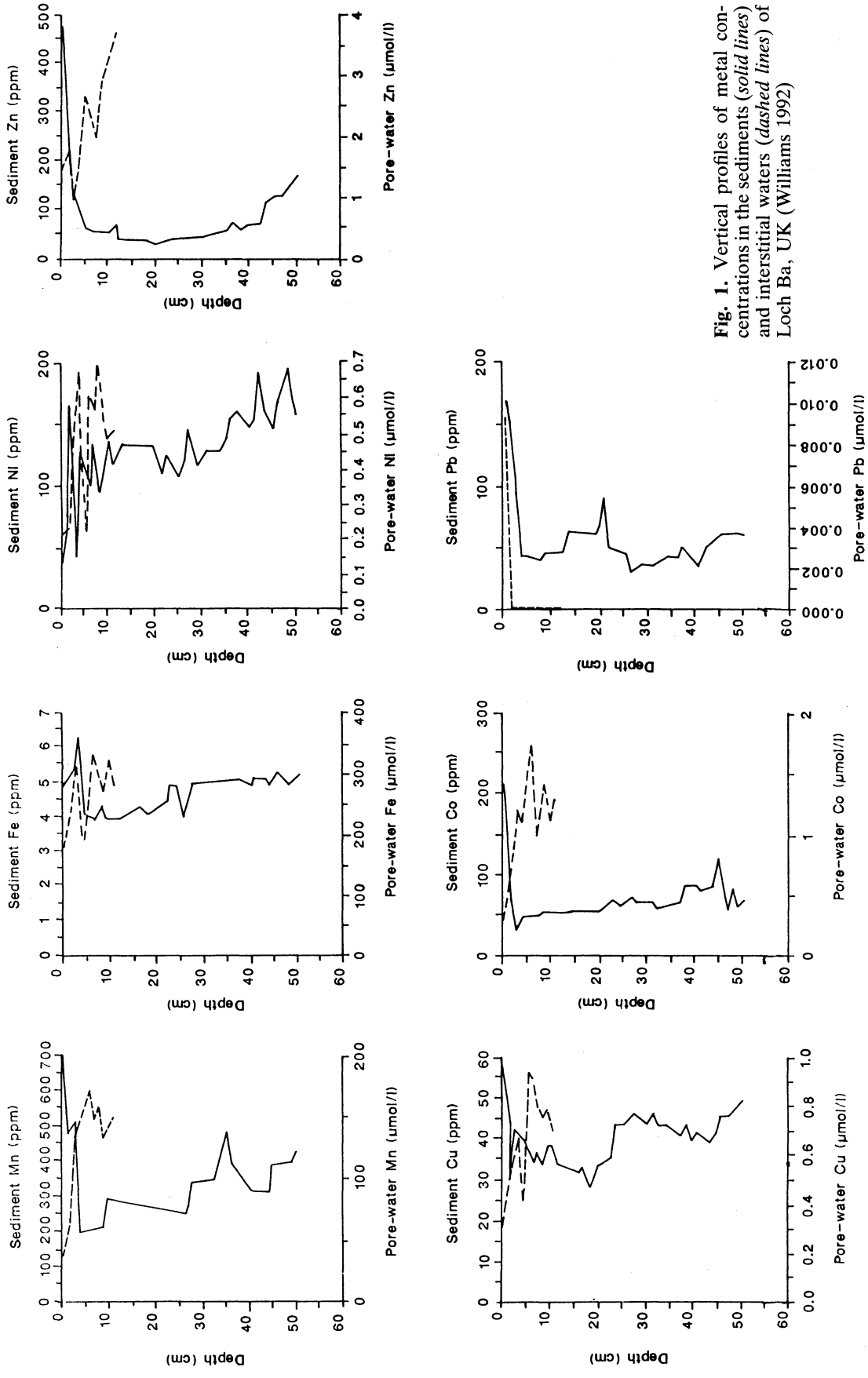


Fig. 1. Vertical profiles of metal concentrations in the sediments (*solid lines*) and interstitial waters (*dashed lines*) of Loch Ba, UK (Williams 1992)

Subsequently, Tessier and coworkers have taken the above approach a step further by the additional use of Teflon sheets to sample discretely the naturally occurring Fe and Mn oxides in lake sediments (Belzile et al. 1989). This goes a considerable way to overcoming the degree of uncertainty arising from the use of sequential leaching to define sediment speciation. The extended approach has been used in a detailed study of Cd binding in the sediments of 38 Canadian lakes (Tessier et al. 1993). A simplified surface complexation model again successfully described metal binding, but it was necessary to introduce an additional sorbent, organic matter, to account fully for the observed data. The study showed that, although significant, Cd binding by Fe oxide was less important than by the organic-sediment fraction.

Water-column profiles of dissolved trace element concentrations in lakes, which link element behavior directly to Fe and Mn oxides, are relatively scarce. Perhaps the clearest association is that between elevated concentrations of dissolved Co and the reductive dissolution of Mn oxide in the hypolimnia of some seasonally anoxic lakes (Hesslein 1987; Balistrieri et al. 1992a). Similar elevated concentrations of dissolved ^{210}Pb and ^{210}Po have been attributed to Fe and Mn oxide dissolution (Benoit and Hemond 1990; see Sect. 6.2). Water-column variations in As have also been linked to Fe and Mn, but these are complicated by As redox transformations [i.e., As(V)–As(III)] and biological methylation (see Sect. 5.1). Distinctive and coherent metal profiles were observed in an Antarctic lake having a saline, permanently anoxic, deep-water layer (Fig. 2), where Mn was dominant over Fe. Cobalt again most closely followed Mn, which was attributed by Green et al. (1989) to the reductive dissolution of Mn oxide and the presence of Co(III) in the Mn oxide lattice. Coincident with secondary maxima of Mn and Co, Ni, Cu, and Cd all showed maxima at a shallower depth. The Ni, Cu, and Cd peaks were also interpreted as being due to release from Mn oxide, but of less strongly bound forms (e.g., adsorbed as opposed to lattice bound). The mechanism of release was linked to the reductive dissolution of the oxide in suboxic waters, although it was noted that soluble complexes may have formed subsequently with the enhanced concentrations of inorganic and organic ligands occurring in the saline deep waters. In fact, the presence of saline waters, the upper boundary of which (48 m) coincided with the upper limit of the trace metal maxima (Fig. 2), provides a number of alternative explanations for the observed metal profiles. The depth zone of increasing salinity was associated with various horizons of high biological activity (e.g., photosynthetic maximum at 58 m; band of nitrifying bacteria at 54 m), a dramatic increase in concentration not only of ligands but also Ca^{2+}, and a decrease in pH from ~8 to ~5.5 (Fig. 2). The deep saline waters comprised essentially a $CaCl_2$ brine, with a Ca concentration of ~0.8 mol l^{-1} compared with ~5×10^{-3} mol l^{-1} at the lake surface. Thus, for instance, the coincident maxima of Ni, Cu, Cd, Mn, and Co at a depth of ~55 m may have been due to displacement of these metals from Mn oxide by H^+ and Ca^{2+} [some of the Mn-associated-with-Mn oxides occurs as adsorbed Mn(II); e.g., Tipping et al. 1984].

Sediment-trap studies have also provided evidence of trace element sedimentation via Fe and Mn oxides. In the permanently anoxic deep waters of a eutrophic, meromictic lake, a clear association was apparent between the "iron wheel" and Cu (Baccini and Joller 1981). Up to 50% of the depositional flux of Cu was thought to be due to Cu bound to sinking Fe oxides, despite the presence of anoxic bottom waters. In Lake Zurich scavenging and sedimentation of Cu, Zn, Pb, Cd, and Cr were linked to biogenic material, and to a lesser extent Fe oxides, whereas Mn oxide, resulting from an active Mn redox cycle, appeared to scavenge Cu, Zn, and Pb from the bottom waters (Sigg et al. 1987).

Thus, from the available data it appears that the relative importance of Fe and Mn oxides as trace element carriers in lake systems is highly variable, both with regard to each other and to other carrier phases (e.g., organic matter), depending on local conditions. Nevertheless, certain generalizations can be made about the relative importance of the two oxides with regard to some elements. Iron oxides appear to have a greater affinity for As (Batterson and McNabb 1983; Lovell and Farmer 1983; Aggett and Roberts 1986; Freeman et al. 1986; Belzile et al. 1989; De Vitre et al. 1991) and Cu (Baccini and Joller 1981; Cornwell 1986; Belzile et al. 1989), whereas Mn oxides appear to have a greater affinity for Ba (Cornwell 1986; Sugiyama et al. 1992), Co (Hesslein 1987; Balistrieri et al. 1992a), Zn (Jaquet et al. 1982; Belzile et al. 1989), and Ni (Kepkay 1985; Belzile et al. 1989; Balistrieri et al.

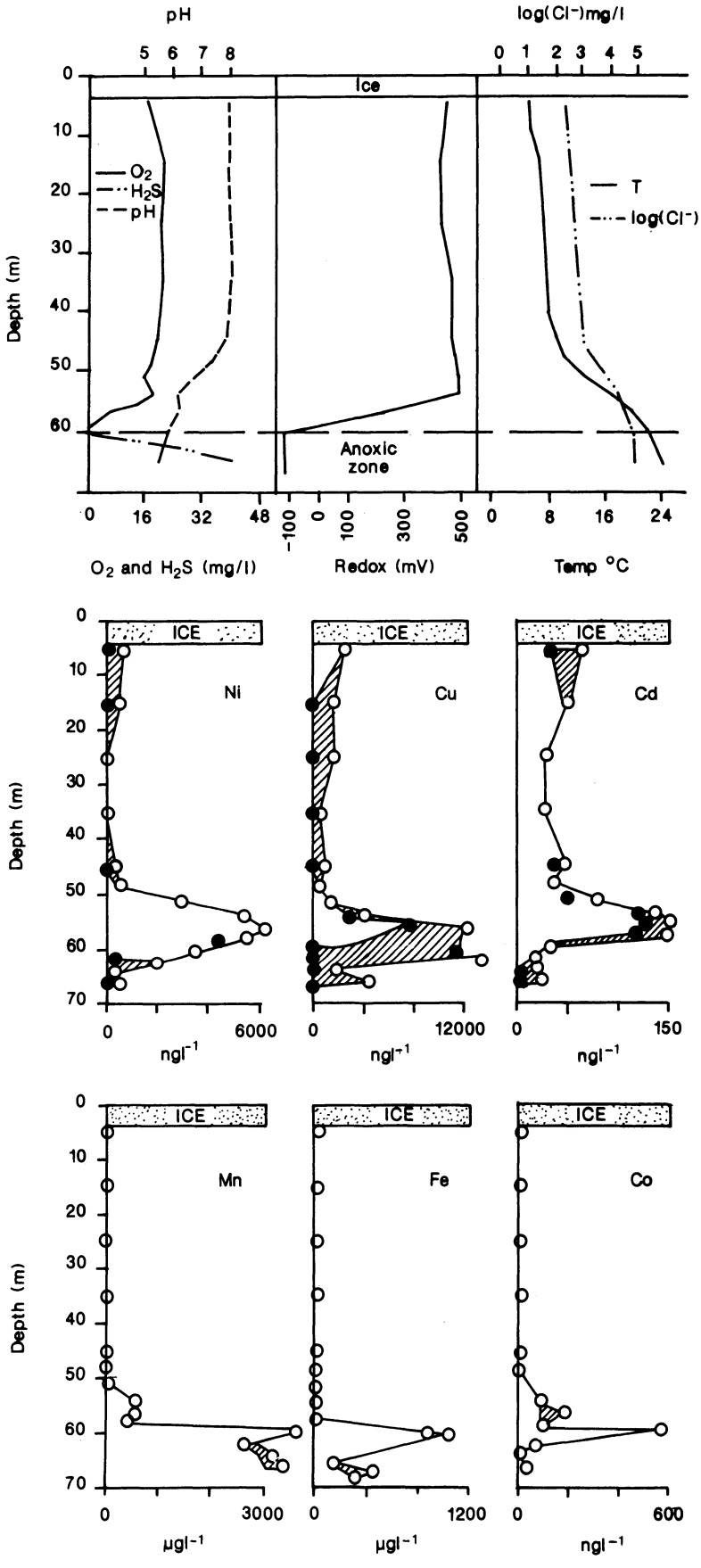


Fig. 2. Vertical profiles of metal concentrations and ancillary data in the water column of a meromictic Antarctic lake, Lake Vanda. Unfiltered metal concentrations are shown as *open circles* and filtered concentrations as *solid circles*, with particulate metal being represented by the *shaded areas*. (Green et al. 1989)

1992a). However, there are inevitably exceptions to such generalizations. For example in Mn-rich Lake Biwa, As is bound predominantly by the Mn oxide fraction (Takamatsu et al. 1985; see also Anderson and Bruland 1991).

3.2.2 Sulfides

The removal of trace metals as sulfides in anoxic lake systems is widely recognized (e.g., Forstner 1982), although direct evidence is limited. Davison et al. (1992) recently published some compositional data on Fe sulfide particles, sampled from anoxic hypolimnetic waters and analyzed using a scanning proton microprobe. This showed that the sulfide particles were richer in Cu (4000 ppm) and Zn (6000 ppm) than Fe oxide precursors. Supporting evidence for metal sulfide precipitation comes mainly from the study of dissolved metals in lake waters and sediments, usually combined with thermodynamic calculations of their solubility, based on one of the commonly used chemical speciation codes (e.g., WATEQ). Elements for which sulfide precipitation has been proposed as an important control include As, Cd, Cu, Co, Ni, Pb, and Zn (Matisoff et al. 1980; Batterson and McNabb 1983; Pedersen 1983; Aggett and O'Brien 1985; Carignan and Nriagu 1985; Carignan and Tessier 1985; Morfett 1988a; Green et al. 1989; Seyler and Martin 1989; Balistrieri et al. 1992a). No clear distinction is generally drawn between precipitation as the pure metal sulfide or coprecipitation with Fe sulfide. Solution conditions rarely appear to approach equilibrium with regard to pure metal sulfides, and the speciation codes commonly indicate oversaturation. Such discrepancies are attributed mainly to complexation, unaccounted for by the speciation code (e.g., organic-metal complexes), solid-solution effects, and detection-limit problems, especially with regard to sulfide measurement.

Various laboratory experiments provide further evidence of metal sulfide precipitation. Frevert (1987) carried out a series of laboratory incubations of undisturbed lake sediment cores, in which H_2S and pH were controlled. Under environmentally realistic anoxic conditions, Zn, Cd, Pb, and Cu were rapidly removed from solution, apparently as a result of sulfide precipitation. Similar experiments with homogenized lake sediments indicated the precipitation of As(III) sulfides (Batterson and McNabb 1983). Di Toro and coworkers (1992) have shown that metal (Cd and Ni) toxicity in lake sediments is mitigated by sulfide precipitation. They linked the effect to the acid volatile sulfide (AVS) content of the sediment, and attributed their observations to the displacement of Fe from its monosulfide by metals having a lower sulfide solubility product (e.g., Ni, Zn, Cd, Pb, Cu, and Hg). A similar correlation with the sulfide solubility product has also been observed in laboratory experiments of trace metal adsorption and coprecipitation by mackinawite, one of the metastable Fe sulfides comprising the AVS pool in sediments (Morse and Arakaki 1993). The extent of removal by both adsorption and coprecipitation occurred in the sequence Ni > Co > Mn. Cadmium, Cr, Cu, and Zn were removed from solution to an even greater extent, but removal associated with mackinawite could not be distinguished from precipitation of the pure metal sulfides.

3.2.3 Other Phases

The Fe and Mn carbonates and various Fe phosphates have been reported in lake systems, but again direct evidence is limited and information on their trace element contents is almost totally lacking. Buffle et al. (1989) characterized colloidal Fe-rich particles from the redox boundary in a eutrophic lake as being a mixed valency Fe(II/III) hydroxophosphate. The Fe and Mn carbonates and phosphates have more commonly been inferred from sediment pore-water studies (e.g., Emerson 1976; Matisoff et al. 1980). One such study suggested that the pore-water concentrations of dissolved Pb in Lake Erie sediments may be controlled by the Pb phosphate, chloropyromorphite (Matisoff et al. 1980).

4 Sediment–Water Interface

The exchange of elements between bottom sediments and the overlying water column is of special interest, because of its significance with regard to the ultimate fate of elements in lakes. The sediment–water interface is characterized by a marked increase in particle concentration and a decrease in diffusive-transport rates compared with the overlying water. Highly reactive particles, such as fresh algal material and metal oxides, tend

to be concentrated there. These can be rapidly broken down and new phases (e.g., sulfides) possibly formed. Trace elements consequently may be released into solution or captured, making this interfacial region a potentially important local source or sink of elements. Consideration of the literature demonstrates a high degree of variability in the direction and relative importance of the diffusive flux of dissolved elements occurring at the sediment–water interface. It also reveals certain difficulties that can arise when interpreting data on sediment–water exchange (see examples given in following sections and case studies on Pu and ^{137}Cs in Sect. 6).

4.1 Diffusive Flux from Sediments

In his earlier overview Sholkovitz (1985) concluded that the alkali (Na, K, and possibly ^{137}Cs) and alkaline-earth (Mg, Ca, and Ba) metals, together with the better known examples of Fe, Mn, P, Si, NH_3, and alkalinity, exhibit enhanced upward fluxes across the sediment–water interface during the seasonal anoxia that occurs in some lakes. These fluxes result in increased element concentrations in anoxic hypolimnia and were attributed by Sholkovitz, in part (Na, K, Mg, Ca, and Ba) or in total, to redox-related processes. Evidence showing similar effects with other elements is scarce, and, furthermore, it is generally difficult to distinguish between diffusion across the sediment–water interface and dissolution of settling particles as the source of such increased concentrations. Examples given in Sect. 3.2.1 of As, ^{210}Pb, and ^{210}Po provide compelling evidence of release from sediments, in that the interpretations are based variously on time- and depth-dependent concentrations in the water column and interstitial waters, sediment-trap data, and mass-budget calculations (Aggett and O'Brien 1985; Benoit and Hemond 1990). In the case of As and ^{210}Pb, however, the situation is complex and a variety of biogeochemical cycling characteristics have been reported (see Sects. 5.1 and 6.2). It is evident from these and the following examples that interpreting such data is by no means straightforward.

Esthwaite Water in Great Britain has been a site of intense study since the pioneering work of Mortimer (1941, 1942), and the early results were pivotal in developing the notion of the reductive dissolution and release of Mn (and Fe) from bottom sediments into overlying waters under anoxic conditions (see Sholkovitz 1985). The initial interpretation of the Esthwaite Water situation was based on time- and depth-dependent water-column Mn concentrations, vertical conductivity profiles in bottom sediments, and laboratory incubation experiments using natural lake sediments and waters (Mortimer 1941, 1942). Subsequent studies, summarized in Davison (1993), have included sediment trapping, porewater measurements, and mass-budget calculations/modeling, and these have led to a fuller understanding of the system. The current interpretation is that although an initial release of Mn occurs from bottom sediments to overlying waters in early spring, it is short-lived. The hypolimnetic sediment in Esthwaite Water is Mn-depleted, and the availability of Mn oxide in the sediment rapidly becomes limiting during summer stratification. Thus, the continuing increase in dissolved Mn concentrations in the water column is supplied by the reductive dissolution of settling Mn oxide particles, and not from the sediments. To the contrary, as a result of the continued increase in hypolimnetic dissolved Mn concentrations, Mn diffuses back into the sediments during the latter part of the stratification period.

The dangers of relying on water-column profiles alone when interpreting possible release from bottom sediments are demonstrated by reference to a series of vertical profiles in Esthwaite Water (Fig. 3). These were obtained during the period of summer stratification following the earlier atmospheric deposition of Chernobyl-derived radionuclides around May 6, 1986 (Davison et al. 1993a). Initial consideration of the profiles suggests a causative link between the elevated ^{137}Cs concentrations below 11 m and those of dissolved Fe in the deoxygenated bottom waters, which are known to result from diffusion from bottom sediments. However, modeling of a detailed time series of surface and bottom water ^{137}Cs concentrations in the lake showed that the similarity of the two profiles was coincidental (Davison et al. 1993a). The initial ^{137}Cs input on May 6 occurred prior to stratification so that the ^{137}Cs was mixed homogeneously throughout the lake. Thereafter, ^{137}Cs concentrations in the well-mixed surface waters were gradually reduced by hydraulic flushing, scavenging by particles, and possible diffusion into bottom sediments, whereas

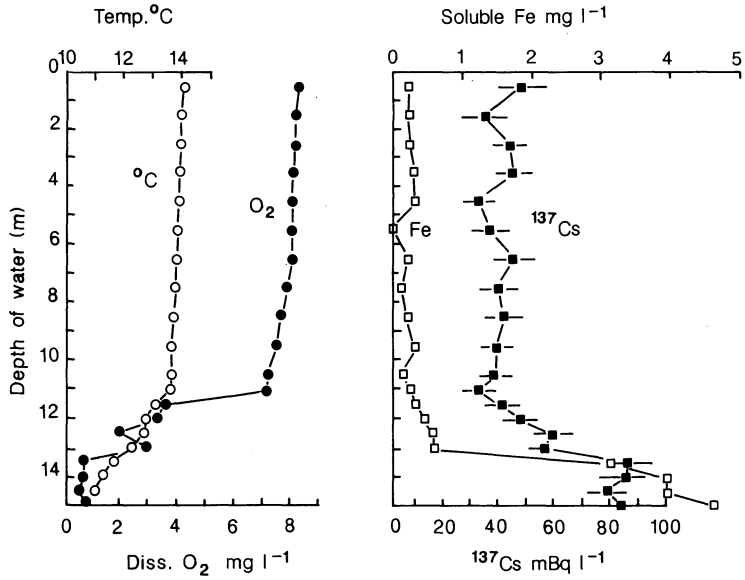


Fig. 3. Variation with water depth of dissolved ^{137}Cs and Fe concentrations, together with temperature and dissolved oxygen, in Esthwaite Water, UK, on 27 August 1986 during the period of summer stratification, following atmospheric deposition of Chernobyl-derived ^{137}Cs in May 1986. (Davison et al. 1993a)

the hypolimnetic ^{137}Cs concentrations were little affected by these processes, thus producing the observed heterograde ^{137}Cs profile.

4.2 Evidence of Little or No Diffusive Efflux from Sediments

Trace elements commonly show evidence of little or no net diffusive transport from sediments into the water column. Many studies based on water-column and pore-water profiles and in situ submerged chamber measurements have shown no significant release of Cu, Pb, and Zn from sediments in lakes when Mn and/or Fe are being released, due to the reductive dissolution of their oxides (Drake and Ackerly 1983; Pedersen 1983; Sakata 1985; Sigg et al. 1987; Morfett et al. 1988; Morfett 1988b; Santschi 1989). This retention is usually attributed to the precipitation of metal sulfides at depth (e.g., Pedersen 1983; Morfett et al. 1988). Figure 4 shows the concentrations of dissolved Fe, Cu, and Zn at the sediment–water interface between July and December, covering the later stages of summer stratification, overturn, and winter mixing in seasonally anoxic, monomictic Esthwaite Water. Contrary to showing remobilization, Cu and Zn concentrations were significantly lower during anoxia (August to early October), which was attributed to sulfide precipitation (Morfett et al. 1988). The lack of evidence for element release from sediments can sometimes be misleading, however, as the released element may be mixed sufficiently rapidly through the water column that no localized increase in concentration can be detected. Thus, hypolimnetic element accumulations may result simply from reduced upward dispersion during stratification (Sholkovitz 1985). For example, Davison et al. (1982) suggested that Mn is released from Esthwaite Water sediments throughout the year, yet shows no apparent bottom-water enhancement in winter, due to the rapid vertical mixing throughout the lake at this time.

4.3 Transient Remobilization

As opposed to systematical seasonal changes in concentration, as seen with Fe and Mn in many lakes, there is some evidence to suggest that trace metal concentrations exhibit various short-lived (days or weeks), localized maxima at the sediment–water interface. Morfett et al. (1988) studied metal concentrations in the interfacial region of the sediment surface of Esthwaite Water in considerable detail. Zinc, and to a lesser extent Cu, showed transient maxima approxi-

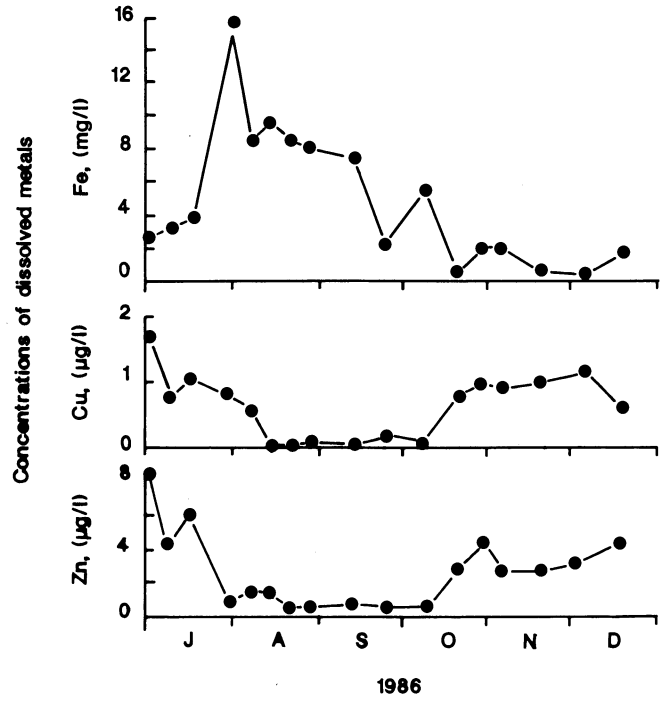


Fig. 4. Dissolved concentrations of Fe, Cu, and Zn at the sediment-water interface in Esthwaite Water, UK, between July and December 1986. The period encompassed the later stages of summer stratification, including a period of hypolimnetic anoxia (August to the overturn on 18 October), and early winter mixing. (Morfett et al. 1988)

mately 1 cm above the sediment–water interface, which were linked to temporal variations in the rates of supply of particulate metal, via sedimentation, and in the rates of vertical mixing in the water column (see Sect. 6.3 for a more detailed discussion). Morfett (1988a) also undertook a series of related laboratory incubations, in which natural Esthwaite sediments and waters were manipulated to mimic environmental conditions as closely as possible. One of the main observations was a transient release of dissolved trace metals as the sediments underwent a redox transition (oxic to anoxic or vice versa), whereas no trace metal (Zn, Cd, or Pb) remobilization generally occurred from cores incubated permanently under either oxic or anoxic conditions. The transient releases were attributed to the partial dissolution of one redox phase prior to the formation of another.

A number of other studies provide support for the occurrence of transient release at the sediment–water interface. Copper and Zn concentration data from seasonally anoxic Lake Biel in Switzerland show short-lived maxima at various times during the year that have no obvious correlation with the reductive remobilization of Mn (Santschi 1989). In a study of the biogeochemical cycling of ^{210}Pb and ^{210}Po in an oligotrophic Wisconsin lake, Talbot and Andren (1984) found that both radionuclides exhibited transient periods of removal from the water column, linked to algal uptake and sedimentation. The ^{210}Pb appeared to be permanently removed to the sediments, whereas ^{210}Po underwent rapid release back to the water column following an algal sedimentation event. Gunkel and Sztraka (1986) observed substantial dissolved trace metal (e.g., Zn, Cr, Cd, and Pb) enhancements over narrow depth intervals (~1.5 cm) at or close to the sediment interface in two urban lakes. These enhancements occurred in the vicinity of marked redox gradients, and although they were linked by the authors to the reductive remobilization of Fe and Mn oxides, a similar supply-based mechanism as for Esthwaite Water cannot be ruled out.

4.4 Diffusive Flux into Sediments

There appear to be a number of circumstances related to redox conditions under which elements diffuse from overlying waters into sediments. The

downward diffusion of Mn during the latter part of the stratification period in some seasonally anoxic lakes has already been discussed (see Sect. 4.1). Another significant example is linked to the effects of pH on element behavior. Lake acidification is often associated with elevated metal concentrations in the water column, and the question of whether acidification leads to metal release from bottom sediments has created considerable interest (e.g., Forstner 1982). Laboratory (Stokes and Szokalo 1977) and in situ mesocosm (Santschi et al. 1986) experiments have both indicated that the release of certain metals (e.g., Zn and Co) from contaminated sediments can be brought about by lowering the pH of the overlying water. In addition, total metal profiles in the sediments of acidic lakes often show depleted concentrations in the uppermost layers, which in some cases have been attributed to acid leaching (see Forstner 1982). In contrast to these findings, in situ pore-water profiles have shown unequivocally that, where the O_2-H_2S boundary occurs at or close to the sediment–water interface, downward diffusive transport into the sediments appears to be the norm for a range of metals, especially in more acidic lakes (Fig. 5; see also Pedersen 1983; Carignan and Nriagu 1985; Carignan and Tessier 1985; Tessier et al. 1989; Pedersen et al. 1993). These include acid-sensitive metals such as Zn and Cd (Carignan and Tessier 1985; Tessier et al. 1989; Pedersen et al. 1993; see also Sect. 6.3). The sedimentary sink is attributed mainly to sulfide precipitation, but also possibly to the knock-on effects of alkalinity generation that accompanies the anaerobic decomposition of organic matter. Thus, the consequent pH gradient across the sediment–water interface of acid lakes (Fig. 5) may result in enhanced sorption and possible gibbsite formation in the sediment (Carignan and Nriagu 1985). The dissolved metal gradients, and hence downward fluxes, tend to be greatest in lakes with overlying acidic waters (pH 4.5–5.5; Carignan and Nriagu 1985; Tessier et al. 1989), although large gradients can also be observed in lakes with a water column pH > 7 (Carignan and Nriagu 1985; Pedersen et al. 1993). The diffusive fluxes can be of major significance in terms of the measured accumulation rates of the metals in the sediments, and therefore will have an important potential effect on the sediment profiles and any subsequent interpretation of the depositional record of trace metals in lakes. The fluxes can particularly lead to the sort of surface or subsurface trace metal maximum in the sediments (see profiles of Cu and Ni in Fig. 5) that has previously been attributed to past changes in anthropogenic inputs or to acid leaching into the water column (Carignan and Nriagu 1985). Such is the effectiveness of reducing sediments, in acting as trace metal sinks in this way, that it has led Pedersen et al. (1993) to speculate on their use as permanent storage sites for waste mine tailings.

It is interesting to consider the possible reasons for the reported differences between the laboratory and mesocosm experiments, involving metal leaching and remobilization on acidification, and the observed pore-water profiles of natural systems, which show metal transfer into sediments. To our knowledge there are in fact little or no data that unequivocally demonstrate metal leaching from lake sediments under "natural" conditions. It may be that under conditions appropriate to a manipulative experiment leaching would occur. Alternatively, there may be inherent differences between the experiments and the natural situations, such as an absence of sulfate reduction and sulfide precipitation in the experiments or differences in dynamic factors. The laboratory and mesocosm experiments were effectively perturbed closed systems, exhibiting non-steady-state conditions. In the mesocosms acid and base were added and conditions monitored within a single 90-day experiment. In the actual lakes conditions were achieved "naturally" over a period of years in an open system. The relatively high metal concentrations in the water column may have been a feature of acid waters entering the lake, and also reflected lower trace metal scavenging within the water column, rather than being the result of remobilization from the sediments. Although of great value in providing insights into possible biogeochemical and transport processes, the discrepancies described highlight some of the possible limitations of the experimental approach when attempting to apply the results to real situations.

5 Pathways Involving Redox Reactions Directly: Case Studies

Sections 5 and 6 provide a series of case studies selected on the basis of their intrinsic interest and the availability of good quality data. The quality criteria employed were either the use of oceanographic-type clean techniques or geo-

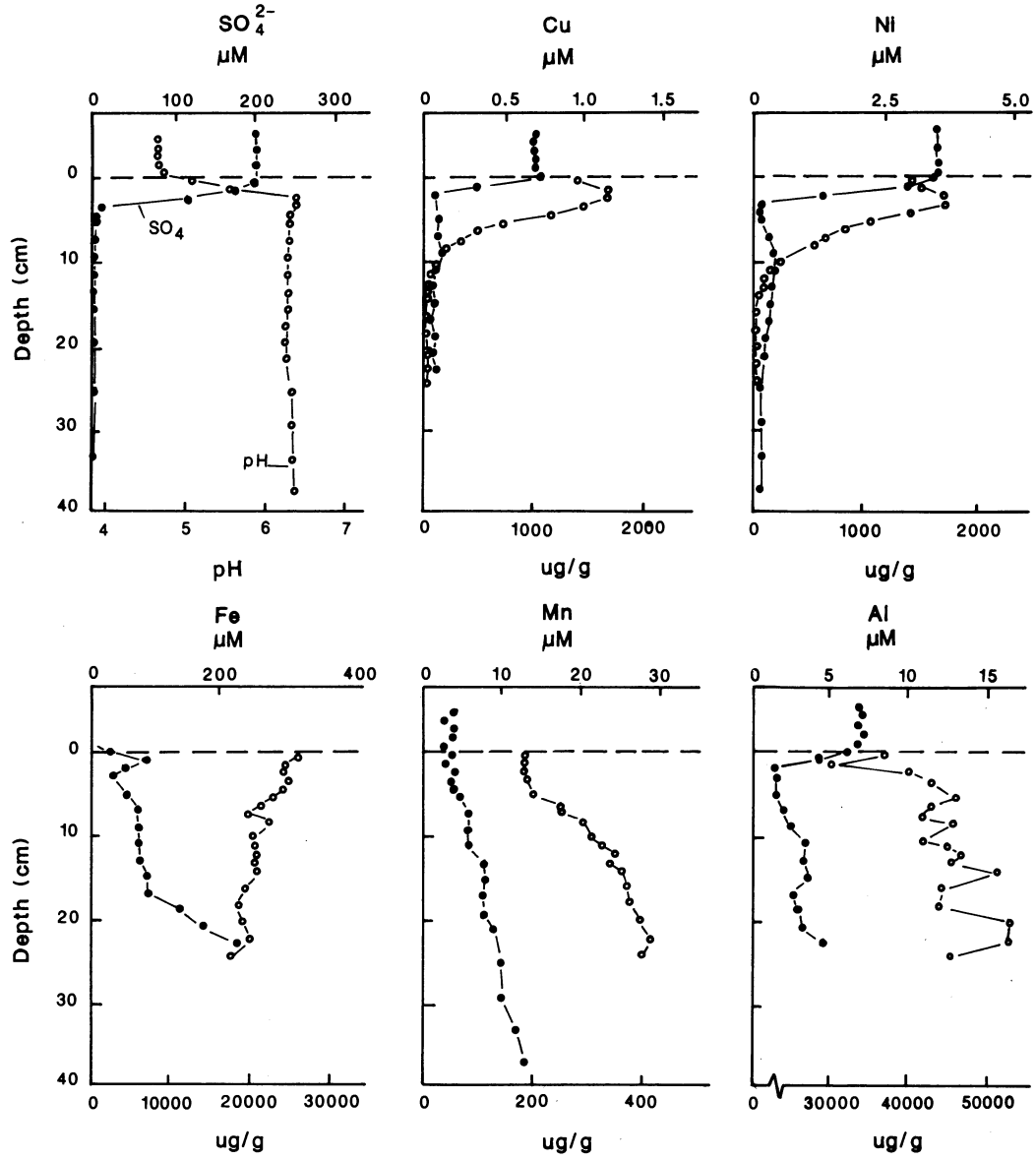


Fig. 5. Vertical profiles of the dissolved (*solid circles*) and total sediment (*open circles*) concentrations of Cu, Ni, Fe, Mn, and Al, together with dissolved SO_4^{2-} and pH, in the sediments and overlying waters at a water depth of 15 m in Clearwater Lake, Ontario. (Carignan and Nriagu 1985)

chemical consistency, i.e., the data are relatively consistent and show coherent trends that can be related to known biogeochemical processes. Table 1 summarizes some of the main features of the redox chemistry in lakes of these and other trace elements, and also provides some key references. The contents of Table 1 reflect the principal observations and conclusions of the cited literature, rather than representing a comprehensive review of biogeochemical characteristics.

5.1 Arsenic

Cullen and Reimer (1989) have reviewed in detail the literature on As speciation in the environment. Considerable advances have been made in recent years in our understanding of the biogeochemical cycling of As in lakes. Much of the progress has centered around the work of Aggett and coworkers in Lake Ohakuri, New Zealand, a seasonally anoxic lake receiving unusually high As inputs derived from geothermal sources

Table 1. Main redox characteristics of selected metals, metalloids, and radionuclides in lakes

Metal	Type	Main carrier phases[a]	Main dissolved forms	Observed water-column variations[b]	References
As	Direct	Fe and possibly Mn oxide for As(V); As(III) sulfide or mixed sulphide	Arsenate, arsenite, monomethylarsonate, dimethylarsenate	Total As generally increases in pore waters and hypolimnion during seasonal anoxia; release from sediment probably important; As(V) –> As(III) during anoxia; redox reactions generally not at equilibrium; methylated forms important: can be dominant seasonally in photic zone	1–4
Ba	Indirect	Mn and Fe oxide, $BaSO_4$, organic matter?	Ba(II) cationic and neutral species	Water-column depletion associated with sorption to Mn oxide; instances of accumulation in seasonally anoxic hypolimnion	5–7
Cd	Indirect	Fe and Mn oxide, organic matter, sulfide	Cd(II) cationic and neutral species[d]; organic-Cd(II) complexes	Little variation; maybe slightly depleted under seasonally anoxic conditions; may sometimes be linked to nutrient (phosphate) distributions	8–11
Co	Indirect?	Mn and Fe oxides, sulfide	Co(II) cationic species[d]; may occur as Co(III) in the Mn oxide	Accumulation in seasonally anoxic hypolimnion with overlying particulate maximum	8, 12–14
Cr	Direct	Cr(VI)-Fe oxide; organic matter; Cr(III) is generally particle-reactive	Chromate, colloidal Cr(III)	Depletion in seasonally anoxic waters probably associated with Cr(VI) –> Cr(III)	8, 13, 15
^{137}Cs	Indirect	Edge/wedge and interlayer sites of illite	Cs^+	Some accumulation in seasonally anoxic hypolimnion	12, 16, 17
Cu	Indirect?	Fe and Mn oxide, organic matter, sufide	Cu(II) cationic and neutral species; organic-Cu(II) complexes; possibly reduced to Cu(I) under anoxia, e.g., CuS^-	Little variation; may show some hypolimnetic depletion, due to Fe oxide scavenging or, under anoxic conditions, due to sulfide precipitation	8, 18–20
Ni	Indirect	Mn and Fe oxide, sulfide	Ni(II) cationic and neutral species[d]	Some evidence of accumulation in seasonally anoxic hypolimnion and depletion in permanently anoxic waters	8, 18, 19, 21
Pb and ^{210}Pb	Indirect	Fe and Mn oxide, organic matter, sulfide	Pb(II) cationic and neutral species[d]; organic-Pb(II) complexes	In some instances accumulation in seasonally anoxic hypolimnion	18, 22–24
^{210}Po	Direct?	Organic matter and Mn oxide?	Po(IV)-Po(II)?	Accumulation in seasonally anoxic hypolimnion	22, 23

Table 1. (*Contd.*)

Metal	Type	Main carrier phases[a]	Main dissolved forms	Observed water-column variations[b]	References
Pu	Direct	Fe oxide; organic matter	Pu(III)?-Pu(IV)-Pu(V)-Pu(VI)?	Apparent accumulation in seasonally anoxic hypolimnion reported in some cases, but redox origin questioned; one report of possible depletion; in a meromictic lake, minimum at redox front associated with Fe oxide scavenging, order-of-magnitude enhancement in anoxic waters	25–28
Se	Direct	Fe and Mn oxide; elemental Se and/or metal selenides under strongly reducing conditions	Selenate, selenite, and various organic (including methylated) forms	Depletion in selenite and selenate in anoxic hypolimnion attributed to in situ reduction to particulate elemental Se; reported instances of release from sediments	12, 29–31
Zn	Indirect	Organic matter, Mn and Fe oxide, sulfide	Zn(II) cationic and neutral species[d]	Instances of enhanced and depleted concentrations under anoxic conditions	8, 12, 19–21, 32–35

[a] Underlined oxide generally more important.
[b] Refers to dissolved concentrations unless otherwise stated.
[c] (1) Aggett and O'Brien (1985); (2) Anderson and Bruland (1991); (3) Freeman et al. (1986); (4) Aggett and Kriegman (1988); (5) Cornwell (1986); (6) Sugiyama et al. (1992); (7) McGrath et al. (1989); (8) Balistrieri et al. (1992a); (9) Sigg et al. (1987); (10) Tessier et al. (1993); (11) Green et al. (1989); (12) Hesslein (1987); (13) Santschi (1988); (14) Williams (1992); (15) Johnson et al. (1992b); (16) Comans et al. (1989); (17) Davison et al. (1993a,b); (18) Carignan and Nriagu (1985); (19) Young and Harvey (1992); (20) Reynolds and Hamilton-Taylor (1992); (21) Belzille et al. (1989); (22) Benoit and Hemond (1990, 1991); (23) Talbot and Andren (1984); (24) White and Driscoll (1985); (25) Alberts and Orlandini (1981); (26) Alberts et al. (1986); (27) Buesseler et al. (1985); (28) Pinder et al. (1992); (29) Cooke and Bruland (1987); (30) Weres et al. (1989); (31) Cutter (1991); (32) Carignan and Tessier (1985); (33) Davison et al. (1992); (34) Tessier et al. (1989); (35) Morfett et al. (1988).
[d] Sulfide species predominant in anoxic waters.

(Aggett and O'Brien 1985; Aggett and Roberts 1986; Freeman et al. 1986; Aggett and Kriegman 1988). The key features of the lacustrine cycling of As are that it can occur in two common oxidation states, As(V) and As(III), its behavior is closely linked to that of Fe and to a lesser extent Mn oxides, and it can undergo biological uptake and methylation (Cullen and Reimer 1989). In solution arsenate typically occurs as the anionic species, $H_2AsO_4^-$ and $HAsO_4^{2-}$, and arsenite as the neutral species, $As(OH)_3$. Both the oxidation of As(III) and the reduction of As(V) can be microbially mediated (Freeman et al. 1986; Cullen and Reimer 1989).

Dissolved As and Fe profiles in Lake Ohakuri during seasonal anoxia illustrate many of the key controlling factors (Fig. 6). The diffusive release of As from the sediments and its consequent enrichment in the anoxic hypolimnion probably result from the reductive dissolution of Fe and Mn oxides. The Fe oxides are generally thought to be the major carrier phase and the sorbed As to be almost exclusively arsenate (Batterson and McNabb 1983; Aggett and Roberts 1986; Aggett and Kriegman 1988; Belzile and Tessier 1990; De Vitre et al. 1991). Detailed information is now available on the exact nature of As(V) binding by Fe oxides (Fuller et al. 1993; Waychunas et al. 1993). Part of the As(V) remobilized from the Fe oxides is reduced to As(III) (Batterson and McNabb 1983; Aggett and Kriegman 1988; Kuhn and Sigg 1993), and hence both oxidation states are seen diffusing from the anoxic sediments in Lake Ohakuri (Fig. 6). The fact that not all the remobilized As(V) is reduced to As(III) in the anoxic pore and hypolimnetic waters indicates that the rate of reduction is similar to the rate of diffusive transport. Thus, As reduction is rate-limited. Kuhn and Sigg (1993) suggested that the reduction of dissolved As(V) to As(III) in the anoxic hypolimnion of Greifensee, Switzerland, was chemical in nature with S(-II) being the most likely reductant. Redox cycling of As, associated with the reductive dissolution of Fe oxides, also occurs where the redox boundary lies within the sediment column (Lovell and Farmer 1983; Belzile et al. 1989; Belzile and Tessier 1990). In Mn-rich lakes, Mn oxides can act as the dominant, or at least a significant, sorbent for As(V) (Takamatsu et al. 1985; Anderson and Bruland 1991).

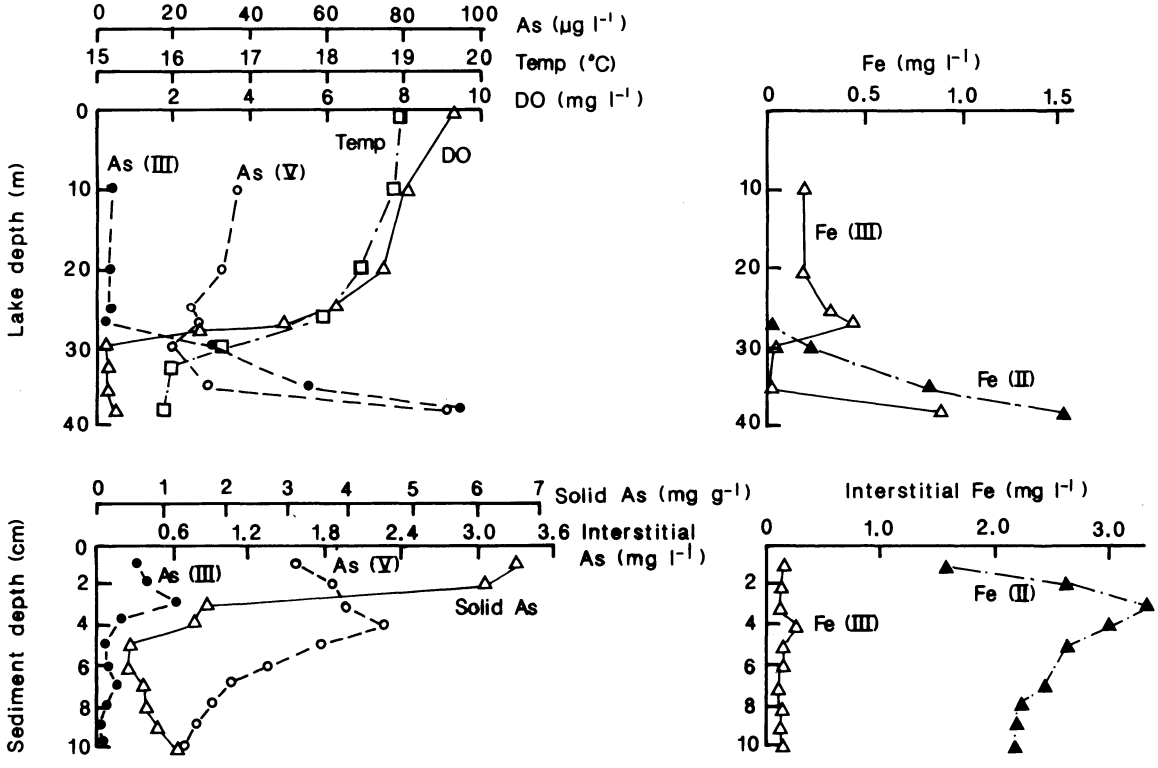


Fig. 6. Vertical distributions of dissolved As and Fe redox species in the water column and interstitial waters of Lake Ohakuri, New Zealand, during summer stratification and hypolimnetic anoxia. (Freeman et al. 1986)

The Mn and amorphous Fe oxides also appear to play an important rule as oxidizing agents in the rapid chemical (i.e., abiological) oxidation of As(III) (Oscarson et al. 1980, 1981; De Vitre et al. 1991). Consequently inorganic As(III), present in anoxic waters, is oxidized by Fe and Mn oxides either during its diffusive transport through overlying oxidized layers or following overturn of the water column. This is probably most efficiently achieved where the oxides occur in surface sediments rather than overlying waters, due to the lower diffusion rates and higher oxide concentrations (see De Vitre et al. 1991). Kuhn and Sigg (1993) attributed the transformation of significant amounts of dissolved As(III) to As(V) in Greifensee, following overturn, to chemical oxidation at the surface of suspended Mn oxide particles.

Field and laboratory studies have shown that under anoxia there is often an initial build-up of As(III), but, subsequently, concentrations may decrease either with depth or time (Batterson and McNabb 1983; Aggett and O'Brien 1985; Anderson and Bruland 1991). This removal is generally attributed, at least within the sediment, to the precipitation of As_2S_3 or a mixed Fe–As sulfide, which generally appear to be supersaturated (Batterson and McNabb 1983; Aggett and O'Brien 1985; Seyler and Martin 1989).

The relative concentrations of As(V) and As(III) do not usually appear to be at chemical equilibrium (see also Cullen and Reimer 1989; Seyler and Martin 1989; Anderson and Bruland 1991; Kuhn and Sigg 1993), suggesting that the observed concentrations result from a dynamic balance between the various biogeochemical and transport processes. Another example of nonequilibrium are the unexpectedly high dissolved As(III) concentrations observed in well-oxygenated surface waters of Lake Ohakuri (see Freeman et al. 1986) and Greifensee (Kuhn and Sigg 1993) during at least part of the spring–summer period and attributed to biological processes. In Greifensee the enhanced As(III) concentrations were preceded by the depletion of dissolved As(V) in the epilimnion, due to algal uptake together with phosphate. Freeman et al. (1986) demonstrated experimentally that under aerobic conditions mixed microbial cultures were able not only to oxidize As(III) to As(V), but also to reduce As(V) to As(III). The ecological logic of microbial As(V) reduction has been explained in terms of a detoxification strategy, aimed at avoiding the consequences of incorporating arsenate instead of phosphate (see Freeman et al. 1986).

An exception to the rule about nonequilibrium of As redox species is provided by Mono Lake, California (Maest et al. 1992). The profiles observed in 1986 (Fig. 7) were from a period (1984–

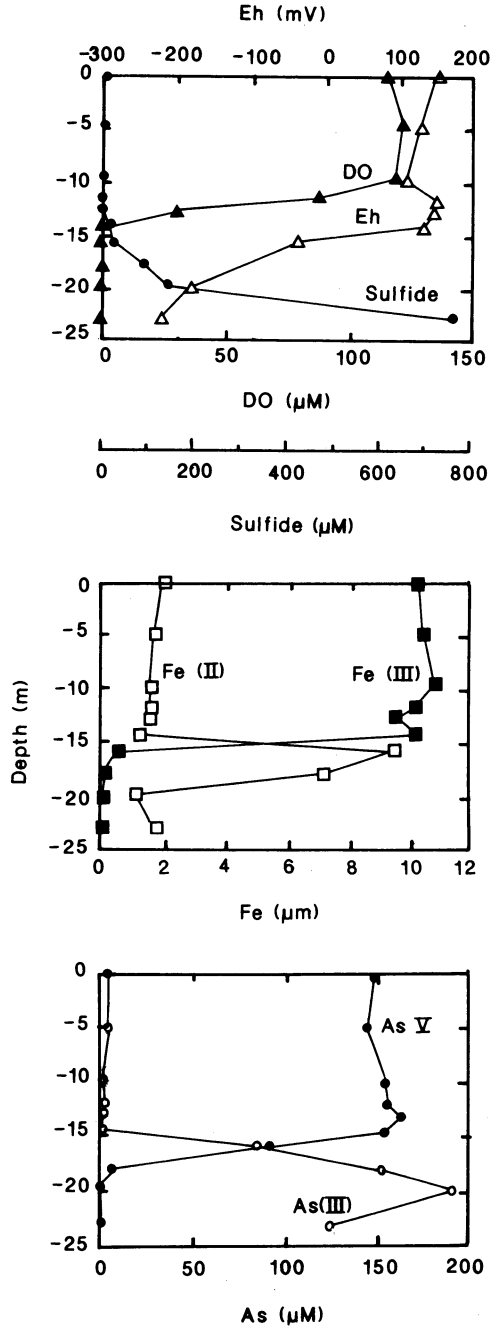


Fig. 7. Vertical distributions of Eh, dissolved oxygen and sulfide, and dissolved Fe and As redox species in the water column of a semipermanently stratified, high-salinity, alkaline lake (Mono Lake) in California. (Maest et al. 1992)

1988) during which this high-salinity (~90‰) alkaline lake was continuously stratified and a stable O_2-H_2S boundary was maintained between 15 and 18 m. There was good correspondence between the measured and predicted redox potentials for Fe(II)/Fe(III), As(III)/As(V), and S(-II)/S(VI) (Maest et al. 1992). This situation appears to be linked to the behavior of As(V), which approached its detection limit with depth in the anoxic zone of Mono Lake. This is in marked contrast to the more commonly observed situation, where As(V) as well as As(III) appears to diffuse from underlying sediments (Fig. 6). This difference may be related to the contrasting time frames of the two systems (i.e., semipermanent anoxia vs seasonal anoxia). More specifically it may be associated with the absence of a source of As(V) at depth in Mono Lake, which, in Lake Ohakuri, is due to the gradual reductive remobilization of Fe oxides in the surface anoxic sediments. The Fe oxides tend to be present in excess in the sediments of seasonally anoxic lakes so that the diffusive flux from the sediments is continuous throughout anoxia (see Sect. 3.1). In Mono Lake the reactive sediment oxide may have been effectively consumed over the preceeding 2-year period of stable anoxia, although some continuous supply via sedimentation can be expected.

There is apparently conflicting evidence for the presence of methylated forms of As in natural freshwaters. No methylated As has been found in the water column and sediment pore waters of Lake Ohakuri (Aggett and O'Brien 1985; Freeman et al. 1986), nor in laboratory experiments with As-contaminated reservoir sediments (Masscheleyn et al. 1991). A comprehensive study of methylated As species has recently been completed in which a regional survey of surface lake and estuarine waters was undertaken together with a detailed study of As speciation in a seasonally anoxic lake in California (Davis Creek Reservoir; Anderson and Bruland 1991). The surface lake samples all showed measurable concentrations of methylated As (average 24%; range 1–59% of total), except for Mono Lake. Minor amounts of methylated As have also been observed in Greifensee (Kuhn and Sigg 1993). Anderson and Bruland (1991) suggested that the apparent lack of methylated As in Mono Lake may be due to its extremely high inorganic As concentration, which could overwhelm the analysis of relatively small concentrations of methylated forms. Another alkaline lake showed the second highest concentration of methylated As among all the surveyed water bodies, yet this corresponded to only ~1% of the total As. In Davis Creek Reservoir dimethylarsinic acid increased to become the dominant form of dissolved As in the surface photic zone during late summer and autumn. Following overturn methylated forms decreased and arsenate increased, suggesting a degradation of dimethylarsinic acid to arsenate. In Greifensee inorganic and methylated As accounted for only ~50% of the total dissolved As (Kuhn and Sigg 1993). The remainder was undetectable by direct hydride generation techniques and was attributed to larger organoarsenic compounds.

5.2 Chromium

The aqueous geochemistry of Cr has recently been reviewed by Rai et al. (1989) and Richard and Bourg (1991). Two oxidation states, Cr(III) and Cr(VI), dominate in natural waters. The most important dissolved species of Cr(III) are $CrOH^{2+}$ below pH 6.3 and $Cr(OH)_3$ at higher pH, whereas for Cr(VI) they are $HCrO_4^-$ and CrO_4^{2-}. Chemically mediated redox reactions are emphasized in the previously mentioned reviews, with no reference to any microbial effects. The Cr(VI) is reduced rapidly by Fe(II) and sulfide. Organic matter, including humic substances, is also an effective reductant (see Saleh et al. 1989). Laboratory experiments indicate that Mn oxide is the most important oxidizing agent, with dissolved O_2 being relatively inefficient. The Cr(III) is more readily scavenged by particles, except possibly at low pH, and exhibits typical metal-like sorption characteristics. Anionic Cr(VI) is adsorbed less readily, with Fe oxide generally being its most important carrier phase.

Two recent studies of seasonally anoxic lakes provide the most detailed insights into Cr cycling in lake systems (Balistrieri et al. 1992a; Johnson et al. 1992b). Figure 8 shows the vertical profiles of Cr species determined by Johnson et al. (1992b) in Greifensee, Switzerland, during periods of mixing and advanced stratification. The Cr(VI) was the predominant dissolved species throughout the year, whereas dissolved Cr(III) was invariably undetectable, probably due to its efficient scavenging. The total "dissolved" Cr fraction (Cr filt in Fig. 8) was also measured following filtration, but

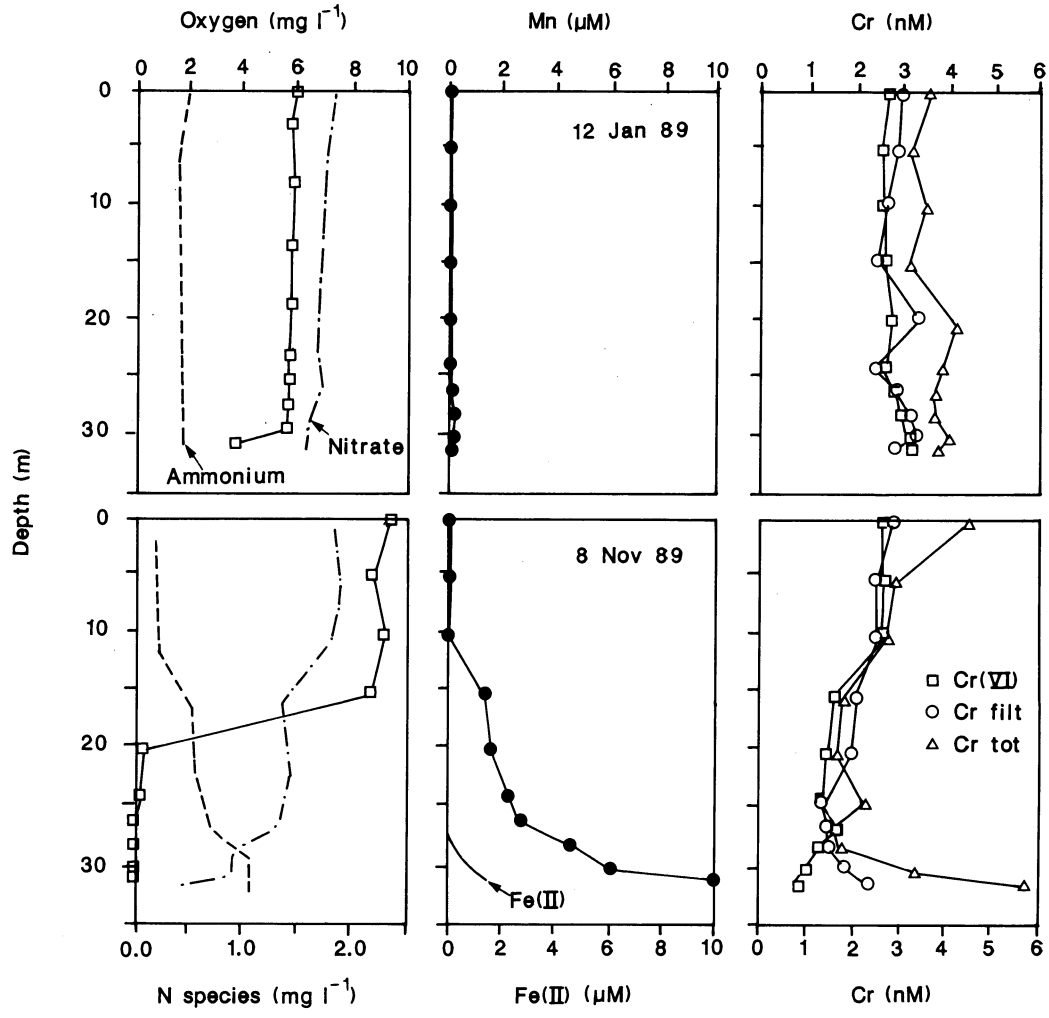


Fig. 8. Vertical profiles of Cr and other redox-sensitive species in the water column of Greifensee, Switzerland. Separate profiles are shown for dissolved *Cr(VI)*, total dissolved Cr(*Cr filt*) and total Cr(*Cr tot*); dissolved Cr(III) was invariably below detection. The *upper series* of profiles was observed during a period of complete mixing and the *lower series* at the height of hypolimnetic anoxia, during a period of stratification that lasted from May to early December. (Johnson et al. 1992b)

exceeded dissolved Cr(VI) only in strongly reducing bottom waters during stratification. This excess was attributed to the occurrence of colloidally bound Cr(III). Total Cr was measured by dilute acid extraction without prior filtration and indicated an increase in particulate (>0.45 μm) Cr above the sediment just before and during the release of Fe(II) and S(-II), possibly linked to the release of Cr(III) from the sediment as Fe oxides were reduced. It was only at the stage where Fe(II) and S(-II) began to accumulate in the hypolimnion that the increased colloidal and particulate Cr and decreased dissolved Cr(VI) concentrations provide any good indication of Cr(VI) reduction to Cr(III). Based on these associations and the results of a complementary laboratory experiment, Johnson et al. (1992b) concluded that Cr(VI) reduction in Greifensee is brought about primarily by reaction with S(-II) and Fe(II), and not with organic matter. However, even when anoxia was well developed in the lake and in the laboratory experiment, more Cr(VI) remained that would have been expected from previous findings on the effectiveness of S(-II) and Fe(II) as reductants (Rai et al. 1989; Saleh et al. 1989; Richard and Bourg 1991).

In addition to the above observations, dissolved Cr(VI) profiles in Greifensee exhibited systematic changes over the period of investigation that indicated its slow removal (i.e., scaveng-

ing) throughout the lake. This was modeled reasonably successfully by considering river inputs and outputs, vertical transport by eddy diffusion, and a first-order rate constant accounting for scavenging. Johnson et al. (1992b) concluded that the scavenging reaction may or may not involve a redox transformation. The fitted rate constant, 0.005 ± 0.002 day^{-1}, was found to be similar to equivalent constants derived from in situ mesocosm experiments in the Experimental Lakes Area (ELA) of northern Ontario, in which ^{51}Cr(VI) and ^{51}Cr(III) were separately used as tracers (Santschi 1988). In the ELA mesocosms the more particle-reactive Cr(III) was removed from solution more rapidly than Cr(VI) through scavenging by biogenic matter. However, the disappearance of both oxidation states from solution was greater than that predicted from laboratory-uptake experiments with surface sediments. Santschi (1988) suggested that the enhanced uptake of Cr(VI) may have been linked to its photoreduction by dissolved organic matter to the more particle-reactive Cr(III). Sigg et al. (1987) also concluded that biogenic material was important in the scavenging of Cr from Lake Zurich, based on a detailed series of sediment-trap data. The photochemical production of dissolved Cr(III) has recently been reported in surface lake waters, based on diurnal field observations of dissolved Cr redox species, light intensity and hydrogen peroxide concentrations, and on controlled photolysis experiments (Kaczynski and Kieber 1993). The authors recognized, however, that the method used for dissolved Cr(III) analysis is subject to interference from colloidal Cr.

In their study of Lake Sammamish, Washington, Balistrieri et al. (1992a) measured dissolved and particulate Cr, but not the two oxidation states. They concluded that Cr is lost seasonally from the bottom waters during the suboxic and anoxic phases, due to reduction of Cr(VI) to the more particle-reactive Cr(III), but did not invoke any general Cr scavenging mechanism. Their total dissolved Cr profiles, however, look very much like the dissolved Cr(VI) profiles seen in Greifensee, where Cr(VI) is more or less equivalent to total dissolved Cr, so that the same mechanisms may be operating in the two lakes.

The findings of Gunkel and Sztraka (1986) in two seasonally anoxic urban lakes are different from those described previously, in that greatly enhanced dissolved Cr concentrations were observed in anoxic bottom waters, attributed to the reductive remobilization of Fe oxides. The reasons for the different pattern of distribution of dissolved Cr in these lakes are unclear.

5.3 ^{239,240}Pu

Plutonium (Pu) is an interesting case study because there has been some disagreement in the literature as to whether Pu is remobilized from lake sediments during seasonal anoxia. In addition, the cited studies highlight some of the difficulties associated with understanding lacustrine trace element data and the usefulness of calculating inventories prior to data interpretation. Consideration of inventories has several advantages over the use of concentrations. These include being readily able to assess both the effect of basin shape on element budgets and the relative importance of a given transformation or flux (e.g., stream and atmospheric inputs and deposition rate) in terms of the overall budget.

The basic chemical characteristics of Pu in natural waters have been summarized by Allard and Rydberg (1983), Morse and Choppin (1986), and Choppin (1991). Plutonium can theoretically exist in aqueous solution in any of four oxidation states: III, IV, V, and VI. The standard redox potentials of the couples relating the latter three are within 0.10 V of each other, so that more than one oxidation state may coexist under oxic conditions. Plutonium (III) is only likely to be of any significance under anoxic conditions. The four oxidation states exhibit very different chemical behavior. Therefore, although a high particle affinity (i.e., K_d) is generally a feature of Pu, its biogeochemistry in lakes can be expected to show significant variation under changing redox conditions. Unfortunately, because of difficulties with analytical methodology and the low concentrations generally found, lake studies have often measured only total dissolved and particulate Pu concentrations. The limited available environmental data indicate that Pu(IV), mainly as hydrolysis products and humic complexes, and Pu(V), mainly as PuO_2^+, are generally the dominant oxidation states in most natural waters. Plutonium (IV) has the higher affinity for particles and is therefore generally the predominant bound form, but it is also more susceptible to complexation by dissolved ligands.

Alberts and Orlandini (1981) concluded that ^{239,240}Pu (hereafter referred to simply as Pu) was

not released from bottom sediments under anoxic conditions, based on laboratory experiments and field observations in a seasonally anoxic lake, Par Pond, located in the Savannah River Site in South Carolina, USA. Shortly afterwards, Sholkovitz et al. (1982) published comparable results from another seasonally anoxic lake, Gull Pond, and reported five times higher fallout Pu concentrations in the anoxic hypolimnion compared with overlying water. Similar observed profiles of stable Fe and ^{55}Fe (also from fallout) led the authors to conclude that, similar to Fe, the excess Pu was derived from sediment release under anoxia, although the exact mechanism was not defined.

Both groups of workers carried out further work in an attempt to resolve the issue. Sholkovitz and coworkers (Buesseler et al. 1985) measured two dissolved Pu profiles in the pore waters of Gull Pond during the period of hypolimnetic anoxia in 1982, incidentally the first such profiles to be determined anywhere. The results were inconclusive, although some evidence of Pu release from the sediments was obtained. The two (June and August) profiles obtained were quite different in character, reflecting the dynamic nature of Pu diagenesis, and showed general similarities with the pore-water Fe and Mn profiles, suggesting a possible link (Buesseler et al. 1985). The estimated diffusive flux of Pu into the overlying waters was, however, insignificant compared with the sediment inventory, and was insufficient to explain the hypolimnetic enrichment seen the previous year (reported in Sholkovitz et al. 1982).

Alberts and coworkers focused their attention on another lake on the Savannah River Site: Pond B, a warm monomictic reservoir affected by local nuclear reactor and processing activities (Alberts et al. 1986; Pinder et al. 1992). Dissolved and particulate water-column concentrations were determined at several depths and time intervals varying from monthly to quarterly between 1983 and 1986. The data revealed coherent patterns of behavior repeated annually. The concentrations were converted to total Pu inventories for (1) the whole water column, (2) the 0- to 6-m layer (equivalent to the oxic zone during summer stratification), and (3) the >6-m layer (the anoxic zone during stratification; Fig. 9). For surface waters the total Pu inventory increased following overturn in November to a maximum in March, followed by a decline until late summer when minimum inventories occurred. For deeper

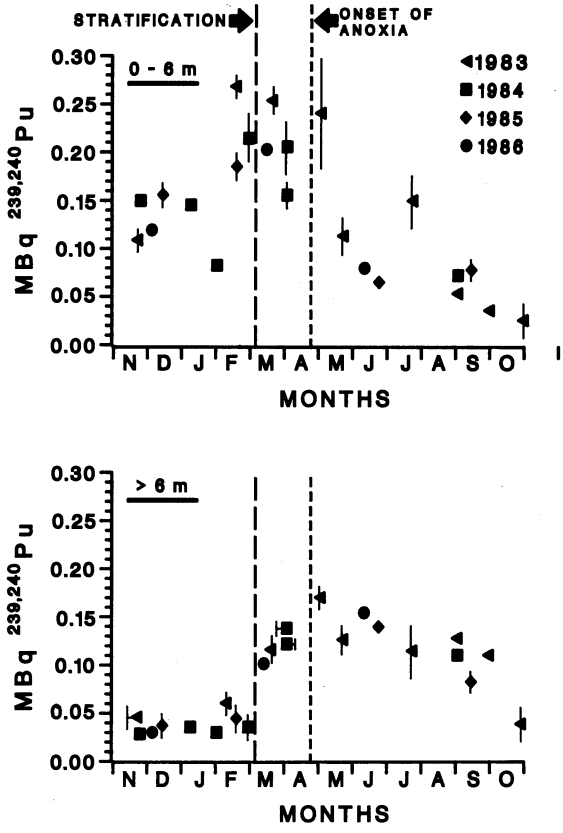


Fig. 9. Inventories of total $^{239,240}Pu$ in the 0–6 m and >6-m-deep sections of the water column in Pond B, a warm monomictic reservoir in the Savannah River Site, South Carolina. Data are plotted from 1 November, the normal time of autumn overturn, and the vertical lines demark the usual dates for the development of stratification (10 March) and the onset of seasonal hypolimnetic anoxia (15 April). (Pinder et al. 1992)

waters the inventory changed little from overturn to stratification, but then increased rapidly to reach a maximum in April and early May, after which the inventory decreased slightly but remained relatively high until turnover. The inventory for the whole water column was similar to that in the 0- to 6-m layer, reaching a maximum around April. The ^{238}Pu : $^{239,240}Pu$ ratios indicated that the cycle involved mainly Pu from sediment sources with little influence from atmospheric sources. Although Pu, Fe, and Mn all showed relatively high concentrations in the seasonally anoxic deep waters, the behavior of Pu was part of a complex cycle that was unrelated to those of Fe and Mn. Alberts and coworkers concluded that (a) the elevated hypolimnetic concentrations during stratification were derived in part from settling of particulate material from the epilimnion

(there was actually a decrease in the total water-column inventory during this period) and (b) the main remobilization of Pu from sediments occurred during well-mixed, fully oxic conditions over the winter period (Alberts et al. 1986; Pinder et al. 1992). This remobilization episode was tentatively linked to sediment resuspension. However, the detailed processes affecting Pu cycling in seasonally anoxic lakes remain obscure.

Other studies have provided information on specific aspects of Pu behavior in lakes (e.g., Orlandini et al. 1990). Complexation by inorganic (especially carbonate) and organic ligands (humic substances) appears to play a particularly important role. The exceptionally high Pu concentrations in the water column of Mono Lake (salinity 90‰; pH ~9.7), relative to those in the sediment (~50% of the Pu inventory remains in the water column), have been attributed to carbonate complexation (Anderson et al. 1982; Simpson et al. 1982). Plutonium in the water column of Mono Lake appears to be predominantly in the IV oxidation state (Nelson et al. 1989), providing an exception to the rule about the high sediment affinity of Pu(IV), and demonstrating that under some conditions the distribution of Pu(IV) is dominated by enhanced solution complexation. Field measurements and laboratory experiments in a variety of aquatic media, including lake waters (e.g., Nelson et al. 1987), have shown that the sediment–solution partitioning of Pu is also affected greatly by the concentration of dissolved or more correctly colloidal humic substances, due to Pu(IV)-humic binding. Further evidence comes from a study of Soap Lake in Washington State (Sanchez et al. 1986). This is another high-salinity alkaline lake, but in contrast to the situation in Mono Lake (Simpson et al. 1982), the vertical profiles of Pu show a clear relation with the O_2-H_2S interface (Fig. 10). The interfacial minimum was attributed to scavenging by Fe oxides and the greatly enhanced concentrations in the permanently anoxic monimolimnion to complexation by carbonate ions and dissolved organic matter. It is this increased complexation capacity, resulting from the long residence time of the bottom waters and other essentially hydrological factors, that is the key to the Pu enhancement in this situation. It is important to remember, however, that the alkalinity, pH, and dissolved organic-carbon concentrations in Soap Lake (Fig. 10) are far greater than would normally be expected. In the pore-water study of Gull Pond cited previously (Buesseler et al. 1985), Pu concentrations showed no correlation with either dissolved organic carbon (max. $15\,mg\,kg^{-1}$) or alkalinity (max. $0.75\,meq\,l^{-1}$).

Plutonium can generally be regarded as an immobile element relative to its sediment inventory except under extreme conditions such as those that exist in saline lakes. Crusius and Anderson (1994) have undertaken a detailed comparison of the mobilities of ^{137}Cs, $^{239,240}Pu$ and ^{210}Pb within sediments for a range of lake types including seasonally anoxic and meromictic water bodies. Although there was some evidence of Pu migration, it was so slight that they recommended the use of $^{239,240}Pu$ as a reliable dating tool for paleolimnological studies, in preference to the more commonly used ^{137}Cs (see Sect. 6.1).

5.4 Selenium

Selenium (Se) has a complicated redox chemistry, closely related to that of S, and is biologically both an essential and a toxic element. The following summary of its main biogeochemical characteristics is taken from several sources (chiefly Cooke and Bruland 1987; Weres et al. 1989; Masscheleyn et al. 1991). In natural waters it can occur in four oxidation states: selenate (VI), selenite (IV), elemental Se (0), and selenide (-II), and as a variety of organic and inorganic compounds. Chemical equilibrium is rarely achieved with regard to the various oxidation states. Selenate should thermodynamically predominate in well-oxygenated surface waters, but this is frequently not the case. Most of the transformations of Se appear to be microbially mediated and its methylation is of both biological and environmental significance. Selenate has a low adsorption affinity for common inorganic solids, and therefore tends to exhibit high mobility. Selenite is more strongly adsorbed, especially by Fe and Mn oxides. The Fe oxide has the greater affinity for selenite and adsorption increases with decreasing pH (Balistrieri and Chao 1990), as expected for an oxyanion. The Se(0) occurs as elemental Se, which is stable over a wide Eh–pH range, and as formally zero-valent atoms in various inorganic and organic compounds and species. Elemental Se is relatively insoluble, but may occur in colloidal form. Selenide occurs most

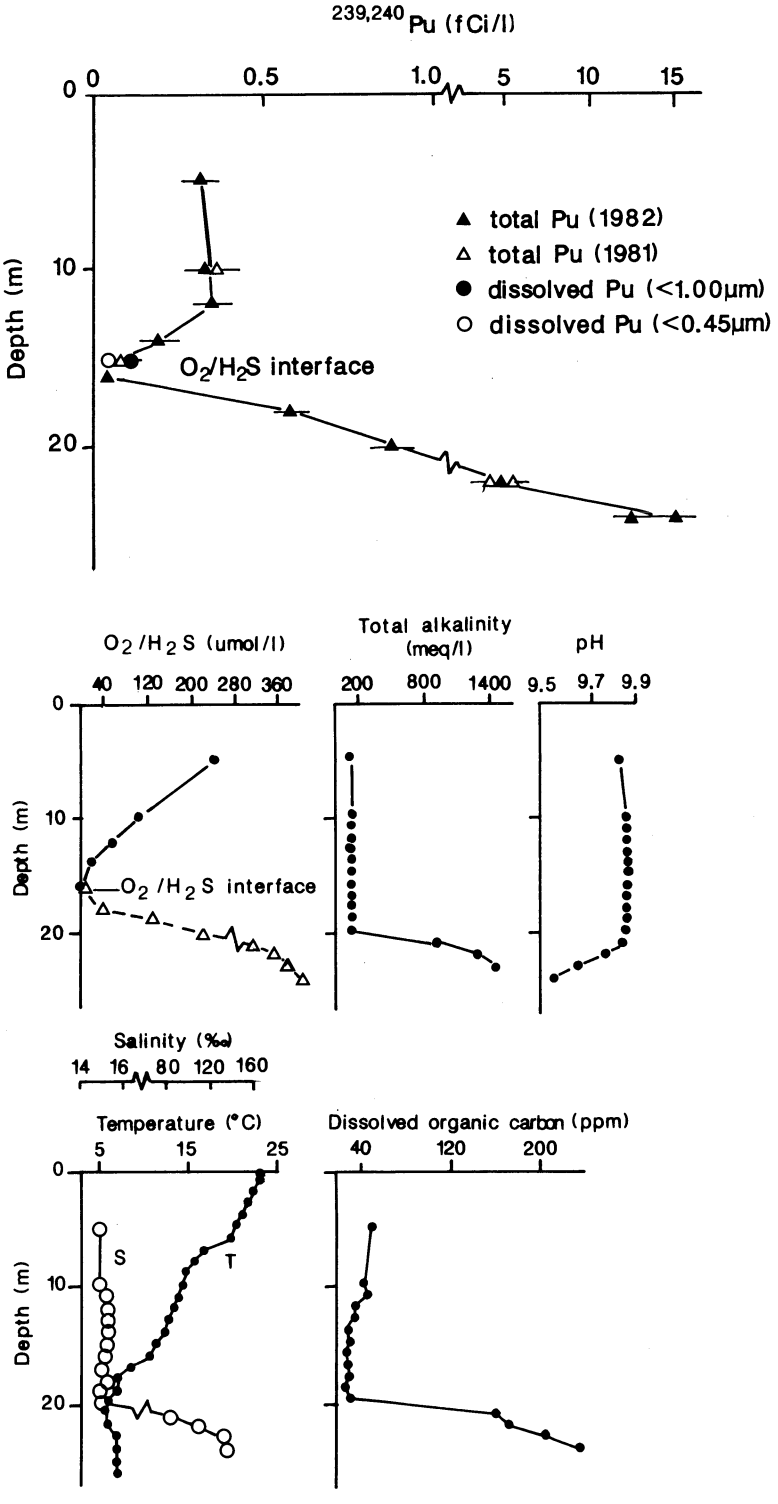


Fig. 10. Vertical profiles of fallout ^{239,240}Pu concentrations and ancillary data in the water column of Soap Lake, Washington State, a saline meromictic lake with permanent deep-water anoxia. (Sanchez et al. 1986)

importantly in various organic forms including seleno amino acids in biota and volatile alkyl species. Selenide also forms insoluble metal selenides, substitutes for sulfide in metal sulfides and dissolved polysulfides, and also forms gaseous hydrogen selenide. Se(0) and Se(-II) are generally not differentiated in existing operational analytical schemes (e.g., Cutter 1991).

Our knowledge of Se behavior in lakes has been advanced substantially by studies of two

American lake systems: (a) a series of reservoirs, some receiving leachates from coal-fired power stations and consequently exhibiting relatively high Se concentrations in waters and sediments (Cutter 1991), and (b) Kesterson Reservoir, a series of ponds that in the past have received drainage waters affected by the weathering of Se-rich marine shales (Cooke and Bruland 1987; Weres et al. 1989). The study by Cutter (1991) provides the most comprehensive lake data, and will be used as the basis for the discussion that follows.

The biogeochemical cycle of Se in lakes, proposed by Cutter (1991), is shown in Fig. 11. The speciation of Se in the inputs varied according to source. Dissolved selenite dominance was associated with coal ash leachates, whereas Se(-II, 0) was the main dissolved form in normal stream inputs. The Se within the reservoirs exhibited a very dynamic cycle, showing seasonally-based, non-steady-state behavior. Scavenging of dissolved Se took place mainly in the epilimnion and was maximal during the summer months, due to uptake by algae. Selenite appeared to be preferentially taken up, and, once incorporated into the algae, was converted to Se(-II). These findings are consistent with Se behavior observed in lacustrine mesocosm experiments and in the oceans (e.g., Santschi 1988). Rapid regeneration ($k = 0.05\ d^{-1}$) of dissolved Se from the algae in the reservoirs was also demonstrated through a series of laboratory experiments (Cutter 1991). The Se(-II, 0) was the predominant species released mainly as dissolved organic selenide. The production and volatilization of dimethyl selenide was tentatively identified as another important removal process in surface waters, based on its detection together with precursor compounds when total Se concentrations were highest. This conclusion is supported by measurements of Se speciation in a range of other surface freshwaters including Kesterson Reservoir (Cook and Bruland 1987).

In the hypolimnia of the various reservoirs regeneration of dissolved Se from decomposing algae was probably an important process. The most dramatic observed effects, however, were greatly decreased dissolved selenite and selenate

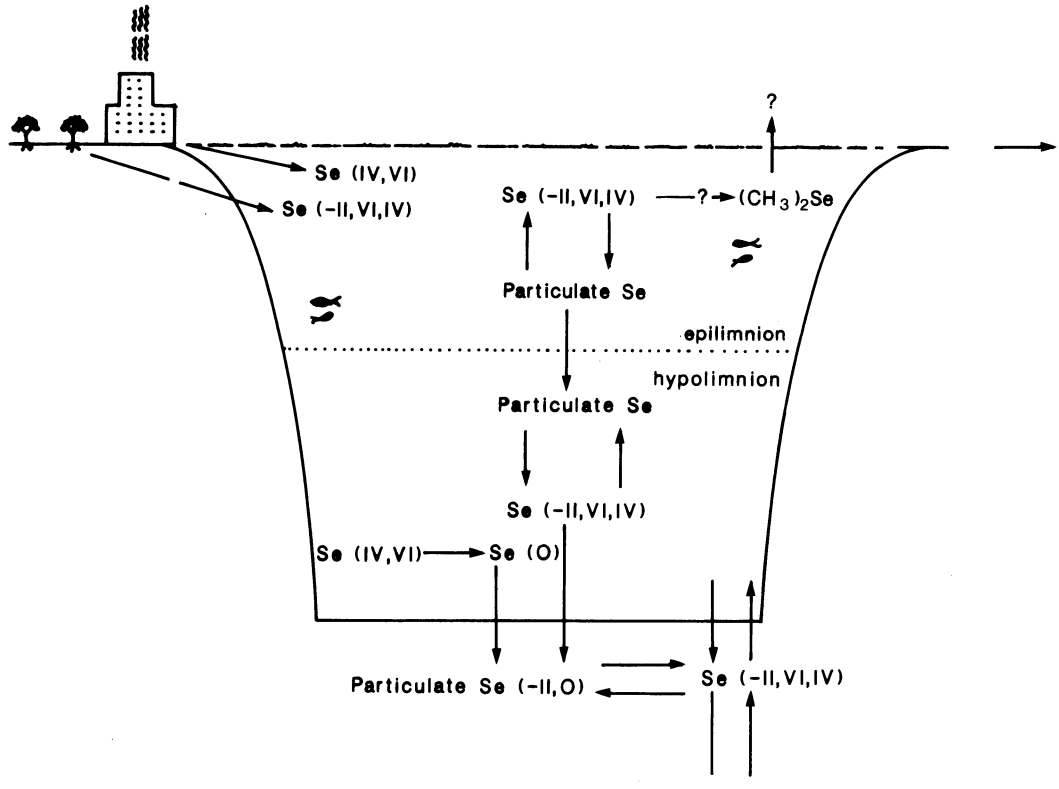


Fig. 11. Biogeochemical cycle of selenium in lakes, proposed by Cutter (1991). Oxidation states of dissolved Se are given in order of decreasing concentration and a description of the pathways is given in the text

concentrations, and increased concentrations of particulate elemental Se during periods of hypolimnetic anoxia. These observation were interpreted as being the result of the in situ reduction of the oxidized species to elemental Se. This transformation, which probably also occurred in the sediments, was thought to be responsible for the observed speciation of sedimentary Se. In the sediments Se was present mainly in a reduced oxidation state, the exact form depending on the redox conditions. Organic selenides dominated in sediments where the hypolimnia remained oxic, whereas elemental Se dominated where hypolimnetic anoxia developed. The conversion to elemental Se under anoxia represented an efficient removal mechanism from the water column, resulting in a lower mobility of sediment-bound Se. Independent laboratory experiments, using sediment from one of the contaminated reservoirs, also indicated that Se solubility was lower under reducing conditions and this was attributed to the formation of elemental Se and/or metal selenides (Masscheleyn et al. 1991). Pore-water data in the reservoir sediments were complicated and provided evidence that Se was diagenetically mobile, and that Se diffused out of or into the sediments depending on oxidation state and local conditions. Somewhat surprisingly, given the above solubility characteristics, there appeared to be a net diffusion of Se out of the sediments during hypolimnetic anoxia. The same behavior was also observed on a small scale in whole-lake radiotracer experiments in the Experimental Lakes Area of northwest Ontario (Hesslein 1987).

Laboratory experiments with lake sediments have been focused on redox transformations, sorption, solubility, and microbial effects including biomethylation, and have confirmed the diverse and complex dynamic behavior of Se (Lipinski et al. 1986, 1987; Oremland et al. 1989; Masscheleyn et al. 1991). It is clear that much remains to be discovered about Se cycling in lakes, particularly with regard to the processes operating in the highly dynamic region around the sediment–water interface. Most Se studies to date have been undertaken on heavily polluted systems, so the question of whether the same processes dominate in lakes with only background Se concentrations needs to be addressed. It is possible that associated differences in dissolved Se speciation may result in somewhat different biogeochemical pathways.

6 Pathways Involving Redox Reactions Indirectly: Case Studies

6.1 ^{137}Cs

In his earlier overview of the redox cycling of elements in lakes, Sholkovitz (1985) provided evidence to suggest that ^{137}Cs exhibits substantial redox-related mobility. He cited the ^{137}Cs enrichments observed in the anoxic hypolimnion of Par Pond (Alberts et al. 1979; Evans et al. 1983) and a number of paleolimnological studies where the ^{137}Cs profile was not entirely consistent with the bomb-fallout record, suggesting postdepositional mobilization. Subsequent work has largely confirmed the mobility of ^{137}Cs and provided support for the mechanism first suggested by Evans et al. (1983). This involves the "ion exchange" of $^{137}Cs^+$ with NH_4^+, produced by the anerobic degradation of organic matter, at various surface and interlayer sites associated with illite and other micaceous minerals. Three types of exchange site were proposed: nonselective surface sites, edge or wedge sites associated with micaceous minerals where cations are selectively bound, and interlayer sites in the micaceous minerals where cations are not readily exchanged. The observed selectivity sequence for the edge and interlayer sites was $NH_4^+ > H^+ > Cs^+ > K^+ > Ca^{2+} > Na^+ = Mg^{2+} > Mn^{2+} = Fe^{2+}$.

Recent work has included a sediment and pore-water study of a well-mixed, permanently oxic Dutch lake with anoxic sediments (Comans et al. 1989). The pore-water concentrations of dissolved ^{137}Cs were 1.5 to 2 times those in the overlying waters, indicating a diffusive flux from the sediments. In addition, the observed distribution coefficient (K_d) for ^{137}Cs showed a linear inverse relationship with the NH_4^+ concentration, which increased with depth, providing support for the proposed ion-exchange mechanism. Cremers et al. (1988) measured ^{137}Cs adsorption isotherms for a range of well-characterized soils and derived information on the concentration and selectivity (with regard to K^+) of the various exchange sites. Other experimental studies have focused more on the kinetics of the sorption mechanism. Pardue et al. (1989) performed sorption experiments and subsequent selective extractions with lake-sediment suspensions under controlled redox conditions over periods of days (up to 170). They were able to interpret their results in terms of the

same three types of exchange sites as suggested by Evans et al. (1983). The results highlighted the complex dynamic interactions that take place between the various types of exchange sites, such that the observed sorption behavior was a function of both the overall solution composition (e.g., concentrations of various competing cations) and the time frame of interest. Again NH_4^+ displaced $^{137}Cs^+$ most effectively followed by K^+, but NH_4^+-extractable ^{137}Cs decreased linearly with time over 160 days, due to "irreversible" fixation at interlayer sites. This slow fixation of ^{137}Cs by micaceous minerals has been reported by many groups, and Comans and Hockley (1992) have described ^{137}Cs sorption by illite using kinetic rather than equilibrium modeling. Their models reflect rapid reversible uptake onto surface and edge sites, followed by slower migration to interlayer sites. The slow interlayer fixation was modeled as an irreversible first-order reaction with a rate constant of $0.004–0.03\,d^{-1}$, depending on model formulation and whether the illite was K- or Ca-saturated. The assumption of irreversibility was not rigorously tested, however, and indeed the authors themselves cited evidence to suggest very slow release from the interlayer sites.

Although there is now widespread acceptance of a possible mechanism for ^{137}Cs remobilization under anoxia, direct field evidence of ^{137}Cs release from sediments is limited. Whole-lake radiotracer experiments showed no significant release of ^{137}Cs during seasonal hypolimnetic anoxia in two separate lake basins (Hesslein 1987). Furthermore, enhanced hypolimnetic concentrations of ^{137}Cs during anoxia should not in themselves be taken as evidence for release from bottom sediments. A study of the fate of Chernobyl-derived ^{137}Cs in Esthwaite Water showed an increase with time and depth of ^{137}Cs concentrations in the anoxic hypolimnion (Davison et al. 1993a). The increased hypolimnetic loading, equivalent to ~0.25% of the ^{137}Cs sediment inventory, was similar to that observed in Par Pond (0.3–0.7%), despite the fact that the clay mineral assemblages are dominated by illite and chlorite in Esthwaite and kaolinite in Par Pond (see Davison et al. 1993a and Evans et al. 1983). A series of laboratory experiments indicated that NH_4^+ and K^+ readily remobilized ^{137}Cs from suspensions of Esthwaite Water sediments (Davison et al. 1993b), in accordance with previous studies. In a series of undisturbed sediment incubations, however, under both oxic and anoxic conditions, ^{137}Cs release was minimal and insufficient to account for the increased hypolimnetic concentrations of Chernobyl ^{137}Cs previously observed during seasonal anoxia. This led Davison et al. (1993b) to suggest that these increased loadings were due to remobilization from sinking particles, rather than from sediment release.

An increasing number of studies have reported major inconsistencies between sediment profiles of ^{137}Cs and atmospheric deposition histories in lakes in North American, Europe, and Australia (Hamilton-Taylor et al. 1993). This has raised questions as to the validity of ^{137}Cs dating, at least under certain conditions. Explanations for the inconsistencies include sediment-mixing effects, changes in sedimentation rate, and delayed inputs from the catchment, as well as recycling of ^{137}Cs in the water column and redistribution of ^{137}Cs due to pore-water diffusion. In their comparative study of radionuclide mobilities in sediments over a range of lake types, including seasonally anoxic and meromictic water bodies with annual varved sediments, Crusius and Anderson (1994) observed that ^{137}Cs penetrated to depths up to 25 cm greater than both $^{239,240}Pu$ and the 1952 horizon when significant fallout began. Because the fallout histories of ^{137}Cs and $^{239,240}Pu$ are so similar, this was attributed to downward diffusion of ^{137}Cs in the pore waters, and not to sediment mixing. In addition, changes in the ^{137}Cs: $^{239,240}Pu$ ratio above their common 1963 fallout peaks suggested upward diffusion of ^{137}Cs from its maximum. Crucius and Anderson were able to exclude a number of possible causes such as reductive dissolution of Fe and Mn oxides and a change in mineralogy. They found that the deep downward penetration of ^{137}Cs, combined with a sharp ^{137}Cs concentration gradient below its peak, were best explained by the existence of two forms of ^{137}Cs in the sediments, namely a dominant nonexchangeable fraction with a high K_d and an exchangeable fraction with a low K_d. The similarity between these conclusions and the known ^{137}Cs binding properties of micaceous minerals, as described previously, is striking. Other factors contributing to the mobility of ^{137}Cs appear to include a high sediment porosity and a low micaceous minerals content (Crusius and Anderson 1993; Spezzano et al. 1993). A substantial body of evidence now clearly exists to suggest that, at least under anoxic conditions, ^{137}Cs can exhibit

significant mobility in lake sediments. Although the position of the 1963 fallout maximum may not be affected by associated pore-water diffusion, due to the relatively small fraction of ^{137}Cs in the pore water, ^{137}Cs dating should be applied with care and preferably only where supported by independent dating evidence.

6.2 Stable Pb, ^{210}Pb, and ^{210}Po

Lead (Pb) is regarded as an element that is very efficiently scavenged by most natural solids (e.g., oxides, sulfides, organic matter, and clay minerals), and subsequently exhibits little tendency to be remobilized. These characteristics are indeed fundamental to the widely used ^{210}Pb dating method for aquatic sediments. Some recent studies nevertheless have provided convincing evidence to suggest that Pb remobilization under anoxia can be significant (e.g., Benoit and Hemond 1990). These conflicting views are used as a focus for a discussion of Pb cycling in lakes. The behavior of ^{210}Po ($t_{1/2}$ = 138 d) is discussed at the same time, because it is the granddaughter of ^{210}Pb ($t_{1/2}$ = 22 y), and the two radionuclides are normally reported together.

Many studies have found little, if any, evidence for the upward release of Pb across the sediment–water interface, irrespective of the relative position of the O_2-H_2S boundary. These have included pore water, water column and benthic-chamber observations, comparisons of sediment trap and sedimentation rates, and various laboratory incubation experiments (e.g., Drake and Ackerly 1983; Hamilton-Taylor et al. 1984; Sakata 1985; Sigg 1985; Frevert 1987; Sigg et al. 1987; Morfett 1988a). Matisoff et al. (1980) referred to the existence of surface maxima of interstitial trace metals in their study of Lake Erie sediments, but the actual data presented show undetectable dissolved Pb values immediately above and below the sediment–water interface. In their study of Lake Superior sediments, which have an oxidized surface layer, McKee et al. (1989a,b) observed a subsurface maximum of dissolved Pb and concluded that Pb could be diffusing from the sediments to the overlying water. It is not clear, however, that this conclusion is justified, because again there appears to be no significant difference between the surface pore-water concentration and that in the water column 1 m above the sediment surface.

There is evidence that Pb is in fact scavenged more efficiently under anoxic than oxic conditions. This has led in some cases to the situation described in Sect. 4.4, where Pb diffuses downward across the sediment–water interface and accumulates in anoxic sediments, presumably due to sulfide precipitation. Figure 12 shows the pore water and overlying dissovled Pb concentrations at three locations in Anderson Lake, Manitoba, a disposal site for sulfide-rick mine tailings (Pedersen et al. 1993). Although the pH of the lake has been lowered from ~8 to ~7 by the disposal operations, the sediments are acting as a sink for Pb, rather than a source, at all locations with various degrees of contamination. Carignan and Nriagu (1985) reported pore-water Pb concentrations generally below the detection limit (5 nmol l^{-1}) in their study of lakes receiving greatly elevated atmospheric inputs of Pb, in the Sudbury region of Ontario, also suggesting efficient removal by anoxic sediments (see Sect. 4.4). Williams (1992) linked the accumulation of Mn, Co, Zn, Cu, and Pb near the sediment surface in Loch Ba to oxidative precipitation following the upward migration of metals from underlying anoxic sediment (see Fig. 1 and Sect. 3.2.1). In contrast to the other metals, however, the dissolved pore-water concentrations of Pb were maximal at the surface and undetectable below 1 cm of depth. The concentration (~10 nmol l^{-1}) in the overlying lake waters was the same as that in the uppermost pore waters, so that the dissolved Pb profile was similar to those shown in Fig. 12. Following the interpretation of Carignan and Nriagu (1985) and Pedersen et al. (1993), dissolved Pb was therefore diffusing into the sediment and then probably precipitating as a sulfide. This mechanism may have contributed to the surface maximum of total Pb in Loch Ba sediments (Fig. 1). There certainly appears to be no indication of leaching of Pb from the sediments under low pH conditions, as was suggested by Williams (1992).

A series of laboratory experiments simulating conditions in Lake Kinneret, Israel, indicated the efficient and rapid removal of Pb under anoxia, which was attributed to sulfide precipitation (Frevert 1987). Similar experiments with sediments and water from Esthwaite Water also showed efficient Pb removal under reducing conditions (Morfett 1988a).

There have been a number of comprehensive field-based studies of stable Pb and ^{210}Pb

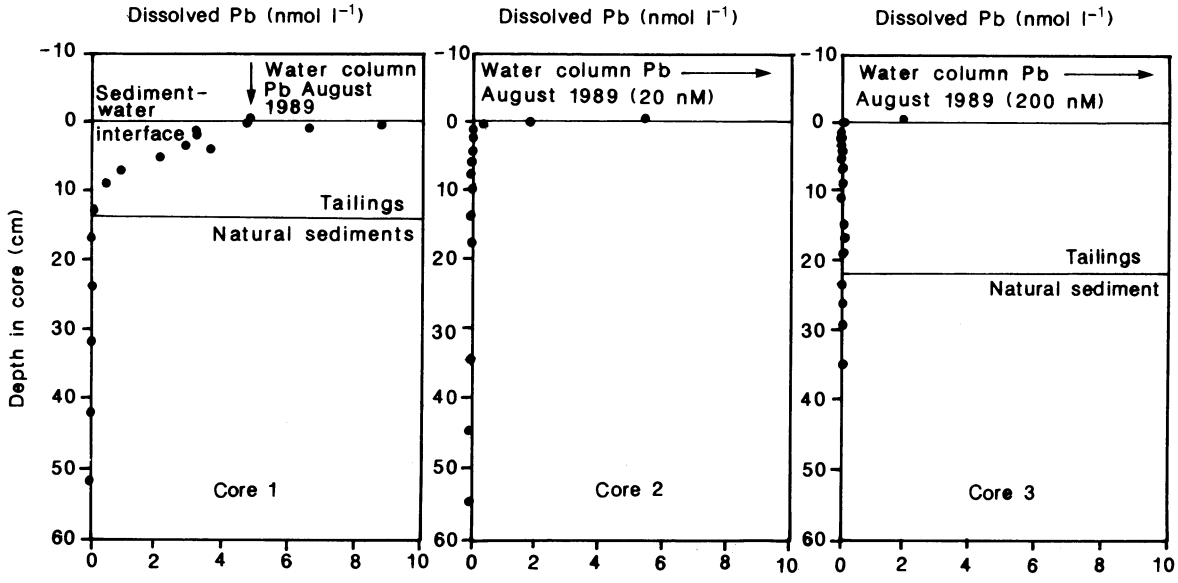


Fig. 12. Vertical profiles of dissolved Pb concentrations in the pore waters of anoxic sediments in Anderson Lake, a productive lake in Manitoba contaminated by sulfide-rich mine tailings. Cores 1 and 3 comprise a mixture of mine tailings and natural organic-rich sediment above ~15 and ~23 cm, respectively, and natural sediment below these depths. Core 2 comprises mainly mine tailings throughout. (Pedersen et al. 1993)

cycling in lakes, and these have demonstrated a surprisingly varied and complex dynamic behavior. White and Driscoll (1985) undertook seasonally based water-column and sediment-trap sampling in an acidic dimictic lake in the Adirondack region of New York State. The hypolimnion became substantially, but not totally, deoxygenated during both summer and winter stratification. A hypolimnetic enrichment of dissolved Pb during the late stages of summer stratification (Fig. 13) coincided with similar elevated concentrations of dissolved organic carbon, Fe, Mn, and Al. It was suggested that mineralization of organic matter coupled with the reductive remobilization of Fe and Mn oxides contributed to the release of Pb from the sediments to the water column. The most important controls on Pb concentrations in the lake, however, were thought to be hydrological factors together with associated pH variations and their effect on gibbsite solubility. The highest dissolved Pb, H^+, and Al concentrations in the lake were associated with elevated river concentrations during periods of high river flow (e.g., during spring snow-melt). The sedimentation of Pb correlated most strongly with that of Al and organic matter, and was greatest during the stratified periods when pH was at a maximum. Supported by thermodynamic calculations, White and Driscoll proposed that Pb was scavenged mainly by organic-rich Al oxide particles precipitated during periods of elevated pH.

Talbot and Andren (1984) measured the seasonal variations in dissolved and particulate ^{210}Pb and ^{210}Po in a noncalcareous (pH ~6) oligotrophic seepage lake (Crystal Lake), having no significant stream in- or outflows. Both radionuclides were rapidly removed from the water column (mean residence times = 0.095 year for ^{210}Pb and 0.26 year for ^{210}Po), although short-term removal rates fluctuated by up to one order of magnitude. The depositional fluxes of both radionuclides were associated with transient periods of high biological productivity, whereas ^{210}Pb was also rapidly removed during autumn overturn. Each period of transient ^{210}Po removal was followed immediately by partial recycling to the water column, attributed to rapid biological scavenging and subsequent release from decomposing organic matter following sedimentation. The redox status of the hypolimnion was not reported. The authors stated that the deep waters of the lake generally remain oxygenated, however, although a reduced zone may form near the sediment–water interface toward the end of stratification. Nevertheless, and in contrast to the behavior of ^{210}Po, ^{210}Pb did not appear to undergo any significant recycling from the sediments.

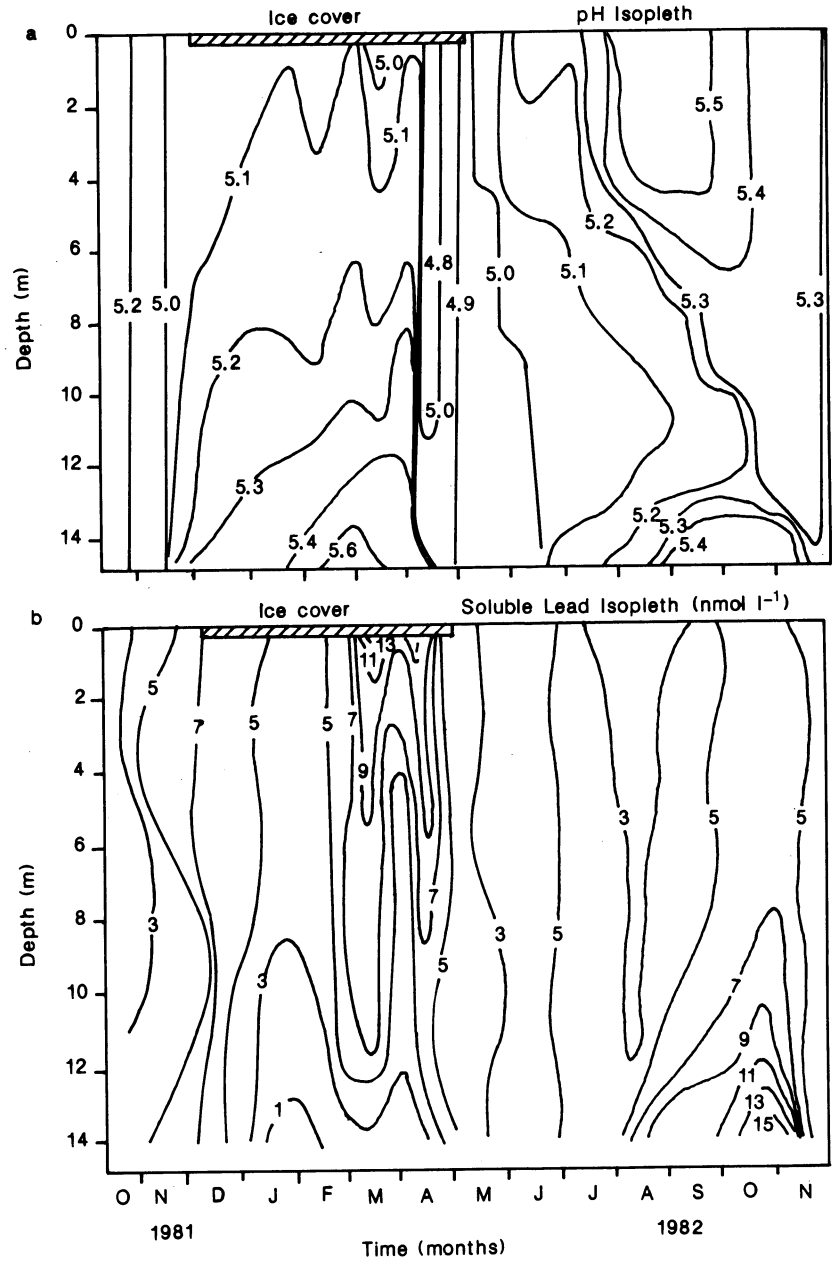


Fig. 13. Temporal and vertical variations in **a** pH and **b** dissolved Pb concentrations in the water column of Darts Lake, an acidic dimictic lake located in Adirondack State Park, New York. (White and Driscoll 1985)

Benoit and Hemond (1990, 1991) measured ^{210}Pb and ^{210}Po in sediment-trap material and in solution and solids of both water column and sediments of Bickford Reservoir, a soft-water dimictic lake in Massachusetts. The lake is seasonally anoxic with a pH ~6.5, approaching 7 in the anoxic hypolimnion. Removal of the radionuclides from the water column was dominated by particle scavenging, the rate of removal being about four times greater in the case of ^{210}Pb. This is similar to the relative difference in mean residence times (~×3) of the two radionuclides observed in Crystal Lake. The most striking feature of the distributions in Bickford Reservoir was the build-up in dissolved (<0.45 μm) and particulate concentrations in the hypolimnion during stratification. Total concentrations are shown in Fig. 14b,c. The sediment-trap data

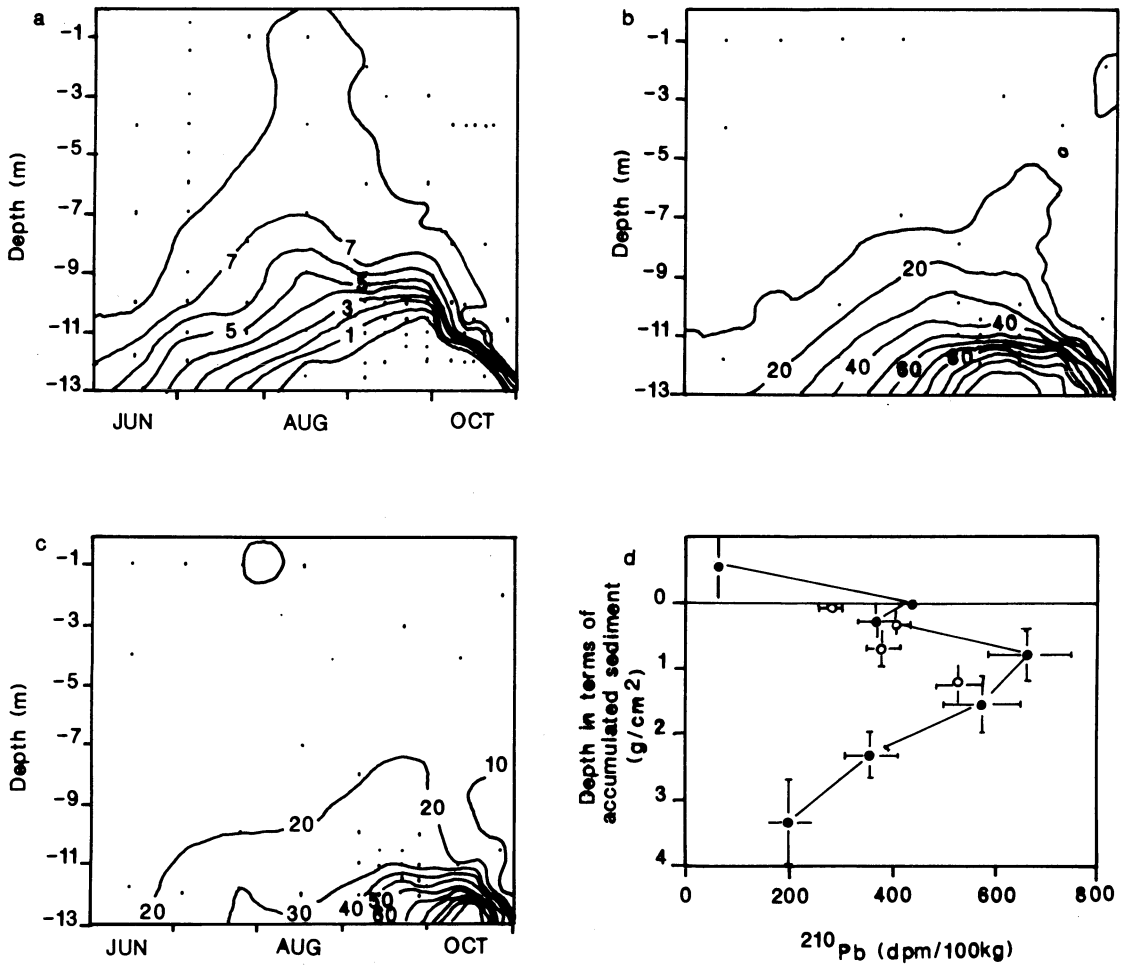


Fig. 14a–d. Distributions of ^{210}Pb and ^{210}Po concentrations in Bickford Reservoir, a seasonally anoxic dimictic lake in Massachusetts. Time-depth distributions in the water column during 1985 of **a** dissolved oxygen with contour intervals of 1 mg l^{-1}; **b** total ^{210}Po with contour intervals of 10 dpm 100 kg^{-1}; **c** total ^{210}Pb with contour intervals of 10 dpm 100 kg^{-1}; and **d** vertical profiles of dissolved ^{210}Pb in the sediment pore waters on 27 August 1985 (*open circles*) and 25 September 1985 (*filled circles*). (Benoit and Hemond 1990, 1991)

and mass-budget calculations indicated that these enrichments were due to release from bottom sediments, rather than from sedimenting particles. Pore-water profiles in August and September revealed a maximum ^{210}Pb concentration located 2–4 cm below the sediment–water interface (Fig. 14d). Pore-water concentrations of ^{210}Pb and ^{210}Po were between one and two orders of magnitude greater than in the overlying water column, confirming that diffusion from the sediments was occurring. Although similar, the hypolimnetic distributions of the two radionuclides showed some significant distinctions. The ^{210}Po was released to a greater extent during the earlier stages of stratification; thus concentrations exceeded those of ^{210}Pb by as much as a factor of 3.8 from mid-August to early September. The presence of such unsupported ^{210}Po is a strong indication of biogeochemical fractionation and remobilization, rather than of hypolimnetic enrichment due to sediment resuspension, which would have released more or less equal activities of the two radionuclides. The buildup of ^{210}Po was restricted predominantly to the period of true anoxia, beginning around mid-August, and in this regard most closely followed the distribution of Fe. Benoit and Hemond (1990) consequently suggested that the hypolimnetic distribution of ^{210}Pb was controlled by its sorption by Fe oxide combined with the classic redox cycling of Fe. Speciation calculations indicated that PbS was probably supersaturated in the anoxic hypolimnion, yet about half of the total ^{210}Pb invariably passed through a 0.45 μm filter. Several possible

explanations were given for this apparent anomaly including the occurrence of colloidal Pb sulfide, Pb binding to other colloidal material, and slow precipitation kinetics. It was justifiably concluded that, whatever the reason, there was clear evidence in the water column of enhanced ^{210}Pb mobility under the anoxic conditions observed. The ^{210}Po behavior was more difficult to understand. The closest temporal association occurred with the redox cycling of Mn, but the direct redox cycling of Po [i.e., Po(II)–Po(IV)] was also considered to be a possibility. The ^{210}Pb appeared to undergo significant remobilization and vertical migration within the sediments as well as between the sediments and the overlying water column. The ^{210}Pb profiles in the sediments were successfully reproduced by a model combining only sediment burial and pore-water diffusion. The model was in effect a feasibility study, however, because it ignored any possible contribution from sediment mixing and assumed that the ^{210}Pb profiles in the pore waters remained constant throughout the year. The fact that pore-water Fe profiles are known to vary greatly, as a function of the supply of organic matter and the mixing and redox conditions in the overlying water column (e.g., Hamilton-Taylor and Morris 1985), raises some doubt about the latter assumption. Benoit and Hemond (1991) concluded that large dating errors can result if diffusive redistribution of ^{210}Pb is neglected. With a ^{210}Pb partition coefficient (K_d) of ~1500, corresponding to the lowest observed K_d in the anoxic pore waters of Bickford Reservoir, Benoit and Hemond calculated that ^{210}Pb dating would be significantly affected by diffusion at sedimentation rates less than ~1 mm y^{-1}.

Stable Pb and ^{210}Pb have also been determined in Lake Sammamish, another seasonally anoxic lake situated near Seattle, Washington (L.S. Balistrieri, pers. comm.; see also Balistrieri et al. 1992a,b). The hypolimnetic inventories of Pb and ^{210}Pb in the lake were well correlated during summer stratification and increased significantly during the latter part of the oxic stage prior to summer anoxia. At this time both forms of Pb were associated mainly with particulate matter. Balistrieri and coworkers attribute these observations to remobilization from the sediment followed by particle scavenging. In contrast to the behavior observed in Bickford Reservoir, the hypolimnetic inventories of Pb and ^{210}Pb then decreased substantially during the anoxic phase. Thermodynamic calculations indicate that the loss of Pb from the water column could be due to the precipitation of PbS. Following overturn in the autumn, the inventories once more increased.

As a final comment in their study of Bickford Reservoir, Benoit and Hemond (1991) wrote that the examination of laminated lake sediments would help in evaluating the potential significance of chemical remobilization to ^{210}Pb dating. This is exactly what has been done by Crusius and Anderson (1993; see also Sects. 5.3 and 6.1) in their recent comparative study of radionuclide mobilities in a range of ELA lakes including seasonally anoxic and meromictic water bodies. They found that ^{210}Pb dating, ^{137}Cs and ^{239,240}Pu peak depths, and varve counts all yielded the same mass accumulation rates; that ^{210}Pb ages agreed with varve ages, and that there was no deep penetration of ^{210}Pb down the core compared with the ^{239,240}Pu profile. No evidence of ^{210}Pb mobility was therefore found in the sediments, in contrast to ^{137}Cs, which showed significant penetration to depths of up to 25 cm deeper than ^{239,240}Pu (see Sect. 6.1). Brunskill and Ludlam (1988) carried out a similar study in Fayetteville Green Lake, New York, a meromictic lake with an anoxic monimolimnion and deep-water sediments comprising annual varves with occasional turbidite layers. Once the variable mass deposition rate down the core was accounted for, there was excellent agreement between the observed ^{210}Pb profile and that predicted from the varve chronology. The predicted half-life for ^{210}Pb was 24 years, with 95% confidence limits of ±2 years, compared with its actual half-life of 22.3 years. The study thus provided a rigorous test of the ^{210}Pb dating method and indicated that there was no significant vertical movement of ^{210}Pb due to either pore-water diffusion or sediment mixing.

The previously mentioned studies provide varied and sometimes contradictory evidence concerning the effect of redox cycling on Pb mobility in lakes. A contributing factor may have been the reliability of some of the dissolved Pb data. Concentrations were close to and often below the limits of detection in some of the cited studies (e.g., Morfett 1988a). It is important that reported detection limits are based on field blanks, which are taken through the entire sampling and analytical protocol. Recent studies, using trace metal clean techniques of the sort developed for oceanographic work, have cast

doubt on much of the published dissolved trace metal data in the Great Lakes, including that on Pb (Nriagu et al. 1993). A selection of the published Pb data for lakes is shown in Table 2 for comparison. Several earlier data sets show coherent and geochemically consistent profiles, although the concentrations are generally higher than those measured using so-called clean techniques. Despite possible concerns over the earlier data, the validity of the general picture presented for Pb in this chapter is supported not only by the coherency of many of the data sets, but also by the fact that many of the conclusions are based on ^{210}Pb. Our understanding of the general behavior of Pb in lakes is currently inadequate to explain the apparent contradictions concerning Pb mobility in sediments and its accumulation or removal from anoxic hypolimnia. The question mark raised over the validity of ^{210}Pb dating (and ^{137}Cs dating; see Sect. 6.1) can be dealt with as a purely practical problem. The relative error in sedimentation rate due to pore-water diffusion is a function of K_d, mass accumulation rate, and porosity. The error increases with decreasing K_d and decreasing mass accumulation rates, and is maximal at a porosity of ~80%, decreasing sharply at higher porosities, especially at mass accumulation rates less than $\sim 0.02\,g\,cm^{-2}\,y^{-1}$ (Benoit and Hemond 1991; Crusius and Anderson 1993). The mass-accumulation rates were $\sim 0.01\,g\,cm^{-2}\,y^{-1}$ in the ELA lakes with high-fidelity sediment records of ^{210}Pb (Crucius and Anderson 1993) and $\sim 0.1\,g\,cm^{-2}\,y^{-1}$ in Bickford Reservoir, where ^{210}Pb dating was suspect (Benoit and Hemond 1991). Hence, the effect of mass accumulation rate seems to have been more than outweighed by a higher K_d ($>10^4$) and porosity (~98%) in the ELA lakes.

6.3 Zinc

As was noted in the Introduction to this chapter simple common patterns of dissolved trace element distribution are rarely seen in lakes, apparently due to their highly dynamic and varied character. This section seeks to demonstrate the variety of controlling factors and the resulting complex distributions of trace elements by reference to Zn, for which a substantial body of lacustrine data is now available. The coverage is meant to be illustrative rather than exhaustive, allowing some of the more coherent, and hence convincing, patterns of behavior to be selected for discussion.

6.3.1 Water-Column Behavior

Studies of suspended particles and their fluxes, determined from trap measurements, have indicated that algal uptake can contribute significantly to Zn removal from lakes (e.g., Baccini and Joller 1981; Sigg 1985; Sigg et al. 1987). Zinc and certain other trace metals in trap samples have often correlated well with carbon, nitrogen, and phosphorus, and this has led Sigg and coworkers to suggest that it may be valid to extend the Redfield stoichiometry describing algal composition to trace metals, e.g., $C_{113}N_{15}P_1Zn_{0.06}Cu_{0.008}Pb_{0.004}Cd_{0.00005}$ in Lake Constance (Sigg 1985) and $C_{97}N_{16}P_1Zn_{0.03}Cu_{0.006}$ in Lake Zurich (Sigg et al. 1987).

Although detailed data are limited, dissolved Zn tends to show varied depth- and time-dependent distributions in lakes that have been linked, for example, to particular circulation patterns (Santschi 1989) and to the seasonal variation in Zn input combined with biological removal (Morfett et al. 1988; Morfett 1988b). Murray (1987) suggested that there might be a limited time window in lakes suitable for observing a clear, biologically mediated relationship between dissolved metals and nutrients when other effects are minimal. He reported two such occurrences between Cd and phosphate in Lake Zurich and Lake Washington during summer stratification, when nutrients and metals were depleted in the epilimnia and enriched in the hypolimnia. The deep-water enhancement of Cd was greater in Lake Washington than in Lake Zurich, and continued through to late summer. Murray attributed the difference to the absence of any extensive Fe and Mn redox cycling in Lake Washington and thus any consequent secondary scavenging by recycled Fe and Mn oxides. Two studies have recently reported similar correlations involving Zn. In Windermere positive correlations were observed throughout the water column between dissolved Zn, phosphate, and silicate, and a negative correlation between dissolved Zn and chlorophyll *a* (Fig. 15), but only during the rapid growth phase of a spring diatom bloom (Reynolds and Hamilton-Taylor 1992). Two independent arguments supported the contention that the observed Zn-nutrient relations were in fact biologically mediated. The stoichiometry derived

Table 2. A comparison of dissolved Pb concentrations in lakes

Dissolved concentration[a] (mean or range in nmol l^{-1})	Sample type	Location	Comments	Reference
<0.2–9	Pore waters (sediments contain mine tailings)	Anderson Lake, Manitoba	Coherent profiles	Pedersen et al. (1993)
5–200	Water column			
<1–15	Water column	Darts Lake, N.Y.	Coherent distributions	White and Driscoll (1985)
0.1–0.4	Water column	Lake Constance	Coherent profiles	Sigg (1985)
0.3–1[b]	Water column	Lake Zurich		
<5–15	Pore waters	Clearwater Lake and McFarlane Lake, Ontario	Mostly below detection limit	Carignan and Nriagu (1985)
<0.6–25	Pore waters	Lake Erie		Matisoff et al. (1980)
5–30	Pore waters	Lake Superior	Reasonably coherent profile	McKee et al. (1989b)
3–10	Pore waters	T Reservoir, Japan		Sakata (1985)
12–28	Pore waters	Various lakes near Sudbury, Ontario		Tessier et al. (1985)
<3–13	Water column and pore waters	Esthwaite Water, UK	Almost all below detection	Morfett (1988a)
4–140	Water column and pore waters	Two urban lakes, Berlin		Gunkel and Sztraka (1986)
<1–10	Pore waters	Lake Ba, UK	Below detection except at sediment surface	Williams (1992)
<5	Water column	Bickford Reservoir, Massachusetts		Benoit and Hemond (1990)
0.11	Water column	Lake Sammamish, Washington	Trace metal clean techniques used	L.S. Balistrieri (pers. comm.)
0.02–0.10	Water column	Lake Ontario	Trace metal clean techniques used	Nriagu et al. (1993)

[a] Concentrations have been converted from original units where appropriate.
[b] Total metal concentration.

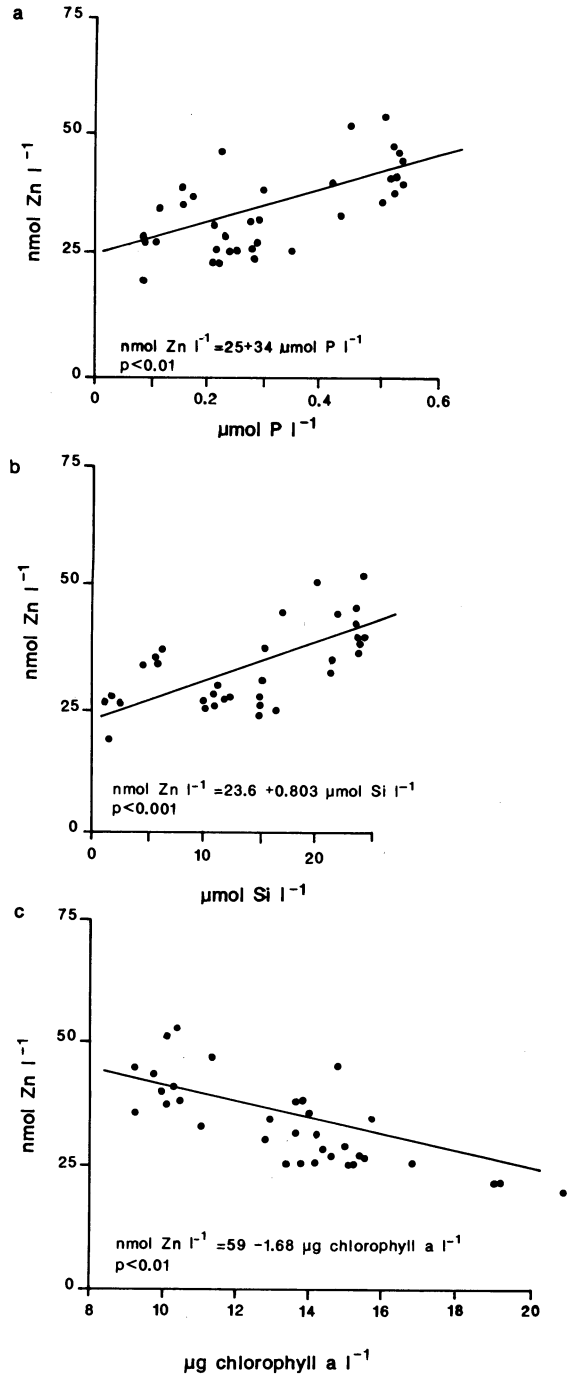


Fig. 15. Dissolved Zn against dissolved nutrients and chlorophyll *a* concentrations for all water depths during the period 2–30 April 1985 in Windermere, UK. (Reynolds and Hamilton-Taylor 1992)

from changes in dissolved concentrations was similar to that obtained from analysis of the standing crop, comprising mainly cells of the diatom *Asterionella*, and to that reported by Sigg for two Swiss lakes (Table 3). Secondly, mass-budget calculations for Windermere during the algal growth phase demonstrated that the loss of dissolved Zn from the water column was similar to the sum of increased Zn associated with the standing crop plus that sedimented out by algae, as measured previously by sediment trapping.

The other report of a significant Zn-nutrient correlation referred to Lake Sammamish, Washington (Balistrieri et al. 1992a). Acid-soluble Zn, which was mainly dissolved, increased with depth and time in the hypolimnion of the lake over the period of summer stratification, and in this respect correlated most closely with the reactive silicate distribution (Fig. 16). The silicate distribution in the lake was associated with the uptake and release of Si by the spring diatom bloom during thermal stratification (Balistrieri et al. 1992b). The Zn:Si atomic ratio in Lake Sammamish (6×10^{-5}) was lower than that in Windermere (8×10^{-4}) and Lake Constance (4×10^{-3}), but different values are not surprising given that the Si content of the standing crop will be highly dependent on its species composition. Perhaps of greater significance is that Zn correlated more strongly with silicate than with other nutrients in Lake Sammamish, as in Windermere and the oceans (Bruland 1980; Bruland and Franks 1983). Interestingly, the Zn–silicate relationship in Lake Sammamish was apparent, despite the intensive redox cycling of Fe and Mn that occurs in this seasonally anoxic lake (Balistrieri et al. 1992b). The distributions of Cd, Co, Cr, Cu, Ni, and Pb were in contrast all affected to various degrees by the cycling of Fe and Mn and the general redox conditions (Balistrieri et al. 1992a; L.S. Balistrieri, pers. comm.). The Cd distribution showed some similarity with that of phosphate in the early stages of stratification, but thereafter the relationship broke down, probably because of phosphate sorption onto Fe oxides and removal of Cd via sulfide precipitation (Balistrieri et al. 1992a).

These results provide some support for the concept of a limited time window for observing metal-nutrient relationships in lakes. In Windermere the Zn–silicate correlation was apparent only during the growth of the diatom bloom in April, whereas in Lake Sammamish the correlation was evident throughout the stratified period. Two differences between the lakes were in the timing of the bloom, relative to the onset of stratification, and in the general magnitude of silicate concentrations. In Lake Sammamish

Table 3. Zinc content of lake algae in terms of atomic ratios

Location	Method	C	P	Si	Zn	Source
Lake Constance	Sediment-trap material	113	1	14	0.06	Sigg (1985)
Lake Zurich	Sediment-trap material	97	1	–	0.03	Sigg et al. (1987)
Windermere	Standing crop analysis	106	1	–	0.04	Reynolds and
(UK)	Regression analysis of dissolved concentrations	–	1	42.4	0.034	Hamilton-Taylor (1992)

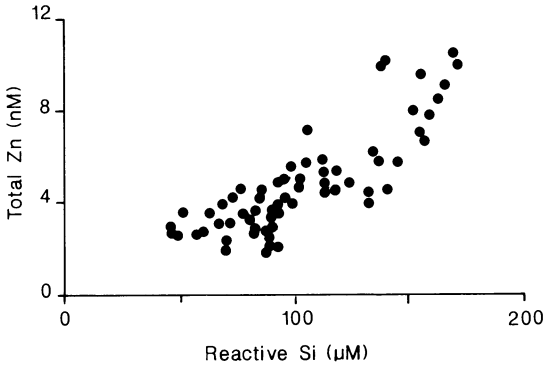


Fig. 16. Total acid-soluble Zn against reactive silicate concentrations for all water depths during the period April–October 1988 in Lake Sammamish, Washington. (Balistrieri et al. 1992a)

much of the growth phase took place in April after the onset of stratification, resulting in a decreasing silicate concentration with time in the epilimnion and relatively high levels in the hypolimnion, where there was no removal and some biogenic release. In Windermere growth of the bloom occurred prior to stratification, which did not begin until early May. Thus, dissolved silicate decreased throughout the water column during the main growth phase in April. The magnitude of the silicate concentrations and the differences in concentration between the epilimnion and hypolimnion were much greater in Lake Sammamish. The epilimnetic and hypolimnetic silicate concentrations differed by less than $5\,\mu mol\,l^{-1}$ in Windermere during May. Based on the observed water-column Zn:Si atomic ratio in Windermere (8×10^{-4}), this corresponds to a difference of approximately $4\,nmol\,l^{-1}$ of Zn. Because the summertime concentrations of Zn in Windermere are $\sim 40\,nmol\,l^{-1}$, it is not surprising that the correlation breaks down during this period when there is little active removal of Si. The Lake Sammamish and Windermere data thus provide compelling evidence to suggest that genuine biologically mediated Zn-nutrient relations can be observed in lakes, but do not represent the norm, because they are usually obscured by other processes. Furthermore, the concept of a universal Redfield stoichiometry for all lakes increasingly appears to be inappropriate. There is good evidence to suggest that even the basic C:N:P ratios of algal material vary widely in lakes as a result of differences in the rates of supply of elements and physical factors (Hecky et al. 1993).

There is no doubt that Fe and Mn oxides also act as carriers for Zn (see Sect. 3.2.1), but Fe and Mn cycling generally has little reported effect on dissolved Zn profiles in the water columns of lakes. Studies of a number of seasonally anoxic basins, including Esthwaite Water (Morfett et al. 1988; Morfett 1988b), Lake Zurich (Sigg et al. 1987), Lake Biel (Santschi 1989) and Lake Sammamish (Balistrieri et al. 1992a), and the permanently anoxic Lake Baldegg (Baccini and Joller 1981), found no changes in Zn concentration that showed any relation with Fe and Mn redox cycling or sulfide precipitation. In other words, there was no evidence for an increase in Zn mobility in the water column that could be linked to the reductive dissolution of Fe and Mn oxides, or of a reduction in Zn mobility, linked to the precipitation of a sulfide. These observations are supported by the results of a whole-lake radiotracer experiment, which showed minimal change in dissolved ^{65}Zn concentrations during anoxia, in contrast to a high degree of redissolution shown by ^{59}Fe, ^{60}Co, and ^{203}Hg (Hesslein 1987). The fact that dissolved Zn distributions appear unaffected by anoxia should not be taken as an indication of the absence of Zn sulphide (co)precipitation, any more than it indicates that Zn is not being transported by Fe and Mn oxides. To the contrary, in Esthwaite Water microprobe analysis of Fe sulfide particles sampled from the

anoxic hypolimnion showed them to be enriched in Zn (6000 ppm; Davision et al. 1992). Overall, however, the observations indicate that redox-related phenomena have a relatively small effect on the vertical distribution of dissolved Zn in lakes.

Some exceptions have been reported where Zn profiles are clearly affected by ambient redox conditions, although all of the cases cited below are unusual in some way. Landing et al. (1991) observed a coherent vertical profile showing a 2.5-fold enrichment in dissolved Zn in the anoxic waters of Jellyfish Lake, a stagnant saline (26–30‰) water body in Palau, Micronesia. It was suggested that the dissolved Zn concentration ($\sim 2.5\,nmol\,l^{-1}$) in the anoxic zone was controlled by the precipitation of a sulfide, but the reason for lower concentrations under oxic conditions was not discussed. In Lake Vanda, a meromictic, permanently anoxic lake in Antarctica, a dissolved Zn maximum was observed around the O_2-H_2S interface (Webster 1992). Based on similarities in the profiles of their dissolved concentrations, the behavior of Zn was linked to redox cycling of Mn oxide, but, in addition, decreased dissolved Zn concentrations at depth in the anoxic zone were attributed to sulfide precipitation. The upper depth limit of the Zn maximum coincided, however, with the top of the zone of enhanced salinity, so that the increase in Zn may have resulted from a number of other possible mechanisms including ion exchange with Ca^{2+} (see Sect. 3.2.1).

6.3.2 Sediment Behavior

A considerable fraction of the algal standing crop of most lakes is deposited at the sediment surface. Published work indicates that Zn in sediments is affected in very different ways by the degradation of this material and by Fe and Mn redox cycling and sulfide precipitation. Data from Esthwaite Water demonstrate how a combination of processes may influence the concentrations of dissolved Zn at the sediment–water interface. The temporal variations observed between 10 and 50 cm above the interface tended to follow those higher in the water column (Fig. 17a). Rather than correlating with any indicator of redox cycling, these variations appeared to be a function mainly of Zn inputs to the lake, via runoff and direct atmospheric deposition, and biological removal. The transient maxima immediately above the sediment surface during the summer (Fig. 17a) again did not correlate with any indicator of redox cycling (e.g., Fe and Mn distributions), but instead appeared to be associated with the sedimentation of algal material. Dissolved Cu showed coincident maxima and values of the associated dissolved Zn:Cu ratio were similar to that in algae. Another short-lived surface maximum occurred earlier the same year in late February–early March (Fig. 17b), but was different in character. It coincided with a rare period (25 Feb.–7 March, 1986) of complete ice cover on Esthwaite Water, during which considerably elevated interfacial concentrations of Zn, Fe, Mn, Cu, Pb, and Cd were observed together. The seasonal onset of enhanced reductive remobilization of Mn and Fe in Esthwaite Water sediments is normally triggered around the end of March by deposition of part of the spring diatom bloom (Hamilton-Taylor and Morris 1985). Morfett et al. (1988) attributed the February–March interfacial maxima in 1986 to the effects of reduced turbulence under ice cover leading to increased sedimentation of particles (e.g., oxides and organic material). The effects of the consequent enhanced remobilization were magnified by the reduced diffusive transport away from the sediment–water interface. An additional factor may have been that, due to the nature of the remobilization event under ice cover, sulfate reduction was not greatly enhanced, so that trace metal scavenging through sulfide precipitation was limited in the surface sediments. Nevertheless, throughout the year dissolved Zn was at a lower concentration in the pore waters than in the water column (Fig. 17), so that Zn always diffused downward either from the transient surface maxima or from the water column proper. The sediments were therefore acting as a sink for Zn, although the transient maxima must result in some rapid recycling into the water column. Although obscured in the detail of the vertical profiles (Fig. 17), there was a clear relationship between the interfacial concentrations of dissolved Zn and the redox conditions in the lake (Fig. 4). Interfacial concentrations were minimal during the period (25 June–10 October) of hypolimnetic anoxia. This observation, together with solubility considerations, led Morfett et al. (1988) to conclude that the removal of Zn in the sediments was due to its precipitation as a sulfide. The fact that Fe sulfide particles in Esthwaite Water

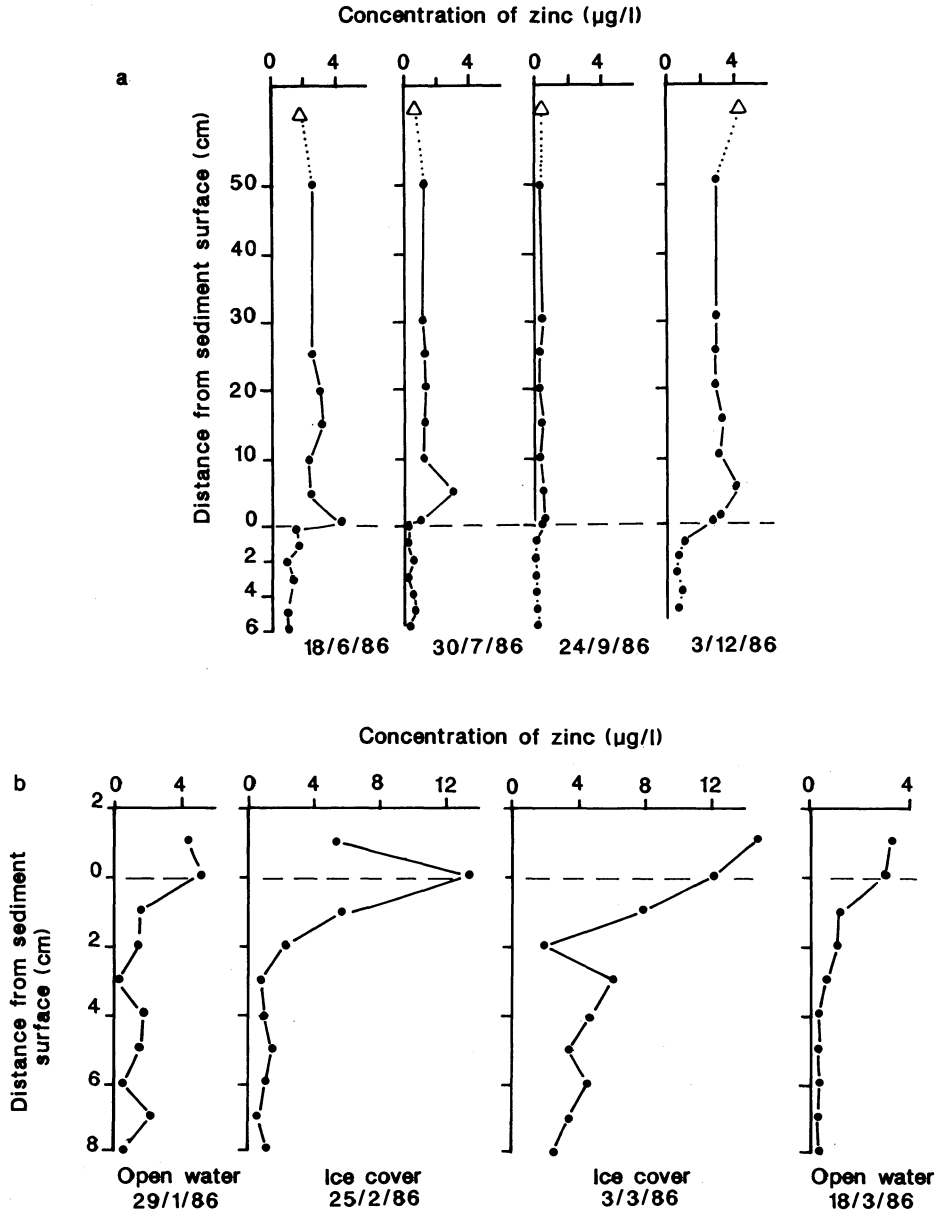


Fig. 17a,b. Vertical profiles of dissolved Zn concentrations in the sediment pore waters and overlying bottom lake waters in Esthwaite Water, a productive seasonally anoxic lake in the UK. **a** A sequence of profiles before (18 June), during (30 July and 24 September), and after (3 December) summer stratification: the mean dissolved Zn concentrations higher in the water column are shown as *open triangles*; **b** a sequence of profiles before, during, and immediately following complete ice cover. (Morfett et al. 1988)

are now known to be enriched in Zn (Davison et al. 1992) adds further weight to this conclusion.

Most other studies on the early diagenesis of Zn in lake sediments are based on cores collected on a single occasion. These results indicate that, as in the sediments of Esthwaite Water, a decreased mobility of Zn due to sulfide precipitation appears to be a dominant factor in lakes where the O_2-H_2S interface is either at the sediment–water interface (Pedersen et al. 1993) or at shallow depth in the sediments (Carignan and Tessier 1985; Tessier et al. 1989). The removal of Zn in this way creates a downward decreasing concentration gradient and results in the diffusive transport of Zn from the water column into the sediments. The same process affects other metals

also, and its occurrence and environmental significance are discussed in more detail in Section 4.4. Tessier et al. (1989) studied sediments with an oxic surface from a large number of oligotrophic lakes of varying pH and degrees of Zn contamination (Fig. 18). They found that downward diffusion of Zn occurred mainly in the more acid lakes (pH < 6). One highly acid lake (Lake Silver with a pH of 4) showed little, if any, change in dissolved Zn concentration across the sediment–water interface, nor any sulfate reduction through the depth sampled (5 cm), suggesting that sulfide precipitation at relatively shallow depth in the sediment is critical for significant removal of Zn in pore waters. In the lakes of pH > 6, the vertical concentration gradients across the sediment–water interface were generally much lower and varied in direction, i.e., downward decreasing, increasing, or no significant gradient (Tessier et al. 1989). These lesser gradients were often associated with localized maxima or minima below the sediment–water interface. Unlike

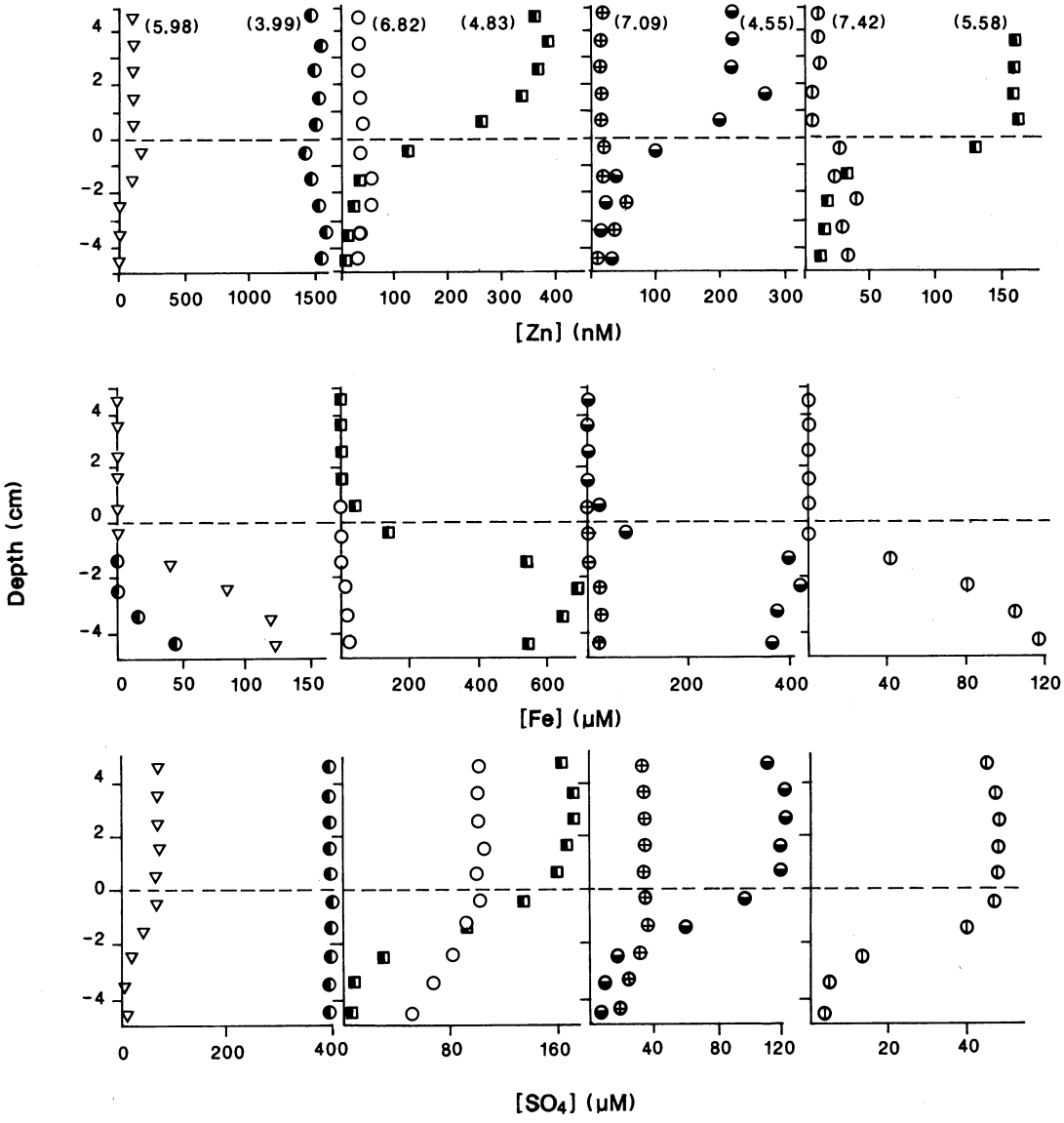


Fig. 18. Vertical profiles of dissolved Zn, Fe, and SO_4 concentrations across the sediment-water interface in lakes of various pH in Quebec and Ontario. *Different symbols* indicate different lakes with bottom lake water pH being shown in *parentheses* on the Zn plots. Lake Silver is shown in the *left-hand series* of profiles with a *circular symbol*. (Tessier et al. 1989)

Esthwaite Water, no dissolved Zn peaks resulting from decomposing algae were observed at the sediment–water interface. This may be linked to the transient nature of such peaks and the one-off sampling strategy used in the Canadian lakes, together with their lower biological productivity.

The Canadian studies also indicated that Zn binding by Fe oxides was of importance in the oxic surface sediments of the lakes surveyed. The dissolved Zn concentrations immediately above the sediment surface in the various lakes showed a strong inverse relationship with pH (Tessier et al. 1989). The associated pH dependency of Zn partitioning (i.e., K_d increased with pH) between these bottom waters and the Fe oxide fraction of the surface sediments agreed reasonably well with a simplified surface complexation model. The binding intensities derived from field data, however, were generally much greater than those obtained from laboratory experiments with Fe oxides. Although the relative importance and role of other sorbents (e.g., Mn oxide and organic matter) was not quantified, the results imply that sorption of Zn by Fe oxides in the sediments is at equilibrium and appears to influence the dissolved Zn concentrations in the lakes. A similar study of oxic lake sediments, also from the Canadian Shield, examined the sediment/pore-water partitioning (i.e., K_d) of Zn together with the speciation of the bound fraction (Young and Harvey 1992). With regard to total leachable Zn the K_d decreased by a factor of ~3 between pH 6.5 and 5.0, which is similar to the decrease observed by Tessier et al. (1989) for Fe oxide binding over the same pH range. The selective extraction of Zn, however, indicated that there was a marked change in the sediment speciation of Zn with pH. The Zn was bound mainly by Mn oxides in the circumneutral lakes, whereas Fe oxides and the organic fraction were relatively more important at low pH. Young and Harvey (1992) suggested that precipitation of Fe-humic compounds at low pH and the concurrent removal of Zn may have been a contributing factor.

There are two other points worth emphasizing concerning the work of Tessier and coworkers on Canadian Shield lakes. Firstly, the role of Fe oxides in the lake sediments was not reflected in the pore-water Zn profiles. Rather than showing enhanced dissolved concentrations at depth due to the reductive remobilization of Fe oxides, the dissolved Zn concentrations were in fact lowered by sulfide precipitation as discussed above (see the contrasting pore-water profiles of Zn and Fe in Fig. 18). The second point relates to the effect of pH and acidification on the behavior of Zn (see also Sect. 4.4). The increase in K_d with pH observed in the surface oxic sediments highlights the well-known pH dependency of Zn sorption. More generally, the sorption edge for Zn binding by natural particles appears to occur within the same pH range (pH 5–8) as that commonly found in lakes (e.g., Mouvet and Bourg 1983; Giusti et al. 1993). This characteristic is illustrated further by the results of an ELA mesocosm experiment, which showed that ^{65}Zn was released from the sediments back into the water column following acidification (Santschi et al. 1986). These findings are not consistent, however, with the studies of the Canadian lake sediments where the high water-column concentrations of dissolved Zn were clearly unrelated to any present-day release from the sediments, because it was the more acid lakes that showed the greatest diffusive fluxes into the sediments (Fig. 18).

An interesting comparison with the above lakes is provided by the Caribou subbasin of Lake Superior, where the Mn redox boundary is considerably deeper at ~12 cm in the sediment column (see Sect. 3.2.1 for a more detailed account). The Zn and organic carbon, but not Fe and Mn, were enhanced in a "fluff" layer at the sediment–water interface. McKee et al. (1989a,b) concluded that the decay of organic matter near the sediment surface releases Zn, which is then sorbed by Fe and Mn oxides.

Further down the core the active redox cycling of Mn, and to a lesser extent Fe, leads to locally elevated Fe and Mn oxide concentrations above their redox boundaries. There was no associated enrichment of total Zn, which McKee et al. (1989a) suggested was due to the lack of a significant source, the most labile organic matter having been degraded near the sediment surface. Furthermore, measurement of sediment speciation indicated that Zn was increasingly associated with sulfides at the expense of the oxide fraction with depth across the Fe and Mn redox boundaries. The Caribou subbasin is therefore similar to Esthwaite Water in that Zn appears to be released from decomposing organic material at or near the sediment–water interface. The position of the redox boundary means, however, that the remobilized Zn is initially scavenged by sedimentary oxides rather than a sulfide.

There is at least one data set that provides

evidence of Zn recycling in association with Fe and Mn. The pore-water and sediment profiles of Zn in Loch Ba, Scotland (Fig. 1), were interpreted as indicating that Zn is released at depth through the reductive dissolution of Mn and probably Fe oxides (Williams 1992). It then diffuses upward to be scavenged once more by the oxides, precipitating above the appropriate redox boundaries. This interpretation was further supported by the results of a sequential extraction procedure, which showed an increase in the adsorbed and hydrous oxide fractions of Zn above the redox boundary. Williams recognized, however, that the increased anthropogenic supply of metals to the lake may have contributed to the maximum in the total Zn concentration at the sediment surface. The recycling of Zn in this way could be readily understood if oxide dissolution at depth was not accompanied by sulfate reduction, but this does not appear to have been the case. Williams reported that the main gradient in redox potential occurred between depths of 2 and 3 cm, and suggested that sulfides were forming below 3 cm. The oxidizable Zn fraction in fact increased significantly below the redox boundary, suggesting that a sulfide may have been forming, so that it is not clear why the dissolved Zn profile was downward increasing, in contrast to the studies described previously. An earlier pore-water study of Lake Erie sediments also indicated that relatively enhanced dissolved Zn concentrations can occur under reducing conditions, although it was again suggested that Zn was being precipitated as a sulfide (Matisoff et al. 1980).

The direction of diffusive transport through the redox boundary is dependent on the relative concentrations and consequently conditions above and below the boundary. There are many possible factors that might have an important influence on the relative concentrations. For example, pH affects metal sorption by oxides above the boundary and sulfide precipitation below the boundary. It is a feature of freshwater lake systems that dissolved sulfide concentrations in anoxic sediments are low and frequently undetectable (e.g., Matisoff et al. 1980; Carignan and Nriagu 1985; Benoit and Hemond 1991). This is not simply because of low sulfate concentrations compared, for instance, to sea water, but generally because the sulfide concentration is controlled by the precipitation of Fe sulfide, and dissolved Fe^{2+} concentrations usually far exceed those of sulfide (e.g., by more than three orders of magnitude (Carignan and Nriagu 1985; see also Davison 1993).

7 Summary and Conclusions

The evidence presented in this overview confirms the diverse behavior of trace elements in lakes under the influence of a spatially or temporally variable redox potential. Given the dynamics of the systems, it is not at all surprising that the sorts of universal trace element profiles seen in the oceans are not generally apparent in lakes, which typically have water-residence times of ~1 year. The diversity appears to be linked to the dynamic character of many of the controlling processes, especially in the vicinity of the sediment–water interface. Furthermore, conditions in many lakes vary significantly during the course of a year on a variety of time scales, so that non-steady-state conditions are commonplace. Important variables include seasonal effects, such as mixing characteristics, biological productivity, and the supply of elements from external sources, and more transient events such as flood discharges and the sedimentation of algal blooms. Seasonal and other short-term variations in input are far more important than in oceans, and may dominate trace element distributions, due in part to the much shorter trace element residence times in lakes (commonly <1 year). Localized transient events at the sediment–water interface appear to be important features of trace element cycling in lakes, and are worthy of more detailed study.

The physical characteristics, such as size and water-residence time, of the world's largest lakes are intermediate between those in more typical lakes and those in oceans. It may be expected that the largest lakes would be the most likely to show ocean-like trace element profiles, although presently there is little or no data to support this suggestion. Lake Baikal is the world's deepest (1632 m) and most voluminous lake with an overall water-residence time of ~330 years. The lake was thought to be dimictic throughout the water column, but recently it was shown that the dimictic circulation is incomplete and the mean deep-water renewal time is ~8 years (Weiss et al. 1991). As a result of the combined effects of slow deep-water renewal and biological cycling, dissolved nutrient profiles exhibit deep-water enrichments similar to those in oceans (Weiss et al. 1991). In contrast, preliminary findings provide

no indication of any associated trace metal enrichments, although there is some doubt over the reliability of the trace metal data, because the water samples were not filtered until more than 2 weeks after collection (Falkner et al. 1991).

An understanding of the redox cycling of trace elements in lakes is best achieved through a combination of approaches (e.g., a time series of water-column and pore-water profiles combined with sediment trapping). Most equivocal of all are interpretations based solely on vertical concentration gradients. In this regard it is clear that hypolimnetic enrichments may be the result of processes other than release from bottom sediments. The interpretational value of field data has been greatly enhanced by a growing tendency for studies to include mass balance calculations, and in some cases more detailed quantitative modeling, and this is to be encouraged. Laboratory and field experiments are valuable tools for gaining detailed insights into processes, but the phenomenological observations need to be applied to real lakes with care. For example, the consequences of experimental additions of acid to lake mesocosms may not be relevant to the longer-term behavior of metals in an acidified lake under seasonally varying redox conditions.

There are three main biogeochemical processes effecting the redox-driven cycling of trace elements in lakes, namely algal production and degradation, Fe and Mn redox cycling, and sulfide precipitation. Other important factors include trace metal complexation with enhanced ligand (e.g., carbonate and humic substances) concentrations and the effects of competition for surface exchange sites arising out of the increased cation (e.g., Ca^{2+}, NH_4^+) concentrations that occur in anoxic waters of lakes. In meromictic lakes the enhanced solute concentrations are generally the cause of anoxia, through increased water-column stability, rather than the result of anoxia, but cause and effect are often inextricably linked.

We are only just beginning to obtain good trace element data sets for lakes, and rationalization of the data into a common set of processes, as achieved for oceans, is still at an early stage. To fully appreciate trace element behavior in lakes more good data sets are required, especially those providing information on the scales of depth and time appropriate to the controlling processes.

Acknowledgments. The chapter was written while J.H.-T. was on sabbatical leave at the Centre for Advanced Analytical Chemistry, CSIRO Division of Coal and Energy Technology, Lucas Heights Research Laboratories, Sydney, Australia. The authors thank CSIRO and particularly Dr. Graeme Batley for their generous provision of office and library facilities to J.H.-T. during this period. We thank Dr. Laurie Balistrieri for providing some unpublished results and Drs. Simon Apte, Gregg Brunskill, and Werner Stumm for commenting on a draft version of the chapter. We also thank Jane Rushton for preparing the figures.

References

Aggett J, O'Brien GA (1985) Detailed model for the mobility of arsenic in lacustrine sediments based on measurements in Lake Ohakuri. Environ Sci Technol 19:231–238

Aggett J, Roberts LS (1986) Insight into the mechanism of accumulation of arsenate and phosphate in Hydro Lake sediments by measuring the rate of dissolution with ethylenediaminetetraacetic acid. Environ Sci Technol 20:183–186

Aggett J, Kriegman MR (1988) The extent of formation of arsenic (III) in sediment interstitial waters and its release to hypolimnetic waters in Lake Ohakuri. Water Res 22:407–411

Alberts JJ, Orlandini KA (1981) Laboratory and field studies of the relative mobility of ^{239,240}Pu and ^{241}Am from lake sediments under oxic and anoxic conditions. Geochim Cosmochim Acta 45:1931–1939

Alberts JJ, Tilly LJ, Vigerstad TJ (1979) Seasonal cycling of cesium-137 in a reservoir. Science 203: 649–651

Alberts JJ, Pinder JE, Bowling JW, Nelson DM, Orlandini KO (1986) ^{239,240}Pu, ^{241}Am and ^{232}Th in lakes: the effects of seasonal anoxia. J Environ Radioactivity 4:167–176

Alberts JJ, Wahlgren MA, Orlandini KA, Durbahn CA (1989) The distributions of ^{239,240}Pu, ^{238}Pu, ^{241}Am, and ^{137}Cs among chemically-defined components of sediments, settling particulates and net plankton of Lake Michigan. J Environ Radioactivity 9:89–103

Allard B, Rydberg J (1983) Behaviour of plutonium in natural waters. In: Carnall WT, Choppin GR (eds) Plutonium chemistry. Am Chem Soc Symp Ser: 216, Washington, pp 275–295

Anderson LCD, Bruland KW (1991) Biogeochemistry of arsenic in natural waters: the importance of methylated species. Environ Sci Technol 25:420–427

Anderson RF, Bacon MP, Brewer PG (1982) Elevated concentrations of actinides in Mono Lake. Science 216:514–516

Baccini P, Joller T (1981) Transport processes of copper and zinc in a highly eutrophic and meromictic lake. Schweiz Z Hydrol 43:176–199

Balistrieri LS, Chao TT (1990) Adsorption of selenium by amorphous iron oxyhydroxide and manganese dioxide. Geochim Cosmochim Acta 54:739–751

Balistrieri LS, Murray JW, Paul B (1992a) The biogeochemical cycling of trace metals in the water column of Lake Sammamish, Washington: Response to seasonally anoxic conditions. Limnol Oceanogr 37:529–548

Balistrieri LS, Murray JW, Paul B (1992b) The cycling of iron and manganese in the water column of Lake Sammamish, Washington. Limnol Oceanogr 37:510–528

Batterson TR, McNabb CD (1983) Arsenic in Lake Lansing, Michigan. Environ Toxicol Chem 2:1–17

Belzile N, Tessier A (1990) Interactions between arsenic and iron oxyhydroxides in lacustrine sediments. Geochim Cosmochim Acta 54:103–109

Belzile N, De Vitre RR, Tessier A (1989) In situ collection of diagenetic iron and manganese oxyhydroxides from natural sediments. Nature 340:376–377

Benoit G, Hemond HF (1990) ^{210}Po and ^{210}Pb remobilization from lake sediments in relation to iron and manganese cycling. Environ Sci Technol 24:1224–1234

Benoit G, Hemond HF (1991) Evidence for diffusive redistribution of ^{210}Pb in lake sediments. Geochim Cosmochim Acta 55:1963–1975

Bruland KW (1980) Oceanographic distributions of cadmium, zinc, nickel, and copper in the North Pacific. Earth Planet Sci Lett 47:176–198

Bruland KW, Franks RP (1983) Mn, Ni, Cu, Zn and Cd in the western north Atlantic. In: Wong CS, Boyle E, Bruland KW, Burton JD, Goldberg ED (eds) Trace metals in seawater. Plenum, New York, pp 395–414

Brunskill GJ, Ludlam SD (1988) The variation of annual ^{210}Pb flux to varved sediments of Fayetteville Green Lake, New York from 1885 to 1965. Verh Int Verein Limnol 23:848–854

Buesseler KO, Benoit G, Sholkovitz ER (1985) A pore water study of plutonium in a seasonally anoxic lake. J Environ Radioactivity 2:283–292

Buffle J, De Vitre RR, Perret D, Leppard GG (1989) Physico-chemical characteristics of a colloidal iron phosphate species formed at the oxic-anoxic interface of a eutrophic lake. Geochim Cosmochim Acta 53:399–408

Calvert SE, Price NB (1977) Shallow water, continental margin and lacustrine nodules: distribution and geochemistry. In: Glasby GP (ed) Marine manganese deposits. Elsevier, Amsterdam, pp 45–86

Carignan R, Nriagu JO (1985) Trace metal deposition and mobility in the sediments of two lakes near Sudbury, Ontario. Geochim Cosmochim Acta 49:1753–1764

Carignan R, Tessier A (1985) Zinc deposition in acid lakes: the role of diffusion. Science 228:1524–1526

Choppin GR (1991) Redox speciation of plutonium in natural waters. J Radioanal Nucl Chem 147: 109–116

Collienne RH (1983) Photoreduction of iron in the epilimnion of acidic lakes. Limnol Oceanogr 28: 83–100

Comans RNJ, Hockley DE (1992) Kinetics of cesium sorption on illite. Geochim Cosmochim Acta 56: 1157–1164

Comans RNJ, Middleburg JJ, Zonderhuis J, Woittiez JRW, De Lange GJ, Das HA, Van Der Weijden CH (1989) Mobilization of radiocaesium in pore water of lake sediments. Nature 339:367–369

Cooke TD, Bruland KW (1987) Aquatic chemistry of selenium: evidence of biomethylation. Environ Sci Technol 21:1214–1219

Cornwell JC (1986) Diagenetic trace-metal profiles in Arctic lake sediments. Environ Sci Technol 20:299–302

Cremers A, Elsen A, De Preter P, Maes A (1988) Quantitative analysis of radiocaesium retention in soils. Nature 335:247–249

Crusius J, Anderson RF (1994) Evaluating the mobility of ^{137}Cs, $^{239+240}$Pu and ^{210}Pb from their distributions in laminated lake sediments. J Paleolimnol (in press)

Cullen WR, Reimer KJ (1989) Arsenic speciation in the environment. Chem Rev 89:713–764

Cutter GA (1991) Selenium biogeochemistry in reservoirs, vol 1. Time series and mass balance results. Electric Power Res Instit, Project 2020-1, Final Rep EPRI EN-7281

Davison W (1991) The solubility of iron sulphides in synthetic and natural waters at ambient temperature. Aquat Sci 35:309–329

Davison W (1993) Iron and manganese in lakes. Earth Sci Rev 34:119–163

Davison W, Seed G (1983) The kinetics of the oxidation of ferrous iron in synthetic and natural waters. Geochim Cosmochim Acta 47:67–79

Davison W, De Vitre R (1992) Iron particles in freshwater. In: Buffle J, van Leeuwen HP (eds) Environmental Particles, vol 1. Lewis, Boca Raton, pp 315–355

Davison W, Woof C, Rigg E (1982) The dynamics of iron and manganese in a seasonally anoxic lake: direct measurement of fluxes using sediment traps. Limnol Oceanogr 27:987–1003

Davison W, Grime GW, Woof C (1992) Characterization of lacustrine iron sulfide particles with proton-induced X-ray emission. Limnol Oceanogr 37: 1770–1777

Davison W, Hilton J, Hamilton-Taylor J, Kelly M, Livens F, Rigg E, Carrick TR, Singleton DL (1993a) The transport of Chernobyl-derived radiocaesium through two freshwater lakes in Cumbria, UK. J Environ Radioactivity 19:125–153

Davison W, Spezzano P, Hilton J (1993b) Remobilization of caesium from freshwater sediments. J Environ Radioactivity 19:109–124

De Vitre R, Davison W (1993) Manganese particles in freshwater. In: van Leeuwen HP, Buffle J (eds) Environmental Particles, vol 2. Lewis, Boca Raton, pp 317–352

De Vitre R, Buffle J, Perret D, Baudat R (1988) A study of iron and manganese transformations at the O_2-S(-II) transition layer in a eutrophic lake (Lake Bret, Switzerland): a multimethod approach. Geochim Cosmochim Acta 52:1601–1613

De Vitre R, Belzile N, Tessier A (1991) Speciation and adsorption of arsenic on diagenetic iron oxyhydroxides. Limnol Oceanogr 36:1480–1485

Diem D, Stumm W (1984) Is dissolved Mn^{2+} being

oxidised by O_2 in absence of Mn-bacteria or surface catalysts? Geochim Cosmochim Acta 48:1571–1573
Di Toro DM, Mahony JD, Hansen DJ, Scott KJ, Carlson AR, Ankley GT (1992) Acid volatile sulfide predicts the acute toxicity of cadmium and nickel in sediments. Environ Sci Technol 26:96–101
Drake JC, Ackerly S (1983) Pore water investigations of Lake Champlain sediments. Proc 26th Conf Great Lakes Res, Oswego, New York, p 38 (Abstr)
Dzombak DA, Morel FMM (1990) Surface Complexation Modelling: Hydrous Ferric Oxide. John Wiley, New York, 393 pp
Emerson S (1976) Early diagenesis in anaerobic lake sediments: chemical equilibria in interstitial waters. Geochim Cosmochim Acta 40:925–934
Evans DW, Alberts JJ, Clark RA (1983) Reversible ion exchange fixation of cesium-137 leading to mobilization from reservoir sediments. Geochim Cosmochim Acta 47:1041–1049
Falkner KK, Measures CI, Herbelin SE, Edmond JM, Weiss RF (1991) The major and minor element chemistry of Lake Baikal. Limnol Oceanogr 36: 413–423
Forstner U (1982) Accumulative phases for heavy metals in limnic sediments. Hydrobiol 91:269–284
Freeman MC, Aggett J, O'Brien G (1986) Microbial transformations of arsenic in Lake Ohakuri, New Zealand. Water Res 20:283–294
Frevert T (1987) Heavy metals in Lake Kinneret (Israel). II. Hydrogen sulfide dependent precipitation of copper, cadmium, lead and zinc. Arch Hydrobiol 109:1–24
Fuller CC, Davis JA, Waychunas GA (1993) Surface chemistry of ferrihydrite: Part 2. Kinetics of arsenate adsorption and co-precipitation. Geochim Cosmochim Acta 57:2271–2282
Giusti L, Hamilton-Taylor J, Davison W, Hewitt CN (1993) Sorption of trace metals (Cu, Pb, Zn) by suspended lake particles in artificial (0.005 M $NaNO_3$) and natural (Esthwaite Water) freshwaters. Geochim Cosmochim Acta (submitted)
Green WJ, Ferdelman TG, Canfield DE (1989) Metal dynamics in Lake Vanda (Wright Valley, Antarctica). Chem Geol 76:85–94
Gunkel G von, Sztraka A (1986) Untersuchungen zum Verhalten von Schwermetallen in Gewässern, II. Die Bedeutung der Eisen- und Mangan-Remobilisierung für die hypolimnische Anreicherung von Schwermetallen. Arch Hydrobiol 106:91–117
Hamilton-Taylor J, Morris EB (1985) The dynamics of iron and manganese in the surface sediments of a seasonally anoxic lake. Arch Hydrobiol/Suppl 72:135–165
Hamilton-Taylor J, Willis M, Reynolds CS (1984) Depositional fluxes of metals and phytoplankton in Windermere as measured by sediment traps. Limnol Oceanogr 29:695–710
Hamilton-Taylor J, Kelly M, Kershaw P, Lambert CE (1993) Radionuclide aquatic pathways. In: Warner FE, Harrison RM (eds) Radioecology after Chernobyl. Wiley, New York, pp 177–274
Harriss RC, Troup AG (1970) Chemistry and origin of freshwater ferromanganese concretions. Limnol Oceanogr 15:702–712
Hart BT (1982) Uptake of trace metals by sediments and suspended particulates: a review. Hydrobiol 91:299–313
Hecky RE, Campbell P, Hendzel LL (1993) The stoichiometry of carbon, nitrogen, and phosphorus in particulate matter of lakes and oceans. Limnol Oceanogr 38:709–724
Hesslein RH (1987) Whole-lake metal radiotracer movement in fertilized lake basins. Can J Fish Aquat Sci 44:74–82
Hilton J, Long GJ, Chapman JS, Lishman JP (1986) Iron mineralogy of sediments. A Mossbauer study. Geochim Cosmochim Acta 50:2147–2151
Jaquet J-M, Nembrini G, Garcia J, Vernet JP (1982) The manganese cycle in Lac Leman, Switzerland: the role of *Metallogenium*. Hydrobiol 91:323–340
Johnson CA, Sigg L, Lindauer U (1992b) The chromium cycle in a seasonally anoxic lake. Limnol Oceanogr 37:315–321
Johnson KS, Coale KH, Jannasch HW (1992a) Analytical chemistry in oceanography. Anal Chem 64:1065A–1075A
Kaczynski SE, Kieber RJ (1993) Aqueous trivalent chromium photoproduction in natural waters. Environ Sci Technol 27:1572–1576
Kephkay PE (1985) Kinetics of microbial manganese oxidation and trace metal binding in sediments: results from an in situ dialysis technique. Limnol Oceanogr 30:713–726
Kuhn A, Sigg L (1993) Arsenic cycling in eutrophic Lake Greifen, Switzerland: influence of seasonal redox processes. Limnol Oceanogr 38:1052–1059
Landing WM, Burnett WC, Lyons WB, Orem WH (1991) Nutrient cycling and the biogeochemistry of manganese, iron, and zinc in Jellyfish Lake, Palau. Limnol Oceanogr 36:515–525
Laxen DPH (1984/1985) Adsorption of Cd, Pb and Cu during the precipitation of hydrous ferric oxide in natural water. Chem Geol 47:321–332
Laxen DPH (1985) Trace metal adsorption/coprecipitation on hydrous ferric oxide under realistic conditions. The role of humic substances. Water Res 19:1229–1236
Laxen DPH, Sholkovitz ER (1981) Adsorption (coprecipitation) of trace metals at natural concentrations on hydrous ferric oxide in lake water samples. Environ Technol Lett 2:561–568
Lipinski NG, Huang PM, Liaw WK, Hammer UT (1986) The effects of chemical treatments on the retention and redox reactions of selenium by selected freshwater sediments. Can Tech Rep Fish Aquat Sci 1462:166–184
Lipinski NG, Huang PM, Hammer UT, Liaw WK (1987) The interaction of selenate and selenite with selected freshwater sediments. Int Rev Ges Hydrobiol 72:107–114
Lovell MA, Farmer JG (1983) The geochemistry of arsenic in the freshwater sediments of Loch Lomond. Heavy Metal Environ, 4th Int Conf, vol 2, CEP Consultants, Edinburgh, pp 776–778
Lovley DR, Phillips EJP, Gorby YA, Landa ER (1991) Microbial reduction of uranium. Nature 350:413–416
Lum KR, Gammon KL (1985) Geochemical availability

of some trace and major elements in surficial sediments of the Detroit River and western Lake Erie. J Great Lakes Res 11:328–338

Maest AS, Pasilis SP, Miller LG, Nordstrom DK (1992) Redox geochemistry of arsenic and iron in Mono Lake, California, USA. In: Kharaka YK, Maest AS (eds) Water-rock interaction, vol 1. Low temperature environments. Proc 7th Int Symp Water-Rock Interaction, Balkema, Rotterdam, pp 507–511

Masscheleyn PH, Delaune RD, Patrick Jr WH (1991) Arsenic and selenium chemistry as affected by sediment redox potential and pH. J Environ Qual 20: 522–527

Matisoff G, Lindsay AH, Matis S, Soster FM (1980) Trace metal mineral equilibria in Lake Erie sediments. J Great Lakes Res 6:353–366

McGrath M, Davison W, Hamilton-Taylor J (1989) Biogeochemistry of barium and strontium in a soft-water lake. Sci Total Environ 87/88:287–295

McKee JD, Wilson TP, Long DT, Owen RM (1989a) Geochemical partitioning of Pb, Zn, Cu, Fe, and Mn across the sediment-water interface in large lakes. J Great Lakes Res 15:46–58

McKee JD, Wilson TP, Long DT, Owen RM (1989b) Pore water profiles and early diagenesis of Mn, Cu, and Pb in sediments from large lakes. J Great Lakes Res 15:68–83

Moffett JW, Zika RG (1983) Oxidation kinetics of Cu(I) in seawater: implications for its existence in the marine environment. Mar Chem 13:239–251

Moffett JW, Zika RG (1987) Reaction kinetics of hydrogen peroxide with copper and iron in seawater. Environ Sci Technol 21:804–810

Morfett K (1988a) Trace metal dynamics in a seasonally anoxic lake. PhD thesis, Lancaster Univ

Morfett K (1988b) The distribution and transport of Cu and Zn in a seasonally anoxic lake. Trace Elem New Zealand: Environ Human Animal, Proc New Zealand Trace Elem Group Conf, Lincoln Coll, Canterbury, pp 57–64

Morfett K, Davison W, Hamilton-Taylor J (1988) Trace metal dynamics in a seasonally anoxic lake. Environ Geol Water Sci 11:107–114

Morse JW, Choppin GR (1986) Laboratory studies of plutonium in marine systems. Mar Chem 20:73–89

Morse JW, Arakaki T (1993) Adsorption and coprecipitation of divalent metals with mackinawite (FeS). Geochim Cosmochim Acta 57:3635–3640

Mortimer CH (1941) The exchange of dissolved substances between mud and water in lakes: I and II. J Ecol 29:280–329

Mortimer CH (1942) The exchange of dissolved substances between mud and water in lakes: III and IV. J Ecol 30:147–201

Mouvet C, Bourg ACM (1983) Speciation (including adsorbed species) of copper, lead, nickel, and zinc in the Meuse River. Water Res 17:641–649

Mudge S, Hamilton-Taylor J, Kelly M, Bradshaw K (1988) Laboratory studies of the chemical behaviour of plutonium associated with contaminated estuarine sediments. J Environ Radioactivity 8:217–237

Murray JW (1987) Mechanisms controlling the distribution of trace elements in oceans and lakes. In: Hites RA, Eisenreich SJ (eds) Sources and fates of aquatic pollutants. Am Chem Soc Adv Chem Ser 216:153–184

Nelson DM, Larsen RP, Penrose WR (1987) Chemical speciation of plutonium in natural waters. In: Environmental research on actinide elements. Proc Conf, Hilton Head, South Carolina, 1983, Dept Energy CONF-841142, pp 27–48

Nelson DM, Orlandini KA, Penrose WR (1989) Oxidation states of plutonium in carbonate-rich natural waters. J Environ Radioactivity 9:189–198

Nriagu JO, Lawson G, Wong HKT, Azcue JM (1993) A protocol for minimizing contamination in the analysis of trace metals in Great Lakes waters. J Great Lakes Res 19:175–182

Oremland RS, Hollibaugh JT, Maest AS, Presser TS, Miller LG, Culbertson CW (1989) Selenate reduction to elemental selenium by anaerobic bacteria in sediments and culture: biogeochemical significance of a novel sulphate-independent respiration. Appl Environ Microbiol 55:2333–2343

Orlandini KA, Penrose WR, Harvey BR, Lovett MB, Findlay MW (1990) Colloidal behaviour of actinides in an oligotrophic lake. Environ Sci Technol 24: 706–712

Oscarson DW, Huang PM, Liaw WK (1980) The oxidation of arsenite by aquatic sediments. J Environ Qual 9:700–703

Oscarson DW, Huang PM, Liaw WK (1981) Role of manganese in the oxidation of arsenite by freshwater lake sediments. Clays Clay Min 29:219–225

Pardue JH, DeLaune RD, Patrick WH, Whitcomb JH (1989) Effect of redox potential on fixation of ^{137}Cs in lake sediment. Health Phys 57:781–789

Pedersen TF (1983) Dissolved heavy metals in a lacustrine mine tailings deposit – Buttle Lake, British Columbia. Mar Pollut Bull 14:249–254

Pedersen TF, Mueller B, McNee JJ, Pelletier CA (1993) The early diagenesis of submerged sulphide-rich mine tailings in Anderson Lake, Manitoba. Can J Earth Sci 30:1099–1109

Pinder JE, Alberts JJ, Bowling JW, Nelson DM, Orlandini KO (1992) The annual cycle of plutonium in the water column of a warm, monomictic reservoir. J Environ Radioactivity 17:59–81

Rai D, Eary LE, Zachara JM (1989) Environmental chemistry of chromium. Sci Total Environ 86:15–23

Reynolds GL, Hamilton-Taylor J (1992) The role of planktonic algae in the cycling of Zn and Cu in a productive soft-water lake. Limnol Oceanogr 37: 1759–1769

Richard FC, Bourg ACM (1991) Aqueous geochemistry of chromium: a review. Water Res 25:807–816

Sakata M (1985) Diagenetic remobilization of manganese, iron, copper and lead in anoxic sediment of a freshwater pond. Water Res 19:1033–1038

Saleh FY, Parkerton TF, Lewis RV, Huang JH, Dickson KL (1989) Kinetics of chromium transformations in the environment. Sci Total Environ 86:25–41

Sanchez AL, Murray JW, Schell WR, Miller LG (1986) Fallout plutonium in two oxic-anoxic environments. Limnol Oceanogr 31:1110–1121

Santschi PH (1988) Factors controlling the biogeochemical cycles of trace elements in fresh and coastal

marine waters as revealed by artificial radioisotopes. Limnol Oceanogr 33:848–866

Santschi PH (1989) Use of radionuclides in the study of contaminant cycling processes. Hydrobiol 176/177: 307–320

Santschi PH, Nyffeler UP, Anderson RF, Schiff SL, O'Hara P, Hesslein RH (1986) Response of radioactive trace metals to acid-base titrations in controlled experimental ecosystems: evaluation of transport parameters for application to whole-lake radiotracer experiments. Can J Fish Aquat Sci 43:60–77

Santschi P, Hohener P, Benoit G, Buchholtz-ten Brink M (1990) Chemical processes at the sediment-water interface. Mar Chem 30:269–315

Schintu M, Kudo A, Sarritzu G, Contu A (1991) Heavy metal distribution and mobilization in sediments from a drinking water reservoir near a mining area. Water Air Soil Pollut 57–58:329–338

Seyler P, Martin J-M (1989) Biogeochemical processes affecting arsenic species distribution in a permanently stratified lake. Environ Sci Technol 23:1258–1263

Sholkovitz ER (1985) Redox-related geochemistry in lakes; alkali metals, alkaline earth elements, and ^{137}Cs. In: Stumm W (ed) Chemical processes in lakes. Wiley, New York, pp 119–142

Sholkovitz ER, Carey AE, Cochran JK (1982) Aquatic chemistry of plutonium in seasonally anoxic lake waters. Nature 300:159–161

Sigg L (1985) Metal transfer mechanisms in lakes; the role of settling particles. In: Stumm W (ed) Chemical processes in lakes. Wiley, New York, pp 283–310

Sigg L, Sturm M, Kistler D (1987) Vertical transport of heavy metals by settling particles in Lake Zurich. Limnol Oceanogr 32:112–130

Sigg L, Johnson CA, Kuhn A (1991) Redox conditions and alkalinity generation in a seasonally anoxic lake (Lake Greifen). Mar Chem 36:9–26

Simpson HJ, Trier RM, Toggweiler JR, Mathieu G, Deck BL, Olsen CR, Hammond DE, Fuller C, Ku TL (1982) Radionuclides in Mono Lake, California. Science 216:512–514

Spezzano P, Hilton J, Lishman JP, Carrick TR (1993) The variability of Chernobyl Cs retention in the water column of lakes in the English Lake District, two years and four years after deposition. J Environ Radioactivity 19:213–232

Stokes PM, Szokalo AM (1977) Sediment-water interchange of copper and nickel in experimental aquaria. Proc 12th Can Symp, Water Pollut Res Can, pp 157–177

Stumm W, Sulzberger B (1992) The cycling of iron in natural environments: considerations based on laboratory studies of heterogeneous redox processes. Geochim Cosmochim Acta 56:3233–3257

Sugiyama M, Hori T, Kihara S, Matsui M (1992) A geochemical study on the specific distribution of barium in Lake Biwa, Japan. Geochim Cosmochim Acta 56:597–605

Sulzberger B, Schnoor JL, Giovanoli R, Hering JG, Zobrist J (1990) Biogeochemistry of iron in an acidic lake. Aquat Sci 52:56–74

Takamatsu T, Kawashima M, Koyama M (1985) The role of Mn^{2+}-rich hydrous manganese oxide in the accumulation of arsenic in lake sediments. Water Res 19:1029–1032

Talbot RW, Andren AW (1984) Seasonal variations of ^{210}Pb and ^{210}Po concentrations in an oligotrophic lake. Geochim Cosmochim Acta 48:2053–2063

Talling JF (1976) The depletion of carbon dioxide from lake water by phytoplankton. J Ecol 64:79–121

Tessier A (1992) Sorption of trace elements on natural particles in oxic environments. In: Buffle J, van Leeuwen HP (eds) Environmental particles, vol 1. Lewis, Boca Raton, pp 425–453

Tessier A, Rapin F, Carignan R (1985) Trace metals in oxic lake sediments: possible adsorption onto iron oxyhydroxides. Geochim Cosmochim Acta 49:183–194

Tessier A, Carignan R, Dubreuil B, Rapin F (1989) Partitioning of zinc between the water column and the oxic sediments in lakes. Geochim Cosmochim Acta 53:1511–1522

Tessier A, Couillard Y, Campbell PGC, Auclair JC (1993) Modeling Cd partitioning in oxic lake sediments and Cd concentrations in the freshwater bivalve *Anodonta grandis*. Limnol Oceanogr 38:1–17

Tipping E, Heaton MJ (1983) The adsorption of aquatic humic substances by two oxides of manganese. Geochim Cosmochim Acta 47:1393–1397

Tipping E, Ohnstad M (1984) Colloid stability of iron oxide particles from a freshwater lake. Nature 308: 266–268

Tipping E, Woof C, Cooke D (1981) Iron oxide from a seaonally anoxic lake. Geochim Cosmochim Acta 45:1411–1419

Tipping E, Thompson DW, Davison W (1984) Oxidation products of Mn(II) in lakes. Chem Geol 44:359–383

Waite TD (1988) Photochemical effects on the mobility and fate of heavy metals in the aquatic environment. Environ Technol Lett 9:977–982

Waychunas GA, Rea BA, Fuller CC, Davis JA (1993) Surface chemistry of ferrihydrite: Part 1. EXAFS studies of the geometry of coprecipitated and adsorbed arsenate. Geochim Cosmochim Acta 57: 2251–2269

Webster JG (1992) Trace metals at the oxic/anoxic-H_2S boundary in Lake Vanda, Antarctica. In: Kharaka YK, Maest AS (eds) Water-rock interaction, vol 1. Low temperature environments. Proc 7th Int Symp Water-Rock Interaction, Balkema, Rotterdam, pp 527–530

Weiss RF, Carmack EC, Koropalov VM (1991) Deep-water renewal and biological production in Lake Baikal. Nature 349:665–669

Weres O, Jaouni A-R, Tsao L (1989) The distribution, speciation and geochemical cycling of selenium in a sedimentary environment, Kesterton Reservoir, California, USA. Appl Geochem 4:543–563

White JR, Driscoll CT (1985) Lead cycling in an acidic Adirondack lake. Environ Sci Technol 19: 1182–1187

Williams TM (1992) Diagenetic metal profiles in recent sediments of a Scottish freshwater loch. Environ Geol Water Sci 20:117–123

Windom HL, Byrd JT, Smith Jr RG, Huan F (1991)

Inadequacy of NASQAN data for assessing metal trends in the nation's rivers. Environ Sci Technol 25:1137–1142

Yagi A (1988) Dissolved organic manganese in the anoxic hypolimnion of Lake Fukami-ike. Jpn J Limnol 49:149–156

Yagi A, Shimodaira I (1986) Seasonal changes of iron and manganese in Lake Fukami-ike – occurrence of turbid manganese layer. Jpn J Limnol 47:279–289

Young LB, Harvey HH (1992) The relative importance of manganese and iron oxides and organic matter in the sorption of trace metals by surficial lake sediments. Geochim Cosmochim Acta 56:1175–1186

9 Comparative Geochemistry of Marine Saline Lakes

F.T. MACKENZIE[1], S. VINK[1], R. WOLLAST[2], and L. CHOU[2]

1 Introduction

Saline lakes may be classified into two groups on the basis of the primary water source for the lake. These groups are the athalassic (nonmarine) and the marine saline lakes. Athalassic saline lakes receive freshwater input and become saline owing to the high evaporation rates of the arid or semiarid climatic regions in which these lacustrine systems are predominantly found. This group of lakes includes most of the small inland salt lakes and playas, as well as larger lakes such as the Dead Sea in Israel and the Great Salt Lake of the United States. The second group of saline lakes is the marine lakes, which are filled primarily with water having a seawater or chemically modified seawater composition. These coastal lakes are usually of small areal extent and are found in a wide variety of climatic regions ranging from temperate to arid. Consequently, marine lakes vary in their characteristics. Only a dozen or so of these lakes have been studied. The most comprehensive studies are of Solar Lake, Sinai (Friedman et al. 1973; Cohen et al. 1977a–c; Krumbein et al. 1977; Jorgensen et al. 1977; Friedman et al. 1982; Lyons et al. 1984) and Mangrove Lake, Bermuda (Neumann 1969; Hatcher 1978; Hatcher et al. 1982; Hatcher et al. 1983; Orem et al. 1986; Sharma et al. 1988; Stolz 1989; Boudreau et al. 1992). Other studies include those of Eil Malk (Jellyfish) lake, Palau (Hamner et al. 1982; Burnett et al. 1989), various ponds found on Christmas Island, Kiribati (Schoonmaker et al. 1985), and several coastal lake systems in western and southern Australia and along the Sinai coast (Warren 1982; Playford 1983; Edward 1983; Burke 1989; Kushnir 1981; Levy 1974, 1977a,b; Gat and Levy 1978).

In this chapter, because there are few comprehensive studies of the hydrogeochemistry and biogeochemical cycling dynamics of marine saline lakes, we emphasize Solar Lake, Sinai, and Mangrove Lake, Bermuda. Furthermore, we take a comparative approach to analysis of these two lacustrine systems in order to provide some feeling for the types and relative importance of the various processes operating in marine saline lakes. In particular, sediment-pore-water processes are emphasized.

2 General Characteristics of Marine Saline Lakes

All marine saline lakes were formed or filled with seawater between approximately 4000 and 6000 years before present (B.P.). At this time the rapid rise in global sea level resulted in the flooding of low-lying coastal areas. The marine lakes were formed in two ways. In the first case, as sea level rose seawater inundated low-lying areas, initially forming lagoons. Over time these lagoons became cut off from direct connection to the ocean, thus becoming seawater lakes. Solar Lake, Ras Mohammad Lake, Bardawil Lagoon and associated sabkhas (all located on the Sinai coast), and many lakes in Australia were formed in this manner. For example, Solar Lake became cut off from the ocean as a bar formed across its mouth. This bar was later stabilized by the formation of a reef on the seaward margin of the lake. The bar still remains porous, and Solar Lake presently receives seawater input by seepage through the bar. In the case of many of the Australian lakes, calcium carbonate sand dunes were deposited at the new coastal margin created by sea-level rise, thereby cutting off the lakes from the ocean. A local fall in sea level or tectonic uplift of an area can also isolate marine lagoons from direct oceanic

[1] Department of Oceanography, School of Ocean and Earth Science and Technology, University of Hawaii, 1000 Pope Road, MSB 525, Honolulu, HI 96822, USA
[2] Laboratoire d'Oceanographie, Universite Libre de Bruxelles, Campus de la Plaine, CP-208, 1050 Brussels, Belgium

connection to form marine lakes. There is evidence that the formation of the hypersaline lakes on Rottnest Island (western Australia) occurred in this manner (Playford 1983).

In the second case, marine saline lakes formed without any initial direct oceanic connection. For example, in areas where there were coastal dune formations, rising sea level caused the seawater dune aquifer level to also rise. The interdune depressions that were below the sea level of 6000 B.P. then became filled with seawater from the aquifer and lakes were formed. This formation history has been documented for lakes in South Australia (Warren 1982) as well as for Mangrove (Neumann 1969) and Lovers lakes in Bermuda. In contrast to other marine lakes, sedimentary evidence from Mangrove Lake suggests that this lake was formed approximately 10000 B.P. as a shallow freshwater lake. This lake, which lies within an interdune depression, became filled with seawater via seepage through the surrounding dunes approximately 4000 B.P. (Hatcher et al. 1982).

Although some lakes presently receive seawater input through large openings, such as the surface channels in Eil Malk (Hamner et al. 1982) as well as the Bardawil Lagoon (Levy 1974) and the underground caves in Lovers Lake, most lakes receive input via seepage alone. No marine lakes have been found to have any permanent freshwater stream input. The hydrology of these lakes is affected by the porosity and permeability of the surrounding bedrock, and processes that change the water level of either the ocean or the lake. The two dominant processes affecting water level are tidal variations in sea level and the rate of evaporation of water from the lake. Variations at a tidal frequency in the water level of several lakes have been recorded. As expected, those lakes with channels connecting to the ocean, e.g., Lovers Lake and Eil Malk, have water pumped to and from the lake in response to the tides. Both of these lakes, however, remain stratified during the tidal cycle, and thus, it is likely that much of the water entering each of these lakes during an incoming tide is removed on the outgoing tide. Tidal oscillations were also recorded in 1971 in Mangrove Lake, which receives input only via seepage (Hatcher et al. 1982). Approximately 10 years later no such changes were observed, however, suggesting that the lithified dunes separating the lake from the ocean had become less permeable owing to cementation by calcium carbonate (Sharma 1988). In all of the previously mentioned cases, oscillations in the lake water level are delayed and damped with regard to tidal variations of the adjacent ocean.

The hydrological cycle of marine lakes that are either located far from the ocean or are separated by a less permeable barrier than those mentioned previously is dominated by the seasonal evaporation/precipitation cycle of the climatic region in which these systems are located. Such a cycle has been described for a number of coastal salidas located on the South Australian coast (Warren 1982). In winter these shallow lakes are filled with brackish water to a level slightly above sea level. During spring and summer lake waters evaporate to levels below the water table of the surrounding dunes. The dune phreatic waters then drain into the salinas. When the dune water table falls below sea level, seawater then seeps into the dunes. By late summer, owing to the extremely high evaporation rates of this area, the water level of these lakes is 20–40 cm below the sediment surface. During autumn and winter, as the evaporation rate decreases and rainfall over the area increases, the water level of these lakes again rises to a level slightly above sea level. Because of the high permeability of the dune sands, the water table of the dunes, and therefore the lake water level, cannot deviate substantially from sea level.

The salinity of marine lakes varies from approximately seawater salinity (31 psu[3]) to greater than 100 psu. Many of the marine lakes that have depths greater than 2 m are stratified throughout most of the year. In the hypersaline lakes the density stratification is determined predominantly by changes in the salinity of the incoming water, rather than ambient temperature changes. Unlike lakes that are stratified by temperature, the stratification in these lakes is most pronounced during periods of increased rainfall and breaks down during dry periods. The annual cycle of stratification and holomixis has been recorded in three lakes on Rottnest Island, Western Australia

[3] psu = practical salinity units defined in terms of the ratio K_{15} of the electrical conductivity of a seawater sample to that of a potassium chloride solution in which the mass fraction of KCl is 32.4356×10^{-6} at 15 °C and 1 atm pressure. By definition $K_{15} = 1$ corresponds to 35 psu (UNESCO Technical Papers in Marine Science No. 36, 1981).

(Bunn et al. 1984) and in Solar Lake, Sinai (Cohen et al. 1977a). The events generally observed in these lakes are as follows: During winter the upper epilimnion is colder and less saline than the lower hypolimnion. As summer progresses the rate of evaporation increases until eventually it is significantly higher than the rate of seawater supply to the lake. This results in a gradual increase in the salinity of the surface layer of the lake. The temperature gradient of the lake disappears. Holomixis occurs and lasts for several weeks in Solar Lake and several months in the Rottnest lakes. Shortly after the first winter rains on Rottnest, stratification again develops as fresher water enters the surface layer of the lake from seeps around the lake. In Solar Lake southerly storms during the rainy season cause seawater to pile up on the seaward side of the porous bar, which separates Solar Lake from the ocean. This local increase in sea level increases hydrostatic pressure on the groundwater system of the bar resulting in increased flow of seawater into the lake. This relatively fresher incoming water overlies the hypersaline water contained in the lake resulting in salinity stratification. The waters of these lakes are extremely clear and consequently sunlight can reach the bottom of the lakes. During winter stratification a thermocline also develops. Solar energy absorbed at and below the pycnocline results in an inverse temperature profile. The bottom layer of these lakes can be up to 50 °C warmer than the surface layer. The density of the hypersaline brine, however, is high enough that the lake does not overturn, although temperature differences between the epilimnion and hypolimnion are extreme. The duration of the mixing and stratification periods can be modified by local and interannual changes in the amount of rainfall and mean temperature; however, the general sequence of events remains the same.

Only one lake, Eil Malk, has been reported to be permanently stratified. This lake is not hypersaline, but is stratified because of salinity variations between the water permanently contained in the lake and the seawater exchanged tidally through the channels that connect the surface waters of the lake to the surrounding ocean. However, this lake does not develop the inverse temperature profile seen in Solar Lake and Rottnest Island lakes. The reason for this difference is probably because tidal exchange of water between the surface of the lake and the ocean removes sufficient heat from the lake so that subsurface heating does not occur.

Perhaps one of the most distinguishing features of marine lakes in comparison with other lakes is the ionic composition of the water. The compositions of several marine lake waters are compared with those of seawater and average river water in Table 1. Because marine lakes are predominantly filled with seawater rather than freshwater, the chemistry of the lake waters is dominated by Na and Cl with lesser, although significant, concentrations of Ca, SO_4, Mg, and K. Although some evaporated freshwater brines have the same constituents present, the relative proportions of the constituents are different. Evaporation of fresh waters will lead to a variety of alkaline lake water compositions, whereas evaporation of marine lake waters follows a path similar to that of evaporative concentration of salts from normal seawater. Calcium carbonate and gypsum are common precipitates that form during evaporative concentration of marine lake waters; salts of higher solubility are not commonly found as evaporative products (Cohen et al. 1977a; Krumbein et al. 1977; Levy 1977; Gat and Levy 1978). Halite, for example, may form seasonally around the perimeter of some marine lakes, but usually redissolves during rainy periods (Levy 1977). In instances where marine lakes become cut off from a seawater source, the composition of the brines filling the lake and the precipitates may vary considerably. For example, calcium chloride brines have developed in the sabkhas located inland of the Bardawil Lagoon, due to the interaction of brines of seawater composition and fine-grained calcium carbonate sediments in the region. This interaction results in the diagenetic formation of dolomite in the sediments of these sabkhas (Levy 1977a,b).

The biological communities of marine lakes, particularly those which are hypersaline, are dominated by prokaryotic organisms, primarily cyanobacteria and sulfur bacteria. Water-column community dynamics have been best studied in Solar Lake and Eil Malk Lake. In these stratified lakes bacterial "plates" usually form in the thermocline. Bacterially mediated processes result in the establishment of a chemocline at approximately the depth of the thermocline in the lakes. In Solar Lake there are alternating layers of predominantly phototrophic (organisms that use light as an energy source) sulfur bacteria or cyanobacteria, as well as chemolithotrophic

Table 1. Major ion composition of surface waters in several marine lakes, surface seawater, and average river water

Lake	Salinity (psu)	Na (mmol/kg)	Mg (mmol/kg)	Ca (mmol/kg)	K (mmol/kg)	Cl (mmol/kg)	SO_4 (mmol/kg)	HCO_3 (mmol/kg)	Br (mmol/kg)	Reference
Solar Lake[a]	70	890	99	21	19	1040	53	3	2	Friedman et al. (1973)
(Sinai)	146	1815	205	47	30	2189	37	4		
Ras Muhammed (Sinai)	244	3394	391	12	72	3903	147	3	5	Friedman et al. (1982)
Bardawil Coastal	140[d]	1857	197	8	43	2146	31	0.8	4	Levy (1977a)
Lagoon[b] (Sinai)		4219	712	28	123	4625	232	5.8	11	
Inland	140[d]	1666	193	31	3	1775	3	0.3	2	Levy (1977a)
		4035	1088	693	92	5124	129	3.5	11	
Christmas	21	279	27	7	5	331	19			Schoonmaker et al. (1985)
Island Ponds[c] (Kiribati)	247	1893	213	17	34	3490	48			
Lake Hayward (Western Australia)	214	3053	90	23	52	3569	106			Burke et al. (1989)
Mangrove Lake (Bermuda)	32			9		480	24	3		Orem et al. (1986); Sharma et al. (1983)
Seawater	35	468	53	10	10	546	28	2	1	Drever (1982)
Average river water	0.110	0.313	0.150	0.368	0.036	0.233	0.120	0.894		Gregor et al. (1988)

[a] Different salinities represent the seasonal variation in salinity and consequent composition found in Solar Lake.
[b] Compositional range determined in various sabkhas located in coastal and inland regions of the Bardawil Lagoon area.
[c] Different salinities represent the range of salinities found in separate ponds on Christmas Island.
[d] Average salinity of various sabkhas calculated from specific gravity determined by Levy (1977a).

(organisms using CO_2 as a carbon source and deriving energy from oxidation of inorganic compounds) and chemoorganotrophic (organisms using organic matter as a carbon source and deriving energy from oxidation of organic compounds) bacteria in the lower layers. The biological composition of Eil Malk Lake is somewhat more varied. In addition to a photosynthetic sulfur bacterial plate at the chemocline, there are also populations of copepods, a species of fish and two species of jellyfish present in the upper water column (Hamner et al. 1982). The increased diversity compared to Solar Lake is probably due to greater water exchange with the ocean and lower salinity of this lake. Mangrove Lake is not stratified and therefore does not develop these types of bacterial plates; however, the biota dominating the water column are cyanobacteria and copepods. Both Eil Malk and Mangrove lakes are highly productive (Hamner et al. 1982; Hatcher et al. 1982).

The sediment/faunal associations that exist in marine saline lakes are very unusual. Few comprehensive studies have been done in this area; the most notable exceptions are those for Mangrove Lake and Solar Lake. The sediments of Mangrove Lake are organic-rich sapropel within which there is a well-defined depth distribution of different bacteria (Stolz 1990). In the top 10 cm there is an abundance of coccoid cyanobacteria, filamentous cyanobacteria, and purple sulfur-oxidizing bacteria with smaller numbers of diatoms and purple and green phototrophic bacteria. Between 10 and 30 cm colonies of purple phototrophic bacteria become more abundant, although coccoid cyanobacteria and sulfur-oxidizing bacteria remain as the most abundant organisms. Sulfate-reducing bacteria are dominant below a depth of 30 cm in the sediments. The presence of sulfur-oxidizing bacteria in the upper layer of these sediments is somewhat surprising. These sediments are extremely anoxic and therefore contain very high concentrations of sulfide. Usually one would expect to find anoxic phototrophic organisms in such environments; however, in this lake, because the sulfur chemocline lies below the light compensation depth, sulfur-oxidizing bacteria are favored.

In Solar Lake, as in other hypersaline marine lakes, sediments are composed of laminated stromatolitic cyanobacterial mats. As seawater is evaporated the lake water becomes oversaturated firstly with carbonate minerals and then with gypsum. These minerals may be precipitated from solution and deposited in the sediments. Because light can penetrate to the bottom of these lakes, salt-tolerant autotrophic organisms can also inhabit the sediment surface. In Solar Lake and Mangrove Lake these organisms are cyanobacteria, although colonies of other bacteria also live on and within the sediments. The high concentrations of sulfate in the water column favor the growth of sulfate-reducing bacteria such as *Desulfovibrio* sp. The activity of *Desulfovibrio* sp. in Solar Lake has been shown to reduce the sulfate concentration of the pore waters to such an extent that gypsum saturation is not reached (Jorgensen et al. 1977). Thus, gypsum can be deposited in the sediments only during periods of reduced algal production in the lake. Consequently, depth profiles through the sediments of these lakes show annual laminations of algal mats, which do not contain gypsum, but do contain bacteriogenically produced carbonates intercalated between layers of precipitated gypsum and carbonates (Krumbein et al. 1977).

3 Comparative Sediment-Pore-Water Reactions

In this section the sediment-pore-water systems of Mangrove Lake, Bermuda, and Solar Lake, Sinai, are discussed in detail. These lake systems were chosen for analysis because of the data base available and the contrasting conditions of the two lacustrine systems (Table 2). Also, sediment types found in these two lakes are very different; consequently, early diagenetic reactions in the two systems, although similar in some regards, are quantitatively different. These differences provide some feeling for the range of sediment-pore-water reactions that can occur in marine saline lakes.

3.1 Mangrove Lake, Bermuda

Mangrove Lake is located on the southern coast of Bermuda in an interdune depression. Lake waters originate primarily from seepage of oceanic waters through the island's porous calcarenite limestone (Hatcher et al. 1982). The ocean shore is approximately 100 m to the southeast of the lake. Hatcher et al. (1982) observed tidal fluctuations of up to 15 cm, demonstrating a fairly substantial exchange of water through the limestone.

Table 2. Comparative characteristics of two marine saline lake systems

Characteristic	Mangrove Lake	Solar Lake
Climate	Subtropical	Arid
Setting	Interdune depression	Sabkha
Formation	Initially freshwater lake	Initially coastal lagoon
Time seawater filled	4000 years bp	2400 years bp
Area	12 000 m^2	7000 m^2
Depth Average	1 m	1.6 m
Maximum	2 m	6 m
Type	Polymictic	Monomictic (holomixis occurs for a few weeks during summer)
Water temperature	18–30 °C	Surface: 16–27 °C Thermocline: up to 60 °C Deep: 27–40 °C
Thermocline depth	None	2–3 m
Salinity	32–34 psu	Surface: 68–170 psu Deep: 170–180 psu
Nutrients	Low	Low
Primary production	High	High
Sediment types	Sapropel	Stromatolitic cyanobacterial mats, shallow lake depths; flocculose cyanobacterial mat at depth in lake; proportion of evaporitically deposited minerals increases with depth
Benthic organisms	Coccoid cyanobacteria Sulfur-oxidizing bacteria Filamentous bacteria Diatoms Purple and green phototrophic bacteria	Coccoid and filamentous cyanobacteria Diatoms Photosynthetic sulfur bacteria Colorless sulfur bacteria Nonphotosynthetic sulfur bacteria Other heterotrophic bacteria
Benthic production	High	High
Pore-water saturation State		
Calcite	Oversaturated	Oversaturated
Aragonite	Undersaturated	Oversaturated
Dolomite	Undersaturated	Oversaturated
Gypsum	Undersaturated	Undersaturated at shallow depths Oversaturated deeper in lake
Sediment accumulation rate	30 cm 100 y^{-1}	5–50 cm 100 y^{-1}

Thus far, no caves connecting the ocean directly to the lake depression have been found acting as efficient conduits of water exchange. The sole source of freshwater is rainfall and subsequent runoff from the surrounding grassy slopes; there are no permanent streams or freshwater springs discharging into the depression. The lake is therefore a saline environment and not a brackish or freshwater water body. Salinity does vary slightly and inversely with rainfall, e.g., an approximately one-part-per-thousand increase in salinity during a 2-week dry spell was recorded by Hatcher et al. (1982).

The water column is clear and generally no deeper than 1.5–2 m throughout the lake. The limestone bedrock of the depression is found at a depth of a few centimeters to 20 m, and is entirely overlain by a stratum of peat, which has an average thickness of 2 m. The sediment overlying the peat stratum consists of horizontal layers of sapropel, which is rich in organic material. The upper layers of the sapropel are flocculent and highly porous

(80–90% porosity); deeper layers have a gel-like consistency. Studies of sediment cores from the lake by Hatcher et al. (1982) include a detailed analysis of the organic composition of the sediments in the upper 5 m of core, deep-pore-water chemistry, and discussion of the possible sources of organic materials.

The littoral zone of the lake is comprised of a thick ring of mangrove trees and patchy distributions of algae, including *Caulerpa* and other green algae. The fauna consist mainly of small fish, including *Gambusia*, worms, gastropods, and mangrove oysters. The plankton community is almost entirely composed of copepods and cyanobacteria. No organisms that could significantly bioturbate or bioirrigate the sediments vertically have been found.

Microorganisms play a major role in the biogeochemical cycling of C, S, and other chemical species. The stratification of the microorganisms in the sediment was described in a previous section. Emphasis in this section is placed on the biogeochemical cycling of carbon and sulfur in the sediment-pore-water system. A model is presented that helps to quantify the relationship between dissolved constituents of the interstitial waters and organic matter decomposition owing to microbiologically mediated sulfate reduction. A similar model was also presented by Boudreau et al. (1992).

3.1.1 Descriptive Pore-Water Chemistry

Pore-water gradients of pH, total alkalinity, total reduced sulfur, bisulfide, and dissolved sulfate for Mangrove Lake sapropel are shown in Fig. 1. It is evident from the sharp gradient in pH observed in the top 5 cm of the sediment that sediment-pore-water reactions proceed rapidly and probably concomitantly with initial deposition of organic-rich sediment. The sharp decrease in pH is due to the presence of CO_2 and H_2S, both "acidic" components, produced as a result of oxidation of organic matter through bacterially mediated sulfate reduction. The nearly monotonic increase in total alkalinity with increasing depth of sediment pore waters shows that dissolved inorganic carbon is added to the pore waters as labile organic carbon is progressively consumed (Fig. 1b). This increase in total alkalinity just balances the electrical-charge deficit of the pore waters brought about by sulfate reduction. This conclusion is clearly documented in Fig. 1c, which shows that nearly all the sulfate has been quantitatively reduced to HS^- and H_2S while dissolved inorganic

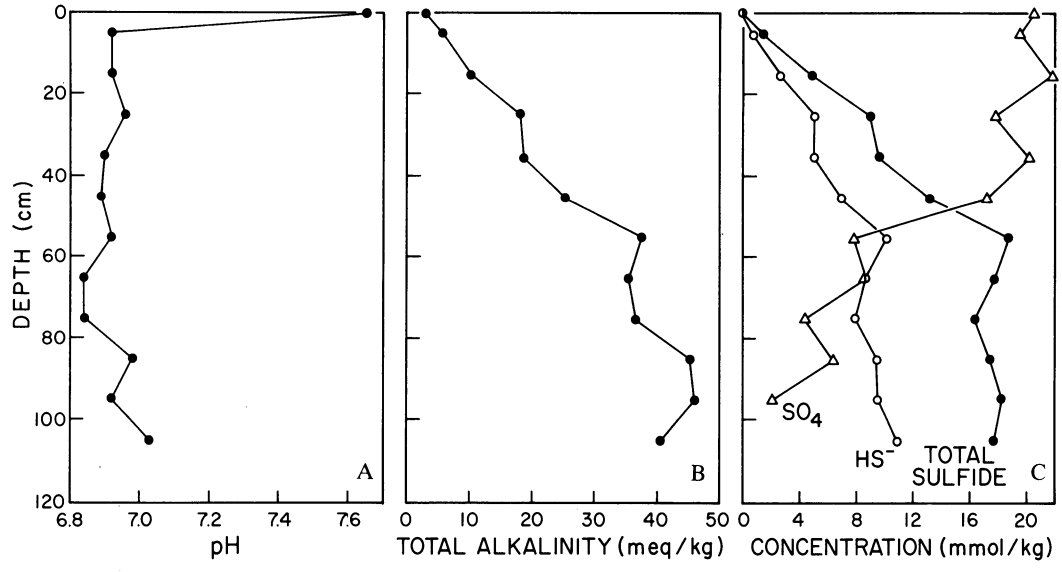


Fig. 1. Pore-water gradients of (A) pH, (B) total alkalinity, and (C) total reduced sulfur (*filled circles*), bisulfide (*open circles*) and dissolved sulfate (*triangles*) measured in the Mangrove Lake sapropel. The sharp decrease in pH and the monotonic increase in total alkalinity indicate that organic matter decomposition proceeds rapidly in the sediments releasing CO_2 into pore waters. The decrease in sulfate and increase in reduced sulfur species show that organic matter decomposition is primarily by sulfate reduction

carbon (mainly HCO_3^-) is produced by oxidation of organic matter (Figs. 1b,c). These reactions are characteristic of many anaerobic sediment-pore-water systems (e.g., Berner 1980). The uniqueness of Mangrove Lake's shallowly buried sediments, however, is that they are nearly pure organic matter and sapropel, and reactions involving siliciclastic and carbonate detritus are quantitatively unimportant, as are chemical reactions leading to production of evaporitic sediments. Thus, these sediments contrast sharply with those of, for example, Solar Lake, Sinai (see Sect. 3.2), and Christmas Island, Kiribati (Schoonmaker et al. 1985), in which evaporitic mineral formation is an important process.

3.1.2 Sediment-Pore-Water Model

The sediment-pore-water system of Mangrove Lake lends itself nicely to development of a quantitative model documenting reactions in the system. Chemical reactions, other than those involving carbon and sulfur biogeochemical cycling, are quantitatively unimportant, and the sediments are nearly a one-component system of highly labile organic matter. The pore-water profiles obtained from the sediments show that the vertical distribution of dissolved constituents is controlled to a significant degree by geochemical reactions involving organic matter degradation owing to bacterially mediated sulfate reduction.

The model described here was first presented by Roland Wollast at the 10th International Symposium on "Chemistry of the Mediterranean Sea" held at Primosten, Yugoslavia, in May 1988. The model is an extension of the work of Ben Yaakov (1973) and Leeper (1975) and quantitatively describes the process of organic matter degradation because of sulfate reduction in a closed geochemical system. Given the distribution of sulfur-oxidizing bacteria overlying sulfate-reducing bacteria in the sediments of Mangrove Lake described previously, the sediment-pore-water system of this lake is almost certainly closed with regard to sulfur species. The reaction describing the overall driving force is

$$2CH_2O + SO_4^{2-} \rightarrow 2HCO_3^- + H_2S. \quad (1)$$

Thus, the respiration of one mole of organic carbon produces one mole of dissolved inorganic carbon and correspondingly one equivalent of alkalinity in the ambient pore water. The distribution of the dissolved inorganic carbon, sulfur, and boron species is controlled by the following equilibrium conditions:

$$H_2CO_3 = HCO_3^- + H^+ \quad (2)$$

$$HCO_3^- = CO_3^{2-} + H^+ \quad (3)$$

$$H_2S = HS^- + H^+ \quad (4)$$

$$H_2O + H_3BO_3 = B(OH)_4^- + H^+ \quad (5)$$

In this system there are eight variables interrelated by the above four equilibrium equations, plus four other mass-balance constraints:

$$B_T = B_T^\circ \quad (6)$$

$$C_T = C_T^\circ + x \quad (7)$$

$$A_T = A_T^\circ + x \quad (8)$$

$$S_T = \frac{x}{2} \quad (9)$$

where B_T is the total concentration of borate; C_T is the total concentration of inorganic carbon; A_T is the total alkalinity; S_T is the total concentration of reduced sulfur species; and x is the number of organic carbon atoms degraded per unit volume of pore water.

The superscript ° denotes the initial values of the concentration of aqueous species in the original entrapped seawater. This system leads to an equation of sixth order with regard to a_H+, which can be easily solved numerically. Thus, it is possible to describe the evolution of the composition of the interstitial waters during the sulfate-reduction process if the geochemical system is nearly closed.

The model may be improved by taking into account the influence of organic nitrogen, which is released as ammonia during organic matter decomposition under anaerobic conditions according to

$$53SO_4^{2-} + C_{106}H_{260}O_{106}N_{16} \rightarrow 106HCO_3^- + 16NH_3 + 53H_2S. \quad (10)$$

Under pH conditions encountered in pore waters, NH_3 is predominantly present as NH_4^+, and the alkalinity increase of the system is further augmented by the reaction

$$NH_3 + H_2O \rightarrow NH_4^+ + OH^- \quad (11)$$

Thus, for an increase of one unit of inorganic carbon added to the system by the degradation of organic matter whose composition has a typical

Redfield ratio C/N of 6.6, the corresponding increase in alkalinity will be 1.15. In the case of Mangrove Lake sediments, the C/N ratio as determined by Hatcher et al. (1982) is equal to 12; thus, the relative increase of alkalinity will be 1.08. We have used this ratio in our model calculations.

The results of the model calculations are shown in Figs. 2–6. The good correlation between measured total alkalinity and total dissolved inorganic carbon is shown in Fig. 2. The fact that the model calculation (straight line) fits the data well indicates that the choice of a C/N ratio of 12 for the decomposing organic matter is reasonable. Furthermore, the C/N ratio of 12, as measured by Hatcher et al. (1982), is that predicted from the relationship between observed total alkalinity and total dissolved inorganic carbon (see also Hatcher et al. 1982).

Figure 3 shows that the increase of total alkalinity is linearly related to the production of total sulfide in the pore waters of Mangrove Lake sapropel. The measured values, although somewhat scattered at high concentrations, fall reasonably close to the linear relation predicted by the model. This correlation further substantiates the assumption of a nearly closed geochemical system as a good approximation. Also, in areas of high sedimentation rates, such as Mangrove Lake, the assumption of a nearly closed sediment-pore-water system is valid in many cases (Berner 1980).

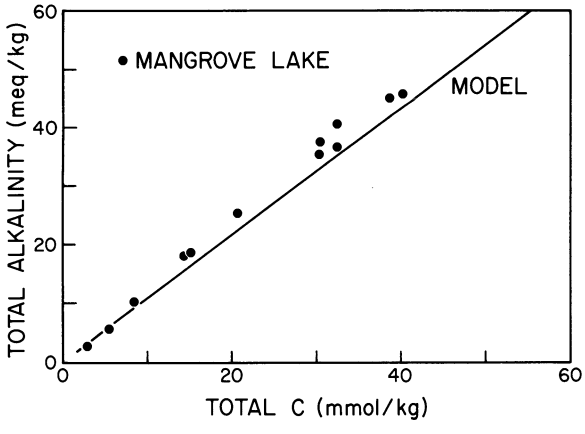


Fig. 2. Relationship between total alkalinity and total dissolved carbon determined from model calculations and pore-water analyses in Mangrove Lake. The close agreement between the model calculations (*line*) and the pore-water analyses (*filled circles*) indicates that the C:N ratio of decomposing organic matter assumed to be close to 12 for model calculations is correct

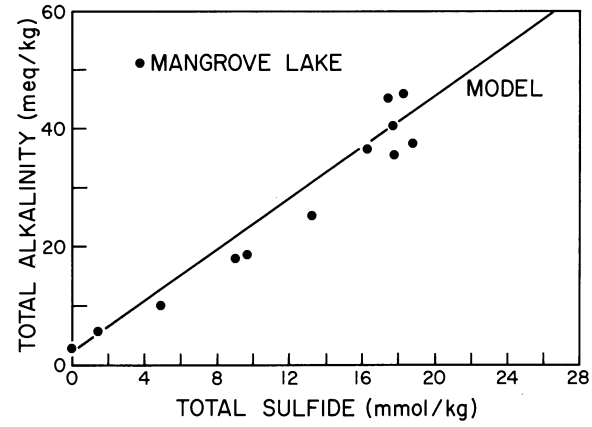


Fig. 3. Relationship between total alkalinity and total reduced sulfur determined from model calculations (*line*) and pore-water analyses in Mangrove Lake (*filled circles*). Pore-water values of total alkalinty and reduced sulfur agree well with the linear relationship predicted from model substantiating the assumption that these sediments can be considered a closed geochemical system

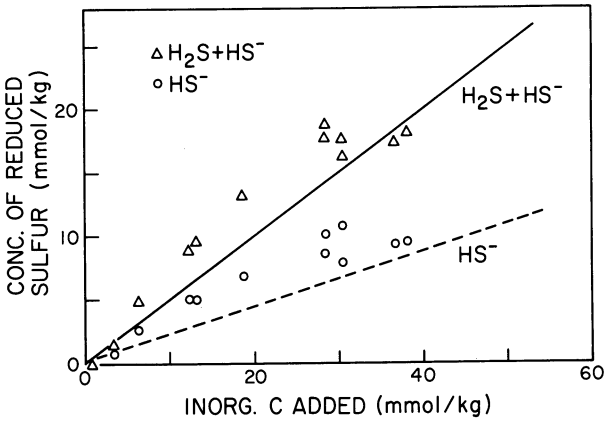


Fig. 4. Distribution of reduced sulfur species in relation to inorganic carbon dissolved in pore waters. Results of model calculations for $H_2S + HS^-$ are shown (*solid line*) and model calculated HS^- concentrations are shown (*dotted line*). Model calculations predict that HS^- and H_2S should be equally abundant in pore waters, and model results compare well with results of pore-water analyses from Mangrove Lake

The speciation of the reduced sulfur species in Mangrove Lake sediment pore waters is also described satisfactorily by the model, as shown in Fig. 4. The model predicts that HS^- and H_2S species should be equally abundant in pore waters. The measured values, although somewhat scattered, follow the trends obtained from the model calculations. It appears that the reduced

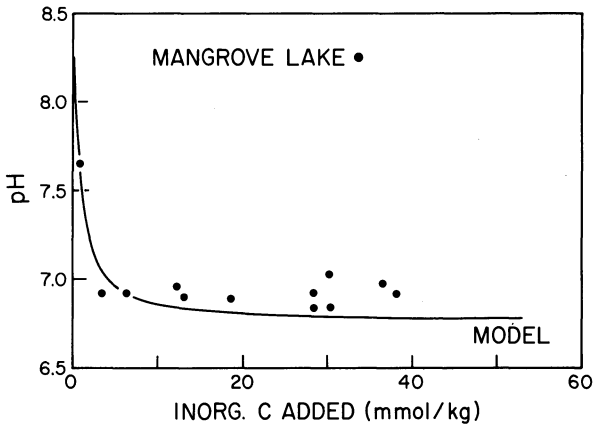


Fig. 5. Model calculations (*line*) show that pore waters of Mangrove Lake should be buffered at pH = 7. The pH measured in pore waters of Mangrove Lake (*filled circles*) agree well with model calculations

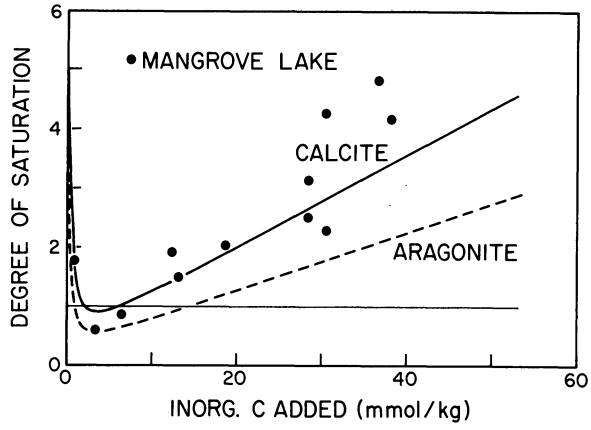


Fig. 6. Effect of the degree of organic matter decomposition on calcite (*line*) and aragonite (*dotted line*) saturation state. Results of model calculation are compared with calculations based on pore-water analyses (*filled circles*) from Mangrove Lake. Pore waters initially become undersaturated with regard to carbonate minerals, due to the production of carbonic acid and HS^- during sulfate reduction of organic matter. Deeper in the sediments pore waters become oversaturated with regard to these minerals, due to the pH buffering of the sulfur system and increased pore-water alkalinity

sulfur system rapidly buffers pore waters to a pH close to 6.9 (Fig. 5). This pH is that predicted from the reaction

$$H_2S = H^+ + HS^-, \quad (12)$$

and is in accord with the accepted value of the equilibrium constant of approximately 7 for Eq. (12) (Stumm and Morgan 1981).

The role of sulfate reduction in precipitation, and recently, dissolution, of calcium carbonate in sediment-pore-water systems has been discussed in the literature (e.g., Ben Yaakov 1973; Leeper 1975; Mackenzie et al. 1981; Morse et al. 1985; Walter 1986; Morse and Mackenzie 1990). Few systems have been investigated in which the sediment is nearly pure organic matter, however, and geochemical reactions are not complicated by moderate-to-abundant siliciclastic or carbonate detritus. The lack of iron in the sediments is especially important, because there is little chance for an iron sulfide mineral to precipitate. The precipitation of such a phase complicates the model calculations including those of pore-water saturation state.

We calculated the degree of saturation of Mangrove Lake sediment pore waters with regard to calcite and aragonite as a function of the degree of degradation of organic matter. The model results and calculations of saturation state based on pore-water chemical analyses (Fig. 6) show that initially the system becomes rapidly undersaturated with regard to both minerals, because of the decrease in pH owing to production of carbonic acid and hydrogen sulfide species. Thus, some calcite, and to a larger extent aragonite and magnesian calcites, could dissolve during the initial stage of sulfate reduction.

During a second phase, corresponding to the deeper parts of the sediment column where sulfate reduction is more complete, the pore waters again become oversaturated with regard to carbonate minerals, because of the invariant pH imposed by reactions involving the sulfur system and the increase of alkalinity. It must be emphasized that the degree of oversaturation remains relatively moderate and is not necessarily high enough to promote the precipitation of calcium carbonate phases in pore waters. The degree of saturation of pore waters with regard to calcium carbonate is very sensitive to the C/N ratio of the organic matter undergoing decomposition.

The observations and modeling of the carbonate saturation state of the pore waters of Mangrove Lake sediments demonstrate unequivocally that organic decomposition by sulfate reduction can lead in the early stages of the reaction to waters undersaturated with regard to carbonate minerals. In some interstitial water environments, carbonate phases may dissolve, and components of the dissolution may be released to overlying marine waters by diffusional or advective processes. This early diagenetic dissolution reaction, and that

related to aerobic oxidation of organic matter (e.g., Moulin et al. 1985) in shallow-water (reef-bank-shelf), carbonate-bearing marine sediments, may account for approximatey 10% of the total carbonate production of this environment (Morse and Mackenzie 1990; Sabine and Mackenzie 1991).

3.2 Solar Lake, Sinai

In contrast to the sapropelic sediments found in Mangrove Lake and some other marine lakes, stromatolitic cyanobacterial mats are characteristic of lake sediments located in more arid regions. These sediments, although they have high organic carbon contents, are commonly complex deposits of evaporitic mineral salts and biogenically produced minerals. The most comprehensively studied example of this type of sediment is that from Solar Lake.

Solar Lake is a small (140 × 50 m), shallow (4–6 m deep) lake located on the Sinai Peninsula. The lake formed from a coastal lagoon, which became closed off from direct contact with the Gulf of Elat approximately 2400 years ago, as a bar formed across the mouth of the lagoon (Cohen et al. 1977a). Seawater presently enters the lake via seepage through this bar. Evaporation rates in the area are extremely high throughout the year, and hence, the waters of the lake are hypersaline. The lake remains stratified throughout most of the year with holomixis occurring for only a few weeks during the summer. During holomixis the salinity is highest (160 psu), and temperatures are typically approximately 27 °C. During stratification, surface salinities vary between 65 and 100 psu, with temperatures between 15–20 °C. At a depth of approximately 2–3 m, the temperature increases to approximately 60 °C, decreasing toward the bottom to 40 °C. Salinities below the thermocline increase from approximately 100 to 160–180 psu with increasing lake depth. Primary productivity in the lake is extremely high, particularly during periods of stratification (Cohen et al. 1977b).

Sediment composition and diagenesis reflect the seasonal and depth-related changes in the water-column characteristics described previously. Colonies of cyanobacteria dominate surface sediments throughout the lake, and in the shallower areas of the lake, bacterial reactions dominate the diagenetic processes. As the lake becomes deeper, bacterial reactions become less important and evaporitic precipitation of minerals increases in importance. Krumbein et al. (1977) described four sediment types within the lake in terms of cyanobacterial mat morphology:

1. Flat shallow-water mat. This mat extends from the lake edge to 1.25 m of depth and consists of well-defined seasonal laminations of different associations of both autotrophic and heterotrophic bacteria and diatoms. Below a depth of approximately 3–5 cm in this mat, there are layers of carbonates intercalated with layers of high organic content. The mat itself is approximately 1 m thick and overlies a gypsum layer that was deposited during an evaporitic event when the lake was in the lagoonal stage of its development.
2. Pinnacle mat. This mat lies at a depth between approximately 1.0–2.5 m in the lake and is an irregularly shaped, loose mat composed of diatoms and coccoid cyanobacteria. There is some gypsum precipitation within this mat that occurred at the onset of stratification.
3. Cyanobacterial and photosynthetic bacterial films. The deeper slope of the lake (between 2.5 and 4.5 m) is covered by a crust composed predominantly of gypsum and carbonate. Thin bacterial films grow on this crust and are preserved within the gypsum and carbonate deposits during diagenesis.
4. Flocculus cyanobacterial mat. Below a depth of approximately 4 m in the lake, the cyanobacteria form a flocculent layer on top of precipitated carbonates and gypsum.

Organic matter diagenesis has been most comprehensively studied in the shallow-water mat. Photosynthesis in the top layers of this mat produces on average of $10\,g\,C\,m^{-2}\,day^{-1}$ (Krumbein et al. 1977). Depth profiles show that the organic carbon content of the mat decreases from 15% dry weight in the top 10 cm to 3% at a depth of 80 cm, and the calcium carbonate content of the sediment increases from less than 10% in the top 10 cm of the mat to 80% at a depth of 80 cm (Krumbein et al. 1977). There is also no calcium carbonate between the surface and a depth of approximately 3–5 cm in the mat (Krumbein et al. 1977). Concomitant with these changes, it is observed that the pore-water concentrations of calcium, sulfate, and strontium are all depleted relative to chloride in the top 25 cm of the sediment-pore-water system (Fig. 7). The

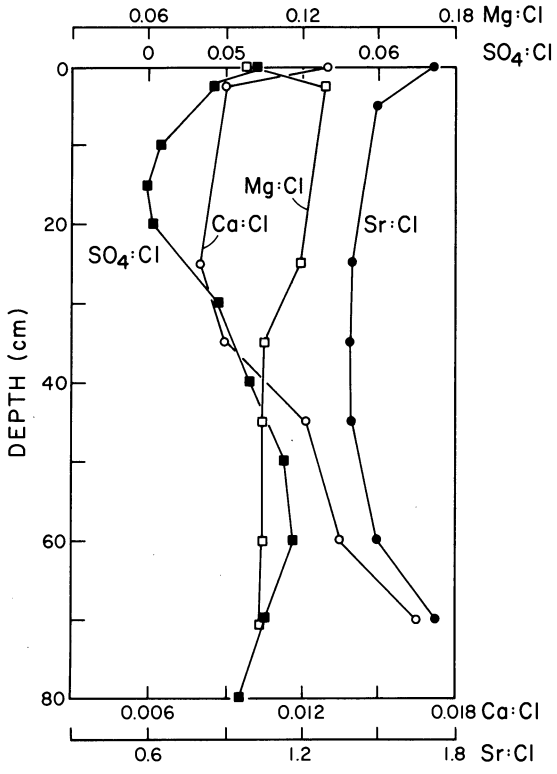


Fig. 7. Pore-water gradients of ratios of major reactive ions with regard to chloride in Solar Lake. The SO_4:Cl ratio (*filled squares*) is that reported by Krumbein et al. (1977), and Mg:Cl (*open squares*), Ca:Cl (*open circles*) and Sr:Cl (*filled circles*) ratios are taken from Lyons et al. (1984). The decrease in calcium, sulfate and strontium relative to chloride are interpreted as indicating carbonate precipitation during sulfate reduction of organic matter in the sediments

concentration of magnesium, however, increases downward in the pore waters relative to the chloride concentration (Lyons et al. 1984). These changes, taken in association with the extremely high rates of sulfate reduction (>100 nmol C m^{-2} day^{-1} in the upper 10 cm of mat, Jorgensen and Cohen 1977), have been interpreted as indicative of carbonate precipitation owing to sulfate reduction and organic matter oxidation (Krumbein et al. 1977; Lyons et al. 1984). Krumbein et al. (1977) also showed SEM evidence of aragonite crystals precipitating on bacteria within the sediments. Lyons et al. (1984) and Krumbein et al. (1977) calculated that less than 1% of the fixed carbon in the mat is converted to $CaCO_3$; thus, 99% of the carbon produced in these sediments is preserved.

Gypsum precipitation within this shallow mat could possibly occur during the period of summer overturn, when the salinity of the surface waters of the lake is greater than 125 psu. However, no gypsum is found preserved in the mat. It appears that the activity of sulfate-reducing bacteria, both in using sulfate to oxidize organic matter and calcium to produce $CaCO_3$, results in undersaturation of pore waters with regard to gypsum.

As the cyanobacterial associations become less structured with depth in the lake, a greater proportion of authigenically precipitated carbonate and gypsum is found in the sediments (Krumbein et al. 1977). Two factors are responsible for this observation: Firstly, the salinity of the overlying water is always high enough to allow evaporitic precipitation of these minerals (Cohen et al. 1977a). Secondly, the conditions of low light and high sulfide concentrations throughout most of the year are extreme conditions for bacterial production, although the species inhabiting this area of the lake can switch from oxygenic to anoxygenic photosynthesis (Krumbein et al. 1977). In the bottom of the lake decomposing organic matter contributes only 4% of the total accumulation rate of sedimentary material.

4 Conclusions

Marine saline lakes vary considerably in their overall characteristics. Few comprehensive studies of these systems are available; however, some general conclusions can be made concerning the biogeochemical processes operating in these systems.

The physical and chemical limnological features of these lakes are strongly affected by the water balance, and therefore, climatic setting of the lake and hydrology of the system. Because of high evaporation rates, some lake waters become hypersaline and may reach saturation with regard to evaporite minerals. Other lakes, located in less arid environments, have water compositions more like that of seawater. Overall, however, the relative proportions of major ions which comprise the waters of marine lakes are very close to those found in seawater (Na- and Cl-dominated), rather than freshwater or evaporitic freshwater systems (Ca- and HCO_3-dominated).

Pore water exchange, particularly when coupled with seasonal climatic changes, can lead to development of stratification within these systems. In some cases water exchange may be slow enough that the hypolimnion may become anoxic. Stratified, hypersaline systems tend to develop a

hypolimnion that is warmer than the epilimnion by up to 50 °C.

Climate and the hydrology of a lake strongly dictate its floral and faunal composition. The biota of lakes found in dry climatic regions is dominated by prokaryotic organisms. Lakes in more temperate regions, provided they are well mixed, have biotic communities more like those found in adjacent coastal marine environments. In all documented cases the benthic biota is dominated by prokaryotic organisms regardless of the physical and chemical properties of the overlying waters in the lake.

Sediment geochemistry in Mangrove Lake, a well-mixed lake located in a temperate environment, was compared with Solar Lake, a hypersaline lake. In both systems bacterial degradation of organic matter is a dominant process. The sediments of Mangrove Lake are unique in that they are composed of an organic-rich sapropel that does not contain significant quantities of siliciclastic or carbonate detritus. Results from pore-water analyses and a sediment-pore-water model suggest that bacterial decomposition of organic matter via sulfate reduction can initially lead to undersaturation of pore waters with regard to carbonate minerals. With continued degradation of organic matter, however, pore waters become oversaturated with respect to carbonate minerals.

In Solar Lake the salinity of pore waters is sufficiently high such that they are oversaturated with regard to both carbonate minerals and gypsum. However, no evidence of gypsum precipitation has been found in the stromatolitic mats that exist in the shallow areas of the lake. In fact, it would appear that sulfate-reducing bacteria in the mats remove sufficient sulfate from pore waters such that gypsum saturation is not reached. There is also evidence that reactions involving these organisms result in precipitation of aragonite in the sediments. With increasing depth in the lake, conditions are such that bacterial production is reduced, and thus, there is an increasing proportion of evaporitically precipitated minerals in the sediments.

Acknowledgments. We especially thank all the students in the course "Biogeochemical Cycling Processes in Coastal Carbonate-Organic Systems" given at the Bermuda Biological Station for Research in 1987 and 1988 for their active participation in the Mangrove Lake studies. Research was partly supported by NSF EAR8816350; School of Ocean and Earth Science and Technology Contribution No. 3468.

References

Ben Yaakov S (1973) pH buffering of pore water of recent anoxic marine sediments. Limnol Oceanogr 18:86–94

Berner RA (1980) Early diagenesis: a theoretical approach. University Press, Princeton, 241 pp

Boudreau BP, Canfield DE, Mucci A (1992) Early diagenesis in a marine sapropel, Mangrove Lake, Bermuda. Limnol Oceanogr 37:1738–1753

Bunn SE, Edward DHD (1984) Seasonal meromixis in three hypersaline lakes on Rottnest Island, Western Australia. Aust J Mar Freshwater Res 35:261–265

Burke CM, Knott B (1989) Limnology of four groundwater fed saline lakes in south-western Australia. Aust J Mar Freshwater Res 40:55–68

Burnett WC, Landing WM, Lyons WB, Orem W (1989) Jellyfish Lake, Palau: a model anoxic environment for geochemical studies. EOS 70:777–783

Cohen Y, Krumbein WE, Goldberg M, Shilo M (1977a) Solar Lake (Sinai). 1. Physical and chemical limnology. Limnol Oceanogr 22(4):597–608

Cohen Y, Krumbein WE, Shilo M (1977b) Solar Lake (Sinai). 2. Distribution of photosynthetic microorganisms and primary production. Limnol Oceanogr 22(4):609–620

Cohen Y, Krumbein WE, Shilo M (1977c) Solar Lake (Sinai). 3. Bacterial distribution and production. Limnol Oceanogr 22(4):621–634

Drever JL (1982) The geochemistry of natural waters. Prentice Hall, Englewood Cliffs, 388 pp

Edward DHD (1983) Inland waters of Rottnest Island. J R Soc West Aust 66:41–47

Friedman GM, Foner HA (1982) pH and Eh changes in sea-marginal algal pools of the Red Sea: and their effect on carbonate precipitation. J Sediment Petrol 52(1):41–46

Friedman GM, Ameil AJ, Braun M, Miller DS (1973) Generation of carbonate particles and laminites in algal mats – example from sea-marginal hypersaline pool, Gulf of Aqaba, Red Sea. Am Assoc Pet Geol Bull 57(3):541–557

Gat JR, Levy Y (1978) Isotope hydrology of inland sabkhas in the Bardawil area, Sinai. Limnol Oceanogr 23(5):841–850

Gregor CB, Garrets RM, Mackenzie FT, Maynard JB (1988) Chemical cycles in the evolution of the earth. John Wiley and Sons, New York, 276 pp

Hamner WM, Gilmer RW, Hamner PP (1982) The physical, chemical and biological characteristics of a stratified, saline, sulfide lake in Palau. Limnol Oceanogr 27(5):896–909

Hatcher PG (1978) The organic geochemistry of Mangrove Lake, Bermuda. NOAA Prof Pap 10:92 pp

Hatcher PG, Simoneit BRT, Mackenzie FT, Neumann AC, Thorstenson DC, Gerchakov SM (1982) Organic geochemistry and pore water chemistry of

sediments from Mangrove Lake, Bermuda. Org Geochem 4:93–112
Hatcher PG, Spiker EC, Szeverenyi NM, Maciel GE (1983) Selective preservation and origin of petroleum forming aquatic kerogen. Nature 305:498–501
Jorgensen BB, Cohen Y (1977) Solar Lake (Sinai). 5. The sulfur cycle of the benthic cyanobacterial mats. Limnol Oceanogr 22(4):657–666
Krumbein WE, Cohen Y, Shilo M (1977) Solar Lake (Sinai). 4. Stromatolytic cyanobacterial mats. Limnol Oceanogr 22(4):635–656
Kushnir J (1981) Formation and early diagenesis of varved evaporite sediments in a coastal hypersaline pool. J Sed Petrol 51(4):1193–1203
Leeper RHJ (1975) Effect of organic decomposition on early diagenesis in anoxic marine sediments. PhD Diss, Southern Methodist University, Dallas
Levy Y (1974) Sedimentary reflection of depositional environment in the Bardawil Lagoon, northern Sinai. J Sediment Petrol 44(1):219–227
Levy Y (1977a) The origin and evolution of brine in the coastal sabkhas, northern Sinai. J Sediment Petrol 47(1):451–462
Levy Y (1977b) Description and mode of formation of the supratidal evaporite facies in northern Sinai coastal plain. J Sediment Petrol 47(1):463–474
Lyons WB, Long DT, Hines ME, Gaudette HE, Armstrong PB (1984) Calcification of cyanobacterial mats in Solar Lake, Sinai. Geology 12:623–626
Mackenzie FT, Ristvet BL, Thorstenson DC, Lerman A, Leeper RH (1981) Reverse weathering and chemical mass balance in a coastal environment. In: Marten JM, Burton JD, Eisma D (eds) River inputs to coastal systems. UNER and UNESCO, Switzerland, pp 152–187
Morse JW, Mackenzie FT (1990) Geochemistry of sedimentary carbonates. Elsevier, New York
Morse JW, Zullig JJ, Bernstein LD, Millero FJ, Milne P, Mucci A, Choppin GR (1985) Chemistry of calcim carbonate rich shallow water sediments in the Bahamas. Am J Sci 285:147–185
Moulin E, Jordens A, Wollast R (1985) Influence of the aerobic bacterial respiration on the early dissolution of carbonates in coastal sediments. Proc Progress in Belgian Oceanographic Research, Brussels, pp 196–208
Neumann AC (1969) Quaternary sea-level data from Bermuda. Resume Commun, VIII Congr, INQUA, Paris, pp 281–229
Orem WH, Hatcher PG, Spiker EC, Szeverenyi NM, Maciel GE (1986) Dissolved organic matter in anoxic porewaters from Mangrove Lake, Bermuda. Geochemica et Cosmochimica Acta 50:609–618
Playford PE (1983) Geological research on Rottnest Island. J R Soc West Aust 66(1, 2):10–15
Sabine C, Mackenzie FT (1991) Oceanic sinks for anthropogenic CO_2. Int J Energy Environ Econ 1(2):119–127
Schoonmaker J, Tribble GW, Smith SV, Mackenzie FT (1985) Geochemistry of saline ponds, Kiritimati (Republic of Kiribati) Proc 5th Int Coral Reef Congr, Tahiti 3:439–444
Sharma P, Mackenzie FT, Wollast R, Teiser M (1988) Biological cycling of carbon and sulfur in Mangrove Lake, Bermuda. Int Phycotalk Symp, Varanasi, India 28–29
Stolz JF (1990) The ecology of phototrophic bacteria. In: Stolz JF (ed) The structure of phototrophic procaryotes, CRC Press, Boca Raton
Stumm WE, Morgan JJ (1981) Aquatic chemistry. An introduction emphasing chemical equilibria in natural water, 2nd edn. John Wiley and Sons, New York, 780 pp
UNESCO Technical Papers in Marine Science (1981) No 36, Paris
Walter LM (1986) Relative efficiency of carbonate dissolution and precipitation during diagenesis: a progress report on the role of solution chemistry. In: Goutier DL (ed) Roles of organic matter in mineral diagenesis. Soc Econ Paleontol Mineral Spec Publ 38:1–12
Warren JK (1982) The hydrological setting, occurrence and significance of gypsum in late Quaternary salt lakes in South Australia. Sedimentology 29(5): 609–637

10 Organic Matter Accumulation Records in Lake Sediments

P.A. MEYERS[1] and R. ISHIWATARI[2]

1 Introduction

The organic-matter content of lake sediments provides information that is important to studies of lacustrine paleoenvironments, the history of climate change, and the effects of humans on local and regional ecosystems. Sediment organic matter yields a record of its sources from biota of the past in its elemental, isotopic, and molecular composition. The types and amounts of alterations that occur to the original contributions of organic matter during and after incorporation into sediments indicate much about the former physical and geochemical environments of lakes. Organic geochemical investigation of the sources and alterations of organic matter in lake sediments is consequently significant to a multitude of disciplines.

Organic matter constitutes a minor, but important, fraction of lake sediments. It is made up of a complex mixture of lipids, carbohydrates, proteins, and other biochemicals that originate from the living tissues of benthic microorganisms, and from the remains of organisms formerly living in the lake and its watershed. Humic substances are diagenetically formed from these biochemical-starting materials and constitute the major part of the complex mixture of organic materials. Studies of the composition of sediment organic matter are fundamental to defining the nutritional value, the redox potential, and the paleoenvironmental information contained in this material. The effects of microbial alteration and selective degradation of organic-matter constituents before they become part of the permanent sediment record are particularly important.

[1] Department of Geological Sciences and Center for Great Lakes and Aquatic Science, University of Michigan, C.C. Little Building, Ann Arbor, MI 48109-1063, USA
[2] Department of Chemistry, Tokyo Metropolitan University, Hachioji-shi, Tokyo, Japan

1.1 Significance of Organic Matter in Lake Sediments

Organic matter forms part of the paleolimnological record preserved in lake sediments. The different types of biota populating a lake and its watershed produce organic matter having distinctive biochemical compositions. Changes in the community structure of these biota create variations in the amounts and types of organic matter deposited at different times in the history of a lake. During the process of deposition in the lake bottom, organic matter is subject to microbial reworking, with the result that its original composition becomes altered. The degree of alteration provides still more information about past lake environments, particularly the amount of water-column mixing that occurred during sediment deposition. Information about these types constitutes part of the records of regional and continental paleoclimates, and studies of the organic-matter compositions of the sediments of lakes from different parts of the world have been important in reconstructing these records.

The organic-matter content of lake sediments participates in a variety of biochemical and geochemical processes. Benthic animals and microbes depend on organic matter for their nutrition. Because many components of organic matter are relatively easily oxidized forms of reduced carbon, the dissolved oxygen concentration of sediment-pore water is controlled largely by the availability of oxidizable organic matter below the sediment/water interface. Furthermore, redox reactions, in which oxidized inorganic species become reduced by interaction with organic matter, are common in sediments. Organic matter is consequently a dynamic biogeochemical component of sediments that influences both living and nonlivng processes in lake bottoms.

Organic-carbon-rich rocks that originate from sediments deposited in ancient lakes are increasingly being recognized as important sources of

petroleum. As examples, Triassic rocks in China, Cretaceous rocks in Brazil, and the Eocene Green River Formation of North America are recognized lacustrine oil-source rocks. A practical application of the study of organic matter in lake sediments is that an understanding of the processes involved in the deposition of modern sediments rich in organic carbon is useful in oil exploration.

1.2 Origins of Organic Matter to Lake Sediments

The primary source of organic matter to lake sediments is from the particulate detritus of plants that have lived in the lake waters and on the surrounding land. The sources of organic matter to lacustrine sediments and the processes modifying it during incorporation into sediments are summarized in Fig. 1. Nearly all organic matter originates from plants; less than 10% comes from animals. Plants can be divided into two geochemically significant groups on the basis of biochemical compositions: (a) nonvascular plants that lack woody and cellulosic tissues such as simple algae, and (b) vascular plants that have these tissues such as grasses, shrubs, and trees. These latter types of plants exist on land and in the shallow parts of lakes as bottom-rooted, emergent vegetation. The relative contributions from these two plant groups is influenced strongly by lake morphology, watershed topography, and the relative abundances of lake and watershed plants. Organic matter in lake sediments covers the spectrum of being predominantly algal in some lakes to being largely land-derived in others.

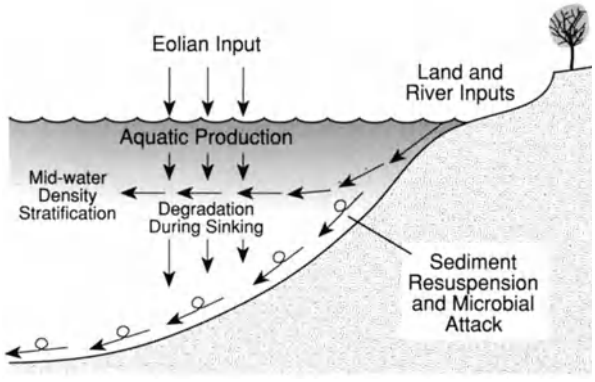


Fig. 1. Representation of the sources of organic matter to lake sediments and of the processes acting to alter and degrade organic matter during its sedimentation. Organic matter from algal production within a lake and from plants within the watershed are the major sources. Airborne material can originate from outside the watershed and is normally a minor contribution. Suspended particles congregate at midwater thermal discontinuities and can be advected laterally. Resuspension and downslope transport moves sediments from shallow locations to basinal depths. Microbial reprocessing of organic matter occurs in the water and in the lake bottom, diminishing the total amount and substituting microbial contributions for original components

Bacteria and other microbes in the water and sediment of lakes, as well as the soil of the lake watershed, continually rework and degrade aquatic and land-derived organic matter. Although some bacteria are capable of photo- or chemosynthesis, lake environments generally contain enough organic matter so that the dominant role of bacteria is the heterotrophic decomposition of organic detritus. An important exception exists in strongly stratified lakes where bacterial can become major producers of primary organic matter. Bacteria biosynthesize characteristic forms of organic matter while breaking down the preformed material remaining from the plants and animals of the lake and watershed.

In addition to these local sources of organic matter, winds commonly transport material, such as pollen, from sources outside the local watershed. The eolian component is typically a small fraction of the total organic mixture, yet it can contain distinctive components potentially useful to paleolimnological and paleoclimatological studies.

An estimate of the sources of organic-matter sources to Lake Michigan, a large oligotrophic freshwater lake, gives an example of the relative contributions from different origins. Approximately 90% of the organic carbon in the waters of the lake originates from algal production, 5% is carried to the lake by rivers, and 5% is brought in with airborne particles and precipitation (Andren and Strand 1981). These contributions of organic matter are subject to selective degradation as they sink to the lake bottom, and therefore the initial source proportions are seldom preserved intact in the sediment record.

1.3 Alterations of Organic Matter During Deposition

A variety of processes act to alter the character of organic matter in the relatively short time between

its origin and its burial in a lake bottom. Foremost among the processes is its degradation during sinking. Sediment-trap studies in Lake Michigan show that only 6% of the organic carbon photosynthetically formed in the surface water of the southern part of this lake reaches the sediment surface 100 m below (Table 1). Nearly 85% of the carbon is oxidized before leaving the epilimnion, the part of the water column above the thermocline (Eadie et al. 1984). The decrease found in the organic-carbon concentration of sinking particles at a location in the center of southern Lake Michigan is illustrated in Fig. 2. Bottom sediments contain less than 10% of the organic-carbon content of surface particulate matter (Meyers and Eadie 1993). In more shallow depths organic matter would have shorter sinking times and consequently shorter exposures to oxidation in the water column. Shallow-water lakes consequently usually have sediments richer in organic matter than that found in deep lakes such as the Laurentian Great Lakes.

Table 1. An estimate of organic-carbon fluxes in Lake Michigan that illustrates the magnitude of organic matter recycling within lacustrine systems

Element of carbon cycle	Flux (g C_{org}/m^2/year)
Primary production	139
Oxidation in epilimnion	−115
Sinking into hypolimnion	24
Oxidation in hypolimnion	−16
Sinking to sediment surface	8
Resuspension into hypolimnion	75

Data are from sediment-trap studies described by Eadie et al. (1984) and assume a 100-m-deep water column.

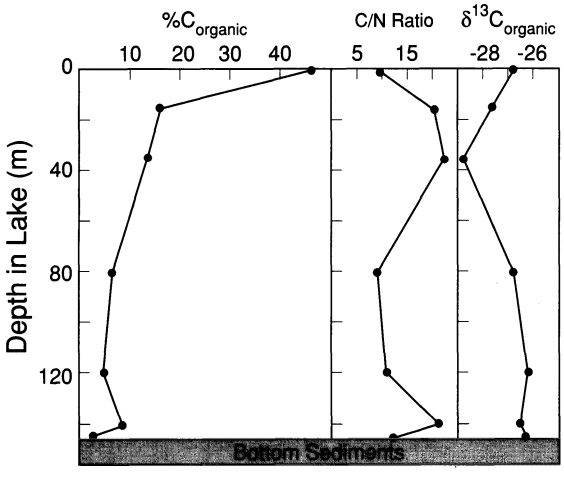


Fig. 2. Organic-carbon concentrations, atomic C/N ratios, and carbon isotopic signatures in phytoplankton, sediment traps at five depths, and surficial sediments in Lake Michigan. Organic-carbon concentrations decrease by a factor of ten, but C/N and isotopic ratios are virtually unchanged between phytoplankton and sediment values. (Meyers and Eadie 1993)

Organic matter continues to be subjected to oxidative alteration and destruction on the lake bottom. Resuspension of sedimented organic matter can be substantial (e.g., 75 g C_{org}/m^2/y at a depth of 100 m in Lake Michigan [Table 1], or nearly ten times the annual flux of organic carbon to the bottom [Eadie et al. 1984; Meyers et al. 1984a; Meyers and Eadie 1993]). Organic matter so resuspended is reexposed to microbial oxidation in the water column. Resuspension is usually greater in large, well-mixed lakes than in small lakes.

Bioturbation, or biological mixing, of surface sediments also prolongs the exposure of organic matter to oxidation and adds to this the degradation due to the nutritional needs of benthic fauna. The depth of bioturbation in the Great Lakes, as an example, averages approximately 10 cm (Robbins and Edgington 1975). Compared to marine studies (Cobler and Dymond 1980), approximately 75% of the organic carbon reaching the surface of bottom sediments is destroyed in the bioturbated layer. Where seasonal or permanent anoxic bottom-water conditions exist, bioturbation is diminished or absent, because benthic animals require dissolved oxygen for respiration. Many temperate-zone lakes experience periods of anoxia during summer thermal stratification, and the sediments of these lakes typically have higher concentrations of organic matter than do permanently oxygenated lakes. Varved sediments particularly indicate little or no resuspension and the absence of bioturbation.

Organic matter is subject to alterations by anaerobic bacteria after burial below the zone of bioturbation. The waters of most lakes contain insufficient dissolved sulfate to make sulfate reduction an important process. Instead, methanogenic bacteria continue degradational processes if the sedimented organic matter contains a sufficient fraction of labile materials to sustain microbial activity. Johnson et al. (1982) surveyed the resulting downcore decrease in organic-carbon concentrations of Lake Superior sendiments. They calculated a half-life of approximately 100

years for organic carbon in the bottom of this large oligotrophic lake.

Less reactive forms of organic matter become more dominant as the more reactive forms are utilized by microbes and by deposit-feeding animals. Components from aquatic sources are generally more sensitive to bacterial-degradative processes than are materials from land sources. Organic matter in lacustrine sediments consequently often have a large and relatively unreactive fraction of land-derived organic residues. Moreover, humic substances and lipids are less reactive than are amino compounds and carbohydrates, and become larger proportions of the organic matter with depth in sediments of Lakes Ontario, Erie, and Huron (Kemp and Johnston 1979). In heavily reworked sediment only the most resistant forms of the original organic mixture remain. Throughout this reprocessing residues of microbially synthesized organic matter are added to the mixture, some to be in turn modified or destroyed, but others to be preserved.

The final result of these multiple processes is that the overall composition of organic matter in sediments is often markedly different from that which is produced by the biota in and around the lake. Furthermore, the amount of organic matter buried in subsurface sediments is a small fraction of that originally introduced into the surface waters.

1.4 Similarities and Differences Between Organic Matter in Sediments of Lakes and Oceans

Sedimentary environments of lakes and oceans are for the most part similar, yet several important differences exist that impact the deposition of organic matter. These differences arise largely because of the contrasts in size and age between the basins of lakes and oceans. Lake basins, being smaller by far than deep ocean basins, receive proportionally more land-derived clastic sediment particles. The result of this is that sedimentation rates in lakes exceed significantly those of oceans, and organic matter is buried more rapidly. Land-derived nutrients accompany the sediments washed into lakes, enhancing lake fertility and aquatic production of organic matter. Lacustrine benthos are not as diverse as those of marine areas, and their depth of bioturbation is less than that of marine fauna. This further diminishes the exposure of organic matter to oxidation. Working against these factors, which enhance preservation of organic matter in lake sediments, is the large amount of turbulent mixing of bottom sediments found in shallow lakes. Turbulent resuspension can be very significant, even in lakes on the order of 100 m deep (e.g., Eadie et al. 1984), and it reexposes organic matter to oxidative processes.

Chemical differences between lakes and oceans ultimately affect organic matter in their sediments. Seawater is rarely devoid of dissolved oxygen, whereas the hypolimnion of most lakes becomes depleted of this atmospheric gas during periods of thermal stratification. The absence of dissolved oxygen impacts the rates and the types of organic matter degradation that can occur. Another difference is that dissolved sulfate is a major ion in seawater, but not in the water of most lakes. Sulfate reduction is an important aspect of the microbial reworking of marine organic matter. Sulfur becomes incorporated into organic matter during this process (e.g., Casagrande et al. 1977) during early diagenesis.

Age differences between ocean and lake basins affect the long-term character of organic matter in these settings. Ocean basins are on the order of hundreds of millions of years old, whereas few lakes are over 10 000 years old. Slow-acting diagenetic processes that become important in marine settings may not appear in younger lacustrine sediments. Because these differences are present, lake sediments generally contain more organic matter than deep-sea sediments. The organic-carbon concentration of lacustrine sediments is commonly several percent, whereas that of ocean sediments is typically a few tenths of a percent. Furthermore, the organic matter of lacustrine sediments typically has a larger land-derived contribution that most marine sediments.

Coastal marine sediments, unlike deep-sea deposits, have strong similarities to lake sediments. They accumulate in relatively shallow water, often receive large proportions of land-derived organic matter, are deposited relatively rapidly, and are geologically young because of the Wisconsin sea-level lowstand. A number of coastal marine basins were in fact freshwater lakes prior to being flooded by seawater as a consequence of the most recent postglacial sea-level rise. Studies of coastal marine sediments and of material from sediment traps deployed in coastal settings have provided important revelations about identification of sources and altera-

tions of organic matter. The results of many of these studies are applicable to lacustrine organic geochemical investigations.

1.5 Dating of Lake-Sediment Records

Lake sediments generally accumulate faster than marine sediments. As a consequence the ages of lake-sediment records are particularly suitable for determination from the decay of relatively short-lived radioisotopes. The two most common radioisotopes employed for this purpose are ^{210}Pb (half-life 22 years) and ^{14}C (half-life 5730 years). The times involved with very short-term sedimentary processes, such as seasonal events or sediment-settling times, are sometimes determined using ^{7}Be (half life 53 days). Radiocarbon ages of sediments are usually determined from their organic-carbon contents. Bulk organic matter in lake sediments typically contains some proportion of recycled detrital organic carbon, which commonly renders ^{14}C ages 1000–2000 years older than actual sediment ages (e.g., Stuiver 1975; Rea et al. 1980; Meyers and Horie 1993). Correction of core ages for the "old" organic matter is difficult, because it is unlikely that the amount of detrital carbon remains constant over time. For this reason it is preferable to determine radiocarbon ages from intact particles of organic matter or from the inorganic carbon contained in the carbonate shells of lake animals, but these materials are not always available.

The ages of lake sediments can also be approximated from evidence of historical events contained within sediment cores. Concentration maxima of long-lived radionuclides, such as ^{137}Cs, are one example. The major modern sources of ^{137}Cs are atomic bomb detonations and nuclear reactors. This radionuclide appears in sediment records starting *ca.* 1945, with peaks during the maximum of bomb testing in 1963–1964, and again in 1986 after the Chernobyl reactor accident (Robins and Edgington 1975; Wieland et al. 1993). Clear-cutting of forested watersheds is typically accompanied by changes in land plants, and therefore the types of pollen delivered to lake sediments. For example, ragweed (*Ambrosia*) proliferated in North America as European settlements pushed westward during the 1800s and cleared land for agriculture, and the *Ambrosia* horizon in lake sediments can be linked to the history of this land-use change. Some lakes contain layers of volcanic ash or tephra that can be related to dated volcanic eruptions. These various event markers are best used to corroborate sediment ages determined from radioactive decay records, rather than as independent age determinants.

2 Indicators of Sources and Alterations of Total Organic Matter in Lake Sediments

Lacustrine accumulations of sedimentary organic matter reflect both the types and amounts of materials from primary sources and the extent of alteration and degradation of the starting material. Lake systems are diverse, and sources and alterations of organic matter are typically variable geographically and temporally. Although the accumulation record of an individual lake is usually unique, studies of different lakes have produced generalizations about the factors influencing the organic-matter contents of lacustrine sediments.

2.1 Source Information Preserved in C/N Ratios of Sedimentary Organic Matter

Origin of organic matter from aquatic as opposed to land sources can be distinguished from the C/N ratios of organic matter in sediments. The presence or absence of cellulose in the plant sources of organic matter influences the sedimentary C/N ratios. Table 2 gives some C/N values of representative plants that contribute organic matter to lake sediments and provides examples of C/N ratios of lake sediments. Nonvascular aquatic plants have low C/N ratios, typically between 4 and 10, whereas vascular land plants, which contain cellulose, have C/N ratios of 20 and greater. Lakes for which the contribution of organic matter from vascular land plants is small relative to water-column production, exemplified by Walker Lake and Lake Michigan, show lower C/N ratios in their sediments than do lakes receiving important amounts of vascular plant debris such as Mangrove Lake and Lake Bosumtwi (Table 2). Ratios of 13–14 for surface sediments of the latter two lakes suggest a mixture of nonvascular and vascular contributions, which is expected for most lakes.

Selective degradation of organic-matter components during early diagenesis can modify elemental compositions, and hence C/N ratios of

organic matter in sediments. C/N ratios of modern wood samples are consistently higher than those of wood that had been buried in sediments (Table 2). A similar change, although much more subtle, accompanies deposition of organic matter. Settling particles in Lake Michigan have a C/N value of 9; the ratio in resuspended bottom sediments is 8. A decrease in C/N ratios has also been observed in soils (e.g., Sollins et al. 1984), where it involves the microbial immobilization of nitrogenous material accompanied by the remineralization of carbon. These changes in the elemental composition of sedimentary organic matter are not commonly large enough, however, to erase the original C/N difference between vascular and nonvascular plants.

Comparison of organic-matter C/N ratios of plankton, sediment-trap contents, and surficial sediment in Lake Michigan suggests that these bulk parameters retain source information, despite large decreases in the total amount of organic matter during sinking (Fig. 2). Although organic carbon concentrations diminish by a factor of ten between plankton and the lake bottom, little difference is evident between the initial and final C/N ratios. Considerable variation is evident, however, in the C/N values of sinking organic matter. These changes in organic-matter elemental composition agree with observed changes in biomarker compositions that show selective losses of algal components in the upper water column and apparent lateral input of algal organic matter at deeper depths (Meyers and Eadie 1993). These changes apparently reflect different diagenetic processes at different depths.

Burial in lake bottoms appears to stabilize

Table 2. Atomic C/N ratios of various plants that contribute organic matter to lake sediments and in sediments of different lakes

Type of sample	C/N	Reference
Land plants		
White oak wood, modern	276	Hedges et al. (1985)
White oak wood, 25 Ky old	111	Hedges et al. (1985)
Red alder wood, modern	264	Hedges et al. (1985)
Red alder wood, 2.5 Ky old	106	Hedges et al. (1985)
Spruce wood, modern	546	Hedges et al. (1985)
Spruce wood, 2.5 Ky old	541	Hedges et al. (1985)
White spruce wood, modern	190	Meyers, unpublished
White spruce wood, 10 Ky old	218	Meyers, unpublished
Willow leaves, modern	38	Meyers (1990)
Cottonwood leaves, modern	22	Meyers (1990)
Pinyon pine needles, modern	42	Meyers (1990)
White spruce needles, modern	43	Meyers, unpublished
White spruce needles, 10 Ky old	46	Meyers, unpublished
Lacustrine plants		
Pyramid Lake plankton	6	Meyers (1994)
Lake Michigan plankton	7	Meyers (1994)
Walker Lake plankton	8	Meyers (1990)
Diatom, *Asterionella formosa*	9	Bourbonniere (1979)
Green alga, *Chlamydamonas sp.*	7	Bourbonniere (1979)
Lake Biwa mixed plankton	6–7	Nakai and Koyama (1991)
Lacustrine samples		
Surface sediment, Lake Biwa	6	Meyers and Horie (1993)
Settling sediment, Lake Michigan	9	Meyers et al. (1984a)
Surface sediment, Lake Michigan	8	Meyers (1994)
Resuspended sediment, Lake Michigan	8	Meyers et al. (1984a)
Surface sediment, Walker Lake	8	Meyers and Benson (1988)
Surface sediment, Pyramid Lake	9	Meyers, unpublished
Surface sediment, Lake Baikal	11	Qiu et al. (1993)
Surface sediment, Coburn Pond	12	Ho and Meyers (1994)
Surface sediment, Mangrove Lake	13	Hatcher et al. (1982)
Surface sediment, Lake Bosumtwi	14	Talbot and Johannessen (1992)

Organic matter from C_3 land plants and algae cannot be distinguished from $\delta\,^{13}C$ values, but organic matter from C_4 plants has a distinctively heavy isotopic composition.

organic matter C/N ratios to further diagenetic alteration. The C/N values of Quaternary sediment samples from the upper 10 m of a core from Mangrove Lake vary irregularly between 11 and 17 (Fig. 3). This variation resembles a similar downcore C/N profile from Lake Yunoko, Japan, which Ishiwatari et al. (1977) interpreted to reflect changes in the source mixture. Indication of preservation of the C/N source signal is also found by Ertel and Hedges (1985), who demonstrated that vascular plant debris isolated from a sediment sample having a bulk C/N of 15 retains the elevated C/N values characteristic of cellulosic plants. The sediment ratio indicates mixing of vascular and nonvascular plant debris, rather than diagenetic alteration. Talbot and Johannessen (1992) similarly conclude that selective diagenesis has had no discernible effect on organic-matter C/N ratios in sediments as old as 27 500 years in Lake Bosumtwi.

Cautious interpretation of C/N ratios consequently can give information about changes in the sources of organic matter to lake sediments in the distant past. Ishiwatari and Uzaki (1987), for example, reported a sharp transition in atomic C/N values from an average of 9 to an average of 13 at the 250 m level in a drilled core of sediment from Lake Biwa, Japan. They interpreted this change as a shift in proportions of organic-matter source from land-plant dominance in deeper sediments to algal dominance in younger sediments. This interpretation is consistent with a change in sediment types from shallow-water sands and gravels to fine-grained deep-water sediment at the 250-m depth. This sediment horizon corresponds to 430 Kya (Meyers et al. 1993). Another example is from the sediments of Pleistocene Lake Karewa, India. Several marked increases to values of 10 or more occur in C/N ratios that typically remain below 4 in sediments deposited between 2.4 My and 400 Ky (Krishnamurthy et al. 1986) and indicate episodes of increased delivery of land-plant material to this ancient lake.

2.2 Source Information from Carbon-Stable Isotopic Compositions

Most photosynthetic plants incorporate carbon into organic matter using the C_3 Calvin pathway, which preferentially incorporates ^{12}C into organic matter, producing a shift of approximately −20‰ from the carbon isotope ratio of the inorganic carbon pool. Some plants use the C_4 Hatch-Slack pathway, and others, mostly succulents, utilize

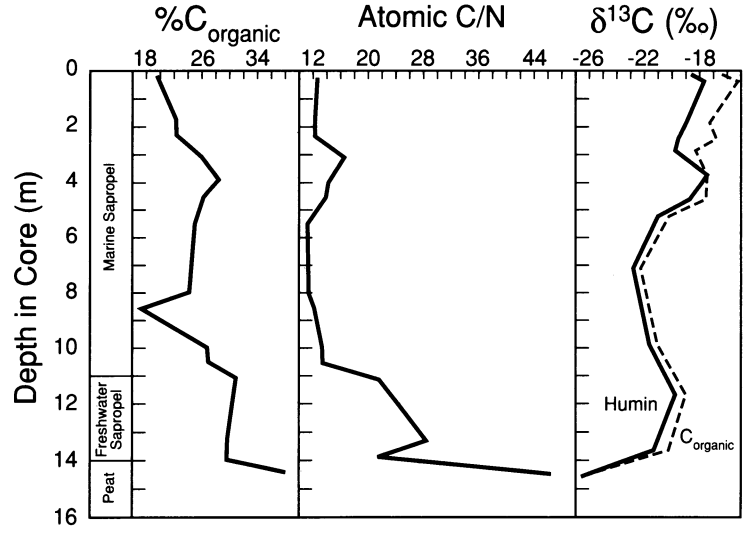


Fig. 3. Organic-carbon concentrations, C/N ratios, and carbon isotope values at different depths in a sediment core from Mangrove Lake, Bermuda. The $\delta^{13}C$ values are relative to the PDB standard. The C/N ratios reflect dominance of organic matter from algal sources in sapropels and from vascular plants in the peat. The convergence of humin total carbon $\delta^{13}C$ values with depth represents selective diagenetic loss of nonhumin carbon with progressively greater sediment age, which is less than 4 Ky. (Data are from Hatcher et al. 1982, 1983)

the crassulacean acid metabolism (CAM) pathway. The isotope shift for the C_4 pathway is −8 to −12‰; that of the CAM pathway can vary from −10 to −20‰. Organic matter produced from atmospheric CO_2 by land plants using the C_3 pathway consequently has an average $\delta^{13}C$ (PDB) value of approximately −28‰, and by those using the C_4 pathway, approximately −14‰ (O'Leary 1988). Lake-derived organic matter is normally isotopically indistinguishable from organic matter from C_3 plants in the surrounding watershed (Table 3). This similarity in the carbon isotopic compositions of lake-derived and land-derived organic matter contrasts with marine situations in which a 7‰ difference exists between algal and continental organic matter (e.g., Jasper and Gagosian 1989; Meyers 1994). This contrast arises from the difference in the abundances and the dominant forms of dissolved carbon in the two types of systems – HCO^- in seawater and CO_2 in freshwater.

The existence of the several isotopic signatures of photosynthetically fixed organic carbon would seem to offer opportunities to trace sources of organic matter in lacustrine food webs and to lake sediments. In the sedimentary organic matter of most lakes, however, the differences originally present in the total carbon isotopic contents of specific flora are lost, because of food web integration of the different carbon sources. For example, photosynthesizers living in Fayetteville Green Lake, New York, have $\delta^{13}C$ (PDB) values ranging from −15 to −41‰. Despite this range among available food sources, most animals in

Table 3. Carbon isotopic compositions of various plants that contribute organic matter to lake sediments and in sediments of different lakes

Type of sample	$\delta^{13}C$(‰)	Reference
C_3 land plants		
Lake Biwa watershed	−25 to −30	Nakai and Koyama (1991)
Willow leaves	−26.7	Meyers (1990)
Cottonwood leaves	−25.0	Meyers (1990)
Aspen leaves	−25.8	Meyers (1990)
Poplar leaves	−27.9	Meyers (1990)
Juniper needles	−22.5	Meyers (1990)
Pinyon pine needles	−24.8	Meyers (1990)
White spruce needles	−25.1	Meyers (1994)
White spruce wood	−23.1	Meyers, unpublished
White spruce bark	−23.5	Meyers, unpublished
C_4 land plants		
Salt grass	−14.1	Meyers (1990)
Tumbleweed	−12.5	Meyers (1990)
Blood grass	−11.1	Talbot and Johannessen (1992)
Wild millet	−10.8	Talbot and Johannessen (1992)
Lacustrine plants		
Lake Biwa mixed plankton	−25 to −28	Nakai and Koyama (1991)
Walker Lake mixed plankton	−28.8	Meyers (1990)
Pyramid Lake mixed plankton	−28.3 + 0.7 (n = 3)	Meyers (1994)
Lake Michigan mixed plankton	−26.8 + 1.4 (n = 7)	Meyers (1994)
Lacustrine sediments		
Lake Biwa surface sediment	−25.3	Meyers and Horie (1993)
Walker Lake surface sediment	−24.2 + 0.8 (n = 30)	Meyers (1990)
Pyramid Lake surface sediment	−26.9	Meyers, unpublished
Coburn Pond surface sediment	−28.4	Ho and Meyers (1994)
Lake Bosumtwi surface sediment	−26.4	Talbot and Johannessen (1992)
Lake Michigan surface sediment	−26.3	Rea et al. (1980)
Lake Michigan settling sediment	−27.5 + 0.9 (n = 6)	Meyers and Eadie (1993)
Lake Baikal surface sediment	−29.9	Qiu et al. (1993)

Organic matter from land plants and from algae can be distinguished on the basis of C/N ratios.

the lake have isotope signatures between −25 and −30‰, and bottom sediments have a $\delta^{13}C$ value of −28‰ (Fry 1986), which is close to the isotopic compositions of organic matter from other lakes (Table 3).

Microbial reworking of organic matter during early diagenesis can potentially modify its bulk carbon isotopic content. Organic matter is a mixture of different types of compounds that deviate differently in isotopic content from the inorganic carbon pool. Amino acids of marine plankton, for example, are depleted in ^{13}C by −17‰ on average, whereas the lipid fraction has a $\delta^{13}C$ value of −28‰ (Degens 1969). Selective loss of more reactive fractions of the total organic matter may create a diagenetic shift in the isotope ratio, which will mask the original source signature. Laboratory decomposition of the C_4 marsh grass, *Spartina alterniflora*, produced progressive losses of isotopically heavy organic material that created an extrapolated isotope shift in bulk organic carbon from −13 to −17‰ (Benner et al. 1987). A similar but smaller shift to lighter carbon isotope values has been documented in organic-carbon-rich sapropelic sediments from Mangrove Lake, a seawater-dominated system in Bermuda (Hatcher et al. 1982). Comparison of the $\delta^{13}C$ ratios of total organic carbon and of the humin fraction of sedimentary organic matter shows a downcore convergence in isotopic values (Fig. 3). This shift apparently is caused at least partly by selective loss of the isotopically heavy carbohydrate fraction of total organic matter (Spiker and Hatcher 1984), but changes in the proportion of land-derived and marine-derived organic matter may also contribute. The possible diagenetic shift in the carbon isotope values is ≈−2‰ over the multi-thousand-year age of these sediments. Despite the possibility of a diagenetic overprint on the isotopic compositions, the overall change in humin $\delta^{13}C$ ratios from −26‰ in the peat layer to −18‰ at the sediment surface clearly reflects a change from land plants to marine algae as the major source of organic matter in Mangrove Lake. The dominance of land-plant contributions is supported by the C/N ratio of 46 in the peat layer (Fig. 3).

Comparison of the organic $\delta^{13}C$ values of plankton, sediment-trap contents, and surficial sediment in Lake Michigan reveals an interesting pattern of isotopic variation that accompanies a large decrease in the total amount of organic matter during sinking (Fig. 2). The initial and final carbon isotopic ratios remain approximately −26 to −27‰, yet values decrease to approximately −29‰ in the upper water column where organic carbon decreases are greated. These changes in organic-matter isotopic composition agree with observed changes in biomarker compositions that show selective losses of algal components in the upper water column (Meyers and Eadie 1993). The isotopic changes apparently reflect progressive diagenetic losses of algal organic matter and eventual survival of the most resistant organic-matter fractions.

Important diagenetic $\delta^{13}C$ shifts with depth are absent in lake sediments in which the bottom organic matter is not dominated by algal contributions. In a core from Lake Michigan, for example, $\delta^{13}C$ values remained at −26‰ from modern to 3500-year-old sediments in which organic carbon concentrations varied between 1 and 3% (Rea et al. 1980). Similarly, Jasper and Gagosian (1989) report that the source of organic matter controls the $\delta^{13}C$ values of a 100 Ky sediment core from the Pygmy Basin on the Louisiana margin of the Gulf of Mexico. Fluctuations from −22.5 to −26.5‰ are caused by shifts in relative proportions of terrigenous and marine inputs. Diagenetic isotope shifts are evidently insignificant in sedimentary settings having low-to-moderate organic-carbon concentrations.

If the possibility of diagenetic effects can be eliminated, then differences between $\delta^{13}C$ values of sediments deposited at different times can provide paleoenvironmental information. The history of productivity enhancement of Lake Ontario is recorded by a shift in organic-carbon $\delta^{13}C$ values from −27‰ in sediments deposited in the mid 1800s to −25‰ in sediments from 1970–1980 (Schelske and Hodell 1991). Periods of desiccation of Walker Lake, Nevada, created shifts in the overall carbon isotopic contents of this saline lake which are preserved as heavier organic-matter $\delta^{13}C$ values in sediments from 2 Kya and 5 Kya (Benson et al. 1991). Similarly, Talbot and Johannessen (1992) have documented organic carbon $\delta^{13}C$ shifts to heavier values in sediments of Lake Bosumtwi, Ghana, that were deposited under the drier conditions that evidently existed near the end of the last glacial maximum 25–10 Kya. Organic matter synthesized by aquatic organisms records times when the waters of both Walker Lake and Lake Bosumtwi were concentrated by evaporation and consequently saltier. A further illustration of the potential paleolimnol-

ogical value of organic $\delta^{13}C$ values is provided by Rau (1978), who shows that episodes of extensive recycling of organic matter within waters can produce algal organic matter that is isotopically light.

A paleolimnological record of the past 9000 years of Lake Baikal in southeastern Siberia is provided by the organic-carbon composition of a sediment core from the northern basin (Qiu et al. 1993). During this time montane glaciers retreated and modern forests became established in the catchment area. C/N values in the postglacial blue clay muds deposited before 6800 years ago vary between 15 and 50, and indicate substantial contributions of vascular land-plant material (Fig. 4). They vary little from approximately 15 in the diatom ooze that has accumulated for the past 6800 years. The change in sediment type from one dominated by glacial flour to one made up of algal remains indicates that lake productivity increased starting approximately 6800 years ago, and this conclusion is strengthened by an increase in sedimentary organic-carbon concentrations (Fig. 4). The drop in more recent C/N ratios indicates that algal organic matter became a larger component of sediment organic matter at this transition. Organic-carbon $\delta^{13}C$ values change from approximately −23‰ in sediments laid down before 6800 years ago to approximately −28‰ since that time. The increase in lake productivity is associated with the advent of a forested watershed, and organic matter derived from these plants probably has accumulated in lake sediments since this time. The change in isotope ratios probably indicates a change in watershed vegetation from C_4 tundra grasses of former times to modern C_3 woody plants (Qiu et al. 1993). The postulated change in type of land vegetation is an example of a special situation that allows land-derived organic matter to be isotopically distinguished from lake-derived organic matter.

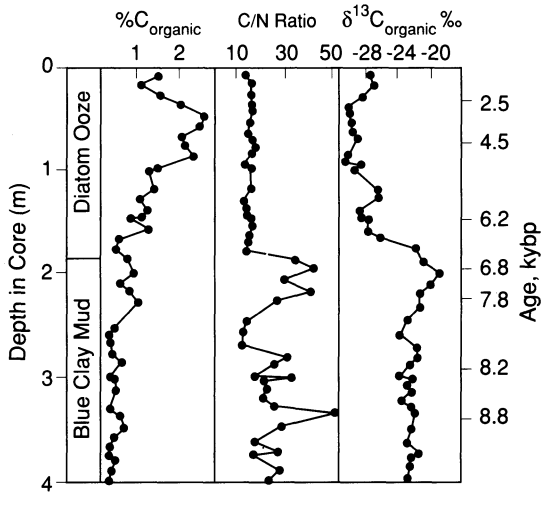


Fig. 4. Organic-carbon concentrations, atomic C/N ratios, and carbon isotopic signatures of sediments from Lake Baikal, Siberia. Decreases in C/N ratios and in organic $\delta^{13}C$ values at the mud/diatom ooze transition indicate an increase in contributions of algal organic matter starting *ca.* 6800 ybp. (Qiu et al. 1993)

2.3 Source Information from Nitrogen-Stable Isotopic Compositions

Important paleolimnological information about the origins and diagenesis of sedimentary organic matter can be obtained from its nitrogen isotopic compositions, yet $\delta^{15}N$ values have not been widely studied. Inorganic nitrogen reservoirs available to land plants and aquatic plants differ in their isotopic contents. Dissolved nitrate has an isotope ratio of +7 to +10‰, whereas atmospheric molecular nitrogen has a $\delta^{15}N$ of approximately 0‰ (Peters et al. 1978). This difference is preserved in the isotopic contents of plankton ($\delta^{15}N$ of +8‰) and C_3 land plants ($\delta^{15}N$ of +1‰), and has been used to trace food chain relationships in a coastal marine marsh by Peterson et al. (1985).

The few investigations of the nitrogen isotope content of lake sediments show that the source information derived from the difference between atmospheric and dissolved forms of nitrogen appears to be preserved. The potential isotopic effects expected from preferential degradation of more reactive organic substances are minor or absent. Pang and Nriagu (1976, 1977) found that sediments in areas of Lakes Superior and Ontario receiving receiving a large proportion of land-derived organic matter have lighter $\delta^{15}N$ values than areas where aquatic organic matter is dominant (+3.7 vs +4.9‰). Significant amounts of downcore degradation of nitrogenous matter occurred relative to total organic matter at all locations in these lakes, increasing the potential for diagenetic isotope shifts. Nevertheless, no differences are evident between $\delta^{15}N$ ratios in surface sediments and those at the bottom of half-meter cores (Fig. 5). Most of the decomposition of organic matter that might cause nitrogen isotope shifts evidently occurs during sinking and prior to sedimentation in the Great Lakes. Meyers

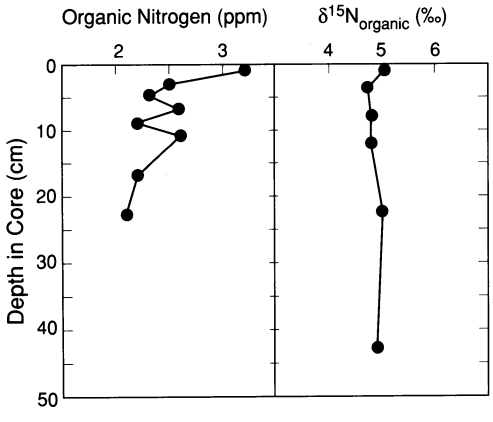


Fig. 5. Organic-nitrogen concentrations (ppm weight of dry sediment) and isotope ratios (air standard) at different depths in a sediment core from Lake Superior. The downcore decrease in concentration indicates degradation of nitrogenous organic matter, yet the isotope ratio is not affected. The relatively heavy isotope values preserve a record of predominantly algal organic-matter deposition at this location. (Data are from Pang and Nriagu 1977)

and Eadie (1993) note a change of −1 to −2‰ in the $\delta^{15}N$ values of sinking particulate organic matter between the near-surface and near-bottom of Lake Michigan. This shift is consistent with the microbial preprocessing of organic material during settling to lake bottoms that is observed in sediment-trap studies.

The sediments of Lake Bosumtwi, which occupies a shallow meteorite impact crater in Ghana and is permanently anoxic, preserves a nitrogen isotopic record of climate variations that have caused the lake level to fluctuate in the past (Fig. 6). Heavier organic $\delta^{15}N$ values appear in sediments deposited during periods of dry glacial-age climate (Talbot and Johannessen 1992). Evaporative losses of isotopically light ammonium nitrogen from the relatively saline and alkaline lake waters occurred during these periods, and the $\delta^{15}N$ excursions reflect aquatic production of organic matter from a modified dissolved nitrogen reservoir.

Organic-matter C/N ratios support the $\delta^{15}N$ evidence for climate change. Values ranging between 15 and 35 in closely spaced sediment intervals record fluctuations in delivery of land-derived organic matter to the lake sediments as climate conditions oscillated. The least variation is found in the sapropel layer, which represents a relatively stable period of high lake level, forested watershed, and wetter climate (Talbot and Johannessen 1992). The transition to this more stable interval occurs in the early Holocene (Fig. 6).

Organic carbon $\delta^{13}C$ values of sedimentary organic matter also record climate-driven changes in the types of land vegetation around Lake Bosumtwi (Talbot and Johannessen 1992). The heavier values in the mixed clastic/carbonate laminated sediments (Fig. 6) reflect contributions from C_4 plants that lived during the drier conditions that existed near the end of the last glacial

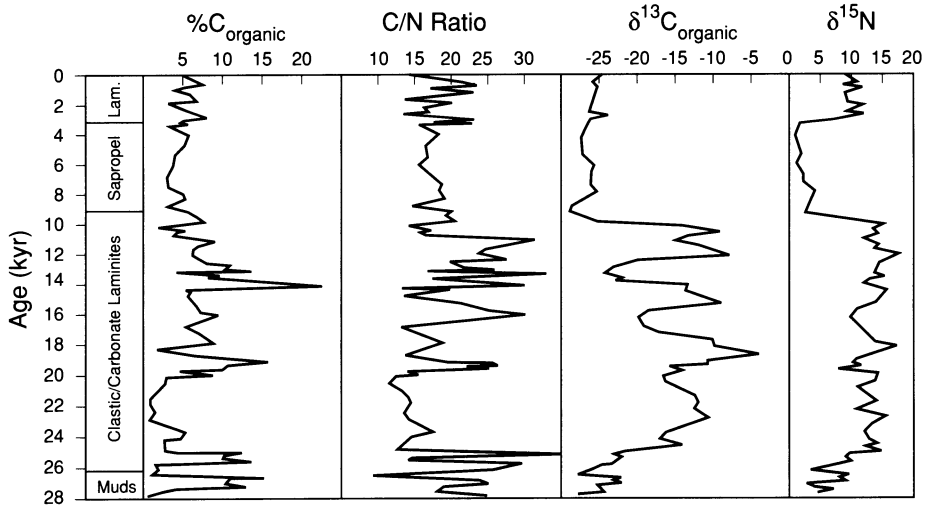


Fig. 6. Organic-carbon concentrations, atomic C/N ratios, and organic $\delta^{13}C$ and $\delta^{15}N$ signatures of sediments from Lake Bosumtwi, Ghana. Decreased C/N ratios and $\delta^{13}C$ and $\delta^{15}N$ values in the sapropel layer record a period of enhanced lake productivity and postulated wetter climate between 9000 and 3000 ybp. (Talbot and Johannessen 1992)

maximum 25–10 Kya. Values of approximately −25‰ in the deep muds and in the upper sedimentary layers indicate delivery of organic matter from C_3 land plants that were present during earlier, wet parts of the lake history, and comprise the forests that surround the lake today.

3 Origin and Alterations of Humic Substances

Humic substances represent between 60 and 70% of the organic matter in young lacustrine sediments and over 90% in older sediments (Ishiwatari 1985). Although humic substances are not easy to characterize, they nonetheless provide information about the sources and alterations of organic-matter-accumulation records. Humic substances are operationally divided into fulvic acid (soluble in base and acid), humic acid (soluble in base but not acid), and humin (insoluble in base and acid). The term "kerogen" is commonly used to describe the nonsoluble fraction of organic matter in sedimentary rocks. This material is equivalent to the humin of younger, nonlithified sediments. Because of this operational and probable precursor-product relationship, the term protokerogen has been applied to humin by some workers.

A number of theories have been proposed to explain the origin of humic substances. Given the diversity of potential-precursor organic substances and the variety of depositional environments, none of these theories is universally adequate. Four hypotheses for the formation of soil humic substances are summarized by Stevenson (1982) and illustrate some of the elements common to various theories: (a) Lignin is progressively degraded by microorganisms to humic acid and then to fulvic acid, (b) lignin is microbially degraded to phenolic monomers, which are reconstituted to form humic substances, (c) cellulose is microbially decomposed to polyphenols, which are then polymerized to form humic substances, and (d) sugars and amino acids condense to form humic substances. Aquatic systems typically have less lignin and cellulose available as potential precursors of humic substances than soil environments. Thurman (1985) overviews additional hypotheses for humic-substance formation where these woody materials are lacking. Leaching of aquatic plant tissues, leaching of watershed soils, photo-oxidation of organic matter dissolved in surface waters, and lysis of algal cells are possible sources of low-molecular-weight compounds which then polymerize to form humic substances. Humic substances in systems containing organic matter derived from woody plants typically are more aromatic in structure than are humics in systems in which lignin and cellulose are not abundant.

The geochemical compounds grouped as humic substances are complex and diverse. As a consequence studies of this organic-matter fraction have traditionally employed general characterizations, such as elemental and spectroscopic analyses, to explore the sources and alterations of humic matter. These procedures, although sometimes crude, are adequate to show that humic substances, themselves products of diagenetic alteration of biogenic organic matter, evidently continue to undergo limited diagenesis in lake sediments.

Short-term changes in the composition of humic substances in lake sediments have been studied. Lake Haruna, Japan, is a small mesotrophic lake in which the source of organic matter is predominantly from algal production (Ishiwatari et al. 1980). The relative contributions of fulvic acid, humic acid, and humin to the total humic matter change with depth in a core that represents approximately 460 years of sediment accumulation. The proportions of fulvic and humic acid decrease, while the proportion of humin increases (Fig. 7). This change is accompanied by a decrease in total organic carbon, indicating that progressive degradation of fulvic and humic acids is probably the underlying cause. Consistent differences in the ratios of acidic and basic amino acids to neutral amino acids in the three humic fractions indicate that they have different histories (Yamamoto and Ishiwatari 1992). The three fractions may represent different stages in the diagenetic condensation of proteins and sugars from a common source, or they may originate from different sources of primary organic matter. The distinctive C/N ratios of the fractions could be explained by either possibility, and these do not change, although the relative contributions of each fraction change with age of the sediment (Fig. 7).

Over multi-thousand-year periods of time, the effects of diagenesis of humic substances continue to be evident in lake sediments. The humin fraction increases from 65% of the total humics at the surface to 85% of the total at the bottom of a 1-m

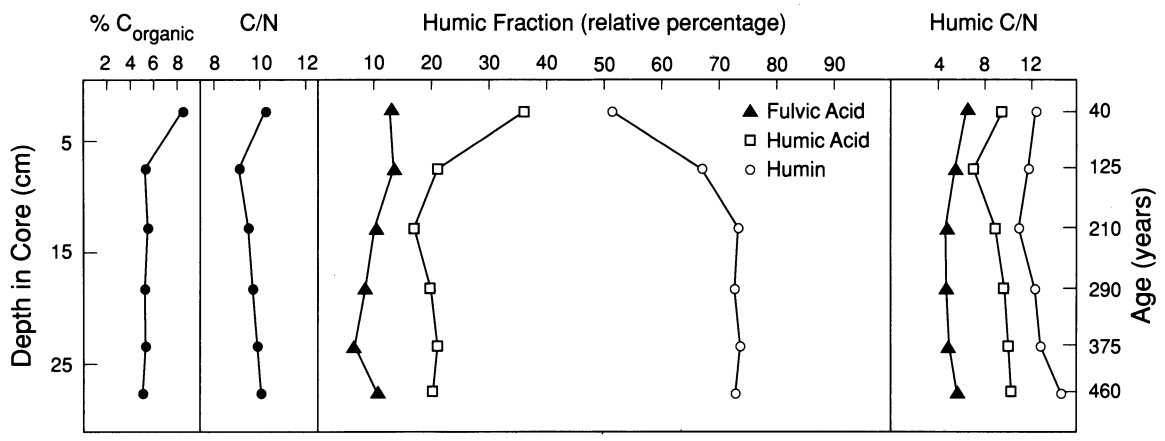


Fig. 7. Composition of humic matter in sediments of Lake Haruna, Japan. Organic matter in these sediments is predominantly algal in origin and is sensitive to early diagenesis. The downcore decrease in organic-carbon concentration is mostly from loss of humic acid, producing a proportional increase in the relative contribution of humin. Atomic C/N ratios are not affected by the diagenetic changes. (Adapted from Yamamoto and Ishiwatari 1992)

core of Lake Michigan sediment, a depth corresponding to approximately 3500 years ago (Rea et al. 1980). Some of this increase may arise from conversion of fulvic and humic acids to humin, but the overall decrease in total sedimentary organic carbon indicates that diagenetic loss of organic matter continues throughout the core, and that preferential degradation of fulvic and humic acids occurs, particularly in younger sediments. Despite evidence of organic-matter degradation in this core, the $\delta^{13}C$ ratio of total organic carbon does not shift from −26.3‰ (Rea et al. 1980). The C/N ratios of both fulvic and humic acids remain approximately 7, and suggest a common origin from aquatic or bacterial sources. In contrast, the humin fraction has a C/N ratio of approximately 15. Humin typically has an atomic C/N value of 14–16 (Ishiwatari 1985), and this ratio suggests an important component of cellulosic land-plant material for humin.

Humic matter from lake sediments has been examined for possible diagenetic exchanges between its component fractions. Bourbonniere and Meyers (1978) used infrared and visible spectroscopy to explore the possible condensation of fulvic acid into humic acid in a half-meter-long core of Lake Huron sediment. They found to evidence for this conversion in the 550-year period represented by this core. This observation supports the postulated selective degradation of fulvic and humic acids seen in the sediments of Lake Haruna and Lake Michigan, as opposed to their interconversion, Furthermore, overall diagenetic effects are minor, inasmuch as H/C ratios of the fulvic acid (approximately 2.2) and the humic acid (approximately 1.6) do not change downcore. The H/C values greater than one reflect the aliphatic nature of the Lake Huron humic substances and a probable origin from algal or bacterial organic matter, rather than from vascular plants. An algal origin for the fulvic and humic acids agrees with the C/N ratios found in sediments of lakes Haruna and Michigan.

Comparisons of samples of wood from modern trees and of wood that has been buried for thousands of years in sediments have been used as proxies for the kinds of diagenetic changes that potentially can occur to humic substances (e.g., Meyers et al. 1980a; Hedges et al. 1985; Spiker and Hatcher 1987). A consistent observation of such studies is that cellulose, made up of aliphatic monomeric units, decreases in relation to lignin, which is a polyaromatic macromolecule. Solid-state ^{13}C nuclear magnetic resonance spectra (Fig. 8) show that well-preserved wood from a log of white cedar buried in a swamp exhibits the strongly aliphatic nature expected from cellulosic material. A microbially decomposed portion of the same log shows selective loss of aliphatic character and resulting enhancement of aromatic character. A similar pattern seems to appear in the humin fraction of sediments from Mangrove Lake (Fig. 8). The shift from predominantly aliphatic character to predominantly aromatic charater has been interpreted to represent a conversion of humic substances to a more stable form

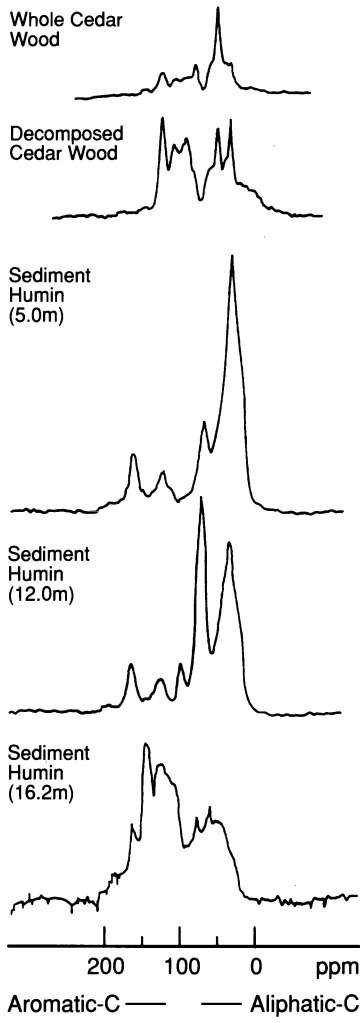


Fig. 8. Solid-state ^{13}C nuclear magnetic resonance (NMR) spectra of buried cedar wood (Great Dismal Swamp, Virginia) and sediment humin samples (Mangrove Lake, Bermuda). The NMR spectra indicate a diagenetic shift from aliphatic carbon in preserved wood to aromatic carbon in degraded wood. The shift in humin spectra with decreasing age of the lake sediments records a change from land-derived to algal organic matter. (Data are from Hatcher et al. 1982; Spiker and Hatcher 1987)

in a period of approximately 10 Ky similar to that found in the wood samples (Hatcher et al. 1982). The change in humin character, however, is also associated with changes in the type of sediment (Fig. 3). It is probable, therefore, that the change reflects different sources of primary organic matter in sediments deposited at different times. The more aromatic character of the oldest and deepest humin (Fig. 8) agrees with an elevated C/N ratio and a light $\delta^{13}C$ value (Fig. 3) in indicating dominance of vascular plant material in this peaty sediment, whereas the aliphatic nature of the 5-m humin is consistent with little contribution of land-plant material in this sapropelic sediment. Humic-matter fractions may consequently preserve evidence of their initial sources of organic matter in their elemental, isotopic, and structural compositions.

4 Sources and Alterations of Lipid Biomarkers

Much has been learned about the sources and diagenetic alterations of organic-matter accumulations in lacustrine sediments from studies of their lipid compositions. Lipids are operationally defined as that fraction of organic matter which can be isolated by extraction with an organic solvent. The term geolipid is sometimes used to describe the materials obtained from sediments, because of the differences that exist between the molecular compositions of unaltered biological matter and the contents of geological samples. The geolipid fraction typically totals between 1 and 10% of sedimentary organic matter. In geologically old and lithified sediments where distinctions between the original biological lipids and diagenetically altered geolipids become greater, the term bitumen is usually employed.

Lipid extraction of lake sediments yields hydrocarbons and the hydrocarbon-like carboxylic acids, alcohols, ketones, aldehydes, and related compounds commonly having ten or more carbon atoms. Many of these compounds have specific biolgical origins, and all of them reflect enzymatic control in their molecular structures. Retention of their biological heritage earns the name biological marker, which is commonly abbreviated to biomarker, for many of these compounds. This characteristic makes the lipid fraction particularly valuable to determinations of organic-matter sources.

Geochemical details about the geolipid contents of young, nonlithified sediments are provided by a number of reviews (Barnes and Barnes 1978; Cranwell 1982; Johns 1986; Müller 1987). We provide examples of studies that illustrate the responses of geolipid biomarker compounds to paleolimnetical changes and to diagenetic alterations. The alterations evident in the biomarker fraction can be used as proxies for the general processes affecting all forms of lacustrine organic

matter, but it is important to remember that lipids total only a few percent of this material.

4.1 Alteration of Lipids During Deposition

Studies of settling particles intercepted by sediment traps indicate that lipids undergo substantial amounts of degradative alteration during sinking to the bottoms of lakes, so that the geolipid compositions of sediments differ from their source compositions. The relative contributions of alkanoic acids and of alkanols become smaller, and molecular distributions change, in settling sediment collected at progressively deeper depths in Lake Michigan (Meyers et al. 1980b, 1984a). The n-C_{16} and n-C_{18} acids and alcohols from algal material become less dominant, whereas the even-chain C_{24}–C_{30} components from the waxy coatings of land plants become proportionally more important. Fatty acid decomposition rates calculated from sediment trap compositions show that n-C_{16} degrades approximately 10 times faster than n-C_{30} (Meyers and Eadie 1993). Similarly, Kawamura et al. (1987) found that distributions of n-alkanes in surficial sediments from Lake Haruna, Japan, were depleted in n-C_{17}, an algal biomarker, relative to the hydrocarbon contents of sediment-trap material in this lake. Aquatic lipid matter is evidently preferentially degraded during the sinking of particulate material, probably because of the relative freshness of this material. In contrast, land-derived organic matter has been microbially reworked before arrival in the lake, and only its most durable lipid components survive to become part of the sedimentary record.

Comparison of the lipid compositions of aquatic organisms with those of underlying sediments shows degradational trends similar to those found in sediment-trap studies. Robinson et al. (1984a) analyzed the lipid contents of bacteria, rotifers, and protozoans from Priest Pot, a eutrophic lake in the English Lake District. They found that shorter-carbon-chain n-alkanols degrade faster than their longer homologs, and that sterols having more than two double bonds do not survive sinking to the lake bottom. Alteration of lipid compositions continues in the sediments of this lake, most intensely in the surface layer. Solvent-extractable lipids become particularly less abundant, and the concentrations of "bound" lipids – those that can be isolated only after acid or base hydrolysis of sediment samples – increase. In several lakes evidence of microbial oxidation of n-alkanes, the least reactive type of aliphatic geolipid, has been found in the appearance of sedimentary n-alkan-2-ones having chain-length distributions similar to those of their precursor hydrocarbons (Cranwell et al. 1987; Rieley et al. 1991a). Preferential degradation of algal components ultimately biases the geolipid record of organic-matter sources retained in the sediments of most lakes. For example, Goossens et al. (1989) show that land-plant lipids dominate the biomarker content of modern sediment from Lake Vechten, The Netherlands, although carbon budgets indicate that land contributions comprise a small part of the total organic-carbon input to the lake system.

4.2 Changes in Sources vs Selective Diagenesis

Geolipid compositions reflect the combined effect of original source inputs and selective diagenesis during and after sedimentation. Within the range of geolipid molecular structures, some are less likely to be altered by diagenesis than others. Comparisons between easily altered and less easily altered molecules help to distinguish diagenetic changes from source changes. Hydrocarbons are generally not as sensitive to diagenetic alteration as oxygen-containing lipids. Within the n-alkane fraction of hydrocarbons, longer-chain-length molecules are less degradable than their shorter-chain-length counterparts, and hence can provide evidence of changes in their sources in sedimentary records. As an illustration the dominant n-alkane shifts from n-C_{27} in pre-1900 sediments to n-C_{31} in more recent sediments of Priest Pot, England, and indicates that marsh and shore grasses replaced trees as the major source of land-derived organic matter (Cranwell et al. 1987). In contrast to the long-chain n-alkanes, the short-chain components in the sediments of this productive lake experience substantial diagenetic losses and generally under-represent the algal contributions of organic matter.

The relative contributions of organic matter from lake and watershed biota are nonetheless at least partially reflected in the biomarker compositions of lake sediments, despite diagenetic biasing toward land-derived components. The n-alkanoic acid distributions in sediments of eutrophic Esthwaite Water and Blelham Tarn, England,

give similar bimodal patterns having maxima at C_{16} and C_{24} (Cranwell 1974), representing characteristic combinations of aquatic and land-plant sources. In contrast, the distribution found in the sediments of oligotrophic Lake Grasmere has a single maximum at C_{26}, indicative of a dominance of land-plant, wax-lipid input. Moreover, *n*-alkane distributions provide an approximate record of watershed plant types. In watersheds where grasses dominate, *n*-C_{31} is the major sediment *n*-alkane, whereas *n*-C_{27} and *n*-C_{29} are more abundant in lake sediments where deciduous tress dominate (Cranwell 1973a). Measurements of the carbon isotopic contents of individual *n*-alkanes isolated from sediments and from leaf waxes allow identifications of geolipid sources to be more specific. Comparisons of the $\delta^{13}C$ values of individual *n*-C_{25} to *n*-C_{29} hydrocarbons extracted from sediments of Ellesmere Lake, England, and from the leaves of trees near the lake, has shown that willow leaves appear to be the major source of these geolipid components (Rieley et al. 1991b).

Selective degradation and replacement of initial biomarker components by microbial contributions alters geolipid distributions in lake sediments. The *n*-alkane distributions in surficial sediments from oligotrophic lakes Motosu and Biwa, Japan, are dominated by the C_{29}, C_{31}, and C_{33} components diagnostic of land-plant waxes (Fig. 9). The *n*-alkanol distributions from these two low-productivity lakes contain dominant-to-large proportions of long-chain, plant-wax components as well (Kawamura and Ishiwatari 1985). The chain-length distributions of the *n*-alkanoic fractions, however, are markedly different. The dominant C_{16} *n*-alkanoic acid in these distributions is ubiquitous in the biosphere; it can be found in land plants, aquatic algae, and bacteria and other microbes. Its dominance in these sediments, where both the *n*-alkanes and the *n*-alkanols record major contributions of land-plant lipids, indicates that microbial utilization and resynthesis of the more-reactive fatty acids has occurred. The sediment from eutrophic Lake Suwa contains a notable amount of the C_{17} *n*-alkane diagnostic of algal production, and the *n*-alkanol and *n*-alkanoic acid fractions are dominated by C_{16} components. The relatively small contributions of long-chain acids and alcohols indicates that contributions of land-plant lipids are small in Lake Suwa compared with the algal contributions.

Some lipid compounds appear to be particularly resistant to diagenetic alteration in lake sediments. For example, Cranwell (1985) reported the presence of C_{37} to C_{39} unsaturated methyl and ethyl ketones in the sediments of three English lakes, but their absence in those of three others. These long-chain compounds have been widely found in marine locations, where they evidently resist diagenetic destruction in sediments as old as Eocene (Marlowe et al. 1984). Although the specific source of these ketones has not been identified in the lacustrine settings, it is probably from prymnesiophyte algae by analogy to the marine source. The difference between the English lake sediments evidently reflects different algal populations in the lakes at the times the sediments were deposited.

Wax esters are also evidently resistant to diagenetic alteration. Fukushima and Ishiwatari (1984) compared the molecular distributions of the component fatty acids and alcohols comprising the wax esters in surface sediments of three lakes in Japan. Those from oligotrophic Lake Motosu are dominated by the C_{24} *n*-alkanoic acids and *n*-

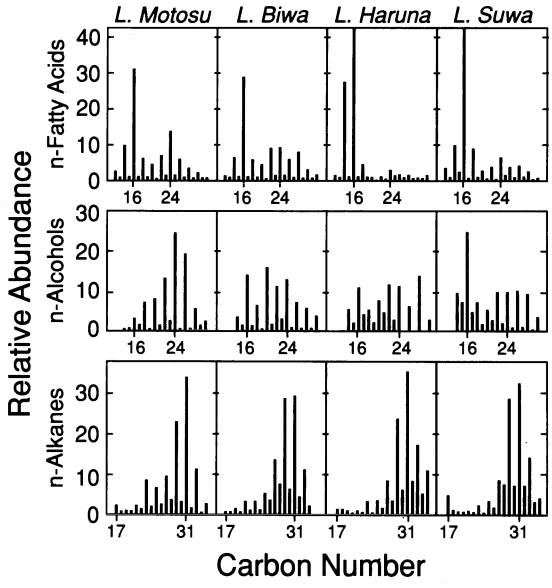


Fig. 9. Chain-length distributions of *n*-alkanes, *n*-alkanols, and *n*-alkanoic acids in surficial sediments from four Japanese lakes. Proportions of the components in each lipid fraction are given as percentage of the total fraction. Long chain-length components originate from land plants, whereas short components are produced by aquatic organisms. The productivities of the lakes increase progressively from oligotrophic Lake Motosu to eutrophic Lake Suwa, and the relative proportions of long-to-short components decrease as lake productivities increase. (Data are from Kawamura and Ishiwatari 1985)

alkanols characteristic of land-plant epicuticular waxes, whereas those from eutrophic Lake Shoji contain a predominance of the n-C_{16} components expected from aquatic plants and few of the long-chain, land-plant materials. The sediment from mesotrophic Lake Haruna displays an intermediate wax ester composition, having the n-C_{16} acid and the n-C_{24} alkanol as the major contributions to their respective distributions. The wax esters, because of their low solubilities and presumably low susceptibilities to microbial utilization, provide improved records of the original proportions of algal and watershed sources of sedimentary lipids.

4.3 Effects of Sediment Grain Size on Geolipid Compositions

Even well-sorted lake sediments contain a range of different-sized mineral and organic particles. Relationships between sediment grain size and geolipid compositions have been investigated by Thompson and Eglinton (1978), who isolated five sediment size fractions from Rostherne Mere, England. The lake is eutrophic, and bottom-water anoxia limits benthic reworking of organic matter. The n-alkane distributions nonetheless contain small amounts of algal components and instead are dominated by the land-derived n-C_{27}, n-C_{29}, and n-C_{31} hydrocarbons, as shown by the long/short ratios significantly greater than one (Table 4). The n-alkanoic acids, however, are nearly equally made up of algal and land-plant components, giving long/short ratios of close to one. The Carbon Preference Index (CPI), devised by Bray and Evans (1961), is used to indicate the degree of diagenetic alteration of straight-chain geolipids. This index is, in essence, a numerical representation of how much of the original biological chain-length specificity is preserved in geological lipids. In fresh lipid material odd-numbered carbon chains dominate hydrocarbon compositions, and even-numbered chains dominate the compositions of fatty acids and alcohols. This chain-length specificity diminishes as diagenesis proceeds and microbial components are substituted for the primary material. Relatively high CPIs (>3–4) of the Rostherne Mere geolipids imply that the biogenic characters of both the hydrocarbons and the alkanoic acids are largely retained. Microbial reprocessing of organic matter, however, has evidently degraded many of the short-chain n-alkanes and has probably replaced much of the original fatty and fraction with microbial acids. The degree to which these

Table 4. Characteristics of organic matter associated with different-size fractions of Rostherne Mere sediment

Organic matter parameter	Whole sediment	Sand fractions		Silt		Clay <5 mm
		>250 mm	250–125 mm	125–66 mm	66–5 mm	
Percent $C_{organic}$	8.4	17.1	14.7	8.7	7.4	12.7
Atomic C/N	14.2	16.0	14.8	14.5	12.9	9.2
Extractable hydrocarbon						
mg aliphatic/g sed	10	24	25	9	10	37
mg UCM/g sed	27	1	9	32	27	64
aliphatic/UCM	0.37	24	2.78	0.28	0.37	0.58
CPI_{16-31}	3.2	4.0	3.4	3.1	2.9	2.5
long/short[a]	3.2	3.1	4.5	3.1	3.0	3.1
Extractable fatty acids						
mg FA/g sed	103	420	220	90	80	750
CPI_{14-27}	7.9	6.6	4.3	2.6	7.4	4.8
long/short[b]	0.6	1.3	1.0	0.5	0.6	1.6
18:1/18:0	0.2	0.3	0.3	0.4	0.2	0.1
16:1/16:0	<0.1	0.1	0.2	0.1	0.1	<0.1
br 15/n15:0	4.3	2.7	3.2	5.4	3.8	2.7

The comparison shows that sediments that become well-sorted by grain size can contain different amounts and types of organic matter. Values are derived from data of Thompson and Eglinton (1978).
[a] (nC27 + nC29 + nC31)/(nC17 + nC19 + nC21).
[b] (n24:0 + n26:0 + n28:0)/(n14:0 + n16:0 + n18:0).

alterations have taken place varies with sediment size fractions. Land-plant lipid character and total extractable geolipid concentrations generally decrease as particle-size diminishes. This pattern is consistent with the decrease in abundance of intact plant detritus and accompanying decrease in C/N ratios in the sediment fractions. The trend toward decreasing concentrations is dramatically reversed in the clay-sized particles, which have the highest loadings of *n*-alkanes and fatty acids. The larger surface area per unit weight and the likelihood of a greater abundance of clay minerals probably provide enhanced sorptive capacities for this size fraction.

Two other size-related changes in the lipid compositions are progressive decreases in the ratio of individual *n*-alkanes to the unresolved complex mixture (UCM) of hydrocarbons and in the proportion of unsaturated n-C_{18} acids to their saturated analog. The UCM indicates contributions of diagenetically derived hydrocarbons, usually from geologically old organic matter such as in eroded sedimentary rocks or residues of petroleum. Microbial reworking of organic matter can also create these complex mixtures of hydrocarbon molecules. The differences evident in the grain-size fractions, combined with the decreases in CPI values, suggest that the lipid contents of the finer-sized particles of sediment have experienced more microbial reworking than those of the coarser particles. Finer-sized particles settle more slowly to lake bottoms than coarser ones, increasing the exposure time of their organic contents to such attack. Diminished aliphatic/UCM ratios, particularly from the finer-sized particles, also indicate the presence of microbially degraded petroleum residues, presumably from run-off of lubricating oil from the roadways in the watershed (Thompson and Eglinton 1978), although some amount of eolian contribution is also possible for the smaller particles. Similarly, Meyers and Takeuchi (1979) found that finer-grain-sized sediments generally contained higher concentrations of extractable aliphatic, aromatic, and UCM hydrocarbons, as well as of extractable fatty acids, than did coarser sediments in Lake Huron. In addition, the size of the UCM component of sediment hydrocarbons decreased with distance from the mouth of the Saginaw River, indicating a principal source from urban run-off of petroleum residues.

4.4 Source Records of Alkanes in Lake Sediments

Alkanes, or saturated hydrocarbons, can record many aspects of the depositional history of organic matter sources in lake sediments, because of their low susceptibility to microbial degradation compared with other types of organic matter. Classical examples of hydrocarbon source records are provided by sediment cores from two lakes in the state of Washington. Sediments of Lake Quinalt, which is surrounded by forests on the Olympic Peninsula, contain low concentrations of hydrocarbons that are dominated by the C_{27} *n*-alkane diagnostic of tree waxes (Fig. 10; Wakeham 1976). No significant difference exists in the *n*-alkane contents of sediments deposited in the early 1800s and in the mid-1970s. In contrast, modern sediments of Lake Washington, which is surrounded by the city of Seattle and its suburbs, have hydrocarbon contents dominated by the UCM indicative of petroleum residues (Fig. 10). Anomalously old radiocarbon ages of 15–20 Ky for the aliphatic hydrocarbon extracts of modern sediments confirm large proportions of fossil hydrocarbons (Wakeham and Carpenter 1976). Furthermore, the contribution of short-chain-length *n*-alkanes derived from algae is equal to the land-plant *n*-alkane contributions, suggesting eutrophication of the waters of Lake Washington. In progressively older sediments the contributions of UCM and short-chain hydrocarbons diminish, until in sediments deposited in the mid-1800s the concentrations and distributions resemble those of Lake Quinalt sediments (Fig. 10). Three sources of hydrocarbons can be identified in these sediments: (a) a natural, low contribution of land-plant *n*-alkanes as found throughout the sedimentary records of both lakes, (b) an input of petroleum residues from urban run-off, which first appears in the Lake Washington record around 1900 and becomes dominant in modern sediments, and (c) an algal input of C_{17} and C_{19} *n*-alkanes, which is usually small in comparison with the land-plant contributions, probably because of selective diagenetic degradation. It becomes large only in the sediments of Lake Washington, which were deposited starting *ca.* 1950, when residential population growth led to a 2-decade period of eutrophication of the lake and large increases in the algal production of n-C_{17}.

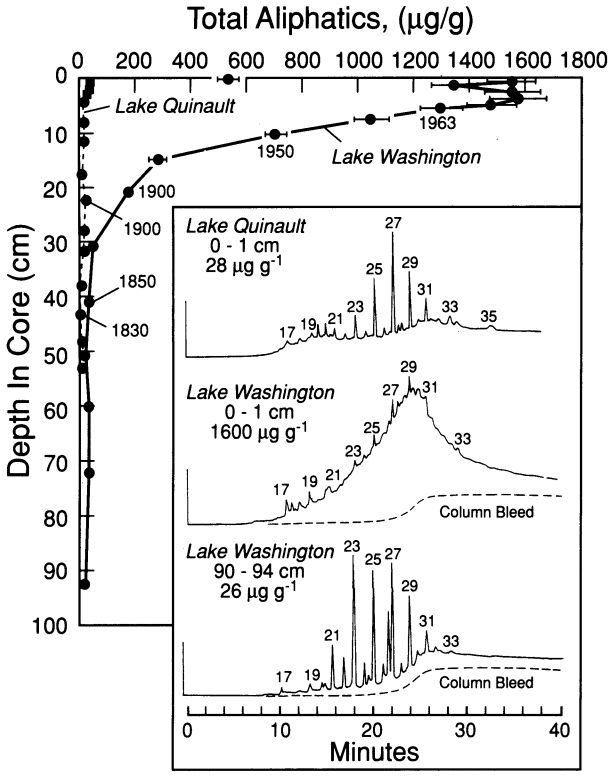


Fig. 10. Concentrations of total extractable aliphatic hydrocarbons in sediment cores from Lake Washington in urban Seattle and Lake Quinalt in rural Washington. Gas chromatographic traces illustrate hydrocarbon distributions in three of these core samples. Carbon numbers of *n*-alkanes are indicated on the traces. The large hump in the trace from surficial sediments in Lake Washington represents an unresolved complex mixture (UCM) of hydrocarbons underlying the individual aliphatic hydrocarbon peaks. Most of the increase in Lake Washington hydrocarbon concentrations since *ca.* 1900 is due to the large addition of petroleum residues, indicated by the UCM, to a low background of land-plant *n*-alkanes, typified by the Lake Quinalt hydrocarbon contents. Core sediment ages shown are from ^{210}Pb dating. (Data are from Wakeham 1976)

4.5 Preservation and Degradation of Fatty Acids in Lake Sediments

Fatty acids are more sensitive to degradation and modification than most types of biogenic lipids, because of their linear structures, carboxylic-acid functionalities, and the frequent presence of carbon-carbon double bonds. Some fatty acids are more susceptible to diagenesis than others; hence, comparisons between different components can help to distinguish diagenetic effects from source changes.

The results of a study by Matsuda and Koyama (1977a,b) illustrate some of the effects of diagenesis and of source change on the fatty acid contents of sediments. Concentrations of total fatty acids and of total organic carbon decrease rapidly over the top 25 cm of a 150-cm-long core from Lake Suwa, Japan (Fig. 11). The ratio of fatty acid carbon to total organic carbon also decreases, showing that fatty acids are degraded more readily than total organic matter. Long-chain components, represented by 24:0, 26:0, and 28:0 (number of carbon atoms:number of double bonds) change little with depth, but short-chain acids, such as 15:0, 16:0, and 18:0, decrease markedly. The degradation rates of these latter acids have been estimated in coastal marine sediments to be 6–7 times faster than for long-chain acids (Haddad et al. 1992). Shorter-chain unsaturated acids, such as 16:1 and 18:1, have higher concentrations than saturated acids of the same carbon chain length in surficial Lake Suwa sediment, but disappear faster than their saturated analogs. In contrast, the concentration of the 24:1 acid appears to experience little change with depth (Fig. 11). Long-chain unsaturated acids are evidently also more resistant to destruction than short-chain acids.

Fatty acids in lake sediments typically originate from several sources. The long-chain components in Lake Suwa sediments are probably from land plants, and as such are the nonreactive survivors of transport of land-derived debris to the lake bottom. The shorter-chain components, particularly the alkenoic acids, are products of algal liposynthesis in the lake. These lipids are easily metabolized by sediment microbes. The *n*-15:0 and *anteiso*-15:0 fatty acids are indicators of microbial biomass (Cranwell 1973b), and they represent in situ production of secondary lipids at the expense of primary organic matter. Most of the concentration changes occur in the top 25 cm of these sediments, corresponding to approximately 60 years (Matsuda and Koyama 1977a). Although the decrease in the contribution of fatty acids to total organic matter (FAC/TOC in Fig. 11) is compelling evidence for diagenetic losses of these lipids, it is also probable that there have been source changes as a result of the documented increasing algal productivity of Lake Suwa over this time. The lower concentrations of C_{16} and C_{18} acids in deeper sediments may arise jointly from formerly lower production and from diagenetic removal. The similar pattern for the C_{15} acids may reflect the presence of larger microbial

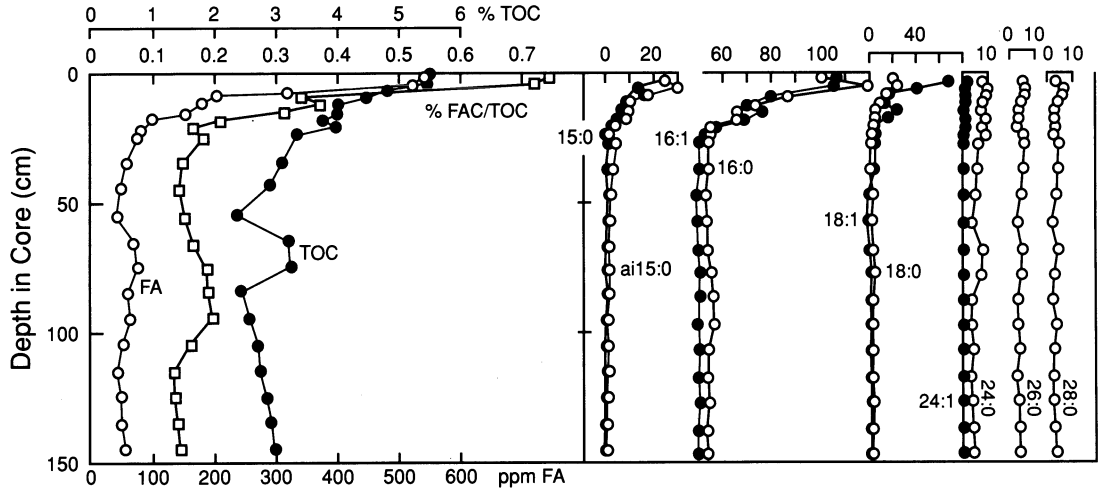


Fig. 11. Downcore concentrations of total fatty acids and of representative components of the total acids in parts per million of Lake Suwa, Japan, sediment. Ratios of total fatty acid carbon to total organic matter are given as FAC/TOC. Major shifts in all parameters at a sediment depth of 20 cm record modern eutrophication of Lake Suwa. Microbial reprocessing of fatty acids in surface sediments is also evident from the distribution of C_{15} acids. (Data are from Matsuda and Koyama 1977a,b)

populations in response to larger amounts of readily metabolized organic matter in younger sediments than in older deposits.

Matsuda and Koyama (1977b) examined the possibility that source changes as well as diagenetic changes impact the downcore fatty acid composition of Lake Suwa sediments. They compared the sediment contents to those of potential source materials, and they explored several measures of source vs alteration effects. The CPI was modified to test for the presence of source changes as well as diagenetic effects. Fatty acids were separated into their lower- (C_{12} to C_{18}) and higher-molecular-weight (C_{22} to C_{32}) groups as CPI_L and CPI_H, respectively. In the lipid content of most plants CPI_L values are high, ranging between 12 and approximately 100; CPI_H values are not as high, ranging between 0.9 and 8, because of the presence of long-chain, odd-carbon acids in some land plants. Bacteria generally have low CPI values, and therefore bacterial reworking of sedimentary organic matter results in lowered CPI values.

The downcore CPI values in the sediments of Lake Suwa are variable, and they are lower than CPI values of potential source materials (Matsuda and Koyama 1977b). The variability indicates that a combination of source changes and of changes in the degree of microbial reworking is involved. The index for all *n*-alkanoic acids, CPI_T, is similar to CPI_L in the upper approximately 20 cm of sediment and becomes more like that of CPI_H in sediments lower than 25 cm in the core. The generally lower CPI values below 25 cm imply that microbial resynthesis of fatty acids has been important in erasing the original compositions. Much of this resynthesis has evidently occurred in the upper part of this core.

A Composition Diversity Index (CDI) was also employed by Matsuda and Koyama (1977b) to evaluate the possibility of changes in sources of fatty acid inputs to Lake Suwa sediments. Higher values are present below approximately 20 cm and indicate a greater diversity of sources. Matsuda and Koyama (1977b) interpreted this pattern to reflect dominance of microbial contributions in the more recent sediment contents. This interpretation is consistent with the downcore CPIs, yet both patterns could also arise from increased algal production in modern times. Higher concentrations of $C_{16:0}$ between 75 and 100 cm in the core accompany higher-percent FAC/TOC, higher CPIs, and lower CDIs. These parameters suggest substantial preservation of the record of fatty acid contributions to the deeper sediments of this lake. On this basis the CPI and CDI trends may record eutrophication as well as microbial inputs. Original fatty acid source indicators appear not to have been totally replaced by microbial components in this example, pro-

bably because of the relatively rapid sedimentation rate in Lake Suwa (ca. 4 mm/year; Matsuda and Koyama 1977a).

Unsaturated fatty acids are generally more susceptible to alteration in sediments than are saturated acids of the same chain lengths. Unsaturated n-C_{16} and n-C_{18} acids are major constituents of the lipids of freshwater algae, and they are rapidly degraded by microbial attack (Cranwell 1976). In a sediment core from Lake Haruna, Japan, the proportions of $C_{16:1}$, $C_{18:1}$, $C_{18:2}$, and $C_{18:3}$ to their corresponding alkanoic acids decrease by a factor of ten in the upper 8 cm of sediment (Kawamura et al. 1980). Little unsaturated acid remained below this depth, corresponding to 120 years of accumulation, and consequently the ratios decreased much more slowly. Similar decreases in the unsaturated-to-saturated ratios of fatty acids are found in Lake Suwa sediments (Fig. 11) and in sediments from Lake Huron (Meyers et al. 1980c). The existence of carbon-carbon double bonds evidently facilitates microbial utilization of these lipids and enhances their degradability.

Variations in environmental factors, such as sedimentation rates and degree of lake water oxygenation, impact the preservation of the relatively reactive fatty acids in sediments deposited under different conditions. Mendoza et al. (1987) reported fatty acid compositions from a core of sediment from Lake Leman, Switzerland, which document the effects of changing sedimentation rates. Concentrations of lower- and higher-molecular-weight acids decrease as expected from diagenetic alteration over the top meter of this core, but they increase in sediments between 2.5 and 3.5 m deep, presumably because of an interlude of higher sedimentation rate. Unsaturated n-C_{16} and n-C_{18} acids show a similar pattern, indicating better preservation during this time of faster removal from microbial degradation. Ho and Meyers (1994) have postulated that fluctuations in concentrations of saturated and unsaturated fatty acids in a 200-year sediment record from Coburn Pond, Maine, similarly reflect varying amounts of microbial reworking of organic matter as the availability of bottom-water oxygen varied.

Rapid burial in lake sediments can dramatically enhance preservation of fatty acids by limiting microbial reworking of this geolipid fraction. Concentrations of total fatty acids increase nearly tenfold with depth, and the proportions of unsaturated acids more than double over the top 25 cm of sediments in Pyramid Lake, Nevada (Fig. 12). The cause of these exceptional patterns is believed to be slumping of deltaic sediments as a result of lowering of the water level of this lake in the early 1900s, thereby protecting surface sediments from aerobic bottom waters (Meyers et al. 1980d). Source changes at this time can be

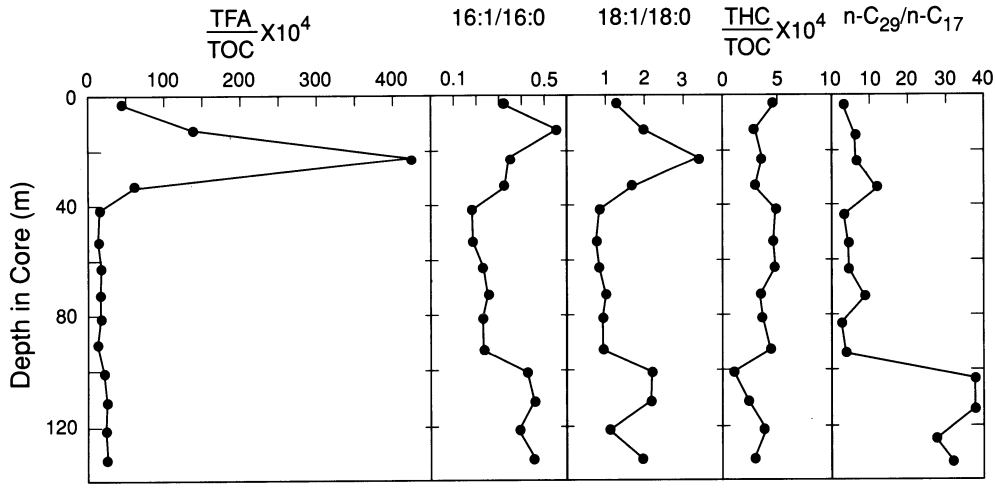


Fig. 12. Evidence of changes in depositional conditions affecting lipid contents of sediments in Pyramid Lake, Nevada. Ratios of concentrations of total fatty acids (*TFA*) and total aliphatic hydrocarbons (*THC*) to total organic carbon (*TOC*), of monounsaturated C_{16} and C_{18} acids to their saturated analogs, and of C_{29}/C_{17} n-alkanes vary at different core depths. Enhanced preservation is indicated by maxima in the fatty acid parameters; enhanced contribution of land-plant hydrocarbons is indicated by the increase in the C_{29}/C_{17} ratio. (Data are from Meyers et al. 1980d)

eliminated, inasmuch as total hydrocarbon concentrations show no enhanced inputs of lipids over this sediment depth range (Fig. 12). The *n*-alkane and fatty acid compositions near the bottom of this core, however, indicate a change to a larger proportion of terrigenous lipids and to better overall lipid preservation at a depth corresponding to 1200–1400 AD. This is a further illustration that changes in depositional parameters can be preserved in the lipid contents of sediments, even by relatively reactive components such as fatty acids.

4.6 Sources and Diagenesis of Sterols in Lake Sediments

Sterols and their derivatives are important geochemical biomarker compounds. The distributions of steroid compounds found in biota and in sediments, as well as some of the diagenetic modifications affecting this class of geolipids, have been the subjects of multiple reviews (e.g., Mackenzie et al. 1982; Brassell et al. 1983; de Leeuw and Baass 1986; Volkman 1986). The molecular structures of several representatives of this family of tetracyclic alcohols are shown in Fig. 13. The presence or absence of double bonds, of methyl groups at various positions on the carbon framework, the length of the branched side chain at the C_{17} position, and the stereochemistry of the substituent bonds create a variety of geochemically useful compounds. Algae, in particular, appear to be capable of synthesizing a wide array of sterols and related cyclic compounds. The structural diversity of sterols and their derivatives can be employed to infer sources and diagenetic pathways of organic matter in sediments.

Sterols extracted from cores of lake sediments have indicated paleolimnological changes that have impacted the sources of these biomarker compounds in sediments deposited at different times. The sources of total organic matter to the sediment presumably also changed, although not necessarily exactly in the same fashion as the sterol sources. In a study of sediments of Lake Leman, Switzerland, Mermoud et al. (1985) noted that epicholestanol (Fig. 13) is present in surficial sections of a core from an anoxic, deep part of this lake, but absent from oxygenated sediments in other parts of the lake and in older parts of the core. They concluded that modern

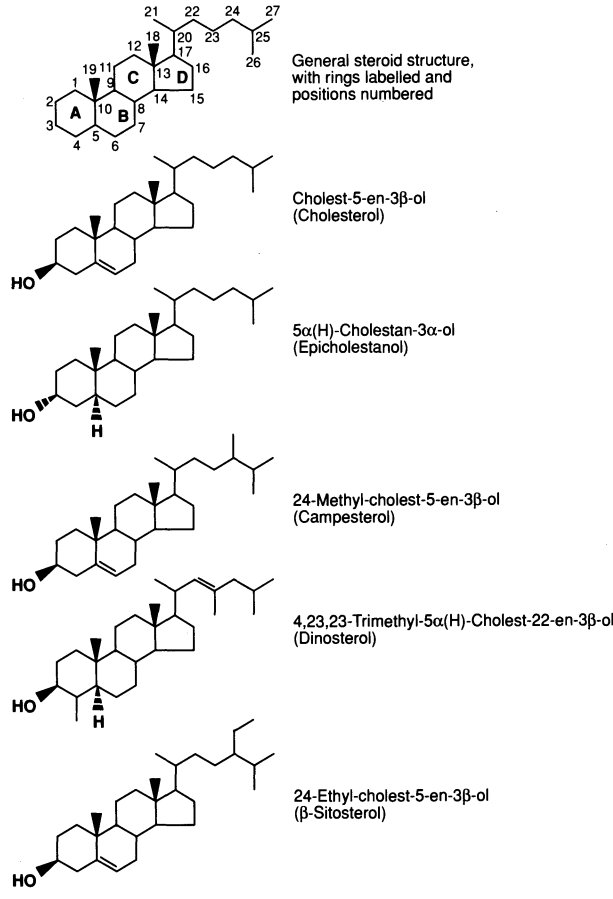


Fig. 13. Representative sterol compounds that have been detected in lacustrine sediments. The C_{27} compounds (e.g., cholesterol) generally dominate the sterol compositions of aquatic plants, whereas C_{29} compounds (e.g., sitosterols) constitute most of the sterols of land plants. Other sterols give greater source specificity. Dinosterol, for example, is indicative of dinoflagellate production

eutrophication of the lake has created seasonal anoxia in the hypolimnion, and has enabled anaerobic bacteria to produce this uncommon sterol. A paleoenvironmentally related change in sterol source has also been reported for Motte Lake, France. Sediments throughout a 6-m core contain gorgostanol, believed to be derived from bacterial reduction of gorgosterol (22,23-methylene-23,24-dimethyl-cholest-5-en-3β-ol), which is probably produced by the dinoflagellate phytoplankton abundant in this lake (Wünsche et al. 1987). The deepest core sections contain aplystanol (24,26-dimethyl-5α(H)-cholestan-3β-ol), for which a source organism is not known in freshwater systems. The absence of aplystanol in younger sediments suggests that the unknown

freshwater organism that synthesized the precursor compound no longer populates Motte Lake.

Sterol compositions have been used to distinguish aquatic contributions of organic matter in sediments from land-derived material. Comparisons of algae and vascular plants from the Lake Suwa (Japan) area showed that cholesterol is the dominant algal sterol, whereas 24-ethylcholesterol (β-sitosterol) is the major sterol in emergent water plants and in watershed plants (Nishimura 1977a; Nishimura and Koyama 1977). Similarly, Rieley et al. (1991a) report that leaf waxes contain C_{28} and C_{29} sterols, but lack C_{27} sterols. This difference has been applied by Nishimura (1977b) to infer that the sediments of alpine, oligotrophic Lake Shirakome-ike contain largely land-derived organic matter, which agrees with known sources of sedimentary mineral components.

The distinction between algal and land-plant sterol compositions has become blurred, however, as new sources of biomarker sterols are identified. Some marine phytoplankton can synthesize ethylcholesterols (e.g., de Leeuw and Baass 1986; Volkman 1986), and some lacustrine algae evidently also have this capability. Matsumoto et al. (1982) have identified 24-ethylcholesterol as the dominant sterol in sediments and epibenthic blue-green algae from saline lakes in Victoria Land, Antarctica. The absence of land vegetation around these lakes rules out contributions of organic matter from living vascular plants to the sediments, yet the ratios of C_{29}/C_{27} sterols (between 1.4 and 7.2) mimic those of temperate-zone lakes known to receive terrigenous organic matter. Dinosterol (Fig. 13) is the major component of a group of 4α-methyl sterols present in freshwater dinoflagellate algae (e.g., Robinson et al. 1984b, 1987). Closely related 4α-methyl sterols have also been identified in marine prymnesiophyte algae (Volkman et al. 1990) and in a submerged vascular plant from Motte Lake (Klink et al. 1992).

Several diagenetic changes occur to the sterol contents of lake sediments. The concentration of sterols decreases relative to total organic carbon (e.g., Nishimura 1977a), although not as fast as the decreases of linear alcohols or fatty acids (Cranwell 1981; Leenheer and Meyers 1983). Another important change is the conversion of stenols, the unsaturated biological form of most sterols, into stanols, the hydrogenated analog. This conversion evidently begins in the water column (e.g., Robinson et al. 1984a, 1986; Wünsche et al. 1987), with the consequence that both stenols and derived stanols are common in surficial lacustrine sediments.

The rapid diagenetic alteration of biological sterols into their geochemical derivatives implies that microbes within the water column and at the sediment/water interface are responsible. A variety of steroid compounds have been identified in the surficial mixed layer of sediments in Lake Haruna, Japan (Fig. 14). Many of these compounds are intermediates in alteration pathways that will lead to either saturation or aromatization of the steroid carbon skeleton, and hence, to improved geochemical stability. Evidence of both reductive and oxidative pathways is present, but simple chemical disproportionation is unlikely in view of the intermediate molecules. Instead, the coexistence of both pathways indicates that a complex microbial assemblage is present in the lacustrine ecosystem. Nearly all of the Lake Haruna steroids are intermediates in the diagenetic pathways described by Mackenzie et al. (1982) and Brassell et al. (1983), except that a steroid diketone is a newly identified compound. Steranes, the hydrocarbons ultimately produced from sterols, are absent in Lake Haruna surficial sediments, and their absence indicates that these derivatives are products of later stages of diagenesis.

Conversion of stenols to stanols and the resulting enhanced stabilization of the sterol carbon skeleton continues deeper in lake sediments. Evidence of this process is illustrated by Fig. 15, which shows the ratio of total unsaturated sterols (stenols) to total saturated sterols (stanols) in sediments of Lake Suwa, Japan. The stenol/stanol ratio is approximately 50 in diatoms from Lake Suwa, but drops to 5 in surficial sediments (Nishimura and Koyama 1976). The stenol/stanol ratio decreases to 2 in the upper 30 cm of the 150-cm-long sediment core and remains constant with greater depth. A similar total organic-carbon pattern suggests that microbial reprocessing of organic matter is largely responsible for the decrease in the stenol/stanol ratio. Microbially mediated hydrogenation of stenols has been postulated to be part of this reprocessing (e.g., Gaskell and Eglinton 1976; Nishimura 1977b; Nishimura and Koyama 1977; Reed 1977; Rieley et al. 1991a). Hydrogenation of the Δ^5 double bond (Fig. 13) yields stanols having 5α(H) and

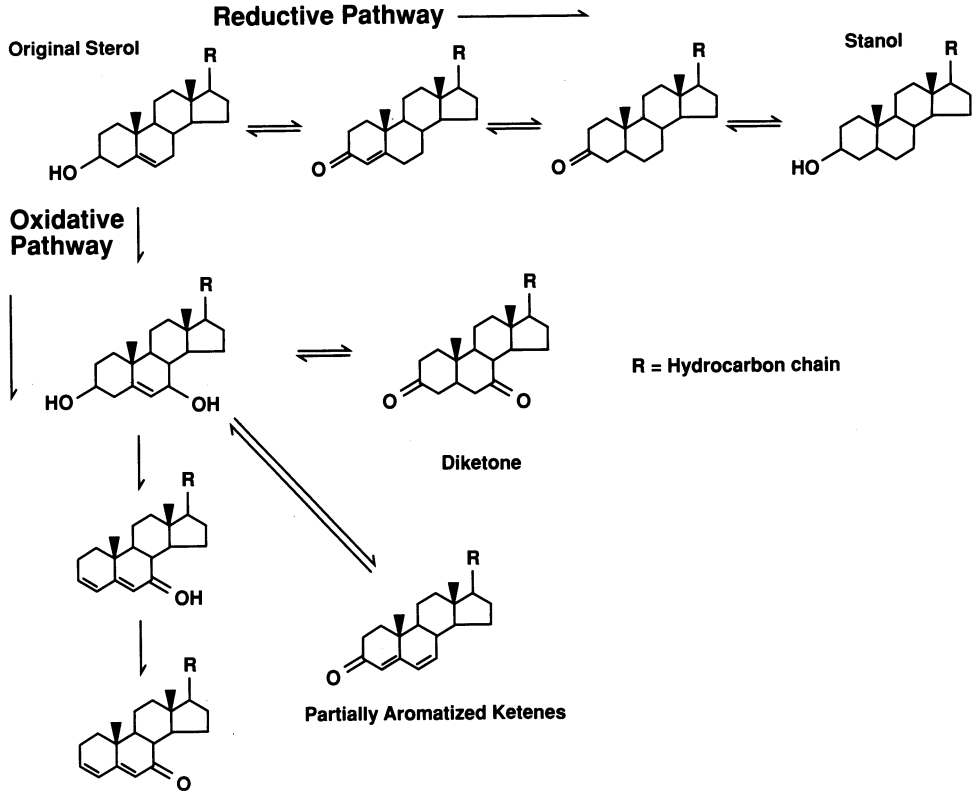


Fig. 14. Preliminary identifications of products of diagenetic alteration of sterol precursors found in the surface sediments of Lake Haruna, Japan, which illustrate the variety of possible compounds and the retention of source-identifying molecular carbon skeleton. Postulated diagenetic routes are indicated. (Ishiwatari, unpubl.)

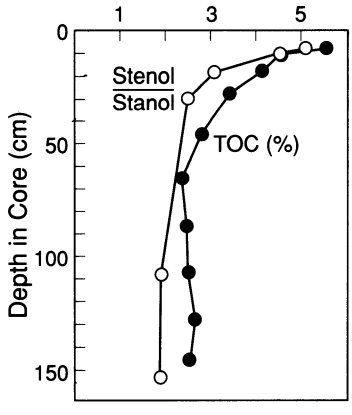


Fig. 15. Downcore changes in the concentration of total organic carbon (TOC) and in ratio of total unsaturated sterols to total saturated sterols (stenol/stanol) in sediments of Lake Suwa, Japan. Similarity of the two depth profiles suggests that much of the change in the stenol/stanol ratio arises from selective preservation of stanols. (Data adapted from Nishimura and Koyama 1976)

5β(H) configurations. Hydrogenation in oxygenated sedimentary environments favors the 5α form (Reed 1977), whereas the 5β form is favored in strongly anoxic sediments (Reed 1977; Nishimura 1982). An additional factor contributing to the decrease in stenol/stanol ratio is preferential preservation of the small amount of stanols synthesized by organisms (Nishimura 1977b, 1978; Nishimura and Koyama 1977; Robinson et al. 1984b). Preferential preservation may also explain why stenol/stanol ratios of aquatic C_{27} sterols decrease more rapidly in sediments than do those of land-derived C_{29} sterols (Nishimura 1978; Leenheer and Meyers 1983).

Sterols and sterol derivatives in sediments provide information about lake conditions of the past. Surface sediments from Rostherne Mere, England, are dominated by cholesterol, campesterol, and β-sitosterol (Fig. 16; Gaskell and Eglinton 1976). In deeper sections the contribution of cholesterol diminishes, indicating that the aquatic productivity was formerly less than the modern eutrophic level. Stenol and stanol dis-

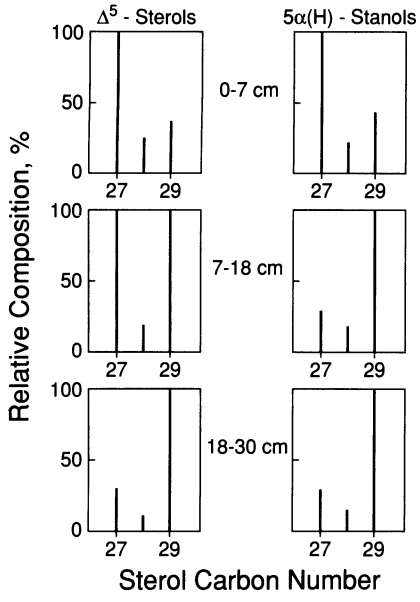


Fig. 16. Relative contributions of C_{27}, C_{28} and C_{29} unsaturated (Δ^5) and saturated [5α(H)] sterols to the sterol contents of sediments from Rostherne Mere, England. Contributions are shown relative to the major component of each sterol fraction. Dominance of C_{27} components in the surface sediment indicates modern eutrophication of this lake. Similarity of stenol and stanol distributions at each depth suggests preservation of source information, despite changes in stenol/stanol ratios. (Data are from Gaskell et al. 1976)

tributions are the same at each sediment-depth horizon, although total sterol concentrations decrease with depth. Stenol/stanol ratios change from 3.1 to 0.2 over the total depth interval, indicating substantial modification from the initial biological material. An overwhelming predominance of 5α(H)-stanols suggests that sterol reduction occurred in oxygenated bottom-water conditions. Retention of the relative molecular proportions nonetheless indicates that sterol biomarker information is preserved, despite overall degradation of these compounds.

4.7 Origins and Significance of Polycyclic Aromatic Hydrocarbons in Lake Sediments

Polycyclic aromatic hydrocarbons (PAHs) are ubiquitous components of both marine and lacustrine sediments (e.g., Laflamme and Hites 1978; Hites et al. 1980), yet these compounds do not occur naturally in organisms. The PAHs are produced by diagenesis and not by biosynthesis. Individual PAHs are created by one of three processes: (a) early diagenesis from biogenic precursors, (b) later diagenesis over long periods of geological time, and (c) high-temperature processes that reconstitute organic-matter fragments into characteristic PAH distributions. Nearly all PAH molecules fit into one of these three categories (e.g., Wakeham et al. 1980a,b; Tan and Heit 1981; Furlong et al. 1987), making these compounds especially useful as indicators of geochemical transport and transformation processes.

The PAH accumulations in lake sediments record contributions from the different source categories. The sediments of Coburn Mountain Pond, Maine, reveal two types of PAH input (Gschwend and Hites 1981; Gschwend et al. 1983). The concentration of perylene increases regularly with depth in a half-meter core, which corresponds to approximately 200 years of time (Fig. 17). Perylene is the diagenetic product of a yet unidentified biogenic precursor, possibly an erythroaphin land-plant pigment (e.g., Aizenshtat 1973). Its increase with depth reflects relatively slow in situ formation via either a first- or second-order reaction requiring anoxic conditions (Gschwend et al. 1983). Surficial sediments consequently contain no perylene. In contrast to the perylene profile, concentrations of pyrolytically derived benzo(a)pyrene, chrysene, and pyrene decrease with depth after peaking at a depositional horizon corresponding to *ca.* 1958 (Fig. 20). The rate of sediment accumulation increases after this time, and changes occur in the concentration and character of sedimentary organic matter (Fig. 17). These changes are postulated to be related to acidification of the water and possible enhanced productivity of this lake (Ho and Meyers 1994). The pyrolytic PAH pattern records the history of coal combustion in the northern United States and airborne transport of combustion products to isolated depositional sites such as Mountain Pond (Gschwend and Hites 1981; Furlong et al. 1987). Acid rain and airborne nutrients may have accompanied these combustion products. The good preservation of the PAH depositional record attests to the low reactivity of aromatic hydrocarbons once they have been formed and incorporated into sediments.

Sediments of Sagamore Lake in Adirondack Park of northern New York State contain three types of downcore PAH patterns (Tan and Heit 1981). Perylene increases in concentration to a

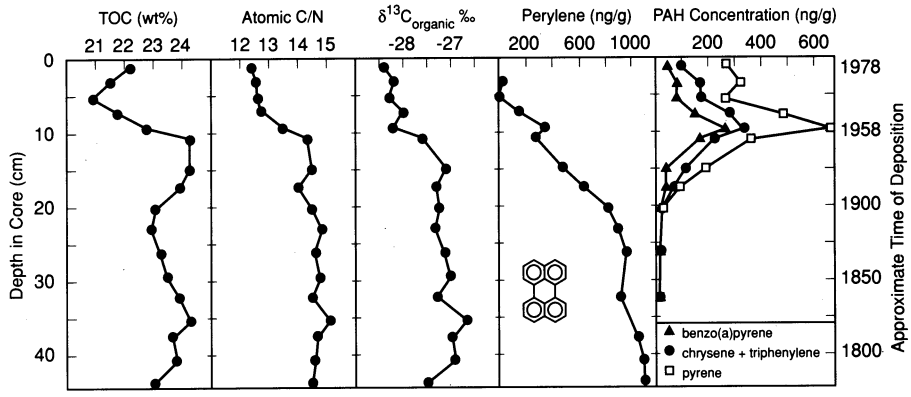


Fig. 17. TOC concentrations, organic C/N ratios, organic $\delta^{13}C$ values, and concentrations of perylene and three pyrolytic polycyclic aromatic hydrocarbons (PAH) in a dated sediment core from Mountain Pond, Maine. Organic matter is predominantly land-derived. Perylene progressively increases in concentration as sediment age increases, indication its diagenetic formation from some precursor material. The concentration maxima of the three pyrolytically formed PAHs coincides with the time of peak coal combustion. Sediments deposited since *ca.* 1958 reflect effects of lake acidification. (Data are compiled from Norton et al. 1981; Gschwend and Hites 1981; Gschwend et al. 1983; Ho and Meyers 1994)

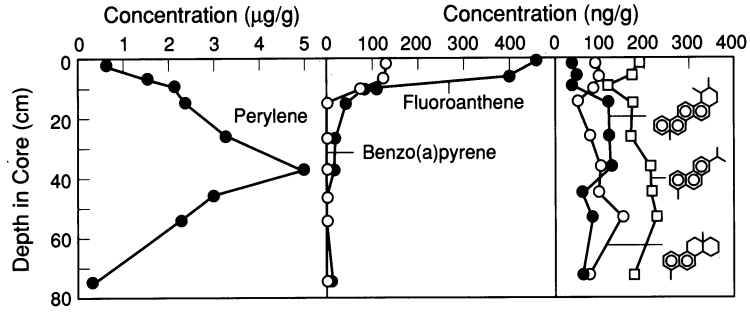


Fig. 18. Concentrations of perylene, two pyrolytic PAHs, fluoranthene and benzo(a)pyrene, and three PAHs derived from biogenic precursors in a sediment core from Sagamore Lake, New York State. The perylene profile suggests that this PAH is slowly formed and that its ultimate concentration is limited by the amount of precursor material. The pyrolytic PAHs reflect the historical combustion of coal. The three PAHs having postulated precursors are evidently formed quickly by diagenesis in surface sediments and not in deeper sediments. (Data are from Tan and Heit 1981)

core depth of 35 cm, corresponding to a sediment age of approximately 85 years, and then decreases to the bottom of the 75-cm core (Fig. 18). The decrease in concentration indicates that older sediments contain less of the unknown precursor to perylene. Diagenetic degradation of perylene is unlikely inasmuch as a similar decrease does not occur in the older Mountain Pond sediments. The perylene profile suggests that a change in the vegetation of the Sagamore Lake watershed occurred around 1890–1900. The concentrations of the pyrolytic PAHs fluoranthene and benzo(a) pyrene are highest at the surface of this 1978 core, and drop to low and nearly constant values by a core depth of 15 cm. The pyrolytic PAH patterns reflect greater fossil-fuel combustion in more modern times. Nonalkylated forms dominate the fluoranthene and pyrene PAH families, clearly identifying a high-temperature source, as opposed to a geologically older, low-temperature source (Tan and Heit 1981).

Concentrations of retene, dimethyl-octahydrochrysene, and trimethyl-tetrahydropicene vary little over the Sagamore Lake sedimentary record (Fig. 18), suggesting that these compounds are produced quickly in sediments and are the relatively stable products of diagenesis. The postulated precursor of retene is abietic acid, a component of pine resin (Simoneit 1977; Wakeham et al. 1980a). The biogenic precursors for chrysene and picene are not confirmed; α-amyrin, present in woody plants, is a possible

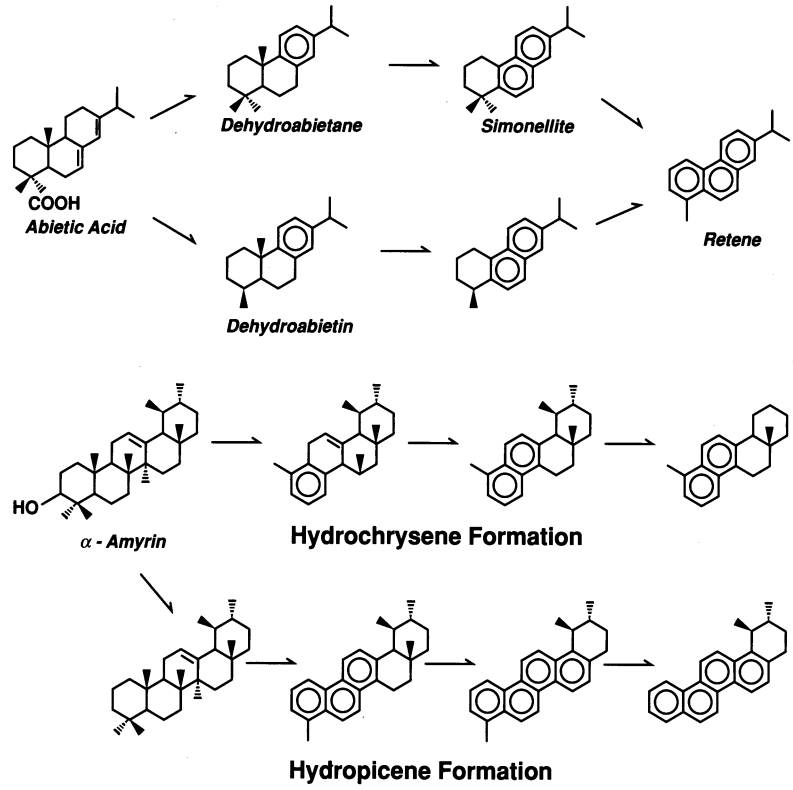


Fig. 19. Postulated diagenetic pathways for the formation of retene, hydrochrysenes, and hydropicenes in sediments (Wakeham et al. 1980a; Tan and Heit 1981). Another likely precursor of hydrochrysene, but not hydropicene, is β-amyrin, the isomeric form of α-amyrin, which differs in the positions of the two methyl groups attached to the E-ring

source (Spyckerelle et al. 1977). Postulated diagenetic pathways for the three types of biogenic PAHs found in Sagamore Lake sediments are summarized in Fig. 19. Many of the intermediate compounds have been identified (Tan and Heit 1981), giving credence to these hypothetical transformations. β-Amyrin can be an additional precursor for hydrochrysene, especially in lakes having a large fraction of deciduous trees in their watersheds. β-Amyrin is abundant in the sediments of Lake Biwa, Japan, and is the major source of hydrochrysene in this lake (Ishiwatari, unpublished results). Hydropicene cannot be derived from β-amyrin, however, because the positions of the two methyl groups on its saturated E-ring clearly reflect an origin from α-amyrin.

4.8 "Free" and "Bound" Geolipid Fractions of Lake Sediments

Many of the lipid components of biological organic matter are biochemically bound into the structural matrices of the cells and cell walls of organisms. Geochemical studies generally ignore such bonds and instead concentrate on the molecules released by hydrolysis of sediment extracts. Important geochemical information, however, can potentially be obtained from geolipids in which the original biochemical bonds are not destroyed during isolation and analysis.

A two-step sediment-extraction procedure is commonly employed to preserve some of the original biochemical associations of geolipids. In the first step traditional solvent extraction is done to obtain the soluble geolipid components. These include truly free molecules having no bonds with other compounds and also molecules that are chemically combined with others, yet can be dissolved in the solvents. This fraction is called the free or solvent-extractable lipids. The second step uses hot acid or base to break hydrolyzable bonds, followed by a second solvent extraction. These lipids are normally called the bound or non-solvent-extractable fraction. The additional lipids obtained by the hydrolysis procedure include materials incorporated into humic substances, retained in biological detritus, and associated

with minerals. The free and bound geolipid fractions of sedimentary organic matter appear to have different sources. The free fraction generally contains a large proportion of land-plant biomarker material, whereas the bound fraction is constituted mostly of algal and bacterial components (Cranwell 1978, 1984; Ishiwatari et al. 1980; Cranwell et al. 1987; Wünsche et al. 1988; Meyers and Ishiwatari 1993).

The ratio of free-to-bound geolipids commonly decreases with depth in lake sediments, indicating that either free components become diagenetically converted into bound forms (e.g., Cranwell et al. 1987), or that components of the free fraction are diagenetically destroyed more easily than the bound components. This pattern is not universally found, however, and complicated source and preservation effects appear to influence the free and bound geolipid fractions in some lake sediments (e.g., Meyers et al. 1984b; Wünsche et al. 1988). As suggested by Cranwell (1978), the bound materials may represent the contents of intact biological debris, and therefore may be strongly influenced by fluctuations in preservational conditions.

The intact esterified geolipid fraction is a specific type of bound material that has been studied for biomarker source information. Compositions of the fatty acid esters of alkanols, sterols, and triterpenols isolated from lake sediments as old as 50 Ky indicate that the ester linkage, combined with the high molecular weights of the esters, enhances the resistance of bound lipids to microbial attack (Cranwell 1986; Cranwell and Volkman 1981). These ester-linked biomarker compounds consequently retain evidence of their respective algal or vascular plant origins. Bacterial biomarkers constitute little of the ester fraction, principally because these organisms do not synthesize large amounts of esters. Selective losses of lower-molecular-weight esters have nonetheless been inferred from surprisingly low contributions of algal ester biomarkers in sediments of Tokyo Bay (Fukushima and Ishiwatari 1984).

5 Sources and Alterations of Pigments in Lake Sediments

Higher plants and algae synthesize a variety of pigmented organic compounds, principally for use in photosythesis. Some of these molecules are biomarkers specific to various types of plants, and their preservation in sedimentary records therefore provides evidence of former biota. Pigments contain chromophore groups, typically conjugated C=C bonds, which absorb portions of the visible solar spectrum and give the molecules their characteristic colors. In addition, many of the pigments have oxygen-containing functional groups (Fig. 20). The double bonds and functional groups provide sites for microbial attack, making these compounds especially sensitive to diagenetic alterations. Despite this liability, a portion of the pigment input to lakes can become diagenetically more stable. The major types of stabilizing alterations are complete aromatization of the chlorophyll tetrapyrrole ring to lead to porphyrins and hydrogenation of carotenoid carbon-carbon double bonds to form isoprenoid alkanes. These stabilized products of diagenesis are found in ancient lake sediments, but not in young sediments. The transformations proceed slowly.

The principal photosynthetic pigments used by plants are the chlorophylls, of which chlorophyll *a* (Fig. 20) is the most common. The various

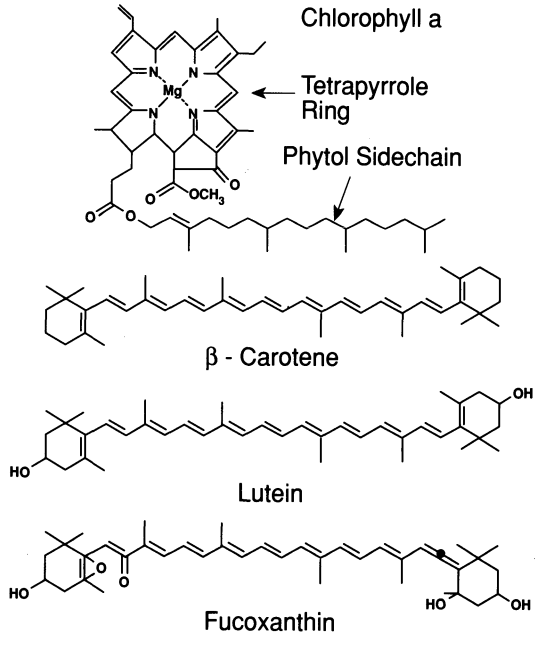


Fig. 20. Molecular structures of representative types of pigments found in lake sediments. Chlorophyll *a* is the dominant chlorophyll, which are the primary photosynthetic pigments and are present in all photosynthetic plants. The carotenes and xanthophylls are secondary pigments and are present in different amounts in different plants, thereby becoming indicators of plant types (Table 5)

chlorophylls differ principally in the alkyl side chains attached to the central tetrapyrrole ring; chlorophyll *a* has the diterpenoid alcohol, phytol, attached by an ester linkage. Chlorophylls absorb solar energy most efficiently in the red portion of the visible spectrum, which are wavelengths that do not penetrate deeply into water. For this reason aquatic plants have evolved different carotenoid compounds, which they utilize as accessory pigments to broaden the range of wavelengths useful for photosynthesis (Table 5). Many of the accessory pigments are characteristic of different algae and can be used to help identify past sources of organic matter in lake sedimentary records.

Both source changes and the effects of diagenesis affect the amounts and types of pigments present in lake sediments. Sanger (1988) and Leavitt (1993) have reviewed the factors important to the accumulation of pigments in lacustrine sediments and note that these organic compounds are seldom preserved intact. Preservation is generally improved in lakes having higher aquatic productivities, with the result that the sedimentary organic matter contains greater proportions of pigments (e.g., Gorham et al. 1974; Gorham and Sanger 1976). Land-derived pigments do not typically survive transport to lakes. Even lake-derived pigments are rapidly degraded if they do not quickly become incorporated into the lake bottom. Carpenter et al. (1986) found that photodegradation of chlorophyll derivatives was virtually complete after only 3 days in the photic zones of lakes in southern Michigan. Increased grazing by zooplankton, which leads to more rapid sedimentation, appears to be the major factor in enhancing preservation of pigments and their derivatives in lacustrine sediments (e.g., Leavitt et al. 1989). After incorporation in lake sediments pigments continue to undergo diagenesis. Keely and Brereton (1986) documented the progressive conversion of chlorophylls *a* and *b* into pheophytins *a* and *b* in a core representing a 100-year accumulation of sediment in Priest Pot, England. The dominance of pheophytins, the demetallized versions of chlorophylls, rather than pheophorbides, in which both magnesium and ester side chains are lost, probably results from the absence of abundant grazing zooplankton in this eutrophic lake, inasmuch as cleavage of this ester linkage typically occurs in food chains that include these animals (Blumer et al. 1971). The interaction of source and preservation factors is complex. Similar changes in the proportions of chlorophyll and carotenoid components of total organic matter in sediments from Brown Pond, Ohio, suggest that both production and preservation are at least loosely linked (Fig. 21). The absence of a progressive diagenetic trend for the pigment contents of these sediments, however, implies that algal production is the dominant factor.

The reactivity of pigments makes them sensitive indicators of changes in lake environments. For

Table 5. Selected pigments indicative of different types of freshwater algae

Pigment	Taxa
Chlorophyll *a*	Plantae
Chlorophyll *b*	Tracheophyta, Chlorophyta, Euglenophyta
Chlorophyll *c*	Chrysophyta, Pyrrophyta
Alloxanthin	Cryptophyta
Fucoxanthin	Chrysophyta
Lutein	Chlorophyta, Charophyta, Euglenophyta
Peridinin	Pyrrophyta
β-carotene	Plantae
Myxoxanthophyll	Cyanophyta
Canthaxanthin	Cyanophyta
Oscillaxanthin	Cyanophyta

Compiled from Schwendinger 1969; Züllig 1981; Leavitt et al. 1989.
The chlorophylls are the primary pigments involved in photosynthesis; the other compounds are accessory pigments that expand the useful wavelengths in the visible portion of the solar spectrum.

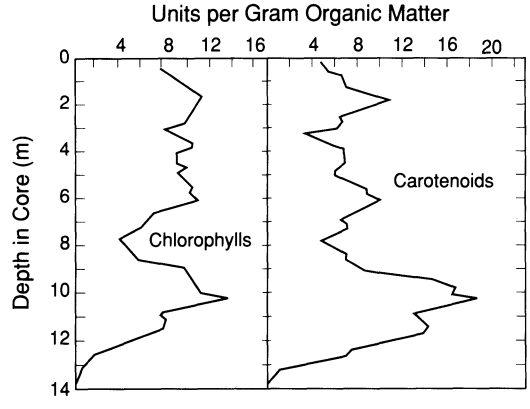


Fig. 21. Downcore contributions of chlorophyll derivatives and carotenoids to total organic matter in sediments of Brown Pond, Ohio. The close similarity of the contributions of the two pigment types suggests common links to production and preservation. (Adapted from Sanger 1988)

example, the diagenetic conversion of chlorophyll to pheophytin is enhanced by acid conditions. This property has been employed by Guilizzoni et al. (1992) to reconstruct the progressive acidification of lakes in the Central Alps. The ratio of chlorophyll to pheophytin is depressed in modern sediments, but increases in older sediments. This pattern is opposite to what would be produced by diagenesis alone, and instead records the onset and increase in acid precipitation in Europe over the past half century.

Changes in past algal populations evidently can be recorded in the pigment compositions of sediments. Progressive eutrophication of Esthwaite Water in the English Lake District is documented by increases in sediment concentrations of the carotenoid pigments characteristic of cyanophytes (Fig. 22). Diminished concentrations in the uppermost, most eutrophic sediments appears to result from replacement of cyanophytes by other algae (Griffiths 1978). This decrease may possibly be due to a preservational effect, but the younger sediments, rather than the older, would be expected to display enhanced preservation. A related history of the development of eutrophication in Zürichsee, Switzerland, is evident in the pigment contents of a century-long core of sediment (Züllig 1981). In this case ten different pigment groups were utilized to identify changes in algal populations as lake conditions changed.

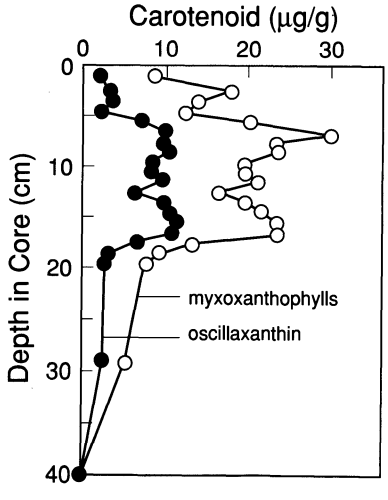


Fig. 22. Concentrations of two carotenoid pigments characteristic of blue-green algae found in sediments of Esthwaite Water, England, by Griffiths (1978). Bottom of core corresponds to ca. 1885. Progressive eutrophication and then remediation of this lake is indicated by the increases of these pigments in younger sediments and following decreases in modern sediments

Although their multiple double bounds make them reactive compounds, pigments can be sufficiently preserved in sediments to record paleolimnological conditions extending back thousands of years. Pigments in the sediments of Kirchner Bog, Minnesota, for example, contain a history of postglacial plant succession spanning nearly 14 Ky (Sanger and Gorham 1972).

6 Sources and Diagenesis of Lignins and Their Derivatives

Lignins are phenolic polymers synthesized by higher plants as part of their vascular systems. Nearly all vascular plants grow on land, and therefore this organic-matter fraction of sediments largely records the contributions and diagenetic alterations of land-derived organic matter. Gymnosperms (nonflowering plants) and angiosperms (flowering plants) synthesize distinctive types of lignin, thus past changes in watershed vegetation can be inferred from the lignin contents of lake sediments. Moreover, lignin is relatively resistant to diagenesis, making its sedimentary record longer-lived than many other forms of primary organic matter.

Characterization of lignin in sediments typically involves oxidative depolymerization to release various phenolic aldehyde, ketone, and acid monomers such as those illustrated in Fig. 23. Monomers have been grouped by Hedges and Mann (1979) to identify the general vascular plant sources of sedimentary lignins (Fig. 24). A measure of the relative contributions of woody and nonwoody land-plant tissues is given by the C/V ratio, which is the sum of *p*-coumaric acid plus ferulic-acid concentrations divided by the sum of the three vanillyl phenols. Gymnosperm sources of land-plant residues are distinguished from angiosperm sources by the S/V ratio, which is the sum of the amounts of the three syringyl phenols divided by the sum of the vanillyl phenols. Oxidative diagenesis of lignin components can be inferred from an increase in the total acid phenols relative to the total aldehyde phenols, expressed as the Ad/Al ratio (Hedges et al. 1982; Ertel and Hedges 1984).

A drilled core of sediment from Lake Biwa, Japan, has provided a unique opportunity to investigate the record of lignin source and diagenetic changes over a long period of time. The core was obtained during 1982–1983, and

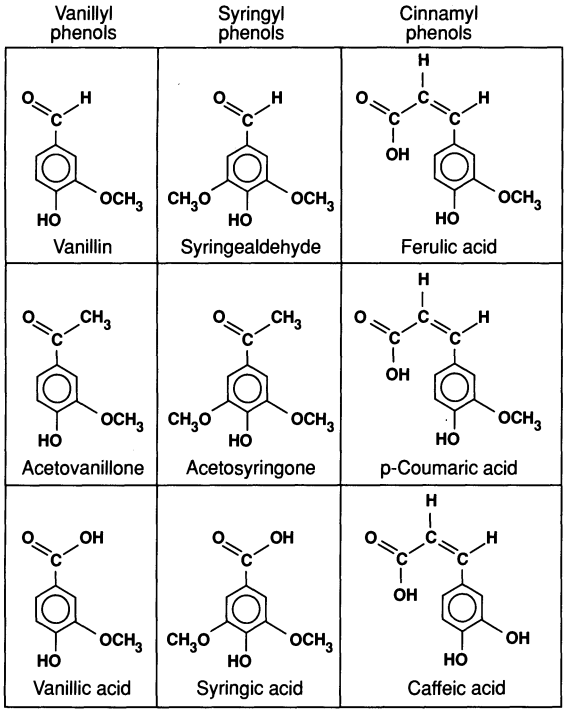


Fig. 23. Molecular structures of phenolic compounds obtained from the oxidative depolymerization of lignins. Caffeic acid is a minor product compared with the other eight compounds

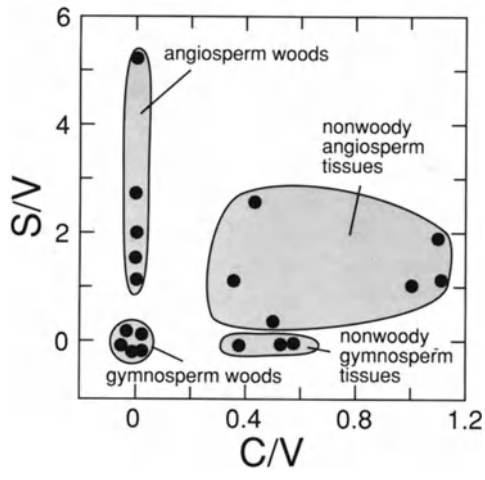


Fig. 24. Lignin parameters S/V vs C/V with their general source assignments indicated. (Data adapted from Hedges and Mann 1979)

430 Kya is the extrapolated basal age of the T Bed, a continuous sedimentary unit representing lake conditions similar to those of the present (Meyers et al. 1993). Lignin contents have been characterized in the T Bed and the underlying S and R Beds by Ishiwatari and Uzaki (1987). The latter two beds are discontinuous and represent shallow-water or fluvial conditions; fission-track dating of an ash layer at 681 m in the R Bed gives an age of 2.4 My (Takemura 1990).

Accumulation of organic matter was fairly uniform over the entire history of the T Bed; organic-carbon concentrations are generally between 0.5 and 1%, and C/N ratios remain approximately 10 (Fig. 25). In the coarser S and R Beds, organic-carbon values are slightly lower, and the higher C/N ratios indicate a greater proportion of land-plant matter. The contribution of lignin to the total organic matter drops steadily with depth in the T Bed, evidently because of diagenesis, inasmuch as the S/V and C/V ratios indicate that the lignin composition does not change. Ishiwatari and Uzaki (1987) calculate a lignin half-life 400 Ky on the assumption that in situ degradation is responsible for this decrease. Their value is based on an earlier estimate of a basal age of 600 Ky for the T Bed; a recalculated half-life is 300 Ky. These values indicate the potential longevity of lignins in lacustrine sediments and their value as a paleoenvironmental indicator.

An increase in the ratio of vanillic acid to vanillin, $(Ad/Al)_v$, shows that diagenesis of lignin components occurs in Lake Biwa sediments (Fig. 25). Vanillic acid is the more oxidized component in this ratio; its increase suggests continued oxidative degradation of lignins. Furthermore, the $(Ad/Al)_v$ ratio is above 0.5 throughout the core, which is substantially higher than in fresh plant material (0.15: Hedges et al. 1982). The elevated $(Ad/Al)_v$ values indicate that the lignins delivered to Lake Biwa have been extensively oxidized prior to deposition. In wood buried in sediments for up to 25 Ky, as much as 30% of the original syringly phenols can be lost from lignins, whereas vanillyl components are preserved better (Hedges et al. 1985). Although these types of selective diagenesis can jeopardize source identification, the low S/V ratios in Lake Biwa sediments agree with pollen data that show a dominance of gymnosperm sources of organic matter to these sediments (Ishiwatari and Uzaki 1987).

7 Diagenesis of Carbohydrates and Proteins in Lake Sediments

Carbohydrates and proteins are two important types of biologically synthesized organic matter.

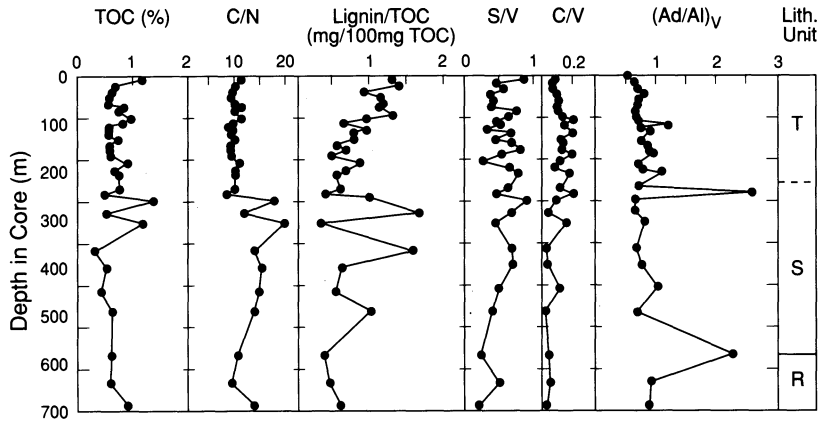


Fig. 25. Downcore comparisons of organic carbon (*TOC*), $\delta^{13}C_{organic}$, atomic C/N ratios, total lignin derivatives, S/V, C/V, and the Ad/Al ratio for syringyl phenols from sediments of Lake Biwa, Japan. The *T* bed is a continuously deposited deepwater clay layer representing the past 430 Ky of lake history. A decrease in the lignin/TOC ratio indicates gradual degradation of lignin. Variations in organic-matter parameters in the *S* and *R* beds reflect varying inputs under shallow-water depositional conditions. The sediment is dated at 2.4 My at a core depth of 681 m. (Data are from Ishiwatari and Uzaki 1987)

Carbohydrates encompass simple sugars, which are water-soluble and reactive compounds, and complex sugars having high molecular weights, which are consequently relatively insoluble and less reactive. The simple sugars are both produced and destroyed rapidly within sediment microcosms, with the result that the source and alteration pathways of these carbohydrate forms are difficult to decipher. Proteins, made up of amino acid units, can be similarly reactive. Interconversion between different amino acids is common, again obscuring information about source and diagenesis. Both carbohydrate and protein compounds decrease relative to total organic carbon in sediments of Mangrove Lake (Hatcher et al. 1982), and these primary-organic-matter fractions generally appear to decompose rapidly in lacustrine sediments (Kemp and Johnston 1979).

Attempts to link amino acid compositions of sediments to those of probable plant sources have not been successful. Casagrande and Given (1980) compared amino acid compositions of peat deposits with those of swamp grass and mangrove trees. Their conclusion was that the bulk of peat amino acids were produced by microbes. Primary source patterns had been erased. The secondary amino acids, however, were produced as part of the sedimentation process, and were therefore approximately the same age as the peat deposits.

The contemporary formation of amino acids by benthic biota permits their use to date sediments through the racemization of the stereochemical specificity of biosynthesized amino acids. This slow-acting process, by which the original L-amino acids are converted to an equilibrium mixture of L- and D-forms, is usually not applicable to lake sediments, because of their geologically limited ages. In some situations, however, it can be useful. For example. McCoy (1987) employed the epimerization of L-isoleucine to D-alloisoleucine in fossil gastropod shells to conclude that some Lake Bonneville sediments date from before 2 Mya, confirming the antiquity of this Plio-Pleistocene precursor to the Great Salt Lake of Utah.

Monosaccharide compositions of potential source organisms have been explored for their potential as tracers of organic-matter inputs to sediments. Cowie and Hedges (1984) examined plankton, bacteria, and land plants for distinctive sugar compositions. They found that aquatic and land sources could be distinguished in coastal marine sediments. A similar source study in two Minnesota lakes found, however, that no correlation existed between the monosaccharides of dominant aquatic plants and those of sediments (Rogers 1965). Concentrations of total sugars in the lake sediments appeared to reflect the amount of postdepositional degradation, rather than initial contributions. The reactivity of even complex carbohydrates is shown by losses of 90–98% of the original polysaccharide contents of wood buried in sediments for approximately 2500 years (Hedges et al. 1985).

8 Paleolimnological Organic Geochemistry

The amounts and types of organic matter in lake sediments provide an integrated history of past life and conditions in and around each lake. Multidimensional organic geochemical studies have been done on sediments from a number of lakes. Indications of changes in the trophic status of these lakes and of changes in the watersheds around them have emerged from the organic-matter records documented by these studies. The effects of both natural and anthropogenic changes are manifested in the types and amounts of organic-matter components of lake sediments deposited over time.

8.1 Organic-Matter Record in the Laurentian Great Lakes of North America

The North American Great Lakes have large surface areas and volumes, but depths that are shallow and watersheds that are small in comparison with their areas. Lake Huron and Lake Michigan share a common water mass, have similarly oligotrophic ecosystems, and are similar in sedimentation processes (Rea et al. 1981; Leenheer and Meyers 1984). Lake Huron is larger in surface area than Lake Michigan (59 530 km^2 vs 57 780 km^2), but the greater depth of Lake Michigan (average 85 m) gives it a larger volume than Lake Huron (average 60 m). The two lakes have been the subjects of a variety of organic geochemical studies.

The large size of Lake Michigan allows study of short-term changes during settling of organic matter to lake bottoms at locations distant from land (e.g., Eadie et al. 1984; Meyers et al. 1980b, 1984a; Meyers and Eadie 1993). Organic-carbon concentrations of settling particles collected in sediment traps decrease with depth, whereas the organic-matter bulk character changes little (Table 6). The measured decreases in concentration agree well with the estimates of substantial oxidation of organic matter during sinking through the epilimnion and hypolimnion (Table 1). The particle-mass flux is markedly higher at all levels in the southern trap array than in the northern (Table 6). The difference in water depth, 145 m in the south as opposed to 171 m in the north, contributes to some of this contrast inasmuch as turbulent resuspension of bottom material is greater in shallower water than in deeper areas. The primary cause, however, is from the greater amount of fine-sized particles delivered to the southern basin by rivers. The small grain size of these clastic particles permits them to travel far into the lake and to be easily resuspended before finally sinking to the bottom. The larger supply of mineral sediment particles dilutes the total organic carbon (TOC) concentrations of the traps in the southern location (Table 6). The TOC mass fluxes nonetheless show that the total amount of organic carbon associated with sinking particles is greater in the southern traps than in the northern. This difference is consistent with the larger fluvial supply of nutrients and organic matter from land areas in the south (Mackin et al. 1980).

Table 6. Organic-matter characteristics of settling particles collected in sediment traps moored in Lake Michigan

Sediment trap	TOC (%)	Atomic C/N	$\delta^{13}C$ (‰)	Long/short *n*-alkanes
Station 4[a]				
15 m	16.0	20	−27.7	5.6
35 m	14.2	23	−28.8	6.2
80 m	6.4	9	−26.8	5.0
120 m	4.8	11	−26.2	1.3
140 m	8.8	21	−26.6	1.9
Station 11[b]				
11 m	38.1	13	−29.2	6.0
31 m	45.8	21	−28.1	7.0
91 m	10.9	17	−27.5	5.0
146 m	4.8	8	−27.4	7.3
166 m	5.7	13	−27.8	7.1

Long/short *n*-alkane ratios are the sum of C_{27} + C_{29} + C_{31} divided by the sum of C_{17} + C_{19} + C_{21} and represent the ratio of land-derived/aquatic hydrocarbons.
TOC, total organic carbon.
[a] Southern Lake Michigan.
[b] Northern Lake Michigan.

The changes occurring to the organic-matter contents of the settling particles are complex, yet information about sources remains evident. The C/N ratios fluctuate with depth, suggesting that land-derived and algal organic matter have different rates of diagenesis, and that lateral inputs of organic matter may occur. In contrast, carbon isotope ratios show little diagenetic or source-change effect. The ratios of long/short *n*-alkanes indicate more land-derived hydrocarbons in the contents of the upper traps at station 4 and in all traps at station 11 in the northern portion of the

lake, which has a forested watershed. Estimates of downward fluxes of *n*-alkanoic acids and *n*-alkanes in traps at two depths indicates that degradation of the acids occurs ten times faster than for hydrocarbons (Meyers and Eadie 1993).

The $\delta^{15}N$ values of particles intercepted by sediment traps indicate that microbial or food-chain preprocessing of their organic matter occurs during sinking. These values are in the range of 3.3 to 5.2‰. Pang and Nriagu (1977) reported $\delta^{15}N$ values of phytoplankton in Lake Superior to average 1.6‰, whereas zooplankton and sedimentary organic matter had average $\delta^{15}N$ values of 5.7 and 5.0‰, respectively. Food-chain processing of organic matter commonly produces a several per mil shift to heavier nitrogen isotope ratios at each trophic level (e.g., Fry 1988), suggesting that the Lake Superior sedimentary organic matter was largely derived from phytoplankton and had been utilized by two or more trophic levels. The same type of processing probably occurs in Lake Michigan, and the sediment-trap values of 3–5‰ in Table 6 indicate that this process occurs mostly in the upper water column where organic-carbon concentartions decrease most rapidly.

The sedimentary record in the Great Lakes dates from the retreat of the Laurentian ice sheet approximately 12 Kya. Although continuous at some locations, the record is often punctuated by hiatuses due to slumping, underlake erosion, and changes in lake level resulting from isostatic rebound and drainage-channel downcutting (Rea et al. 1980, 1981). Sediment cores from sites located close to each other often contain very different spans of lake history, and therefore allow interesting comparisons. One location in southern Lake Huron, for example, provides a continuous record of the most recent 400 years of sediment accumulation, whereas another location less than 7 km away is made up almost entirely of glaciolacustrine clay deposited 12 Kya (Meyers et al. 1980c). Fine-sized sediments generally contain higher concentrations of organic carbon, *n*-alkanoic acids, and *n*-alkanes than those found in coarser sediments (Thompson and Eglinton 1978; Meyers and Takeuchi 1979). The glaciolacustrine clays of core 58 are nonetheless poorer in organic carbon, fatty acids, and hydrocarbons than the modern silty clays of core 12 (Fig. 26). Dilution of organic matter by high sedimentation rates of the glaciolacustrine clays probably caused the low concentrations. In addition, the productivity of the surrounding land areas immediately following glacial retreat was probably lower than in subsequent periods. Indeed, the low C_{29}/C_{17} *n*-alkane ratio in core 58 indicates that little land-derived hydrocarbon material reached this site. In contrast, variations in the C_{29}/C_{17} ratios in core 12 show that the proportions of land-plant and algal hydrocarbons have fluctuated repeatedly over the past 400 years, and that land-derived hydrocarbons have often been dominant. Diagenesis of core 12 fatty acids is indicated by downcore

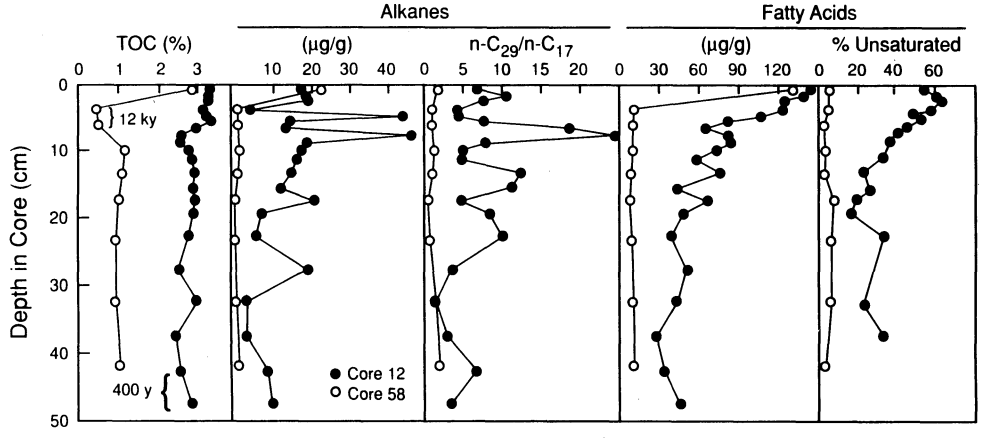


Fig. 26. Comparison of downcore changes in TOC, total *n*-alkane and fatty acid concentrations, $n\text{-}C_{29}/n\text{-}C_{17}$ alkane ratio, and percentage of unsaturated components of the total fatty acids in two sediment cores from southern Lake Huron. The sediments differ drastically in age, and consequently their lipid contents are markedly different. The 400-year age of the basal section of core 12 is extrapolated from ^{210}Pb dating. Core 58 consists of a veneer of modern sediment overlying glaciolacustrine clay 12 Ky in age. (Data are from Meyers et al. 1980c)

decreases in their total concentration and in the proportion of unsaturated acids (Fig. 26). Both of these parameters are low in core 58, because diagenesis is further advanced in these much older sediments.

Over the past 200 years sources of organic matter to the Great Lakes have been successively modified by replacement of native watershed vegetation by farmland, urbanization of the near-lake areas, industrialization of the region, and eutrophication of some nearshore areas of the lakes. These changes are recorded in the organic-matter contents of lake sediments. A shift in organic-carbon $\delta^{13}C$ values from $-27‰$ in Lake Ontario sediments deposited before *ca.* 1830 to values of $-24‰$ in younger sediments has been interpreted by Sackett et al. (1986) to record the replacement of native C_3 plants by agricultural C_4 plants in the watershed of this lake. The carbon isotope change is accompanied by the appearance of *Ambrosia* (ragweed) pollen in the sediment record, which records the deforestation of surrounding land areas *ca.* 1830. A subsequent interpretation of the shift to heavier organic-carbon isotopic ratios in sediments from the Rochester Basin of Lake Ontario is that enhanced algal productivity is the principal cause (Schelske and Hodell 1991), although a change in watershed vegetation has occurred.

Several factors make Lake Ontario especially sensitive among the Laurentian Great Lakes to environmental change. Lake Ontario is approximately one-third the area and volume of either Lake Huron or Lake Michigan, and is consequently impacted more easily than these larger lakes. Its area is 19 000 km^2 and its mean depth is 86 m. The lake is also the final basin in the flow pattern which sees water exit the Great Lakes system via the St. Lawrence River. Therefore, it is ultimately affected by changes that have occurred to any of the lakes.

The organic-matter contents of sediments from Lake Ontario record some of the historical changes that have occurred in the Great Lake ecosystem. Early settlement and forest clearance by European settlers in the mid-nineteenth century produced an increase in lake productivity that is marked by enhanced silica and organic-carbon delivery to lake sediments (Schelske et al. 1983, 1988). Urbanization of the Ontario watershed after 1940 dramatically increased delivery of nutrients to the lake. Organic-carbon delivery doubled and inorganic-carbon accumulation increased by a factor of ten (Schelske et al. 1988; Schelske and Hodell 1991). These alterations of the formerly pristine lake system left their imprints on the geolipid composition of lake sediments. The contributions of extractable hydrocarbons and fatty acids to the total sedimentary organic content have markedly increased in recent sediments (Fig. 27). Contributions of land-derived organic matter typically contain higher proportions of *n*-alkanes than those from aquatic algae (Cranwell et al. 1987; Goossens et al. 1989). The proportion of land-derived long-chain *n*-alkanes to algal short-chain *n*-alkanes also increases in the more recent sediments (Fig. 27). Land-derived long-chain *n*-alkanoic acids degrade significantly slower than algal fatty acids (Haddad et al. 1992; Meyers and Eadie 1993). The twentieth century

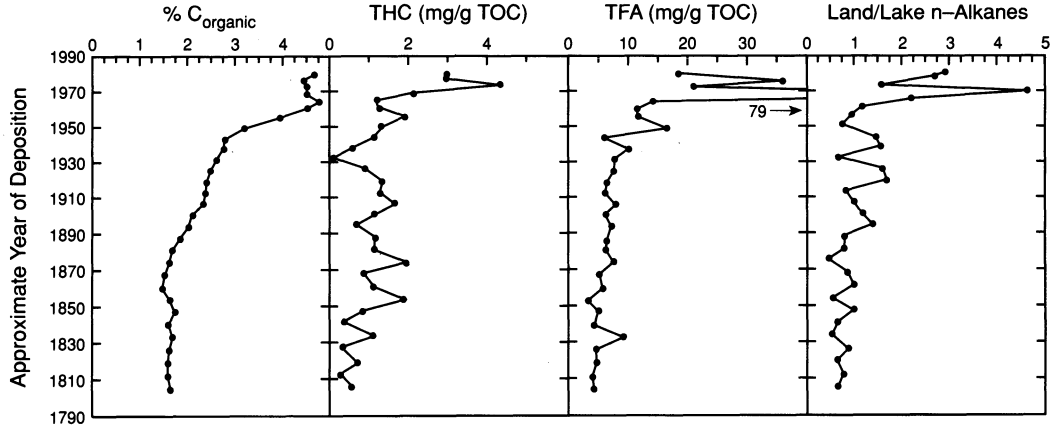


Fig. 27. Concentrations of organic carbon, hydrocarbons (THC), and fatty acids (TFA) in sediments core from the Rochester Basin of Lake Ontario. The proportion of land- to lake-derived *n*-alkanes is represented by the ratio of $(C_{27} + C_{29} + C_{31})/(C_{17} + C_{19} + C_{21})$ components

Lake Ontario sediments evidently record progressively larger deliveries of land-derived organic matter to this lake. This pattern reflects the increasingly urbanized character of the watershed, which has accelerated land runoff from paved roadways and from domestic waste waters. Paradoxically, this factor has also increased nutrient supply to the lake flora and has eutrophied the lake waters (e.g., Schelske et al. 1983; Schelske and Hodell 1991).

Some parts of the Laurentian Great Lakes have been particularly impacted by environmental changes caused by humans. Sediments of Saginaw Bay, Lake Huron, contain a geolipid record of both urbanization of the local land area and eutrophication of the bay. Contributions of aquatic geolipid biomarkers have increased since *ca.* 1900 (Meyers and Takeuchi 1981), and the relative proportions of land-plant *n*-alkanols, sterols, and *n*-alkanes have consequently become smaller (Fig. 28). Phytol concentrations correlate with chlorophyll and hence with algal biomass (Schultz and Quinn 1974), whereas dihydrophytol is eroded from land and has a constant concentration in Saginaw Bay sediments. The increase in the phytol/dihydrophytol ratio indicates enhanced algal inputs (Fig. 28). These changes record progressive eutrophication of the waters of Saginaw Bay.

Petroleum residues at the same time become the dominant hydrocarbons in the bay sediments, presumably from road runoff as also seen in Lake Washington (Wakeham 1976). The unresolved complex mixture (UCM) changes from a minor to the major part of the total aliphatic hydrocarbon concentrations (Fig. 28). The UCM concentrations diminish as distance from land increases (Meyers and Takeuchi 1979; Meyers 1984), indicating fluvial sources for the petroleum residues. The heavily industrialized and urbanized watershed of the Saginaw River is the most likely origin of these contaminants.

Petroleum hydrocarbons generally appear to be transported in association with suspended sediment particles in Lakes St. Clair, Erie, and Ontario. Highest concentrations are found in sediments close to major cities and in areas where fine-sized sediment particles can settle to lake bottoms (Nagy et al. 1984). Western Lake Erie, which receives tha discharge from the heavily industrialized and urbanized Detroit River, has the largest accumulation of petroleum hydrocarbons. The sediments of shallow Lake St. Clair (approximately 6 m) contain low concentrations of petroleum hydrocarbons (Nagy et al. 1984), yet Meyers (1984) notes that UCM components constitute nearly 80% of the total hydrocarbons in a 20-cm core of sediment from this lake. The organic-matter characteristics of this core closely resemble those of core 58 from southern Lake Huron, which is made up of glaciolacustrine clay estimated to be 12 Ky old. Radiocarbon dating of organic matter in the Lake St. Clair core gives an age of 24 Ky, indicating the presence of a sizable fraction of geologically ancient organic matter. Meyers (1984) suggests that the bulk of the sedi-

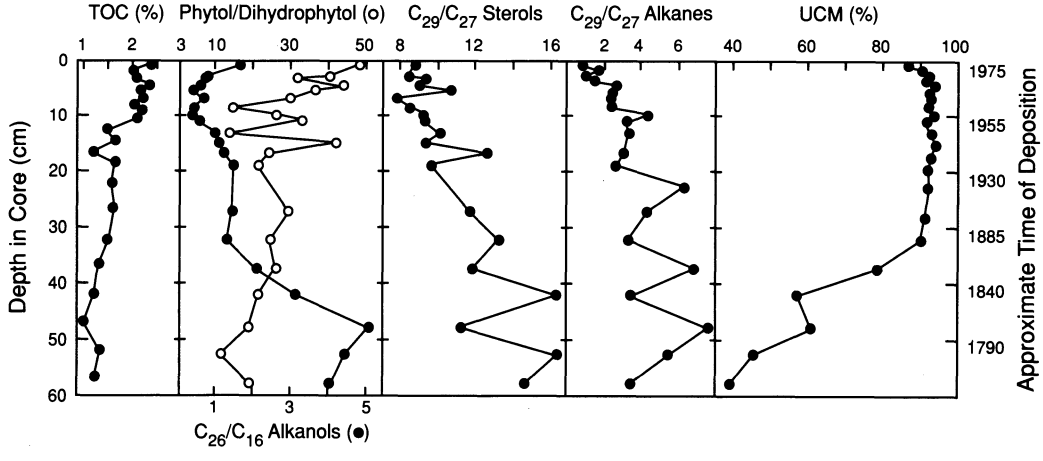


Fig. 28. Downcore changes in TOC concentration and in lipid characteristics in a core of Saginaw Bay sediment. Modern eutrophication of this bay is evident from increase in TOC, phytol/dihydrophytol, and C_{16} alkanol inputs since 1955. Impact of petroleum pollution is recorded by dominance of UCM of hydrocarbons since the late 1800s. Dates are extrapolated from ^{210}Pb dating. (Adapted from Meyers and Takeuchi 1981)

ments in this shallow lake are relict postglacial clays, and that they incorporated petroleum hydrocarbons long ago from natural oil seeps in nearby Canada. Little modern sediment accumulates under the shallow, wind-mixed, turbulent waters of Lake St. Clair.

8.2 Organic-Matter Record in Lake Biwa, Japan

Lake Biwa, the largest lake in Japan, has been the subject of paleolimnological studies since the 1950s. Much of the watershed is forest or farmland, but the areas of human settlement have grown greatly during recent decades. The maximum water depth is 102 m, and the surface area of the lake is 674 km^2. The lake has existed for approximately 6 My, although major tectonic reorganizations of its basin have evidently occurred (e.g., Takemura 1990), which have interrupted the sedimentary record. Organic geochemical studies have concentrated on the upper 250 m of sediments, which is an apparently continuous sedimentary record of the past approximately 430 Ky (Meyers et al. 1993). The results of many of these investigations were reviewed by Ishiwatari and Ogura (1984) and Ishiwatari (1991).

Organic-carbon $\delta^{13}C$ values change from −25.5‰ in near-surface sediments to approximately −28‰ at 200 m (Fig. 29). A progressive change in organic-matter source or diagenesis is not evident from organic-carbon concentrations, C/N ratios, or C/V and S/V ratios, all of which remain virtually unchanged (Fig. 25). Nakai (1972) postulated that the local climate has become progressively warmer over the past 400 Ky, warming the surface waters of the lake and decreasing the kinetic isotopic fractionation by algae, but the pollen record does not confirm this suggestion. The carbon isotope shift is nonetheless intriguing and suggests that some sort of progressive paleoenvironmental change has occurred.

Several episodes of comparatively short-term paleolimnological change are recorded in Lake Biwa sediments. Organic-carbon concentrations are typically approximately 1%, but rise to approximately 2% at two core intervals, between 3 and 15 m as well as 80 and 90 m (Fig. 29). Maximum pollen concentrations and heavier carbon isotope values also occur at the 80- to 90-m depth (Fig. 29). Total *n*-alkane concentrations similarly increase with depth to a maximum between 3 and 15 m, and increase again between 80 and 90 m. The *n*-alkane distributions are dominated by C_{29} or C_{31} (Kawamura and Ishiwatari 1984), which are diagnostic of land-plant waxes from trees or shrubs (C_{29}) or grasses (C_{31}).

Possible changes in the sources of the *n*-alkanoic acids in these sediments have been explored by dividing them into two groups (Kawamura and

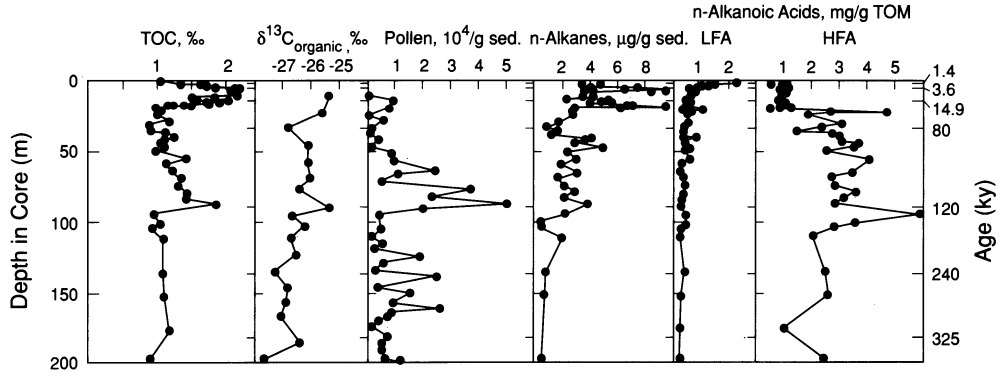


Fig. 29. Concentrations of TOC, total pollen, total *n*-alkanes, lower-molecular-weight fatty acids (LFA), and higher-molecular-weight fatty acids (HFA) in the 200-m core of sediment from Lake Biwa, Japan. LFA and HFA are given as mg of *n*-alkanoic acid per g total organic matter (TOM), which is estimated as TOC × 1.67. Enhanced contributions of HFA suggest that larger amounts of land-plant lipids were delivered to the lake sediments at times in the past that were coincident with enhanced pollen inputs. Enhanced contributions of LFA, in contrast, suggest larger amounts of lake-derived lipids, most notably during the past 15 Ky. Lipid data are from Kawamura and Ishiwatari (1984). Organic $\delta^{13}C$ (PDB) data from Ishiwatari and Uzaki (1987) show a persistent yet unexplained trend to heavier values in younger sediments. Sediment ages are from Meyers et al. (1993)

Ishiwatari 1984). The lower-molecular-weight fatty acids indicative of algae (C_{12} to C_{19}) are the first group (LFA), and the higher-molecular-weight acids (C_{20} to C_{32}) corresponding to land-plant contributions are the second group (HFA). Concentrations of the LFAs decrease with depth relative to total organic matter, whereas HFA concentrations peak at approximately 100 m. The agreement between pollen concentrations and land-plant contributions of *n*-alkanes and *n*-alkanoic acids in sediments between 80 and 90 m indicates that inputs of organic matter from watershed vegetation were elevated during this time. Meyers et al. (1993) have concluded that this sediment interval corresponds to the interglacial episode *ca.* 120 Kya and a wetter climate than during the subsequent glacial period.

Important features of the upper 20 m of Lake Biwa sediments include peak values of organic carbon and LFAs (Fig. 29), and the maximum concentration of diatom frustules (Mori and Horie 1975). These features, combined with C/N values averaging 8.5 in this interval (Kawamura and Ishiwatari 1981), indicate that aquatic production has been the principal source of sediment organic matter. Long-chain *n*-alkanoic acids (HFA) change little relative to total organic matter, but the C_{12} to C_{19} acids (LFA) decrease by a factor of four (Fig. 29), indicating that diagenetic losses are severe for the LFAs. Kawamura and Ishiwatari (1981) noted that some oxidation of *n*-alkanoic acids to hydroxy acids and dicarboxylic acids may occur over the top 5 m of this core, but most of the loss of LFAs is from microbial alteration to non-fatty-acid forms of carbon. Conversion of fatty acids from free to bound forms does not occur during the 20–30 Ky period represented by the upper 20 m of these sediments.

A piston core of the upper 12 m of the Lake Biwa sedimentary record has provided a high-resolution record of global and regional environmental changes that accompanied the most recent glacial–interglacial transition (Meyers and Horie 1993). Organic-carbon concentrations remain generally between 1 and 2.5% throughout the detailed sediment record (Fig. 30). The C/N ratios vary over the narrow range of approximately 6–10. Nakai and Koyama (1991) have determined that the C/N ratios are 7–8 in samples of mixed plankton from Lake Biwa, and are over 30 in plants from surrounding land areas. The correspondence between lake sediment C/N ratios and those of plankton samples indicates that the dominant source of organic matter to lake sediments has been phytoplankton throughout the cored sediment record.

In contrast to the record of no change in source of organic matter to Lake Biwa sediments, a major shift of approximately −4‰ occurs in organic $\delta^{13}C$ values at the Pleistocene–Holocene boundary (Fig. 30). Biota selectively incorporate ^{12}C during synthesis of organic matter, and the amount of discrimination against ^{13}C depends on the concentration of dissolved CO_2 available to phytoplankton (O'Leary 1981; Freeman and Hayes 1992). The isotopic content of organic matter synthesized by aquatic organisms consequently provides an indirect record of fluctuations in atmospheric CO_2 concentrations (Rau et al. 1991). An increase in atmospheric CO_2 would lead to increased equilibrium concentrations of CO_2 dissolved in lake waters and increased discrimination by phytoplankton against ^{13}C. The shift to lighter organic $\delta^{13}C$ values in Lake Biwa sediments consequently appears to preserve a record of the glacial–interglacial increase from 200–280 ppm in atmospheric pCO_2 that has been measured in air bubbles occluded in ice cores spanning the Pleistocene–Holocene transition (Neftel et al. 1982; Barnola et al. 1987).

Important changes occur in the molecular compositions of the high-resolution Lake Biwa sedimentary organic-matter record. The ratio of unsaturated-to-saturated *n*-fatty acids, represented by the $C_{18:2}/C_{18:0}$ ratio, is low in Late Pleistocene sediments, and it increases more than tenfold in postglacial sediments (Fig. 30). Much of this increase probably results from enhanced rates of algal productivity and sediment accumulation (Meyers et al. 1993), which would improve preservation of the normally reactive unsaturated fatty acids. Kawamura and Ishiwatari (1981) proposed that the ratio of sedimentary *n*-$C_{18:2}$ and *n*-$C_{18:0}$ acids may also record the paleotemperatures of lake waters. They note that variations in this ratio coincide with variations in the proportion of boreal conifer pollen in Holocene sediments. If diagenesis were the dominant factor, then a continual decrease in the unsaturated/saturated ratio would be present. The proportion of polyunsaturated acids commonly increases in algae as water temperatures decreases as a biochemical response to maintain fluidity of cell membranes. The $C_{18:2}/C_{18:0}$ ratio appears to record periods of cooler surface water in the most recent history of Lake Biwa, but the

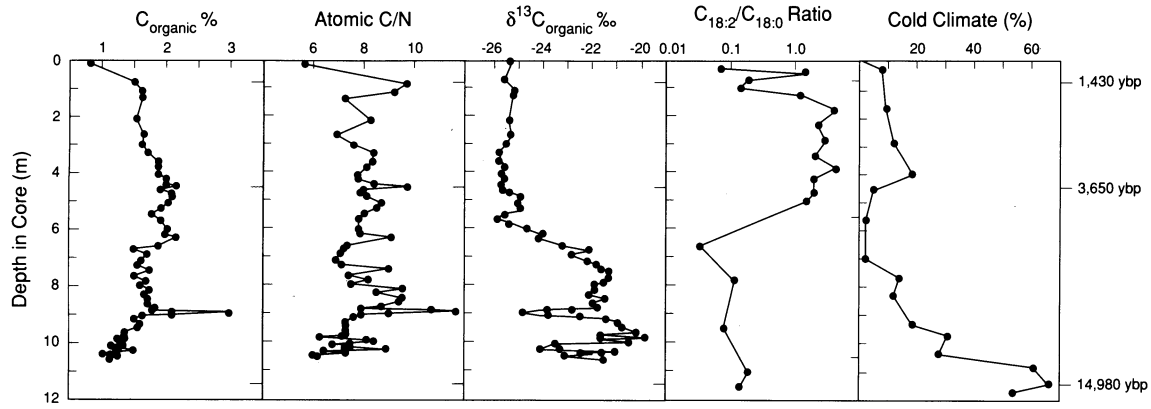


Fig. 30. Organic-carbon concentrations, atomic C/N ratios, and organic $\delta^{13}C$ values of samples from a 12-m piston core of Lake Biwa sediment (Meyers and Horie 1993). Climate record is inferred from pollen contents of lake sediments (Horie 1991). Increases in postglacial productivity and sediment accumulation rates improved preservation of unsaturated C_{18} fatty acids. Small-scale variations in the $C_{18:2}/C_{18:0}$ ratio in postglacial sediments may also record biochemical responses of algae to episodes of cooler water temperatures (Kawamura and Ishiwatari 1981). Organic carbon ^{14}C ages are from Horie et al. (1971)

ratio ultimately diminishes, due to preferential degradation of the unsaturated acid with greater age of the sediment.

8.3 Organic-Matter Record in Greifensee, Switzerland

Greifensee is a small eutrophic lake that is located in a heavily populated region 12 km east of Zürich, Switzerland. it has a surface area of 8.6 km^2 and a maximum depth of 32 m. A 6.4-m-long core from near the center of Greifensee contains three main stratigraphic units: a sapropelic mud from 0 to 60 cm, a carbonate ooze from 60 to 350 cm, and a postglacial clay from 350 to 640 cm.

Concentrations of organic carbon generally decrease with depth in this core, but the most significant downcore changes are found in the compositions of the hydrocarbons in each of the three layers (Fig. 31). In the upper sediment unit, n-C_{17} is the cominant alkane and reflects the high rates of algal production in this eutrophic lake. Concentrations of this algal biomarker decrease in deeper sediments and record times when the lake evidently was oligotrophic. Part of the decrease in contributions of n-C_{17}, however, is due to diagenetic loss of this algal biomarker relative to the long-chain, plant-wax hydrocarbons (Giger et al. 1980). Important contributions of long-chain n-alkanes, represented by n-C_{29} in Fig. 31, are present throughout the 6.4-m core. High CPI values (Bray and Evans 1961) of the long-chain hydrocarbons verifies that their origin is from contemporary watershed plants, inasmuch as ancient n-alkanes would have lost much of their odd/even predominance. The dominance of n-C_{29} at all sediment levels except the topmost, most eutrophic level indicates that deciduous trees have been the major watershed plant type (Cranwell 1973a), which is consistent with what is known of the historical record.

The isoprenoid hydrocarbon phytane, derived through diagenesis from the phytol side chain of chlorophyll a (Fig. 20), is found at all sediment depths, but pristane, a related isoprenoid, is present only in the postglacial clays and in small amounts in some samples of the sapropelic mud. Pristane is common in most modern sediments and is a by-product of zooplanktonic digestive processing of chlorophyll a (Blumer et al. 1971). Its absence in some modern lacustrine sediments reflects the absence of calanoid copepods in the food chains of these lakes (Ho and Meyers 1993). Both phytane and pristane are produced from slow-acting diagenetic reworking of phytol, and become common constituents of the hydrocarbon contents of ancient sedimentary rocks. Giger et al. (1980) interpreted the pristane in the postglacial clays to indicate that hydrocarbons from erosion of Miocene sedimentary rocks in the watershed were incorporated into the lake bottom at this time. With the development of forests in

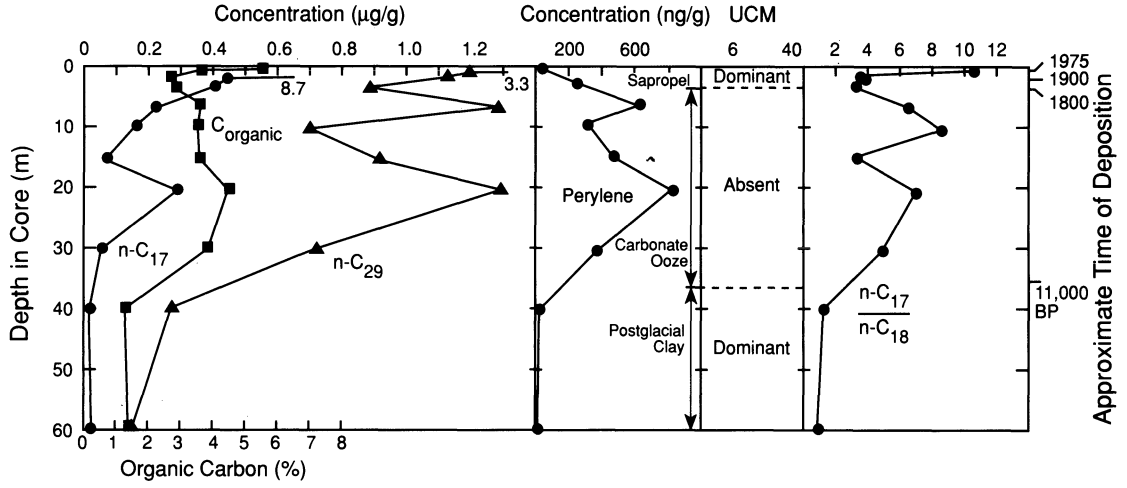


Fig. 31. Downcore concentrations of organic carbon and two biomarker *n*-alkanes in sediments of Greifensee, Switzerland. Perylene concentrations and unresolved mixture of aliphatic hydrocarbons (UCM) are shown at different core depths. Changes in the whole lake environment, recorded in changes in the sediment types, appear also in the hydrocarbon molecular compositions. (Data are from Giger et al. 1980; Wakeham et al. 1980a)

the watershed after approximately 11 Kya, erosion became negligible, and pristane inputs essentially disappeared.

The downcore profiles of the diagenetically formed polycyclic aromatic hydrocarbon perylene and the C_{29} *n*-alkane are very similar (Fig. 31). The principal difference is in the topmost portion of the core, where perylene concentrations are low and increase with depth, whereas the C_{29} *n*-alkane concentrations decrease from their maximum value. Most of this difference results from the time lag in the diagenetic production of perylene (Gschwend et al. 1983), and the overall similarities support the hypothesis of a land-plant precursor for perylene (Aizenshtat 1973).

A UCM of hydrocarbons is a major component of the sapropelic muds and the postglacial muds, but not the carbonate oozes (Fig. 31). The UCMs are common in geologically old hydrocarbon distributions, such as those found in petroleum and in ancient sedimentary rocks, and represent a huge variety of diagenetically formed hydrocarbons. The UCM hydrocarbons in the postglacial clays originate from erosion of Miocene watershed rocks, like the pristane in these sediments (Giger et al. 1980). Deposition of ancient hydrocarbons is also evident in the lack of odd/even predominance of C_{17} to C_{21} *n*-alkanes in the postglacial muds, as represented by the C_{17}/C_{18} ratios. The predominance is high in the surface sediment where algal inputs are large, but low deep in the sediments where geologically old *n*-alkanes are major contributors (Fig. 31).

The hydrocarbon compositions of the three major sedimentary units record differences in the sources of organic matter to Greifensee. Sediments deposited in this century contain a mixture of plant-wax *n*-alkanes, algal biomarkers, and a complex mixture of geologically old hydrocarbons. These components derive in turn from watershed biotic input, modern eutrophication of the lake waters, and a combination of enhanced land erosion and petroleum residues from urbanization of the watershed. Sediments laid down between the year 1800 and approximately 11 000 years ago are dominated by hydrocarbons produced by plants in and around the lake. Their *n*-alkane distributions show evidence of selective degradation of shorter-chain components (Giger et al. 1980). Prior to 11 Kya, sediments are postglacial clays in which geologically old hydrocarbon mixtures from erosion of surrounding rock formations are major components.

The progressive modern eutrophication of Greifensee is recorded in the concentration and isotopic composition of sedimentary organic matter. High nutrient/CO_2 ratios in the lake water have lead to enhanced preservation of aquatic organic matter as bottom-water anoxia has become more strongly developed. At the same time organic-matter $\delta^{13}C$ values have become heavier as the availability of dissolved

CO_2 has been diminished by algal uptake (Hollander et al. 1992).

8.4 Organic-Matter Record in Lake Washington, Washington, USA

Lake Washington is surrounded by the Seattle, Washington, metropolitan area. It is larger (surface area 87.6 km^2) and deeper (maximum 60 m) than Greifensee and is presently oligotrophic, but like Greifensee, it has been heavily impacted by human activities. The lake was eutrophic in the 1950s and early 1960s. Lake productivity has subsequently diminished as a result of controls on nutrient inputs and of changes made in lake-flushing patterns. An 11-m-long core from northern Lake Washington contains several layers of different types of fine-sized gyttja deposited over a 1.5-m-thick layer of glaciolacustrine clay. Pollen and lignin compositions record a 14 Ky postglacial watershed plant succession (Hedges et al. 1982; Leopold et al. 1982). Pollen compositions indicate that an early pine-dominated forest was replaced *ca.* 10 Kya by an alder and fern bracken mixture (Fig. 32). Since *ca.* 7 Kya dominance of western red-cedar pollen records a cooler, more moist climate. A potential problem with pollen paleoclimate reconstructions is that pollen can be easily transported by winds from distant areas. Lignin residues are contained in water-carried plant debris, and they consequently give a better record of local, rather than distant, types of vegetation.

The watershed succession interpreted from the lignin components of Lake Washington sediments generally agrees with the pollen reconstruction, except for the interval dominated by pine. A sequence of four watershed types is indicated by compositional changes within the lignin-derived phenols. In the basal meter of the core, low S/V and C/V ratios (Fig. 32) result from an approximately equal mixture of woody and nonwoody gymnosperm (conifers and ferns) plant tissues (Hedges et al. 1982). Low concentrations of total lignin-derived phenols relative to organic carbon indicate that small inputs of land-plant organic matter occurred at this time. In contrast, C/N values are between 11 and 15 here and throughout the core, and suggest an approximately equal mixture of land and algal material. These elemental ratios are less specific than the lignin parameters. Between 10 and 8 m in the core, high S/V and C/V ratios record a predominance of nonwoody angiosperm tissues, probably originating from marsh or grassland sources. The lignin plant reconstruction in this interval contradicts the pollen data, leading Leopold et al. (1982) to conclude that the pine-pollen dominance is an artifact resulting from eolian transport from regions outside the watershed. High S/V and low C/V ratios from 7 to 4 m suggest large contributions of angiosperm wood, a conclusion that is consistent with the abundance of alder pollen (Fig. 32). The decrease in the S/V ratio while the C/V ratio holds constant between 4 m to the core top indicates a gradual replacement of deciduous trees by conifers. This interpretation also agrees with the pollen reconstruction.

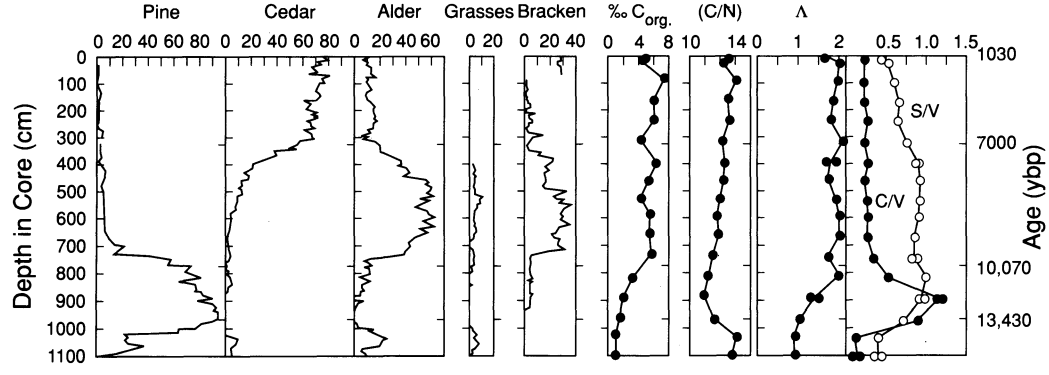


Fig. 32. Postglacial pollen stratigraphy and ligninderived phenolic compounds from various depths of a sediment core from Lake Washington. Lambda represents the total lignin phenols per 100 mg organic carbon; S/V and C/V are the ratios of syringyl and cinnamyl phenols relative to vanillyl phenols, respectively. Pollen and lignin indicators of watershed plants agree well, except between 10 and 8 m, where airborne pine pollen appear in the core record. (Data are from Hedges et al. 1982; Leopold et al. 1982)

Hydrocarbon compositions from a core from near the center of Lake Washington record a variety of environmental changes in organic-matter sources. Recent eutrophication of the lake and introduction of land runoff petroleum residues are evident in aliphatic hydrocarbon distributions (Fig. 10). Deforestation of the watershed during the past century has been recorded in peaks in specific polycyclic aromatic hydrocarbons (Fig. 33). The diterpenoid PAH retene is derived from abietic acid (Fig. 19), a common constituent of conifer sap (Simoneit 1977). Accelerated erosion of soil during logging of the conifer-covered watershed of Lake Washington since the early 1900s created a pulse of abietic acid to the lake sediments (Wakeham et al. 1980a). Concentration profiles of several triterpenoid PAHs are similar to the retene profile (Fig. 33). Probable precursors of these PAHs are α-amyrin and β-amyrin (Fig. 19), which are found in conifer bark. Logging and associated enhanced erosion of forest products has evidently increased the delivery of these PAH precursors to Lake Washington sediments as well.

Concentrations of the pentacyclic aromatic hydrocarbon perylene change differently than those of the four PAH molecules derived from conifer precursors (Fig. 33). The delay that is typically found in lacustrine sedimentary records (Figs. 17 and 18) between addition of the perylene precursor and the diagenetic production of this PAH is evident in the Lake Washington record as well. Absence of either increase or decrease with core depth indicates that the input of the unspecified perylene precursor to Lake Washington has remained constant over the past 3000 years.

8.5 PAH Records of Greifensee and Lake Washington Sediments

Greifensee and Lake Washington are temperate-zone lakes that have experienced similar post-glacial changes in watershed vegetation and aquatic productivity over the past 14 Kya. The PAH contents of their sediments record both similarities and differences in source inputs. In both lakes PAH compositions increase markedly in concentration and complexity in sediments deposited since *ca.* 1900 (Fig. 34). These changes arise from a combination of street runoff of petroleum residues and airborne input of combustion-derived PAH (Wakeham et al. 1980b). Both of these anthropogenic sources have increased in magnitude during the past century, and have overwhelmed the natural contributions of PAHs derived from biogenic precursors.

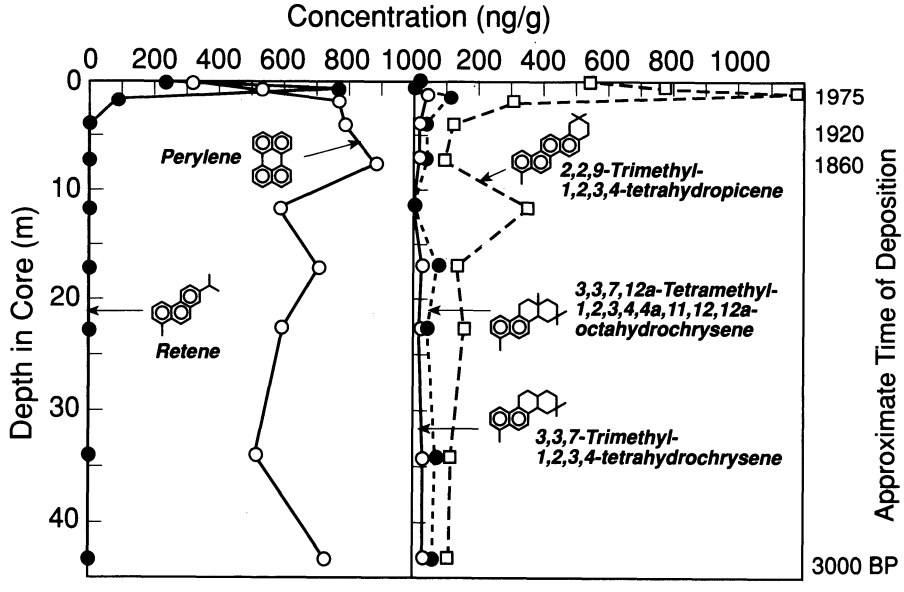


Fig. 33. Downcore concentrations of three types of diagenetically produced polycyclic aromatic hydrocarbons in sediments of Lake Washington. Perylene is gradually formed in sediments until the unknown precursor material is depleted. Retene is formed from abietic acid, a component of conifer sap, and picene and chrysene hydrocarbons are formed from amyrin precursors, found in conifer bark. Widespread logging temporarily enhanced the availability of the conifer precursors. (Data are from Wakeham et al. 1980a)

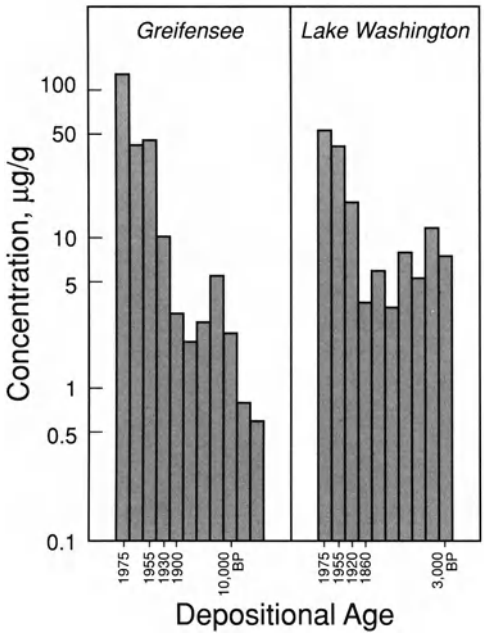


Fig. 34. Concentrations of total polycyclic aromatic hydrocarbons (PAH) deposited at different times in the sediments of Greifensee, Switzerland, and Lake Washington. Both increased erosion of watershed areas and increased urban pollution are responsible for the 50- to 100-fold magnifications of concentrations in modern sediments. (Data are from Wakeham et al. 1980b)

Natural differences in watershed biota also affect the sedimentary diagenetic PAH contents of these two lakes. Sediments of Lake Washington contain large concentrations of retene, whereas those of Greifensee contain negligible amounts of this derivative of abietic acid (Wakenham et al. 1980a). Similarly, pimanthrene, for which resin-derived pimaric acid is the probable precursor, and a wide range of triterpenoid hydrocarbons derived from amyrin precursors are abundant in the sediments of Lake Washington, but not in those of Greifensee. These differences reflect the fact that conifers are abundant around Lake Washington, but not around Greifensee. The perylene profiles also differ in the two lakes. After the initial diagenetic lag, sedimentary concentrations are constant in Lake Washington, but variable in Greifensee (Figs. 31 and 33). This contrast may indicate that the types of watershed vegetation, and therefore the sources of the perylene precursor, have varied more around Greifensee than around Lake Washington.

9 Organic Geochemical Records of Ancient Lakes

Although the majority of biosynthetic organic matter is remineralized or degraded during sinking and early sedimentation in lakes, a small portion survives to become buried deeply in lacustrine sediments. If the sedimentary layers become part of the long-term geological record, then their organic matter contents can provide a comprehensive history of lacustrine biological production and depositional conditions extending millions of years into the past. Both the isotopic signature of reworked organic matter and the preserved carbon skeletons of individual biomarker compounds record information about former biota and environments.

Two ancient lacustrine sedimentary deposits are especially noteworthy because of their rich organic-matter contents – the Messel shale of Germany and the Green River shale of Wyoming, Utah, and Colorado. Both of these formations were created during parts of the Eocene epoch (58 Mya to 36 Mya). The Messel shale was deposited in a relatively short period *ca.* 47 Mya at the bottom of an anoxic lake. The Green River Formation comprises a number of units, each representing a different phase in the evolution of this 6-km-thick accumulation of lacustrine sediments. The whole Green River Formation included three main lakes, which varied in size and depth during the existence of this lacustrine system. During some intervals anoxic conditions prevailed, and organic-carbon-rich sediments were deposited. These two examples illustrate some of the types of paleolacustrine information that can be obtained from the organic matter of ancient lacustrine deposits.

Porphyrins are diagenetic products derived from the chlorophylls of plants and the heme molecules in the blood of animals. They are found widely in ancient sedimentary rocks. Their carbon contents consist almost entirely of the intact tetrapyrrole ring (Fig. 20) inherited from their biological precursor compounds. As such, carbon isotope compositions of the porphyrins are protected from possible diagenetic effects, and they are believed to record accurately the carbon isotope signatures of their source organisms. Carbon isotope measurements made on porphyrins isolated from the Messel shale give $\delta^{13}C$ values averaging −23.4‰ (Hayes et al. 1987; Freeman et al. 1990). The porphyrins were derived from

chlorophylls *a*, *c*, and *d* based on the positions and structures of their tetrapyrrole ring side chains. The isotope ratio and the chlorophyll types suggests that the organic matter in this lacustrine deposit was synthesized primarily by a combination of algae and photosynthetic bacteria, although abundant land-plant fossils and biomarkers are present in the shale. Among other algae, dinoflagellate production particularly was evidenced by the presence of 4-methyl stanols. The significance of the photosynthetic bacteria is that they indicate that part of the photic zone of the lake was anoxic. Further evidence of important microbial contributions of photosynthesized organic matter to the Messel paleoenvironment is given by a series of tetraterpenoid hopanes and the presence of lycopane, but not β-carotene (Kimble et al. 1974). Acyclic carotenoids, such as lycopene, are found in photosynthetic bacteria, but they are not major pigments in algae. The organic geochemical evidence for bacterial photosynthesis indicates that the epilimnion of this lake was very shallow and that the photic zone extended into the anoxic hypolimnion.

Kerogen is the lithified-sediment equivalent of humic substances and constitutes the bulk of organic matter in ancient rocks. Recombination and condensation of biological precursor molecules is believed to contribute to construction of the kerogen macromolecular matrix. The incorporation of biomarker compounds into kerogen can enhance their preservation. Geochemical studies can selectively disassemble this matrix, releasing recognizable biomarker fragments. Such analyses have been done on samples of Green River shales. Some biomarker compounds that have been isolated include porphyrins and isoprenoid fatty acids (Burlingame and Simoneit 1968), steranes (Gallegos 1975), and bicyclic carotenoid components (Machihara and Ishiwatari 1987). These biomarkers have been obtained from different parts of the Green River Formation, and hence represent different paleolacustrine environments. Comparisons of alkanoic acids released from Green River shale by extraction and by kerogen pyrolysis by Kawamura et al. (1986) show that incorporation of fatty acids into protokerogen during early diagenesis enhances preservation of the paleolacustrine information provided by these biomarker compounds. The kerogen-bound acids possess high CPIs, indicating retention of their biological character (Bray and Evans 1961; Matsuda and Koyama 1977a), and have distributions dominated by $C_{16:0}$, recording microbial or algal synthesis. Kimble et al. (1974) found that the major tetraterpane in extracts of Green River shale is perhydro-β-carotene. This hydrocarbon is derived from the important algal accessory pigment carotene (Table 5); its dominance indicates that algal photosynthesis was evidently the primary source of organic matter to the Green River paleolimnologic system. Determination of $\delta^{13}C$ values of biomarker compounds isolated from Green River kerogen has also shown that photoautotrophs were responsible for much of the production of organic matter in this ancient lake system (Collister et al. 1992). Some biomarker compounds, however, have $\delta^{13}C$ values of approximately $-80‰$, and these extremely light carbon isotopic ratios are evidence that methanotrophs were also important contributors of organic matter. The organic compounds produced by bacteria that consumed isotopically light methane are forms of secondary organic matter, created from the anoxic alteration and recycling of primary, photosynthetically produced organic matter. The evidence for methanotrophy confirms that this lacustrine paleoenvironment experienced sustained periods of anoxia, during which methane was produced by methanogenic bacteria. These periods probably resulted from sustained intervals of enhanced photosynthesis within ancient lakes, and they created conditions that led to improved preservation of organic matter in lake sediments.

10 Summary

The organic-matter-accumulation records of lacustrine sediments are affected by many variables. Biota living in the lake and its watershed are the sources of organic compounds initially contributed to the lake system. Microbial reworking of these materials during sinking and early sedimentation markedly diminishes the total amount of organic matter while replacing many of the primary compounds with secondary compounds. Much of the organic-matter content of sediments is the product of this microbial reprocessing.

Despite the generally low survival rate for most primary organic compounds, various organic-matter components of lake sediments nevertheless retain source information and thereby become important parts of paleolimnological records. Progressive eutrophication, changes in watershed

vegetation, and the advent of urban pollution of lacustrine systems are some of the paleoenvironmental aspects that can be inferred from the elemental, isotopic, and molecular compositions of sedimentary organic matter. Carbon/nitrogen ratios of total organic matter reflect original proportions of algal and land-derived material. Carbon isotopic compositions indicate the history of lake productivity and carbon recycling. Biomarker compounds provide important information about contributions from different biota. Sterol compositions and chain-length distributions of *n*-alkanes, *n*-alkanoic acids, and *n*-alkanols help distinguish different algal and watershed sources, and also record diagenetic alterations. Stabilization of functional-group-containing biomarkers by conversion into saturated or aromatic hydrocarbons or by incorporation into bound forms improves their preservation, and hence record of source information. Lignin components provide important evidence of watershed plant cover in former times, and pigments in the sediment record reflect compositions of algal assemblages of the past.

Acknowledgments. We could not have prepared this overview of lacustrine organic geochemistry without the experience and knowledge gained from working with many colleagues and students over the past several decades. We collectively thank these many collaborators in our lake studies, and we acknowledge their contributions to advancing understandings of the processes that impact the organic geochemistry of lake sediments. This summary has benefited particularly from the careful reading and thoughtful suggestions for improvement contributed by B.J. Eadie.

References

Aizenshtat Z (1973) Perylene and its geochemical significance. Geochim Cosmochim Acta 37:559–567

Andren AW, Strand JW (1981) Atmospheric deposition of particulate organic matter and polyaromatic hydrocarbons in Lake Michigan. In: Eisenreich SJ (ed) Atmospheric pollutants in natural waters. Ann Arbor Science, Ann Arbor, pp 459–479

Barnes MA, Barnes WC (1978) Organic compounds in lake sediments. In: Lerman A (ed) Lakes-chemistry, geology, physics, Springer, Berlin Heidelberg New York, pp 127–152

Barnola JM, Raynaud D, Korotkevich YS, Lorius C (1987) Vostok ice core provides 160 000-year record of atmospheric CO_2. Nature 329:408–414

Benner R, Fogel ML, Sprague EK, Hodson RE (1987) Depletion of 13C in lignin and its implications for stable carbon isotope studies. Nature 329:708–710

Benson LV, Meyers PA, Spencer RJ (1991) Change in the size of Walker Lake during the past 5000 years. Palaeogeogr Palaeoclimatol Palaeoecol 81:189–214

Blumer M, Guillard RRL, Chase T (1971) Hydrocarbons of marine plankton. Mar Biol 8:183–189

Bourbonniere RA (1979) Geochemistry of organic matter in Holocene Great Lakes sediments. Thesis, University of Michigan, Ann Arbor, 373 pp

Bourbonniere RA, Meyers PA (1978) Characterization of sedimentary humic matter by elemental and spectroscopic methods. Can J Spectrosc 23:35–41

Bourbonniere RA, Meyers PA (1983) Characterization of sedimentary humic matter by alkaline hydrolysis. Org Geochem 5:131–142

Brassell SC, Eglinton G, Maxwell JR (1983) The geochemistry of terpenoids and steroids. Biochem Soc (UK) Trans 11:575–586

Bray EE, Evans ED (1961) Distribution of n-paraffins as a clue to the recognition of source beds. Geochim Cosmochim Acta 27:1113–1127

Burlingame AL, Simoneit BRT (1968) Isoprenoid fatty acids isolated from the kerogen matrix of the Green River Formation (Eocene). Science 160:531–533

Carpenter SR, Elser MM, Elser JJ (1986) Chlorophyll production, degradation, and sedimentation: Implications for paleolimnology. Limnol Oceanogr 31: 112–124

Casagrande DJ, Given PH (1980) Geochemistry of amino acids in some Florida peat accumulations. II. Amino acid distributions. Geochim Cosmochim Acta 44:1493–1507

Casagrande DJ, Siefert K, Berschinski C, Sutton N (1977) Sulfur in peat-forming systems of the Okefenokee Swamp and Florida everglades: origins of sulfur in coal. Geochim Cosmochim Acta 41: 161–167

Cobler R, Dymond J (1980) Sediment trap experiment on the Galapagos spreading center, equatorial Pacific. Science 209:801–803

Collister JW, Summons RE, Lichtfouse E, Hayes JM (1992) An isotopic biogeochemical study of the Green River oil shale. Org Geochem 19:265–276

Cowie GL, Hedges JI (1984) Carbohydrate sources in a coastal marine environment. Geochim Cosmochim Acta 48:2075–2087

Cranwell PA (1973a) Chain-length distribution of *n*-alkanes from lake sediments in relation to post-glacial environmental change. Freshwater Biol 3:259–265

Cranwell PA (1973b) Branched-chain and cyclopropanoid acids in a recent sediment. Chem Geol 11: 307–313

Cranwell PA (1974) Monocarboxylic acids in lake sediments: indicators, derived from terrestrial and aquatic biota, of paleoenvironmental trophic levels. Chem Geol 14:1–14

Cranwell PA (1976) Decomposition of aquatic biota and sediment formation: lipid components of 2 blue-green algal species and of detritus resulting from microbial attack. Freshwater Biol 6:481–488

Cranwell PA (1978) Extractable and bound lipid components in a freshwater sediment. Geochim Cosmochim Acta 42:1523–1532
Cranwell PA (1981) Diagenesis of free and bound lipid components in terrestrial detritus deposited in a lacustrine sediment. Org Geochem 3:79–89
Cranwell PA (1982) Lipids of aquatic sediments and sedimenting particulates. Progr Lipid Res 21:271–308
Cranwell PA (1984) Lipid geochemistry of sediments from Upton Broad, a small productive lake. Org Geochem 7:25–37
Cranwell PA (1985) Long-chain unsaturated ketones in recent sediments. Geochim Cosmochim Acta 49: 1545–1551
Cranwell PA (1986) Esters of acyclic and polycyclic isoprenoid alcohols: Biochemical markers in lacustrine sediments. Org Geochem 10:891–896
Cranwell PA, Volkman JK (1981) Alkyl and steryl esters in a recent lacustrine sediment. Chem Geol 32:29–43
Cranwell PA, Eglinton G, Robinson N (1987) Lipids of aquatic organisms as potential contributors to lacustrine sediments. II. Org Geochem 11:513–527
Degens ET (1969) Biogeochemistry of stable carbon isotopes. In: Eglinton G, Murphy MTJ (eds) Organic geochemistry – methods and results. Springer, Berlin Heidelberg New York, pp 304–329
Eadie BJ, Chambers RL, Gardner WS, Bell GE (1984) Sediment trap studies in Lake Michigan: resuspension and chemical fluxes in the southern basin. J Great Lakes Res 10:307–321
Ertel JR, Hedges JI (1984) The lignin composition of humic substances: distribution among soil and sedimentary humic, fulvic, and base-insoluble fractions. Geochim Cosmochim Acta 48:2065–2074
Ertel JR, Hedges JI (1985) Sources of sedimentary humic substances: vascular plant debris. Geochim Cosmochim Acta 49:2097–2107
Freeman KH, Hayes JM (1992) Fractionation of carbon isotopes by phytoplankton and estimates of ancient CO_2 levels. Global Biogeochem Cycles 6:185–198
Freeman KH, Hayes JM, Trendel JM, Albrecht P (1990) Evidence from carbon isotope measurements for diverse origins of sedimentary hydrocarbons. Nature 343:254–256
Fry B (1986) Sources of carbon and sulfur nutrition for consumers in three meromictic lakes of New York State. Limnol Oceanogr 31:79–88
Fry B (1988) Food web structure on Georges Bank from stable C, N, and S isotopic compositions. Limnol Oceanogr 33:1182–1190
Fukushima K, Ishiwatari R (1984) Acid and alcohol compositions of wax esters in sediments from different environments. Chem Geol 47:41–56
Furlong ET, Cessar LR, Hites RA (1987) Accumulation of polycyclic aromatic hydrocarbons in acid sensitive lakes. Geochim Cosmochim Acta 51: 2965–2975
Gallegos EJ (1975) Terpane-sterane release from kerogen by pyrolysis gas chromatography-mass spectrometry. Anal Chem 47:1524–1528
Gaskell SJ, Eglinton G (1976) Sterols of a contemporary lacustrine sediment. Geochim Cosmochim Acta 40:1221–1228
Giger W, Schaffner C, Wakeham SG (1980) Aliphatic and olefinic hydrocarbons in recent sediments of Greifensee, Switzerland. Geochim Cosmochim Acta 44:119–129
Goossens H, Duren RR, Leeuw JW de, Schenck PA (1989) Lipids and their mode of occurrence in bacteria and sediments. II. Lipids in the sediment of a stratified, freshwater lake. Org Geochem 14:27–41
Gorham E, Sanger JE (1976) Fossilized pigments as stratigraphic indicators of cultural eutrophication in Shagawa Lake, northeastern Minnesota. Geol Soc Am Bull 87:1638–1642
Goreham E, Lund JWG, Sanger J, Dean WE Jr (1974) Some relationships between algal standing crop, water chemistry, and sediment chemistry in the English lakes. Limnol Oceanogr 19:601–617
Griffiths M (1978) Specific blue-green algal carotenoids in sediments of Esthwaite Water. Limnol Oceanogr 23:777–784
Gschwend PM, Hites RA (1981) Fluxes of polycyclic aromatic hydrocarbons to marine and lacustrine sediments in the northern United States. Geochim Cosmochim Acta 45:2359–2367
Gschwend PM, Chen PH, Hites RA (1983) On the formation of perylene in recent sediments: kinetic models. Geochim Cosmochim Acta 47:2115–2119
Guilizzoni P, Lami A, Marchetto A (1992) Plant pigment ratios from lake sediments as indicators of recent acidification in alpine lakes. Limnol Oceanogr 37:1565–1569
Haddad RI, Martens CS, Farrington JW (1992) Quantifying early diagenesis of fatty acids in a rapidly accumulating coastal marine sediment. Org Geochem 19:205–216
Hatcher PG, Simoneit BRT, Mackenzie FT, Neumann AC, Thorstenson DC, Gerchakov SM (1982) Organic geochemistry and pore water chemistry of sediments from Mangrove Lake, Bermuda. Org Geochem 4:93–112
Hatcher PG, Spiker EC, Szeverenyi NM, Maciel GE (1984) Selective preservation and origin of petroleum-forming aquatic kerogen. Nature 305:498–501
Hayes JM, Takigiku R, Ocampo R, Callot HJ, Albrecht P (1987) Isotopic compositions and probable origins of organic molecules in the Eocene Messel shale. Nature 329:48–51
Hedges JI, Mann DC (1979) The characterization of plant tissues by their lignin oxidation products. Geochim Cosmochim Acta 43:1803–1807
Hedges JI, Ertel JR, Leopold EB (1982) Lignin geochemistry of a Late Quaternary core from Lake Washington. Geochim Cosmochim Acta 46:1869–1877
Hedges JI, Cowie GL, Ertel JR, Barbour RJ, Hatcher PL (1985) Degradation of carbohydrates and lignins in buried woods. Geochim Cosmochim Acta 49: 701–711
Hites RA, Laflamme RE, Windsor JG Jr (1980) Polycyclic aromatic hydrocarbons in marine/aquatic sediments: their ubiquity. Adv Chem Ser 185:289–311

Ho ES, Meyers PA (1994) Variability of early diagenesis in lake sediments: evidence from the sedimentary geolipid record in an isolated tarn. Chem Geol 112:309–324

Hollander DJ, McKenzie JA (1991) CO_2 control on carbon-isotope fractionation during aqueous photosynthesis: a paleo-pCO_2 barometer. Geology 19: 929–932

Hollander DJ, McKenzie JA, Haven HL (1992) A 200 year sedimentary record of progressive eutrophication in Lake Greifen (Switzerland): implications for the origin of organic-carbon-rich sediments. Geology 20:825–828

Ishiwatari R (1973) Chemical characterization of fractionated humic acids from lake and marine sediments. Chem Geol 12:113–126

Ishiwatari R (1985) Geochemistry of humic substances in lake sediments. In: McKnight DM (ed) Humic substances in soil, sediment, and water: geochemistry, islation, and characterization. John Wiley, New York, pp 147–180

Ishiwatari R (1991) Die organischen Substanzen in den Biwa-See-Sedimenten als Informationstrager über Paläoumweltbedingungen. In: Horie S (ed) Die Geschichte des Biwa-Sees in Japan, Universitätsverlag Wagner, Innsbruck, pp 187–201

Ishiwatari R, Ogura K (1984) Organic geochemistry. In: Horie S (ed) Lake Biwa. Junk, Dordrecht, pp 557–577

Ishiwatari R, Uzaki M (1987) Diagenetic changes of lignin compounds in a more than 0.6 million-year-old lacustrine sediment (Lake Biwa, Japan). Geochim Cosmochim Acta 51:321–328

Ishiwatari R, Ogura K, Horie S (1980) Organic geochemistry of a lacustrine sediment (Lake Haruna, Japan). Chem Geol 64:261–280

Ishiwatari R, Takamatsu N, Ishibishi T (1977) Separation of autochthonous and allochthonous materials in lacustrine sediments by density differences. Jpn J Limnol 38:94–99

Ishiwatari R, Ogura K, Horie S (1980) Organic geochemistry of a lacustrine sediment (Lake Haruna, Japan). Chem Geol 29:261–280

Jasper JP, Gagosian RB (1989) Glacial-interglacial climatically-forced sources of sedimentary organic matter to the late Quaternary northern Gulf of Mexico. Nature 342:60–62

Johns RB (ed) (1986) Biological markers in the sedimentary record. Elsevier, Amsterdam

Johnson TC, Evans JE, Eisenreich SJ (1982) Total organic carbon in Lake Superior sediments: comparisons with hemipelagic and pelagic marine environments. Limnol Oceanogr 27:481–491

Kawamura K, Ishiwatari R (1981) Polyunsaturated fatty acids in a lacustrine sediment as a possible indicator of paleoclimate. Geochim Cosmochim Acta 45:149–155

Kawamura K, Ishiwatari R (1984) Fatty acid geochemistry of a 200 m sediment core from Lake Biwa, Japan. Early diagenesis and paleoenvironmental information. Geochim Cosmochim Acta 48:251–266

Kawamura K, Ishiwatari R (1985) Distribution of lipid-class compounds in bottom sediments of freshwater lakes with different tropic status, in Japan. Chem Geol 51:123–133

Kawamura K, Ishiwatari R, Yamazaki M (1980) Identification of polyunsaturated fatty acids in surface lacustrine sediments. Chem Geol 28:31–39

Kawamura K, Ishiwatari R, Ogura K (1987) Early diagenesis of organic matter in the water column and sediments: Microbial degradation and resynthesis of lipids in Lake Haruna. Org Geochem 11:251–264

Kawamura K, Tannenbaum E, Huizinga BJ, Kaplan IR (1986) Long-chain carboxylic acids in pyrolysates of Green River kerogen. Org Geochem 10:1059–1065

Keely BJ, Brereton RG (1986) Early chlorin diagenesis in a Recent aquatic sediment. Org Geochem 10:975–980

Kemp ALW, Johnston LM (1979) Diagenesis of organic matter in the sediments of Lakes Ontario, Erie, and Huron. J Great Lakes Res 5:1–10

Kimble BJ, Maxwell JR, Philp RP, Eglinton G, Albrecht P, Ensminger A, Arpino P, Ourisson G (1974) Tri- and tetraterpenoid hydrocarbons in the Messel oil shale. Geochim Cosmochim Acta 38: 1165–1181

Klink G, Dreier F, Buchs A, Gulaçar FO (1992) A new source for 4-methyl sterols in freshwater sediments: *Utricularia neglecta* L. (Lentibulariaceae). Org Geochem 18:757–763

Krishnamurthy RV, Bhattacharya SK, Kusumgar S (1986) Palaeoclimatic changes deduced from $^{13}C/^{12}C$ and C/N ratios of Karewa lake sediments, India. Nature 323:150–152

Laflamme RE, Hites RA (1978) The global distribution of polycyclic aromatic hydrocarbons in recent sediments. Geochim Cosmochim Acta 42:289–303

Leavitt PR (1993) A review of factors that regulate carotenoid and chlorophyll deposition and fossil pigment abundance. J Paleolimnol 9:109–127

Leavitt PR, Carpenter SR, Kitchell JF (1989) Whole-lake experiments: the annual record of fossil pigments and zooplankton. Limnol Oceanogr 34: 700–717

Leenheer MJ, Meyers PA (1983) Comparison of lipid compositions in marine and lacustrine sediments. In: Bjoroy M (ed) Advances in organic geochemistry 1981. John Wiley, Chichester, pp 309–316

Leenheer MJ, Meyers PA (1984) Comparison of lipid character of sediments from the Great Lakes and the northwestern Atlantic. Org Geochem 7:141–150

Leeuw J de, Baass M (1986) Early-stage diagenesis of sterols. In: Johns RB (ed) Biological markers in the sedimentary record, Elsevier, Amsterdam, pp 101–123

Leopold EB, Nickman R, Hedges JI, Ertel JR (1982) Pollen and lignin records of Late Quaternary vegetation, Lake Washington. Science 218:1305–1307

Machihara T, Ishiwatari R (1987) Possible carotenoid-derived structures in fossil kerogens. Geochim Cosmochim Acta 51:207–211

Mackenzie AS, Brassell SC, Eglinton G, Maxwell JR (1982) Chemical fossils: the geologic fate of steroids. Science 217:491–504

Mackin JE,Owen RM, Meyers PA (1980) A factor

analysis of elemental associations in the surface microlayer of Lake Michigan and its fluvial inputs. J Geophys Res 85:1563–1569

Marlowe IT, Brassell SC, Eglinton G, Green JC (1984) Long chain unsaturated ketones and esters in living algae and marine sediments. Org Geochem 6:135–141

Matsuda H, Koyama T (1977a) Early diagenesis of fatty acids in lacustrine sediments. I. identification and distribution of fatty acids in recent sediment from a freshwater lakes. Geochim Cosmochim Acta 41:777–783

Matsuda H, Koyama T (1977b) Early diagenesis of fatty acids in lacustrine sediments. II. A statistical approach to changes in fatty acid composition from recent sediments and source materials. Geochim Cosmochim Acta 41:1825–1834

Matsumoto G, Torii T, Hanya T (1982) High abundance of algal 24-ethylcholesterol in Antarctic lake sediment. Nature 299:52–54

McCoy WD (1987) Quaternary aminostratigraphy of the Bonneville Basin, western United States. Geol Soc Am Bull 98:99–112

Mendoza YA, Gulaçar FO, Hu Z-L, Buchs A (1987) Unsubstituted and hydroxy substituted fatty acids in a recent lacustrine sediment. Int J Environ Anal Chem 31:107–127

Mermoud F, Gulaçar FO, Buchs A (1985) 5α(H)-Cholestan-3α-ol in sediments: characterization and geochemical significance. Geochim Cosmochim Acta 49:459–462

Meyers PA (1984) Petroleum contaminants in the Great Lakes. In: Nriagu JO, Simmons MS (eds) Toxic contaminants in the Great Lakes. John Wiley, New York, pp 147–162

Meyers PA (1990) Impacts of regional Late Quaternary climate changes on the deposition of sedimentary organic matter in Walker Lake, Nevada. Palaeogeogr, Palaeoclimatol Palaeoecol 78:229–240

Meyers PA (1994) Preservation of elemental and isotopic source identification of sedimentary organic matter. Chem Geol 114:289–302

Meyers PA, Takeuchi N (1979) Fatty acids and hydrocarbons in surficial sediments of Lake Huron. Org Geochem 1:127–138

Meyers PA, Benson LV (1988) Sedimentary biomarker and isotopic indicators of the paleoclimatic history of the Walker Lake basin, western Nevada. Org Geochem 13:807–813

Meyers PA, Eadie BJ (1993) Sources, degradation, and recycling of organic matter associated with sinking particles in Lake Michigan. Org Geochem 20:47–56

Meyers PA, Horie S (1993) An organic carbon isotopic record of glacial-interglacial change in atmospheric pCO_2 in the sediments of Lake Biwa, Japan. Palaeogeogr Palaeoclimatol Palaeoecol 105:171–178

Meyers PA, Ishiwatari R (1993) The early diagenesis of organic matter in lacustrine sediments. In: Engel M, Macko SA (eds) Organic geochemistry, Plenum, New York, pp 185–209

Meyers PA, Takeuchi N (1981) Environmental changes in Saginaw Bay, Lake Huron, recorded by geolipid contents of sediments deposited since 1800. Environ Geol 3:257–266

Meyers PA, Leenheer MJ, Erstfeld KM, Bourbonniere RA (1980a) Changes in spruce composition following burial in lake sediments for 10 000 years. Nature 287:534–536

Meyers PA, Edwards SJ, Eadie BJ (1980b) Fatty acid and hydrocarbon content of settling sediments in Lake Michigan. J Great Lakes Res 6:331–337

Meyers PA, Bourbonniere RA, Takeuchi N (1980c) Hydrocarbons and fatty acids in two cores of Lake Huron sediments. Geochim Cosmochim Acta 44: 1215–1221

Meyers PA, Maring HB, Bourbonniere RA (1980d) Alkane and alkanoic acid variations with depth in modern sediments of Pyramid Lake. In: Douglas AG, Maxwell JR (eds) Advances in Organic Geochemistry 1979, Pergamon, Oxford, pp 365–374

Meyers PA, Leenheer MJ, Eadie BJ, Maule SJ (1984a) Organic geochemistry of suspended and settling particulate matter in Lake Michigan. Geochim Cosmochim Acta 48:443–452

Meyers PA, Kawka OE, Whitehead DR (1984b) Geolipid, pollen, and diatom stratigraphy in postglacial lacustrine sediments. Org Geochem 6:727–732

Meyers PA, Takemura K, Horie S (1993) A reinterpretation of Late Quaternary sediment chronology of Lake Biwa, Japan, from correlation with marine glacial-interglacial cycles. Quat Res 39:154–162

Mori S, Horie S (1975) Diatoms in a 197.2 meters core sample from Lake Biwa-ko. Proc Jpn Acad 51:675–679

Müller H (1987) Hydrocarbons in the freshwater environment: a literature review. Arch Hydrobiol Behandlung, Ergebnisse der Limnologie 24:1–69

Nagy E, Mudroch P, Mudroch A, Thomas RL (1984) Hydrocarbons in the surficial sediments of Lakes St. Clair, Erie, and Ontario. Environ Geol Water Sci 6:31–37

Nakai N (1972) Carbon isotopic variation and the paleoclimate of sediments from Lake Biwa. Proc Jpn Acad 48:516–521

Nakai N, Koyama M (1991) Die Rekonstruktion von Paläoumweltbedingungen unter Berucksichtigung der anorganischen Bestandteile, des C/N- und des Kohlenstoff-Isotopenverhaltnisses am Beispiel des 1400-m-Bohrkerns aus dem Biwa-See. In: Horie S (ed) Die Geschichte des Biwa-Sees in Japan Universitätsverlag Wagner, Innsbruck, pp 149–160

Neftel A, Oeschger H, Schwander J, Stauffer B, Sumbrun R (1982) Ice core sample measurements give atmospheric CO_2 content during the past 40 000 yr. Nature 295:220–223

Nishimura M (1977a) The geochemical significance in early sedimentation of geolipids obtained by saponification of lacustrine sediments. Geochim Cosmochim Acta 41:1817–1823

Nishimura M (1977b) Origin of stanols in young lacustrine sediments. Nature 270:711–712

Nishimura M (1978) Geochemical characteristics of the high reduction zone of stenols in Suwa sediments and the environmental factors controlling the conversion of stenols into stanols. Geochim Cosmochim Acta 42:349–357

Nishimura M (1982) 5β-isomers of stanols and stanones

as potential markers of sedimentary organic quality and depositional paleoenvironments. Geochim Cosmochim Acta 46:423–432
Nishimura M, Koyama T (1976) Stenols and stanols in lake sediments and diatoms. Chem Geol 17:229–239
Nishimura M, Koyama T (1977) The occurrence of stanols in various living organisms and the behavior of sterols in contemporary sediments. Geochim Cosmochim Acta 41:379–385
Norton SA, Hess CT, Davis RB (1981) Rates of accumulation of heavy metals in pre- and post-European sediments in New England lakes. In: Eisenreich SJ (ed) Pollutants in natural waters. Ann Arbor Science, Ann Arbor, pp 409–421
O'Leary MH (1988) Carbon isotopes in photosynthesis. Bioscience 38:328–336
Pang PC, Nriagu JO (1976) Distribution and isotope composition of nitrogen in Bay of Quinte (Lake Ontario) sediments. Chem Geol 18:93–105
Pang PC, Nriagu JO (1977) Isotopic variations of the nitrogen in Lake Superior. Geochim Cosmochim Acta 41:811–814
Peters KE, Sweeney RE, Kaplan IR (1978) Correlation of carbon and nitrogen stable isotope ratios in sedimentary organic matter. Limnol Oceanogr 23:598–604
Peterson BJ, Howarth RW, Garritt RH (1985) Multiple stable isotopes used to trace the flow of organic matter in estuarine food webs. Science 227: 1361–1363
Qiu L, Williams DF, Gvorzdov A, Karabanov E, Shimaraeva M (1993) Biogenic silica accumulation and paleoproductivity in the northern basin of Lake Baikal during the Holocene. Geology 21:25–28
Rau G (1978) Carbon-13 depletion in a subalpine lake: carbon flow implications. Science 201:901–902
Rau GH, Froelich PN, Takahashi T, Des Marais DJ (1991) Does sedimentary organic $\delta^{13}C$ record variations in Quaternary ocean [CO_2(aq)]? Paleoceanography 6:335–347
Rea DK, Bourbonniere RA, Meyers PA (1980) Southern Lake Michigan sediments: changes in accumulation rate, mineralogy, and organic content. J Great Lakes Res 6:321–330
Rea DK, Owen RM, Meyers PA (1981) Sedimentary processes in the Great Lakes. Rev Geophy Space Phys 19:635–648
Reed WE (1977) Biogeochemistry of Mono Lake, California. Geochim Cosmochim Acta 41:1231–1245
Rieley G, Collier RJ, Jones DM, Eglinton G (1991a) The biogeochemistry of Ellesmere Lake, U.K. I. Source correlation of leaf wax inputs to the sedimentary record. Org Geochem 17:901–912
Rieley G, Collier RJ, Jones DM, Eglinton G, Eakin PA, Fallick AE (1991b) Sources of sedimentary lipids deduced from stable carbon-isotope analyses of individual compounds. Nature 352:425–427
Robbins JA, Edgington DN (1975) Determination of recent sedimentation rates in Lake Michigan using Pb-210 and Cs-137. Geochim Cosmochim Acta 39: 285–304
Robinson N, Eglinton G, Brassell SC (1984b) Dinoflagellate origin for sedimentary 4α-methylsteroids and 5α(H)-stanols. Nature 308:439–441
Robinson N, Cranwell PA, Finlay BJ, Eglinton G (1984a) Lipids of aquatic organisms as potential contributors to lacustrine sediments. Org geochem 6:143–152
Robinson N, Cranwell PA, Eglinton G, Brassell SC, Sharp CL, Gophen M, Pollinger U (1986) Lipid geochemistry of Lake Kinneret. Org Geochem 10:733–742
Robinson N, Cranwell PA, Eglinton G, Jaworski GHM (1987) Lipids of four species of freshwater dinoflagellates. Phytochemistry 26:411–421
Rogers MA (1965) Carbohydrates in aquatic plants and associated sediments from two Minnesota lakes. Geochim Cosmochim Acta 29:183–200
Sackett WM, Eadie BJ, Meyers PA (1986) Stable carbon isotope studies of organic matter in Great Lakes sediments. Transactions, American Geophysical Union 76:1058 (Abstr)
Sanger JE (1988) Fossil pigments in paleoecology and paleolimnology. Palaeogeogr Palaeoclimatol Palaeoecol 62:343–359
Sanger JE, Goreham E (1972) Stratigraphy of fossil pigments as a guide to the postglacial history of Kirchner Marsh, Minnesota. Limnol Oceanogr 17:840–854
Schelske CL, Hodell DA (1991) Recent changes in productivity and climate of Lake Ontario detected by isotopic analysis of sediments. Limnol Oceanogr 36:961–975
Schelske CL, Stoermer EF, Conley DJ, Robbins JA, Glover RM (1983) Early eutrophication in the Lower Great Lakes: New evidence from biogenic silica in sediments. Science 222:320–322
Schelske CL, Robbins JA, Gardner WS, Conley DJ, Bourbonniere RA (1988) Sediment record of biogeochemical responses to anthropogenic perturbations of nutrient cycles in Lake Ontario. Can J Fish Aquat Sci 45:1291–1303
Schultz DM, Quinn JG (1974) Measurement of phytol in estuarine suspended organic matter. Marine Biol 27:143–146
Schwendinger RB (1969) Carotenoids. In: Eglinton G, Murphy MTJ (eds) Organic geochemistry. Springer, Berlin Heidelberg New York, pp 425–437
Simoneit BRT (1977) The Black Sea, a sink for terrigenous lipids. Deep-Sea Res 24:813–830.21
Sollins P, Spycher G, Glassman CA (1984) Net nitrogen mineralization from light-fraction and heavy fraction forest soil organic matter. Soil Biol Biochem 16: 31–37
Spiker EC, Hatcher PG (1984) Carbon isotope fractionation of sapropelic organic matter during early diagenesis. Org Geochem 5:283–290
Spiker EC, Hatcher PG (1987) The effects of early diagenesis on the chemical and stable carbon isotopic composition of wood. Geochim Cosmochim Acta 51:1385–1391
Spyckerelle C, Greiner A, Albrecht P, Ourisson G (1977) Hydrocarbons aromatiques d'origine geologique, III. Un tetrahydrochrysene, derive de triterpenes, dans des sediments recents et anciens: 3,3,7-trimethyl-1,2,3,4-tetrahydrochrysene. J Chem Res (M) 3746–3777
Stevenson FJ (1982) Humus chemistry. John Wiley and

Sons, New York
Stuiver M (1975) Climate versus changes in ^{13}C content of the organic component of lake sediments during the Quaternary. Quat Res 5:251–262
Talbot MR, Johannessen T (1992) A high resolution palaeoclimatic record for the last 27500 years in tropical West Africa from the carbon and nitrogen isotopic composition of lacustrine organic matter. Earth Planet Sci Lett 110:23–37
Talbot MR, Livingstone DA (1989) Hydrogen index and carbon isotopes of lacustrine organic matter as lake level indicators. Palaeogeogr Palaeoclimatol Palaeoecol 70:121–137
Takemura K (1990) Tectonic and climatic record of the Lake Biwa, Japan, region provided by the sediments deposited since Pliocene times. Palaeogeogr Palaeoclimatol Palaeoecol 78:185–193
Tan YL, Heit M (1981) Biogenic and abiogenic polynuclear aromatic hydrocarbons in sediments from two remote Adirondack lakes. Geochim Cosmochim Acta 45:2267–2279
Thompson S, Eglinton G (1978) The fractionation of a Recent sediment for organic geochemical analysis. Geochim Cosmochim Acta 42:199–207
Thurman EM (1985) Organic geochemistry of natural waters, Martinus Nijhof/Junk, Dordrecht
Volkman JK (1986) A review of sterol markers for marine and terrigenous organic matter. Org Geochem 9:83–99
Volkman JK, Kearney P, Jeffrey SW (1990) A new source of 4-methyl sterols and 5α(H)-stanols in sediments: prymnesiophyte microalgae of the genus *Pavlova*. Org Geochem 15:489–497
Wakeham SG (1976) A comparative survey of petroleum hydrocarbons in lake sediments. Mar Pollut Bull 7:206–211
Wakeham SG, Carpenter R (1976) Aliphatic hydrocarbons in sediments of Lake Washington. Limnol Oceanogr 21:711–723
Wakeham SG, Schaffner C, Giger W (1980a) Polycyclic aromatic hydrocarbons in Recent lake sediments. II. Compounds derived from biogenic precursors during early diagenesis. Geochim Cosmochim Acta 44:415–429
Wakeham SG, Schaffner C, Giger W (1980b) Polycyclic aromatic hydrocarbons in Recent lake sediments – I. Compounds having anthropogenic origins. Geochim Cosmochim Acta 44:403–413
Wieland E, Santschi PH, Höhener P, Sturm M (1993) Scavenging of Chernobyl ^{137}Cs and natural ^{210}Pb in Lake Sempach, Switzerland. Geochim Cosmochim Acta 57:2959–2979
Wünsche L, Gulaçar FO, Buchs A (1987) Several unexpected marine sterols in a freshwater environment. Org Geochem 11:215–219
Wünsche L, Mendoza YA, Gulaçar FO (1988) Lipid geochemistry of a post-glacial lacustrine sediment. Org Geochem 13:1131–1143
Yamamoto S, Ishiwatari R (1992) A study of the formation mechanism of sedimentary humic substances. III. Evidence for the protein-based melanoidin model. Sci Total Environ 117/118:279–292
Züllig H (1981) On the use of carotenoid stratigraphy in lake sediments for detecting past developments of phytoplankton. Limnol Oceanogr 26:970–976

Subject Index

abietic acid 304, 305, 320
absorption 170
acid lakes 185–213, 229, 245, 255, 256
acid neutralizing capacity 190
acid precipitation 186
acid volatile sulfide 225
acidification 229, 256
acidity
  ion exchange 194
  redox processes 197
acidity generation 185
adiabatic temperature gradient 93
advection 83
aerosols 172
age of lakes 24
air-water exchange
  double-resistance theory 167, 168
air-water partition coefficient 168
algae
  as particulate matter 173
alkaline lakes 235, 239
alkalinity 190, 192, 194
alkanes 293, 312
alkanols and alkanones (n-) 293
alkenones 294
aluminium 211
amino acid dating 300
ammonia 189
amyrin (α-) 305, 320, 321
anisotropic diffusion 126, 127
annual stratification 129, 131
aspect ratio 85
atmospheric deposition 185–213

bacteria
  anaerobic 281, 322
  products 280
balance
  for stable isotopes in lake 143, 146
bank storage 54, 59
baroclinic waves 104
barotropic waves 105
Batchelor Scale 103
Be-7 283
benzo(a)pyrene 303
biomarkers
  algal 293, 300, 301, 307
  definition 292
  land-plant 293, 301, 311
  microbial 297
bioturbation 281
bottom currents 116
bottom-boundary layer 115–119
boundary mixing 115
Brunt-Väisälä frequency *see* stability frequency
buoyancy flux 97, 99, 121, 130
  benthic boundary layer 98
  local 97, 101
  mixed layer 98, 99
  surface 98, 99, 109, 110

C/N ratio
  organic matter 283–285, 289
cabbeling 91, 128, 132
campesterol 300, 302
cappilary waves 105
carbon cycle 281
carbon isotopes
  C_3 plants 284, 286
  C_4 plants 284, 286
  leaf *n*-alkanes 295
  plankton 284
carbon preference index (CPI) 295, 298, 322
carbonate deposits 140, 161
carotenoids 307, 322
chemical weathering 208
chemolithotrophic organisms 267
chemoorganotrophic organisms 268
chlorophyll 306, 307
chlorophyll spectra 133
cholesterol 300, 302
chrysene 303, 305, 320
climate 19
climate change 74
  effect on stable isotopes 78
  effect on surface elevation 78, 79
  effect on water temperature 75–77
closure approximation 88
  local 88, 125
  nonlocal 88
coastal lagoons 14, 18
condensation 96
constant stress layer 100, 108, 116
continuity equation 86
convective mixing 110
Coriolis acceleration 86, 106, 132
Cox Number 109, 113
CPI definition 295
crater lakes 13, 18, 25
critical length scale for reactive species 134
Cs-137 283
  Chernobyl derived 226, 243
  dating 243, 249
cyanobacterial mats 275
  morphology 275

d-(excess) parameter for stable isotopes 142, 152, 153
delta lakes 13
density current 128, 132
density gradients, horizontal 131, 132
density of lakes (number per area) 5
density of water 91, 92
  influence of dissolved or suspended substances 92
density ratio *see* stability ratio
deposition
  dry 173
  wet 174
differential diffusion 132
differential heating and cooling 100, 128
differential mixing 128, 132
diffusion
  between water and air 169
  molecular 83
  turbulent 89
diffusive regime of double diffusion 120–122
diffusive sublayer 117
dimictic lake 147, 148
dinosterol 300, 301
dissipation
  turbulent kinetic energy 100, 101, 108, 125
diurnal winds 131
double diffusion 120
drag coefficient *see* wind stress coefficient

eddy diffusion *see* turbulent diffusion
eddy viscosity 89, 117
emissivity 96, 97
  of atmosphere 97
endorheic lakes 21
energy budget 63
  equations for components 70
  equations for ice 72
  equations for water 69, 70
energy fluxes
  kinetic 95, 98
  potential 95, 97
  thermal 95–97
enthalpy of vaporization 168
ephemeral lake 150, 157–160
epilimnion 147, 148
equation of state of water 91, 128
Eulerian representation 86
eutrophication 300, 313, 318
evaporation 15, 64, 96, 110, 170
  Craig and Gordon model 141, 154
  evaporation isotope flux 141, 152
  evaporation lines 142, 154, 156
  evaporation methods 40–43, 59
  evaporation pan 143, 144
evapotranspiration 145, 152, 153

fatty acid (FAC)
  carbon preference index 298
  composition diversity index 298
  relative degradation rates 293, 297
ferromanganese concretions 221
Fick's Law 83, 89, 108, 169, 171
finger regime of double diffusion 120–122
floodplain lakes 13
fluvial lakes 12, 18, 31
Flux Richardson Number 99, 101
forest
  acidity 195
  nitrogen saturation 201
form drag 119
friction velocity 171
  bottom boundary layer 116
  of wind 99, 108
fulvic acid
  C/N ratios 291
  definition 290
  H/C ratios 291

geothermal heat flux 97, 98, 118, 123
glacial lakes 8, 18, 25, 31
Gradient Richardson Number 99, 107, 112, 114
gradient-flux model 89
gravity 86
gravity waves 104, 106
groundwater 37, 38, 40, 45–62
gypsum precipitation 276

haline contraction, coefficient of 92, 94
halocline 157
heat content
  annual variation 85, 95
heat flux 85, 96, 111
heavy metals 198
Henry's Law constant 168
Holocene 25
humic acid
  C/N ratios 291
  definition 290
  H/C ratios 291
humin
  C/N ratios 291
  definition 290
  NMR spectra 292
hydraulic conductivity 49, 52, 58
hydraulic loading 85, 100
hydrological budget 63–65
  equations for 67, 68
hydrostatic equation 89
hypolimnion 147, 148, 157

incompressible flow 87
index lake
  for stable isotope balance 144
inertial circle 106
inertial frequency 105–107
inertial subrange 102, 125
inertial-convective subrange 103, 126, 133
internal friction 86
internal waves 107, 129, 130
interstitial waters 161
intrusion 127
isopycnal diffusion 123–129
  models 125, 126
isopycnal surface 128
isotope enrichment 140, 143, 148
isotope fractionation
  equilibrium effect 139
  kinetic (transport) effect 139, 141
  salinity effect 155, 156
isotropic turbulence 102, 125

Karman constant 99
Kelvin waves 105, 106
Kelvin-Helmholtz instability 107, 112
kinetic energy 98
  from rivers 100
Kolmogorov Scale 102, 125, 132

Lagrangian representation 86
lake level fluctuativa 25, 64, 65
land plants
  biomarkers 293, 301, 311
  C/N ratios 284
  carbon-isotope ratios 286
  nitrogen-isotope ratios 288
landslide lakes 25
Langmuir circulation 111, 133
law of the wall 108, 116
lead 199
level change of lakes 25
lignin
  Ad/Al ratio 309
  C/V ratio 308, 319
  S/V ratio 308, 319
limnic ratio 7
load, critical 202
logarithmic layer 108, 116
Lorentzian function 180
Lotka-Volterra 133, 134

marine saline lakes 265, 266
  characteristics 276
  chemocline 267
  composition 267, 268
  epilimnion 267
  holomixis 267
  hydrological cycle 266
  hypolimnion 267
  mineral precipitates 267, 269, 274–276
  organisms 267, 268
mass balance
  role of air-water exchange 176, 177
mass transfer coefficient
  air-water 171
meromictic lake 147, 148, 154
meromictic lakes 223, 232, 239, 248, 253, 258
meromixis 123, 129, 132
meteoric water line (MWL)
  for stable isotopes 139, 151–153
methylation of trace elements 223, 231, 232, 233, 235, 239
mixed layer 110
  models 73
mixing 83
  diapycnal 112–115
  isopycnal 123–129
  spatial scales 134
  time scales 129
  turbulent 83
mixing efficiency 101, 110, 112
mixing time
  convectively driven 130
  wind-driven 130
models
  lake-level 68
  thermal 73, 74
moisture, effective 63, 66
moisture exchange between water and atmosphers effect on stable isotopes 141, 142

Monin-Obukhov Length 99, 102, 109, 111
monomictic lake 147, 148

Navier-Stokes equation 87
neutral surface 128
nitrate 212
nitrogen isotopes 288, 289
nonlocal exchange 89, 90

octanol-water partition coefficient 173
Okubo diagram for horizontal mixing 126, 134
organic carbon partition coefficient 175
overturn 147, 148, 157
oxygen isotopes 78
Ozmidov Scale 102, 109, 113

PAHs (polycyclic aromatic hydrocarbons) 176
paleolimnology 161
paleotemperatures 316
particulate matter
  in air 172
  in water 172
  role of algae 173
partition coefficient
  air-water 168
  octanol-water 173
  organic carbon 175
patchiness 133
  of biomass 134
Pb-210 dating 244, 248, 249
PCB (polychlorinated biphenyls) 174, 176
perylene 303, 304, 318, 320
petroleum residues 292, 314, 318, 320
pheophorbide 307
pheophytin 307, 308
photoadaptation 134
photochemical oxidation/reduction 219, 237
photosynthesis 134
phototrophic organisms 267
phytane 317
picene 304, 320
planetary waves 105
plankton
  biomarkers 293, 300, 301, 307
  C/N ratios 284
  carbon-isotope ratios 284
  nitrogen-isotope ratios 288
Poincaré waves 105, 106
pore water
  calcite saturation 274
  carbon and sulfur species 271
  chemical model 272
  concentration 275
  sulfate reduction 274
porphyrins 321, 322
potential energy 97
potential temperature 94
potential vorticity 105, 106
potentiomanometer 46, 56, 57, 59
precipitation 64
  acid 186
precipitation methods 38–40
pressure gradient 86
pristane 317
pycnocline 115
  diurnal 130
  seasonal 131
pyrene 303, 304

radiation
  long wave 96
  short wave 69, 96
radiocarbon dating
  organic-carbon 283, 315
ragweed pollen 283, 313
rain water 192
reaction time 132
Redfield stoichiometry/ratios 249, 252, 273
reservoirs 32
resuspension of sediment particles 119
retene 304, 320, 321
Reynolds' decomposition 87
Reynolds Number 116
Reynolds' stress 88
  production of turbulent kinetic energy 99, 101
Richardson Number *see* Flux or Gradient Richardson Number
river input 98, 123, 131
Rn-222 119
Rossby waves 105
roughness length 116
runoff 64

sabkhas (ephemeral salt lakes) 157–160
saline lakes 14, 21, 154, 159, 223, 239, 253
salinity 23, 92, 266
salt fingers 121
sapropel 269, 273
sediment-traps
  C/N ratios 284, 311
  carbon-isotope ratios 286, 311
  fatty-acid decomposition 293
  nitrogen-isotope ratios 289
  organic-carbon decrease 281, 311
sedimentation 179
sediments
  dating 283
  laminated 249
seepage meter 38, 46, 57, 59
seiche pumping 132
Seiches 105
  Defant procedure 107
  horizontal modes 107, 132
  internal 107, 114, 129, 130
  Merian formula 105, 107
  vertical modes 107, 131
shear diffusion 126, 127
shear of velocity 113, 115
sitosterol (β-) (2,4-ethylcholesterol) 300, 302
skin friction 119
solar radiation 96
solubility 168
specific expansion coefficient 91
specific heat 87, 99
stability
  global 93
  local 93, 120
  vertical of water column 91
stability frequency 90, 94, 99, 122
stability ratio 120, 122
standard mean ocean water (SMOW) 142
Stefan-Boltzmann Law 96
stenol/stanol ratio 301, 303
stirring 83, 110
Stokes' drift 106
stratification 85, 267
  potential energy 95
stream gaging 44
string of lakes 151, 152
sulfate 206
sulfur bacteria 130
sulfur dioxide 189
sulfurhexafluoride (SF_6) 132
surface waves 104, 106, 129

tectonic lakes 8, 18, 25, 31
temperature
  fluctuations 113
  microstructure 113, 119
temperature of maximum density 91
  influence of pressure 91
  influence of salinity 93
terminal lake 150
thermal bar 128, 129, 132
thermal expansivity 91, 92
  influence of salinity 93
thermals 121
thermobaricity 91, 128
thermocline 147
  models 73
Thorpe-displacement 102, 113
topographic Rossby waves 105, 106
trace elements
  pore waters 221, 227, 229, 238, 242, 244, 247, 248, 250, 253–256
trace metal-nutrient relationships 249, 251, 252

trace metals
  analysis 217, 229, 248
  effect of ice cover 253
tracer, artificial 124
transilient turbulence theory 89, 90
transport
  advective 83, 123
  diffusive 83, 123
turbidity currents 129
turbulence cascade 102
turbulent diffusion
  diapycnal 109, 111, 112, 114
  momentum 117
  horizontal 126
  isopycnal 123–129
  vertical 99, 109, 111
turbulent fluctuation 87
turbulent kinetic energy (TKE) 99, 100
  balance for double diffusion 122
  dissipation 101, 103, 108, 134
  rate of production by wind 108
  spectrum 102
turbulent velocity 129
typology of lakes 18, 31

unresolved complex mixture (UCM)
  definition 296
  sediment records 296, 314, 318
unsaturated ketones 294
uranin, fluorescent dye 123, 124

vapor pressure 168
viscosity 87
viscous sublayer 115–117
  energy dissipation 116
volatilization 170

wash-out ratio
  for chemical deposition in water 174
water balance 143, 144
watershed manipulation 210
watershed models 44, 45, 47, 59
  IHDM 48
  ILWAS 45
  U.S. Geological Survey 44
  Variable Source Area Simulator 48
waves 104–107
wax esters 294
weathering 208
wind friction velocity 99, 108
wind speed
  influence on air-water exchange 171
wind stress 86, 108, 130
  coefficient 100
wood
  C/N ratios 284
  carbon-isotope ratios 286
  lignin degradation 309
  NMR spectra 292

Lake Index

Abaya 8
Abert 65
Abhe 8, 26, 28
Agaziz (ancient) 26, 27
Alakol (or Alakul, Kazakstan) 8
Albert 1, 8, 9
Alpnachersee 109, 114, 116
Amazonian lakes 150
Anderson 244, 245, 250
Aral Sea 1–3, 6, 8, 9, 15, 20–25, 27, 29, 30, 32, 63
Asal 8, 15, 28
Atitlan 8, 14, 24

B, Pond, Savannah River Site 238
Ba, Loch 222, 244, 250, 257
Baghrash 21
Baikal 8, 9, 24, 29, 85, 94, 113, 128, 132, 148, 257
Balaton 30
Baldeggersee 119, 252
Balkhash 9, 15, 21–23, 29
Baltic Ice Lake (ancient) 27
Bardawil (Lagoon and sabkhas) 160, 161, 265–268
Bataklik (ancient) 25
Becharoff 12
Bickford Reservoir 246–250
Bielersee (Bienne) 85, 228, 252
Biwa 7, 8, 24, 31, 225, 284–286, 294, 308–310, 315–317
Bolsena 14
Bonneville (ancient) 27, 310
Botsumvi 14, 24, 284, 286, 287, 289
Bracciano 14
Brown Pond 307
Burdur 29

Cadagno 130
Canadian Shield lakes 256
Caspian Sea 1, 2, 6, 8, 9, 14, 15, 20–25, 27, 29, 30, 63, 85
Chad 5, 8, 9, 15, 21, 22, 26, 28, 78, 154
Champlain 8, 10, 12
Chao 12
Chilka 14
Clearwater 196, 230, 250
Coburn Pond 284, 286, 299, 303
Coipasa (salt pan) 26, 27
Constance 249–252
Crater (Oregon) 14, 24, 85
Crater (Quebec) 14, 24
Cristallina 208–210
Crystal 245, 246

Dakataua 14
Darts 246, 250
Davis Creek Reservoir 235
Dead Sea 5, 8, 9, 14, 15, 27, 85, 92, 95, 132, 154, 155, 157, 158, 161, 265
Dieri (ancient) 28
Dong Ting (Tung Ting) 9, 12, 13

Eagle 65
Ebi 21
Edku 13
Edward 1, 8, 9
Eil Malk (Jellyfish) 253, 265–267, 269
Ekoln 58
Ellesmere 294
Erie 6, 64, 65, 220, 225, 244, 250, 257, 282, 314
Esthwaite Water 226–228, 243, 244, 250, 252–254, 256, 308
Experimental Lakes Area (ELA) 196, 197, 201, 237, 242, 248, 249, 256
Eyre 2, 9, 15, 21, 22, 24, 25, 28

Fayetteville Green 248
Frome 21, 28

Gaggade-Asal-Sukalol (ancient) 26, 28
Gairdner 21
Geneva (Léman) 7, 299, 300
George 8, 24
Gersauersee 132
Ghoubbat (ancient) 26
Giuiletti 157
Goose 65
Grand Coulee, lakes of the 151
Grasmere 294
Great Bear 12
Great Salt 1, 8, 15, 21, 26, 27, 64–66, 161, 265
Great Slave 1
Green 286
Green Bay (Lake Michigan) 179, 182
Gregory 28
Greifensee 233–237, 317, 318, 320, 321
Grosswald (ancient) 27
Gull Pond 238, 239

Hanle-Dobi (ancient) 26
Harney-Malheur 76, 77
Haruna 291, 293, 295, 299, 301
Hayward 268
Helmand 21
Hong Ze (=Hung Tse) 12, 13
Hovsgol (Khubsugul) 1, 8
Hulun 13
Huron 6, 12, 282, 291, 294, 299, 312, 314

Ikeda 14
Iliamna 12
Issyk-Kul 1, 7–9, 15, 24

Jellyfish (Eil Malk) 253, 265–267, 269

Kainji reservoir 144
Kara Bogaz 14, 15
Kesterson Reservoir 241
Kinneret (also Tiberias) 146–149, 157, 159, 244
Kiribati 265, 268, 272
Kivu 1, 8, 9, 24, 26, 28, 120–122
Kucharo 14

Ladoga 7, 10, 11
Lahontan (ancient) 27, 65, 66, 78, 79
Lake 223 (ELA) 201
Lake 227 (ELA) 196, 197
Lanao 24, 30
Laurentian Great Lakes 24, 64, 151–154, 249
Le Bouchet 24, 25
Léman (Geneva) 7, 299, 300
Lisan (ancient) 27, 158, 161
Longmu 29
Lop Nor 29
Lovers 266
Luang 14

Lucerne 123–125, 131

Mai Ndombe 13
Makarikari (salt pan) 22, 26
Malawi (former Nyasa) 1, 8, 9, 21, 23, 148
Managua 9
Mangrove 265–277, 284–286, 292, 310
Manitoba 26, 27
Manzalah 13, 21
Maracaibo 8, 9, 14, 24, 25
Mashu 14
McFarlane 250
Mega Chad (ancient) 28
Michigan 6, 10–12, 85, 106, 179, 182, 220, 280, 281, 284, 286, 287, 293, 307, 311, 312
Minchin (ancient) 26, 27
Mississippi Lakes 24
Mono 234, 235, 239
Montriond 25
Motosu 294
Motte 300, 301

New Euxine (ancient) 27, 29
Nicaragua 8, 9

Ohakuri 221, 230, 233–235
Ohrid 24
Ojibway (ancient) 26, 27
Okavango swamp 28, 144, 145
Onega 10, 11
Ontario 6, 12, 125, 127, 182, 250, 282, 287, 313, 314
Ossa 14

Pangong 8
Par Pond 238, 242, 243
Persian Gulf sabkhas 160
Piccolo Naret 208
Ponchartrain 13
Poopo 14, 15, 21, 26, 27
Poyang 12, 13
Prespa 24
Priest Pot 293, 307
Pur Mensi 27
Pyramid 8, 21, 26, 27, 70, 71, 76, 78, 79, 284, 286, 299

Quinalt 296

Raak Plain dry lakes 158, 159
Ras Muhammed (Mohammad) 265, 268
Red 10, 27
Rostherne Mere 295, 302
Rotorua 14
Rottnest lakes 267
Rudolf (Turkana) 1, 8
Rukwa 9

Sagamore 303–305
Saint Clair 314
Sallie 46
Sammamish 237, 248, 250–252
Sarez (Pamir) 24
Sarykamish 2, 7, 22, 23
Searles 161
Sempachersee 111
Shikotsu 14
Shirakome-ike 301
Shoji 295
Shorkul 29
Silver 65, 255
Siskiwit 167, 176–178, 182
Snake 55
Soap 239, 240
Solar 265, 267–270, 272, 275–277
Sparkling 148, 150
Summer 65
Sumxi 29
Superior 6, 12, 154, 176–178, 180–182, 221, 244, 250, 256, 281, 289
Suwa 294, 297–299, 301

T Reservoir, Japan 250
Taal 14
Tahoe 8, 21, 24, 103, 133
Tai 12, 13
Tanganyika 1, 8, 9, 21, 23, 24, 26, 28, 148
Tauca 26, 27
Taupo 8
Taymir 8, 12
Tazawa 14, 85

Tiberias (also Kinneret) 146–149, 157, 159, 244
Titicaca 1, 5, 9, 14, 21, 22, 26, 27
Toba 7, 8, 14, 24, 31
Tonle Sap (Grand Lac) 2, 13
Torrens 9, 21
Towada 14
Toya 14
Trasimeno 14
Turkana (former Rudolf) 1, 8, 9, 15, 23, 26, 28
Tuz 29

Urmia 8, 9, 14, 15, 29
Urnersee 114, 115, 132
Urs 4
Uyuni (salt pan) 24, 26, 27

Val Sabbia 208
Vallon 24, 25
Van 15, 29
Vanda 148, 224, 253
Vechten 293
Vico 14
Victoria 1, 8, 9, 24
Viti 24, 25

Walker 26, 27, 65, 284, 286, 287
Wapamunga 159
Washington 249, 296, 319–321
Weishan 13
Williams 38–43, 55–57
Windermere 249, 251, 252
Winnemucca 65
Winnipeg 26, 27
Winnipegosis 27
Wisdom 1, 14, 24
Woods (Australia) 28
Woods (Canada) 27

Yellowstone 74–76
Yunoko 285

Zota 208, 210
Zugersee 114, 115, 131
Zürichsee (L. Zurich) 96, 98, 106, 223, 237, 249, 250, 252, 308